



PHASE EQUILIBRIA STUDIES ON CHEMICAL MIXTURES ENCOUNTERED IN THE NATURAL GAS INDUSTRY

By

Paul Zwawanda

MTech Eng (Gubkin University, Russia),

BTech (Hons) Eng (Chinhoyi University of Technology, Zimbabwe)

Submitted in fulfilment of the degree Doctor of Philosophy in Chemical Engineering

University of KwaZulu-Natal

February 2022

APPROVALS FOR THESIS SUBMISSION

As the candidate's supervisor, I, Prof P Naidoo, have approved this thesis for submission.



Prof. Paramespri (Prathieka) Naidoo

09 February 2022

Date

As the candidate's supervisor, I, Dr. Wayne Michael Nelson, have approved this thesis for submission.

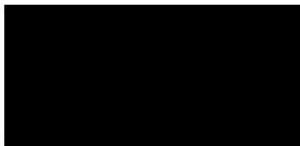


Dr. Wayne Michael Nelson

09/02/2022

Date

As the candidate's supervisor, I, Dr Kuveneshan Moodley, have approved this thesis for submission.



Dr. Kuveneshan Moodley

09-02-2022

Date

DECLARATION 1: PLAGIARISM

This thesis is submitted in fulfilment of the academic requirements for the degree PhD in Chemical Engineering.

I, Paul Zvawanda, student number (218084291) declare that:

1. The research reported in this thesis, except where otherwise indicated, is my original research.
2. This thesis has not been submitted for any degree or examination at any other university.
3. This thesis does not contain other persons' data, pictures, graphs or other information, unless specifically acknowledged as being sourced from other persons.
4. This thesis does not contain other persons' writing, unless specifically acknowledged as being sourced from other researchers. Where other written sources have been quoted, then:
 - a. Their words have been re-written but the general information attributed to them has been referenced
 - b. Where their exact words have been used, then their writing has been placed in italics and inside quotation marks, and referenced.
5. This thesis does not contain text, graphics or tables copied and pasted from the Internet, unless specifically acknowledged, and the source being detailed in the thesis and in the References sections.

Signed

09 February 2022

.....

.....

Paul Zvawanda

Date

DECLARATION 2: PUBLICATIONS

DETAILS OF CONTRIBUTION TO PUBLICATIONS that form part and/or include research presented in this thesis (include publications in preparation, submitted, *in press* and published and give details of the contributions of each author to the experimental work and writing of each publication)

Publication 1: Paul Zvawanda, Paramespri Naidoo, Wayne Michael Nelson, and Kuveneshan Moodley
“*P-T-x* Measurement and modelling of Methane or Carbon dioxide +2,2'-[ethane-1,2-diylbis(oxy)] di(ethan-1-ol) (TEG)/methanol Systems from $T = 298.15$ to 323.15 K”,
Journal of Chemical and Engineering Data, 14 April 2022,
<https://doi.org/10.1021/acs.jced.2c00061>.

Publication 2: Paul Zvawanda, Paramespri Naidoo, Wayne Michael Nelson, and Kuveneshan Moodley
“*P-T-x* Measurement and modelling of Methane + propane + methanol; Methane + propane + TEG; Methane + propane + methanol + TEG systems”, *in preparation*.

Publication 3: Paul Zvawanda, Paramespri Naidoo, Wayne Michael Nelson, and Kuveneshan Moodley
“*P-T-x* Measurement and modelling of 5/6 component systems (Methane + propane + methanol + water + TEG; Methane + propane + carbon dioxide + methanol + water + TEG) typical to those encountered in natural gas industry”, *in preparation*.

Signed

09 February 2022

.....

.....

Paul Zvawanda

Date

ACKNOWLEDGEMENTS

Firstly, I would like to thank the Lord Almighty, who made this happen and kept me safe throughout my studies.

Secondly, much appreciation goes to my supervisors: Prof P Naidoo, Dr W Nelson and Dr K Moodley, for their guidance and support was unmatched. Special mention goes to:

- i) Prof P Naidoo for accepting my application to join the Thermodynamics Research Unit (TRU).
- ii) Dr W Nelson for the design and development of the equilibrium cell used in this study. Prof Dominique Richon is also appreciated for his assistance and expertise led to the development of the equipment used in this study. Furthermore, the funds to purchase the material and build the unit was from Prof Deresh Ramjugernath's research funding and he is also much appreciated.
- iii) Dr K Moodley for much guidance on writing and modelling.

Thirdly, I would like to thank Sivanna Naicker, the laboratory technician Mr Ayanda Khanyile, and all the technical support staff in the chemical engineering discipline for their help, guidance, teachings were of great significance in this study.

Much appreciation also goes to the NRF (National Research Foundation) and the SARChI (South African Research Chair Initiative) for without their financial support, this study would not have been a success.

I would also like to thank my colleagues Paul Ngcobo, Phakamile Ndlovu, Edward Marondedze, Dr Mojgan Ebrahimejadhasanabadi and Dr Marcin Durski for their inspiration and support.

Lastly, special appreciation goes to my family for their unwavering support throughout these four years. Special mention goes to my parents Mr and Mrs C Zvawanda, my wife Palocia and my son Nyashadzashe for being my pillar of strength and motivation throughout my studies.

ABSTRACT

Natural gas processing involves removing impurities from the gas streams. These impurities include carbon dioxide, nitrogen, hydrogen sulphide, water vapour, mercury, and others. These impurities must be eliminated from the gas streams, often using solvents, to meet sales specifications, enhance calorific value, lessen corrosion and blockages in pipelines due to hydrate formation and to allow for cryogenic gas processing. Solvents such as methanol and the lower molecular weight glycols have the most suitable characteristics to be employed as hydrate inhibitors, whilst 2,2'-[Ethane-1,2-diylbis(oxy)] di(ethan-1-ol) (triethylene glycol (TEG)) is mostly used in dehydration plants.

In this study, phase equilibria data for mixtures of six chemical species commonly encountered in the processing of natural gas were studied. Phase equilibrium measurements were performed using a combined static (synthetic or analytic) apparatus. The apparatus comprises a horizontal cylindrical sapphire tube fitted with a movable piston that can be used to adjust the cell volume, thereby fixing/controlling the pressure in the process. A mobile Rapid Online Sampler Injector (ROLSI™) was fitted to the equilibrium cell for sampling both the vapour and the liquid phases. Vapour- liquid equilibrium (TP_{xy}) data were measured and modelled for the following test systems, carbon dioxide + n-hexane and carbon dioxide + n-decane over a temperature range of 313.15 to 319.23 K. Bubble point (TP_x) data were measured and modelled for the following test systems: carbon dioxide + methanol; carbon dioxide + TEG; methane + methanol; methane + TEG; carbon dioxide + aqueous TEG systems over a temperature range of 298.10 to 323.15 K. Generally, good agreement was observed between the reported literature data and the experimental data measured in this work, thus validating the experimental techniques used. New TP_x data were measured and modelled for seven novel systems of this study, namely: methane + propane + methanol; methane + propane + TEG; methane + methanol + TEG; carbon dioxide + methanol + TEG; methane + propane + methanol + TEG; methane + propane + methanol + water + TEG; methane + propane + carbon dioxide + methanol + water + TEG over a temperature range of 283.15 to 323.15 K and in selected composition regions. The composition ranges and conditions are typical of those found in gas pipelines and gas dehydration units.

The experimental data were modelled in Aspen Plus V11-12 using appropriate thermodynamic models, i.e., Peng Robinson (PR), Soave-Redlich-Kwong (SRK), Peng Robinson Wong Sandler (PRWS), Perturbed-Chain Statistical Associating Fluid Theory (PC-SAFT), and the Cubic Plus Association (CPA) models. The maximum absolute average relative deviation (AARD) in pressure on all the modelled data were 4.89%, 8.67%, 7.39%, 9.63% and 19.7% for the PRWS, SRK, CPA, PR, and PC-SAFT models, respectively, indicating that the PRWS model best described most of the systems.

The measured data contributes to the information required for the process design, control and monitoring of methanol and/or TEG in gas conditioning systems. Furthermore, the data helps refine thermodynamic models that can predict phase behaviour in multicomponent systems in applications mentioned earlier, including gas hydrate inhibition, subsea gas processing, carbon capture, and storage.

Table of Contents

APPROVALS FOR THESIS SUBMISSION	ii
DECLARATION 1: PLAGIARISM	iii
DECLARATION 2: PUBLICATIONS.....	iv
ACKNOWLEDGEMENTS	v
ABSTRACT.....	vi
List of Figures.....	xv
List of Tables	xx
Nomenclature	xxv
CHAPTER 1: PROJECT BACKGROUND	1
1.0 INTRODUCTION.....	1
1.1. Gas dehydration.....	3
1.2. Aim and objectives.....	5
1.3. Changes encountered in this study	7
1.4. Thesis structure.....	8
CHAPTER 2: REVIEW ON SYSTEMS INVESTIGATED IN THIS STUDY	10
2.0 INTRODUCTION.....	10
2.1. Chemicals selected in this study.....	11
2.1.1. Triethylene glycol (TEG).....	12
2.1.2. Methanol	13
2.1.3. Water.....	13
2.1.4. Carbon dioxide.....	14
2.1.5. Methane.....	14
2.1.6. Propane	15
2.1.7. n-Hexane	16
2.1.8. n-Decane	17
2.2. Intermolecular forces.....	17
2.2.1. Hydrogen bonding and the hydrophobic effect.....	18
2.3. Published phase equilibria data for components related to this study.....	20
2.3.1. Binary systems data	20
2.3.1.1. Methane + TEG system.....	20
2.3.1.2. Propane + TEG system	22
2.3.1.3. Carbon dioxide + TEG system.....	23

2.3.1.4. Water + TEG system.....	25
2.3.1.5. Methanol + TEG system	26
2.3.1.6. Methane + methanol system	26
2.3.1.7. Propane + methanol system	28
2.3.1.8. Carbon dioxide + methanol system.....	29
2.3.1.9. Water + methanol system.....	30
2.3.1.10. Methane + water system	31
2.3.1.11. Propane + water system	32
2.3.1.12. Carbon dioxide + water system.....	33
2.3.1.13. Methane + carbon dioxide system.....	34
2.3.1.14. Propane + carbon dioxide system	35
2.3.1.15. Methane + propane system	36
2.3.2. Ternary systems data.....	37
2.3.2.1. Methane + propane + carbon dioxide system	37
2.3.2.2. Methane + carbon dioxide + methanol system	38
2.3.2.3. Methane + carbon dioxide + water system	38
2.3.2.4. Methane + water + methanol	39
2.3.2.5. Propane + carbon dioxide + methanol	40
2.3.2.6. Propane + water + methanol	40
2.3.2.7. Carbon dioxide + water + TEG system.....	41
2.3.2.8. Carbon dioxide + water + methanol system.....	42
2.3.2.9. Ternary systems with no reported data	43
2.3.3. Quaternary systems	43
2.3.4. Five-component (quinary) systems	44
2.3.5. Six-component (senary) system	45
2.4. Summary of chapter 2	45
CHAPTER 3: REVIEW OF THERMODYNAMIC PRINCIPLES FOR HPVLE MODELLING	46
3.0 INTRODUCTION.....	46

3.1 Overview of the key principles in phase equilibrium thermodynamics	46
3.1.1. Fugacity and vapour-liquid equilibrium for pure components	46
3.1.2. Fugacity and vapour-liquid equilibrium for mixtures	47
3.1.2.1 The ideal solution and ideal gas approaches	48
3.1.2.2. Gamma-Phi modelling	50
3.1.2.3. Phi-Phi modelling	51
3.2. Thermodynamic models applied in this work	51
3.2.1. Cubic equations of state used in this study	51
3.2.2. Activity coefficient model	55
3.2.2.1. Overview of G^E models	55
3.2.3. Mixing rules that combine an EOS with an activity coefficient model	56
3.2.3.1. Wong Sandler (WS) mixing rules	56
3.2.3.2. Peng-Robinson Wong Sandler (PRWS)	57
3.2.4. Association models	58
3.2.4.1. Overview of association models	58
3.2.4.1.1. Association schemes	58
3.2.4.2. The Perturbed-Chain Statistical Associating Fluid Theory (PC-SAFT) model	60
3.2.4.3. Cubic Plus Association (CPA) EOS	61
CHAPTER 4: REVIEW OF EXPERIMENTAL METHODS AND APPARATUS USED FOR VAPOUR-LIQUID EQUILIBRIA MEASUREMENTS	64
4.0 INTRODUCTION	64
4.1. Classification of HPVLE experimental techniques	64
4.1.1. The static and dynamic method of classification	65
4.1.1.1 Static methods	66
4.1.1.2 Description of the static analytic method	66
4.1.1.3 Description of the static synthetic method	68
4.1.1.4. List of apparatus that employ a combination of the static analytic, static synthetic method, with either temperature or pressure control	70
4.1.1.5 List of other static apparatus with variable volume view cells	70
4.2. Preparation methods for synthetic mixtures	83

4.2.1. Gas mixtures	83
4.2.2. Preparation of liquid solutions	84
CHAPTER 5: EXPERIMENTAL WORK	85
5.0 INTRODUCTION.....	85
5.1. Equipment set up and equilibrium cell description	85
5.2. Experimental procedure.....	91
5.2.1. Temperature probe calibration	91
5.2.2. Pressure transducer calibration	92
5.2.3. GC detector calibration	93
5.2.4. VLE (TP_{xy}) measurement procedure: binary system	96
5.2.5. Bubble point measurements	98
5.2.5.1 Preparation of a binary liquid mixture	98
5.2.5.2 Preparation of a ternary liquid mixture	99
5.2.5.3 Bubble point (TP_x) measurement procedure.....	100
CHAPTER 6: RESULTS AND DISCUSSION	102
6.0 INTRODUCTION.....	102
6.1 Chemicals used	102
6.1.2 Water content in methanol and triethylene glycol	105
6.2 Calibrations	105
6.2.1 Temperature sensors calibration results	105
6.2.2 Pressure transducer calibration results	107
6.2.3. GC detector calibration results.....	109
6.2.3.1 GC calibration carbon dioxide (1) + n-hexane (2) test system	109
6.2.3.2 GC calibration carbon dioxide (1) + n-decane (2) test system.....	111
6.3. VLE test system measurements and modelling	113
6.3.1 Carbon dioxide (1) + n-hexane (2) test system	115
6.3.2 Carbon dioxide (1) + n-decane (2) test system	119
6.3.3 Carbon dioxide (1) + methanol (2) test system.....	122
6.3.4 Methane (1) + methanol (2) test system.....	125
6.3.5 Methane (1) + TEG (2) test system.....	128

6.3.6 Carbon dioxide + TEG and its aqueous test systems	131
6.3.6.1 Carbon dioxide (1) + (water (2) / TEG (3) 10/90 wt.%) test system.....	135
6.3.6.2 Carbon dioxide (1) + (water (2) / TEG (3) 3.5/96.5 wt.%) test system.....	138
6.4 New systems: VLE data measurement and modelling.....	141
6.4.1 New system 1: (methane (1) /propane (2) 95/5 mol%) + methanol (3).....	141
6.4.1.1 Comparison of the methane + methanol system and the propane-free (methane / propane 95/5 mol%) + methanol system at 303.15 K.....	149
6.4.2 New system 2: (methane (1) /propane (2) 95/5mol%) + TEG (3)	150
6.4.2.1 Comparison of the propane-free (methane/propane 95/5 mol%) + TEG system and the methane + TEG system at 323.16 K	157
6.4.3 New system 3: methane (1) + (methanol (2) / TEG (3) 3.33/96.67 wt.%).....	158
6.4.3.1 Comparison of the methanol-free (methane + (methanol / TEG 3.33/96.67 wt.%) system and the methane + TEG system	165
6.4.4 New system 4: Carbon dioxide (1) + (methanol (2) /TEG (3) 3.33/96.67 wt.%).....	166
6.4.4.1 Comparison of the (carbon dioxide + TEG) and methanol-free (Carbon dioxide + (methanol/TEG 3.33/96.67 wt.%) system.....	172
6.4.5 New system 5: (methane (1)/propane (2) 95/5mol%) + (methanol (3) /TEG (4) 3.33/96.67 wt.%).....	174
6.4.5.1 Comparison of the propane-free (methane /propane 95/5 mol %) + (methanol /TEG 3.33/96.67 wt.%) system and the (methane + (methanol /TEG 3.33/96.67 wt.% system)).....	188
6.4.6 New system 6: (methane (1)/propane (2) 95/5 mol%) + ((water (3) /TEG (5) 5/95 wt.): methanol (4) 3.33 wt.%)	189
6.4.6.1 Comparison of the water-free (methane / propane 95/5 mol%) + ((water /TEG 5/95 wt.): methanol 3.33 wt.%) system and the (methane /propane 95/5 mol %) + (methanol /TEG 3.33/96.67 wt.%) system.....	205
6.4.7 New system 7: (methane (1)/propane (2)/carbon dioxide (3) 90.22/4.60/5.18 mol%) + ((water (4) /TEG (6) 5/95 wt.): methanol (5) 3.33 wt.%)	207
6.4.7.1 Comparison of the (methane /propane /carbon dioxide 90.22/4.60/5.18 mol%) + ((water /TEG 5/95 wt.): methanol 3.33 wt.%) system and the (methane / propane 95/5 mol%) + ((water /TEG 5/95 wt.): methanol 3.33 wt.%) system.....	215
CHAPTER 7: CONCLUSIONS	226

CHAPTER 8: RECOMMENDATIONS	230
REFERENCES	232
APPENDIX A	250
Uncertainty estimation	250
APPENDIX B: TABLES AND GRAPHS OF RESULTS	258
B.1. Vapour pressure measurement results	258
B.1.1. Water vapour pressure	260
B.1.2. Methanol vapour pressure results	261
B.1.3. n-Hexane vapour pressure results	262
B.1.4. Carbon dioxide vapour pressure results	263
B.2. Gas mixture composition validation	265
B.3. Pure component parameters	267
B.4 Vapour liquid equilibria measurement results: test systems	267
B.5. Vapour liquid equilibria measurement results: novel systems	271
APPENDIX C: P-y PLOTS	277
C.1 Carbon dioxide + n-hexane system	277
C.2 Carbon dioxide (1) + n-decane (2) system	278
APPENDIX D. DESCRIPTION OF THERMODYNAMIC MODELS APPLIED IN THIS WORK	279
D.1. Equations of state (EsOS) models	279
D.1.1. Cubic equations of state	279
D.1.1.1. Classical mixing rules	283
D.2. Activity coefficient models	284
D.2.1 The Non-random two liquid (NRTL) activity coefficient model	284
D.3. Wong Sandler (WS) mixing rules and its application in the PRWS model	285
D.4 Association models	287
D.4.1. The Perturbed-Chain Statistical Associating Fluid Theory (PC-SAFT) model	287
D.4.1.1. Mixtures	292
D.4.2. Cubic Plus Association (CPA) EOS	293
APPENDIX E MODELLING RESULTS	296
E.1. CPA analysis and flash results comparison using either literature k_{ij} or k_{ij} from this work for binary systems of interest	296
E.2. Graphical representation of the statistical significance of k_{ij} on the methane + methanol system	300

E.3. CPA multicomponent systems bubble point predictions using k_{ij}s reported in table 6-19	303
APPENDIX F: CPA PURE COMPONENT VAPOUR PRESSURE AND DENSITY PREDICTIONS	316

List of Figures

Figure 1-1: Natural gas value chain: from the wells to the consumers	1
Figure 1-2: Process flow diagram for a glycol dehydration unit	4
Figure 2-1: Structural formula of TEG	12
Figure 2-2: Structural formula of methanol	13
Figure 2-3: Structural formula of water	133
Figure 2-4: Structural formula of carbon dioxide	14
Figure 2-5: Structural formula of methane	15
Figure 2-6: Structural formula of propane	16
Figure 2-7: Structural formula of n-hexane	16
Figure 2-8: n-Decane structural formula.....	17
Figure 2-9: Implications of the hydrophobic effect	20
Figure 3-1: Advantage of combining a cubic equation of state with an activity coefficient model	57
Figure 4-1: Experimental methods for phase equilibrium measurements	65
Figure 4-2: Basic layout of the static analytic method.....	66
Figure 4-3: Generic drawing of a static synthetic apparatus layout.....	69
Figure 4-4: Pressurising process of the synthetic type apparatus	70
Figure 5-1: Schematic of the apparatus for measuring high-pressure vapour liquid equilibria data ...	86
Figure 5-2: Photograph of the combined static analytic, static synthetic apparatus used in this study	88
Figure 5-3: Photograph of the dismantled apparatus showing different components.....	89
Figure 5-4: Photograph of the cell system side flange with the rolsitm attached to it	90
Figure 5-5: Set up used to prepare binary and ternary liquid mixtures.....	99
Figure 5-6: Set up of a prepared liquid mixture in a glass round-bottom flask, being loaded to the equilibrium cell	100
Figure 6-1: Plot (1) of the deviation between the standard temperature and calculated calibrated temperature for the probes used in this work	106
Figure 6-2: Plot (2) of the deviation between the standard temperature and calculated calibrated temperature for the probes used in this work.....	107
Figure 6-3: Plot (1) of the deviation between the pressure standard and the calculated pressure for the pressure transducer used in this work	108
Figure 6-4: Plot (2) deviation between the pressure standard and the calculated pressure for the pressure transducers used in this work.....	108
Figure 6-5: GC detector calibration chart for the CO ₂ (1) + n-hexane (2) mixture, CO ₂ dilute region	109
Figure 6-6: GC detector calibration chart for the CO ₂ (1) + n-hexane (2) mixture, CO ₂ rich region	110

Figure 6-7: GC detector calibration chart for the CO ₂ (1) + decane (2) mixture, CO ₂ dilute region.	111
Figure 6-8: GC detector calibration chart for the CO ₂ (1) + n-decane (2) mixture, CO ₂ rich region	112
Figure 6-9: TPxy plot of CO ₂ (1) + n-hexane (2).	116
Figure 6-10: Relative volatility versus composition of CO ₂ (1) + n-hexane (2) system.	117
Figure 6-11: TPxy plot for the CO ₂ (1) + decane (2) system.	120
Figure 6-12: Relative volatility for the CO ₂ (1) + decane (2) test system.	121
Figure 6-13: TPxy data for CO ₂ (1) + CH ₃ OH (2) system.	123
figure 6-14 TPxy data for CO ₂ (1) + CH ₃ OH (2) system	124
Figure 6-15: TPx graph for the CH ₄ + CH ₃ OH test system	125
Figure 6-16: TPx graph for the CH ₄ + TEG test system.	128
Figure 6-17: Thermodynamic modelling of the CH ₄ + TEG test system.	129
Figure 6-18: TPx plot of CO ₂ (1) + TEG (2) test system at 298.15 k.	132
Figure 6-19: TPx plot of the CO ₂ + (H ₂ O /TEG 10/90 wt %) at 298.15 k	136
figure 6-20: TPx graph for the CO ₂ (1) + (H ₂ O (2) /TEG (3) 3.5/96.5 wt %) at 322.04 k	139
Figure 6-21: TPx graph for the (CH ₄ (1)/ C ₃ H ₈ (2) 95/5 mol%) + CH ₃ OH (3) novel system.	142
Figure 6-22: Thermodynamic modelling of the (CH ₄ (1) / C ₃ H ₈ (2) 95/5 mol%) + CH ₃ OH (3) system.	144
Figure 6-23: Comparison of the TPx data at 303.15 K for: CH ₄ + CH ₃ OH; (CH ₄ / C ₃ H ₈ 95/5 mol%) + CH ₃ OH systems	150
Figure 6-24: TPx plot for the (CH ₄ (1) / C ₃ H ₈ (2) 95/5 mol%) + TEG (3) novel system.	151
Figure 6-25: Thermodynamic modelling of the (CH ₄ / C ₃ H ₈ 95/5 mol%) + TEG system.	152
Figure 6-26: Comparison of the TPx data at 323.16 k for: CH ₄ + TEG; (CH ₄ / C ₃ H ₈ 95/5 mol%) + TEG	158
Figure 6-27: TPx graph for the CH ₄ (1) + (CH ₃ OH (2) / TEG (3) 3.33/96.67 wt %)) system.	159
Figure 6-28: Thermodynamic modelling of the CH ₄ + (CH ₃ OH/TEG 3.33/96.67 wt%) system.	160
Figure 6-29: Comparison of the TPx data at 323.15 K for: CH ₄ + TEG; CH ₄ + (CH ₃ OH /TEG 3.33/ 96.67 wt %)	165
Figure 6-30: TPx graph for the CO ₂ (1) + (CH ₃ OH (2) /TEG (3) 3.33/96.67 wt%) system	166
Figure 6-31: Thermodynamic modelling of the CO ₂ (1) + (CH ₃ OH (2) /TEG (3) 3.33/96.67 wt%) system.	167
Figure 6-32: Comparison of the TPx data at T = 323.15 K for: CO ₂ + (CH ₃ OH/TEG 3.33/96.67 wt %); CO ₂ + TEG	173
Figure 6-33: TPx graph for the (CH ₄ /C ₃ H ₈ 95/5mol%) + (CH ₃ OH /TEG 3.33/96.67 wt%) system.	175
Figure 6-34: TPx graph for the (CH ₄ /C ₃ H ₈ 95/5mol%) + (CH ₃ OH /TEG 3.33/96.67 wt%) system:	177
Figure 6-35: Thermodynamic modelling of the (CH ₄ /C ₃ H ₈ 95/5mol%) + (CH ₃ OH /TEG 3.33/96.67 wt%) system at 283.16 K	179

Figure 6-36: Thermodynamic modelling of the (CH ₄ /C ₃ H ₈ 95/5mol%) + (CH ₃ OH /TEG 3.33/96.67 wt%) system at 303.16 K.....	180
Figure 6-37: Thermodynamic modelling of the (CH ₄ /C ₃ H ₈ 95/5mol%) + (CH ₃ OH /TEG 3.33/96.67 wt%) system at 323.15 K.	182
Figure 6-38: Comparison of the TPx data at $T = 323.15$ K for: (CH ₄ /C ₃ H ₈ 95/5 mol %) + (CH ₃ OH /TEG 3.33/96.67 wt% system); and CH ₄ + (CH ₃ OH /TEG 3.33/96.67 wt% system)	189
Figure 6-39: TPx graph for the (CH ₄ (1) / C ₃ H ₈ (2) 95/5mol%) + ((H ₂ O (3) /TEG (5) 5/95% wt): CH ₃ OH (4) 3.33 wt%) system.....	190
Figure 6-40: TPx graph for the (CH ₄ (1) /C ₃ H ₈ (2) 95/5mol%) +((H ₂ O (3) /TEG (5) 5/95% wt): CH ₃ OH (4) 3.33 wt%) system:.....	193
Figure 6-41: Thermodynamic modelling of the (CH ₄ (1)/C ₃ H ₈ (2) 95/5mol%) + ((H ₂ O (3) /teg (5) 5/95% wt): CH ₃ OH (4) 3.33 wt%) system at 283.16 K.	194
Figure 6-42: Thermodynamic modelling of the (CH ₄ (1) /C ₃ H ₈ (2) 95/5mol%) + ((H ₂ O (3) /TEG (5) 5/95% wt): CH ₃ OH (4) 3.33 wt%) system at 303.16 K.	196
Figure 6-43: Thermodynamic modelling of the (CH ₄ (1) /C ₃ H ₈ (2) 95/5mol%) + ((H ₂ O (3) /TEG (5) 5/95% wt): CH ₃ OH (4) 3.33 wt%) system at 323.15 K.	197
Figure 6-44: comparison of the TPx data at $T = 323.15$ k for (CH ₄ / C ₃ H ₈ 95/5 mol%) + ((H ₂ O /TEG 5/95% wt): CH ₃ OH 3.33 wt%) system ; and the (CH ₄ /C ₃ H ₈ 95/5 mol %) + (CH ₃ OH /TEG 3.33/96.67 wt%) system.....	206
Figure 6-45: TPx graph for the(CH ₄ /C ₃ H ₈ /CO ₂ 90.22/4.60/5.18 mol%) + ((H ₂ O /TEG 5/95% wt): CH ₃ OH 3.33 wt%)	208
Figure 6-46: TPx graph for the (CH ₄ (1) /C ₃ H ₈ (2) /CO ₂ (3) 90.22/4.60/5.18 mol%) + ((H ₂ O (4) /TEG (6) 5/95 wt%): CH ₃ OH (5) 3.33 wt%) system:	210
Figure 6-47: Thermodynamic modelling of (CH ₄ (1) /C ₃ H ₈ (2) /CO ₂ (3) 90.22/4.60/5.18 mol%) + ((H ₂ O (4) /TEG (6) 5/95% wt): CH ₃ OH (5) 3.33 wt%) system at 283.15 K.	212
Figure 6-48: Thermodynamic modelling of (CH ₄ /C ₃ H ₈ /CO ₂ 90.22/4.60/5.18 mol%) + ((H ₂ O /TEG 5/95% wt): CH ₃ OH 3.33 wt%) system at 303.15 K.....	213
Figure 6-49: Thermodynamic modelling of (CH ₄ (1) /C ₃ H ₈ (2) /CO ₂ (3) 90.22/4.60/5.18 mol%) + ((H ₂ O (4) /TEG (6) 5/95 wt%): CH ₃ OH (5) 3.33 wt%) system at 323.15 k.	214
Figure 6-50: Comparison of the TPx data at $T = 323.15$ K for (CH ₄ /C ₃ H ₈ /CO ₂ 90.22/4.60/5.18 mol%) + ((H ₂ O /TEG 5/95% wt): CH ₃ OH 3.33 wt%) system ; and the (CH ₄ /C ₃ H ₈ 95/5 mol%) + ((H ₂ O /TEG 5/95 wt%): CH ₃ OH 3.33 wt%) system.	216
Figure B.1-1: Plot (3) of deviation between the standard temperature and calculated calibrated temperature for the probes used in this work.	259
Figure B.1-2: Plot (3) of the deviation between the standard pressure and the calculated calibrated pressure for the transducers used in this work.	260
Figure B.1-3: Water vapour pressure measurement results	261

Figure B.1-4: Methanol vapour pressure measurement results.....	262
Figure B.1-5: n-Hexane vapour pressure measurement results	263
Figure B.1-6: CO ₂ vapour pressure measurement results:	264
Figure C-1: P-y plot of CO ₂ (1) + n-hexane (2) system:	277
Figure C-2: P-y plot for the CO ₂ (1) +n- decane (2) test system:	278
Figure E-1.1: CPA flash and analysis results comparison for thermodynamic modelling of the CO ₂ + CH ₃ OH test system at 298.10 K.....	296
Figure E-1.2: CPA flash and analysis results comparison for thermodynamic modelling of the CH ₄ + CH ₃ OH test system at 298.15 K.....	297
Figure E-1.3: CPA flash and analysis results comparison for thermodynamic modelling of the CH ₄ + TEG test system at 298.15 K	298
Figure E-1.4: CPA flash and analysis results comparison for thermodynamic modelling of the CO ₂ + TEG test system at 298.15 K	299
Figure E-2.1: PRWS thermodynamic modelling of the CH ₄ + CH ₃ OH test system at 298.15 K.	300
Figure E-2.2: CPA thermodynamic modelling of the CH ₄ + CH ₃ OH test system at 298.15 K	301
Figure E-2.3: PC-SAFT thermodynamic modelling of the CH ₄ + CH ₃ OH test system at 298.15 K	302
Figure E-3.1: CPA Thermodynamic modelling of the CO ₂ + (H ₂ O /TEG 10/90 wt% TEG) at 298.15 K	303
Figure E-3.2: CPA Thermodynamic modelling of the CO ₂ (1) + (H ₂ O (2) /TEG (3) 3.5/96.5 wt.%) at 322.04 K	304
Figure E-3.3: CPA Thermodynamic modelling of the (CH ₄ (1) / C ₃ H ₈ (2) 95/5 mol%) + CH ₃ OH (3) system.	306
Figure E-3.4: CPA Thermodynamic modelling of the (CH ₄ / C ₃ H ₈ 95/5 mol%) + TEG system.	307
Figure E-3.5: CPA Thermodynamic modelling of the CH ₄ + (CH ₃ OH (2) / TEG (3) 3.33/96.67 wt.%) system.	308
Figure E-3.6: CPA Thermodynamic modelling of the CO ₂ (1) + (CH ₃ OH (2) /TEG (3) 3.33/96.67 wt.%) system	309
Figure E-3.7: CPA Thermodynamic modelling of the (CH ₄ (1) /C ₃ H ₈ (2) 95/5mol%) + (CH ₃ OH (3) /TEG (4) 3.33/96.67 wt.%) system	311
Figure E-3.8: CPA Thermodynamic modelling of the (CH ₄ (1)/C ₃ H ₈ (2) 95/5mol%) + ((H ₂ O (3) /TEG (5) 5/95% wt.): CH ₃ OH (4) 3.33 wt.%) system.	31259

Figure E-3.9: CPA Thermodynamic modelling of the (CH ₄ (1)/C ₃ H ₈ (2)/CO ₂ (3) 90.22/4.60/5.18 mol%) + ((H ₂ O (4) /TEG (6) 5/95 wt.%): CH ₃ OH (5) 3.33 wt.%) system	315
Figure F-1: Carbon dioxide pure component properties.	316
Figure F-2: Water pure component properties	317
Figure F-3: Methanol pure component properties.	318
Figure F-4: TEG pure component properties.	319
Figure F-5: Hexane pure component properties	320
Figure F-6: Decane pure component properties.	321

List of Tables

Table 1-1: Gas sales specification.....	2
Table 2-1: Chemical and physical properties of carbon dioxide	14
Table 2-2: Physical and Chemical Properties of Methane	15
Table 2-3: Chemical and physical properties of propane	16
Table 2-4: Intermolecular forces	18
Table 2-5: Reported VLE data for Methane and TEG binary system	21
Table 2-6: Binary system data for TEG and propane	22
Table 2-7: Phase equilibria data for TEG and carbon dioxide	24
Table 2-8: VLE data for water + TEG	25
Table 2-9: VLE data for methane + methanol system	28
Table 2-10: VLE data for propane + methanol system	29
Table 2-11: VLE data for carbon dioxide + methanol system	30
Table 2-12: VLE data for water + methanol system	31
Table 2-13: VLE data for methane + water system	32
Table 2-14: VLE data for propane + water system	32
Table 2-15: VLE data for Carbon dioxide + water system	33
Table 2-16: VLE data for methane + carbon dioxide system	34
Table 2-17: Binary VLE data for propane + carbon dioxide	35
Table 2-18: Binary VLE data for methane + propane.....	36
Table 2-19: Phase equilibria data for the methane + propane + carbon dioxide system	37
Table 2-20: Phase equilibria data for the methane + carbon dioxide + methanol system	38
Table 2-21: Phase equilibria data for the methane + carbon dioxide + water system	39
Table 2-22: Phase equilibria data for the methane + water + methanol system.....	39
Table 2-23: Phase equilibria data for the propane + carbon dioxide + methanol system	40
Table 2-24: Phase equilibria data for the propane + water + methanol system	41
Table 2-25: Phase equilibria data for the carbon dioxide + water + TEG system	41
Table 2-26: Phase equilibria data for the carbon dioxide + water + methanol system	42
Table 2-27: Ternary systems of interest with no reported data	43

Table 2-28: Quaternary systems of this study	44
Table 3-1: Binary interaction coefficients k_{ij} for the Peng-Robinson EOS for components of this study	52
Table 3-2: Binary interaction coefficients k_{ij} for the SRK EOS, components of this study	53
Table 3-3: Association schemes for associating compounds based on the terminology of (Huang & Radosz, 1990)	59
Table 3-4: Binary interaction coefficients k_{ij} for the PC-SAFT EOS and components investigated in this study	60
Table 3-5: CPA literature k_{ij} parameters for components of this study	63
Table 4-1: List of combined static analytic, static synthetic equipment with either temperature or pressure control.....	71
Table 4-2: List of static equipment with variable volume view cells	73
Table 5-1: GC parameters for detector calibration and VLE measurements	96
Table 6-1: Details of chemicals used for this study	103
Table 6-2: GC chemical purity checks	104
Table 6-3: Measured values for refractive index, density, and viscosity for the liquid components	104
Table 6-4: Results of water content determination in methanol and TEG	105
Table 6-5: Calibration polynomials for the temperature probes T102 and T104, July 2018	105
Table 6-6: Calibration polynomials for the temperature probes T102 and T104 recalibration.....	106
Table 6-7: P122 Pressure transducer calibration polynomials	107
Table 6-8: GC split ratios, mole fractions, peak areas and deviations for the CO ₂ (1) + n-hexane (2) GC detector calibration, CO ₂ dilute region	110
Table 6-9: GC split ratios, mole fractions, peak areas and deviations for the CO ₂ (1) + n-hexane (2) GC detector calibration, CO ₂ rich region	111
Table 6-10: GC split ratios, mole fractions, peak areas and deviations for the CO ₂ (1) + n-decane (2) GC detector calibration, CO ₂ dilute region.....	112
Table 6-11: GC split ratios, mole fractions, peak areas and deviations for the CO ₂ (1) + n-decane (2) GC detector calibration, CO ₂ rich region	113
Table 6-12: Regressed model parameters and deviations for the CO ₂ (1) + n-hexane (2) system .	118
Table 6-13: Regressed model parameters and deviations for the CO ₂ (1) + n-decane (2) system .	122
Table 6-14: Regressed model parameters and deviations for the CO ₂ (1) + CH ₃ OH (2) system	125
Table 6-15: Regressed binary interaction parameter (k_{12}) for the CH ₄ (1) + CH ₃ OH (2) system	127
Table 6-16: Regressed binary model parameters and deviations for the CH ₄ (1) + TEG (2) system	131
Table 6-17: Model parameters for the CO ₂ (1) + TEG (2) system	134

Table 6-18: Regressed model parameters and deviations for the CO ₂ (1) + (H ₂ O (2) 10 wt % + TEG (3) 90 wt %) system	137
Table 6-19: CPA model parameters used in multicomponent systems bubble predictions in this study	138
Table 6-20: Model parameters for the CO ₂ (1) + (H ₂ O (2) /TEG (3) 3.5/96.5 wt %) system	141
Table 6-21 (a): Regressed model parameters and deviations for the (CH ₄ (1) 95mol% + C ₃ H ₈ (2) 5mol%) + CH ₃ OH (3) system	145
Table 6-21 (b): Regressed model parameters and deviations for the (CH ₄ (1) 95mol% + C ₃ H ₈ (2) 5mol%) + CH ₃ OH (3) system cont	146
Table 6-22 (a): Regressed model parameters and deviations for the (CH ₄ (1) 95mol% + C ₃ H ₈ (2) 5mol%) + TEG (3) system	153
Table 6-22 (b): Regressed model parameters and deviations for the (CH ₄ (1) 95mol% + C ₃ H ₈ (2) 5mol%) + TEG (3) system cont	154
Table 6-23 (a): Regressed binary parameters and deviations for the various models employed for the CH ₄ (1) + (CH ₃ OH (2) /TEG (3) 3.33/96.67 wt.% system)	161
Table 6-23 (b): Regressed binary parameters and deviations for the various models employed for the CH ₄ (1) + (CH ₃ OH (2) /TEG (3) 3.33/96.67 wt.% system) cont	161
Table 6-24 (a): Regressed binary parameters and deviations for the CO ₂ (1) + (CH ₃ OH (2) / TEG (3) 3.33/96.67 wt.%) system	169
Table 6-24 (b): Regressed binary parameters and deviations for the CO ₂ (1) + (CH ₃ OH (2) / TEG (3) 3.33/96.67 wt.%) system cont.....	169
Table 6-25 (a): Regressed binary parameters and deviations for the (CH ₄ (1)/C ₃ H ₈ (2) 95/5 mol %) + (CH ₃ OH (3) /TEG (4) 3.33/96.67 wt.%) system	183
Table 6-25 (b): Regressed binary parameters and deviations for the (CH ₄ (1)/C ₃ H ₈ (2) 95/5 mol %) + (CH ₃ OH (3) /TEG (4) 3.33/96.67 wt.%) system cont.....	183
Table 6-26 (a): Regressed binary parameters and deviations for the (CH ₄ (1)/ C ₃ H ₈ (2) 95/5 mol%) + ((H ₂ O (3) /TEG (5) 5/95% wt.): CH ₃ OH (4) 3.33 wt.%) system	199
Table 6-26 (b): Regressed binary parameters and deviations for the (CH ₄ (1)/ C ₃ H ₈ (2) 95/5 mol%) + ((H ₂ O (3) /TEG (5) 5/95 wt.): CH ₃ OH (4) 3.33 wt.%) system cont	200
Table 6-27 (a): Regressed binary parameters and deviations for the (CH ₄ (1)/C ₃ H ₈ (2)/CO ₂ (3) 90.22/4.60/5.18 mol%) + ((H ₂ O (4) /TEG (6) 5/95 wt.): CH ₃ OH (5) 3.33 wt.%) system .	216
Table 6-27 (b): Regressed binary parameters and deviations for the (CH ₄ (1)/C ₃ H ₈ (2)/CO ₂ (3) 90.22/4.60/5.18 mol%) + ((H ₂ O (4) /TEG (6) 5/95 wt.): CH ₃ OH (5) 3.33 wt.%) system cont	218
Table 6-28: Summary of the maximum AARD % in pressure for the data measured in this work ..	225
Table A-1: Values of standard uncertainties used in this study.	252
Table B.1-1: Calibration polynomials for the temperature probes T104 and T105, low pressure equipment	259
Table B.1-2: Pressure transducer calibration polynomials	259

Table B.1-3: Vapour pressure measurement results for water	260
Table B.1-4: AAD and AARD for water between this work and literature data of (Louder, et al., 1924)	261
Table B.1-5: Vapour pressure measurement results for methanol	261
Table B.1-6: AAD and AARD for methanol between this work and literature data from NIST TDE (Lemmon, et al., 2021)	262
Table B.1-7: Vapour pressure measurement results for n-hexane	262
Table B.1-8: AAD and AARD for n-hexane between this work and literature data from NIST TDE (Lemmon, et al., 2021)	263
Table B.1-9: Vapour pressure measurement results for CO ₂	264
Table B.1-10: AAD and AARD for CO ₂ between this work and literature data from NIST TDE (Lemmon, et al., 2021).....	264
Table B.2-1: CH ₄ + C ₃ H ₈ gas mixture validation	265
Table B.2-2: CH ₄ + CO ₂ + C ₃ H ₈ gas mixture validation	265
Table B.2-3: GC equipment conditions	266
Table B.3-1: Critical properties and acentric factors for components of interest in this study	267
Table B.3-2: Critical properties and acentric factors for components of interest in this study	267
Table B.3-3: Mathias Copeman alpha function parameters	267
Table B.4-1: Experimental VLE data, relative volatility (α_{12}), and uncertainty information for the CO ₂ (1) + n-hexane (2) system	268
Table B.4-2: Experimental VLE data, relative volatility, and uncertainty information for the CO ₂ (1) + n-decane (2) system at 319.22	269
Table B.4-3: Experimental VLE data and uncertainty information for the CO ₂ (1) + methanol (2) system	269
Table B.4-4: Experimental VLE data and uncertainty information for the CH ₄ (1) + CH ₃ OH system	270
Table B.4-5: Experimental VLE data and uncertainty information for the CH ₄ + TEG system	270
Table B.4-6: Experimental VLE data and uncertainty information for the CO ₂ + TEG test system	270
Table B.4-7: Experimental VLE data and uncertainty information for the CO ₂ (1) + H ₂ O (2) + TEG (3) test systems	271
Table B.5-1: Experimental VLE data and uncertainty information for the (CH ₄ (1) /C ₃ H ₈ (2) 95/5 mol%) + CH ₃ OH (3) system	272
Table B.5-2: Experimental VLE data and uncertainty information for the (CH ₄ (1) 95 % mol + C ₃ H ₈ (2) 5 % mol) + TEG (3) system	272
Table B.5-3: Experimental VLE data and uncertainty information for the CH ₄ (1) + (CH ₃ OH (2) 3.33 wt.% +TEG (3) 96.67 wt.% (3) system	273

Table B.5-4: Experimental VLE data and uncertainty information for the CO ₂ (1) + (CH ₃ OH (2) 3.33 wt.% +TEG (3) 96.67 wt. % (3) system	273
Table B.5-5: Experimental VLE data and uncertainty information for the (CH ₄ (1) /C ₃ H ₈ (2) 95/5 mol%) + (CH ₃ OH (3) /TEG (4) 3.33/96.67 wt.%) system	274
Table B.5-6: Experimental VLE data and uncertainty information for the (CH ₄ /C ₃ H ₈ 95/5 mol%) + ((H ₂ O /TEG 5/95 wt.%): CH ₃ OH 3.33 wt.%)	275
Table B.5-7: Experimental VLE data and uncertainty information for the (CH ₄ (1)/C ₃ H ₈ (2)/CO ₂ (3) 90.22/4.60/5.18 mol%) + ((H ₂ O (4) /TEG (6) 5/95 wt.%): CH ₃ OH (5) 3.33 wt.%) system	276
Table D-1: SRK and PR EOS	280
Table D-2: Parameters for the SRK and PR EOS	280
Table D-3: Parameters of the attractive parameter	282
Table D-4: Parameters of the co-volume parameter	282
Table D-5: Pure component parameters for the PC-SAFT EOS	292

Nomenclature

Symbols

a	attraction force /attractive parameter of an EOS
A	Helmholtz free energy
A_{ij}	NRTL parameters
b	is the maximum error induced by type B uncertainty or co volume parameter
c	gas composition uncertainty
CPAM	M parameter of the alpha function of the CPA model
CPAPC	critical pressure for the CPA model
CPATC	monomer critical temperature for the CPA model
D	Debye
d	delta/change
Exp	experimentally measured value
$F(r)$	Force
(f)	Fugacity
G^E	excess molar Gibbs free energy
H^E	excess enthalpy
i	denotes a chemical species
j	denotes another type of chemical specie
k	coverage factor
K_i	Equilibrium ratio for component i
k_{ij}	Binary interaction parameter
L	length
m	mass
(m)	the segment number, or the number of segments per chain
mb	mass balance
min	minute
n	number of moles
N	number of data points
n_D	refractive index

P	Pressure
P_c	critical pressure
prep	preparation
o	composition of gas mixture
R	the universal gas constant
S	entropy
T	Temperature
T_c	critical temperature
T_r	reduced temperature
u	standard uncertainty
U	expanded uncertainty
ub	mass balance precision
$u(r)$	the potential energy of interactions
ν	viscosity
V	molar volume of a fluid
wt	weight
x	liquid mole fraction
y	vapour mole fraction
z	either liquid or vapour phase
Z_c	compressibility factor

Greek letters

ρ	density
φ	Fugacity coefficient
γ	is the activity coefficient of a given component
μ	Chemical potential
μ	micro
σ	standard deviation or segment diameter
θ	the parameter under consideration
α	quantities or alpha function of a cubic equation of state or relative volatility

ω	acentric factor
τ_{ij}	is a parameter in the NRTL activity coefficient model representing interaction between component i and j .
(ε)	segment energy parameter
$(\beta^{A_i B_i})$	association volume parameter
$(\varepsilon^{A_i B_i})$	association energy parameter

Subscripts

calc	calculated value
calib	calibration
calib cor	calibration correlation
max	maximum
mix	mixture
rep	repeatability
std	standard

Superscripts

as	association
chn	chain contribution
$disp$	dispersion term
E	excess property
Id	ideal solution
Ig	ideal gas
hs	hard sphere
liq	liquid phase
nst	data retrieved from NIST TDE in Aspen Plus V12
®	registered trademark
R	Residual property
TM	trademark

vap vapour phase

Overbars

- Partial molar property
^ Thermodynamic property of a component in a mixture.

Abbreviations

AAD	Absolute Average Deviation
AARD	Absolute Average Relative Deviation
amu	Atomic Mass Unit
APACT	Associated-Perturbed-Anisotropic-Chain Theory
CS	Cross-Section
csgm	Calibration Standard Gas Mixture
CPA	Cubic Plus Association equation
sCPA	simplified Cubic Plus Association
DEA	Diethanolamine
DGA	Diglycolamine
EF EOS	Excess Function equation of state
EOS	Equation of State
EOS-CR	Equation of State Chemical Recticular
ESD	Elliot-Suresh-Donohue equation
EsOS	Equations of State
FID	Flame Ionization Detector
FS	Full Scale
FSO	Full Scale Output
GC	Gas Chromatography

GC-MS	Gas Chromatography-Mass Spectrometry
GE	Gibbs Energy model
GERG-2008	Groupe European de Recherche Gaziere
HPVLE	High Pressure Vapour-Liquid Equilibria
HV	Huron-Vidal mixing rule
ID	Internal Diameter
KK	Krichevsky-Kasarnovsky equation
LC	Local Composition model
LLE	Liquid-Liquid Equilibria
LNG	Liquefied Natural Gas
MC	Mathias Copeman alpha function
MDEA	Methyl Diethanolamine
MEA	Monoethanolamine
MHV1	Modified Huron-Vidal mixing rule
NC	Number of Components
NDG	Number of Data Groups
NGL	Natural Gas Liquids
NIST	National Institute of Standard and Technology
NRTL	Non-random Two Liquid model
$Obj F$	Objective Function minimised by data regression
OD	Outside diameter
PC-SAFT	Perturbed Chain Statistical Associating Fluid Theory
PR	Peng-Robinson
PR/NDD	Non-Density Dependent approach to Peng Robinson
PTFE	Polytetrafluoroethylene
PRWS	Peng Robinson Wong Sandler

Rel.S.D	Relative Standard Deviation
RMSD	Root Mean Square Deviation
ROLSI TM	Rapid Online Sampler
RSS	Root of Sum Squares
SAFT-VR	Statistical Associating Fluid Theory for potentials of Variable Range
SLE	Solid Liquid Equilibria
SRK	Soave-Redlich-Kwong
SS	Stainless Steel
TEG	Triethylene Glycol
TCD	Thermal Conductivity Detector
TRU	Thermodynamics Research Unit
UKZN	University of KwaZulu-Natal
UNIQUAC	Universal Quasichemical
VLE	Vapour Liquid Equilibria
VLLE	Vapour Liquid Liquid Equilibria
VdW	Van der Waals
VOC	Volatile Organic Compounds
ws	Working Standard
WS	Wong-Sandler mixing rule

CHAPTER 1: PROJECT BACKGROUND

1.0 INTRODUCTION

Natural gas is composed of mainly methane (above 85% by volume) with ethane, propane, butanes, and some impurities (Manning and Thompson, 1991; Mokhatab et al., 2006). The compositions vary from reservoir to reservoir. Before it is available to the market, natural gas must be produced from natural gas wells, treated and transported (Mokhatab et al., 2006). The value chain of natural gas from the wells to the consumers is depicted in Figure 1-1.

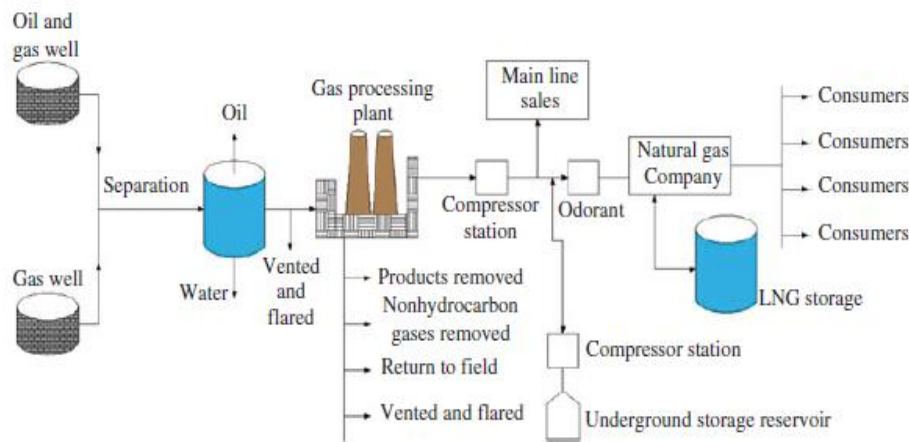


Figure 1-1: Natural gas value chain: From the wells to the consumers. Taken from (Nasr and Connor, 2014).

Gas processing involves removing vapour phase impurities from the gas streams. These impurities include carbon dioxide, nitrogen, hydrogen sulphide, water vapour, mercury, and others (Kohl and Nielsen, 1997; Manning and Thompson, 1991; Mokhatab et al., 2006). These impurities must be separated from the gas streams to meet sales stipulations, enhance calorific value, lessen corrosion and blockages in pipelines and to allow for cryogenic gas processing. Raw gas containing the vapour phase impurities of hydrogen sulphide (H_2S) is technically known as sour gas, and purified natural gas free from H_2S is referred to as sweet gas (Mokhatab et al., 2019, 2006). Once a gas stream is extracted, as shown in Figure 1.1, hydrate inhibitors such as methanol are injected into the gas stream at wellheads, then the gas is transmitted via pipelines to the gas processing plant.

Gas processing involves several unit operations, the order of which varies from plant to plant. The first step in natural gas treatment is the separation of the gas stream from oil and water using separators. Then water vapour impurities in the gas stream are eliminated through dehydration, in which glycols

are usually used. Furthermore, during this gas processing stage, an acid gas removal unit is responsible for eliminating H_2S and CO_2 (Shimekit & Mukhtar, 2012). The acid gas removal unit makes use of alkanolamines. Other important process units used during gas processing include: the demethanizer for separating methane from natural gas liquids (NGL); and fractionators for separating NGLs in the gas streams (Shimekit and Mukhtar, 2012). After the gas processing stage, as indicated in Figure 1-1, the gas may be compressed and then sent to the final consumers via pipelines or other transportation modes. An example of the allowable impurities in natural gas for US pipeline transportation are presented in Table 1-1.

Table 1-1: Gas sales specification. (Shimekit and Mukhtar, 2012) .

Components	US pipeline specification
H_2O	$< 0.1 \text{ g/m}^3$ ($< 120 \text{ ppm}$)
H_2S	$< 4 \text{ ppm}$
CO_2	$< 2 \text{ mol } \%$
C_{3+}	$35.4 - 39.1 \text{ MJ/m}^3$, dew point -293.15 K
Total inerts (He, Ar, N_2 , etc)	$< 4 \text{ mol } \%$

When choosing a natural gas purification/treatment process, there are many factors one must consider. These include (i) types and compositions of impurities in the gas; (ii) selectivity of acid gas elimination needed; (iii) pressure, temperature, volume, and makeup of the gas needing processing; and (iv) the desire and extent of sulphur recovery needed considering environmental issues or process economics (Burr and Lyddon, 2008; Manning and Thompson, 1991; Mokhatab et al., 2006).

If there is a high concentration of heavy hydrocarbons in the feed like C_{5+} , then chemical solvents would be the best option. This is because if physical solvents are used, there may be co-absorption of these heavy hydrocarbons, which is undesirable (Burr and Lyddon, 2008). Also, physical solvents are generally utilised over chemical solvents if the concentration of impurities and acid gases is high (Burr and Lyddon, 2008).

Some processes are carried out with selective absorption of H_2S from the gas stream, letting the CO_2 slip with the overhead gases (Burr and Lyddon, 2008). One chemical solvent which offers such selectivity is methyl diethanolamine (MDEA). The absorption of carbon dioxide is highly influenced by either the partial pressure of CO_2 or the pressure of the feed gas. The higher the partial pressure of the acid gas $\geq (50 \text{ psia or } 0.34 \text{ MPa})$, the more preferable it is to use physical solvents and vice versa (Burr and Lyddon, 2008; Mokhatab et al., 2006). This is because, at low feed gas pressures, the cost of compressing the gas for physical absorption is high (Burr and Lyddon, 2008).

Based on the interaction between absorbate and absorbent, absorption processes can be classified as either chemical absorption or physical absorption.

In physical absorption processes, the component being absorbed dissolves in the liquid absorbent more than any other constituent of the gas stream, and no chemical reaction takes place between the absorbate and the absorbent (Kohl and Nielsen, 1997). Examples of such solvents are methanol and triethylene glycol (TEG). To regenerate physical solvents, no heat addition is required to strip off the impurities; only a reduction in pressure favours this (Burr and Lyddon, 2008).

In the chemical absorption process (in which reversible reactions occur), a chemical reaction occurs between a component of the liquid phase and the gaseous component being absorbed, forming a weakly bonded reaction product (Kohl and Nielsen, 1997). Ethanolamines (MEA, diethanolamine (DEA), MDEA, diglycolamine DGA, etc.) and hot potassium carbonate are all examples of chemical solvents. Chemical solvents are usually regenerated by the application of heat (Burr and Lyddon, 2008).

As presented in Table 1-1, the gas stream should be kept above the dew point to prevent formation of hydrates and corrosion from occurring. Dew point refers to the temperature and pressure at which the first droplet of water condenses out of the vapour phase. The removal of water vapour from gas streams, leads to the decrease of the dew point temperature; hence it is important to always keep the water vapour impurity at a minimum, especially in cold environments.

1.1. Gas dehydration

This study is mainly related to systems encountered in TEG dehydration; hence a brief description of the glycol dehydration process is presented. If hydrate prevention methods are not adequate, it is necessary to directly remove water from the gas streams. Removal of water from the gas streams is termed dehydration and the two most common methods are absorption and adsorption

In comparison with adsorption, absorption with glycols is currently the most preferred dehydration method because: these are cheaper than adsorbents; require less energy for regeneration as compared to adsorbents; more expensive to replace an adsorption bed than replacing glycol solvent, and whilst changing an adsorption bed requires a total shutdown, glycol can be changed continuously (Christensen, 2009).

Glycol dehydration units consist of a contactor and a regenerator. Nearly 95% of glycol dehydration units use TEG (Mostafazadeh et al., 2009). Glycols are used in operations where the dew point

depression of the order of 60 to 120 °F (33 to 67 K) are needed (Price et al., 2004). The compressed wet gas is treated in glycol dehydration plants, where TEG is predominantly used to absorb water vapour from the gas stream, thus lowering the dew point temperature (Jerinić et al., 2008).. Ghafri et al. (al Ghafri et al., 2014) states that pipeline operating conditions are in a temperature range between 253.15 and 323.15 K, with pressure ranging from 5 to 25 MPa, an envelope that includes states in which hydrates can form. According to Haji (Hajiw, 2014) for safety reasons, gas is compressed, transported and delivered under a single dense phase at pressures from 1.4 to 8.3 MPa. Natural gas flows are generally over 1 million std m³; hence losses of treatment fluids can be costly (Jerinić et al., 2008).

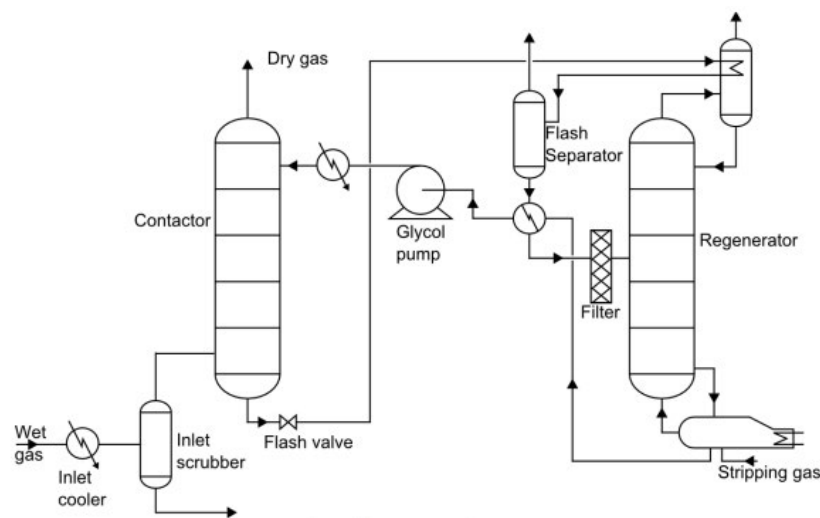


Figure 1-2: Process flow diagram for a glycol dehydration unit. Taken from (Christensen, 2009).

As shown in Figure 1-2, the wet gas passes through the inlet cooler, which reduces the gas temperature to the desired feed temperature in the contactor (299.82 to 310.93 K) (Manning and Thompson, 1991). This cooling condenses liquid hydrocarbons and some water out of the gas stream. The condensed liquids are removed from the gas stream in the inlet scrubber. The wet gas then enters the contactor and flows upwards, counter current to the downflowing TEG. Absorption of the water vapour from the gas stream to the downflowing TEG takes place in the contactor, and the dehydrated gas exits through the top of the contactor column. The rich glycol is withdrawn from the bottom of the contactor, passing through a flash valve which reduces the pressure to regenerator pressure. The rich glycol flows through the reflux condenser coil to the flash separator where most of the soluble gas is flashed off. The rich glycol then flows through the rich-lean heat exchanger and a filter into the regenerator (Price et al., 2004)). Regeneration of TEG takes place in the regenerator, which is basically a distillation column that operates just above atmospheric pressure. A reboiler provides the energy required to separate the water and glycol. Operating temperature range of the regenerator column is 360.93 to 477.49 K

(Manning and Thompson, 1991). Water vapour leaves through the top of the regenerator column. The regenerated lean glycol mixture is directed back to the absorber column via a heat exchanger and then pumped via a glycol cooler. Lean TEG at the top of the contactor column will be at a temperature (3 to 11 K) higher than the wet gas entering the contactor to reduce condensation of hydrocarbons into the TEG. TEG can dehydrate natural gas at a temperature range of 283.15 to 327.59 K, with 299.82 to 310.93 K being the preferred range (Manning and Thompson, 1991). Below 283.15 K, TEG becomes too viscous such that the dehydration efficiency is significantly reduced, while above 316.48 K, the water content of the feed gas is too high, which reduces the dehydration capability of TEG (Manning and Thompson, 1991). The maximum recommended temperature for the regenerator column is 477.59 K since thermal decomposition of TEG occurs above this temperature. Once the lean TEG composition is known, the TEG circulation rate and the number of trays or the height of packing can be established (Price et al., 2004) . Most economical designs use circulation rates of approximately 16.69 l TEG/ kg of water to 41.73 l TEG/ kg of water absorbed (Price et al., 2004) .

1.2. Aim and objectives

The aim of this project was to measure and model the high-pressure vapour-liquid equilibria (HPVLE) data for mixtures of key components present in the natural gas streams, such as methane, propane, carbon dioxide, water, methanol and TEG. Such data are necessary for the gas processing industries to understand the interaction between these components in a mixture and the plant design and operations.

The objectives comprised:

- i. To perform a literature review on published phase equilibria data for systems of interest, the experimental techniques and procedures used to analyse such systems.
- ii. To validate the experimental apparatus and the experimental procedure for analysis of such systems.
- iii. To measure the VLE data for water-methanol - TEG – carbon dioxide-hydrocarbon systems, representative of those encountered in natural gas processing
- iv. To model the phase behaviour using the rigorous thermodynamic approach.

In this study, phase equilibria data of up to six-component systems representative of those encountered in natural gas processing were measured. Propane has been selected in this study instead of ethane due to the existence of literature data for mixtures involving ethane. Since oil and gas mixtures are complex such that all components are not known, the trend has been to study simpler systems that represent characteristics of real mixtures. Only experimental solubility data of single natural gas components (methane, ethane, propane) in aqueous TEG are presented in the open literature (Jerinić et al., 2008). Few data sets are available in the open literature for glycol related systems (Kruger et al., 2018). After

an extensive review of the data in the available literature, it is observed that VLE data for multicomponent mixtures containing methane (CH_4), propane (C_3H_8), carbon dioxide (CO_2), methanol (CH_3OH), water (H_2O), TEG at high-pressure conditions typical to natural gas treating and transportation systems are not reported or probably confidential and not published on open source.

TP_{xy} data were measured for the following test systems, carbon dioxide + n-hexane and carbon dioxide + n-decane over a temperature range of 313.15 to 319.23 K. TP_x data were also measured and modelled for the carbon dioxide + methanol; carbon dioxide + TEG; methane + methanol; methane + TEG; carbon dioxide + aqueous TEG systems over a temperature range of 298.10 to 323.15 K. These test system data aided in establishing the experimental techniques and associated accuracy of the equipment. New TP_x data were measured and modelled for seven new systems of this study namely: methane + propane + methanol; methane + propane + TEG; methane + methanol + TEG; carbon dioxide + methanol + TEG; methane + propane + methanol + TEG; methane + propane + methanol + water + TEG; methane + propane + carbon dioxide + methanol + water + TEG over a temperature range of 283.15 to 323.15 K.

It is vital to understand the distribution of production chemicals in natural gas streams, oil and water since that information is key in estimating the quantities of chemicals needed for a specific facility (Fonseca, 2010; Frost et al., 2015). To highlight the significance of phase equilibria studies for multicomponent systems related to the present study, Filho et al. (Filho et al., 2021) performed new solubility measurements for a natural gas mixture comprised of carbon dioxide + propane ethane + methane in TEG and TEG aqueous solutions. Filho et al. (Filho et al., 2021) performed their measurements at a temperature range of 273.15 to 353.15 K and pressures up to 40 MPa. This recent publication is similar to the systems investigated in this work. Filho et al. (Filho et al., 2021) makes it a point that the phase equilibria data for these systems is of industrial importance in the following applications: gas hydrate inhibition, carbon capture storage, subsea processing and gas dehydration. In another study inclined to this work, Kruger et al. (Kruger et al., 2018) measured phase equilibria data for a ternary system of methane + water + ethylene glycol between 6 to 12.5 MPa, a temperature range of 288 to 323 K, with a glycol content from 90 to 99 wt.%. In their study, Filho et al. (Filho et al., 2021) modelled their data using the simplified (CPA) model, a non-density dependent approach to Peng Robinson (PR/NDD) model and a Huron-Vidal SRK equation coupled with the NRTL Gibbs energy expression (SRK/HV/NRTL). The SRK/HV/NRTL model was not satisfactory in correlating the experimental methane solubility. The simplified (CPA) and the PR/NDD models successfully described the methane + TEG phase behaviour, and both failed for the TEG aqueous solutions. Another method that made use of binary interaction parameters dependent on the liquid phase composition (xk_{ij}) yielded

fair to satisfactory results, especially for the simplified (CPA). With this latter approach, in the case of multicomponent systems, the simplified (CPA) yielded consistent predictions compared to the PR/NDD approach, particularly for total gas solubility. Overall, Filho et al. (Filho et al., 2021) concluded that the models failed to yield satisfactory results based only on binary interaction parameters.

Carbon dioxide capture, transportation and storage has been of growing significance over the last decades as the world seeks a wide range of technology solutions to mitigate the effects of global warming. Additionally, carbon dioxide dehydration for enhanced oil recovery has been of importance. Best (Best, 1981) reported carbon dioxide + TEG contactor conditions of $T = 309.25$ to 313.15 K and pressures up to 13 MPa. Hence in addition to the stated above reasons, it has become imperative to understand the phase behaviour of TEG in carbon dioxide/ and or water (Wise and Chapoy, 2016). The solubility data are vital in fine-tuning binary interaction parameters utilised to predict inhibitor distribution in multicomponent systems (Wise and Chapoy, 2016). Experimental VLE data are important since all equations of state used for phase equilibria predictions require at least one binary interaction parameter obtained from experimental data (Webster and Kidnay, 2001; Wei et al., 1995). Generally, all predictive models presume a large number of accurate binary systems VLE database; however, such data are not enough since predictions must approximate reality (Wei et al., 1995).

The thesis therefore serves to fill in the gaps in mixture combinations and provide new data on systems that have not been previously measured. Therefore, this work is associated with the philosophy of creating a databank for the thermophysical properties of polar solvents in hydrocarbons at high pressures, which is vital for knowledge generation and in the design of separation processes.

1.3. Changes encountered in this study

The initial proposed topic for this study was “The distribution of methanol in aqueous amine natural gas treating systems”. This topic was aligned to the GPA midstream project 131 (GPA, 2017; Grybat et al., 2017). Due to many constraints, the aim and objectives were modified to focus on physical solvents (TEG and methanol) in gas treating systems instead of the amines, and the measurement and modelling of VLE data of water-methanol-TEG- hydrocarbon systems, representative of those encountered in natural gas processing. This is partly aligned to the GPA midstream project 161 (GPA, 2017).

1.4. Thesis structure

The thesis is comprised of seven chapters. The second chapter focuses on the description of chemical components of interest in this study. Their uses, physical and chemical properties are discussed. Moreover, a brief discussion on intermolecular forces and hydrogen bonding is presented as this is essential in selecting a suitable thermodynamic model and the understanding of phase behaviour. In addition to that, the chapter also presents literature phase equilibria data for systems of interest in this study, systems where there are no reported data and those with data that could not be found in open literature.

Chapter three presents a review of thermodynamic principles for HPVLE modelling. Two cubic equations of state (PR and SRK) applied in this study are reviewed, together with reported binary interaction parameters. A combination of a cubic equation of state and an activity coefficient model (PRWS) applicable to this study is also presented. The association models (PC-SAFT and CPA) all applied in this study are also reviewed.

Chapter four focuses on the review of experimental methods and techniques used for HPVLE measurement. Emphasis was placed on the review of static analytic, static combined apparatus employed in this study. Analytical methods that have been used for multicomponent systems similar to the present study are also reviewed. This was necessary as it provided a guide on the development of analysis techniques employed in this study.

Chapter five presents a detailed narrative of the experimental apparatus and procedures that were used in this work. Procedures used for calibrating temperature probes, pressure transducers, and the GC detector are outlined. Furthermore, procedures for the measurement of phase equilibria data in this study, both TP_{xy} and TP_x , are presented.

Chapter six presents the results and discussion of the experimental work conducted in this study. Results on the measurement of physical properties of interest for components in this study are presented together with reported literature data. In addition to that, results on temperature probes, pressure transducers and GC detector calibrations are presented and discussed. Furthermore, measured and modelled phase equilibria data for systems of interest in this study are presented and discussed.

Chapter seven presents conclusions made in this study.

Chapter eight presents recommendations made out of this study.

CHAPTER 2: REVIEW ON SYSTEMS INVESTIGATED IN THIS STUDY

2.0 INTRODUCTION

This section gives a detailed description of each of the chemical components of this study, some explanations on intermolecular forces that are anticipated in the mixtures, and a literature review on published phase equilibria data for components of interest. Furthermore, systems with phase equilibria data that have not been reported and those without data available in the open literature are discussed.

A summary of the systems of interest include:

(i) Binary systems

	methane	propane	carbon dioxide	methanol	TEG	water
methane						
propane	x					
carbon dioxide	x	x				
methanol	x	x	x			
TEG	x	x	x	x		
water	x	x	x	x	x	

x represents a binary system comprising of a component listed on the top row + a component listed on the left column.

(ii) Ternary systems

	methane	propane	carbon dioxide	methanol	TEG	water
methane + propane			x	x	x	x
methane + carbon dioxide				x	x	x
propane + carbon dioxide				x	x	x
methanol + TEG	x	x	x			
water + methanol	x	x	x		x	
water + TEG		x	x			

x represents a ternary system comprising of components listed on the left column + a component on the top row.

(iii) Quaternary systems

Mixture	methane	propane	carbon dioxide	methanol	TEG	water
(a)	×	×	×	×		
(b)	×	×	×		×	
(c)	×	×	×			×
(d)	×	×		×	×	
(e)	×	×			×	×
(f)	×		×	×	×	
(g)	×		×	×		×
(h)		×	×	×	×	
(i)		×	×	×		×
(j)		×	×	×		×
(k)	×			×	×	×
(l)		×		×	×	×
(m)			×	×	×	×

x represents individual components listed in the top row, that are merged to make quaternary mixtures listed (a) to (m) on the left column.

(iv) Quinary systems

Mixture	methane	propane	carbon dioxide	methanol	TEG	water
(a)	×	×	×	×	×	
(b)	×	×	×	×		×
(c)	×	×	×		×	×
(d)	×	×		×	×	×
(e)	×		×	×	×	×
(f)		×	×	×	×	×

x represents individual components listed on the top row that are merged to form quinary systems (a) to (f) listed on the left column.

V. Senary system:

Methane + propane + carbon dioxide + methanol + water + TEG

2.1. Chemicals selected in this study

While the six main chemical components selected for this study were: methane, propane, carbon dioxide, water, methanol and triethylene glycol, n-hexane and n-decane were used for test system measurements only.

2.1.1. Triethylene glycol (TEG)

Triethylene glycol (chemical formula $C_6H_{14}O_4$) is a transparent, colourless, low-volatility, moderate-viscosity, water-soluble liquid. TEG is completely miscible with water and many organic liquids and is preferentially used in applications that require a higher boiling point glycol than diethylene glycol. Glycols are, however, slightly soluble in hydrocarbon liquid phases and are non-volatile; hence they are insignificantly present in the vapour phase of natural gas mixtures under vapour-liquid equilibrium conditions. The oil and gas industry use TEG to dehydrate natural gas and also as a gas hydrate inhibitor. In addition to that, TEG has been used as a dehumidifier in air conditioning systems, as an intermediate in the manufacture of polyols and polyester resins, as well as a vinyl plasticizer (Carvalho et al., 2015). Furthermore, TEG has been used in carbon dioxide dehydration for enhanced oil recovery purposes or carbon capture transportation and storage purposes. TEG is a polar molecule that can participate in hydrogen bonding in the presence of other associating molecules or on its own since it is a self-associating molecule. The structural formula of TEG is presented in Figure 2-1. Glycols are the most widely used chemicals in gas dehydration because they are (Stewart and Arnold, 2011):

- Highly hygroscopic (readily absorb and retain water)
- Easily regenerated in stripper units.
- Low vapour pressure chemicals, thus glycol loss, are minimal in the dry gas stream and the regeneration system.
- Non corrosive and non-foaming at normal conditions.
- Stable with regard to chemical and thermal decomposition.

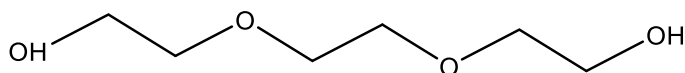


Figure 2-1: Structural formula of TEG.

The CAS number and physical properties for TEG of interest in this study are listed in Tables 6-1 to 6-4 in chapter 6.

2.1.2. Methanol

Methanol (chemical formula CH_3OH) is amongst valuable solvents in the gas processing industry. Its application as a commercial solvent for hydrate inhibition, gas sweetening, dehydration and natural gas liquids recovery spans over decades (Mokhatab et al., 2006). The ability of methanol to exist as a liquid phase between the temperatures of 175.35 K to 337.85 K allows it to find application in low-temperature processes where TEG cannot be used. Methanol is mostly used as a hydrate inhibitor since it is non-corrosive, does not react chemically with any constituent of the gas and is completely soluble in water (Stewart and Arnold, 2011). The only unfavourable physical property of methanol relative to other solvents is its higher vapour pressure (Mokhatab et al., 2006). Figure 2-2 presents the structural formula of methanol.

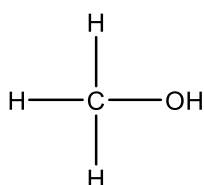


Figure 2-2: Structural formula of methanol.

Methanol is a polar molecule that is completely soluble in water at 298.15 K (National Center for Biotechnology Information, 2018a). Methanol is a hydrogen bonding molecule similarly to TEG. Other important chemical and physical properties of methanol relevant to this study are listed in Tables 6-1 to 6-4 in Chapter 6.

2.1.3. Water

Water (chemical formula H_2O) is a clear, odourless, nontoxic liquid that is comprised of two hydrogen atoms and one oxygen atom and is usually found associated with oil and gas from their reservoirs. In the present study, it was used to form an aqueous solution of TEG, representative of that found in gas dehydration plants. Its structural formula is presented in Figure 2-3, whilst the physical and chemical properties are listed in Tables 6-1 to 6-3 in chapter 6.

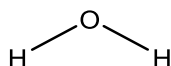


Figure 2-3: Structural formula of water.

Water is a polar molecule able to form hydrogen bonds and is soluble in ethanol, methanol, and acetone (National Center for Biotechnology Information, 2018b).

2.1.4. Carbon dioxide

Carbon dioxide (chemical formula CO₂) is a colourless, odourless gas at atmospheric temperatures and pressures (National Center for Biotechnology Information, 2018c). Carbon dioxide is relatively nontoxic and non-flammable. It is soluble in water and forms carbonic acid; hence the term acid gas is used referring to gaseous components that contain carbon dioxide. The structural formula of carbon dioxide is presented in Figure 2-4, whilst most of the chemical and physical properties are tabulated in Tables 2-1, 6-1 and 6-2.

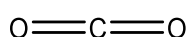


Figure 2-4: Structural formula of carbon dioxide.

Table 2-1: Chemical and physical properties of carbon dioxide. Source: (National Center for Biotechnology Information, 2018c).

Property	Quantity, units
Molar mass	44.01 g·mol ⁻¹
Melting point	216.55 K (Triple point)
Boiling point	194.65 K (Sublimes)
Vapor pressure	5.73 MPa (at 293.15 K)
Polarity	Is a non-polar molecule
IUPAC name	Carbon dioxide
CAS	124-38-9
Solubility in water	88ml CO ₂ /100ml H ₂ O at (293.15 K, 760 mm Hg or 0.1 MPa)
Miscibility with HCs	Miscible with hydrocarbons and most organic liquids.
Vapour Pressure	5720 kPa at 293.15 K
Viscosity	21.29 uPa·s (at 300 K, 6710 kPa)
Heat of Vaporization	16.7 KJ·mol ⁻¹ at 288 K ^b
Index of refraction	1.6630 at 297.15 K

^b NIST TDE (Lemmon et al., 2021)

2.1.5. Methane

Methane (chemical formula CH₄) is a highly flammable, colourless and odourless gas that is the main constituent of natural gases. It consists of one carbon atom and has a tetrahedral shape. Like other

normal alkanes, it is a non-polar molecule, soluble in slightly polar or non-polar solvents. Its structural formula is presented in Figure 2-5, whilst the relevant physical and chemical properties are tabulated in Table 2-2.

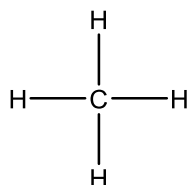


Figure 2-5: Structural formula of methane.

Table 2-2: Physical and Chemical Properties of Methane. Source: (National Center for Biotechnology Information, 2018d).

Property	Quantity
Molecular weight	16.043 g/mol
IUPAC name	Methane
CAS	74-82-8
Boiling point	112.15 K
Melting point	90.15 K
Flash point	85.15 K, closed cup (Flammable gas)
Water solubility	3.3ml CH ₄ /100ml H ₂ O at 293.15 K
Solubility in methanol	Slightly soluble
Vapor pressure	62128.2325 kPa (466000 mmHg) at 298.15 K
Viscosity	108.7 uP at 293.15 K
Heat of vaporisation	8.19 kJ·mol ⁻¹
Refractive index	1.000444 at 273.15 K, 101.325 kPa ^b

^b (Haynes et al., 2014a)

2.1.6. Propane

Propane (chemical formula C₃H₈) is one of the components of natural gas, which is usually present in much smaller quantities than methane. It is the main constituent of liquefied petroleum gas (LPG) used for domestic purposes. Propane gas is an alkane that consists of three carbon atoms bonded to eight hydrogen atoms (Mentzer, 2018). Its structural formula is presented in Figure 2-6, whilst its relevant physical and chemical properties are shown in Table 2-3.

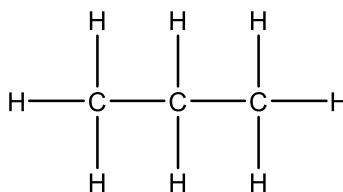


Figure 2-6: Structural formula of propane.

Table 2-3: Chemical and physical properties of propane. Source: (National Center for Biotechnology Information, 2018e).

Property	Quantity
Molecular weight	44.097 g·mol ⁻¹
IUPAC name	Propane
CAS	74-98-6
Boiling point	321.15 K
Melting point	83.45 K
Flash point	169.15 K
Solubility in water	0.007 g·(100cm ³) ⁻¹ at 293.15 K
Density (liquid propane)	0.493 g·cm ⁻³ at 298.15 K
Vapour pressure	840 kPa at 293.15 K
Viscosity	8.3 uPa·s at 300 K
Heat of vaporisation	14.79 kJ·mol ⁻¹ at 298.15 K
Index of refraction	1.2898 at 293.15 K

2.1.7. n-Hexane

Normal hexane (n-hexane) (chemical formula C₆H₁₄) is a six-carbon straight-chain saturated alkane made from refining crude oils. It is a colourless, highly flammable, volatile liquid that is immiscible with water and less dense than water (National Center for Biotechnology Information, 2021a). n-Hexane has a wide range of applications, including being used as a drying agent, fuel and fuel additive, paint and coating additive, anti-scaling agent and corrosion inhibitor, and a solvent for rubber, glues, cement, adhesives, inks, and varnishes (National Center for Biotechnology Information, 2021a). Other relevant physical and chemical properties of n-hexane are presented in Tables 6-1 to 6-3. Figure 2-7 illustrates the structural formula of n-hexane.

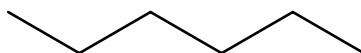


Figure 2-7: Structural formula of n-hexane.

n-Hexane is a non-polar molecule and is soluble in non-polar and slightly polar solvents (Nuñez-Rodriguez, 2020).

2.1.8. n-Decane

Normal decane (n-decane) (chemical formula $C_{10}H_{22}$) is a saturated alkane consisting of 10 carbon atoms and is a product of crude oil distillation. It is a non-polar molecule; hence it is immiscible with water. However, it is soluble in slightly polar or non-polar solvents (Nuñez-Rodriguez, 2020). n-Decane is a colourless, flammable liquid, and its vapours are heavier than air and is a component of petrol and kerosene (Patil, 2018). n-Decane has been mainly used as a solvent to make other chemicals, has been used in jet fuel research as a standardised hydrocarbon; thus, it can also be used as a fuel and fuel additive (National Center for Biotechnology Information, 2021b). Other relevant physical and chemical properties of n-decane are presented in chapter 6, Tables 6-1 to 6-3. The structural formula of n-decane is shown in Figure 2-8.

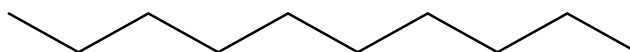


Figure 2-8: n-Decane structural formula.

2.2. Intermolecular forces

Knowledge of the intermolecular forces between chemicals in a mixture is crucial in chemical thermodynamics studies for many aspects such as (Kontogeorgis and Folas, 2010) :

- Selecting a suitable thermodynamic model
- Understanding and interpreting phase behaviour
- Development and improvement of thermodynamic models through improved mixing rules and better terms for equations of state.

Intermolecular forces lead to non-ideality in systems; thus, it is necessary to understand these. Atoms obey the repulsive-attractive relation (Soo, 2011). Accordingly, the distance between intermolecular centres (r) governs the interaction between molecules (Soo, 2011). A useful way of representing the relation between the force $F(r)$ and the potential energy of interactions $u(r)$ is as follows (Soo, 2011):

$$F(r) = - \frac{du(r)}{dr} \quad (2-1)$$

The total potential energy $u(r)$ can be broken down into two components (the attractive and repulsive parts).

$$u(r) = u_{attractive} + u_{repulsive} \quad (2-2)$$

Table 2-4 lists some of the forces of importance in the biochemical/chemical industry. A distinct section is dedicated to hydrogen bonding and other quasi chemical forces that are usually stronger than the Van der Waals and other forces presented in Table 2-4.

Table 2-4: Intermolecular forces.

Force type	Specific description
Coulomb	electrostatic
Van der Waals	General
Van der Waals	Dispersion (London)
Van der Waals	Polar (Keesom)
Van der Waals	Induction (Debye)
Dipole-quadrupole	
Quadrupole-quadrupole	
Induction-quadrupole	

The most predominant physical forces are the van der Waals forces (all variants listed in Table 2-4). They are weaker than chemical forces, and their interactions occur over long ranges (Soo, 2011). Coulombic forces are important in electrolyte solutions and are insignificant to this study.

Kontogeorgis and Folas (Kontogeorgis and Folas, 2010) made the following comments on the significance of van der Waals forces:

- Dispersion forces cannot be considered negligible and are usually quite significant.
- Induction forces are the weakest of the three Van der Waals forces and rarely exceed 7% of the total attractive force, even for polar molecules.
- For highly polar molecules, especially with dipole moment above 1 D, dipolar forces are significant.
- Quadrupole effects are much smaller; however, they are significant in special cases such as carbon dioxide, nitrogen and more components with high quadrupole moments.

2.2.1. Hydrogen bonding and the hydrophobic effect

Hydrogen bonds are formed between a hydrogen atom and electronegative atoms such as O, N, F and these bonds are stronger than physical forces (Kontogeorgis and Folas, 2010; Soo, 2011). However, these bonds are less strong than chemical (covalent) bonds. This work focuses on hydrogen bonding between oxygenated molecules that can either self-associate or cross associate.

Water has strong hydrogen bonds; hence its many unique properties, such as maximum density at 277.15 K and having a hydrophobic effect (Kontogeorgis and Folas, 2010). If foreign non-polar particles such as alkanes are introduced into water, the hydrogen bonds form well-defined voids (like gas hydrates). Thus, water molecules tend to glue to each other away from the foreign particles, particularly non-polar molecules (Kontogeorgis and Folas, 2010). Figure 2-9 illustrates the hydrophobic effect. The hydrophobic interaction occurs hand in hand with the hydrophobic effect. Hydrophobic interaction is the interaction of non-polar molecules (hydrophobic) on water surfaces. Van der Waals forces fail to account for the hydrophobic effect as they usually predict the opposite effect (Kontogeorgis and Folas, 2010). The interaction of non-polar molecules on water surfaces is much stronger than their interaction in free space (Kontogeorgis and Folas, 2010).

Categories of hydrogen bonding

Hydrogen bonding can be classified into three categories, namely (Kontogeorgis and Folas, 2010):

1. Intermolecular or self-association. This type of bonding occurs between two like molecules. (water, methanol, TEG).
2. Intramolecular association, which occurs between a hydrogen atom and an electronegative atom like oxygen of the same chemical species for instance in methanol molecules.
3. Solvation or cross association between two different chemical species such as (methanol-water; water-TEG; methanol-TEG).

A thermodynamic model short of hydrogen bonding contributions struggles to portray the phase equilibria of hydrogen bonding fluids, and the Peng-Robinson equation of state is a good example of such a model (Soo, 2011).

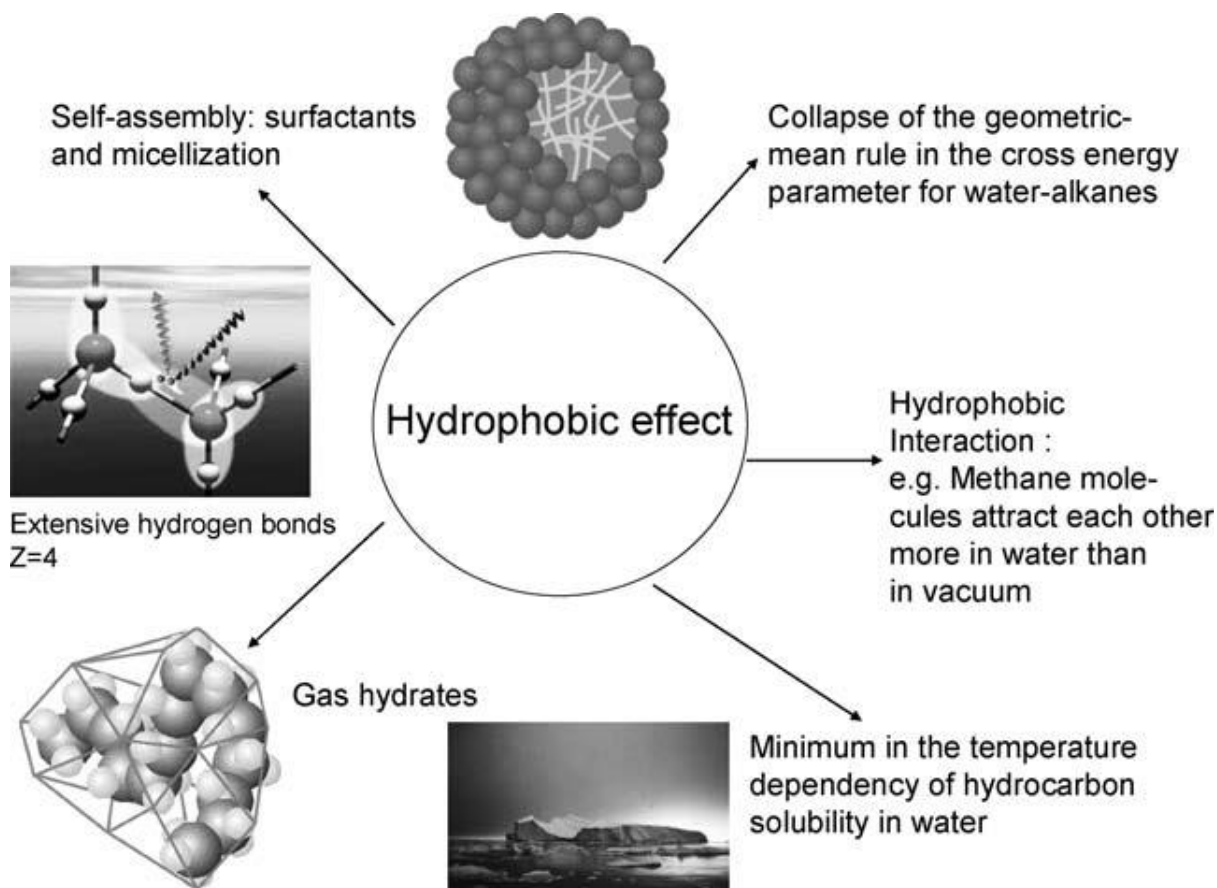


Figure 2-9: Implications of the hydrophobic effect. Source: (Kontogeorgis and Folas, 2010).

2.3. Published phase equilibria data for components related to this study.

The published phase equilibria data for different systems of interest related to this study are presented. In cases where there exists many datasets for a particular system, only a select few systems are presented.

2.3.1. Binary systems data

2.3.1.1. Methane + TEG system

There are few phase equilibrium data for the methane + TEG system in the open literature. TEG absorbs small amounts of methane (0.0006 to 0.0840 methane mole fraction) over a pressure range of 0.11 to 20.20 MPa (Jou et al., 1987; Rasoolzadeh et al., 2020a; Wilson et al., 1989), air pollutants, and volatile organic compounds (VOC), which are eventually emitted into the atmosphere from the glycol regenerator unit (Arya et al., 2014). Thus, the solubility of lower hydrocarbons in TEG is vital since the dissolved lower alkanes constitute a loss to the TEG dehydration process (Jou et al., 1987). Reported phase equilibrium data for the TEG + methane system are presented in Table 2-5.

Table 2-5: Reported phase equilibria data for Methane + TEG binary system.

Reference	T (K)	u T (K)	P (MPa)	u P (MPa)	N
(Jou et al., 1987) ^a	298.15; 323.15; 348.15; 373.15; 398.15	0.50	0.11-20.20	0.08	51
(Wilson et al., 1989) ^{a,nst}	273.15; 298.14		3.44-17.30		16
(Rasoolzadeh et al., 2020a) ^a	343.16 – 444.95	0.02	2.39-12.94	0.01	61
(Jerinić et al., 2008) ^b	298.15; 316.75	0.10	0.16-8.61	0.002	12
(Filho et al., 2021) ^a	273.15; 282.93; 297.87; 298.15; 312.81; 342.69; 352.65	0.03	3.60-47.21	0.02	38

^a- Only TP_x data reported; ^b- only TP_y data reported; N – number of data points; u – standard uncertainty; ^{nst} - obtained from NIST TDE in Aspen Plus V12; all data in Table 2-5 are isothermal except the data of Rasoolzadeh (Rasoolzadeh et al., 2020a) which was measured at constant methane compositions (isopleths); hence T range is presented.

Table 2-5 shows that only five literature sources reported VLE data for the TEG + methane binary system. For the reported TP_x data, the liquid mole fraction of methane ranged from 0.0006 to 0.119 over pressure ranges of 0.11 to 47.21 MPa. This indicates the difficulty with which methane dissolves in TEG. The TP_y data of Jerinić et al. (Jerinić et al., 2008) showed that the vapour mole fraction of methane is approximately equal to one, indicating the low volatility of TEG. Jou et al. (Jou et al., 1987) measured their data in a windowed Jerguson cell, using the vapour recirculation method. For the data of Jou et al. (Jou et al., 1987), uncertainty in pressure increased with an increase in the mole fraction of methane in the system. The measured data of Jou et al. (Jou et al., 1987) were correlated with a form of the Peng-Robinson (PR) equation of state, and binary interaction parameters were determined for this system. In their study, Jou et al. (Jou et al., 1987) found out that the PR EOS was inaccurate when applied to systems containing components with strong intermolecular interactions like TEG, hence it was inaccurate for the methane + TEG system. Jerinić et al. (Jerinić et al., 2008) used a static saturation apparatus with volume displacement to measure the solubility of TEG in supercritical methane. Jerinić et al. (Jerinić et al., 2008) modelled their data using the PR and SRK equations of state, combined with the quadratic mixing rule. The mean logarithmic deviation for TEG solubility (TEG vapour mole fraction) in methane for the data of Jerinić et al. (Jerinić et al., 2008) was 4.6% for the SRK EOS and 24.7% for the PR EOS. Jerinić et al. (Jerinić et al., 2008) reported that the solubility data of TEG in methane is vital for the design of glycol dehydration units and improving the accuracy of state equations in calculating glycol condensation in transmission pipelines. There is thus the need for more measurements of the methane + TEG data. A common trend is that the solubility of a gas in a liquid decrease with increasing temperature, which is not the case for the binary system of methane + TEG (Rasoolzadeh et al., 2020a). The solubility of methane in TEG increases with an increase in temperature

(an inverse solubility phenomenon). The inverse solubility phenomenon observed for the methane + TEG binary system is due to the expansion of the TEG solvent, which leads to the formation of large free voids, onto which methane molecules are encapsulated (Rasoolzadeh et al., 2020a). Rasoolzadeh et al (Rasoolzadeh et al., 2020a) modelled their data using the PR EOS coupled with different mixing rules including: the Wong-Sandler (WS), Van der Waals (VdW), Huron-Vidal (HV) and modified Huron-Vidal (MHV1) mixing rules. The excess Gibbs energy mixing rules were used with either the UNIQUAC or the NRTL activity coefficient model. In their work, Rasoolzadeh et al (Rasoolzadeh et al., 2020a) concluded that the PR EOS with the VdW mixing rules with a temperature-dependent binary interaction parameter yielded the most accurate results with AARD in pressure of 1.53%. The AARD% in pressure for the WS, MHV1 and HV mixing rules with the UNIQUAC activity coefficient model were 2.10, 3.99 and 1.64 respectively (Rasoolzadeh et al., 2020a). The AARD% in pressure for the WS, MHV1 and HV mixing rules with the NRTL activity coefficient model were 4.71, 10.04 and 5.38 respectively, indicating that the UNIQUAC activity coefficient model yielded better results than the NRTL activity coefficient model (Rasoolzadeh et al., 2020a). This might be because the NRTL activity coefficient model is only an energetic model, whereas the UNIQUAC activity model considers the molecule sizes (Rasoolzadeh et al., 2020a).

2.3.1.2. Propane + TEG system

Knowledge about the solubilities of natural gas components in TEG is necessary since TEG absorbs some of these components, such as propane, during the gas dehydration process. This solubility knowledge is necessary for energy management, hydrocarbon recovery optimisation, minimisation of TEG recirculation rate, hydrocarbon loss minimisation, economic savings, and the design of TEG regeneration units (Rasoolzadeh et al., 2020b). Table 2-6 presents the reported data in the literature for the propane + TEG system

Table 2-6: Binary system data for TEG and propane.

Reference	T (K)	u T (K)	P (MPa)	u P (MPa)	N
(Jou et al., 1987) ^a	298.15; 323.15; 348.15; 373.15; 398.15	0.50	0.02-6.45	0.07	40
(Rasoolzadeh et al., 2020b) ^a	352.86-448.99	0.02	0.82-7.06	0.01	39

^a- TPx data only; N- Number of data points; u – standard uncertainty. Rasoolzadeh et al. (Rasoolzadeh et al., 2020b)'s data are isopleths data (hence only the covered T range is presented); while Jou et al. (Jou et al., 1987)'s data are isothermal.

Despite the fact that natural gas is composed of many components, the phase behaviour can be studied through simple mixtures such as the propane + TEG binary system. In a similar manner, all components of natural gas can be studied to obtain the necessary binary interaction parameters. The modelling of real multicomponent mixtures is therefore possible by implementing the mutual binary interaction parameters of all the components

Table 2-6 shows that only two literature sources reported the VLE data of the propane + TEG binary mixture. For the reported data, liquid mole fraction of propane ranged from 0.0007 to 0.1096 mole fraction over a pressure range of 0.02 to 7.06 MPa. For the data of Jou et al. (Jou et al., 1987), similar equipment to the one presented for the methane + TEG data was used. Rasoolzadeh et al. (Rasoolzadeh et al., 2020b) measured the solubility data of propane in TEG using the Cailletet equipment through bubble points measurements. At a propane mole fraction of 0.1096, the data of Rasoolzadeh et al. (Rasoolzadeh et al., 2020b) indicates an inverse temperature dependency for propane solubility in TEG, which is not the common trend. At this propane composition of 0.1096, increasing the temperature decreases the solubility pressure, indicating increasing propane solubility at higher temperatures. The unusual behaviour could be due to the solvent forming free voids at higher temperatures, thus allowing more propane to dissolve into the solvent (Rasoolzadeh et al., 2020b). Rasoolzadeh et al. (Rasoolzadeh et al., 2020b) modelled their data using the PR EOS with the UNIQUAC G^E model using various mixing rules such as WS, and HV, where the WS mixing rule yielded the best results with an AARD of 5.06% in bubble point pressure calculations. The AARD% in pressure for the PR EOS with the VdW mixing rules with temperature-dependent binary interaction parameter and the PR Huron Vidal models were 8.88 and 6.31 respectively (Rasoolzadeh et al., 2020b). An increase in the number of adjustable parameters usually leads to better model correlations (Rasoolzadeh et al., 2020b).

A comparison of the solubility of methane in TEG and propane in TEG using the data presented by researchers listed in Tables 2-5 and 2-6 showed that propane has a higher solubility in TEG than methane. The higher solubility of propane in TEG is most likely attributed to the more alkane carbon chains; hence the VdW intermolecular bonds and attractions are much stronger between propane and TEG as compared to methane and TEG. Table 2-6 shows that there are only two independent sources of experimental solubility data for propane in TEG. Furthermore, based on the limited data sets there is a need for more measurements for this system.

2.3.1.3. Carbon dioxide + TEG system

Carbon dioxide capture, transportation, and storage has been of growing significance over the last decades as the world seeks methods to limit global warming. Additionally, carbon dioxide dehydration for enhanced oil recovery has been of importance. TEG has been the solvent of choice for dehydration of carbon dioxide streams; hence it is vital to understand the phase behaviour of carbon dioxide + TEG

systems since this is important in the design of the dehydration units. Best (Best, 1981) reported carbon dioxide + TEG contactor conditions of $T = 309.25$ to 313.15 K and pressures up to 13 MPa. Generally, glycol losses are higher for carbon dioxide dehydration than in natural gas dehydration systems, especially at pressures above 6.21 MPa (Price et al., 2004). The solubility of TEG in dense phase carbon dioxide causes these losses. There is considerable VLE data for carbon dioxide + TEG binary system in the open literature. The reported data for the carbon dioxide + TEG system are presented in Table 2-7.

Table 2-7: Phase equilibria data for TEG and carbon dioxide.

Reference	T (K)	u T (K)	P (MPa)	u P (MPa)	N
(Jou et al., 1987) ^a	298.15; 323.15; 348.15; 373.15; 398.15	0.5	0.13-20.25	0.01	40
(Wise and Chapoy, 2016) ^a	273.15; 283.15; 298.15; 343.15	0.05	0.42-37.40	0.04	29
(Yonemoto et al., 1989) ^{b, nst}	313.14; 323.14; 333.14		2.76-11.03		18
(Kaminishi et al., 1989) ^b	313.15; 333.15	0.05	4.48-15.43	0.01	30
(Jiang et al., 2019) ^a	273.15; 293.15; 313.15; 333.15; 353.15	0.1	0.50-3.50	0.001	38
(Skylogianni et al., 2020) ^a	303.10; 313.10; 323.10; 333.10; 343.20; 353.20; 363.10; 373.20; 383.20; 393.10	0.1	0.19-0.34	0.0009	10
(Takahashi et al., 1984) ^a	297.04; 310.93; 322.04		2.52-8.03		10

^a -Only TP_x data reported; ^b -Only TP_y data reported; N- number of data points; u – standard uncertainty; ^{nst} – data retrieved from NIST TDE in Aspen Plus V12; all data in Table 2-7 are isothermal.

Using data presented by researchers listed in Table 2-7, it was observed that the vapour phase of this carbon dioxide + TEG binary system contains very small quantities of TEG. This might be due to the low vapour pressure of TEG, which makes it difficult to measure such data. Wise and Chapoy (Wise and Chapoy, 2016) used a pressure rocking cell for their measurements. It is important to note that the phase equilibria data reported by Wise and Chapoy (Wise and Chapoy, 2016) are comprised of both VLE and LLE data. The data of Wise and Chapoy (Wise and Chapoy, 2016) are categorised as follows:

1. $T = 273.15$; x_{CO_2} 0.075 – 0.343 (VLE data) and x_{CO_2} 0.465-0.506 (LLE data)
2. $T = 283.15$; x_{CO_2} 0.047- 0.448 (VLE data), and x_{CO_2} 0.466-0.489 (LLE data)
3. $T = 298.15$; x_{CO_2} 0.048- 0.419 (VLE data), and x_{CO_2} 0.433-0.468 (LLE data)

Wise and Chapoy (Wise and Chapoy, 2016) modelled their data with the CPA using a single binary parameter, and the AARD was 2.55% with respect to carbon dioxide composition.

2.3.1.4. Water + TEG system

The VLE data for the water + TEG binary system is limited in the open literature. Knowledge of the phase equilibria data for the binary system of water + TEG is important. This is useful in the design and simulation of natural gas dehydration units, where water vapour impurities are removed from the gas stream by TEG solvent. Aqueous glycol mixtures have multiple industrial uses such as being used as conditioning agents, lubricants, hygroscopic agents and in the manufacture of solvents (Aniya et al., 2015). Townsend (Townsend, 1955) reported phase equilibria data for 95, 98 and 99.5 wt.% TEG aqueous solutions over a temperature range of 294.26 to 305.37 K, a pressure range of 3.45 to 17.24 MPa. Porter and Reid (Porter and Reid, 1950) reported phase equilibrium data for (water/TEG 5/95 wt. %) in contact with a sample of natural gas over a temperature range of 288.71 to 310.93 K, pressure range of 3.45 to 13.79 MPa. In the past, the equilibrium ratio (K) values for (water/TEG 5/95 wt. %) solution were generally used as the basis for the design of glycol dehydration units (Scauzillo, 1961). These reported water/TEG wt.% ratios motivated the selection of the water/TEG wt.% ratios used in this study, as well as the temperature and pressure ranges. Reported phase equilibria data for the water + TEG system are presented in Table 2-8.

Table 2-8: VLE data for water + TEG.

Reference	T (K)	u T (K)	P (MPa)	u P (MPa)	N
(Mostafazadeh et al., 2009) ^a	371.55-421.25	0.10	0.09	0.01	18
(Aniya et al., 2015) ^b	356.16-559.01	0.05	0.05-0.10	0.00003	60
(Chung and Luo, 1999) ^c	298.15; 303.15; 308.15; 313.15		0.002-0.003		4
(Ishiguro and Matsumotu, 1947) ^c	303.15; 308.15;313.15; 318.15; 323.15; 328.15; 333.15;338.15; 343.15				54
(Chouireb et al., 2018) ^b	355.05-420.64	1	0.05-0.10	0.005	51
(Piemonte et al., 2012) ^b	317.25-536.44	0.10	0.007-0.053	0.0001	68

^a – Only TP_{xy} data reported; ^b – Only TP_x (isobaric) data reported; ^c-Only vapour pressure data reported; N – number of data points; u – standard uncertainty; all data presented in Table 2-8 are isobaric; hence only covered T range are presented

Table 2-8 shows only four literature sources reported isobaric phase equilibria data for the water + TEG binary systems at low pressures. The other two literature sources reported vapour pressure data for water + TEG binary system. Mostafazadeh et al. (Mostafazadeh et al., 2009) conducted isobaric VLE measurements for the water + TEG binary system in a modified Othmer still, and samples were analysed

using GC and titration methods. Mostafazadeh et al. (Mostafazadeh et al., 2009) correlated their data using the UNIQUAC, NRTL and Van Laar models which were all in good agreement with the experimental data. Mostafazadeh et al. (Mostafazadeh et al., 2009) reported the root mean square deviations (RMSD) in activity coefficient as 0.032, 0.016 and 0.002 for the NRTL, UNIQUAC and Van Laar activity coefficient models respectively for the water + TEG system. The data presented by listed researchers in Table 2-8 showed that the vapour phase is mostly water. This is due to the low vapour pressure of TEG compared to that of water since TEG is a higher boiling point component. Aniya et al. (Aniya et al., 2015) measured isobaric VLE data for the binary mixture of water + TEG using a modified Sweitoslawsky-type ebulliometer. The data of Aniya et al. (Aniya et al., 2015) were correlated using the NRTL and Wilson models. For their model comparison, Aniya et al. (Aniya et al., 2015) reported maximum RMSD in temperature of 0.4602 and 0.7665 for the Wilson and NRTL activity coefficient models respectively. This shows that the Wilson activity coefficient model better describes the phase equilibria data for water + TEG systems compared to the NRTL activity coefficient model. Water and TEG are both polar molecules and hence their interactions are strong. Aniya et al. (Aniya et al., 2015) reports that the water + TEG system exhibits non-ideal behaviour due to strong hydrogen bonding and has a negative deviation from Raoult's Law. The presented literature review shows that, more data are needed for the water + TEG binary system, especially high-pressure data since this has not been reported in the open literature.

2.3.1.5. Methanol + TEG system

No literature VLE data were obtained for the methanol + TEG binary pair in Aspen plus V12 and on the Dortmund Data Bank (DDBST GmbH, 2019). Under normal dehydration conditions, 40-60% of methanol in the feed gas is absorbed by TEG (Price et al., 2004). Hence it is crucial to understand the phase equilibria data of methanol + TEG systems. Thus, there is a need to measure phase equilibria data for the methanol + TEG system.

2.3.1.6. Methane + methanol system

There are abundant phase equilibria data for the methane + methanol system in the open literature. Methanol is an industrial solvent that is used to purify natural gas streams from sour gases (Vetere, 1986). Furthermore, methanol has attracted some interest since it is also used in the treatment of synthesis gas produced from coal gasification and as a gas hydrate inhibitor. Therefore, the coexistence of methane + methanol at very low to medium temperatures under pressure has been a frequent occurrence that requires phase equilibria descriptions for the methane + methanol system, acid gas-methane + methanol, methane + methanol + water (Hong et al., 1987). Some of the published data for the methane + methanol system includes the data of Yarym-Agaev et al. (Yarym-Agaev et al., 1985),

Brunner et al. (Brunner et al., 1987), Wang et al. (Wang et al., 2003), and Frost et al. (Frost et al., 2015). Hong et al. (Hong et al., 1987) confirmed the existence of a two-liquid phase for the methane + methanol system below the critical temperature of methane. Brunner et al. (Brunner et al., 1987) measured their data using two experimental approaches, namely:

1. Use of gas chromatography (analytical method) to determine composition at low methanol mole fractions.
2. Use of two high-pressure optical cells (synthetic method) for moderate to high methanol mole fractions (thus bubble point and dew point determination).

Frost et al. (Frost et al., 2015) employed an analytical isothermal cell for their measurements. A variable volume high-pressure equilibrium cell with a 360° sapphire window was used for these measurements. A ROLSI™ was used for sampling, an Agilent 6890 GC equipped with HP PLOT Q capillary column and a thermal conductivity detector (TCD) coupled in series with a flame ionization detector (FID).

Hong et al. (Hong et al., 1987) used a vapour recycle type of apparatus in their measurements. Schlichting et al. (Schlichting et al., 1993) used the dynamic continuous accumulative method in their measurements, and their data were correlated with the Redlich-Kwong-Soave equation of state. Schlichting et al. (Schlichting et al., 1993) measured the solubility of methanol in methane at conditions prevailing at the top of high-pressure absorbers, since the higher the concentration of the liquid solvent in the overhead gas reflects, the greater the loss of the solvent and the contamination of the overhead gas with the solvent. Ukai et al. (Ukai et al., 2002) used a static-circulation type apparatus for their measurements. Wang et al. (Wang et al., 2003) measured their data using ROP and RUSKA PVT units. Besides measuring the phase equilibria data for methane + methanol binary mixture, Wang et al. (Wang et al., 2003) also measured the phase equilibria data for the multicomponent mixture of (methane/ethane 90.13/9.87 mol%) in water/pure alcohol (methanol/ethylene glycol)/ aqueous solution of (methanol/ethylene glycol) in a pressure range of 5 to 40 MPa, with the intention that the data be used for testing/improving thermodynamic models. Frost et al. (Frost et al., 2014) used the CPA EOS for phase equilibria calculations where a good agreement was witnessed between the experimental and the predicted data. Frost et al. (Frost et al., 2014) conducted their measurements in an analytical isothermal cell with variable volume. Frost et al. (Frost et al., 2015) additionally measured phase equilibria data for the multicomponent mixture of methane + methanol + n-hexane + water at 296.2 K and pressure ranges of 6 to 10 MPa. Table 2-9 presents some of the published literature data for the methane + methanol binary system. Kapatech et al. (Kapatech et al., 2016) modelled their data using the CPA model and reported an AARD of 5.31% in methane composition over their full data range, which indicated the reliability of their approach.

Table 2-9: VLE data for methane + methanol system.

Reference	<i>T</i> (K)	<i>u T</i> (K)	<i>P</i> (MPa)	<i>u P</i> (MPa)	N
(Yarym-Agaev et al., 1985) ^{a,nst}	298.14; 313.14; 338.13		2.50-12.50	0.04	15
(Vetere, 1986) ^a	213.2; 233.2; 273.2		1.08-6.97		16
(Brunner et al., 1987) ^a	298.15; 323.15; 373.15	0.2	5.45-100.00	1.08	71
(Hong et al., 1987) ^a	200; 220; 250; 273.15; 290; 310; 330		1.34-41.37	0.08	83
(Ukai et al., 2002) ^a	280.15	0.01	2.11-11.41	0.001	9
(Wang et al., 2003) ^a	283.2; 293.2; 303.2	0.10	5.05-40.05	0.01	24
(Frost et al., 2014) ^a	298.87	0.01	5.24-18.01	0.05	9
(Frost et al., 2015) ^a	298	0.01	3.72-15.51	0.05	5
(Kapateh et al., 2016) ^a	273.15	0.05	1.71-46.99	0.04	10
(Lazalde-Crabbtree et al., 1980) ^b	227.55; 273.15; 295.65	0.2	4.61-5.68	0.01	6
(Schlichting et al., 1993) ^b	242.60; 262.00; 282.70	0.10	2.00-10.00		17

^a – *TP_{xy}* data reported; ^b – Only *TP_y* data reported; N – number of data points; *u* – standard uncertainty; ^{nst} – retrieved from NIST TDE in Aspen Plus V12; all data in Table 2-9 are isothermal.

2.3.1.7. Propane + methanol system

Phase equilibria data for the alkane-methanol system is important in the design of gas separation processes and the development of thermodynamic models. Few literature sources reported the phase equilibria data for the propane + methanol binary system. Galivel-Solastiouk et al. (Galivel-Solastiouk et al., 1986) measured phase equilibria data for propane + methanol system using three different apparatus, two of them based on the static analytic method, and the third one of variable volume (static synthetic) was used to measure a single data point based on the bubble point measurement technique. The different sets of equipment were used to ensure reliability of their measurements. Furthermore, Galivel-Solastiouk et al. (Galivel-Solastiouk et al., 1986) measured *TP_{xy}* data for the ternary system of propane + methanol + carbon dioxide presented in section 2.3.3.5. Leu et al (Leu et al., 1992) performed their measurements in a variable volume cell with a transparent sapphire window cylinder fitted between two steel headers. Joung et al. (Joung et al., 2004) performed their measurements in a circulating apparatus with a view cell. Joung et al. (Joung et al., 2004) reported that the propane + methanol system exhibits a highly non-ideal behaviour due to the associating behaviour of methanol. Lee and Tan (Lee and Tan, 1998) used a dual recirculation technique for their measurements. They correlated their data using the PR and SRK equations of state, which yielded satisfactory correlations for this system. Reported data for the propane + methanol system are presented in Table 2-10.

Table 2-10: VLE data for propane + methanol system.

Reference	T (K)	u T (K)	P (MPa)	u P (MPa)	N
(Galivel-Solastiouk et al., 1986) ^a	313.1; 343.1; 373.1	0.10	0.35-4.30	0.01	31
(Leu et al., 1992) ^a	310.7; 352.2; 393.0; 474.3	0.10	0.03-8.66	0.04	39
(Joung et al., 2004) ^a	313.55; 327.95; 343.21	0.10	0.28-2.58	0.01	31
(Lee and Tan, 1998) ^a	343.1		0.86-2.53	0.06	3
(Yesavage et al., 1968) ^{a, nist}	210.38-349.85		1.72- 4.83	0.70	4
(Kretschmer and Wiebe, 1952) ^b	273.15; 298.15; 323.15		0.06-0.10	0.0011	5

^a – TP_{xy} data reported; ^b – Only TP_x data presented; ^{nist} – retrieved from NIST TDE in Aspen Plus V12; N – number of data points; u – standard uncertainty.

With the increase in propane mole fraction in the mixture, the uncertainty in pressure decreased for the data of Joung et al. (Joung et al., 2004).

2.3.1.8. Carbon dioxide + methanol system

Published VLE data for the carbon dioxide + methanol system are abundant in the open literature, thus making this an appropriate test system based on the device available for measurements. Some of the reported data for the carbon dioxide + methanol binary system are presented in Table 2-11. The equilibrium data of carbon dioxide + methanol has been of importance due to the application of carbon dioxide in supercritical fluid extraction and the application of methanol in acid gas absorption. Much of the data provides the basis for designing and optimising acid gas treatment systems that utilise methanol as a solvent.

Some of the published data for the carbon dioxide + methanol system includes the data of Ohgaki and Katayama (Ohgaki and Katayama, 1976), Naidoo et al. (Naidoo et al., 2008), Xie et al. (Xie et al., 2005), Chang and Rousseau (Chang and Rousseau, 1985), and Brunner et al. (Brunner et al., 1987). It is also important to note that Chang and Rousseau (Chang and Rousseau, 1985) reported phase equilibria data for the ternary mixture of methanol + water + carbon dioxide at temperatures between 243.15 to 298.15 K, presented in section 2.3.2.8. Brunner et al. (Brunner et al., 1987) reported error in pressure measurements as ± 0.002 MPa of the pressure value. Xie et al. (Xie et al., 2005) performed their measurements utilising a variable volume windowed equilibrium cell. Additionally, Xie et al. (Xie et al., 2005) measured phase equilibria data for the ternary system of hydrogen + carbon dioxide + methanol. Naidoo et al. (Naidoo et al., 2008) measured VLE data for the carbon dioxide + methanol system at a temperature range of 263.15 to 373.15 K and pressures up to 12 MPa. Pt 100 Ω sensors

measured the temperature inside the cell with an accuracy of 0.05%, whilst pressure measurements were performed by a Sensotec TJE pressure transducer of rated accuracy 0.25%.

Table 2-11: VLE data for carbon dioxide + methanol system.

References	T (K)	u T (K)	P (MPa)	u P (MPa)	N
(Ohgaki and Katayama, 1976) ^a	298.15; 313.15		0.58-8.06	0.001	17
(Chang and Rousseau, 1985) ^b	243.15; 258.15; 273.15; 298.15	0.1	0.19-5.45		26
(Brunner et al., 1987) ^a	298.15; 323.15; 373.15; 423.15; 473.15	0.2	0.41-16.08		84
(Xie et al., 2005) ^b	313.2	0.2	0.93-7.93	0.007	7
(Naidoo et al., 2008) ^a	263.15; 273.15; 313.15; 363.15; 373.15	0.2	0.79-12.06		33
(Hong and Kobayashi, 1988) ^a	230; 250; 273.15; 290; 310; 330		0.69-10.65		64
(Suzuki et al., 1990) ^a	313.4	0.2	0.68-7.71	0.02	8
(Leu et al., 1991) ^a	323.2; 352.6; 394.2; 477.6	0.1	0.45-14.03	0.03	40
(Qureshi et al., 2017) ^a	298.15	0.03	2.97-5.64	0.01	7
(Höhler et al., 2018) ^b	258.2; 272.9; 288.0; 298.3	0.1	0.22-5.73	0.01	57

^a – TP_{xy} data reported; ^b – Only TP_x data reported; N – number of data points; u is the standard uncertainty; all data in Table 2-11 are isothermal.

Additionally, Hohler et al. (Höhler et al., 2018) measured phase equilibria data for carbon dioxide + methanol + water ternary mixture. Qureshi et al. (Qureshi et al., 2017) modelled their data using the PC-SAFT, Polar PC-SAFT, PR and SRK equations of state. Chang and Rousseau (Chang and Rousseau, 1985) correlated their data using the SRK equation of state with a Mathias' polar correction factor and obtained excellent correlations to the experimental data. The RMSD % in pressure for the data Chang and Rousseau (Chang and Rousseau, 1985) using the SRK EOS was reported to be 4.61.

2.3.1.9. Water + methanol system

Published phase equilibria data for the water + methanol system are abundant in the open literature. Sentenac et al. (Sentenac et al., 1998) performed their measurements using an equilibrium cell that had bellows and two sapphire windows for visual observations. Some of the published phase equilibria data for the water + methanol system are presented in Table 2-12.

Table 2-12: VLE data for water + methanol system.

References	T (K)	u T (K)	P (kPa)	u P (kPa)	N
(Zielkiewicz and Oracz, 1990) ^a	313.15	0.02	8.48-32.85	0.004	14
(Bao et al., 1995) ^{a, nst}	353.15; 373.15; 388.15; 403.15		64-815		36
(Kurihara et al., 1995) ^a	323.15; 328.15; 333.15	0.01	29.11-72.83	0.03	52
(Mokbel et al., 1995) ^{b, nst}	243.75; 258.69; 278.58; 288.58; 298.55; 308.57		0.29-28.28		36
(Sentenac et al., 1998) ^{b, nst}	363.15; 383.15; 403.15; 424.15; 442.15	0.05	117-2093	10	25
(Yao et al., 1999) ^a	318.15	0.01	14.76-42.78	0.01	11
(Bernatová et al., 2006) ^{a, nst}	323.15	0.02	12.35-55.61		14

^a – TP_{xy} data reported; ^b – Only TP_x data reported; N – number of data points; u – standard uncertainty; ^{nst}- data retrieved from NIST TDE in Aspen Plus V12; all data in Table 2-12 are isothermal.

Yao et al. (Yao et al., 1999) conducted their measurements using a two-phase recirculating still. Bernatová et al. (Bernatová et al., 2006) used a recirculating still for their measurements, and the data were correlated using the NRTL model, which showed good agreement between the experimental and the calculated values. Kurihara et al. (Kurihara et al., 1995) correlated their data for the water + methanol system using the NRTL activity coefficient model with good accuracy. The AARD in pressure of Kurihara et al. (Kurihara et al., 1995) using the NRTL model was 2.35%.

2.3.1.10. Methane + water system

Data for methane + water system are abundant in the open literature. Natural gas reservoirs contain methane and water as major components (Shmonov et al., 1993). Therefore, the combination of methane + water is of practical significance since the phase behaviour of this binary system is vital for optimising methane recovery (Shmonov et al., 1993). Shmonov et al. (Shmonov et al., 1993) performed their bubble point measurements using a variable volume view cell made of high strength nickel base non-corrosive alloy, with a sapphire window at one end. Kiepe et al. (Kiepe et al., 2003) performed their measurements using a static synthetic method. Frost et al. (Frost et al., 2014) also measured phase equilibria data for the ternary mixture of methane + methanol + water presented in section 2.3.2.4. Böttger et al. (Böttger et al., 2016) performed their measurements using a constant volume static synthetic apparatus comprised of a high-pressure cylinder with two sapphire windows at its ends. Table 2-13 presents some of the published phase equilibria data for the methane + water system.

Table 2-13: VLE data for methane + water system.

Reference	<i>T</i> (K)	<i>u T</i> (K)	<i>P</i> (MPa)	<i>u P</i> (MPa)	N
(Gillespie and Wilson, 1982) ^{a,nst}	323.14		1.37-13.79		6
(Yarym-Agaev et al., 1985) ^{a,nst}	298.14; 313.14; 338.13		2.50-12.50	0.04	15
(Wang et al., 1995) ^b	283.15; 288.15; 293.15; 298.15		1.12-5.18		21
(Gao et al., 1997)	324.15; 375.15	0.1	10.24-58.00	0.01	14
(Kiepe et al., 2003) ^b	313.35; 353.18; 373.29		0.01-9.25		29
(Wang et al., 2003) ^b	283.2; 293.2; 303.2	0.10	2.00-40.03	0.01	17
(Frost et al., 2014) ^a	283.89; 298.31; 313.11; 323.56	0.01	4.78-19.49	0.05	22
(Böttger et al., 2016) ^b	283.14; 298.15	0.02	1.15-10.36	0.04	14
(Shmonov et al., 1993) ^b	627; 631; 633; 635	1.00	132-298	0.5	23

^a – *TP_{xy}* data reported; ^b – Only *TP_x* data reported; N – number of data points; *u* - standard uncertainty; ^{nst}-p data retrieved from NIST TDE in Aspen Plus V12; all data in Table 2-13 are isothermal.

2.3.1.11. Propane + water system

Phase equilibria data for propane + water system is important in the design and operation of natural gas and liquefied petroleum gas (LPG) facilities. In addition, hydrocarbon solubility in water is an essential aspect from the environmental point of view due to limitations of hydrocarbon content in water disposal (Chapoy et al., 2004). Only a few studies report the phase equilibria data for propane + water system which are listed in Table 2-14.

Table 2-14: VLE data for propane + water system.

Reference	<i>T</i> (K)	<i>u T</i> (K)	<i>P</i> (MPa)	<i>u P</i> (MPa)	N
(Kobayashi and Katz, 1953) ^{b, nst}	310.88; 338.67; 360.87; 369.67; 383.18 399.78; 421.98		0.49-19.33		86
(Sanchez and Coll, 1978) ^{a, nst}	473.11; 523.11; 573.11		23-200		18
(de Loos et al., 1980)(De Loos, et al., 1980) ^b	586.5-663.2	0.02	17.37-187.17	0.05	256
(Chapoy et al., 2004) ^b	277.62; 278.09; 280.14; 283.06; 288.13; 293.13; 298.12; 308.13; 323.13; 338.15; 353.18; 368.16	0.04	0.36-3.90	0.001	61

^a – *TP_{xy}* data reported; ^b – Only *TP_x* data reported; N – number of data points; *u* - standard uncertainty; ^{nst}- data retrieved from NIST TDE in Aspen Plus V12; all data in Table 2-14 are isothermal except for the data of De Loos et al. (de Loos et al., 1980) which are isopleths (constant composition) hence only covered *T* range is presented.

De Loos et al. (de Loos et al., 1980) conducted their experiments in a high-pressure autoclave with sapphire windows. Chapoy et al. (Chapoy et al., 2004) performed their measurements using a static analytic apparatus. Chapoy et al. (Chapoy et al., 2004) modelled their data using the Valderrama modification of the Patel–Teja equation EOS combined with the non-density dependent mixing rules and obtained good agreement between measured and calculated data.

2.3.1.12. Carbon dioxide + water system

There is abundant experimental solubility data for carbon + water in the open literature. This phase equilibria data is significant for applications such as storage of carbon dioxide in depleted oil fields or deep aquifers and carbon dioxide enhanced oil recovery. Furthermore, phase behaviour data for carbon dioxide + water and hydrocarbon mixtures are crucial inputs to reservoir simulations which are important in the evaluation and development of reservoir plans, design of process plants and surface facilities, interpretation of well test data, and establishing water dew point in carbon dioxide (al Ghafri et al., 2014). Some of the data published in the last decade are listed in Table 2-15. It is important to note that Serpa et al. (Serpa et al., 2013) also measured phase equilibria data of a ternary system of carbon dioxide + MEG + water, which is related to components in this study.

Table 2-15: VLE data for carbon dioxide + water system.

Reference	T (K)	u T (K)	P (MPa)	u P (MPa)	N
(Han et al., 2011) ^b	313; 323; 333	0.10	0.36-1.99	0.05	15
(Lucile et al., 2012) ^b	298.15; 323.15; 348.15; 373.15; 393.15	0.06	0.54-5.14	0.01	30
(Hou et al., 2013) ^a	298.15-448.15		1.08-17.55		30
(Serpa et al., 2013) ^{b, nst}	303	0.10	0.12-0.41	0.02	5
(al Ghafri et al., 2014) ^b	323.15	0.05	2.07-18.68	0.005	8
(Mohammadian et al., 2015) ^b	333.15; 353.15	0.05 ^{<i>U</i>}	0.1-21.3	0.02 ^{<i>U</i>}	30
(Muromachi et al., 2015) ^b	286.15; 292.15; 298.15	0.44	0.20-4.0	0.06	17
(Yuan et al., 2017) ^b	308.2	0.10	0.45-1.62		5
(Meyer and Harvey, 2015) ^{c, nst}	283.15; 294.83; 303.14; 313.17; 333.19; 353.15		0.50-5.00		57

^a – TP_{xy} data reported; ^b – Only TP_x data reported; ^c – Only TP_y data reported; N – number of data points; u – standard uncertainty; ^{nst} - data retrieved from NIST TDE in Aspen Plus V12; U is the combined expanded uncertainty; all data in Table 2-15 are isothermal.

Ghafri et al. (al Ghafri et al., 2014) performed phase equilibria measurements for the carbon dioxide + water system using a phase recirculating technique in a high-pressure quasi-static analytic apparatus with two diametrically opposite sapphire windows. Ghafri et al. (al Ghafri et al., 2014) also measured phase equilibria data for the methane + carbon dioxide + water ternary system presented in section 2.3.2.3. For the data of Hou et al. (Hou et al., 2013), the uncertainty $u(P)$ of = 0.04% of pressure readings was reported. Han et al. (Han et al., 2011) correlated their data using two models namely, the PR-Duan and the modified Setschenow equations, which yielded average relative deviation of (3.90 and 4.06) % respectively with respect to carbon dioxide solubility.

2.3.1.13. Methane + carbon dioxide system

There is abundant phase equilibria data for the methane + carbon dioxide binary system in the open literature. This is because carbon dioxide is present in natural gas, though the composition varies from field to field. Therefore, phase equilibria data for methane + carbon dioxide is of great importance for the proper design of separation equipment in the gas processing industry and enhanced oil recovery systems. Xu et al. (Xu et al., 1992), Bian et al. (Bian et al., 1993), Webster and Kidnay (Webster and Kidnay, 2001) correlated their data using the PR EOS.

Table 2-16: Binary VLE data for methane + carbon dioxide system.

Reference	$T(K)$	$u T (K)$	$P (MPa)$	$u P (MPa)$	N
(Donnelly and Katz, 1954) ^{a, nst}	209.31; 219.30; 223.74; 241.51; 259.83; 271.48		1.48-7.90		54
(Kaminishi et al., 1968) ^{a, nst}	253.15		5.23-8.11		5
(Arai et al., 1971) ^{a, nst}	273.15; 253.14; 288.15		5.71-8.28		21
(Devlikamov et al., 1982) ^{a, nst}	273.15; 278.14; 283.14; 288.15; 293.14; 298.14		4.10-8.10		32
(Xu et al., 1992) ^a	288.50; 293.40	0.01	5.12-8.15	0.02	23
(Bian et al., 1993) ^a	301.0	0.05	6.860-7.56		6
(Wei et al., 1995) ^a	230; 250; 270	0.02	0.89-8.38		60
(Webster and Kidnay, 2001) ^a	230; 270	0.01	0.89-8.42		43

^a – TP_{xy} data reported; N – number of data points; u – standard uncertainty; ^{nst}- data retrieved from NIST TDE in Aspen Plus V12; all data in Table 2-16 are isothermal.

The AARD in pressure for the data of Xu et al. (Xu et al., 1992) using the PR EOS was 1.2%, and the AAD in the vapour phase was 0.0009 methane mole fraction, indicating a good agreement between the calculated and the experimentally measured data. Bian et al. (Bian et al., 1993) used a vapour circulation

apparatus for their measurements. For the data of Bian et al. (Bian et al., 1993), the AARD in pressure was 4% for the PR EOS and 18% for the SRK EOS. Webster and Kidnay (Webster and Kidnay, 2001) also measured the VLE data for the ternary system of methane + propane + carbon dioxide system at 230 and 270 K. Some of the reported phase equilibria data for the methane + carbon dioxide system are listed in Table 2-16.

For the data of Bian et al. (Bian et al., 1993), the uncertainty in the pressure measurement was estimated to be 0.5%. Wei et al. (Wei et al., 1995) modelled their data using the PR EOS, and the results were satisfactory. Carbon dioxide has substantial quadrupole moment and as a result, simple EOS such as the PR is less accurate when modelling carbon dioxide systems (Wei et al., 1995).

2.3.1.14. Propane + carbon dioxide system

There is abundant phase equilibria data that have been published for the propane + carbon dioxide binary system and some of the selected data are shown in Table 2-17. Mixtures of propane and carbon dioxide have been proposed as promising refrigerants (Kim and Kim, 2005).

Table 2-17: Binary VLE data for propane + carbon dioxide

Reference	$T(K)$	$u T (K)$	$P (MPa)$	$u P (MPa)$	N
(Reamer et al., 1951) ^{a, nst}	277.59; 294.25; 310.91; 327.57; 344.23	0.03	0.54-6.91		150
(Niesen and Rainwater, 1990) ^a	311.05; 327.75; 344.43; 361.15	0.1	1.30-6.67		90
(Yucelen and Kidnay, 1999) ^a	240; 270; 330	0.1	0.15-5.85		43
(Webster and Kidnay, 2001) ^a	230; 270	0.01	0.097-3.21		71
(Kim and Kim, 2005) ^a	253.15; 263.15; 273.15; 283.15; 293.15; 303.15; 313.15; 323.15	0.02	0.24-6.28	0.001	77
(Tanaka et al., 2009) ^a	260; 265; 270; 280; 283.150; -290	0.002	0.60-3.92	0.002	33

^a – TP_{xy} data reported; N – number of data points; u – standard uncertainty; ^{nst} - data retrieved from NIST TDE in Aspen Plus V12; all data in Table 2-17 are isothermal.

Niesen and Rainwater (Niesen and Rainwater, 1990) modelled their data using the SRK EOS, which yielded good correlations. Yucelen and Kidnay (Yucelen and Kidnay, 1999), Kim and Kim (Kim and Kim, 2005) modelled their data using the PR EOS with the VdW one fluid mixing rules and obtained

satisfactory results. For the data of Kim and Kim (Kim and Kim, 2005), the relative deviation between the experimental and calculated pressure with the PR EOS was 3.5%. Kim and Kim (Kim and Kim, 2005) performed their measurements in a circulation-type of equipment with a view cell. For the data of Niesen and Rainwater (Niesen and Rainwater, 1990), pressure values were accurate to within $\pm 0.05\%$ of the pressure readings. Tanaka et al. (Tanaka et al., 2009) modelled their data using the SRK and PR EOS, where the bubble point pressure deviations were minimised by the least-squares method. Tanaka et al. (Tanaka et al., 2009) reported the AAD in pressure of 2.74% and 2.53% for the PR and SRK models respectively.

2.3.1.15. Methane + propane system

There is considerable published phase equilibria data for the methane + propane system in the open literature. Some of the published literature data are presented in Table 2-18. Sage et al. (Sage et al., 1934) conducted phase equilibria measurements for the methane + propane mixture at a temperature range of 293.15 to 363.15 K and pressure range of 0.10 to 20.23 MPa, conditions which typically resembles those that exist in petroleum formations.

Table 2-18: Binary VLE data for methane + propane.

Reference	T (K)	u T (K)	P (MPa)	u P (MPa)	N
(Sage et al., 1934) ^{a, nst}	293.18; 313.18; 328.18; 343.17; 353.17	0.10	1.01-9.63	0.01	38
(Reamer et al., 1950) ^{a, nst}	277.59; 294.23; 310.91; 327.57; 344.23; 360.90	0.03	0.54-10.16		128
(Akers et al., 1954) ^{a, nst}	157.62; 194.86; 213.20; 226.52; 241.58; 256.49; 273.15		0.69-9.65		71
(Price and Kobayashi, 1959) ^{a, nst}	227.63; 255.39; 283.14		0.69-8.96		23
(Webster and Kidnay, 2001) ^a	230; 270	0.01	0.10-9.29		81
(May et al., 2015) ^a	243.62	0.15	0.89-8.32	0.02	9
(McLinden and Richter, 2016) ^{b, nst}	273.15	0.05	0.66-2.36	0.002	6

^a – TP_{xy} data reported; ^b – Only TP_y data reported; N – number of data points; u - standard uncertainty; ^{nst}- data retrieved from NIST TDE in Aspen Plus V12; all data in Table 2-18 are isothermal.

Phase equilibria data is also of crucial importance in the design of LNG facilities. One of the key units in a LNG processing plant is the cryogenic distillation column known as the demethanizer, or the scrub

column (May et al., 2015). Accurate simulation of the demethanizer requires the calculation of VLE for multicomponent mixtures at high pressures from approximately 4 to 6 MPa, over a temperature range of 223 to 303 K (May et al., 2015). May et al. (May et al., 2015) modelled their data using two models namely the Groupe European de Recherche Gaziere (GERG-2008) multiparameter EOS and the PR EOS. For the data of May et al. (May et al., 2015), the maximum relative deviation in methane liquid mole fraction was close to 10% for the PR EOS, with the GERG-2008 EOS yielding better results than those of the PR EOS.

2.3.2. Ternary systems data

A literature survey was conducted for published phase equilibria data for all possible ternary combinations for the main components of this study. The results of this literature survey are presented in this section.

2.3.2.1. Methane + propane + carbon dioxide system

There are few reported phase equilibria data for the methane + propane + carbon dioxide system in the open literature. Published data for this ternary system are presented in Table 2-19. The data are important for the cryogenic separation of hydrocarbon gases from natural gas. Webster and Kidnay (Webster and Kidnay, 2001) modelled their data using the PR EOS, which yielded satisfactory predictions.

Table 2-19: Phase equilibria data for the methane + propane + carbon dioxide system.

Reference	T (K)	$u T$ (K)	P (MPa)	$u P$ (MPa)	N
(Kurata and Im, 1971) ^{a, nst}	150.21; 165.21; 185.21; 200.21; 205.21; 208.21	0.3	0.46-2.36	0.003	12
(Im and Kurata, 1972) ^{b, nst}	150.2; 165.2; 185.2; 200.2; 205.2; 208.2	0.2	0.46-2.36	0.003	12
(Webster and Kidnay, 2001) ^a	230; 270	0.01	0.80-8.01		75
(Kurata, 1974) ^{a, nst}	150.16; 165.16; 185.16; 200.16; 205.16; 208.16		0.76-2.36		12
(Acosta et al., 1984) ^c	199.8 - 289.1	0.05	0.10-5.51	0.02	25

^a – TP_{xy} data reported; ^b - Only TP_x data reported; ^c – Only TP_y data reported; N – number of data points; u - standard uncertainty; ^{nst} - data retrieved from NIST TDE in Aspen Plus V12; all data in Table 2-19 are isothermal except the data of Acosta et al. (Acosta et al., 1984) which are isopleths, hence T range is presented.

The binary interaction parameters k_{ij} from the possible binary pairs of the ternary mixture were used to predict data for the methane + propane + carbon dioxide mixture (Webster and Kidnay, 2001). The predictions of the ternary data were most accurate at low pressures and less accurate at high pressures around 8 MPa, which is close to the critical points. Im and Kurata (Im and Kurata, 1972) modelled their data using the Wilson equation to an accuracy of ± 4 mol% in the solubility of carbon dioxide in the multicomponent mixture. Im and Kurata (Im and Kurata, 1972) modelled their data using binary interaction parameters from the possible binary pairs of the ternary mixture.

2.3.2.2. Methane + carbon dioxide + methanol system

Only one literature source reported the phase equilibria data for the methane + carbon dioxide + methanol ternary system. The reported data are presented in Table 2-20.

Table 2-20: Isothermal phase equilibria data for the methane + carbon dioxide + methanol system.

Reference	T (K)	P (MPa)	N
(Schmid, 2011)	313.39	2.11-15.43	35

TPxy data reported; N – number of data points; data retrieved from NIST TDE in Aspen Plus V12.

More phase equilibria data measurements for this ternary system are necessary, especially at isotherms other than 313.39 K, the only isotherm reported in Table 2-20.

2.3.2.3. Methane + carbon dioxide + water system

There are few reported phase equilibria data for methane + carbon dioxide + water system. The available data for this ternary system are presented in Table 2-21. The data for this ternary system are useful in reservoir simulations and in carbon dioxide enhanced oil recovery, among other applications (al Ghafri et al., 2014). Additionally, the data for this system might be of future use in emerging technologies like the usage of gas hydrates in gas mixtures separations (Kastanidis et al., 2017). Ghafri et al. (al Ghafri et al., 2014) modelled their VLLE data for the methane + carbon dioxide + water ternary system using the statistical associating fluid theory for potentials of variable range (SAFT-VR). The pure component parameters and binary mixtures parameters were used to predict this ternary phase equilibria data and the SAFT-VR was used in conjunction with the square well potentials (al Ghafri et al., 2014). The SAFT-VR model predictions for the ternary system were not satisfactory as the predicted data was too small by a large margin to the experimental data (al Ghafri et al., 2014).

Table 2-21: Phase equilibria data for the methane + carbon dioxide + water system.

Reference	T (K)	u T (K)	P (MPa)	u P (MPa)	N
(Song and Kobayashi, 1989) ^{c, nst}	288.71 - 323.15		5.72-13.79		51
(Dhima et al., 1999) ^{b, nst}	344.15		10-100		9
(Qin et al., 2008) ^b	324.00; 375.80; 376.20	1.00	10.5-50.6	1.00	21
(al Ghafri et al., 2014) ^a	323.15; 373.15; 423.15	0.05	1.91-18.00	0.005	16
(Kastanidis et al., 2017) ^{a, nst}	275.7 - 290.4		2.47-12.15		47

^a – TP_{xy} data reported; ^b – Only TP_x data reported; ^c – Only TP_y data reported; N – number of data points; u – standard uncertainty; ^{nst} – data retrieved from NIST TDE in Aspen Plus V12; the data of Dhima et al. (Dhima et al., 1999); Ghafri et al. (al Ghafri et al., 2014) and Qin et al. (Qin et al., 2008) are isothermal and those of Kastanidis et al. (Kastanidis et al., 2017); Song and Kobayashi (Song and Kobayashi, 1989) are isopleths hence T ranges are presented.

2.3.2.4. Methane + water + methanol

There are few reported phase equilibria experimental data for the methane + water + methanol system. The data for this system are important for flow assurance purposes in the gas industry. The available data for this ternary system are presented in Table 2-22. Wang et al. (Wang et al., 2003) measured the solubility of methane in aqueous solutions of methanol, where the concentration of methanol in the aqueous phase were: 20 to 100 wt.% in increments of 20. For the data of Frost et al. (Frost et al., 2014), the feed composition was 0.250 mol% methane, 0.287 mol% methanol and 0.463 mol% water. Frost et al. (Frost et al., 2014) and Wise et al. (Wise et al., 2016) modelled their data using the CPA EOS where the results of the model predictions were in good agreement with the experimental data.

Table 2-22: Phase equilibria data for the methane + water + methanol system.

Reference	T (K)	u T (K)	P (MPa)	u P (MPa)	N
(Wang et al., 2003) ^b	283.2; 293.2; 303.2	0.10	5.05-40.05	0.01	120
(Frost et al., 2014) ^a	280.25; 298.77; 313.45	0.01	5.14-13.12	0.05	9
(Wise et al., 2016) ^b	293.15	0.05	0.54-35.35	0.04	17
(Ng and Robinson, 1983) ^{a, nst}	267.77; 280.65		4.20-18.57		3
(Blanco et al., 2000) ^{c, nst}	248.71 – 282.93	0.4	0.16-9.49		282

^a – TP_{xy} data reported; ^b – Only TP_x data reported; ^c – Only TP_y data reported; N – number of data points; u – standard uncertainty; ^{nst} – data retrieved from NIST TDE in Aspen Plus V12; the data of Frost et al. (Frost et al., 2014); Wang et al. (Wang et al., 2003) and Wise et al. (Wise et al., 2016) are isothermal; the data of Blanco et al. (Blanco et al., 2000) are isopleths hence only T range is presented

Wise et al. (Wise et al., 2016) measured the solubility of methane in 70 wt.% methanol aqueous solution where the overall AAD in methane mole fraction was 20.70% from the results of the CPA model prediction. For the data of Blanco et al. (Blanco et al., 2000), the accuracy of pressure measurements were $\pm 0.2\%$ of the pressure readings.

2.3.2.5. Propane + carbon dioxide + methanol

There are limited reported phase equilibria data for the propane + carbon dioxide + methanol system. The available data for this ternary system are presented in Table 2-23. The data were not modelled.

Table 2-23: Isothermal phase equilibria data for the propane + carbon dioxide + methanol system.

Reference	T (K)	u T (K)	P (MPa)	u P (MPa)	N
(Galivel-Solastiouk et al., 1986)	313.1; 343.1	0.1	0.510 – 3.203	0.005	58

TP_{xy} data reported; N– number of data points; u – standard uncertainty.

Table 2-23 shows that only one literature data source reported phase equilibria data for the propane + carbon dioxide + methanol system at two isotherms only of 313.1 and 343.1 K and pressures below 3.3 MPa. The equipment used by Galivel-Solastiouk (Galivel-Solastiouk et al., 1986) has been mentioned earlier in section 2.3.1.7. The data for this system are important in the design of absorption systems that employ methanol as a solvent of choice, such as the Rectisol process (Galivel-Solastiouk et al., 1986). Acid gas treating processes that employ methanol, as in the Rectisol process operates at temperatures lower than 273.15 K, in the range of up to 202.65 K (Burr and Lyddon, 2008). This indicates the need for more phase equilibria measurements on this system over wide temperature ranges to as low as 202.65 K and high-pressure ranges.

2.3.2.6. Propane + water + methanol

There are few open literature sources with experimental phase equilibria data for the propane + water + methanol ternary system (see Table 2-24). The recent data set has extensive data points compared to the first source. A temperature range is presented for the data of Blanco et al. (Blanco et al., 2001) since this are non-isothermal data. Blanco et al. (Blanco et al., 2001) measured dew point data for this ternary mixture using a dew point generator. The data of Blanco et al. (Blanco et al., 2001) were modelled using

EOS–CR method (equation of state – chemical reticular), which accurately reproduced the experimental dew point temperature data with an AAD in the range of 0.8 to 3.2 K.

Table 2-24: Phase equilibria data for the propane + water + methanol system.

Reference	<i>T</i> (K)	<i>P</i> (MPa)	N
(Ng and Robinson, 1983) ^{a, nst}	270.35	0.23	1
(Blanco et al., 2001) ^{b, nst}	254.20 – 280.90	0.10-0.54	237

^a – *TP_{xy}* data reported; ^b – Only *TP_y* data reported; N – number of data points; ^{nst}– data retrieved from NIST TDE in Aspen Plus V12; all data in Table 2-24 are isopleths; hence *T* ranges are presented.

The data presented in Table 2-24 is limited to low pressures below 1 MPa, and also to temperatures below 281 K. Therefore, it is necessary that more data be measured for this system for pressures higher than 1 MPa, and for temperature ranges other than those reported in Table 2-24.

2.3.2.7. Carbon dioxide + water + TEG system

There are few reported phase equilibria experimental data for the carbon dioxide + water + TEG ternary system. Reported data are presented in Table 2-25. The phase equilibria data are necessary since they provide essential information required to design dehydration processes for carbon dioxide-rich gases. Examples of key industries that require such data are refining processes, petrochemical, synthetic fuels, and enhanced oil recovery projects. Takahashi et al. (Takahashi et al., 1984) measured the solubility data of carbon dioxide in TEG aqueous solutions with a water content of 3.5 and 7 wt.%, at a temperature range of 297.15 to 322.15 K and pressures up to 8 MPa. Wise and Chapoy (Wise and Chapoy, 2016) also measured the solubility of carbon dioxide in TEG and its aqueous solutions (96.5, 90, 60, and 40 wt.% TEG) for a temperature range between 263.15 to 343.15 K and pressure range between 0.3 to 37 MPa.

Table 2-25. Phase equilibria data for the carbon dioxide + water + TEG system.

Reference	<i>T</i> (K)	<i>u T</i> (K)	<i>P</i> (MPa)	<i>u P</i> (MPa)	N
(Takahashi et al., 1984)	296.98; 310.93; 322.04	0.1	2.51-8.03	0.01	30
(Wise and Chapoy, 2016)	263.15; 273.15; 297.04; 298.15; 310.93; 322.04; 343.15	0.05	0.22-30.13	0.04	59

Only *TP_x* data reported; N – number of data points; *u* – standard uncertainty; all data in Table 2-25 are isothermal.

The solubility data of carbon dioxide in TEG and its aqueous solutions has been of interest for the past six decades. The data of (Takahashi et al., 1984) was modelled with the Krichevsky-Kasarnovsky (KK) equation, which yielded good agreement with the experimental data, with an AAD of < 2% in carbon dioxide liquid mole fraction. The data of Wise and Chapoy (Wise and Chapoy, 2016) was modelled using the CPA EOS with a single binary interaction parameter. The CPA model was unsatisfactory in describing the phase behaviour for this ternary system, except for the pure carbon dioxide + TEG binary system data.

2.3.2.8. Carbon dioxide + water + methanol system

The phase equilibria data for the carbon dioxide + water + methanol is vital in supercritical fluid extraction. Chang and Rousseau (Chang and Rousseau, 1985) used the SRK EOS with Mathias's polar correction factor to model their data. There was excellent agreement between the measured and the correlated data of Chang and Rousseau (Chang and Rousseau, 1985). The RMSD % in pressure for the data Chang and Rousseau (Chang and Rousseau, 1985) using the SRK EOS was reported to be 8.46 when both binary interaction parameters k_{ij} and c_{ij} were regressed and 12.45 with the k_{ij} only. Yoon et al. (Yoon et al., 1993) used the SRK and Patel-Teja EOS incorporated with Huron Vidal mixing rules and obtained excellent agreement between the measured and the experimental data Yoon et al. (Yoon et al., 1993) used a recirculation type of apparatus for their measurements. The reported data are presented in Table 2-26.

Table 2-26: Phase equilibria data for the CO₂ + H₂O + CH₃OH system.

Reference	T (K)	u T (K)	P (MPa)	u P (MPa)	N
(Chang and Rousseau, 1985) ^a	243.15; 258.15; 273.15; 298.15	0.10	0.008-0.017		35
(Yoon et al., 1993) ^a	305.15; 308.15; 311.15; 313.15		0.7-12		110
(Xia et al., 2004) ^a	313.75; 354.35; 395.0	0.10	0.14-9.93	0.01	221
(Höhler et al., 2018) ^a	258.3; 272.9; 273.0; 288.1; 298.3	0.10	0.44-5.45	0.01	78
(Jarne et al., 2004) ^b	246-288.90	0.40	0.2-4.31		192

^a-Only TP_x data reported; ^b- Only TP_y data reported; N – number of data points; u – standard uncertainty; the data of Jarne et al. are isopleth data (constant water composition); hence only T range is presented, the rest are isothermal data

Xia et al. (Xia et al., 2004) measured the solubility of carbon dioxide in aqueous methanol solutions, where the methanol mole fraction in the solvent mixture was any of the following: 5, 10, 25, 50, 75, 90,

95 and 100%. Xia et al. (Xia et al., 2004) conducted their measurements in a high-pressure cell of stainless steel, fitted with sapphire windows at opposite ends for viewing purposes. Jarne et al. (Jarne et al., 2004) modelled their data using the predictive excess function–equation of state (EF–EOS), where the measured dew point temperature was reproduced with an AAD in the range 0.0 to 2.7 K.

2.3.2.9. Ternary systems with no reported data

Table 6-27 presents ternary systems of this study. A review of the information on Dortmund data bank (DDBST GmbH, 2019) and NIST ThermoData Engine in Aspen Plus V11-12 revealed that no data has been reported for the following ternary systems***:

Table 2-27: Ternary systems of interest with no reported data.

	methane	propane	carbon dioxide	methanol	TEG	water
methane + propane			X	***	***	***
methane + carbon dioxide				X	***	X
propane + carbon dioxide				X	***	***
methanol + TEG	***		***			***
water + methanol		X	X		X	
water + TEG		***	X			

x denotes a ternary system with reported data; *** denotes a ternary system with no reported data. Hence there is need for phase equilibrium data measurements on these systems.

2.3.3. Quaternary systems

The proprietary Dortmund Data Bank (DDBST GmbH, 2019) was used to search for all possible possible quaternary systems that could result from the main six components of this study (see Table 2-28). A review of the information on the data bank showed that no data were available for the methane + propane + methanol + TEG quaternary system. It was further revealed on the same data bank that data were available for the following quaternary systems:

Table 2-28: Quaternary systems of this study.

Mixture	methane	propane	carbon dioxide	methanol	TEG	water
(a)	×	×	×	×		
(b)	×	×	×		×	
(c)	×	×	×			×
(d)	*	*		*	*	
(e)	×	×			×	×
(f)	×		×	×	×	
(g)	×		×	×		×
(h)		×	×	×	×	
(i)		×	×	×		×
(j)		×	×	×		×
(k)	×			×	×	×
(l)		×		×	×	×
(m)			×	×	×	×

x represents individual components listed in the top row, that are merged to make quaternary mixtures listed on the left column with reported data; * represents individual components listed in the top row, that are merged to make quaternary mixture (d) listed on the left column with no reported data.

However, none of the reported data was available in the open literature. This proves that measurements of phase equilibria data for these systems are required to fill this knowledge gap in the open literature.

2.3.4. Five-component (quinary) systems

A literature survey was conducted to investigate if there has been reported literature data on any possible five-component system combination for the main components of this study. A review of information on the proprietary Dortmund Data Bank (DDBST GmbH, 2019) showed that data were available for all of the following systems:

methane + propane + carbon dioxide + water + methanol;

methane + propane + carbon dioxide + water + TEG;

methane + propane + carbon dioxide + methanol + TEG;

methane + propane + water + methanol + TEG;

methane + carbon dioxide + water + methanol + TEG;

propane + carbon dioxide + water + methanol + TEG

However, none of the data was available in the open literature. Hence research and publication of the data on these systems are necessary to make the data easily accessible.

2.3.5. Six-component (senary) system

A literature survey was conducted to investigate if there has been any reported phase equilibria data for the six-component system of this study. A review of information on the proprietary Dortmund Data Bank (DDBST GmbH, 2019) showed that data were available for the methane + propane + carbon dioxide + water + methanol + TEG; however, the data could not be obtained from open literature. This shows that more measurements are required on this system so that the data can be easily accessible.

2.4. Summary of chapter 2

The chapter highlighted each of the main components of this study, with the important physical and chemical properties listed. The type bonding and interactions expected on each of the items was briefly described. From the presented information, it is expected that highly polar components of this study namely TEG, methanol and water would effect stronger forces on mixtures due to either self or cross associations. Quadruple effects are expected to be significant in mixtures where carbon dioxide is one of the components. Weak van der Waals forces are expected in normal alkane dominated systems (methane and propane). Also, the hydrophobic effect is anticipated in systems containing alkane + water. The phase equilibria data for all possible mixtures for components of interest in this study were investigated. Reported phase equilibria data were presented along with systems where data were not present in the open literature. Systems with reported phase equilibria data that were limited were identified.”. The reported water/TEG wt.% ratios motivated the selection of the water/TEG wt.% ratios used in this study, as well as the temperature and pressure ranges. Furthermore, thermodynamic models that were used to model most of the reported data and the equipment used were revealed. Generally, the following models, PR, SRK, PRWS, CPA, PC SAFT, NRTL, UNIQUAC were revealed to have modelled most of the reported data with greater accuracy. For ternary and higher-order mixtures, the models were less accurate as in either correlating or predicting the experimental data as compared to the binary systems. The literature review helped to reveal gaps in experimental phase equilibria data on certain chemical mixtures of importance to the gas industry. It also helped to inform some of the possible thermodynamic models that can be used on chemical mixture combinations of this work.

CHAPTER 3: REVIEW OF THERMODYNAMIC PRINCIPLES FOR HPVLE MODELLING

3.0 INTRODUCTION

This section focuses on the description of thermodynamic models relevant to this study. Modelling of phase equilibria data is important because it enables adjustment of binary interaction for correlation of the experimental data, which can be used in predicting phase equilibria data for the systems of interest at other conditions, thus leading to model performance improvement. Thermodynamic models can aid the design processes by reducing the number of experimental data points required for a particular design challenge (Dohrn and Brunner, 1995). In simulation studies, computational and experimental methods are necessary; however, the experimental data have a conclusive role in validating theoretical methods and correcting parameters in correlations (Frost et al., 2014). Modelling high-pressure vapour liquid equilibrium (HPVLE) involves data regression (i.e., parameter fitting) for data correlation via prediction. In addition, predictions were performed via associating theory models, which are discussed in this section.

3.1 Overview of the key principles in phase equilibrium thermodynamics

3.1.1. Fugacity and vapour-liquid equilibrium for pure components

“Fugacity (f) is a measure of the molar Gibbs energy of a real gas” (Ahmed, 2010). Fugacity can be viewed as a vapour pressure adjusted to denote the likelihood of molecules to diffuse from one phase into the other (Ahmed, 2010). Components diffuse from a phase with a high component fugacity to the phase with a lower component fugacity until equal fugacities of each component in either phase is achieved. For a system with both liquid and vapour phases, vapour-liquid equilibrium occurs when there are equal fugacities of components in either of the phases. This implies a zero-net transfer of all components between the phases; hence the system is in thermodynamic equilibrium. The thermodynamic equilibrium condition can be expressed as:

$$f_i^{vap} = f_i^{liq} \quad (3-1)$$

Where f_i^{vap} is the fugacity of component i in the vapour phase (Pa); f_i^{liq} is the fugacity of component i in the liquid phase (Pa).

For any fluid, the fugacity coefficient of component i in the fluid is a function of the fugacity of the component, system pressure and mole fraction (Ahmed, 2010). Given a vapour phase, the fugacity coefficient of component i in this phase is expressed as:

$$\phi_i^{vap} = \frac{f_i^{vap}}{y_i P} \quad (3-2)$$

Where ϕ_i^{vap} is the fugacity coefficient of component i in the vapour phase; y_i is the mole fraction of component i in the vapour phase; and P is the system pressure.

For component i in the liquid phase, the fugacity coefficient can be mathematically expressed as:

$$\phi_i^{liq} = \frac{f_i^{liq}}{x_i P} \quad (3-3)$$

Where ϕ_i^{liq} is the fugacity coefficient of component i in the liquid phase; x_i is the liquid mole fraction of component i .

Equations (3-1 to 3-3) can be arranged to produce:

$$P y_i \phi_i^{vap} = P x_i \phi_i^{liq} \quad (3-4)$$

This can be further simplified to:

$$y_i = x_i \frac{\phi_i^{liq}}{\phi_i^{vap}} \quad (3-5)$$

Further simplification leads to:

$$y_i = K_i x_i \quad (3-6)$$

Where K_i is the equilibrium ratio for component i

It is important to highlight that phase equilibrium, either for a binary system or multicomponent system, is characterised by:

- uniform temperature in the system

$$T_i^{Phase\ 1} = T_i^{Phase\ 2} \quad (3-7)$$

- uniform pressures in the system

$$P_i^{Phase1} = P_i^{Phase\ 2} \quad (3-8)$$

- uniform chemical potentials of components in each phase

$$\mu_i^{Phase1} = \mu_i^{Phase\ 2} \quad (3-9)$$

3.1.2. Fugacity and vapour-liquid equilibrium for mixtures

In practical petroleum engineering applications, concern is on the phase behaviour of hydrocarbon gas mixture, which will be in equilibrium with a hydrocarbon liquid mixture at specific temperature and pressure conditions (Ahmed, 2010). The fugacity in solution of component i (in a mixture) can be described via equation (3-10) (Dahm and Visco, 2015).

$$d\mu_i = RTd \ln \hat{f}_i \quad (3-10)$$

Where d represents change (delta); μ_i is the chemical potential for component i in the mixture; T is the temperature; R is the universal gas constant; \hat{f}_i is the fugacity in solution of component i in the mixture.

The symbol for chemical potential is the same whether component i is in a mixture or not, thus after some integration of equation (3-10) as shown in (Dahm and Visco, 2015), confusion can be avoided by substituting the pure component chemical potential by the pure component excess molar Gibbs free energy G^E , thus:

$$\mu_i(T, P, x) = G^E + RT \ln \left[\frac{\hat{f}_i(T, P, x)}{f_i(T, P)} \right] = \bar{G}_i \quad (3-11)$$

Where \bar{G}_i is the partial molar Gibbs free energy of component i in the mixture.

Using equation (3-11), two of the most crucial models for VLE modelling can be explored and these are the ideal gas for the vapour phase and the ideal solution for the liquid phase (Dahm and Visco, 2015).

3.1.2.1 The ideal solution and ideal gas approaches

The fugacity of component i in a mixture modelled as an ideal solution is equivalent to the pure component fugacity at the mixture pressure and temperature, multiplied by its mole fraction, and this is the Lewis Randall rule, which can be expressed as (Dahm and Visco, 2015):

$$\hat{f}_i^{Id}(T, P, x) = x_i f_i(T, P) \quad (3-12)$$

Where the superscript Id reflects the ideal solution.

The same approach used for the ideal solution can be applied to the ideal gas. The ideal gas chemical potential for component i , is the same as the ideal gas partial molar Gibbs free energy of component i , hence after some computations and inspections as outlined in (Dahm and Visco, 2015), equation (3-13) can be obtained.

$$\hat{f}_i^{Ig}(T, P, y) = y_i f_i^{Ig}(T, P) \quad (3-13)$$

Where the superscript Ig reflects the ideal gas.

As stated in section 3.1.1 that pure component fugacity in an ideal gas is equivalent to the system pressure; thus, the fugacity of component i in a mixture, when modelled as an ideal gas can be expressed as:

$$\hat{f}_i^{Ig}(T, P, y) = Py_i \quad (3-14)$$

Real mixture behaviour is explained in terms of departures from equations (3-12 and 3-13) (Dahm and Visco, 2015; Orbey and Sandler, 1998) since only few mixtures are ideal.

Excess properties are used to capture deviations from ideal solutions. Thus, the excess chemical potential of component i in a mixture can be evaluated as (Dahm and Visco, 2015):

$$\mu_i^E(T, P, x) = RT \ln \left[\frac{\hat{f}_i(T, P, x)}{f_i(T, P)} \right] = RT \ln \gamma_i \quad (3-15)$$

Where γ_i is the activity coefficient of component i in the mixture; superscript E represents the excess term of the chemical potential.

The activity coefficient is the ratio of the fugacity coefficient of component i in a mixture to its ideal solution value; thus, it captures the deviation from the ideal solution. In other words:

$$\hat{f}_i(T, P, x) = \hat{f}_i^{Id} \gamma_i = x_i f_i(T, P) \gamma_i \quad (3-16)$$

Residual properties are used to account for the departure from ideal gas in the vapour phase. Thus; the residual chemical potential of a component i in solution can be calculated as follows:

$$\mu_i^R(T, P, y) = RT \ln \left[\frac{\hat{f}_i(T, P, y)}{P y_i} \right] = RT \ln[\hat{\phi}_i] \quad (3-17)$$

Where $\hat{\phi}_i$ is fugacity coefficient of component i in solution.

The fugacity coefficient of a component i in a mixture can be described “as the ratio of the fugacity of component i in the mixture to its ideal gas value” (Dahm and Visco, 2015). Therefore, the fugacity coefficient accounts for the deviation from the ideal gas behaviour, hence;

$$\hat{f}_i(T, P, y) = \hat{f}_i^{Ig} \hat{\phi}_i = y_i P \hat{\phi}_i \quad (3-18)$$

Thus, the activity coefficient and fugacity coefficient can be used to model VLE. Just like the pure component result, the mixture chemical equilibrium condition is equal to that for the mixture fugacity condition, thus:

$$\hat{f}_i(T, P, x)^{Phase\ 1} = \hat{f}_i(T, P, x)^{Phase\ 2} \quad (3-19)$$

Using equation (3-19) and substituting equation (3-18), for the fugacity coefficient in a mixture, the following expressions are obtained:

$$\hat{f}_i(T, P, z)^{Phase\ 1} = \hat{f}_i(T, P, z)^{Phase\ 2} \quad (3-20)$$

$$z_i^{Phase\ 1} P \hat{\phi}_i^{Phase\ 1} = z_i^{Phase\ 2} P \hat{\phi}_i^{Phase\ 2} \quad (3-21)$$

At equilibrium, pressure will be the same in both phases; hence equation (3-21) reduces to:

$$z_i^{Phase\ 1} \hat{\phi}_i^{Phase\ 1} = z_i^{Phase\ 2} \hat{\phi}_i^{Phase\ 2} \quad (3-22)$$

Note that for equations (3-20 to 22), z can be either liquid or vapour phase composition.

Therefore, when using the fugacity coefficient in a mixture, the chemical equilibrium condition includes the mole fraction (Dahm and Visco, 2015). For a mixture at chemical equilibrium, the mole fractions in the different phases are mostly not equal except at an azeotrope. There still remains a problem of reducing the fugacity expressions (equations 3-19 to 20) to equations explicit in pressure, composition, and temperature. This is performed in different approaches for different phase equilibria scenarios.

3.1.2.2. Gamma-Phi modelling

For modelling phase equilibrium in mixtures, a component in a mixture will have the same fugacities in both phases it appears (Dahm and Visco, 2015); thus, equation (3-19) may be written for the case of a vapour-liquid equilibria mixture as:

$$\hat{f}_i^{vap} = \hat{f}_i^{liq} \quad (3-23)$$

Where *vap* and *liq* represents the vapour and liquid phases respectively.

In the gamma phi approach, description of the fugacity coefficient of component i in a mixture for the liquid phase is accomplished by using the ideal solution as a reference (Dahm and Visco, 2015); thus, equation (3-16) may be presented as:

$$\hat{f}_i^{liq}(T, P, x) = x_i f_i(T, P) \gamma_i \quad (3-24)$$

Where deviations from ideal solution behaviour are taken care of by the activity coefficient, gamma (γ).

The fugacity coefficient of component i in a mixture for the vapour phase is described using the ideal gas reference; thus, equation (3-25) is obtained from equation (3-18).

$$\hat{f}_i^{vap}(T, P, y) = y_i P \hat{\phi}_i \quad (3-25)$$

Where departure from ideal gas behaviour is accounted by the fugacity coefficient of component i in the mixture, phi ($\hat{\phi}_i$).

Using equation (3-24) for the right-hand side of equation (3-23), and equation (3-25) for the left-hand side, the following expression is obtained:

$$y_i P \hat{\phi}_i = x_i f_i(T, P) \gamma_i \quad (3-26)$$

Equation (3-26) is the gamma-phi equation which is has been useful for modelling the VLE behaviour of mixtures (Dahm and Visco, 2015).

3.1.2.3. Phi-Phi modelling

With the phi-phi approach, both the vapour and liquid phases are modelled utilising an equation of state (EOS). Thus, the following expressions can be presented:

$$\hat{f}_i^{liq}(T, P, x) = x_i P \hat{\phi}_i^{liq} \quad (3-27)$$

$$\hat{f}_i^{vap}(T, P, y) = y_i P \hat{\phi}_i^{vap} \quad (3-28)$$

Substituting equations (3-27) and (3-28) into equation (3-23) results in:

$$y_i P \hat{\phi}_i^{vap} = x_i P \hat{\phi}_i^{liq} \quad (3-29)$$

Since pressure is equal in both phases at equilibrium, it is cancelled out from equation (3-29) to obtain:

$$y_i \hat{\phi}_i^{vap} = x_i \hat{\phi}_i^{liq} \quad (3-30)$$

Equation (3-30) requires an equation of state that can describe both the vapour and liquid phases, for instance, cubic equations of state. For further reading on derivations and descriptions of equations presented in this section 3.1, the reader is referred to (Dahm and Visco, 2015; Orbey and Sandler, 1998).

3.2. Thermodynamic models applied in this work

In this work, no modifications were made to the thermodynamic models used. Rather the interest was in their application to systems measured and those reported in the literature. Hence, the models are discussed briefly in this section, with more descriptions of the equations presented in Appendix D. Also, the reader is referred to (Dahm and Visco, 2015; Kontogeorgis and Folas, 2010; Orbey and Sandler, 1998) for a detailed description of the models.

3.2.1. Cubic equations of state used in this study

Cubic equations of state are conventional high-pressure models (Kontogeorgis and Folas, 2010), capable of describing both the liquid and vapour phases. High-pressure vapour-liquid equilibrium (HPVLE) can often be more complicated than low-pressure VLE due to the non-ideality behaviour of both phases at high pressures. This study made use of the Peng-Robinson (PR) and the Soave-Redlich-Kwong (SRK) cubic equations of state (EsOS). These were used because they are both the primary model choices of the chemical and petroleum industries, such as the gas processing industry, petrochemicals, air separation, and others (Kontogeorgis and Folas, 2010). Both models have been previously used for systems related to this study, as highlighted in chapter 2. Equations for the PR and SRK models and their parameters are presented in Appendix D.1.1.

Binary interaction parameters

According to Best (Best, 1981), the binary k_{ij} interaction parameter is a rough estimate of how strong the interactions are between two components i and j . The larger the absolute value of k_{ij} between components i and j , the stronger the interaction between those components (Best, 1981). If the absolute value of k_{ij} is very small, it means the chemical system is close to ideal (Best, 1981); hence the interactions are minimum. Table 3-1 shows literature k_{ij} values for the PR EOS for components of interest in this study. In this work, unless otherwise stated, literature k_{ij} values are presented for purposes of comparison with the regressed k_{ij} values from experimental data of this work. The presented literature k_{ij} values are in the temperature range covered in this study.

Table 3-1: Binary interaction coefficients k_{ij} for the Peng-Robinson EOS, components of this study.

Component <div style="display: inline-block; vertical-align: middle;"> $i \rightarrow$ $j \downarrow$ </div>	CO ₂	CH ₄	C ₃ H ₈	C ₆ H ₁₄	C ₁₀ H ₂₂	CH ₃ OH	H ₂ O	TEG
CO ₂		0.105 ^a	0.125 ^a	0.115 ^a	0.115 ^a	0.075 ^b 0.012 to 0.068 ^c	0.2186 ^c	0.07203 ^e
CH ₄			0.010 ^a	N/C	N/C	0.01 ^a	0.4850 ^d	0.03418 ^e
C ₃ H ₈				0.010 ^a	0.005 ^a	0.026 0.03 ^b	0.5525 ^d	0.13314 ^e
C ₆ H ₁₄					0.00	N/C	N/C	N/C
C ₁₀ H ₂₂						N/C	N/C	N/C
CH ₃ OH							0.0435 ^c ; -0.0778 ^c	f
H ₂ O								f
TEG								

$$k_{ij} = k_{ji}$$

N/C represents binary systems not considered in this study.

a:(Ahmed, 2010); b : (Robinson et al., 1985), $T = 323.15$ K for CO₂ + CH₃OH system, $T = 310.98$ K for CH₃OH + C₃H₈ system; c : (Ye et al., 2011), T dependent; d: (Li et al., 2015); e: Obtained at 298.15 K using equation 3.30 provided by Jou et al. (Jou et al., 1987); f: parameters not available.

Table 3-1 shows that no binary interaction parameters were reported in literature for TEG + methanol and TEG + water binary pairs using the PR EOS. This highlights the need to obtain suitable parameters applicable to the PR EOS to model such binary pairs. The majority of the measurements are taken at low pressures, hence the activity coefficient approach would have been used in most cases. For the multicomponent systems it is not possible to use different models for different component pairs. Hence one is forced to model this system with a single model, because of the many components which exist

in the mixture. For the carbon dioxide + water + TEG ternary system, the k_{ij} values between each binary pair are usually large since water and TEG are highly polar and can form hydrogen bonds (Best, 1981). Carbon dioxide + TEG parameters vary slightly with temperature or pressure, hence Best (Best, 1981) employed a temperature-independent k_{ij} . The binary interaction parameter for the water + carbon dioxide system varies greatly with temperature but not with pressure (Best, 1981). Bamberger et al. (Bamberger et al., 2000) asserts that correlating experimental data of water + carbon dioxide requires temperature-dependent binary interaction parameters. Jou et al. (Jou et al., 1987) asserts that the PR EOS temperature-dependent binary interaction parameters for the solute + TEG binary system, which shows a linear relationship with temperature can be evaluated using equation (3-31).

$$k_{ij} = A_0 + A_1 * T \quad (3-31)$$

Where A_0 and A_1 are parameters presented in the paper of Jou et al. for the solute of concern, in this case carbon dioxide, methane and propane.

The SRK EOS binary interaction parameters for components of this study are presented in Table 3-2.

Table 3-2: Binary interaction coefficients k_{ij} for the SRK EOS, components of this study.

Component i → j ↓	CO ₂	CH ₄	C ₃ H ₈	C ₆ H ₁₄	C ₁₀ H ₂₂	CH ₃ OH	H ₂ O	TEG
CO ₂		X	X	X	X	0.0100 ^c 0.0356 ^c 0.0547 ^c	0.193 ^a	g
CH ₄	0.093 ^a 0.1 _{nc} ^b ; 0.06 _c ^b 0.1243 ^d		X	N/C	N/C	g	0.52 ^a	
C ₃ H ₈	0.1358 ^c 0.1235 ^d	0.0068 ^d		N/C	N/C	0.0043 ^c	g	
C ₆ H ₁₄	0.1021 ^d	N/C	N/C		N/C	N/C	N/C	N/C
C ₁₀ H ₂₂	0.1361 ^{e,f}	N/C	N/C	N/C		N/C	N/C	N/C
CH ₃ OH	X	g	X	N/C	N/C		g	g
H ₂ O	-0.1224 ^a	-0.3678 ^a	g	N/C	N/C	g		g
TEG	g	g	g	N/C	N/C	g	g	

a: (Austegard et al., 2006); b: (Thiery et al., 1994) where subscripts nc represents the non-critical region, c represents the critical region. c: (Chang et al., 1983) 0.0356 at 298.15 K, 0.0547 at 313.15 K; d: (de Guido et al., 2014); e: (Nourozieh et al., 2013) at 373.2 K, up to 6 MPa pressure; f: (Nourozieh et al., 2013) at 323.15 K, up to 6 MPa; g: parameters not available; X represents binary system where either k_{ij} or k_{ji} are presented in Table 3.2; N/C represents binary systems not considered in this study

Austegard et al. (Austegard et al., 2006) compared the experimental solubility data of the carbon dioxide + water + methane system using the SRK VdW model. In that work, the SRK VdW model yielded two different values for the binary interaction parameters k_{ij} and k_{ji} .

Table 3-2 shows that no literature binary interaction parameters were reported for the following binary pairs: methane + methanol; water + propane; water + methanol; carbon dioxide + TEG; methane + TEG; propane + TEG; methanol + TEG; and water + TEG using the SRK EOS. This highlights the need to obtain suitable parameters applicable to the SRK EOS to model such binary pairs. For the carbon dioxide + water and, water + methane binary pairs, the temperature-dependent binary interaction parameters were estimated following the equations (3-32) and (3-33) respectively presented by (Austegard et al., 2006).

$$k_{ij} = -0.527 + 1.67 * 10^{-3} * T - 1.05 * 10^{-6} * T^2 \quad (3-32)$$

$$k_{ji} = -1.50 + 4.85 * 10^{-3} * T - 3.53 * 10^{-6} * T^2 \quad (3-33)$$

T is in Kelvin

Thiery et al. (Thiery et al., 1994) asserts that the SRK EOS can accurately predict vapour-liquid equilibria data in the critical and non-critical regions for the carbon dioxide + alkanes binary pairs, provided the binary interaction parameters used are different for each region. For the critical region, the binary interaction parameters should be established from experimental data specific to the conditions.

Chang et al. (Chang et al., 1983) employed the SRK EOS to predict phase equilibria data for mixtures found in typical treatment processes of produced gases from coal processing. The temperature-dependent binary interaction parameters for the methanol + carbon dioxide system were estimated using equation (3-34) presented by (Chang et al., 1983).

$$k_{ij} = -0.0972 + 0.4741 * 10^{-3} * T \quad (3-34)$$

The drawback of the PR and SRK EOS is that they have difficulties describing phase behaviour of substances such as water, high polar molecules, and hydrogen bonding molecules (Kontogeorgis and Folas, 2010; Ozigagu and Duben, 2019). Ozigagu and Duben (Ozigagu and Duben, 2019) observed that both models overestimate the pressure of the system by a factor of two and underestimate the composition of methane in the vapour phase by approximately 2-3% for the methane + methanol system. For the methane + TEG system, Ozigagu and Duben (Ozigagu and Duben, 2019) demonstrated that both models (PR and SRK) underestimate the experimental pressure, and their results were approximately a third of those reported in the experiments.

3.2.2. Activity coefficient model

3.2.2.1. Overview of G^E models

The mathematical flexibility of activity coefficient models has made them applicable to systems that exhibit high liquid phase non-ideality (Mathias and Copeman, 1983). The activity coefficient models work well up to moderate pressures and at reduced temperatures where the liquid is considered incompressible (Mathias and Copeman, 1983). In this work, no activity coefficient model was used alone but instead used in combination with an equation of state model. Since the equation of state models applied to this work have already been described, this section is devoted to the activity coefficient model employed in this work and the mixing rules used to combine a cubic EOS with an activity coefficient model. As mentioned in section 3.2 although cubic EsOS utilising the VdW one fluid theory have been successful for modelling mixtures containing non-polar to slightly polar compounds, their drawback lies in the fact that they have difficulties in describing the phase behaviour of substances such as water, high polar molecules, and hydrogen bonding molecules. This limitation of cubic equations of state prompted the widespread usage of the gamma-phi approach described in section 3.1, where an activity coefficient model (excess Gibbs energy (G^E)) describes the liquid phase, while an EOS describes the vapour phase (Kontogeorgis and Folas, 2010).

Activity coefficient models are classified into two main categories: random-mixing models such as van Laar, Margules; and the local composition models (LC) such as NRTL (Non-random Two Liquid), Wilson and so on (Kontogeorgis and Folas, 2010). For further details about these, the reader is referred to Kontogeorgis and Folas (Kontogeorgis and Folas, 2010), only the NRTL model used in this work is discussed. This was because the NRTL provides best fits on all mixtures provided the non-randomness parameter is properly selected for each binary pair (Renon and Prausnitz, 1968). As the size difference between two components increases, the activity coefficient also increases; hence activity coefficients accounts for departures from ideality in a solution (Kontogeorgis and Folas, 2010). The relationship between the excess Gibbs energy G^E and activity coefficients is expressed in equation (3-36).

$$G^E = H^E - TS^E \quad (3-35)$$

$$RT \ln \gamma_i = \left(\frac{\partial nG^E}{\partial n_i} \right)_{T,P,n_j \neq n_i} \quad (3-36)$$

Where H^E is the excess enthalpy; S^E is excess entropy.

Therefore, developing an excess Gibbs energy model requires knowledge about the energetic effect due to dissimilarities in intermolecular forces and the entropic effect characterised by excess entropy

(Kontogeorgis and Folas, 2010). The different activity coefficient models formulated begin from an expression of G^E (Kontogeorgis and Folas, 2010).

One of the most challenging tasks is to decide upon the most appropriate activity coefficient model to be used and the values of the chosen model parameters. Earlier studies by other researchers determined that the NRTL model yielded the best fit for aqueous organic mixtures compared with other activity coefficient models (Orbey and Sandler, 1998). For that reason, the NRTL model was used in this study since there are aqueous organic mixtures for most of the systems. For more details about the NRTL model, the reader is referred to Appendix D.2, Renon and Prausnitz (Renon and Prausnitz, 1969, 1968).

3.2.3. Mixing rules that combine an EOS with an activity coefficient model

Mixing rules are required to model complex phase behaviour of extremely non-ideal systems since such systems cannot be satisfactorily described by the common Van der Waals one fluid mixing rules (Wong and Sandler, 1992). Several authors proposed different mixing rules; however, only the mixing rules of Wong and Sandler (Wong and Sandler, 1992) denoted as (WS) were utilised in this work. The WS mixing rules were used in this work because, unlike other mixing rules such as the Huron-Vidal, which could not satisfy the condition that “*second virial coefficients be a quadratic function of composition and were not consistent with statistical mechanical theory*” (Wong and Sandler, 1992), the WS mixing rules satisfies that condition. As a result, the WS mixing rule made it feasible to obtain accurate results at both high and low density limits without being density-dependent (Wong and Sandler, 1992). Furthermore, the WS mixing rule produced much better results for polar moderately symmetric mixtures such as water + propanol (Kontogeorgis and Folas, 2010).

3.2.3.1. Wong Sandler (WS) mixing rules

Wong and Sandler, in 1992, proposed a mixing rule linking an EOS with an excess Gibbs free energy model, which allows for extrapolation over wide ranges of pressures. The mixing rule of Wong and Sandler (Wong and Sandler, 1992) equates the excess Helmholtz free energy A^E at infinite pressure from an equation of state to that of an activity coefficient model (Kontogeorgis and Folas, 2010). Some details about the derivations for the equations for the WS mixing rule are presented in Appendix D.3 and (Wong and Sandler, 1992).

3.2.3.2. Peng-Robinson Wong Sandler (PRWS)

Combining the cubic EOS with an activity coefficient model has been made possible by mixing rules for the energy parameter of the cubic EOS. Detailed descriptions about the derivations for the PRWS model are presented in (Wong and Sandler, 1992). These mixing rules allow incorporating an expression for the excess Gibbs energy G^E inside the cubic equation of state, thus enabling it to be applied for high pressure and polar systems (Kontogeorgis and Folas, 2010). Figure 3-1 illustrates the advantages of combining an activity coefficient model with a cubic equation of state. This allows phase equilibria description using a single model for both polar and non-polar mixtures, either at low, moderate or high pressures. In this work, the excess Gibbs energy in the WS mixing rule was estimated via the NRTL (Non-Random Two-Liquid) activity coefficient model (Renon and Prausnitz, 1968). NRTL parameter is represented as A_{ij} and the non-randomness parameter was fixed at 0.3. The non-randomness parameter was fixed at 0.3 since, according to (Kontogeorgis and Folas, 2010), this value has been used with success for water-polar systems as well as non-polar components. The Mathias-Copeman (MC) (Mathias and Copeman, 1983) alpha function was employed for both the PR and PRWS models in this work.

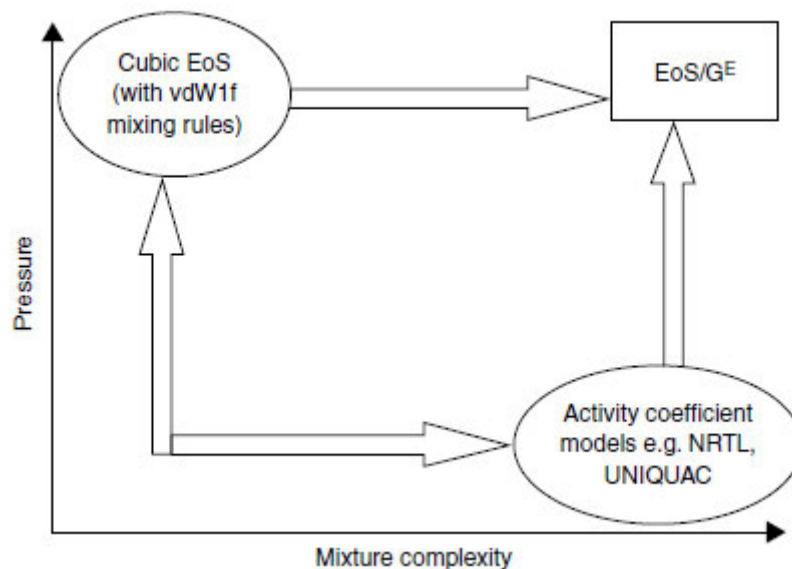


Figure 3-1: Advantage of combining a cubic equation of state with an activity coefficient model.

Source: (Kontogeorgis and Folas, 2010).

3.2.4. Association models

3.2.4.1. Overview of association models

Association models can account for the effects of hydrogen bonding in mixtures. These models are applicable in describing phase equilibria of associating molecules such as glycols, water, alcohols, phenols, acids, amines, and others capable of forming hydrogen bonds (Kontogeorgis & Folas, 2010). Kontogeorgis and Folas (Kontogeorgis and Folas, 2010) reported that the association theories are mainly classified into three main categories, namely:

- Perturbation theories : (The statistical associating fluid theory (SAFT), The cubic plus association equation (CPA), and The Elliot-Suresh-Donohue equation (ESD))
- Lattice fluid theories
- Chemical theories: The associated-perturbed-anisotropic-chain theory (APACT).

The PC-SAFT and the CPA association models were used in this work due to their wide use in process simulation software and industry. In the perturbation theories, the total energy of hydrogen bonding is evaluated from statistical mechanics, and the crucial parameter for hydrogen association is the number of bonding sites per molecule (Kontogeorgis and Folas, 2010). To express the association theories in the form of a thermodynamic model, two contributions are needed which are the physical term and the association term. The association term accounts for the effects of hydrogen bonding and other quasi-chemical interactions, whilst the physical term accounts for the non-ideality caused by physical forces (Kontogeorgis and Folas, 2010). For these associating theories, the compressibility factor Z is expressed as follows (Kontogeorgis and Folas, 2010):

$$Z = Z^{ph} + Z^{as} \quad (3-37)$$

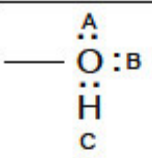
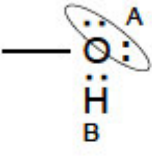
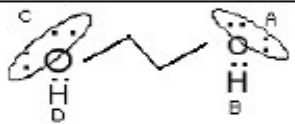
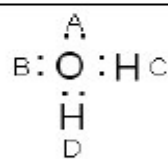
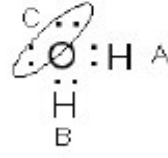
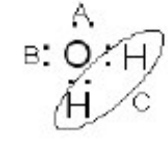
Where Z is the compressibility factor, ph represent the physical contribution and as represent the association contribution to the compressibility factor.

3.2.4.1.1. Association schemes

The association term in the CPA EOS and PC-SAFT EOS represents hydrogen bonding by considering a specific site-site interaction. “*Association exists only between (donor) hydrogen and (acceptor) oxygen sites*” (Wu and Prausnitz, 1998). Table 3-3 provides a schematic explanation of association schemes relevant to the present study. For these association models, various molecules are characterised by distinct association schemes. The one-site 1A scheme is applied to acids, whilst the two-site 2B or three-site 3B schemes are applied to amines and alcohols (Kontogeorgis et al., 2006). In the 3B scheme for alcohols, sites A and B belong to oxygen lone pairs, while site C belongs to a hydrogen atom (Kontogeorgis et al., 2006). The association is not symmetrical; hence, the fraction of nonbonded hydrogen atoms (X^C) is unequal to the fraction of nonbonded lone pairs (X^A or X^B) (Kontogeorgis et al., 2006), see Table 3-3. For the 2B association scheme, the two lone-pair oxygens are regarded as a single

site (Kontogeorgis et al., 2006). Typical association fluids, water and glycols are normally allocated the 4C association (Afzal et al., 2012; Kontogeorgis et al., 2006), though water can be assigned either of the two variants of 3B association, see Table 3-3. When water is assigned to the 3B association scheme as shown in Table 3-3, the two hydrogen atoms may be considered to be a single site labelled C. Alternatively, the two lone pair electrons of the oxygen atom are considered as one site. The 2B association scheme (one proton donor + one proton acceptor) was used for methanol, while the 4C scheme (two proton donors + two proton acceptors) was used for both water and glycols by (Tsivintzelis and Kontogeorgis, 2016).

Table 3-3: Association schemes for associating compounds based on the terminology of (Huang and Radosz, 1990). Taken from: (Riaz, 2011).

Species	Formula	Type	Site fractions (X)
Alcohol		3B	$X^A = X^B; X^C = 2X^A - 1$ $X_1 = X^A X^B X^C$
		2B	$X^A = X^B$ $X_1 = X^A X^B$
Glycols		4C	$X^A = X^B = X^C = X^D$ $X_1 = X^A X^B X^C X^D$
Water		4C	$X^A = X^B = X^C = X^D$ $X_1 = X^A X^B X^C X^D$
		3B	$X^A = X^B; X^C = 2X^A - 1$ $X_1 = X^A X^B X^C$
		3B	$X^A = X^B; X^C = 2X^A - 1$ $X_1 = X^A X^B X^C$

It is important to note that the initial step towards obtaining the parameters of the PC-SAFT and CPA models is to allocate the association scheme to each associating molecule. In this work, inbuilt association schemes in Aspen Plus V12 were used.

3.2.4.2. The Perturbed-Chain Statistical Associating Fluid Theory (PC-SAFT) model

The PC-SAFT model was developed by Gross and Sadowski (Gross and Sadowski, 2001). The PC-SAFT EOS has proved to show very good predictive capabilities and precise correlation when applied to the VLE of mixtures (Gross and Sadowski, 2001). The PC-SAFT model has been used to correlate and predict LLE and VLE in mixtures comprising of hydrocarbons, glycol oligomers, water, aromatic hydrocarbon, methane, nitrogen, and carbon dioxide (Grenner et al., 2007), hence its application to the systems measured in this work. The parameters and equations for the PC-SAFT model are presented in Appendix D.4.1. It is important to note that the critical point is usually overestimated when using the PC-SAFT model (Kontogeorgis and Folas, 2010).

Table 3-4: Binary interaction coefficients k_{ij} for the PC-SAFT EOS and components investigated in this study.

Component t i j	CO ₂	CH ₄	C ₃ H ₈	C ₆ H ₁₄	C ₁₀ H ₂₂	H ₂ O	CH ₃ OH	TEG
CO ₂		0.065 ^a 0.048 ^d 0.0356 ^m	0.109 ^a ; 0.1063 ^b 0.0724 ⁱ	0.1294 ^b 0.1267 ^c 0.0711 ^j	0.1269 ^b 0.1417 ^c 0.0631 ^k	g	0.048 ^d	0.084573 ^e
CH ₄	0.0856 ^h		0.0033 ^b	N/C	N/C	- 385226 ^e	X	0.075449 ^e
C ₃ H ₈	X	0.0117 ^l		N/C	N/A	- 349218 ^e	X	0.060651 ^e
H ₂ O	g	X	X	N/C	N/C		X	X
CH ₃ OH	0.119607 ^f	0.042 ^d	0.05 ^d	N/C	N/C	-0.06 ^d		g
TEG	X	X	X	N/C	N/C	-0.12 ^d	g	

Literature values: a(Gross and Sadowski, 2001); b: obtained from (Teymouri, 2016) for the temperature range 90 – 360.93 K ; c: Obtained from (Justo-García et al., 2008) for a temperature range of 277-510 K; d: (Fouad and Berrouk, 2013); e: calculated at 303.15 K using the equation obtained from(Teymouri, 2016); f: calculated at 303.15 K using the equation obtained from (Gil et al., 2012) ; g: no parameters available; h: (Perez et al., 2017) for a temperature range of 143-301 K; i: (Perez et al., 2017) for a temperature range of 210-366 K; j: (Perez et al., 2017) for a temperature range of 238-393 K; k: (Perez et al., 2017) for a temperature range of 277-583 K; l: (Perez et al., 2017) for a temperature range of 90-360 k; m: (Perez et al., 2017) for a temperature range of 143-301 K; N/C represents binary pairs not of considered in this study; X represents a binary system where either k_{ij} or k_{ji} are presented in Table 3.4

Furthermore, the SAFT models underestimate the solubility of hydrocarbon in water since they do not take into account the hydrophobic effect (Wu and Prausnitz, 1998). Table 3-4 presents some of the reported PC-SAFT binary interaction parameters for components of this study.

Table 3-4 shows that no reported literature binary interaction parameters were obtained for the following binary pairs: carbon dioxide + water; methanol + TEG using the PC-SAFT equation. This highlights the need to obtain suitable parameters applicable to the PC-SAFT equation for modelling such binary pairs. According to Teymouri (Teymouri, 2016) temperature-dependent binary interaction parameters are fitted to a second-order polynomial equation (3-38), of which coefficients are reported in (Teymouri, 2016). This equation was employed by Teymouri (Teymouri, 2016) for the water + alkane systems and glycol + non-associating systems.

$$k_{ij}(T) = A_2 * T^2 + A_1 * T + A_0 \quad (3-38)$$

For water + methane, Teymouri (Teymouri, 2016) reported an AAD % of 3.5 in composition of solute, and an AAD % of 5.07 in composition for approximately 200 data points on each of the systems over the temperature range of 273.15 to 523.15 K. This range covers the experimental range of this work; hence their parameters could be used when modelling similar systems in the present work.

For glycol-non-associating compounds, the binary interaction parameters showed a linear trend with temperature (Teymouri, 2016). Furthermore, Teymouri (Teymouri, 2016) reported AAD % of 2.16 for the TEG + carbon dioxide system, 1.63 for the TEG + methane system, and 7.71 for the TEG + propane system after utilising the binary interaction parameters obtained from equation (3-38).

For carbon dioxide + methanol, the literature temperature-dependent binary interaction parameters were evaluated using equation (3-39) from Gil et al. (Gil et al., 2012) and are presented in Table 3-4.

$$k_{ij}(T) = -0.0323 + 2.88 * 10^{-4} T \quad (3-39)$$

3.2.4.3. Cubic Plus Association (CPA) EOS

The CPA (cubic plus association) EOS was proposed by Kontogeorgis et al. (Kontogeorgis et al., 1996) to better represent the phase behaviour of associative compounds. The association term from Wertheim's theory is employed in these CPA EOS. It accounts for the hydrogen bonding between associating components. In this equation, the SRK EOS was combined with the attractive term of Wertheim's theory, which is similar to that presented for the PC-SAFT equations. The usage of CPA EOS for modelling (acid gases + glycol) systems has been studied previously. Tsivintzelis and

Kontogeorgis (Tsivintzelis and Kontogeorgis, 2016) modelled a system of MEG + water + methane + hydrogen sulphide; (MEG + water 60/40 wt.%) + (methane + carbon dioxide 78.6/21.421.4 mol%) using the CPA EOS and various modelling approaches. Folas et al, (Folas et al., 2006) presented isothermal P_{xy} CPA model prediction for the MEG + methane + propane + water and water + MEG + methane + propane + toluene systems. The CPA equation of Kontogeorgis et al. (Kontogeorgis et al., 1996) has been applied with success to several complex phase equilibria, such as mixtures comprising of water, glycols, hydrocarbons, alcohols, glycols and others (Kontogeorgis et al., 2006). The focus of Kontogeorgis et al. (Kontogeorgis et al., 2006) was on systems of industrial importance such as gas dehydration and glycol regeneration units, systems with gas hydrate inhibitors (glycol and methanol), and alcohol separation. Filho et al. (Filho et al., 2021), in a study more closely related to this work, modelled phase equilibria data for multicomponent systems comprising typical natural gas mixtures and TEG. This study focuses on VLE studies of carbon dioxide + hydrocarbon gases + aqueous TEG + methanol similar to those encountered in gas processing hence the use of the CPA model. The CPA EOS of Kontogeorgis et al. (Kontogeorgis et al., 1996) reduces to a pure cubic equation of state if no hydrogen bonding is involved, a practice which the oil and gas industry has widely accepted (Kontogeorgis et al., 2006). The parameters and equations for the CPA model are presented in Appendix D.4.2.

Limitations of the CPA

The limitations on the use of the model are related to the critical region. The model overshoots the critical region in all cases (Kontogeorgis et al., 2006). Also, the CPA requires distinct combining rules to describe various types of phase equilibria (SLE, VLE, and LLE) (Kontogeorgis et al., 2006). Table 3-5 presents reported CPA binary interaction parameters for components of this study.

Table 3-5 shows that no reported binary interaction parameters were obtained from the literature for the methanol + TEG and methane + propane binary pairs, using the CPA model. This highlights the need to obtain suitable parameters applicable to the CPA equation for modelling these binary pairs.

Table 3-5: CPA literature k_{ij} parameters for components of this study.

Component <i>i</i>	Component <i>j</i>	<i>T</i> : K	k_{ij}
methanol	water	298.15	-0.094 ^{h, k} -0.045 ^a
methanol	water	313.15 333.15	-0.008 ^a -0.055 ^k
TEG	water	297.60	0.211 ^k
TEG	water	332.60	-0.201 ^k -0.1911 -18.40/ <i>T</i> ^b
TEG	methanol	n	n
TEG	methane		0.000 ^f 0.1371+ 8.31/ <i>T</i> ^b
TEG	propane		0.153 – 8.31/ <i>T</i> ^b
TEG	carbon dioxide	273-398 273.15-373.15	0.0027 ^e 0.035 ^d 0.324 – 59.35/ <i>T</i> ^b 0.0183 ^c
methanol	methane		0.0134 ^a
methanol (2B association scheme)	propane	293.05 313.1 352.2	0.026 ^l 0.059 ^l 0.067 ^l
methanol	carbon dioxide	230- 313.15	0.0384 ^g
water	methane	298.15 313.15 323.15	-0.045 ^a -0.008 ^m 0.0088 ^m 0.7988 -236.5/ <i>T</i> ^b 0.00979 ^j
water	propane	278-366	0.1135 ^a 0.4809-130.5/ <i>T</i> ^b
water	carbon dioxide	323-444	0.0046+0.000331 <i>T</i> ^b 0.1 ^g 0.0098 ⁱ
methane	propane	n	n
methane	carbon dioxide		0.0882 ^e
propane	carbon dioxide		0.1552 ^e
carbon dioxide	n-hexane		0.1200 ^e
90 wt% TEG	carbon dioxide	263.15-343.15	0.0893 ^c

Literature: a:(Folas et al., 2006); b : (Arya et al., 2014); c: (Wise and Chapoy, 2016); d: (Afzal et al., 2012); e:(Tsivintzelis and Kontogeorgis, 2016); f: (Breil and Kontogeorgis, 2009); g : (Kontogeorgis and Folas, 2010); h : (Folas et al., 2005); i : (Tsivintzelis et al., 2014); j : (Tsivintzelis and Kontogeorgis, 2015). k:(Derawi, 2002); l:(Folas, 2006); m:(Derawi et al., 2003); n: parameters not available.

CHAPTER 4: REVIEW OF EXPERIMENTAL METHODS AND APPARATUS USED FOR VAPOUR-LIQUID EQUILIBRIA MEASUREMENTS

4.0 INTRODUCTION

The purpose of this review is to discuss the equipment published in literature for the measurement of high-pressure vapour-liquid equilibria (HPVLE) data. More emphasis is given to the combined static analytic equipment and static synthetic equipment which is employed in the present study. Analytical methods which have been used for the study of multicomponent systems similar to those in the present study are also presented. Furthermore, preparation methods for synthetic fluid mixtures are briefly discussed. High-pressure phase equilibria data are essential in comprehending chemical processes that occur at high pressures (Fonseca et al., 2011). Usually, when referring to the expression “high pressure” in VLE studies, 1 MPa is chosen as the lower limit (Dohrn et al., 2010; Dohrn and Brunner, 1995). Although computational methods are valuable for predicting phase equilibria, the experimental measurement of VLE data is still of great importance, especially for complex systems or high-pressure systems (Fonseca, 2010), where models fail to accurately describe the behaviour.

4.1. Classification of HPVLE experimental techniques

Authors have classified equipment for the measurement of HPVLE differently in the literature. A variety of methods are used to measure high-pressure phase equilibria data since there is no universal method that can determine the different behaviour (Dohrn et al., 2010; Laugier and Richon, 1986). One of the bases for choosing an experimental technique is the pressure and temperature conditions. For low pressures less than 0.101MPa, the experimental technique that is employed is the ebulliometric (Chapoy, 2004; Dohrn and Brunner, 1995) or the dynamic method. However, Olson (Olson, 1989) argues that ebulliometry can be used for high-pressure systems up to 2 MPa. According to Chapoy (Chapoy, 2004), high-pressure phase equilibria experimental methods are classified depending on:

- the method used for composition determination: these are either analytical methods where there is a direct sampling of components or synthetic methods, sometimes known as indirect methods (Dohrn et al., 2010; Dohrn and Brunner, 1995).
- the manner in which equilibrium is achieved: this could be either the dynamic method where at least one of the phases circulates or the static method where there is stirring of the phases. The circulation and stirring of the phases ensures that compositions in the phases are uniform, thus helping to attain phase equilibrium.

4.1.1. The static and dynamic method of classification

Figure 4-1. shows the experimental methods using descriptors by several principal researchers of the Thermodynamics Research Unit (TRU) at the University of KwaZulu-Natal and other researchers (Bengesai, 2016; Reddy, 2006). Under dynamic methods, a single vapour or both liquid and vapour phases pass through the equilibrium cell until equilibrium is attained (Dohrn and Brunner, 1995), or phase recirculation where the phases recirculates through the equilibrium cell/chamber until equilibrium is attained. It is possible to combine both the static and the dynamic method into static-dynamic combined methods. In this work, the apparatus used can be classified under the static synthetic-analytic combined method, since it allowed measurements to be performed either through the static synthetic method or the static analytic method.

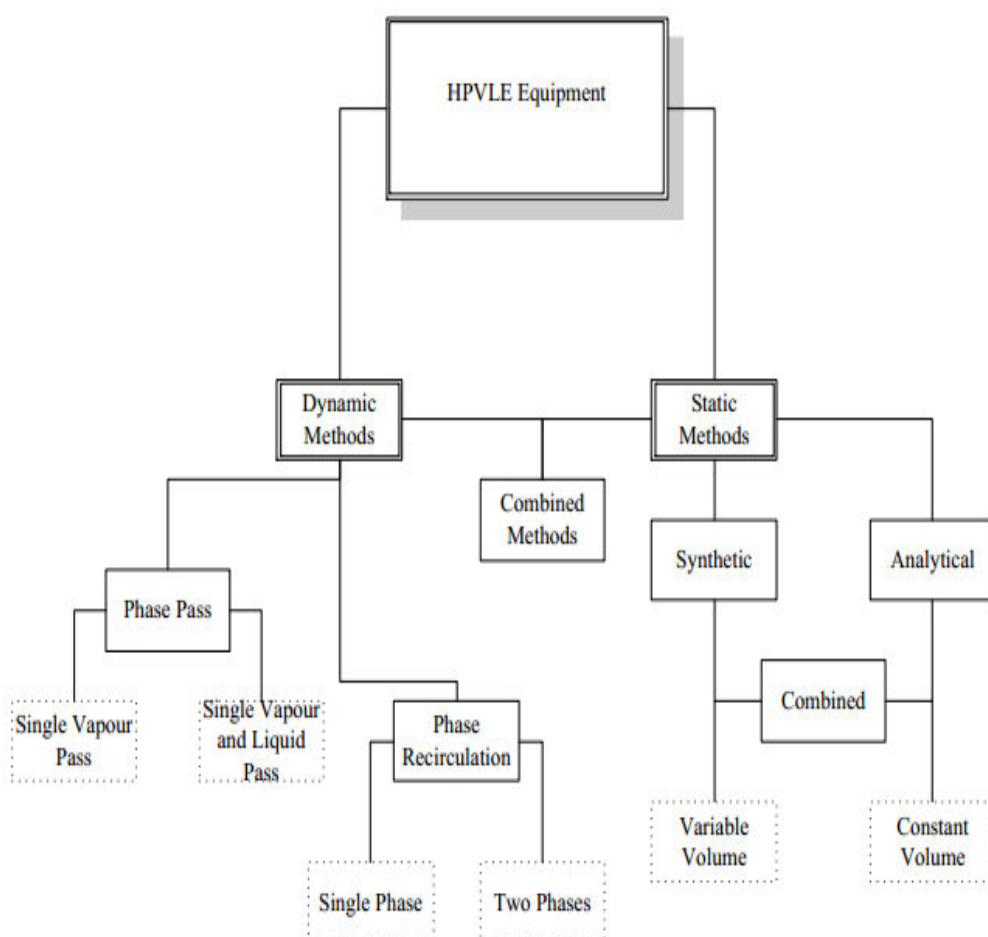


Figure 4-1: Experimental methods for phase equilibrium measurements. Source: (Reddy, 2006).

4.1.1.1 Static methods

Static methods are classified as either synthetic or analytic methods or could be a combination of the synthetic and the analytic method commonly termed the combined methods. Under this, the cells could be either variable or fixed/ constant volume. The basic layout of the static analytic method is shown in Figure 4-2.

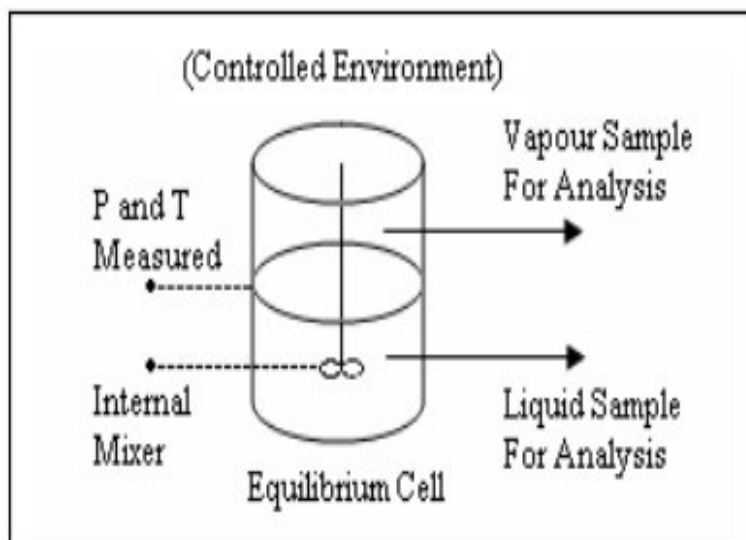


Figure 4-2: Basic layout of the static analytic method: Source: (Raal and Mühlbauer, 1994).

The basic layout of a static analytic method is presented in Figure 4-2. The main features presented are:

- The temperature-controlled environment or bath usually consists of either a water bath, glycol or mixture of water and glycol, air and so on
- The equilibrium cell in which vapour-liquid equilibrium is attained.
- A mixer that speeds up the attainment of equilibrium
- Pressure transducers and temperature sensors for measuring cell conditions.
- A sampling method or mechanism to sample the liquid or vapour phase for analysis purposes.
- A method or means for sample analysis which include chromatographic methods and so on.

4.1.1.2 Description of the static analytic method

The static analytic method involves charging the equilibrium cell with binary or multicomponents under pressure, which are then mixed with the help of a stirrer or a rocking device for quick achievement of

equilibrium (Dohrn and Brunner, 1995; Nelson, 2008). Firstly, the equilibrium cell is degassed by a vacuum pump and then an amount of the degassed liquid component is loaded into the cell. Then the gaseous component is loaded into the cell after the feeding lines have been purged. This mixture is then immersed into a liquid bath where a temperature controller controls temperature. The mixture is thoroughly stirred until the attainment of equilibrium. Equilibrium is established when conditions are met such that the temperature attains the desired value or is satisfactorily stable and remains at this plateau for at least thirty minutes, coinciding with pressure stabilisation, and no macroscopic change in the composition in the fluid (Dohrn et al., 2010). The pressure difference between the equilibrium cell and the chromatographic circuit provides the driving force for the movement of the sample from the cell to the chromatographic circuit. Higher pressure is maintained inside the cell than the chromatographic circuit and hence the sample flows through the stem of the sampling valve. At equilibrium, multiple liquid and vapour samples are sampled from the mixture in the equilibrium cell for analysis using a gas chromatograph. The areas A_1 , A_2 recorded by the GC detectors are proportional to the amount of the respective components in the mixture. They thus are subjected to the calibration correlation to determine either the vapour y_1 or the liquid composition x_1 being measured. This procedure produces a single VLE data point. To produce a complete phase envelope (P - x - y) curve, repetitive loading of different masses and sampling is necessary (Nelson, 2008). With this system, it is possible to study multicomponent systems; hence this allows for the study of real-life systems typical of industrial problems (Fonseca, 2010).

The drawback of this method is the complexity of the setup. The analytical component requires prior optimisation of the analytical techniques and often requires time-consuming calibrations (Fonseca, 2010). Analytical techniques, tools, and diagnostic processes are of no value if the samples fail to accurately represent the composition of mixtures under analysis (Peper & Dohrn, 2012). Withdrawing a sample from a high-pressure equilibrium cell, handling in transfer lines, analysis and the back coupling of the sampling due to pressure drop on the remaining system are major sources of error (Peper et al., 2019; Peper and Dohrn, 2012). Careful attention must be taken with respect to the choice of the sampling position, method of sampling, for instance, isobaric sampling or sampling by pressure drop, sample analysis, and the back coupling of the sampling on the remaining system (Peper and Dohrn, 2012). Regarding the analytical method, sampling is the stage where largest errors may occur (Peper and Dohrn, 2012). Careful attention should be applied to avoid sample adsorption in transfer lines, columns and seals, especially when sampling in the trace region of components such as water, methanol and others (Peper and Dohrn, 2012). Direct sampling from equilibrium cells is only achieved by pressure drop, utilising special valves such as the ROLSI™, a combination of metering and lock valves and other mechanisms (Peper and Dohrn, 2012). A limitation of the direct sampling method using the ROLSI™ is that only the GC analytical method is feasible, unlike other sampling methods where several analytical methods maybe employed concurrently. The ROLSI™ operates from cryogenic temperatures

up to 523.15 K (MINES ParisTech, 2000) and this poses a potential limitation for analysis of higher boiling components. One of the components of this study, TEG, boils at 561.15 K; hence difficulties in its vapourisation might occur during sampling.

4.1.1.3 Description of the static synthetic method

This method is mostly employed where the use of static analytic method presents challenges, like in scenarios where coexisting phases are of similar densities, hence phase separation is difficult (Dohrn and Brunner, 1995; Fonseca, 2010). Multiphase equilibria can be investigated using visual synthetic method, and this has been the most commonly used of all methods for phase equilibria measurements (Dohrn et al., 2010). The difficulty in analysing phase behaviour of fluids is replaced by the difficulty in synthesising them (Dohrn and Brunner, 1995). In this method, the composition of the components in a mixture is usually predetermined by weighing, and the phase behaviour is established by measuring temperature and pressure at an equilibrium state. Usually, in this method, variable volume view cells equipped with a piston that divides the cell into two sections, namely the system side and the hydraulic side are used. A hydraulic fluid is either fed or drained/vented from the hydraulic side and this pushes the piston in the cell, thereby altering the volume and thus pressure of the cell. Figure 4-3 presents a generic drawing of the basic layout for a static synthetic apparatus. This method is based on phase transition, where the evolution of the new phase is noticed by pressure change and confirmed visually (Fonseca, 2010). Initially, conditions are made such that a single phase exists, and thereafter variation of the pressure and volume causes the appearance of another phase (Dohrn and Brunner, 1995). This method has been used for dew point, bubble point and critical point measurement by several authors. Lee et al. (Lee et al., 2000) measured the critical points and bubble point pressures of chlorodifluoromethane mixtures + carbon dioxide using the same method. Tsuji et al. (Tsuji et al., 2004) measured the bubble point of the carbon dioxide + n-decane system using the static synthetic method. In 2016, Williams-Wynn et al. (Williams-Wynn et al., 2016) verified VLE measurements of the + n-hexane + carbon dioxide system by measuring bubble point pressures of the same system using a static synthetic system and comparing them to data from the static analytic method.

The cell is enclosed by a bath of either water or air to keep the system temperature constant. Firstly, the equilibrium cell is evacuated using a vacuum pump. Several composition determinations by weighing are outlined by different authors depending on their equipment set up. According to Williams Wynn et al. (2016), the mass of the empty cell was measured by a mass balance. Then degassed liquid component is charged into the cell system side since they are of low vapour pressures as compared to the gaseous components and the loaded cell is reweighed. Then the volatile component is loaded into the cell either as a gas or sometimes as liquid after the cell has been initially cooled and then reweighed again.

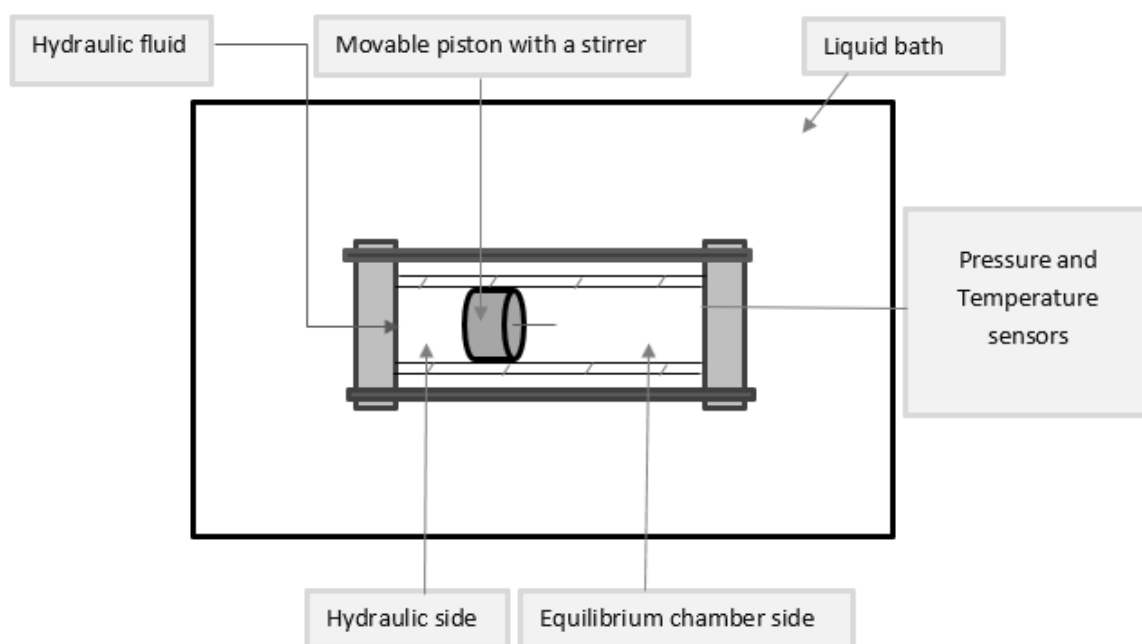


Figure 4-3: Generic drawing of a static synthetic apparatus layout.

Hydraulic fluid, which could be either water, nitrogen gas, carbon dioxide and so on, is fed to the hydraulic side of the cell, causing the piston to move towards the equilibrium chamber side, thus reducing the volume of the equilibrium chamber side and consequently increasing the pressure of equilibrium chamber system side. As the piston continues to reduce the volume of the equilibrium chamber side, thorough mixing is induced by the aid of a stirrer. The system pressure and temperature are monitored and recorded in a computer via a data logger (Tsuji et al., 2004). Eventually, a stage is reached where the last bubble vanishes, and the solution becomes a single homogeneous phase. The pressure at which this bubble disappears is termed the bubble point pressure. For Tsuji et al. (Tsuji et al., 2004), the bubble point was ascertained by the inflexion point as shown in Figure 4-4. Alternatively, some authors prefer that the single homogeneous mixture turns into two phases. This is achieved by ensuring that the initially formed single homogeneous phase has attained thermal stability and then gradually reducing the pressure until the emergence of the first small bubble. The pressure when this bubble appears is termed the bubble point pressure (Williams-Wynn et al., 2016). The cell and bath are usually designed so that their contents are visible through a window. Lee et al. (Lee et al., 2000) repeated each measurement at least twice, whilst Williams-Wynn et al. (Williams-Wynn et al., 2016) repeated each measurement at least three times to confirm consistent measurements, thereafter a new composition was charged into the cell and the process was repeated to complete the P-x curve.

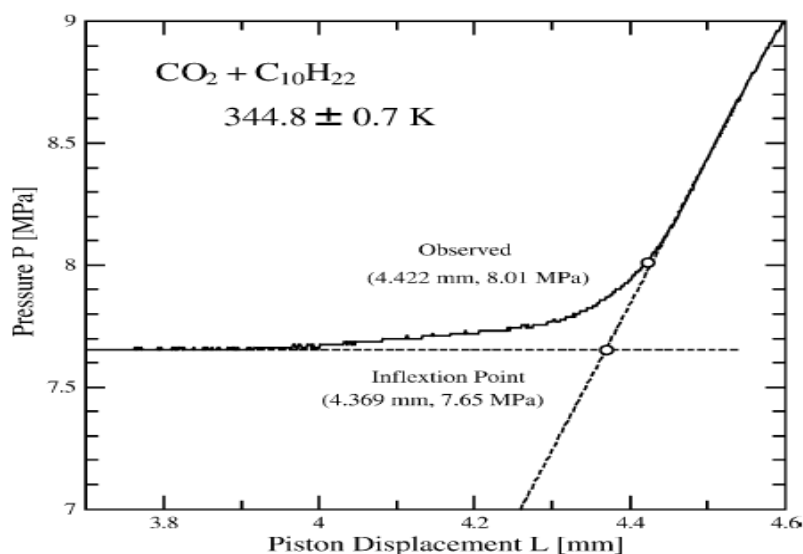


Figure 4-4: Pressurising process of the synthetic type apparatus. $\text{CO}_2 + \text{C}_{10}\text{H}_{22}$, $x_1 = 0.5221$: (Tsuji et al., 2004).

4.1.1.4. List of apparatus that employ a combination of the static analytic, static synthetic method, with either temperature or pressure control

Only a few apparatuses have been described in the open literature that are capable of high pressure isobaric, isothermal measurements (Nelson et al., 2021). Other than the equipment of Nelson et al. (Nelson et al., 2021) that has been used in this work and is described in detail in chapter 5, Table 4-1 lists equipment that has been explicitly reported in literature to be of the combined static analytic, static synthetic equipment with either temperature or pressure control.

4.1.1.5 List of other static apparatus with variable volume view cells

Some selected literature for other static equipment with variable volume view cells that have been used by other researchers are presented in Table 4-2. Most of the apparatus have been described as fit for the static analytic method, though some may have the possibility of being used in the static synthetic mode. A few of the equipment are for the static synthetic method only.

Table 4-1: List of combined static analytic, static synthetic equipment with either temperature or pressure control.

Author	Equipment description: (Material of Construction, Volume, Windows or not, Systems measured.	Sampling/ sample volume for both liquid and vapour	GC-FID/TCD – column used, /IR/Spectroscopy	Pressure rating (MPa)- Device used.	Temperature range, device used.	Type of Bath, Temperature regulation, and stability.	Stirring mechanism /device/ Comments on systems relevant to this study.
Chen et al. (Chen et al., 1993)	A horizontal variable volume view cell. Has a moving piston for pressure control. The Cell was made up of SS 304, with a total variable volume of 17 cm ³ , excluding the piston. L = 9.55 cm, ID = 1.91 cm. A sapphire window enclosed the cell at one end. Viton O rings provided sealing within the cell. Piston O rings were made of Teflon impregnated with Viton.	Six-way valves withdrew samples into sampling lines (3 of them, top, bottom and middle position)	Analytic method: Mass Spectrometer (MS), (UTI Co. Model 100C). The atomic mass unit range of the spectrometer was (1-300 amu). The mass spectrum is stored and analysed in a PC. In cases where the MS was not applicable, a GC was used. Synthetic mode: A video screen via a boroscope allowed for visual observation of phase transitions.	Pressure readings were checked against a dial gauge (Heise Model CM)	Pt-100 Ω temperature sensors with a precision of 0.1 K were used for monitoring temperature inside the equilibrium cell	A nitrogen purged oven, fitted with a fan for uniform temperature distribution. Oven temperature is regulated to within ± 0.1 K.	A stirring bar under the cell that is activated by a rotating magnet and driven by an air pump was used to fasten attainment of equilibrium.

Table 4-1: List of combined static analytic, static synthetic equipment with either temperature or pressure control cont.

Author	Equipment description: (Material of Construction, Volume, Windows or not, Systems measured.	Sampling/ sample volume for both liquid and vapour	GC-FID/TCD – column used, /IR/Spectroscopy	Pressure rating (MPa)- Device used.	Temperature range, device used.	Type of Bath, Temperature regulation, and stability.	Stirring mechanism /device/ Comments on systems relevant to this study.
Zilnik et al. (Žilnik et al., 2016)	<p>The cell is made up of alloy cast steel Hastelloy C₄, of a cylindrical form, ID 50 mm. Sealing of the cell is achieved by the use of perfluoroelastomere ‘O’ rings.</p> <p>The equipment can be utilised with either a fixed volume (150 cm³), where both ends are enclosed with a sapphire window or with a variable volume (186 - 222 cm³) where one end is enclosed with a sapphire window and the other with a membrane bellows.</p> <p>VLE data of toluene + carbon dioxide and carbon dioxide + n-decane</p> <p>A digital camera was used to observe the cell contents.</p>	<p>Valves are used for sampling the vapour and liquid phases.</p> <p>Alternatively, automatically controlled valves fixed to the cell and , coupled to the GC could be used for composition analysis.</p>	<p>Synthetic methods: were utilised to measure bubble point pressure and determine critical point pressure.</p> <p>Analytical method: sampling was conducted at isobaric conditions. The liquid component was condensed out of the sample, and weighed using an analytical balance to determine its quantity. The measurement uncertainty of the analytical balance was 0.05 mg at k = 2. The gaseous component in the liquid sample was gathered in a gas mouse, while a 20 dm³ expansion vessel gathered gas from the gas sample. Uncertainty in volume was 0.01%. The quantity of the gaseous component in the sample was computed using the PR and SRK EoS, based on pressure increase in the gas mouse or expansion vessel at known volume and temperature.</p>	<p>A pressure transducer of the type Omegadyne PX1004, was utilised for pressure measurements within the range of 0.1 and 17.2 MPa.</p> <p>The expanded uncertainty of the measurement was 0.003 MPa for a 95% level of confidence.</p>	<p>Pt-100 Ω sensors, enables the measurements of equilibrium cell temperature within an expanded uncertainty range of ± 0.1 K for a 95% level of confidence.</p>	<p>A thermostat Julabo Presto LH46, pumps the hot or cold oil HL 40 through the double jacket of the cell.</p>	<p>A magnetic stir bar in the cell helped to attain equilibrium quickly.</p>

Table 4-2: List of static equipment with variable volume view cells.

Author	Equipment description: (Material of Construction, Volume, Windows or not, Systems measured.	Sampling/ sample volume for both liquid and vapour	GC-FID/TCD – column used, /IR/Spectroscopy	Pressure rating (MPa)- Device used.	Temperature range, device used.	Type of Bath, Temperature regulation, and stability.	Stirring mechanism /device/ Comments on systems relevant to this study.
Li et al. (Li et al., 1981)	<p>A variable volume view cell, made of A286 SS, with a maximum cell volume of 600 cm³. The cell dimensions are roughly: ID ~ 5.08 cm, OD ~ 11.43 cm enclosed with a metal plug at one end. The other end was enclosed by quartz view window, ~ 6.98 cm diameter and a thickness of ~ 2.54 cm.</p> <p>Mixtures under study were confined by a floating piston that had “Karlrez” O ring on its ends. Silicon oil on the backside of the piston was used as the hydraulic fluid, thereby regulating the system pressure.</p> <p>Equipment was used to measure VLE of n-hexaane + carbon dioxide.</p>	Liquid and vapour phases were sampled using sampling valves.	A varian model 3700 GC-TCD was used for sample analysis. A porapak N on Chromosorb G column packed column was used.	A pressure transducer attached to the cell body was used for pressure measurements inside the cell. Accuracy of pressure readings were estimated to be within ± 0.01 MPa.	Pt resistance thermometers attached to the cell body were used for temperature measurements. Accuracy of temperature measurements was within ± 0.05 K.	An air bath was used.	A rocking mechanism on the air bath enhanced the attainment of equilibrium.

Table 4-2: List of static equipment with variable volume view cells cont.

Author	Equipment description: (Material of Construction, Volume, Windows or not, Systems measured.	Sampling/ sample volume for both liquid and vapour	GC-FID/TCD – column used, /IR/Spectroscopy	Pressure rating (MPa)- Device used.	Temperature range, device used.	Type of Bath, Temperature regulation, and stability.	Stirring mechanism /device/ Comments on systems relevant to this study.
<p>Scurto et al. (Scurto et al., 2001),</p> <p>Lopez-Castillo et al. (Lopez-Castillo et al., 2006)</p>	<p>A variable volume view cell which is made of a tubular reactor (HIP TOC7-20) with a quartz window at one end was used.</p> <p>A N₂(g) powered piston separated the system side and the pressurisation side and was able to move freely in the cell. Viton O rings provided sealing between the piston and the cell, and the two ends enclosing the cell.</p> <p>VLE data for carbon dioxide + Methanol binary system. Dew points of carbon dioxide + trichloromethane</p>	<p>Valco sampling valves were utilised for sampling the vapour and liquid phases.</p> <p>A 9.6 µl loop was used for sampling the vapour phase whilst a 6.03 µl sample loop was for the liquid phase.</p>	<p>A Varian 3800 gas chromatograph was used to determine the fluid composition.</p> <p>This equipment had a TCD detector and the GC column used was a HayeSep Q 80/100 packed column.</p>	<p>A Serta 1505 pressure transducer was used for pressure measurements . On the pressure side, the transducer was equipped with Cole-Parmer 94785-00 digital meter +/- 0.08 MPa, whilst on the system side a Heise Model 901 A digital pressure indicator +/-0.02 MPa was connected.</p>	<p>Temperature inside the cell was measured by type K thermocouple</p>	<p>An air bath was used to control the temperature of the apparatus. A Pt resistor was used as a sensor for the air bath, and a 300W light bulb as the heating source. The temperature of the bath was regulated by (Omega CS 6071-APc)</p>	<p>Attainment of equilibrium was enabled by the use of a magnetic stirrer which was mounted on the system side of the cell.</p>

Table 4-2: List of static equipment with variable volume view cells cont.							
Author	Equipment description: (Material of Construction, Volume, Windows or not, Systems measured.	Sampling/ sample volume for both liquid and vapour	GC-FID/TCD – column used, /IR/Spectroscopy	Pressure rating (MPa)- Device used.	Temperature range, device used.	Type of Bath, Temperature regulation, and stability.	Stirring mechanism /device/ Comments on systems relevant to this study.
Secuianu et al. (Secuianu et al., 2003)	A high pressure visual static analytic apparatus, with variable volume (25-60 cm ³) was used. The cell had two sapphire windows, one of which acted as a piston. VLE data for carbon dioxide + 2-propanol binary mixture.	Vapour and liquid samples were collected by manually operated valves which allowed for the depressurization and expansion of the samples into glass traps.	The quantity of carbon dioxide in both the liquid and vapour phase were determined by expansion into a glass bottle of calibrated volume. Liquid samples of both phases were weighed with a balance with an accuracy of 0.0001 g.	This apparatus was designed to operate below 30 MPa. A pressure gauge (Type S 10, WIKA, Germany; accuracy 0.5% was used for pressure measurements	Design operational temperature range of 273 to 353 K. A Ni- Cr-Ni thermocouple accuracy (0.1 K) was used for temperature measurements within the cell.	The cell is heated electrically, and its temperature is controlled by a circulating thermostat connected to the heating jacket.	Achievement of equilibrium was enabled by the use of a stirrer which was mounted onto the cell.
Naidoo et al. (Naidoo et al., 2008)	A variable volume cell static analytic apparatus, fitted with sapphire windows for viewing was used. The cell is made up of type 316 stainless steel. The internal volume of the cell is roughly 200 cm ³ VLE data for a binary system of methanol + carbon dioxide.	Six port GC valves were utilised for sampling of the phases. Sample volume was approximately 0.17 cm ³ .	A Chrompack CP 9000 GC system was used for analysis purposes. The column used was a stainless-steel column with either Q packing or Porapak N packing. A thermal conductivity detector (TCD) was used for detection of the components.	A Sensotec TJE pressure transducer (certified to accurate to within 0.25%) of rating 12MPa was used for measuring equilibrium pressure inside the cell.	Pt-100 Ω temperature sensors (0.05%) accuracy were used for monitoring temperature inside the equilibrium cell for the range 250 K - 393 K.	An air bath was used. Pt-100 Ω resistors were the temperature sensors for the bath.	Attainment of equilibrium was facilitated by the use of stirrer. The systems studied with the apparatus i.e. carbon dioxide + methanol is very relevant to the present study.

Table 4-2: List of static equipment with variable volume view cells cont.							
Author	Equipment description: (Material of Construction, Volume, Windows or not, Systems measured.	Sampling/ sample volume for both liquid and vapour	GC-FID/TCD – column used, /IR/Spectroscopy	Pressure rating (MPa)- Device used.	Temperature range, device used.	Type of Bath, Temperature regulation, and stability.	Stirring mechanism /device/ Comments on systems relevant to this study.
Sergiu et al. (Sima et al., 2011), Feroiu et al. (Feroiu et al., 2013), Sergiu et al (Sima et al., 2018)	The authors used the same equipment as described by Secuianau et al. (2003), although there were some differences in the sampling system and analysis system. The authors measured VLE data for carbon dioxide + ethanol system. In 2017, Sergiu et al. (2018) measured VLE for carbon dioxide + 1,2-dimethoxyethane using the same experimental equipment similar to those used by Sergiu et al. (2011).	Two rapid on-line sampler injectors (ROLSI™) were used for sampling the vapour and the liquid samples respectively. At least six samples of each phase were analysed to check for repeatability.	A GC (Perichrom) system equipped with a TCD was used for analysis of the samples. An HP Plot Q column of 30 m long and 0.530 mm diameter was used for separation of the components. Helium gas of flow rate of 30 cm ³ /min was used as the GC carrier gas.	Same as that of Secuianau et al. (2003).	Same as that of Secuianau et al. (2003).	Same as that of Secuianau et al. (2003).	Same as that of Secuianau et al. (2003).

Table 4-2: List of static equipment with variable volume view cells cont.							
Author	Equipment description: (Material of Construction, Volume, Windows or not, Systems measured.	Sampling/ sample volume for both liquid and vapour	GC-FID/TCD – column used, /IR/Spectroscopy	Pressure rating (MPa)- Device used.	Temperature range, device used.	Type of Bath, Temperature regulation, and stability.	Stirring mechanism /device/ Comments on systems relevant to this study.
Fonseca and Solms (Fonseca and von Solms, 2012)	<p>The equipment has a variable-volume cell of stainless steel, and has a 360° sapphire window.</p> <p>The cell volume can be altered between 116 cm³ and 207 cm³.</p> <p>The apparatus was designed for the measurement of multi-phase equilibria data in systems containing water, hydrate inhibitors and hydrocarbons. Measurement of binary VLE data for methane + water was used to validate the quality of the apparatus.</p>	Three ROLSI™ samplers were used for sampling of the phases.	An Agilent 6890 GC System equipped with an automatic injector (for calibrations) was used in this work. HP-PLOT Q capillary column was used for the separation of all the compounds. For detection purposes, a TCD coupled in series with an FID were used.	A pressure transmitter Keller 33X, Switzerland, was used for monitoring pressure inside the cell. Its rated to operate for up to 50 MPa with an accuracy of 0.1% of the full scale.	Pt-100 Ω temperature sensors with a precision of 0.01 K were used for monitoring temperature inside the equilibrium cell for the range 213 K - 353 K. These were in turn connected to an Agilent data accusation unit.	A custom-made temperature chamber was used in this case for maintaining the temperature of the cell.	A Neodymium–iron–boron magnetic stirrer was used for enhancing homogeneity within the mixture. This is applicable to the current study.

Table 4-2: List of static equipment with variable volume view cells cont.							
Author	Equipment description: (Material of Construction, Volume, Windows or not, Systems measured.	Sampling/ sample volume for both liquid and vapour	GC-FID/TCD – column used, /IR/Spectroscopy	Pressure rating (MPa)- Device used.	Temperature range, device used.	Type of Bath, Temperature regulation, and stability.	Stirring mechanism /device/ Comments on systems relevant to this study.
Frost et al. (Frost et al., 2014)	A variable-volume equilibrium cell, fitted with a 360° sapphire window. A high-pressure syringe pump was utilised to vary the volume of the cell. The equipment was developed for measurement of phase equilibria data of polar chemicals and hydrocarbons. VLE data for binary systems of methane + water, methane + methanol and, the ternary system of water + methane + methanol was measured on this apparatus.	Two ROLSI™ samplers were used for sampling of the phases. The ROLSI™ samplers and the GC carrier gas line were heated to 523 K, for instant vaporisation of the samples. At equilibrium, between 5 and 10 samples were withdrawn.	An Agilent 6890 GC System, equipped with an automatic injector was used for analysis. An HP-PLOT Q capillary column, and a TCD coupled in series with an FID were employed. Calibration of the GC detectors was performed using chromatographic syringes with mole numbers uncertainties of 2 % in the FID and 3 % in the TCD.	A pressure transmitter Keller 33XSwitzerland, for measurements up to 50 MPa with an accuracy of 0.1 % of the full scale 0.05 MPa was used for pressure measurement inside of the cell.	Two platinum resistance thermometers Pt100 (class 1/10 DIN), placed on opposite ends of the sapphire were used for cell temperature measurement. The precision of these sensors was reported to be 0.01 K. Data was measured for a temperature range of 283.15 to 323.15 K.	A custom-made temperature chamber was used in this case for maintaining the temperature of the cell.	Establishment of equilibrium was enhanced by the use of a stirrer. This is applicable to the current study.

Table 4-2: List of static equipment with variable volume view cells cont.							
Author	Equipment description: (Material of Construction, Volume, Windows or not, Systems measured.	Sampling/ sample volume for both liquid and vapour	GC-FID/TCD – column used, /IR/Spectroscopy	Pressure rating (MPa)- Device used.	Temperature range, device used.	Type of Bath, Temperature regulation, and stability.	Stirring mechanism /device/ Comments on systems relevant to this study.
Legoix et al. (Legoix et al., 2017)	<p>A static analytic equipment of variable volume view cell. The cell is made up of 316 Ti and with a piston made from stainless steel and is enclosed with a sapphire window on both ends.</p> <p>The cell volume can be varied between 20.8 (± 0.6) and 65.4 (± 0.3) cm³</p> <p>VLE data for methane + carbon dioxide system and, water + methane + carbon dioxide + mixtures were measured.</p>	A ROLSI TM sampler was used for sampling of the phases.	GC-MS equipped with TCD-FID was employed for analysis of samples. The GC-MS data were processed with the MSDChem software and the Chemstation integrator.	Operates up to 60 MPa	Has been operated between 253 and 473 K	In this case, temperature regulation was achieved with the aid of a cooling circulator (ministat 230, Huber) filled with a mixture of 50% Water/ 50% Ethanol Vol%.	A stirrer attached at the bottom port of the cell to helped to attain equilibrium quickly.

Table 4-2: List of static equipment with variable volume view cells cont.							
Author	Equipment description: (Material of Construction, Volume, Windows or not, Systems measured.	Sampling/ sample volume for both liquid and vapour	GC-FID/TCD – column used, /IR/Spectroscopy	Pressure rating (MPa)- Device used.	Temperature range, device used.	Type of Bath, Temperature regulation, and stability.	Stirring mechanism /device/ Comments on systems relevant to this study.
Ngema et al. (Ngema et al., 2014), equipment was used by Williams-Wynn et al. (Williams-Wynn et al., 2016) in a modified version.	<p>A static synthetic variable volume view cell utilised for bubble point measurement. The cell is comprised of a crystal sapphire tube, which is enclosed on both ends by 316 stainless steel flanges. Sealing between the sapphire tube and the flanges was accomplished by nitrile 'O' rings.</p> <p>A 316 stainless steel piston which is driven by a hand pump alters the volume of the cell.</p> <p>Sealing between the cell and the piston was accomplished by two nitrile 'O' rings that were set in grooves on the piston head. The maximum cell volume was roughly 10 cm³.</p> <p>Bubble point measurement of carbon dioxide + n-hexane system</p>	N/A	N/A	<p>A 0 to 12 MPa P-10 pressure transducer is used for pressure measurements of the cell. A CPC Mensor 8000 automated high-pressure calibrator equipped with a barometric reference provided the atmospheric pressure. The maximum uncertainty this barometric reference is 0.005 kPa (0.01% of full range).</p>	<p>Two Pt-100 Ω sensors were used to measure the equilibrium cell temperature. Each of the flanges (top and bottom) had a well onto which the temperature sensors were inserted. T range 273.15 to 323.15 K, the maximum error for the probes was determined at 0.06 K</p>	<p>A stainless-steel water bath is used to maintain cell temperature. Water bath temperature was regulated by a Grant TX 150 thermostat and circulator. The water bath has two viewing windows to allow for the viewing of the cell when it is submerged in the water.</p>	<p>An upper cylindrical PTFE mixer together with its bottom mixer paddle helps to attain equilibrium. The mixers are magnetically linked with Neodymium Magnets.</p>

Table 4-2: List of static equipment with variable volume view cells cont.							
Author	Equipment description: (Material of Construction, Volume, Windows or not, Systems measured.	Sampling/ sample volume for both liquid and vapour	GC-FID/TCD – column used, /IR/Spectroscopy	Pressure rating (MPa)- Device used.	Temperature range, device used.	Type of Bath, Temperature regulation, and stability.	Stirring mechanism /device/ Comments on systems relevant to this study.
Hajiw (Hajiw, 2014)	<p>Bubble Point measurement equipment:</p> <p>A static synthetic cell with variable volume was utilised. This was a rocking cell of volume 300 cm³. The cell is made up of titanium and it has a mixing ball inside, in addition to the piston.</p> <p>Measurement was done for a multicomponent mixture containing:</p> <p>CO₂, CO, O₂, Ar, CH₄, H₂, N₂</p>	N/A	N/A	Maximum operating pressure of cell is 70 MPa. Pressure was measured by a Quartzdyne pressure transducer, with an accuracy of ± 8 kPa.	Operating temperature range of the cell is 265.15 K to 353.15 K. The temperature is measured by a platinum resistance thermometer, which is inserted in the cooling jacket, with accuracy of ± 0.1 K.	Cell temperature is maintained by a cooling jacket which is insulated with polystyrene.	Attainment of equilibrium is enhanced by the rocking mechanism.

Table 4-2: List of static equipment with variable volume view cells cont.							
Author	Equipment description: (Material of Construction, Volume, Windows or not, Systems measured.	Sampling/ sample volume for both liquid and vapour	GC-FID/TCD – column used, /IR/Spectroscopy	Pressure rating (MPa)- Device used.	Temperature range, device used.	Type of Bath, Temperature regulation, and stability.	Stirring mechanism /device/ Comments on systems relevant to this study.
Hajiw (Hajiw, 2014)	VLE measurement: A static analytic apparatus was used in this case. VLE measurement was done for a multicomponent mixture containing: H ₂ S, CO ₂ , CH ₄ , C ₂ H ₆ , C ₃ H ₁₀ , Cyclopentane, Benzene, Toluene, m-Xylene.	Vapour and liquid phases were sampled with either one of the two capillary samplers.	Sample composition analysis was done by a GC Perichrom model PR-2100, equipped with both the FID and the TCD. An RT-Q plot column was used to separate all compounds	System pressure was measured by a pressure transducer for the range 0 to 16 MPa, with an estimated accuracy of ± 8 kPa.	Two Pt-100 Ω sensors located on opposite ends of the cell were used to measure the equilibrium cell temperature. Estimated accuracy was ± 0.1 K.	A liquid bath maintained the cell temperature.	The use of a stirrer device enhanced the attainment of equilibrium.

4.2. Preparation methods for synthetic mixtures

4.2.1. Gas mixtures

Preparation of gas mixtures is not an easy task, and it requires skilled personnel and very accurate equipment. Generally, standard gas mixtures similar to gas mixtures used in this work are prepared gravimetrically following the ISO 6142 standard (Brewer et al., 2014; Budiman et al., 2018; ISO, 2015). Brewer et al. (Brewer et al., 2014) gravimetrically prepared and validated a standard gas mixture of methane + carbon dioxide. Brewer et al. (Brewer et al., 2014) used a GC equipped with a methaniser and a flame ionisation detector (FID) to validate their prepared gas mixture. It is vital to have reliable, accurate and traceable gas measurement results, and to achieve this, calibration standard gas mixtures (csgm) are used as references to working standard (ws) gas mixtures (Budiman et al., 2018). Budiman et al. (Budiman et al., 2018) gravimetrically prepared a csgm of CO₂/N₂ 960 µmol/mol following the ISO 6142 in a one dilution step and a GC-TCD was used for verification of the csgm. A carbon dioxide calibration curve was generated by plotting the carbon dioxide peak areas as a function of the mole fraction of the csgms. The obtained R² coefficient after the least-squares fit linear regression was 0.9994 which is > 0.995; hence the gravimetric values of the csgms were consistently demonstrated (Budiman et al., 2018). The composition of carbon dioxide in a ws gas mixture was certified via a bracketing technique (two-point method) which produced more accurate results than other methods such as the one point, three-point and four-point methods (Budiman et al., 2018). The carbon dioxide composition of the prepared ws was determined by fitting results from the GC-TCD to a calibration curve yielded by a series of csgms (Budiman et al., 2018). Budiman et al. (Budiman et al., 2018) used various calibration approaches for their csgm namely the single point, two point, three point and multipoint and made a comparison of these methods. In this work, binary and ternary gas mixtures were purchased from Afrox, and their composition validated via the comparison of peak areas for parent gases to those of specific gas specie in the gas mixture injected at a constant volume. These are discussed in Appendix. B.2.

The detailed preparation of the csgm is discussed in the ISO 6142 standard (ISO, 2015, 2001) hence it is briefly discussed here. Precise gas mixtures like csgm are prepared gravimetrically by “*weighing the smallest mass of a gas component and adding it to a mixture with minimal uncertainty*” (Budiman et al., 2018). The gas mixtures composition is expressed in mole fraction (ISO, 2001) which are obtained on the basis of the purity of parent gases, the molar mass and the mass of gas loaded into a high-pressure cylinder (Budiman et al., 2018). The mass of each gas component is evaluated by subtracting the mass of the cylinder before a gas component was loaded, from that when the gas component was loaded in the cylinder. The quality of the gas mixture prepared depends on the gas filling technique, weighing technique and the quality of cylinders used; and the pros of the gravimetric method are low uncertainties and a wide range of varying gas mixture compositions that can be prepared (Budiman et al., 2018).

4.2.2. Preparation of liquid solutions

Binary solution of liquid components can be prepared gravimetrically (Ebrahimejadhasanabadi, 2019; Gherwi et al., 2006; Najdanovic-Visak et al., 2002). A set up similar to that used by Ebrahimejadhasanabadi (Ebrahimejadhasanabadi, 2019) was used in this study and this is discussed in detail in chapter 5, section 5.2.5.

CHAPTER 5: EXPERIMENTAL WORK

5.0 INTRODUCTION

The experimental work dealt with the measurement of saturation pressure of some pure fluids with a low-pressure equipment (see Appendix B.1.) and of VLE of mixtures with a high-pressure equipment presented in Chapter 5. The HPVLE measurements in this study were conducted using a combined static analytic, static synthetic apparatus. In this work, the static analytic mode was used for TP_{xy} measurements, whilst the static synthetic mode was used for TP_x measurements.

5.1. Equipment set up and equilibrium cell description

The schematic of the equipment is shown in Figure 5-1 and is comprised of a cylindrical sapphire of the following dimensions: internal diameter (ID) 31.90 mm, outer diameter (OD) 54.88 mm and length 70 mm. Stainless-steel (SS) 316L flanges enclosed the cylindrical sapphire at its two ends. The flanges were connected by four metric 8 (M8) (SS) shoulder bolts and eight M8 nuts, where four nuts were on each of the flanges. Figures 5-2, 5-3, and 5-4 presents photographs of the apparatus. The length of the shoulder bolts was 122 mm, with a shoulder size of 64 mm. The widths of the flanges were 99.18 mm, height 75.64 mm. The thickness of the system side flange was 20.46 mm and had five inlet/outlet ports for the pressure transducer (PT), the feeding and evacuation (LP) valves, the capillary sampler, and the other well, which was plugged by Valco fittings. These inlet/outlet ports are wells drilled into the flange. The thickness of the hydraulic flange was 16.38 mm and had one inlet/outlet port for connecting a feeding valve for the pressurising fluid. Sealing between the cylindrical sapphire and the stainless-steel flanges was accomplished using polyurethane O-rings with the following dimensions: ID 40 mm, and cross-section (CS) 3.10 mm, which were inserted into grooves on each of the flanges. Polyurethane O-rings were used because they are resistant to high impact, high-pressure hydraulic fluids, and abrasion. A unique feature of the apparatus is a movable piston inside the cell, which can be used to adjust the volume of the cell, thereby fixing/controlling the pressure in the process. For static analytic measurements of this work, the piston was driven by nitrogen gas (C) which was fed to the hydraulic side of the equilibrium cell via the pressure controller (PC) Mensor CPC 8000. The pressure controller, when set to operate in the control mode, helped maintain equilibrium pressure since on sampling of the phases, some minor pressure drops occur, which are taken care of by the pressure controller through volume variation. In cases where pressure drops were observed for the CO_2 + n-hexane system, the pressure drop was on average 0.004 MPa for the vapour phase and 0.006 MPa for the liquid phase sampling after purging several times and over a time frame of roughly thirty minutes of sampling. For the CO_2 + n-decane system, the observed pressure drop was 0.005 MPa for both the vapour and liquid phase sampling. Also, there are many cases when the pressure was stable such that there was no need

guide ring (see Figure 5-3) encased on a groove at the posterior side of the piston acted as a piston guide so that the piston would be positioned correctly and in a balanced position in the sapphire cell. The piston was coupled to a magnet stirrer which enhances the attainment of equilibrium for the components under investigation. The stirrer was driven by an external rotating rod which was coupled to a DC motor (OS). A pressure transmitter (PT) model P-10 from WIKA was used for pressure measurements inside of the cell. As described by the manufacturer, its operating range is 0 to 10 MPa and has a rated accuracy of 0.05% full scale (FS). This pressure transmitter was sealed with copper O-ring OD 18.46 mm connected to a stainless-steel Swagelok tube fitting, female connector, 6 mm tube OD x $\frac{1}{4}$ inch ISO thread size female BSP. The pressure transmitter was inserted into one of the inlet/outlet ports of the flange on the system side of the equilibrium cell. For high-pressure measurements above 10 MPa, another pressure transducer model P-10 from WIKA, of working range 0 to 35 MPa and accuracy of 0.05% of the measurement span, replaced the 0 to 10 MPa transducer. The 35 MPa transducer was sealed via a copper O-ring OD 21.70 mm, ID 13 mm, 2.40 mm thick into a stainless-steel Swagelok tube fitting, female connector, 6 mm tube OD x $\frac{1}{4}$ inch ISO thread size female BSP. Two Pt-100 Ω temperature sensors (WIKA 1/10 DIN, accuracy ± 0.03 K), were used for monitoring the cell temperature. The temperature sensors covered with SS316 have a 90° bend, with a diameter of 3 mm, insertion length of 100 mm, and a total length of 350 mm. Ideally, the tip of the temperature probes is inserted into wells drilled on each of the two flanges, and the bend allows them to fit into the water bath. The pressure and temperature probes were connected to a data logger (Agilent model 34970A), not shown in Figure 5-1. The Agilent data logger was connected to a computer, thus allowing real-time recording of temperature and pressure measurements. Approximately 20 dm³ of distilled water was used in the bath (LB). The water bath temperature and thus the equilibrium cell was regulated by a TX grant controller, model (Optima TX 150).

A mobile Rapid Online Sampler Injector (ROLSI™) (R) was fitted to the equilibrium cell for sampling both the liquid and vapour phases. The ROLSI™ was connected to the equilibrium cell through a flange on the system side (see Figure 5-4), in which a well was drilled such that the capillary of the sampler would go through into the equilibrium cell. A PTFE gland packing was used for sealing the ROLSI™. A differential screw adjuster enabled the movement of the ROLSI™ capillary through the cell. Basically, the ROLSI™ capillary's position could be adjusted to any vertical position in the cell, that sampling of either the vapour phase or multiple liquid phases can be achieved. The ROLSI™ was linked to the GC via a 1/16" SS 316 line which was insulated. ROLSI™ allows researchers to take repeatable and representative in situ samples from the isolated system without any contamination (MINES Paris Tech, 2014). The process temperatures of the ROLSI™, sampling lines, and the GC line were controlled by Shinko ACS 13 A digital controllers (not shown in Figure 5-1). All lines were heated with nichrome

wires of diameter 0.5 mm, resistance 5.617 Ω/m a product of Rescal (Aperam alloys, France) and the ROLSI™ was heated using a heating cartridge of 6 mm diameter, 60 mm length, 160 W and 230 V. This integrated heating system allows for the instant vaporisation of liquid samples or maintaining high temperatures for vapour samples.

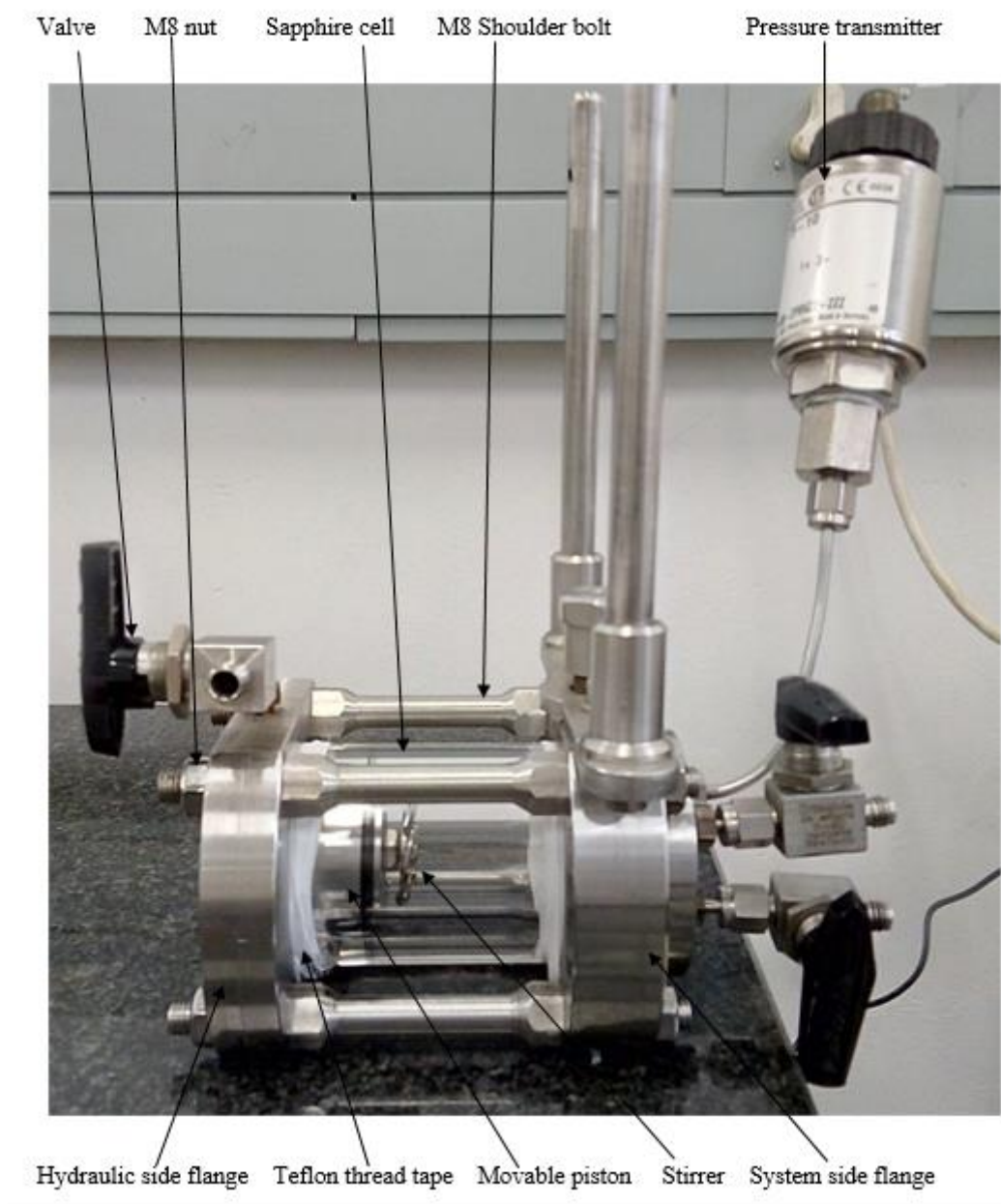


Figure 5-2: Photograph of the combined static analytic, static synthetic apparatus used in this study.

The operating parameters for the ROLSI™ are dependent on the type of polymer used. In this study it was applicable to a temperature range from cryogenics to 523.15 K and a pressure range of 0 to 60 MPa

(MINESParisTech, 2000). The temperature limitation is due to Viton O-rings used in the ROSLI™, which cannot withstand temperatures greater than 523.15 K. The maximum operating temperature poses a potential limitation to the current study since one of the components (TEG) boils at 561.15 K; hence there was a chance that difficulties in its vaporisation would occur. Other specific O rings that can withstand higher temperatures have been sought but to no avail, and time limitation was also a contributing factor. A remedy considered for this limitation was bubble point measurements which do not require the ROSLI™. For bubble point measurements, a plug stuffed with Teflon was used to seal the capillary well on the system side flange, see Figure 5-3.

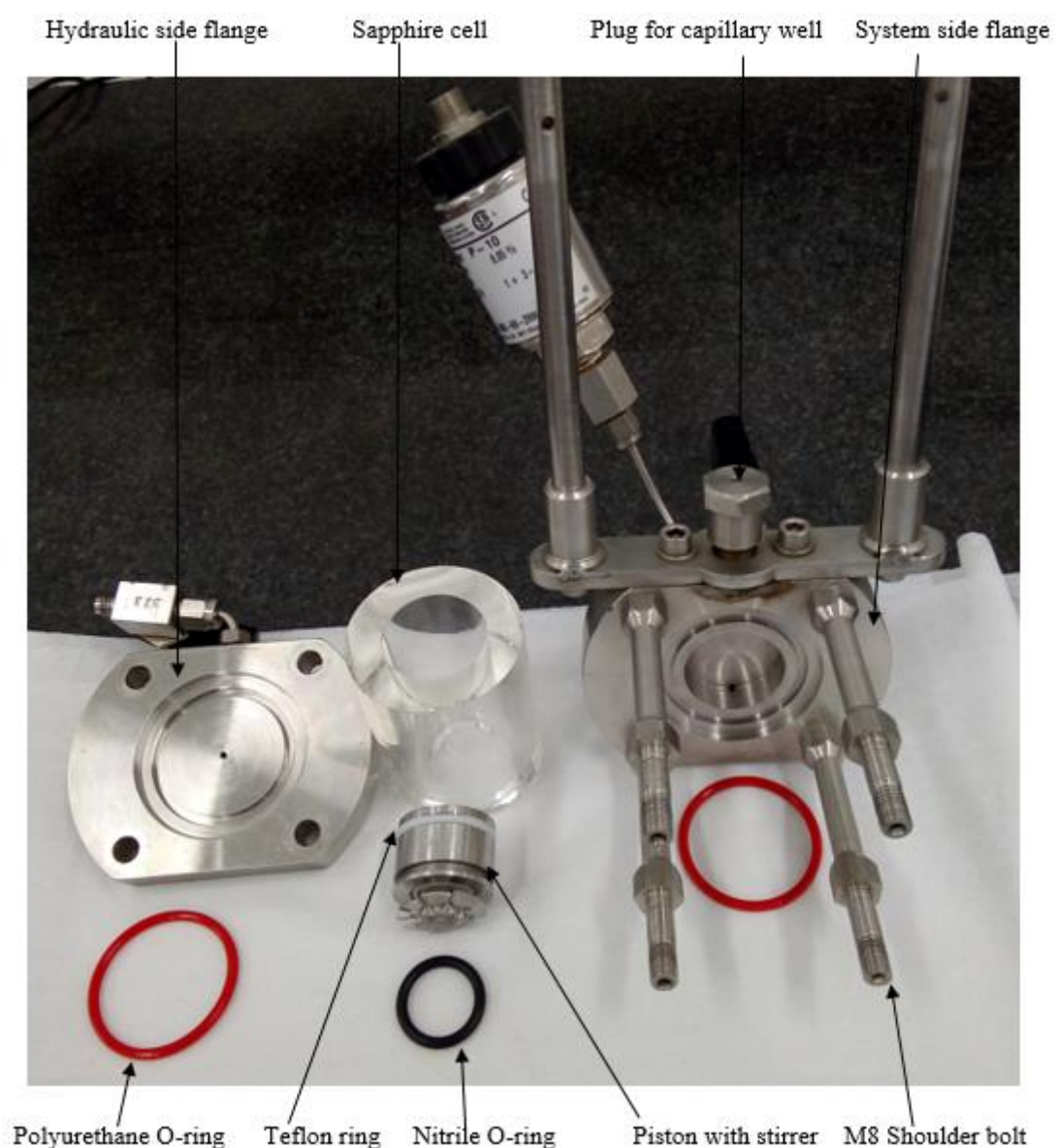


Figure 5-3: Photograph of the dismantled apparatus showing different components.

Furthermore, for the static synthetic measurements of this study, a syringe pump connected to the hydraulic side flange instead of the gas cylinder, pressure controller and buffer tank connections presented in Figure 5-1 was used to drive the piston with water as the hydraulic fluid. Voltage controllers (not shown in Figure 5-1) were utilised to supply the necessary potential difference. A manual jack was used to lift the bath up and down for the purposes of either submerging the cell in the bath or removing the cell out of the bath. Evacuation of the cell and degassing of the liquid components was achieved by using a vacuum pump (not shown in Figure 5-1). To preserve the cell considering the brittleness of sapphire material, Teflon thread tape (12 mm width and 0.1 mm thickness) covered the cell's outer edges as presented in Figure 5-2.



Figure 5-4: Photograph of the cell system side flange with the ROLSI™ attached to it.

5.2. Experimental procedure

Before commencement of measurements, calibration of the pressure transducer, temperature probes and the GC detector were performed. The procedure used has been presented by several authors such as Tochigi et al. (Tochigi et al., 2010), Naidoo et al. (Naidoo et al., 2008), Williams-Wynn et al. (Williams-Wynn et al., 2016), Nelson et al. (Nelson et al., 2021) and others, though the equipment used in the different studies might have slight differences. This experimental procedure generally includes pressure and temperature calibrations, GC calibrations, equilibrium cell preparation, pure component vapour pressure, and phase equilibrium measurements. Details on vapour pressure measurement procedures are presented in Appendix B.1.

5.2.1. Temperature probe calibration

Temperature probe calibration was conducted for the two temperature probes for a temperature range from 273.15K – 333.15K with the help of a temperature standard WIKA, CTH6500 which was inserted into a WIKA CTB 9100 stirred liquid bath of silicone oil M20. The standard was calibrated by WIKA instruments. The internal uncertainty of the standard probe was 0.02 K. The temperature of the thermo-regulated silicon oil was gradually increased in steps of 10 K from 273.15 K to 333.15 K and was then gradually decreased over the same range. The stepwise increment and decrement of temperature allowed to check for hysteresis within the instrument. At each stabilised set temperature, the temperature of the T102 and T104 probes were recorded via a data logger for at least three minutes. The measured values of the temperature standard were read from the unit display and recorded manually. All the recorded values were averaged. The data were fitted to either a first-order (equation 5.1) or a second-order polynomial (equation 5.2), depending on which of the two gave a better fit of the calibration data.

$$Y = mX + C \quad (5-1)$$

$$Y = lX^2 + mX + C \quad (5-2)$$

Where Y is the calculated temperature, l is a coefficient of X^2 , m is the gradient, X is the measured temperature value, C is the y intercept or a constant. The l , m and C values in this case were determined using the LINEST function in MS Excel which uses the least-squares method to calculate the statistics of a straight line or a second-order polynomial and returns an array describing that line. The standard uncertainty of the temperature calibration was the largest deviation between the calculated temperature using the calibration equation and the actual temperature. The calibration equation was used to compute the true experimental temperatures from the temperatures displayed by the temperature probes. Extra

care has to be taken when handling the temperature probes since minor damage such as probe bending may lead to changes in the internal resistance of the probe. Hence recalibration may be required, and thus it is recommended to periodically check the calibrations. The temperature standard should be calibrated at least once a year.

The procedure outlined herein was also used when calibrating the T104 and T105 temperature probes on the low-pressure equipment used only for liquid component vapour pressure measurements in this work.

5.2.2. Pressure transducer calibration

The pressure transmitter was calibrated against a CPC Mensor 8000 high-end pressure controller, a product of WIKA, which acts as either a pressure standard and can also be used for pressure control. The working range for the CPC 8000 pressure standard is 0-25 MPa, which has been calibrated by WIKA instruments and has a stated accuracy of 0.010% full scale.

On the CPC Mensor 8000, the pressurising N₂ cylinder was connected to the supply inlet, and the measure /control inlet was connected to the system side of the equilibrium cell. Nitrogen gas was charged into the equilibrium cell. Subsequently, the reference WIKA transducer was connected to the discharge port of the equilibrium cell. Then the cell was submerged into the bath, and the temperature was maintained at 313.15 K to prevent temperature variation during calibration. This was necessary because pressure transducers respond not only to pressure changes but also to temperature changes. The pressure measured by the reference transducer was zeroed prior to the beginning of the calibration as it exhibited a minor offset at atmospheric conditions. The hysteresis check was also conducted for this instrument by uniformly raising and lowering the pressure in the cell over the operating range for the performed measurements. After every 1 MPa pressure interval within the operating range, the pressure in the cell was set to stabilise, and the data recorded by the Agilent were gathered and averaged. Pressure values from the reference transducer were recorded manually from the transducer display after stabilisation. The gathered data were then fitted to either a first-order or a second-order polynomial, which satisfies the general equations (5-1) and (5-2) respectively, where in this case Y is the calculated pressure, m is the gradient, X is the measured pressure value, C is the y intercept of a constant and l is the coefficient of X^2 . The l , m and C values in this case were determined with the aid of the LINEST function in MS Excel. The standard uncertainty of the pressure calibration was the largest deviation between the pressure estimated by the calibration equation and the true pressure. The calibration equation was utilised to compute the true experimental pressures from the pressures displayed by the

pressure transducer. Likewise, the pressure transducer standard should be periodically recalibrated. For the purposes of preserving the cell and also due to limitations on the maximum pressure the cylinders had, the 35 MPa transducer was calibrated up to 17.6 MPa. In this work, no measurements were conducted beyond 17.6 MPa.

The same procedure outlined herein was also used when performing calibrations for transducers P121 and P122 on the low-pressure equipment used for liquid components vapour pressure measurements. The only difference was that steps of 10 kPa were used during increment or decrement of the pressure over the entire calibration range of 0-100 kPa.

5.2.3. GC detector calibration

This step is necessary for VLE measurements. The calibration procedure used in this work was well described by Nelson et al. (Nelson et al., 2021), and it follows the standard solution method of Raal and Mühlbauer (Raal and Mühlbauer, 1999). The procedure presented below is for a binary mixture consisting of a liquid and gas.

The first step requires the preparation of standard solutions by mass, by the following steps:

- The empty equilibrium cell was initially cleaned by either acetone or ethanol, ensuring that the chosen solvent does not interact and affect the O-rings.
- The cell was evacuated for at least an hour with the help of a vacuum pump to remove residual gases or solvents or any material which could have been dissolved in the O-rings or piston PTFE, since these may lead to errors in the experimental pressure measurements.
- The equilibrium cell was then weighed with an Ohaus mass balance model PX5202 (maximum capacity 5200g) of estimated accuracy ± 0.03 g, with a resolution of 0.01 g, for four replicates at different angles and the average was taken as the mass of the cell. This was done so that the centre of mass is distributed evenly throughout the measurements since the equilibrium cell is not of even shape.
- Then liquid component was charged into the system side of the cell manually using a 10 cm³ healthcare plastic syringe (a product of Neomedic Pty Ltd) compatible with chemicals of this study.
- When enough liquid has been charged, the cell was connected to a vacuum pump, which evacuates all volatiles from the liquid component for approximately three to ten minutes, depending on the volatility of the liquid component. More volatile liquid components were

evacuated for a few minutes. This was necessary since residual gases and volatiles may lead to large errors in pressure readings (Aim, 1978).

- The loaded cell was weighed again to determine the mass of the liquid component. This was repeated four times at different angles and the average was taken as the new mass of cell plus liquid component; hence the mass of the liquid component could be determined by subtracting the mass of the empty cell from that of the loaded cell with liquid component.
- Then gas was loaded to the system side of the cell from the gas cylinder after purging the feeding lines. Mass of the loaded cell, now with gas and the liquid component, was weighed as described above. Mass of the loaded gas was thus determined by subtracting the mass of cell loaded with liquid from the mass of loaded cell with liquid and gas mixture. Therefore, the exact composition of the loaded liquid component and gas component was determined. For dilute regions of n-hexane, more carbon dioxide or volatile components were loaded into the cell with the help of stirring and cooling the cell using an ice bath. This was so because, according to Henry's Law, the absorption of a gas into a liquid solvent is favourable at low temperatures and high pressures. High total pressures prevent evaporation of the solvent; thus, it reduces solvent losses. In cases where carbon dioxide was loaded by lowering cell temperature using ice, the cell was dried afterwards using a hairdryer and subsequently cleaned using pressurised air to make sure there were no droplets of water or debris on the surface of the cell or any part of the cell that would affect the accurate measurement of the mass of gas loaded.

After loading the equilibrium cell and determining the composition by mass, the cell was mounted to the liquid bath. A GC was connected to the equilibrium cell to analyse the components after purging the sampling lines at least five times. The GC operating parameters for the n-hexane + carbon dioxide test system are shown in Table 5-1. The GC system was turned on and left for approximately two hours to stabilise the baseline. A gas, either carbon dioxide or nitrogen, was loaded to the cell's hydraulic side, gradually displacing the movable piston towards the system side, thus altering the volume and pressurising the cell system side until a single phase was achieved. The calibration procedure employed in this work would not work for a bi-phasic mixture (for instance, a liquid-liquid system) (Nelson et al., 2021). Mixing of the components was accomplished with the aid of a stirrer so that system homogeneity could be accomplished quickly, and sampling was done whilst the mixer was on. No temperature and pressure recordings were necessary at this stage. Peak areas recorded during calibrations provide a range/limits under which peak areas during VLE measurements should lie.

The response of the thermal conductivity detector (TCD) is calibrated by injecting known quantities of a single component or known compositions for binary mixtures since the TCD's response does not provide any information about the exact quantity of material passing through. The ROLSI™ and the GC line temperatures were set such that the sample would remain in vapour phase thus enabling all of the sample to be transferred for accurate analysis. For the same mixture, sampling was done at different split ratios such as 150, 100, 50 and 20 using a ROLSI™ sampler and two peaks were recorded by the TCD. The different split ratios allowed for a broad range of peak areas to be recorded at any given standard solution since, the higher the split ratio, the lower the peak area, and vice versa. The average area ratios A_1/A_2 for each of the split ratios should be almost the same within ± 0.003 of the averaged values at other split ratios, and this data was recorded for different standard mixtures. The multiple binary mixtures created cover the compositions expected from the vapour phase and liquid phase compositions.

The response factor (F) of a TCD detector is defined as the proportionality constant between the number of moles for a given component (n) passing through the detector to its peak area (A), hence given a binary mixture of components 1 and 2, the following expressions can be written:

$$n_1 = F_1 A_1 ; n_2 = F_2 A_2 \quad (5-3)$$

If i represents either of the components 1 or 2, then n_i is the number of moles of component i , F_i is the detector response factor for component i , and A_i is the integrated peak area for component i .

$$\frac{n_1}{n_2} = \frac{x_1}{x_2} = \left(\frac{F_1}{F_2}\right) \left(\frac{A_1}{A_2}\right) \quad (5-4)$$

“In practice, the mole number ratios x_1/x_2 are more linearly proportional to their peak area ratios A_1/A_2 than mole numbers n_1 are to their peak areas A_1 in the presence of $A_{1 \neq 2}$ ” (Soo, 2011), as shown in equation (5-4). Using the LINEST function in MS Excel (which employs the least squares method), the x_1/x_2 and A_1/A_2 data can then be fitted to either first-order or second-order polynomial depending on which of these two gives the best result fit of the calibration data. This resulted in a calibration curve that was split in this study for the vapour phase and the liquid phase regions, respectively. Raal and Mühlbauer (Raal and Mühlbauer, 1999) suggested that the calibration be divided into the dilute and concentrated region to account for the potential non-linearity of the detector, especially in the dilute region. The limiting condition that $x_1=0$ at $A_1 = 0$ was respected in this study.

For the carbon dioxide (1) + n-hexane (2) system, GC detector calibration has been performed for carbon dioxide mole fraction range of 0.204 to 0.992. The calibration was split into two for x_1 0.204 to 0.883 for the liquid phase and y_1 0.883 to 0.992 for the vapour phase.

For the carbon dioxide (1) + n-decane (2) system, the GC detector calibration has been performed for the carbon dioxide mole fraction range of 0.304 to 0.948. The calibration was split into two for x_1 0.112 to 0.887 for the liquid phase and y_1 0.992 to 0.999 for the vapour phase. Table 5-1 presents the GC parameters for detector calibration and VLE measurements.

Table 5-1: GC parameters for detector calibration and VLE measurements.

Column	Zebron™ Phase: ZB-WAX: CO ₂ + n-hexane	Zebron™ Phase: ZB-WAX: CO ₂ + n-decane
Column specifications	L = 60 m, ID = 0.3 mm, df = 0.5 μ m	L = 60 m, ID = 0.3 mm, df = 0.5 μ m
Carrier gas	Hydrogen	Hydrogen
Operating conditions		
Split ratios	150; 100; 50 and 20	150; 100; 75;50; 20;10;7 and 5
Inlet pressure (MPa)	0.054	0.1851
Injector temperature (K)	473.15	473.15
Column temperature (K)	333.15	373.15
Detector temperature (K)	473.15	473.15
Linear Velocity (cm/s)	30	40
Current (mA)	70	70
Makeup flow (cm ³ /minute)	15	15

5.2.4. VLE (TP_{xy}) measurement procedure: binary system

Having obtained the calibrations for the temperature probe, pressure transducer, and the TCD responses for both the vapour and liquid phases, VLE measurements were then undertaken.

TP_{xy} measurements were performed for the following test systems:

- Carbon dioxide + n-hexane at 313.15 K
- Carbon dioxide + n-decane at 319.15 K

The equilibrium cell was initially leak tested after being charged with N₂ gas to a pressure of approximately 10 MPa. Snoop® was applied to all connections and nuts to check the presence of bubbles, which would signify a leak. If many tiny bubbles are observed on a connection, tightening of the nuts is recommended until no more bubbles are observed, or complete replacement of an O-ring if the leak is detected where there is an O-ring seal. N₂ gas was then vented out of the equilibrium cell, which was subsequently cleaned by solvents such as ethanol or acetone. The cleaned cell was then

evacuated using a vacuum pump for at least 30 minutes to eliminate any residual gases /volatiles that might be present in the seals.

An unknown mass of the liquid component was loaded into the cell, followed by evacuation for approximately three to five minutes to remove any volatile gases. Then feeding lines 1/8" stainless-steel connected to a gas cylinder with the more volatile component, carbon dioxide, in this case, were purged. These lines were then connected to the feeding valve on the equilibrium cell's system side while being purged. The volatile component was then loaded into the cell by gradually opening the valve until the desired gas was loaded. The valve was closed, and the lines disconnected from the cell. The cell was then submerged into a water bath, and the VLE measurements were performed at a constant temperature. The mixture was thoroughly stirred with the help of the stirrer until vapour liquid equilibrium was reached, which was assumed by attaining a constant temperature and pressure for at least ten minutes. The movable ROLSI™ sampler shown in Figure 5-4 was adjusted so that it was able to sample either the vapour phase or the liquid phase, and sampling was done when the stirrer was switched off. A slight pressure drop within the uncertainty of the pressure measurements was observed on moving the sampler from the liquid to the vapour phase. The stirrer was switched off to allow for clear separation of the phases and as a safety measure for avoiding the blockage of the ROLSI™ by potential attrited O-ring pieces since these would have settled down. On sampling either of the phases, the system was initially purged five times before the data was recorded. Each time a sample was withdrawn from the cell, some minor or sometimes negligible pressure drops would occur and this was compensated with the aid of the pressure controller as described in section 5.1. The split ratio and the ROLSI™ opening time were adjusted and set so that the peak areas recorded were within the calibration range. A minimum of ten samples per phase was taken and analysed and the peak areas were recorded. The recorded peak areas A_1, A_2 for each sample were subjected to a calibration polynomial to determine the actual composition. An average value of the composition for the recorded samples on either of the vapour or liquid phase was taken as the composition of that mixture (x_1 or y_1) where x_1 represents the mole fraction of the volatile component in the liquid phase, and y_1 , the mole fraction of the volatile component in the vapour phase. This would produce a single TP_{xy} data point. To obtain a complete TP_{xy} phase envelope, successive loading of the more volatile component into the cell was performed so as to increase the overall gaseous composition. The standard error (standard deviation divided by the average) of the samples should be less than 1%, although higher standard errors may be expected in the dilute region (Nelson, 2012). The absolute pressure value recorded during VLE measurements was a sum of the atmospheric pressure and the pressure recorded by the pressure transducer, which will have been subjected to a pressure calibration polynomial. Upon completing the VLE measurements, the discharge valve was slowly opened in a fume board to vent off the gaseous component. Lastly, the liquid component was collected in waste bottles.

5.2.5. Bubble point measurements

These were performed using the versatile equipment of Nelson et al. (Nelson et al., 2021). The capillary well on the system side flange of the equilibrium cell was plugged by PTFE, as presented in Figure 5-3. Bubble point measurements were performed following the methods presented by Lee et al. (Lee et al., 2000), Tsuji et al. (Tsuji et al., 2004), and Williams-Wynn (Williams-Wynn et al., 2016) and have been discussed in section 4.1.1.3. The equilibrium cell was leak-tested, cleaned and evacuated following the procedure described for VLE measurements. A gravimetric method was then used to prepare a binary mixture of known composition following the same procedure described for the TCD calibration and also described by Nelson et al. (Nelson et al., 2021). For multicomponent mixtures of more than two components, the two-component liquid or three-component liquid solutions were, prepared gravimetrically to the desired compositions. The two-component or three-component gas mixture was ordered from Afrox.

5.2.5.1 Preparation of a binary liquid mixture

The method used in this case is almost similar to the method employed by (Ebrahiminejadhasanabadi, 2019) for the preparation of hybrid solvents. Two glass round bottom flasks were loaded, each with a different liquid. The loaded liquid components were dried under vacuum, and the high vacuum valves on each glass round bottom flask were closed. The mass of each empty glass round bottom flask was initially weighed by an Ohaus mass balance with an expanded uncertainty of ± 0.003 g, resolution 0.001 g, model PA423C (maximum capacity 420 g). The loaded glass round bottom flask was reweighed after loading and drying each of the liquid components to determine the exact mass of the loaded liquid. A T-piece fitting connected to a valve on its outlet was used to connect these two round bottom flasks. The flask with less viscous liquid was made to be vertically positioned on top of the other flask with a more viscous liquid, as shown in Figure 5-5. A vacuum pump was connected to the T-piece via a hose fitting. The valve connected to the T-piece was opened for approximately 30 seconds to purge any air in the line connections, after which the valve is closed. The high vacuum valve on the bottom flask containing the more viscous liquid was slightly opened. This allowed liquid from the top flask to pass through it and making sure that it was not fully open to prevent outside air from leaking into the flask. Then likewise, the high vacuum valve on the top flask was opened such that it allowed the less viscous liquid to flow through it under vacuum into the round bottom flask at the bottom. When all of the less viscous liquid has been loaded into the flask containing the more viscous liquid as described above, the two high vacuum valves were closed, starting with the one on the bottom flask and lastly the one on the top flask. The T-piece fitting was then disconnected such that each flask stands on its own, with the flask containing the liquid mixture sealed by the high vacuum valve. Some manual agitation was performed by gently shaking the round bottom flask containing the liquid mixture. The flask with the liquid mixture was weighed, and the new mass was recorded on the Ohaus mass balance model

PA423C to determine the exact mass of the less viscous liquid that will have been added to this flask. Afterwards, this flask with the liquid mixture was connected to the equilibrium cell through fittings, as shown in Figure 5-6. Although the cell was under vacuum, the connecting lines had to be re-evacuated when the valve connecting the glass round bottom flask to the cell was opened to evacuate to the flask exit. The valve connecting the cell to the vacuum pump was then closed, followed by a careful slight opening of the high vacuum valve on the round bottom flask. This allowed the passage of the liquid mixture into the cell while preventing any air from the outside to leak through. Furthermore, this ensured that the composition of the prepared liquid solution was not altered as it was transferred from the round bottom flask to the equilibrium cell. The valve connecting the cell to the round bottom flask was closed after loading the equilibrium cell with this liquid mixture of predetermined composition. The round bottom flask was disconnected from the cell.

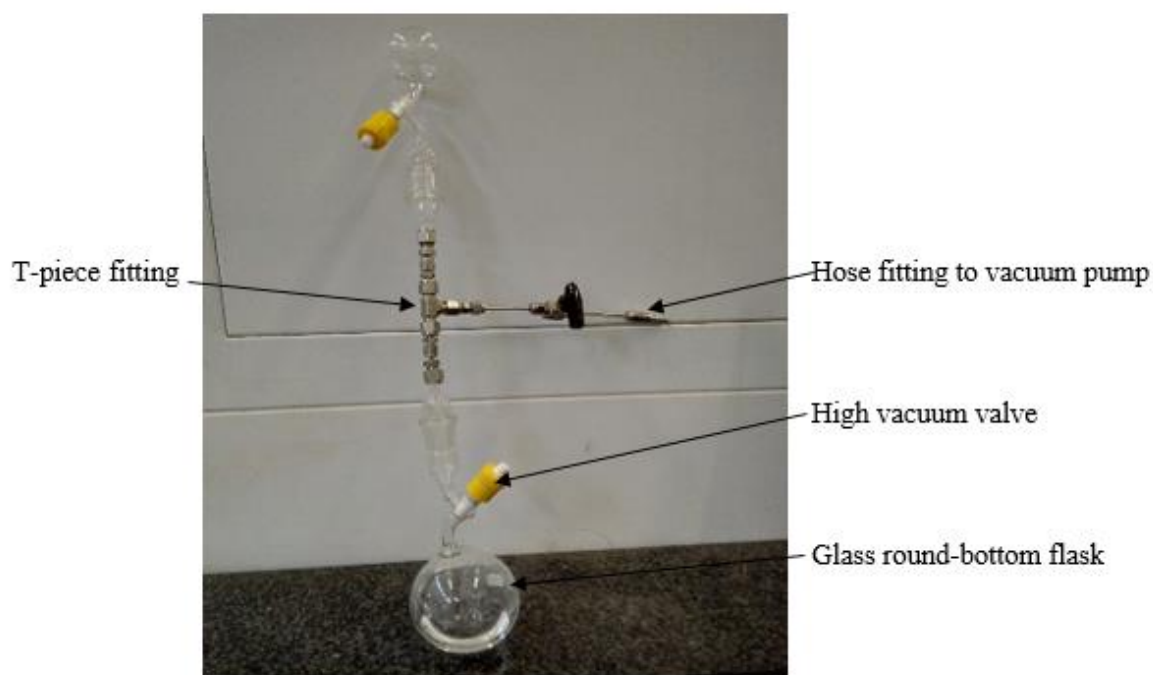


Figure 5-5: Set up used to prepare binary and ternary liquid mixtures.

5.2.5.2 Preparation of a ternary liquid mixture

For a ternary liquid mixture, the liquid preparation procedure is the same as mentioned for the binary mixture, except that initially, two liquid components are prepared, and then the third one requires an additional clean round bottom flask. The clean glass round bottom flask was loaded by the third liquid, and following the same procedure mentioned above, this new flask was connected to the flask already containing the two liquid mixture which is positioned via a T-piece fitting. After evacuation of the T-piece and connections to these assembled flasks, the third liquid was loaded into the round bottom flask

containing the already synthesised binary liquid mixture. The glass round bottom flask containing the new ternary mixture was reweighed again to determine the exact mass of the third liquid. This ternary mixture was then loaded into the equilibrium cell using the same procedure mentioned above for the binary liquid mixture.



Figure 5-6: Set up of a prepared liquid mixture in a glass round-bottom flask, being loaded to the equilibrium cell.

5.2.5.3 Bubble point (TP_x) measurement procedure

On loading the components, the less volatile liquid component or components are loaded, followed by the gas component as has been described above. For bubble points measurements, the loaded cell was submerged in a water bath which was maintained at a constant temperature within ± 0.11 K. A syringe pump model 100DX (ISCO) controlled by SFX™ 200 controller (ISCO), was set to operate at a constant flow mode. This pump was filled with water, after which it was connected to the hydraulic side of the equilibrium cell via 1/8" stainless steel lines. The syringe pump, which can also operate at constant pressure mode, can handle pressures of up to 68 MPa, hence pressure limits were set so that the pressures would not exceed the ratings of either of the pressure transducers used in this work. The working volume of the equilibrium cell can be varied from approximately 3 cm³ to approximately 33 cm³ with a piston, using hydraulic fluid on the backside, water in this case.

The mixture was initially compressed to almost bubble point where only just one or a few bubbles were observed and let to mix for approximately 5 minutes. Then water was pumped/pushed into the hydraulic side of the cell at a constant volumetric flow rate of $0.01 \text{ cm}^3/\text{minute}$. The piston moved towards the system side, thus pressurizing the cell until a single homogeneous phase was formed. This proceeded whilst the components were being stirred as the stirrer was connected to a groove inside the movable piston. The bubble point pressure was the point where the last bubble disappeared from the mixture on the system side of the cell as water was slowly pumped to the hydraulic side. Pressure readings were taken from the data logger and presented as visual; thus, phase transition from two phase to one homogeneous phase was used to detect the bubble point pressure. Also, the pressure curve from the data logger was observed, and at a point where there is a sudden rapid increase in pressure (break-point or inflection point), the pressure reading was recorded. The recorded pressures (visual or break-point) were then fitted to the calibration equation, and atmospheric pressure was added as well to determine the actual bubble point pressure. Therefore, this apparatus allowed two forms of phase transition detection, one visual since the apparatus is transparent and graphically from pressure recordings. There was a good agreement between the data recorded using either of the two methods as the data was within an estimated accuracy of 0.01 MPa. After obtaining the bubble point pressure, the cell was then depressurized by refilling the syringe pump at a rate of $10 \text{ cm}^3/\text{minute}$ until some bubbles reappear again in the mixture on the system side. When a single bubble or a few of them reappears in the cell, the stop button of the syringe pump was pressed, and thereafter the pump was run again, thus repeating the pressurization of the system side until a single homogeneous phase was observed and pressure readings were taken for the bubble point pressure. For each point, the measurements were repeated an average of three times to ensure the repeatability of the measurements, with both visual and breaking point recordings being undertaken. For each mixture loaded in the equilibrium cell, a single P - x data point was recorded at a constant temperature. In some cases, multiple isotherms of the same loaded mixture compositions were measured consecutively by either decreasing or increasing the bath temperature, thus saving time for dismantling and cleaning the cell and limiting chemical costs. After each measurement the cell was cleaned and reloaded with a different composition until the whole range of the T - P - x data were measured.

CHAPTER 6: RESULTS AND DISCUSSION

6.0 INTRODUCTION

This section presents the results and discussion of this study. This includes chemical purities, temperature, pressure, and GC detector calibrations, test systems phase equilibria measurements, novel systems phase equilibria measurements, and modelling results. It is important to note that the same equipment was used either in static synthetic mode or in static analytic mode; hence the term combined static apparatus.

The test systems measured were:

1. TP_{xy} measurements for the carbon dioxide + n-hexane system at 313.19 K – static analytic/static synthetic method
2. TP_{xy} measurements for the carbon dioxide + n-decane at 319.23 K – static analytic method
3. TP_x measurements carbon dioxide + methanol /TEG systems (298.10 to 313.15 K) – static synthetic method
4. TP_x measurements for the methane + methanol /TEG systems (298.15 to 323.15 K) – static synthetic method
5. TP_x measurements for the carbon dioxide + water + TEG system (298.15 to 322.04 K) – static synthetic method

TP_x data were measured for all new systems using the static synthetic method and these were:

1. Methane + propane+ methanol at 283.15, 303.15, and 323.15 K
2. Methane + propane + TEG at 303.16 and 323.16 K
3. Methane + methanol + TEG at 303.15 and 323.15 K
4. Carbon dioxide + methanol + TEG at 303.15 and 323.15 K
5. Methane + propane + methanol + TEG at 283.15, 303.15 and 323.15 K
6. Methane + propane + methanol + water + TEG at 283.15, 303.15 and 323.15 K
7. Methane + propane + carbon dioxide + methanol + water + TEG at 283.15, 303.15 and 323.15 K.

Thermodynamic modelling of the measured data included data correlation and prediction using five thermodynamic models and their combinations: the PR, SRK, PRWS, CPA, and the PC-SAFT. Detailed descriptions of these models were presented in chapter 3 and Appendix D.

6.1 Chemicals used

All the chemicals utilised in the present study, their suppliers' details, CAS and CAT numbers are presented in Table 6-1. Chemical purity checks were performed for all components. The purity checks

were performed through GC injections for each component and the measurement of physical properties such as refractive index, viscosity and density for the liquid components. The results are presented in Tables 6-2 and 6-3. Vapour pressure measurements were also conducted for the liquid components except for TEG and n-decane, results of which are presented in Appendix B, section B.1. The vapour pressure values of this work are in good agreement with literature data. For methanol and TEG, the water content was also checked using a Karl Fischer titration unit. Gas mixture composition validation for the propane + methane and methane + carbon dioxide + propane gas mixtures was performed by comparing the GC peak areas for either methane/carbon dioxide in the mixtures to the peak area of individual component injections. Further details on the gas mixture composition validation are presented in Appendix B.2.

Table 6-1: Details of chemicals used for this study.

List of chemicals	Supplier	CAS Number	CAT Number/Lot Number
2,2'-(ethane-1,2-diylbis(oxy))diethanol) or Triethylene Glycol (TEG)	Sigma-Aldrich	112-27-6	BCBW8450, STBJ4922, STBJ6265
Methanol (CH ₃ OH)	Sigma-Aldrich	67-56-1	STBH0784, STBH6445
Water (H ₂ O) distilled, deionized	ELGA Purelab Option-Q	7732-18-5	N/A
Methane (CH ₄)	Afrox	74-82-8	541403-SE-C
(Methane: propane) gas mixture	Afrox		803867-IJ-A (GOC MIX 3357 (S)).
(Methane:propane:carbon dioxide) gas mixture	Afrox		804360-IJ-A (GOC MIX 3684)
Carbon dioxide (CO ₂)	Afrox	124-38-9	514103-RC-C
n-Hexane (C ₆ H ₁₄)	Sigma-Aldrich	110-54-3	STBH9152, STBJ1404
n-Decane (C ₁₀ H ₂₂)	Sigma-Aldrich	124-18-5	WXBC6468V

All pure component purities were shown to be 99.0% or more. All gases were used without further purification, whilst liquid components were all dried under a vacuum.

Table 6-2: GC chemical purity checks.

Chemicals	Supplier stated purity: (wt. fraction purity)	Relative GC Peak Area: (Exp)	Normal boiling Temperature: K*	Molecular Weight: g/mol *
TEG	≥ 0.9990	≥ 0.9914	561.729 ^{a,f}	150.2 ^{a,f}
Methanol	≥ 0.9990	≥ 0.9970	337.6843 ^f	32.04 ^{b,f}
Water		≥ 0.9990	373.15 ^{c,i}	18.02 ^{c,i}
Methane	≥ 0.9995	≥ 0.9924	111.6558 ^f	16.043 ^f
Carbon dioxide	≥ 0.9990	≥ 0.9991	185.24 ^f	44.01 ^{d,f}
n-Hexane	≥ 0.9900	≥ 0.9970	341.8608 ^f	86.18 ^f
n-Decane	≥ 0.9900	≥ 0.9979	447.236 ^f	142.29 ^f
Methane:propane gas mixture nominal ratio	$\geq 0.95:0.05^e$	0.9428:0.05.72 ^h		
Methane:propane:carbon dioxide gas mixture nominal ratio	0.9022:0.0460:0.0518 ^g	0.9014: 0.0494: 0.0492 ⁱ		

Exp refer to experimental values; * Literature (ref); a: (Kohl and Nielsen, 1997) ; b: (National Center for Biotechnology Information, 2018a); c: (National Center for Biotechnology Information, 2018b) ; d: (National Center for Biotechnology Information, 2018c); e: (mole fraction $\pm 0.26\%$ of CH₄; $\pm 5\%$ of C₃H₈); f: Obtained from NIST ThermoData Engine (TDE version 10.2, database version 10.12) in Aspen Plus V11; g:(mole fraction $\pm 0.22\%$ of CH₄, $\pm 2\%$ of C₃H₈, $\pm 2\%$ of CO₂); h : (experimental composition validation : mole fraction $\pm 0.85\%$ of CH₄, $\pm 0.65\%$ C₃H₈); i: (experimental composition validation :mole fraction $\pm 0.83\%$ of CH₄, $\pm 0.98\%$ of C₃H₈, $\pm 1.01\%$ of CO₂).

Table 6-3: Measured values for refractive index, density, and viscosity for the liquid components.

Component	Refractive index (n_D)		Density (ρ): g·cm ⁻³		Viscosity (ν): mPa·s	
	Lit*	Exp	Lit*	Exp	Lit*	Exp
Water	1.333 ^c	1.33251	0.9971 ^a	0.9971	0.899 ^b	0.8989
Methanol	1.3265 ^d	1.32667	0.7866 ^{d,e}	0.7866	0.563 ^f	0.5640
TEG	1.4559 ^h ; 1.456 ⁱ	1.45538	1.1225 ^g	1.12288	49.0 ^h ; 48.05 ⁱ	
n-Hexane	1.3727 ^j	1.37229	0.6606 ^j ; 0.6553 ^k	0.65608	0.2943 ^k	
n-Decane	1.4090 ^m	1.40989	0.7255 ^m ; 0.7269 ⁿ	0.72733	0.864 ^o	

$U_\rho = 0.0002 \text{ g·cm}^{-3}$; $U_{(n_D)} = 0.001$; $U_{(\nu)} = 0.0103 \text{ mPa·s}$ and $U_{(T)} = 0.01 \text{ K}$

Exp refer to experimental values; * Literature (ref); a: data at 298.15 K (Moosavi and Rostami, 2017); b: data at 298.15 K (Rodríguez-Escontrela et al., 2015); c: Data at 298.15 K , (National Center for Biotechnology Information, 2018b); d: (National Center for Biotechnology Information, 2018a); e: data at 298.15 K (Yang et al., 2017); f: data at 298.15 K (Moosavi et al., 2015); g: data at 293.15 K (Rastorguev and Gazdiev, 1969); h: Data at 293.15 K , (DOW chemical company, 2018) ; i: data at 293.15 K (Carvalho et al., 2015); j: (Haynes, 2010) at 298.15 K; k: data at 298.15 K (Mascato et al., 2000) ; l: data at 298.15 K (Guerrero et al., 2011); m : data at 298.15 K (Haynes et al., 2014b); n: data at 298.15 K (Bried and Hemmion, 1938); o: data at 298.15 K (Qin et al., 2014).

As observed in Table 6-3, the experimental values for the refractive index, density and viscosity match well with literature data.

6.1.2 Water content in methanol and triethylene glycol

The water content was measured using the C10S coulometric Karl Fischer (KF) titrator (Mettler Toledo), which made use of the KF electrolyte A and C (products of ROMIL LTD) as the KF reagents. These are pyridine free reagents, that are produced to a water specification of less than 50 ppm (0.0050%). Calibration was done with a KF calibrant that contained 0.1% water (1.0mg/g) in an anisole/propylene carbonate matrix. The results in Table 6.4 show that the water content was well below 0.1%. The water content standard deviation for the methanol sample was 0.012%, whilst for the TEG sample it was 0.015%.

Table 6-4: Water content in methanol and TEG.

Component	% Water content	mg of water/g of sample
Methanol	0.071	0.707
Triethylene glycol	0.061	0.607

6.2 Calibrations

6.2.1 Temperature sensors calibration results

Two Pt100 stainless steel probes were used on the HPVLE apparatus. More details about probes T102 and T104 and their location on the equipment are outlined in chapter 5, section 5.1. In addition to that, the calibration procedure was outlined in section 5.2.1, which was conducted twice. The second calibration was necessitated due to the fact that measurements were noticed to deviate off from their usual values at given setpoints. The calibration correlation, Pearson product-moment correlation coefficient (r-squared fit), and maximum errors are presented in Tables 6-5, 6-6 and Figures 6-1, 6-2.

Table 6-5: Calibration polynomials for the temperature probes T102 and T 104.

Probe	Correlation	R ² value	ΔT (max): K
T102	Y =0.997X-1.637	R ² = 1.000	0.03
T104	Y =0.999X-1.435	R ² = 1.000	0.04

Calibration performed July 2018; Y represents calculated temperature (K); X represents the temperature displayed for the specific probe (K)

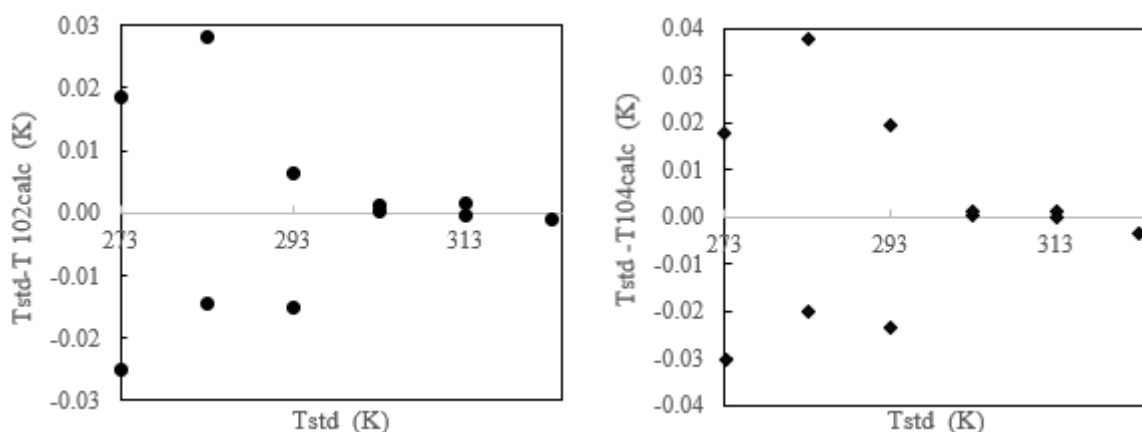


Figure 6-1: Plot of the deviation between the standard temperature (Tstd) and calculated calibrated temperature (Tcalc) for the probes used in this work.
(Left) probe T102; (Right) probe T104.

The calibration polynomial for probe T102 gave a maximum deviation reading of ± 0.03 K. Calibration polynomial for probe T104 gave a maximum deviation reading of ± 0.04 K.

The T102 and T104 temperature probes were recalibrated in August 2020, and checks were performed regularly. The data were fitted to a second-order polynomial, and the results are presented in Table 6-6.

Table 6-6: Calibration polynomials for the temperature probes T102 and T 104 recalibration.

Probe	Correlation	R ² value	ΔT (max): K
T102	$Y = -0.0003X^2 + 1.0197X - 2.6907$	$R^2 = 1.000$	0.12
T104	$Y = -0.0001X^2 + 1.0106X - 1.5791$	$R^2 = 1.000$	0.11

Calibration performed in August 2020; Y represents calculated temperature (K); X represents the temperature displayed for the specific probe (K)

The calibration polynomial for probe T102 gave a maximum deviation reading of ± 0.12 K. Calibration polynomial for probe T104 gives a maximum deviation reading of ± 0.11 K. All values of standard uncertainties used in this study are presented in Table A-1 (Appendix A). The large difference in the deviation readings between the July 2018 and the August 2020 calibration polynomials might probably have been caused by loss of sensitivity due to external factors. Suspected external factors are alterations on the tip of the sensors, probably due to wear and tear.

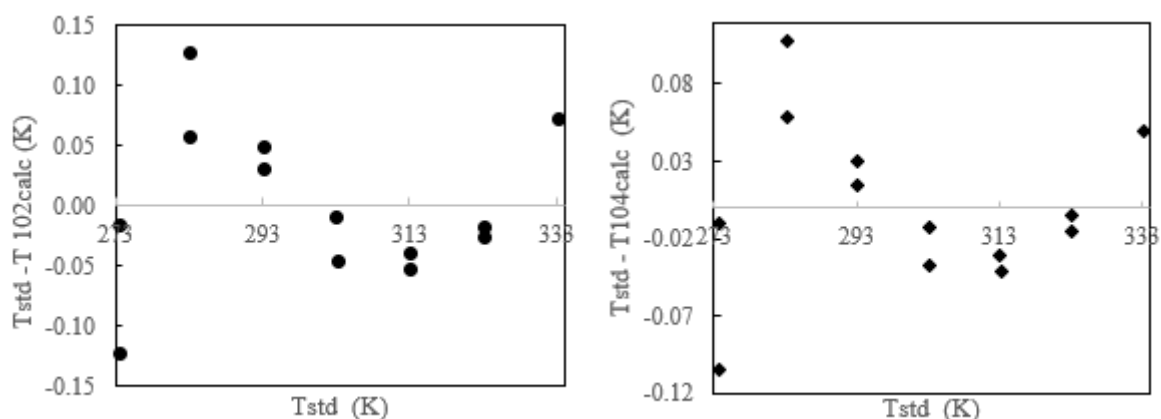


Figure 6-2: Plot of the deviation between the standard temperature (Tstd) and calculated calibrated temperature (Tcalc) for the probes used in this work.
(Left) probe T102; (Right) probe T104.

6.2.2 Pressure transducer calibration results

Pressure transducer calibrations were carried out as described in chapter 5, section 5.2.2. The data were fitted to either first-order or second-order polynomial depending on which of the two would give minimum errors. Two pressure transducers (0 to 10 MPa) and (0 to 35 MPa) were used separately on the same equipment throughout this work. Since one transducer was used at a time, the same channel (P122) was used by either the 10 or the 35 MPa transducer. The 35 MPa transducer was calibrated up to 17.6 MPa, as in this work, no measurement was performed beyond 17.6 MPa. The original plan was to conduct measurements up to 20 MPa; however, one of the sapphire cells developed some dents on its edges due to the brittleness of the sapphire material. Eventually, that cell exploded into pieces at approximately 25 MPa. As a result, pressures were limited to approximately 15 MPa maximum pressure to preserve the spare sapphire cell. The calibration polynomials and the errors are presented in Table 6-7 and Figures 6-3 to 6-4, respectively.

Table 6-7: P122 Pressure transducer calibration polynomials.

Pressure transducer range	Date performed	Correlation	R ² value	ΔP max: MPa
P122 [10 MPa]	(June 2019)	$Y = 1.000X + 0.4528$	$R^2 = 1.000$	0.0009
P 122 [10 MPa]	(December 2019)	$Y = 0.9999X - 0.5505$	$R^2 = 1.000$	0.0012
P122 [10 MPa]	(July 2020)	$Y = 8E-05X^2 + 0.9988X - 0.15402$	$R^2 = 1.000$	0.0005
P122 [35 MPa]	(Sept 2020)	$Y = 0.9998X - 0.1880$	$R^2 = 1.000$	0.0013

Y represents the calculated pressure value (MPa); X represents the displayed pressure value for the specific pressure transducer.

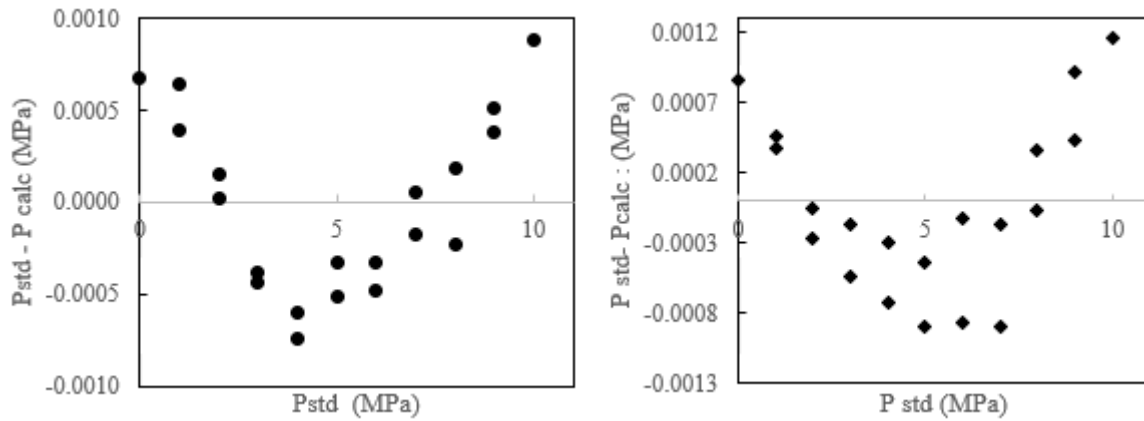


Figure 6-3: Plot of the deviation between the pressure standard (Pstd) and the calculated pressure (Pcalc) for the pressure transducer used in this work.
P122; (Left): June 2019; (Right): December 2019.

For the June 2019 calibration, the calibration polynomial yielded a maximum deviation reading of ± 0.0009 MPa, whilst for the December 2019 calibration, the calibration polynomial yielded a maximum deviation reading of ± 0.0012 MPa.

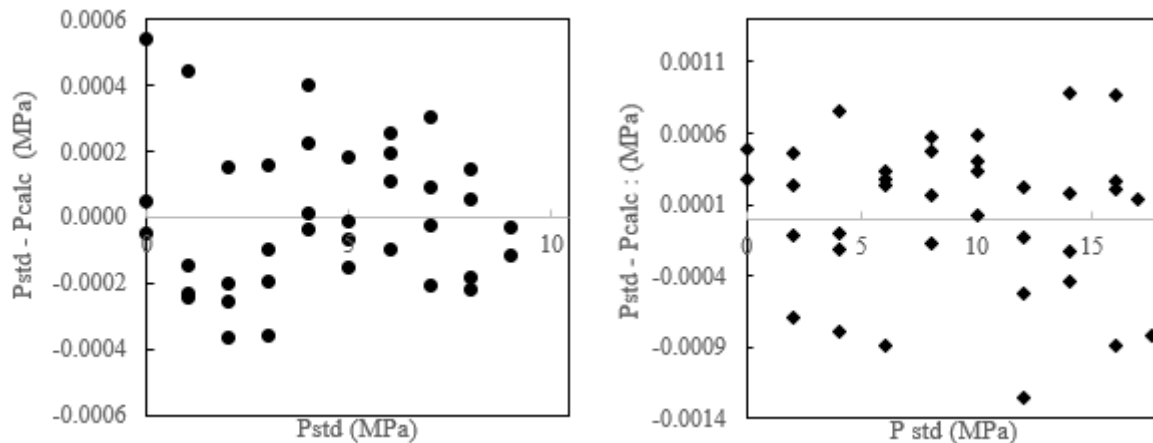


Figure 6-4: Plot deviation between the pressure standard (Pstd) and the calculated pressure (Pcalc) for the pressure transducers used in this work.
P122; (Left): July 2020; (Right): September 2020 (35 MPa transducer).

For the July 2020 calibration, the calibration polynomial yielded a maximum deviation reading of ± 0.00054 MPa, whilst for the September 2020 calibration, the calibration polynomial yielded a maximum deviation reading of ± 0.0013 MPa.

6.2.3. GC detector calibration results

This was conducted for the carbon dioxide + n-hexane test system and the carbon dioxide + n-decane test system using a Shimadzu GC 2010 with a TCD detector and a ZB Wax capillary column. The GC detector calibration deviations for both systems are presented in Tables 6-8 to 11.

6.2.3.1 GC calibration carbon dioxide (1) + n-hexane (2) test system

For the carbon dioxide (1) + n-hexane (2) system, GC detector calibration was performed for the x_1 (CO_2) mole fraction range of 0.204 to 0.992. This was conducted for split ratios of 150, 100, 50, and 20 for each mixture that was prepared. The calibration was performed using a gravimetric method with the masses of the components having been determined by weighing the newly designed equilibrium cell. The data were fitted to a second-order polynomial. This was because the second order polynomial yielded lower relative composition errors as compared to the first order polynomial. The GC calibration procedure was outlined in chapter 5, section 5.2.3. The calibration was split into two regions for x_1 over 0.204 to 0.883 for the carbon dioxide dilute region and y_1 of 0.883 to 0.992 for the carbon dioxide-rich region. The opening time for the ROLSITM was set at 0.01 seconds and the time between samples was 54 seconds. The GC detector calibration chart for the carbon dioxide dilute region is presented in Figure 6-5.

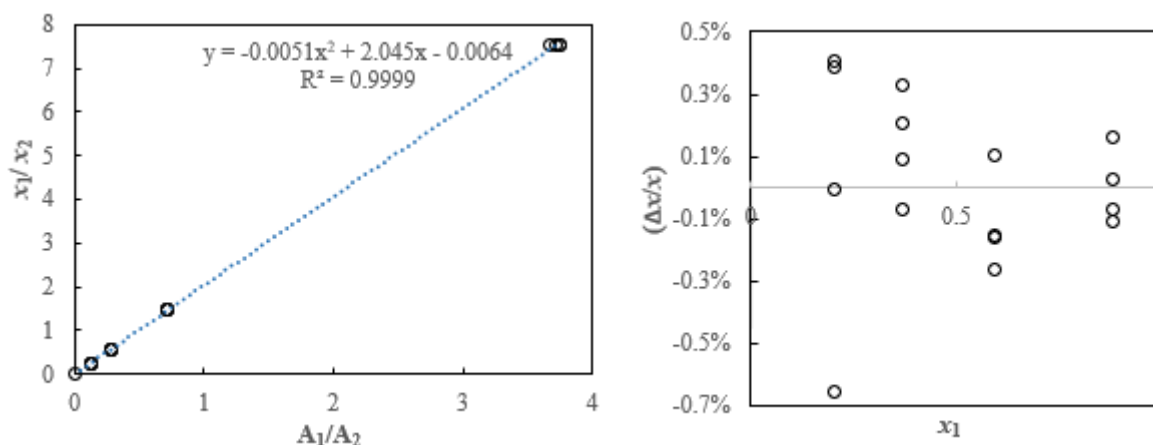


Figure 6-5: GC detector calibration chart for the CO_2 (1) + n-hexane (2) mixture.
(Left): CO_2 dilute region; (Right): Relative compositional errors in x_1 (%).

A maximum relative composition error of 0.66 % carbon dioxide was determined after fitting the data to a second-order polynomial.

Table 6-8: GC split ratios, mole fractions, peak areas and deviations for the CO₂ (1) + n-hexane (2) GC detector calibration, CO₂ dilute region.

Split ratio	x_1	x_2	A_1	A_2	x_1/x_2 calc	x_1 calc	Δx_1	$(\Delta x_1/x_1)\%$
150	0.5931	0.4069	7623	10587	1.46	0.5941	-0.0009	-0.16
100	0.5931	0.4069	9648	13363	1.47	0.5947	-0.0016	-0.26
50	0.5931	0.4069	17265	23973	1.46	0.5941	-0.0010	-0.16
20	0.5931	0.4069	35555	49695	1.45	0.5925	0.0006	0.11
150	0.3665	0.6335	5382	18857	0.58	0.3658	0.0008	0.21
100	0.3665	0.6335	6624	23113	0.58	0.3668	-0.0003	-0.07
50	0.3665	0.6335	10657	37276	0.58	0.3662	0.0003	0.09
20	0.3665	0.6335	22618	79412	0.58	0.3653	0.0012	0.33
150	0.2040	0.7960	742	5799	0.26	0.2032	0.0008	0.41
100	0.2040	0.7960	909	7106	0.26	0.2033	0.0008	0.39
50	0.2040	0.7960	1967	15177	0.26	0.2054	-0.0013	-0.66
20	0.2040	0.7960	4516	35132	0.26	0.2041	0.0000	-0.01
150	0.8828	0.1172	20051	5461	7.43	0.8814	0.0014	0.16
100	0.8828	0.1172	26573	7157	7.52	0.8826	0.0003	0.03
50	0.8828	0.1172	43287	11523	7.60	0.8838	-0.0009	-0.11
20	0.8828	0.1172	119504	31917	7.58	0.8834	-0.0006	-0.07

The GC detector calibration chart for the carbon dioxide-rich region is presented in Figure 6-6

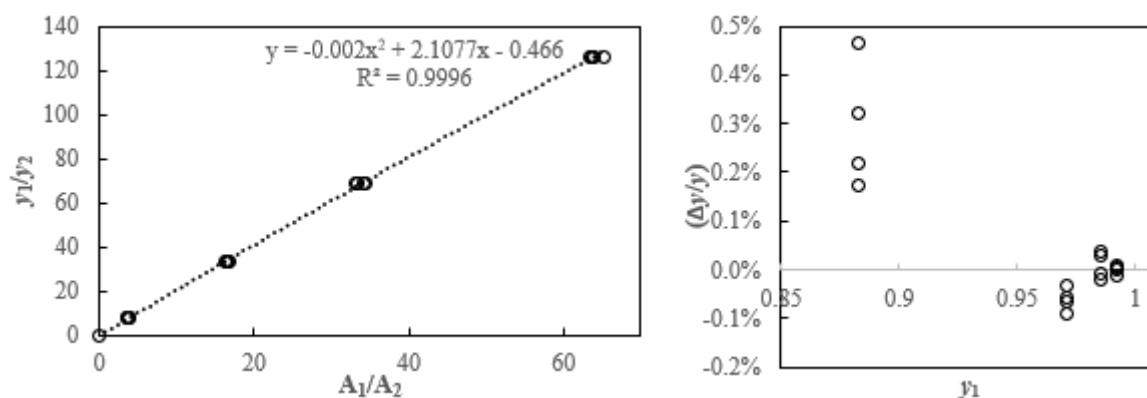


Figure 6-6: GC detector calibration chart for the CO₂ (1) + n-hexane (2) mixture.
(Left): CO₂ rich region; (Right): Relative compositional errors in y_1 (%).

A maximum relative composition error of 0.47% carbon dioxide was determined after fitting the data to a second-order polynomial.

Table 6-9: GC split ratios, mole fractions, peak areas and deviations for the CO₂ (1) + n-hexane (2) GC detector calibration, CO₂ rich region.

Split ratio	y ₁	y ₂	A ₁	A ₂	y ₁ /y ₂ calc	y ₁ calc	Δy ₁	(Δy ₁ /y ₁)%
150	0.8828	0.117	20051	5461	7.25	0.8787	0.0041	0.47
100	0.8828	0.117	26573	7157	7.33	0.8800	0.0028	0.32
50	0.8828	0.117	43287	11523	7.42	0.8813	0.0015	0.17
20	0.8828	0.117	119504	31917	7.40	0.8809	0.0019	0.22
150	0.9708	0.029	25979	1582	33.60	0.9711	-0.0003	-0.03
100	0.9708	0.029	38663	2335	33.88	0.9713	-0.0006	-0.06
50	0.9708	0.029	70193	4195	34.24	0.9716	-0.0009	-0.09
100	0.9708	0.029	169892	10240	33.95	0.9714	-0.0006	-0.06
150	0.9857	0.014	15298	443	69.92	0.9859	-0.0002	-0.02
100	0.9857	0.014	21823	638	69.32	0.9858	-0.0001	-0.01
50	0.9857	0.014	43206	1298	67.49	0.9854	0.0003	0.03
20	0.9857	0.014	100889	3044	67.20	0.9853	0.0004	0.04
150	0.9921	0.008	19307	296	128.40	0.9923	-0.0001	-0.01
100	0.9921	0.008	26164	413	125.01	0.9921	0.0001	0.01
50	0.9921	0.008	45268	707	126.34	0.9921	0.0000	0.00
20	0.9921	0.008	123413	1941	125.44	0.9921	0.0001	0.01

6.2.3.2 GC calibration carbon dioxide (1) + n-decane (2) test system

For the carbon dioxide (1) + n-decane system (2) system, GC detector calibration has been done for the x_1 (CO₂) mole fraction range of 0.304 to 0.948. The calibration was split into two for x_1 0.112 to 0.887 for the carbon dioxide dilute region and y_1 0.992 to 0.999 for the carbon dioxide-rich region. The GC detector calibration chart for the carbon dioxide dilute region is presented in Figure 6-7.

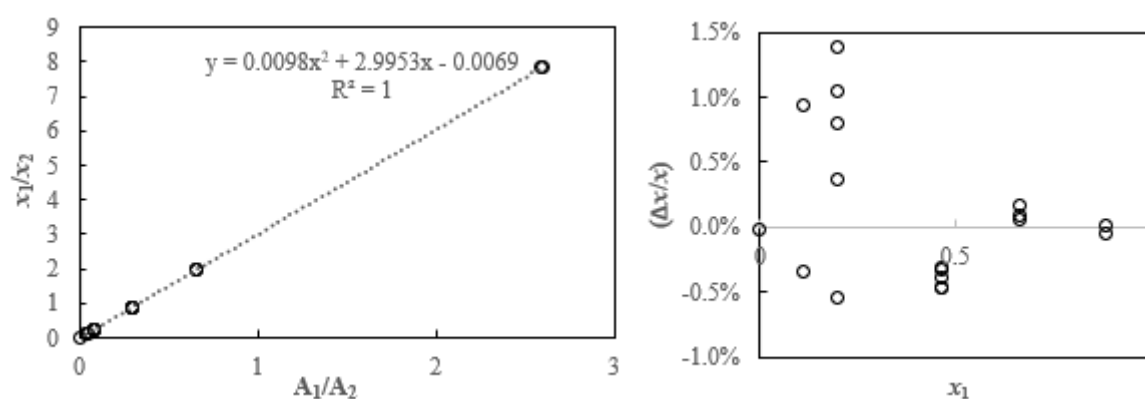


Figure 6-7: GC detector calibration Chart for the CO₂ (1) + n-decane (2) mixture.
(Left): CO₂ dilute region; (Right): Relative compositional errors in x_1 (%).

A maximum relative composition error of 1.39 % for carbon dioxide was determined after fitting the data to a second-order polynomial.

Table 6-10: GC split ratios, mole fractions, peak areas and deviations for the CO₂ (1) + n-decane (2) GC detector calibration, CO₂ dilute region.

Split ratio	x ₁	x ₂	A ₁	A ₂	x ₁ /x ₂ calc	x ₁ calc	Δx ₁	(Δx ₁ /x ₁) %
100	0.887	0.113	37439	14391	7.8524	0.8870	-0.0002	-0.02
50	0.887	0.113	69057	26645	7.8224	0.8867	0.0002	0.02
50	0.663	0.337	46747	70868	1.9732	0.6637	-0.0003	-0.05
20	0.663	0.337	102046	155698	1.9605	0.6622	0.0011	0.17
15	0.663	0.337	129898	197767	1.9648	0.6627	0.0006	0.10
100	0.468	0.532	7163	24293	0.8772	0.4673	0.0003	0.06
50	0.468	0.532	16378	54997	0.8860	0.4698	-0.0022	-0.47
20	0.468	0.532	42036	141370	0.8847	0.4694	-0.0018	-0.39
12	0.468	0.532	64215	215632	0.8860	0.4698	-0.0022	-0.47
10	0.468	0.532	82691	278525	0.8833	0.4690	-0.0014	-0.31
100	0.196	0.804	2790	33158	0.2452	0.1969	-0.0006	-0.32
50	0.196	0.804	5132	61825	0.2418	0.1947	0.0016	0.80
20	0.196	0.804	12111	145160	0.2431	0.1956	0.0007	0.37
10	0.196	0.804	23141	279649	0.2411	0.1942	0.0020	1.05
150	0.196	0.804	1891	22412	0.2459	0.1974	-0.0011	-0.55
50	0.112	0.888	998	22908	0.1236	0.1100	0.0015	1.39
20	0.112	0.888	1837	41395	0.1261	0.1120	-0.0004	-0.34
7	0.112	0.888	6719	153512	0.1243	0.1105	0.0010	0.93

The GC detector calibration chart for the carbon dioxide-rich region is presented in Figure 6-8.

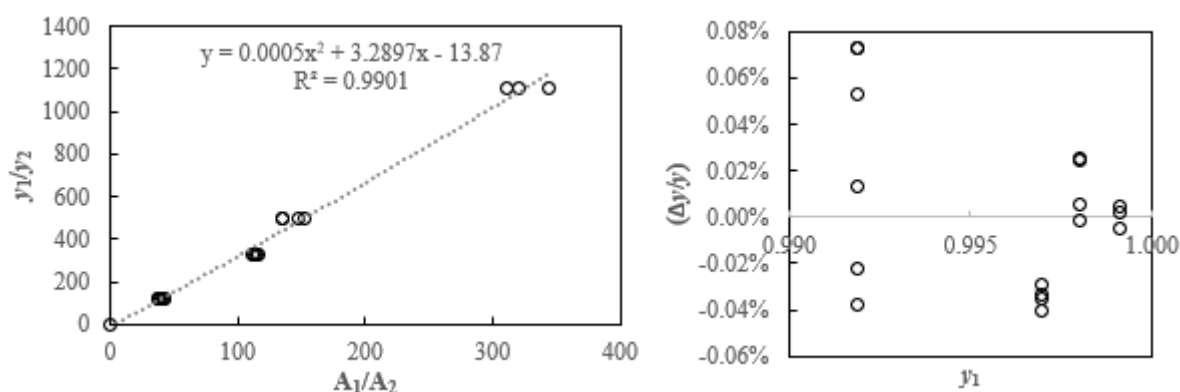


Figure 6-8: GC detector calibration Chart for the CO₂ (1) + n-decane (2) mixture.
(Left): CO₂ rich region; (Right): Relative compositional errors in y_1 (%).

A maximum relative composition error of 0.07% for carbon dioxide was obtained after fitting the data to a second-order polynomial.

Table 6-11: GC split ratios, mole fractions, peak areas and deviations for the CO₂ (1) + n-decane (2) GC detector calibration, CO₂ rich region.

Split ratio	y ₁	y ₂	A ₁	A ₂	y ₁ /y ₂ calc	y ₁ calc	Δy ₁	(Δy ₁ /y ₁)%
150	0.992	0.008	26000	684	111.93	0.9911	0.0007	0.07
100	0.992	0.008	35126	923	111.99	0.9911	0.0007	0.07
50	0.992	0.008	70783	1824	114.53	0.9913	0.0005	0.05
5	0.992	0.008	640613	14954	127.95	0.9922	-0.0004	-0.04
20	0.992	0.008	160788	3820	125.47	0.9921	-0.0002	-0.02
10	0.992	0.008	343720	8499	119.98	0.9917	0.0001	0.01
150	0.997	0.003	28375	244	375.78	0.9973	-0.0004	-0.04
100	0.997	0.003	40887	360	366.54	0.9973	-0.0003	-0.03
50	0.997	0.003	72182	643	361.45	0.9972	-0.0003	-0.03
10	0.997	0.003	301045	2633	368.69	0.9973	-0.0003	-0.03
75	0.998	0.002	42867	316	441.54	0.9977	0.0002	0.02
50	0.998	0.002	60312	447	439.01	0.9977	0.0003	0.03
10	0.998	0.002	302363	2046	483.06	0.9979	0.0001	0.01
7	0.998	0.002	406891	2674	497.93	0.9980	0.0000	0.00
50	0.999	0.001	87120	280	1054.97	0.9991	0.0000	0.00
20	0.999	0.001	191009	596	1091.28	0.9991	0.0000	0.00
10	0.999	0.001	385266	1118	1177.72	0.9992	0.0000	0.00

6.3. VLE test system measurements and modelling

Before measurements of the new VLE data for systems of interest could commence, test systems were measured using the newly designed VLE equipment to test its reliability and gain expertise on the techniques. The equipment used allowed measurements to be conducted on either the static analytic mode or the static synthetic mode (for bubble point measurements). The sections which follow present the experimental data along with the literature and model results. Error bars affecting pressures and molar fractions of the measured VLE data (for both test and new systems) are systematically added in the figures, but sometimes these are not visible because of the small values.

The thermodynamic modelling applied used five models, namely the cubic plus association (CPA), (Peng Robinson) (PR), Peng Robinson Wong Sandler (PRWS) and Soave-Redlich-Kwong (SRK)

equations of state, and the perturbed-chain statistical associating fluid theory (PC-SAFT). This was conducted using Aspen Plus V11 and subsequently Aspen Plus V12. This was due to some issues with running the V11 software. Temperature-dependent binary interaction parameters for all the models have been used and are represented as k_{ij} , where i and j represent specific components. Unless otherwise stated, all regressed parameters are in SI units. The maximum-likelihood objective function was used for data correlation with either the Deming or New Britt-Luecke algorithm and the Deming or the Weighted least squares initialization method. Details of the algorithms used can be found in the Aspen Plus V12 support files. The expressions for the maximum-likelihood objective functions that were used for the TPx data and $TPxy$ data are presented in equations (6-1) and (6-2), respectively. Additionally, the Predictive Soave-Redlich-Kwong (PSRK) model proposed by Holderbaum and Gmehling (Holderbaum and Gmehling, 1991) was used to predict phase equilibria data on binary systems of this study.

$$Obj F = \sum_{n=1}^{NDG} w_n \sum_{i=1}^N \left[\left(\frac{T_{Calc,i} - T_{Exp,i}}{\sigma_{T,i}} \right)^2 + \left(\frac{P_{Calc,i} - P_{Exp,i}}{\sigma_{P,i}} \right)^2 + \sum_{j=1}^{NC-1} \left(\frac{x_{Calc,i,j} - x_{Exp,i,j}}{\sigma_{x,i,j}} \right)^2 \right] \quad (6-1)$$

$$Obj F = \sum_{n=1}^{NDG} w_n \sum_{i=1}^N \left[\left(\frac{T_{Calc,i} - T_{Exp,i}}{\sigma_{T,i}} \right)^2 + \left(\frac{P_{Calc,i} - P_{Exp,i}}{\sigma_{P,i}} \right)^2 + \sum_{j=1}^{NC-1} \left(\frac{x_{Calc,i,j} - x_{Exp,i,j}}{\sigma_{x,i,j}} \right)^2 + \sum_{j=1}^{NC-1} \left(\frac{y_{Calc,i,j} - y_{Exp,i,j}}{\sigma_{y,i,j}} \right)^2 + \right] \quad (6-2)$$

Where: $Obj F$ is the objective function minimised by data regression

NDG is the number of data groups in the regression case

w_n is the weight of the data group n

N is the number of data points in group n

NC is the number of components present in the data group

T, P, x, y represents the temperature, pressure, liquid mole fraction and vapour mole fraction

$Calc$ represents calculated data

Exp represents experimentally measured data

i is data for data point i

j is fraction data for component j

σ is the standard deviation of the data.

For all the models assessed in this work, the quality of the data fit was quantified by using either the absolute average deviation (AAD) or the absolute average relative deviation (AARD), and these are defined as:

$$AAD(\theta) = \frac{1}{N} * \sum |Exp(\theta) - Calc(\theta)| \quad (6-3)$$

$$AARD(\theta) = \left(\frac{1}{N}\right) * \sum \frac{|Exp(\theta) - Calc(\theta)|}{Exp(\theta)} \quad (6-4)$$

Where θ is the parameter under consideration, Exp is the experimentally measured value, Calc is the calculated value, N is the number of data points.

Pure component parameters (critical pressure, critical temperature, and acentric factor) for components of this study are presented in Tables B.3-1 to 2 (Appendix B). Table B.3-3 presents the MC alpha function parameters. The CPA pure component properties predictions (vapour pressure and density) are also presented in Appendix F.

6.3.1 Carbon dioxide (1) + n-hexane (2) test system

Several binary VLE measurements for the carbon dioxide (1) + n-hexane (2) system have been undertaken by numerous authors; hence there is significant literature data on this system. This informed its choice as one of the test systems of this study to prove the functionality of the newly designed static analytic/synthetic visible horizontal variable volume cell and the research methodologies applied thereof for further use in the novel systems measurements of the study. The VLE measurement and model prediction results for the carbon dioxide + n-hexane system are displayed in Figure 6-9, along with the reported data from literature and listed in Table B.4-1 (Appendix B). For this system, both the static synthetic method (bubble point measurement) and the static analytic method were used. The GC method used for the analytic method is outlined in section 5.2.3.

The VLE data that has been measured in this work is labelled *This work* with extensions to classify whether this was bubble point data (visual point) or analytical data. Figure 6-9 shows a comparison of the experimentally measured data and data reported in the literature.

The P - x data from this work matches well to literature data of (Williams-Wynn et al., 2016) measured by the static analytic apparatus, although there are some slightly higher pressures on the bubble point data points between 0.2 and 0.4 moles compared to the bubble point data measured by (Williams-Wynn et al., 2016) with the static synthetic apparatus used in that study. It is also notable that both the bubble point data (TP_x synthetic) and the (TP_{xy} analytic) data measured in this work agrees well with the TP_{xy} data measured by (Chen and Chen, 1992; Li et al., 1981; Nelson et al., 2021; Wagner and Wichterle,

1987) and the PSRK-model as shown in Figure 6-9. The associated uncertainties for the measured variables are also presented in Table B.4-1 (Appendix B).

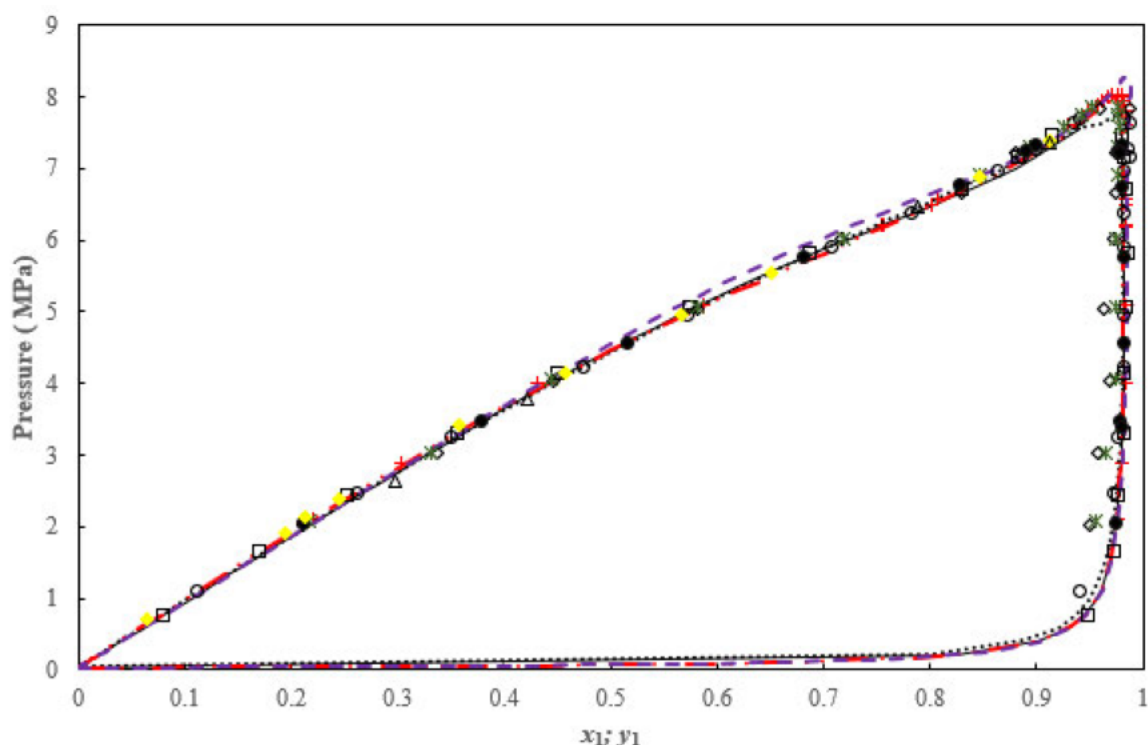


Figure 6-9: TP_{xy} plot for the CO_2 (1) + n-hexane (2) system.

This work analytic at 313.19 K (\bullet); This work, visual point (P-x) at 313.20 K (\blacklozenge); (Williams-Wynn et al., 2016) at 313.12 K (\circ); (Chen and Chen, 1992) at 313.15 K (\diamond); (Li et al., 1981) at 313.14 K (\square); (Wagner and Wichterle, 1987) at 313.14 K (\otimes); (Nelson et al., 2021) at 313.15 K ($+$); (Williams-Wynn et al., 2016) bubble point at 313.21 K (Δ); PSRK model at 313.15 K (Solid continuous black line); CPA model at 313.20 K ($- - -$); PRWS model at 313.20 K ($- \cdot -$); PC-SAFT model at 313.20 K (\cdots).

For the data of Li et al. (Li et al., 1981), temperatures were estimated to be accurate to ± 0.05 K, reported pressures are estimated to be accurate to ± 0.0138 MPa and for composition, the maximum average absolute deviation was reported as 3.3%. For the data of Wagner and Wichterle (Wagner and Wichterle, 1987), temperatures were estimated to be accurate to ± 0.002 K, reported pressures were estimated to be accurate to ± 0.002 MPa, and accuracy of composition determination was 1% of the smallest mole fraction in the mixture. The data of Williams-Wynn et al. (Williams-Wynn et al., 2016) has been reported with an expanded uncertainty in temperature $U(T)$ of 0.08 K, expanded uncertainty in pressure $U(P)$ of 0.010 MPa, and the expanded uncertainty in liquid and vapour composition $U(x_1)$ of 0.008 and $U(y_1)$ of 0.0025 respectively. The data of Nelson (Nelson et al., 2021) has been reported with an expanded uncertainty in temperature $U(T)$ of 0.08 K, expanded uncertainty in pressure $U(P)$ of 0.002 MPa ($P > 0.5$ MPa); $U(P)$ of 0.4 kPa ($P < 0.5$ MPa).

For the vapour phase data, it can be noted that there are significant discrepancies between the literature sources. This is illustrated in the relative volatility plots versus composition (Figure 6-10) and the expanded P-y plot (see Figure C-1 in Appendix C). This indicates the difficulty in calibration, sampling, and analysis of the vapour phase (Nelson et al., 2021) .

Figure 6-10 shows that the relative volatility data for this work agrees well with the literature data by Li et al. (Li et al., 1981), Nelson et al. (Nelson et al., 2021), and the PSRK model. There is a slight deviation of approximately 5% between the data of this work and that of Williams-Wynn et al. (Williams-Wynn et al., 2016) at x_1 below 0.3. The relative volatility data for this work does not match the data of (Chen and Chen, 1992; Wagner and Wichterle, 1987) except for x_1, y_1 above 0.8 as can be observed in Figure 6-10.

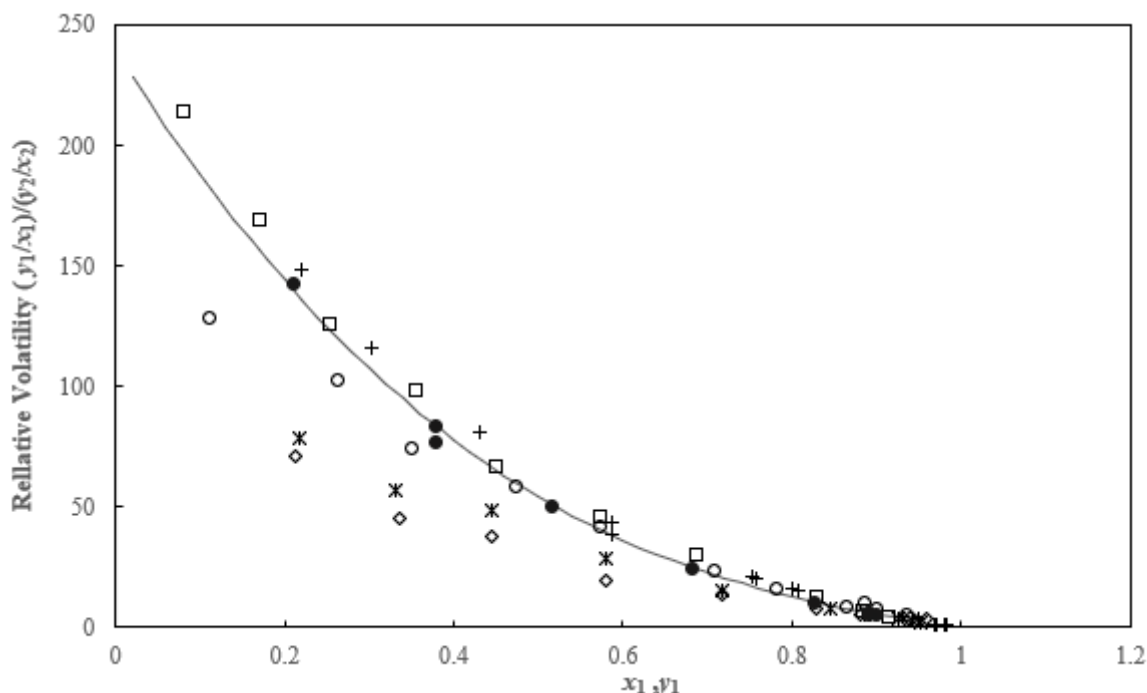


Figure 6-10: Relative volatility versus composition of CO₂ (1) + n-hexane (2) system.

This work at 313.19 K (●) ; Williams-Wynn et al. (Williams-Wynn et al., 2016) at 313.12 K (○); Chen and Chen (Chen and Chen, 1992) at 313.15 K (◇); Li et al. (Li et al., 1981) at 313.14 K (□); Wagner and Wichterle (Wagner and Wichterle, 1987) at 313.14 K (*); Nelson et al. (Nelson et al., 2021) at 313.15 K (+); PSRK model at 313.15 K (Solid continuous black line).

The trends observed in Figure 6-10 are similar to those of Figure C-1 in Appendix C. Figure C-1 shows an excellent agreement between the data of this work and that of Li et al. (Li et al., 1981), Nelson et al. (Nelson et al., 2021), and the PSRK model, with some slight deviation to the data of Williams-Wynn et al. (Williams-Wynn et al., 2016). Figure C-1 shows that most of the data measured by (Chen and Chen,

1992; Wagner and Wichterle, 1987) do not agree with the data measured in this work, except for two data points. Table B.4-1 (Appendix B) presents relative volatility uncertainty for the carbon dioxide (1) + n-hexane (2) system.

Figure 6-9 shows that there is good agreement between the experimental data and model predictions via the PSRK, CPA, PRWS, and PC-SAFT models. The regressed model parameters and deviations are presented in Table 6-12. The AARD % in pressures for all the models (PC-SAFT, PRWS and CPA) are below 1%, indicating an excellent prediction of the phase equilibria data for the carbon dioxide + n-hexane system by the models. Figure C-1 also shows a good comparison between the data of this work and that of the PSRK model prediction.

Table 6-12: Regressed model parameters and deviations for the CO₂ (1) + n-hexane (2) system.

PC-SAFT		PRWS		CPA	
$T = 313.19 \text{ K}$		$T = 313.19 \text{ K}$		$T = 313.19 \text{ K}$	
Parameter	Value	Parameter	Value	Parameter	Value
k_{12}	0.0164	k_{12}	0.5451	k_{12}	0.1219
m_1	3.1737	A_{12}	2.5853		
δ_1	2.5278	A_{21}	-0.2858		
ϵ_1	134.7839				
m_2	5.5145				
δ_2	2.5624				
ϵ_2	178.7767				
$\beta^{A_i B_i}$	0				0
$\epsilon^{A_i B_i}$	0				0
AAD P (MPa)	0.01		0.01		0.04
AARD P %	0.02		0.30		0.79
AAD x_1	0.0005		0.0008		0.0017
AARD x_1 %	0.11		0.18		0.44
AAD y_1	0.0009		0.0009		0.0038
AARD y_1 %	0.10		0.09		0.39
AAD T (K)	0.07		0.59		0.68
AARD T %	0.19		1.47		1.69

Model parameters are defined in Appendix D. All values are in S.I units.

Aspen Plus V12 was used for the PRWS modelling and the regressed binary interaction parameter k_{12} of this work of 0.5451 is comparable to the reported k_{12} of 0.5628 by Nelson et al. (Nelson et al., 2021).

For the PC-SAFT model, the regressed binary interaction parameter k_{12} of this work of 0.0164 is not comparable with the value reported by Teymouri (Teymouri, 2016) of 0.1294 which the authors applied to a wide temperature range of 90 to 360.93 K. The regressed pure component parameter $m_1 = 3.1737$

is comparable to the reported literature value of 2.782 by Gross and Sadowski (Gross and Sadowski, 2001), as well as the m_2 parameter of this work 5.5145 is comparable to 4.6627 reported by Gross and Sadowski (Gross and Sadowski, 2001). The m and δ pure component parameters of this work in Table 6-12 can be compared with literature reported values in Appendix D, Table D-5.

For the CPA model, the regressed binary interaction parameter k_{12} of this work of 0.1219 is comparable to the literature reported data by Tsivintzelis and Kontogeorgis (Tsivintzelis and Kontogeorgis, 2016) of 0.1200.

6.3.2 Carbon dioxide (1) + n-decane (2) test system

The carbon dioxide + n-decane system was chosen as a test system as n-decane has a much higher boiling point than carbon dioxide and a high viscosity than water. These features are similar to the TEG and carbon dioxide system in this work, albeit the boiling point and the viscosity of TEG is significantly higher than n-decane. Measurement of the phase behaviour of the test system was to provide an insight into how the equipment and the experimental method would relate to higher boiling point solvents due to the high relative volatility of the systems and the effect of the substantial viscosity on the stirring in the cell. The study of systems containing hydrocarbon + carbon dioxide is important for the petrochemical industry, chemical industry, and enhanced oil recovery (Jiménez-Gallegos et al., 2006). There is not much published VLE literature data for this system at 319.15 K, a temperature range within this study's scope. Jimenez-Gallegos et al. (Jiménez-Gallegos et al., 2006) and Zilnik et al. (Žilnik et al., 2016) measured VLE data for the carbon dioxide + n-decane system at 319.15 K, and their published data are provided in Figure 6-11 together with new experimental data from this study. Jimenez-Gallegos et al. (Jiménez-Gallegos et al., 2006) obtained their experimental data using a static analytic method that made use of a GC (HP 6890) with a TCD and a Porapak Q-packed column for analysis. Zilnik et al. (Žilnik et al., 2016) obtained their experimental data using a versatile apparatus that made it possible to use different methods such as synthetic and analytic methods. Their apparatus was used with either a fixed volume or a variable volume and it allowed visual observation of the entire contents of the equilibrium cell. For the data of Zilnik et al. (Žilnik et al., 2016), the temperature was measured within an expanded uncertainty of $U(T)$ of 0.04 K, pressure measurements were estimated within an expanded uncertainty ($U(P)$) of 0.005 MPa, and the composition expanded uncertainties were within ± 0.0005 for both the liquid and vapour composition. For this system, the static analytic method was used and the GC method used is outlined in section 5.2.3. Experimental VLE data for the carbon dioxide + n-decane system are listed in Table B.4-2 (Appendix B) and displayed in Figure 6-11.

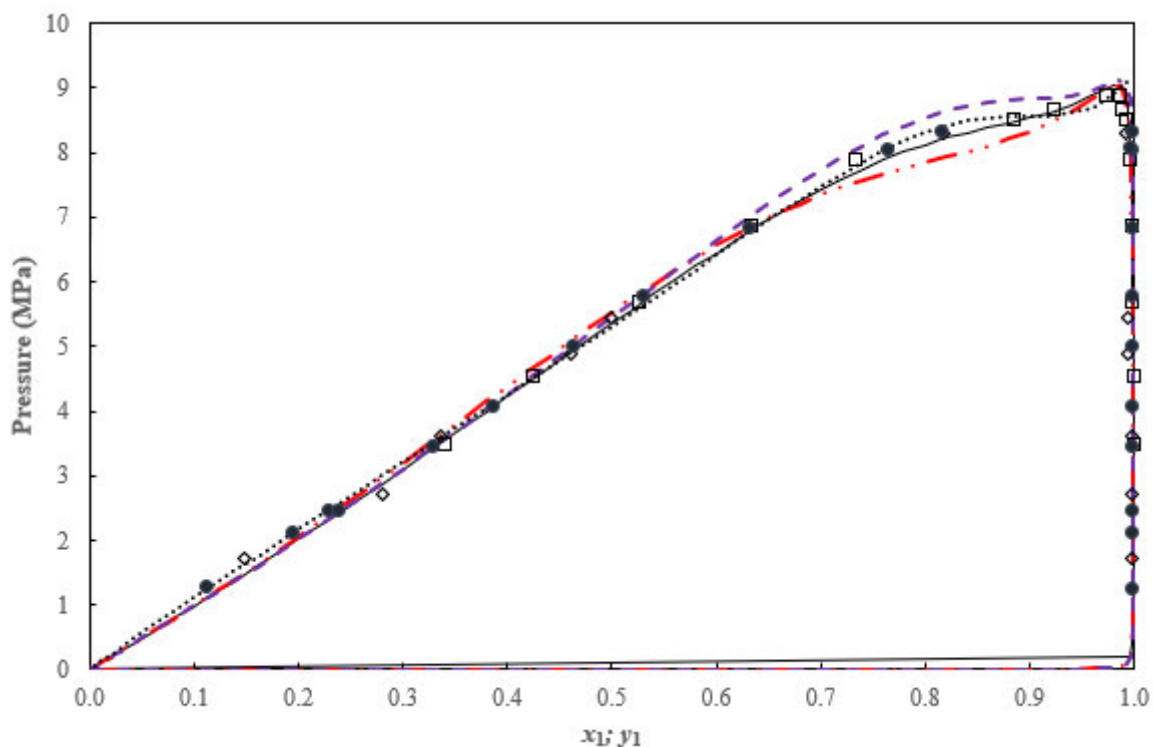


Figure 6-11: TP_{xy} plot for the CO_2 (1) + n-decane (2) system.

This work at 319.23 K (●); (Jiménez-Gallegos et al., 2006) at 319.11 K (□); (Žilnik et al., 2016) at 319.10 K (◇); PSRK model at 319.15 K (continuous solid black line); PC-SAFT model (····); PRWS model at 319.23 K (- · - ·); CPA model at 319.23 K (- - -).

Figure 6-11 shows a comparison of the experimentally measured and reported data. The liquid phase data (P - x) measured in this work matches well with the literature data of Jimenez-Gallegos et al. (Jiménez-Gallegos et al., 2006), and Zilnik et al. (Žilnik et al., 2016). The data of Jimenez-Gallegos et al. (Jiménez-Gallegos et al., 2006) and that of Zilnik et al. (Žilnik et al., 2016) were correlated with the cubic spline interpolation and this was then used to interpolate carbon dioxide mole fractions at the same pressures as those of this work. Comparison showed that there was a 3.7% overall absolute average relative deviation between the data of Jimenez-Gallegos et al. (Jiménez-Gallegos et al., 2006) and that of this work, and 3.1% overall AARD between the data of Zilnik et al. (Žilnik et al., 2016) and that of this work. The discrepancies are most likely attributed to the slight differences in temperatures between the data of this work and the reported literature data.

The vapour phase P - y data was analysed with the aid of Figure C-2 (Appendix C) and the relative volatility vs composition plot (Figure 6-12). Figure C-2 shows that the vapour phase data (P - y) agrees well with literature data of Jimenez- Gallegos et al. (Jiménez-Gallegos et al., 2006) and the PSRK despite a slight deviation on some of the data points. In addition, it is evident from Figure C-2 that there

are discrepancies between the vapour phase data presented by Jimenez-Gallegos et al. (Jiménez-Gallegos et al., 2006) and Zilnik et al. (Žilnik et al., 2016).

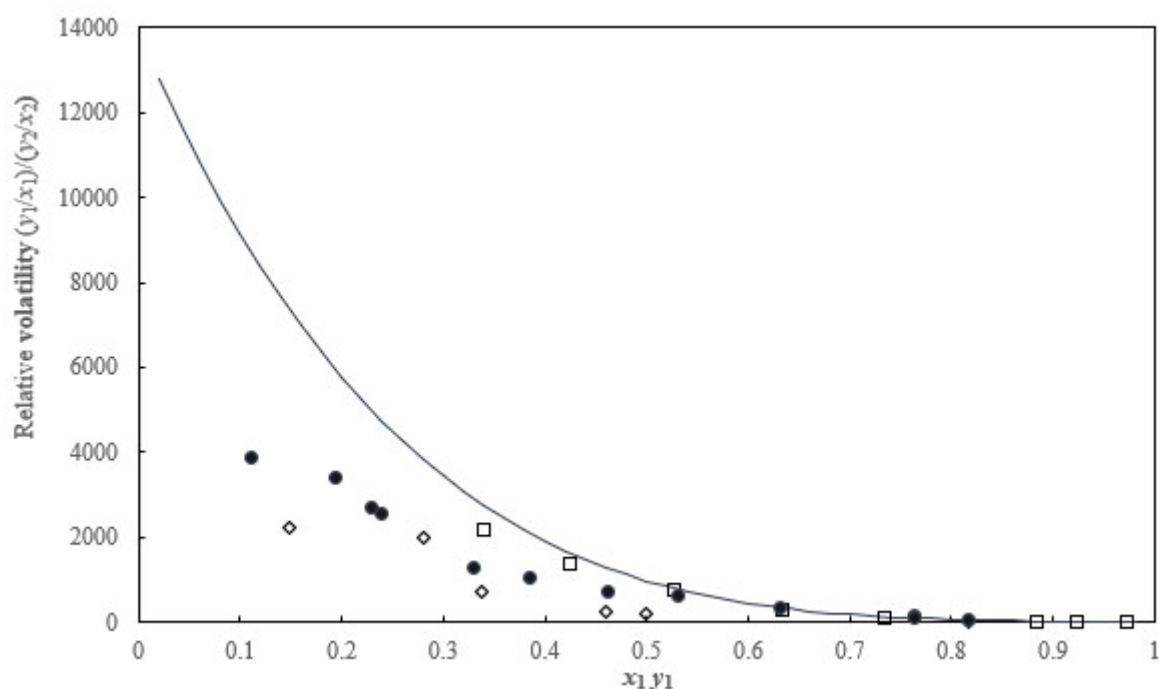


Figure 6-12: Relative volatility for the CO₂ (1) + n-decane (2) test system.

This work at 319.23 K (●); Jimenez-Gallegos et al. (Jiménez-Gallegos et al., 2006) at 319.11 K (□) ; Zilnik et al. (Žilnik et al., 2016) at 319.10 K (◇); PSRK model at 319.15 K (continuous solid black line).

Figure 6-12 shows that for x_1, y_1 greater than 0.5, the relative volatility calculated for this work matches well to the PSRK model prediction and the data of Jimenez-Gallegos et al. (Jiménez-Gallegos et al., 2006). For x_1, y_1 between 0 and 0.5 there is a deviation of the relative volatility data from the majority of the literature data considered in this work. Relative volatility data is also presented in Table B.4.2 (Appendix B).

Figure 6-11 shows that there is good agreement between the experimental data and model predictions via the PSRK, CPA, PC-SAFT and PRWS models. In addition, Figure 6-11 shows that there is some slight deviation for the PRWS model prediction from the experimental data of this work and other literature sources. The PRWS gives poor prediction near the critical point for this system between x_{CO_2} of 0.7 to 0.9, which is a known deficiency of the model. For the PRWS, modelling was performed using Aspen Plus V12. There was a 0.5% overall AARD (P) between the PSRK model and the data of this work. This shows that the data measured in this work is in good agreement with the models considered. The pressure, temperature, and composition uncertainty data are presented in Table B.4.2 (Appendix B). Table 6-13 shows the regressed model parameters and deviations. The AARD in pressures for the

CPA, PC-SAFT models are all below 1%. The AARD for the PRWS model is 1.62%. All this suggests a good agreement between the model predictions and the data of this work.

Table 6-13: Regressed model parameters and deviations for the CO₂ (1) + n-decane (2) system.

PC-SAFT		PRWS		CPA	
T = 319.23 K		T = 319.23 K		T = 319.23 K	
Parameter	Value	Parameter	Value	Parameter	Value
k_{12}	0.1628	k_{12}	0.6934	k_{12}	0.1148
m_1	0.4673	A_{12}	4.7486		
δ_1	5.8128	A_{21}	-0.2912		
ε_1	254.6				
m_2	1.0553				
δ_2	6.6144				
ε_2	580.1933				
$\beta^{A_i B_i}$	0				
$\varepsilon^{A_i B_i}$	0				
AAD P (MPa)	0.03		0.08		0.08
AARD P %	0.70		1.62		1.71
AAD x_1	0.0016		0.0025		0.0028
AARD x_1 %	0.49		0.84		1.01
AAD y_1	0.0002		0.0006		0.0007
AARD y_1 %	0.02		0.06		0.07
AAD T (K)	0.84		1.60		2.26
AARD T %	1.81		3.48		4.91

All values in SI units

The regressed binary interaction parameter k_{ij} for the PC-SAFT model of 0.1628 is comparable to the literature value of 0.1417 reported by Justo-Gar'cia et al. (Justo-García et al., 2008) for a temperature range of 277-510 K.

6.3.3 Carbon dioxide (1) + methanol (2) test system

Besides TEG, methanol is also one of the main liquid components of the current study; hence a test system involving methanol was considered. As highlighted in section 2.3.1.7, there is a significant number of reported phase equilibria data for the carbon dioxide + methanol system in the open literature, thus making it a good test system. In this work, for the carbon dioxide + methanol system, bubble point measurements were performed at 298.10 K and 313.15 K using the static synthetic method, and the results are listed in Table B.4-3 (Appendix B) and displayed in Figures 6-13 and 6-14, respectively. The uncertainty of such a system was estimated at a 95% level of confidence.

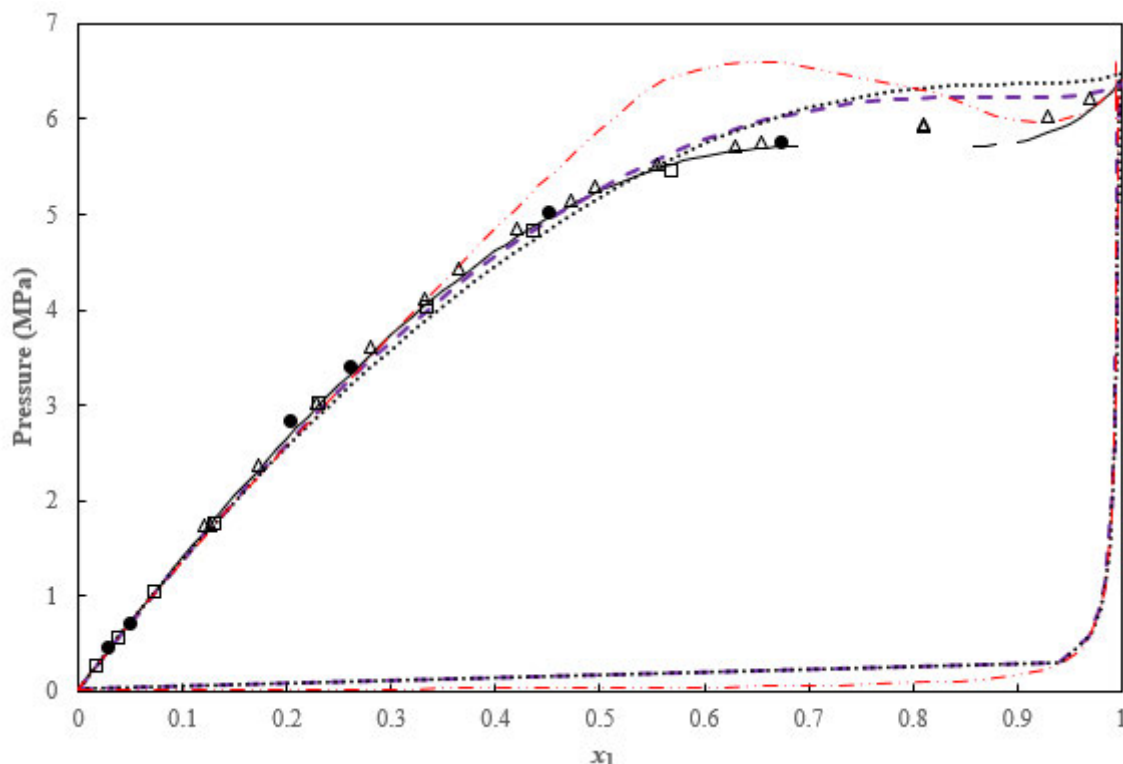


Figure 6-13: TP_{xy} data for CO_2 (1) + CH_3OH (2) system.

This work at 298.10 K (●); Chang and Rousseau (Chang and Rousseau, 1985) at 298.14 K (□); Brunner et al. (Brunner et al., 1987) at 298.14 K (Δ); PSRK model (—); PC-SAFT model (····); PRWS model (— · —); CPA model (— — —).

Figure 6-13 shows a very good comparison of the experimentally measured and reported data by Brunner et al. (Brunner et al., 1987), Chang and Rousseau (Chang and Rousseau, 1985). Furthermore, the Figure shows that there is good agreement between the experimental data and model predictions via the PSRK, CPA, and PC-SAFT models. For the PRWS model prediction, there is a noticeable deviation from the measured data in this work, especially between x_1 of 0.45 to x_1 of 0.9, with relatively good agreement on the rest of the phase envelope. Overall, all models show reasonable agreement with the data of this work as is shown in Table 6-14 where the AAD and AARD in pressures and composition from the correlated experimental data are listed. It can be noted that the AARD in pressure for all the three models is less than 1% (see Table 6-14).

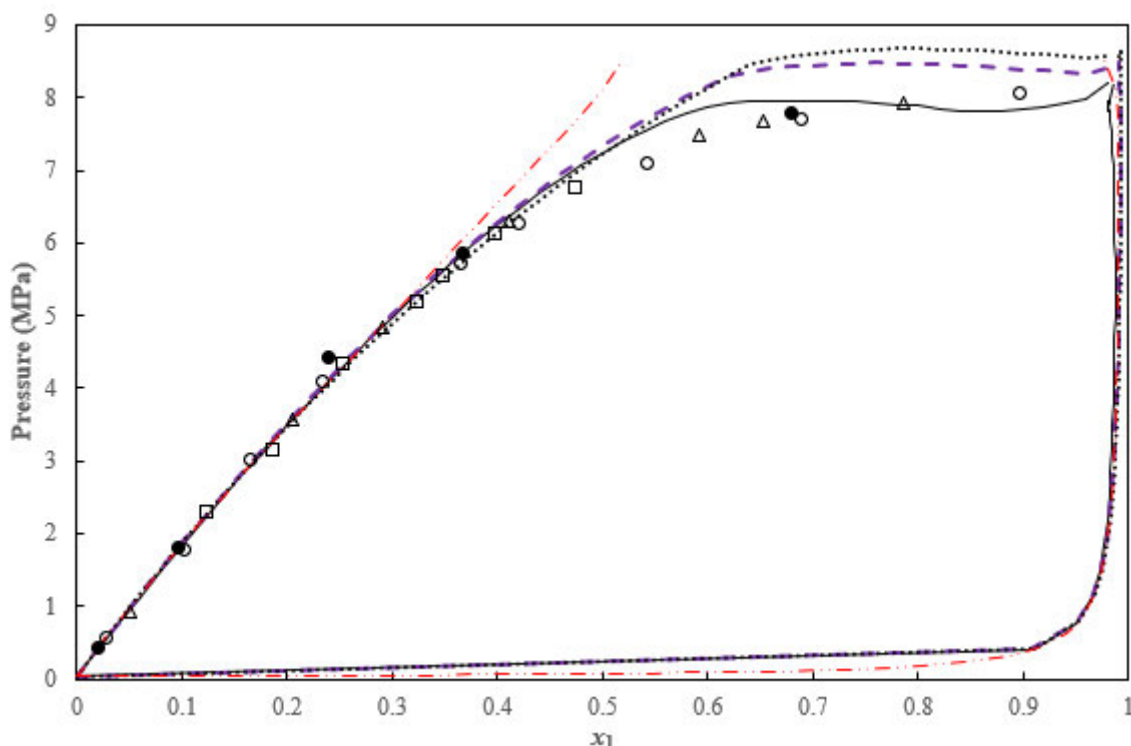


Figure 6-14: TP_{xy} data for CO_2 (1) + CH_3OH (2) system.

This work at 313.15 K (●); (Ohgaki and Katayama, 1976) at 313.09 K (○); (Naidoo et al., 2008) at 313.15 K (□); (Xie et al., 2005) at 313.2 K (Δ); PSRK model at 313.15 K (continuous solid black line); PC-SAFT model (····); PRWS model at 313.15 K (— · —); CPA model at 313.15 K (— — —).

Figure 6-14 shows a very good comparison of the experimentally measured and reported data by Naidoo et al. (Naidoo et al., 2008), Ohgaki and Katayama (Ohgaki and Katayama, 1976) and Xie et al. (Xie et al., 2005). Moreover, the Figure shows that there is good agreement between the experimental data and model predictions via the PSRK, CPA, PC-SAFT, and PRWS models. Model parameters employed in this work are presented in Table 6-14 together with the AAD and AARD in pressures and composition. Despite providing a good fit, the PRWS model does not predict the critical point very well for this system, as illustrated in Figures 6-13 and 6-14. Generally, most models are not able to perform the correlations in the critical region due to similar densities of the phases; hence the two-phase fluid becomes a one-phase fluid.

For the PRWS model, Aspen V12 was used and the maximum likelihood objective function with the Deming algorithm and the Deming initialisation method was used. Constraints were not tightly satisfied for the results produced by the Britt-Luecke algorithm, hence the use of the Deming algorithm. For all three models (PRWS, CPA and PC-SAFT), there is a decrease in the absolute value of k_{ij} with an increase in temperature (see Table 6-14).

Table 6-14: Regressed model parameters and deviations for the CO₂ (1) + CH₃OH (2) system.

PRWS model			CPA model		PC-SAFT model		
<i>Parameter</i>	<i>T</i> = 298.10 K	<i>T</i> = 313.15 K	<i>T</i> = 298.10 K	<i>T</i> = 313.15 K	<i>Parameter</i>	<i>T</i> = 298.10 K	<i>T</i> = 313.15 K
k_{12}	0.5401	0.5138	-0.1128	-0.11593	k_{12}	-0.00524	0.000607
A_{12}	-0.7936	-0.5917			$(\epsilon^{A_2B_2})$	6562.473	
A_{21}	1.4531	1.2845			$(\beta^{A_2B_2})$	0.00000015	
AAD <i>P</i> (MPa)	0.01	0.02	0.02	0.03	AAD <i>P</i> (MPa)	0.03	0.04
AARD <i>P</i> %	0.38	0.55	0.58	0.58	AARD <i>P</i> %	0.75	0.82
AAD x_1	0.0056	0.0009	0.0009	0.0008	AAD x_1	0.0014	0.0012
AARD x_1 %	6.14	0.39	0.42	0.35	AARD x_1 %	0.62	0.61
AAD <i>T</i> (K)	0.01	3.26	0.01	2.02		0.01	2.29
AARD <i>T</i> %	0.46	1.04	0.00	0.65		0.00	0.73

For the CPA modelling, using the Aspen Plus Analysis function and flash calculations, the results for the CO₂ + CH₃OH system at 298.10 K were compared using either the k_{ij} reported in this work or the literature k_{ij} of 0.0384 reported by (Kontogeorgis and Folas, 2010). The results are displayed in Figure E-1.1 Appendix E. In both cases the Analysis and flash results match well, and those obtained using k_{ij} of this work are close to the experimental data. As a result, the binary k_{ij} from this work, can be extended to model multicomponent mixtures involved in this study.

6.3.4 Methane (1) + methanol (2) test system

There is considerable literature data for the methane + methanol system as shown in section 2.3. In this work, bubble point measurements were conducted for the methane + methanol system at 298.15 K and 303.15 K, using the static synthetic method, the results of which are listed in Table B.4-4 (Appendix B) and displayed in Figure 6-15.

Figure 6-15 shows a very good comparison of the experimentally measured and reported data. Only data for one literature source (Wang et al., 2003) for this system at 303.15 K is presented in the open literature.

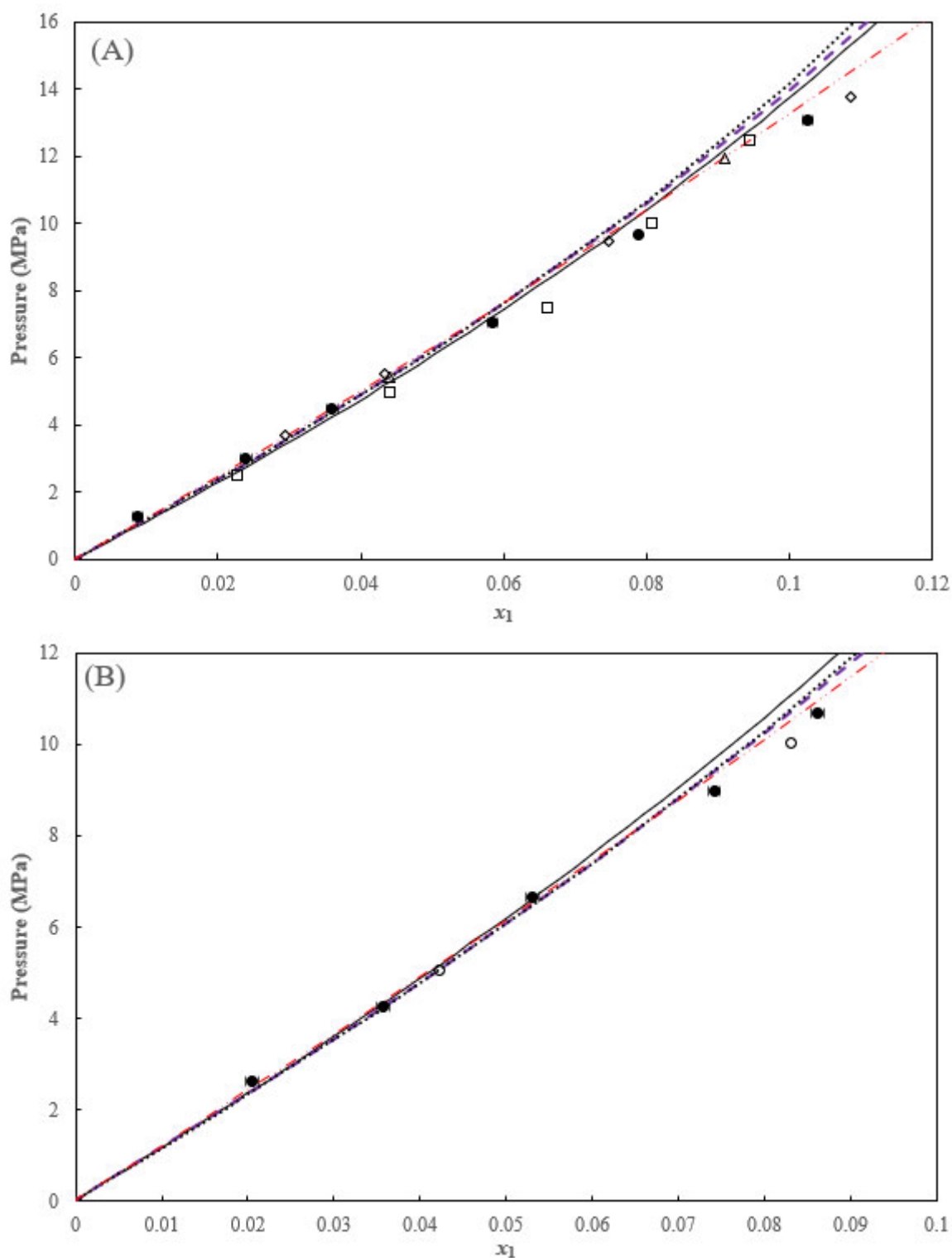


Figure 6-15: TPx graph for the CH_4 (1) + CH_3OH (2) test system.

(A): data at 298.15 K, (●) This work; (□) Yarym-Agaev et al. (Yarym-Agaev et al., 1985); (○) Brunner et al. (Brunner et al., 1987); (◇) Frost et al. (Frost et al., 2015) ; (B) data at 303.15 K; (●) This work; (○) Wang et al. (Wang et al., 2003). For both figures; solid continuous lines represent the PSRK model; CPA model (---); PRWS model (- · - ·); PC-SAFT model (····).

The data were modelled in Aspen Plus V12. Figure 6-15 shows that there is good agreement between the experimental data and model predictions via the PSRK, CPA, PRWS, and PC-SAFT models. The regressed model parameters and deviations are presented in Table 6-15. The AARD in pressures for all the models (PC-SAFT, PRWS and CPA) are below 3.5 %, indicating good prediction of the phase equilibria data for the CH₄ + CH₃OH system by the models. The PRWS model performed much better than the association models (PC-SAFT and CPA) since the AARD % in pressure are all below 2% for the PRWS model. The regressed binary interaction parameters k_{ij} for the PRWS model increase with an increase in temperature. However, for the PRWS, the regressed k_{ij} values are not statistically different since a similar trend can be observed when the k_{ij} from the regressed data at 303.15 K was used to predict the data at 298.15 K, see Appendix E, Figure E.1. For both the CPA and PC-SAFT models, the binary interaction parameters decrease with an increase in pressure. The regressed k_{ij} for the CPA and PC-SAFT models seems to be statistically different considering that there are slight differences in the trends when the k_{ij} from the regressed data at 303.15 K was used to predict the data at 298.15 K. However, the k_{ij} from regressed data at 303.15 K seems to yield a better fit to the experimental data at 298.15 K than the regressed k_{ij} at 298.15 K, see Appendix E, Figures E.1 and E.2. The regressed binary interaction parameters for the PC-SAFT model presented in Table 6-15 are comparable to the reported k_{ij} value of 0.042 by (Fouad and Berrouk, 2013).

Table 6-15: Regressed binary interaction parameter (k_{12}) for the CH₄ (1) + CH₃OH (2) system.

PRWS model			CPA model		PC-SAFT model		
	$T = 298.15 \text{ K}$	$T = 303.15 \text{ K}$	$T = 298.15 \text{ K}$	$T = 303.15 \text{ K}$		$T = 298.15 \text{ K}$	$T = 303.15 \text{ K}$
k_{12}	0.3178	0.3423	0.0550	0.0462	k_{12}	0.0549	0.0498
A_{12}	14.1634	13.9922			$(\epsilon^{A_2B_2})$		
A_{21}	1.2922	1.1915			$(\beta^{A_2B_2})$		
AAD P (MPa)	0.09	0.09	0.16	0.12	AAD P (MPa)	0.18	0.12
AARD P %	1.86	1.65	3.07	2.04	AARD P %	3.32	2.14
AAD x_1	0.0008	0.0006	0.0015	0.0010	AAD x_1	0.0017	0.0010
AARD x_1 %	2.63	1.16	4.00	1.65	AARD x_1 %	4.31	1.79
AAD T (K)	2.56	1.60	3.17	2.09		3.25	2.42
AARD T %	0.86	0.53	1.06	0.69		1.09	0.80

The CPA modelling, that is the Aspen Plus Analysis function and flash calculations results for the CH₄ + CH₃OH system at 298.15 K was compared using either the k_{ij} of this work (0.04045) or the literature k_{ij} of 0.01 reported by (Yan et al., 2007). The results are displayed in Figure E-1.2 Appendix E. In both

cases the analysis and flash results are matching, and those obtained using k_{ij} of this work are close to the experimental data. As a result, the binary k_{ij} from this work, can be extended to model multicomponent mixtures involved in this study.

6.3.5 Methane (1) + TEG (2) test system

There is limited data for this system in the open literature, as shown in chapter 2, section 2.3. It was necessary to measure data for this system despite the few reported data since methane and TEG are key components in the present study. The binary phase equilibria data for the methane + TEG system also forms the basis for comparing multicomponent systems that consist of these components.

In this work, bubble point measurements were performed for the methane + TEG system at 298.15 K and 323.15 K using the static synthetic method. The VLE data measured for this test system is displayed in Figure 6-16 together with the reported literature data. The data of this work is also presented in Table B.4-5 (Appendix B), together with the associated uncertainties for the measured variables.

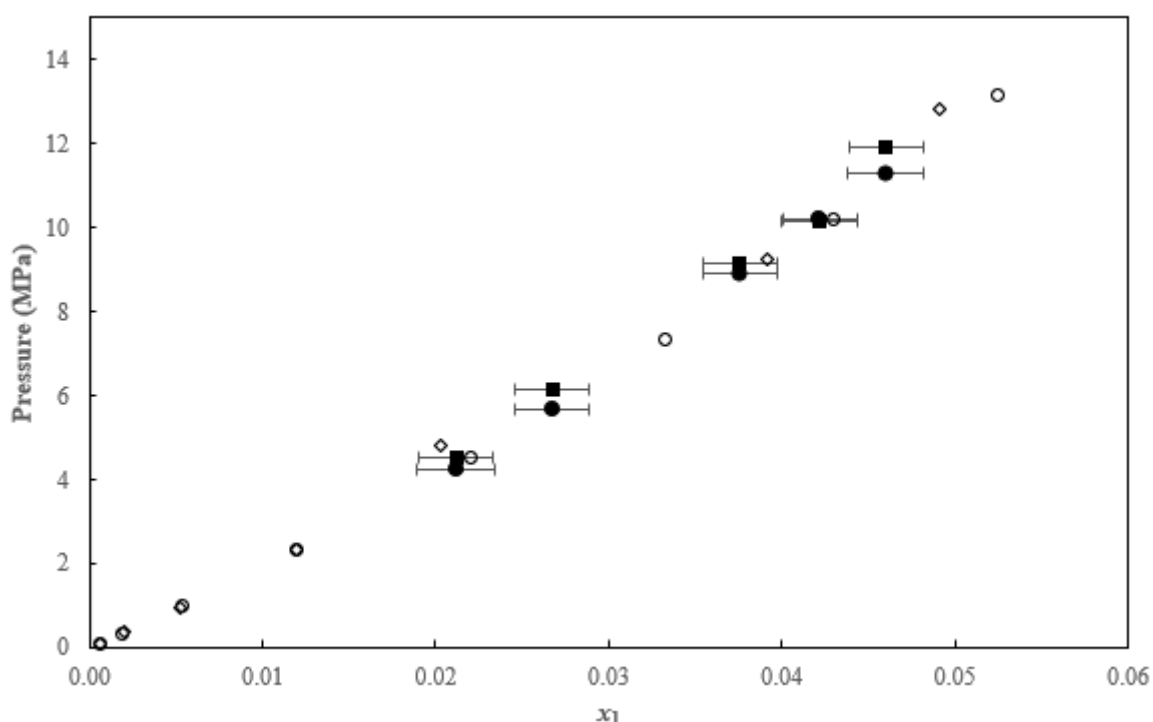


Figure 6-16: TPx graph for the CH_4 (1) + TEG (2) test system.

This work 298.15 K (■); This work 323.15 K (●); Jou et al. (Jou et al., 1987), at 298.15 K (◇); Jou et al. (Jou et al., 1987) , 323.15 K (○).

The composition uncertainty for methane is represented by error bars in Figure 6-16. Compositional errors for methane are significant due to the inherent significance of the mass balance uncertainty which is set at 0.01 g, considering that the masses of methane loaded in the methane + TEG mixture are very small.

Figure 6-16 shows a very good comparison of the experimentally measured and reported data of Jou et al. (Jou et al., 1987). It is also important to note that there has been some scatter in the data of Jou et al. (Jou et al., 1987) at 298.15 K, and the data of this work for both isotherms. However, despite the scatter, the data of Jou et al. (Jou et al., 1987) lie within the composition uncertainty of this work as indicated by the error bars, suggesting good agreement between the data sets.

The data was modelled in Aspen Plus V12 and is presented in Figure 6-17. The regressed model parameters and deviations are presented in Table 6-16. Figure 6-17 both (A) and (B) shows that there is good agreement between the experimental data and model predictions via the CPA, PRWS, and PC-SAFT models. Figure 6-17, both (A) and (B) also shows that the agreement between the experimental data and the PSRK model prediction is not that good, especially at higher pressures. The AARD in pressures for all the models (PC-SAFT, PRWS and CPA) are below 5 % for both isotherms, whilst the AARD in methane composition are all above 5%, with the highest being 9.73% for the PC-SAFT model, indicating the difficulty in the prediction of the phase equilibria data for the methane + TEG system. The model prediction trends observed in Figure 6-17, especially for the PSRK model might be due to the fact the TEG boils at very high temperatures, whereas methane at very low temperatures. TEG is a polar molecule and thus forms hydrogen bonds with itself, whilst methane is a non-polar molecule, hence does not dissolve easily in TEG.

Jou et al. (Jou et al., 1987) reported that for mixtures that contain components with strong intermolecular interactions, simple EoS with common mixing rules are not satisfactory for describing the phase behaviour of methane + TEG system as the PR EOS failed to yield satisfactory correlations in that study. The regressed binary interaction parameters k_{ij} for the CPA and PC-SAFT models increase with an increase in temperature as can be observed in Table 6-16, whilst for the PRWS, the binary interaction parameter decreases with an increase in temperature. The regressed binary interaction parameters for the CPA model presented in Table 6-16 are comparable to the evaluated k_{ij} value of 0.1649 at 298.15 K using the formula presented by Arya et al. (Arya et al., 2014). TEG is a self-associating molecule.

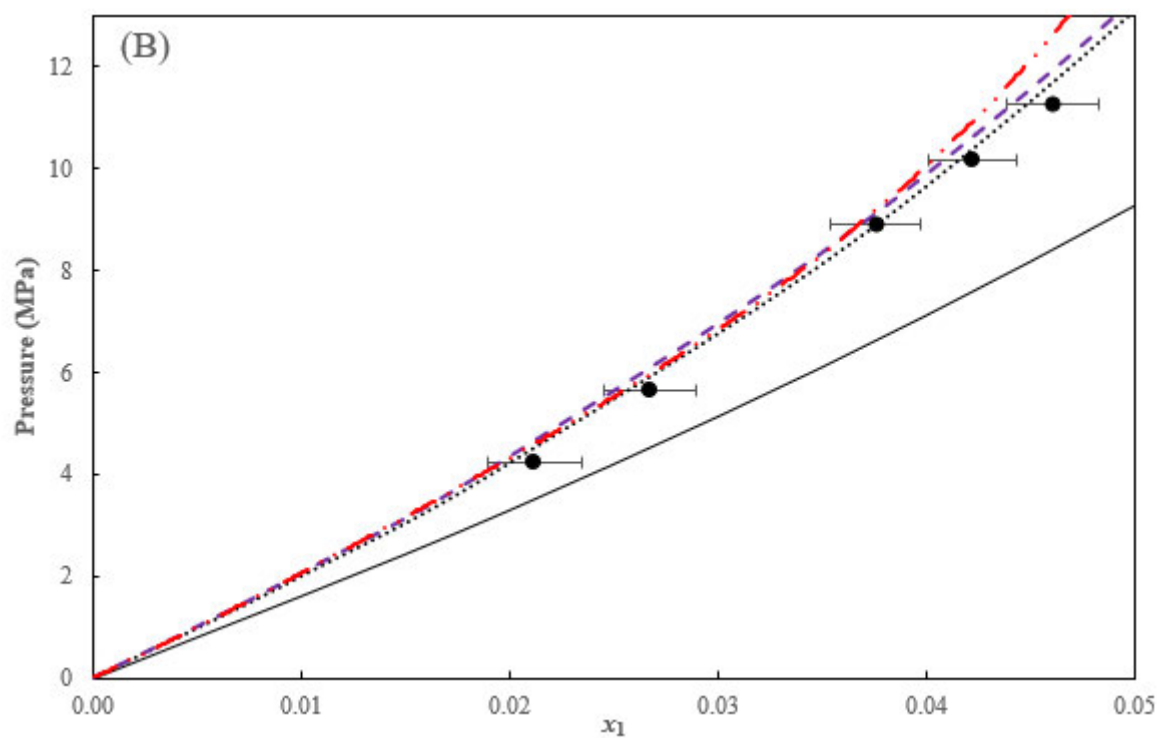
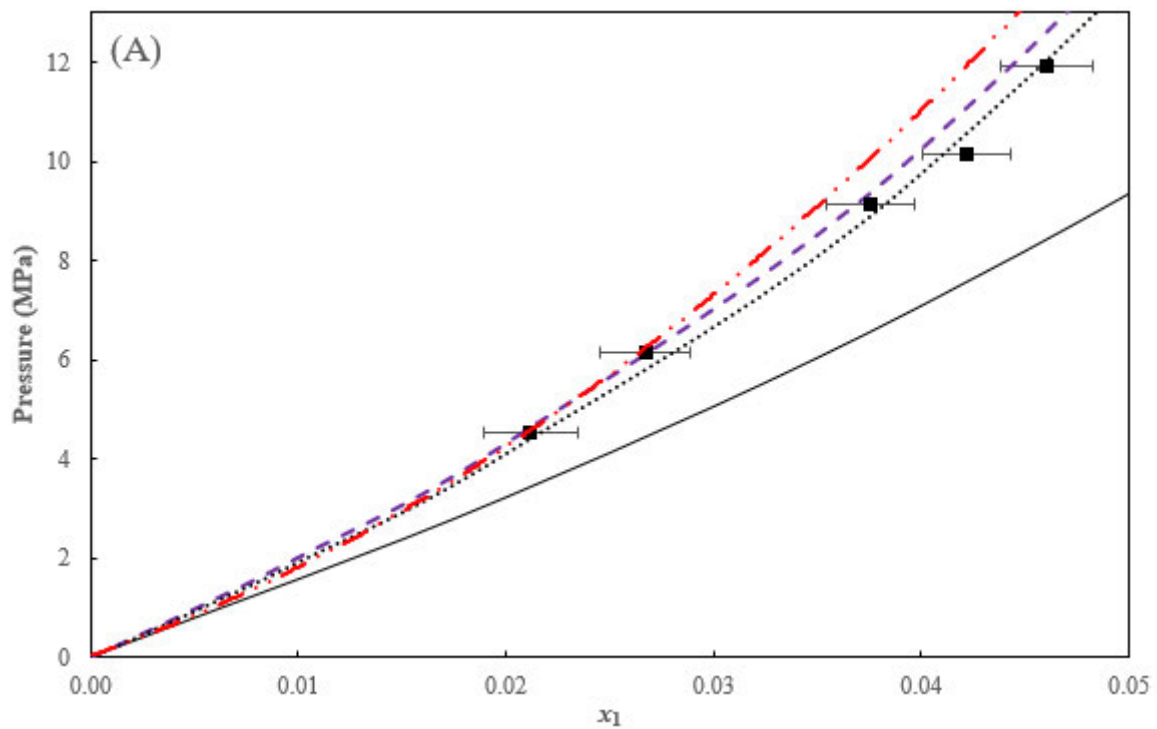


Figure 6-17: Thermodynamic modelling of the CH₄ (1) + TEG (2) test system.
 (A) data at 298.15 K, This work (■); (B) data at 323.15 K, This work (●); and modelling results: solid continuous lines represent the PSRK model; CPA model (---); PRWS model (- · -); PC-SAFT model (····).

The CPA and PC-SAFT models are able to account for the hydrogen bonding in the self-associating TEG molecule, hence the improvement in the modelling compared to the PRWS model as can be observed in Figure 6-17.

Table 6-16: Regressed binary model parameters and deviations for the CH₄ (1) + TEG (2) system.

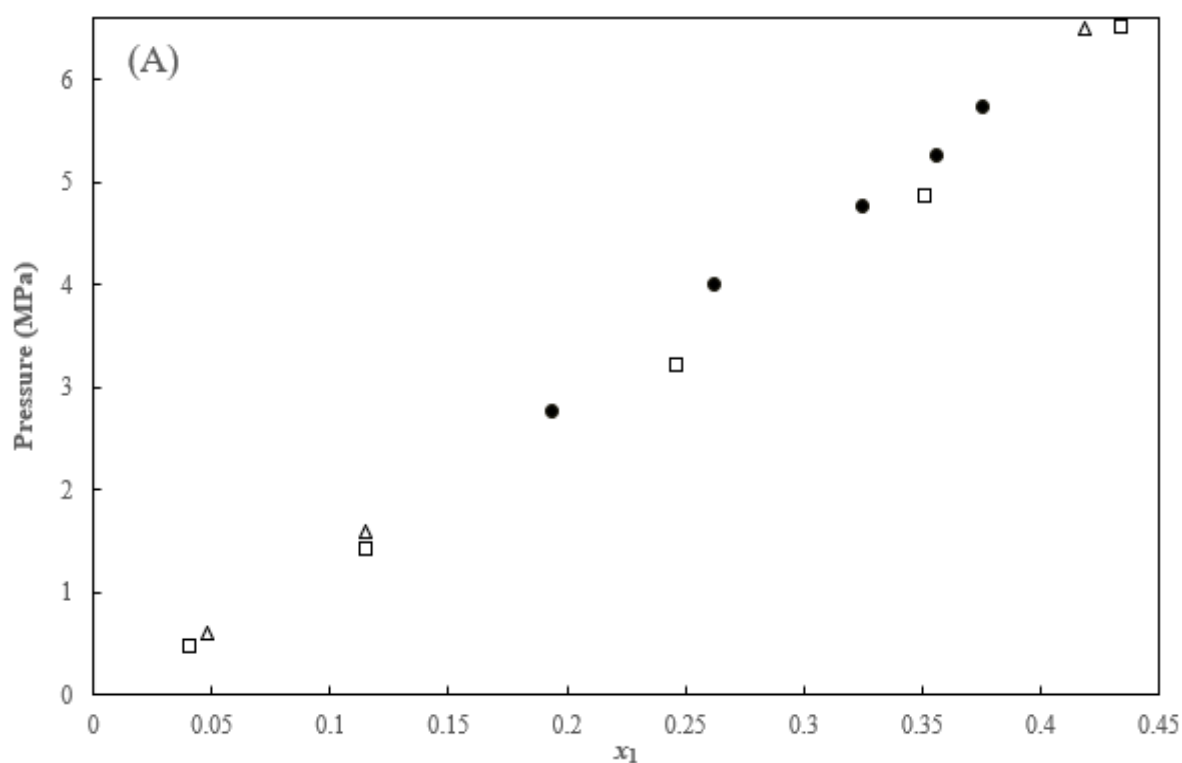
PRWS model			CPA model		PC-SAFT model		
	$T = 298.15 \text{ K}$	$T = 323.15 \text{ K}$	$T = 298.15 \text{ K}$	$T = 323.15 \text{ K}$		$T = 298.15 \text{ K}$	$T = 323.15 \text{ K}$
k_{12}	0.5773	0.5363	0.1734	0.2046	k_{12}	0.01699	0.03302
A_{12}	67.3695	37.9757			$(\epsilon^{A_2B_2})$		
A_{21}	1.6222	1.5973			$(\beta^{A_2B_2})$		
AAD P (MPa)	0.16	0.20	0.11	0.17	AAD P (MPa)	0.13	0.11
AARD P %	2.48	4.90	3.46	4.48	AARD P %	4.21	3.93
AAD x_1	0.0023	0.0011	0.0016	0.0012	AAD x_1	0.0021	0.0014
AARD x_1 %	6.25	6.55	7.71	6.97	AARD x_1 %	9.73	7.67
AAD T (K)	11.62	8.98	5.98	3.54		5.89	3.65
AARD T %	3.90	2.78	2.01	1.09		1.97	1.13

Using the CPA modelling in Aspen Plus, in particular with the Analysis function and flash calculations, the results for the CH₄ + TEG system at 298.15 K were compared using either the k_{ij} of this work (0.1734) or the literature k_{ij} of 0.1726 reported by (Kontogeorgis et al., 2011). The results are displayed in Figure E-1.3 Appendix E. In both cases the analysis and flash results match well, although these over-predict the total pressure values especially for methane mole fraction above 0.025. As a result, the binary k_{ij} from this work, can be extended to model multicomponent mixtures involved in this study.

6.3.6 Carbon dioxide + TEG and its aqueous test systems

These test systems are important in the present study since all the components are part of the new multicomponent systems measured in this study. For the systems with aqueous TEG, the solution was prepared in the laboratory; therefore, measurement of similar systems would confirm the precision of the experimental techniques used in this work.

The thermodynamic data for this system is scarce in the open literature. In this work, the static synthetic method was used. The bubble point measurement and model prediction results for the carbon dioxide + TEG system are displayed in Figure 6-18, along with the reported data from literature and listed in Table B.4-6 (Appendix B). No P - y data was found from the literature. This might be due to the low vapour pressure of TEG, which makes it difficult to measure such data. Jou et al. (Jou et al., 1987) measured the solubility of carbon dioxide in TEG in the temperature range of 298.15 to 398.15 K and pressures up to 20 MPa. Wise and Chapoy (Wise and Chapoy, 2016) also measured the solubility of carbon dioxide in TEG and its aqueous solutions (90, 60, and 40 % weight (wt.%) in TEG) for a temperature range between 263.15 K to 343.15 K and pressure range between 0.3 MPa to 37 MPa.



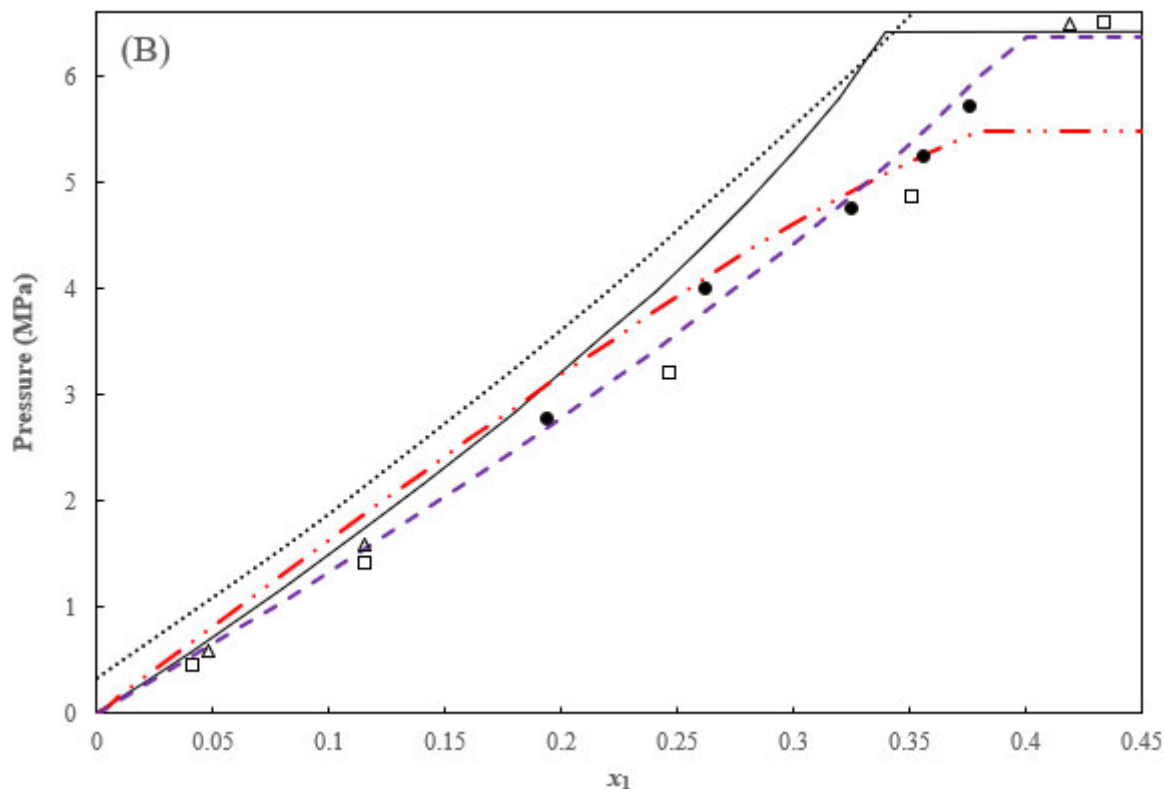


Figure 6-18: TPx plot of CO_2 (1) + TEG (2) test system at 298.15 K.

(A): Experimental data and reported literature data. (B): Experimental data, literature data, and model predictions. This work (●); Wise and Chapoy (Wise and Chapoy, 2016) (Δ); Jou et al. (Jou et al., 1987) (□); and modelling results: solid continuous lines represent the PSRK model; CPA model (---); PRWS model (- · - ·); PC-SAFT model (····).

Figure 6-18 (A) shows a very good comparison of the experimentally measured data and reported data from literature, especially that of Wise and Chapoy (Wise and Chapoy, 2016). There seems to be some minor discrepancy between the reported literature data. The error bars in carbon dioxide composition for the data of this work are not visible in Figure 6-18 since the carbon dioxide composition uncertainty of $U(x_1) = 0.0005$ is very small. Wise and Chapoy (Wise and Chapoy, 2016) reported large carbon dioxide uncertainty of $0.029 U(x_1)$ which if plotted covers the data of this work and that of Jou et al. (Jou et al., 1987). This suggests that the data of this work and that of Jou et al. (Jou et al., 1987) are within the experimental uncertainty of the data of Wise and Chapoy (Wise and Chapoy, 2016).

The cubic plus spline interpolation was used to correlate the data of Wise and Chapoy (Wise and Chapoy, 2016) and Jou et al. (Jou et al., 1987) with that of this study with respect to pressure. The interpolation was used to predict the mole fraction of carbon dioxide at the composition measured in this work. The absolute average deviation between the data of Wise and Chapoy (Wise and Chapoy,

2016) and this work was determined to be 2.6% and 8.2% between the data of Jou et al. (Jou et al., 1987) and this work.

Figure 6-18 (B) shows comparison of the experimentally measured data and the model predictions by the CPA, PRWS. The PC-SAFT model produced the worst fit to the experimental data, as shown in Figure 6-18 (B). The PRWS modelling was performed using Aspen Plus V12. From Figure 6-18 B, it can be observed that the PSRK, CPA and PRWS model predictions all tend to reach a point (inflection point) where the pressure suddenly changes to almost a constant whilst the liquid mole fraction of carbon dioxide increases. Wise and Chapoy (Wise and Chapoy, 2016) described this inflection point as a point where there is a phase change of carbon dioxide from VLE to LLE. The CPA model is in good agreement with the data of this work as well as the literature data presented in this work. Wise and Chapoy (Wise and Chapoy, 2016) also correlated their experimental data for the carbon dioxide + TEG system at 298.15K using the CPA model and good agreement was observed between the experimental data and the model results. For Wise and Chapoy (Wise and Chapoy, 2016), the CPA showed an average absolute deviation of 2.55% for their data. Pure component parameters for the PC-SAFT model, in this case, were obtained from Grenner et al. (Grenner et al., 2007). For the PC-SAFT data and CPA model, P_{xy} data were regressed at 298.15 K. Regressed model parameters and deviations are presented in Table 6-17. From Table 6-17, it can be observed that the AARD % in pressure is 3.71, 8.72, and 19.7 for the PRWS, CPA and PC-SAFT model predictions, respectively.

Table 6-17: Model parameters for the CO₂ (1) + TEG (2) system.

PC-SAFT		PRWS		CPA	
T = 298.15 K		T = 298.15 K		T = 298.15 K	
Parameter	Value	Parameter	Value	Parameter	Value
k_{12}	0.16046	k_{12}	0.0984	k_{12}	0.0498
m_1	2.2075	A_{12}	5.9585		
δ_1	3.1986	A_{21}	0.4012		
ε_1	111.7083				
m_2	1.9444				
δ_2	3.7538				
ε_2	185.9075				
$(\beta^{A_2B_2})$	-0.022				
$(\varepsilon^{A_2B_2})$	1682.252				
AAD P (MPa)	1.01		0.18		0.17
AARD P %	19.7		3.71		3.66
AAD x_1	0.0392		0.0128		0.0454
AARD x_1 %	13.8		4.17		13.42
AAD T (K)			3.59		
AARD T %			1.20		

Using the CPA modelling, that is the Aspen Plus Analysis function and flash calculation results for the CO₂ + TEG system at 298.15 K were compared using either the k_{ij} of this work (0.0498) or the literature k_{ij} of 0.0390 reported by (Kontogeorgis et al., 2011). The results are displayed in Figure E-1.4 Appendix E. In both cases the analysis and flash results match well, and those obtained using k_{ij} of this work are close to the experimental data. As a result, the binary k_{ij} from this work, can be extended to model multicomponent mixtures involved in this study.

6.3.6.1 Carbon dioxide (1) + (water (2) /TEG (3) 10/90 wt.%) test system

Besides validating the experimental technique, the objective of these measurements was to provide additional basic data for the development of the technology for the preparation of carbon dioxide-rich gases in EOR and reprocessing such gases for reinjection into reservoirs. As previously highlighted in chapter 2, section 2.3.2.7, the phase equilibria data for this system is scarce in the open literature, indicating the need for more research. The water 10 wt.% + TEG 90 wt.% mixture was prepared following the method explained in chapter 5, section 5.2.6.1. The static synthetic method was used to conduct bubble point measurements, the results of which are displayed in Figure 6-19 together with the reported data. The experimental data are also listed in Table B.4-7 (Appendix B) together with uncertainty data for the measured variables.

Figure 6-19 (A) shows that the experimentally measured data is not in perfect agreement with the data of Wise and Chapoy (Wise and Chapoy, 2016). This could be due to the different equipment setup and techniques used to prepare the aqueous TEG solution. Most of the data measured in this work at 298.15 K indicate a greater solubility of carbon dioxide in TEG than the work of Wise and Chapoy (Wise and Chapoy, 2016). The error bars for compositional uncertainty of carbon dioxide are not visible in Figure 6-19 (A). However, despite the discrepancies in the data, the data of this work is within the compositional uncertainty $U(x) = 0.033$ of the data of Wise and Chapoy (Wise and Chapoy, 2016). This indicates that the measurements performed in this work are acceptable.

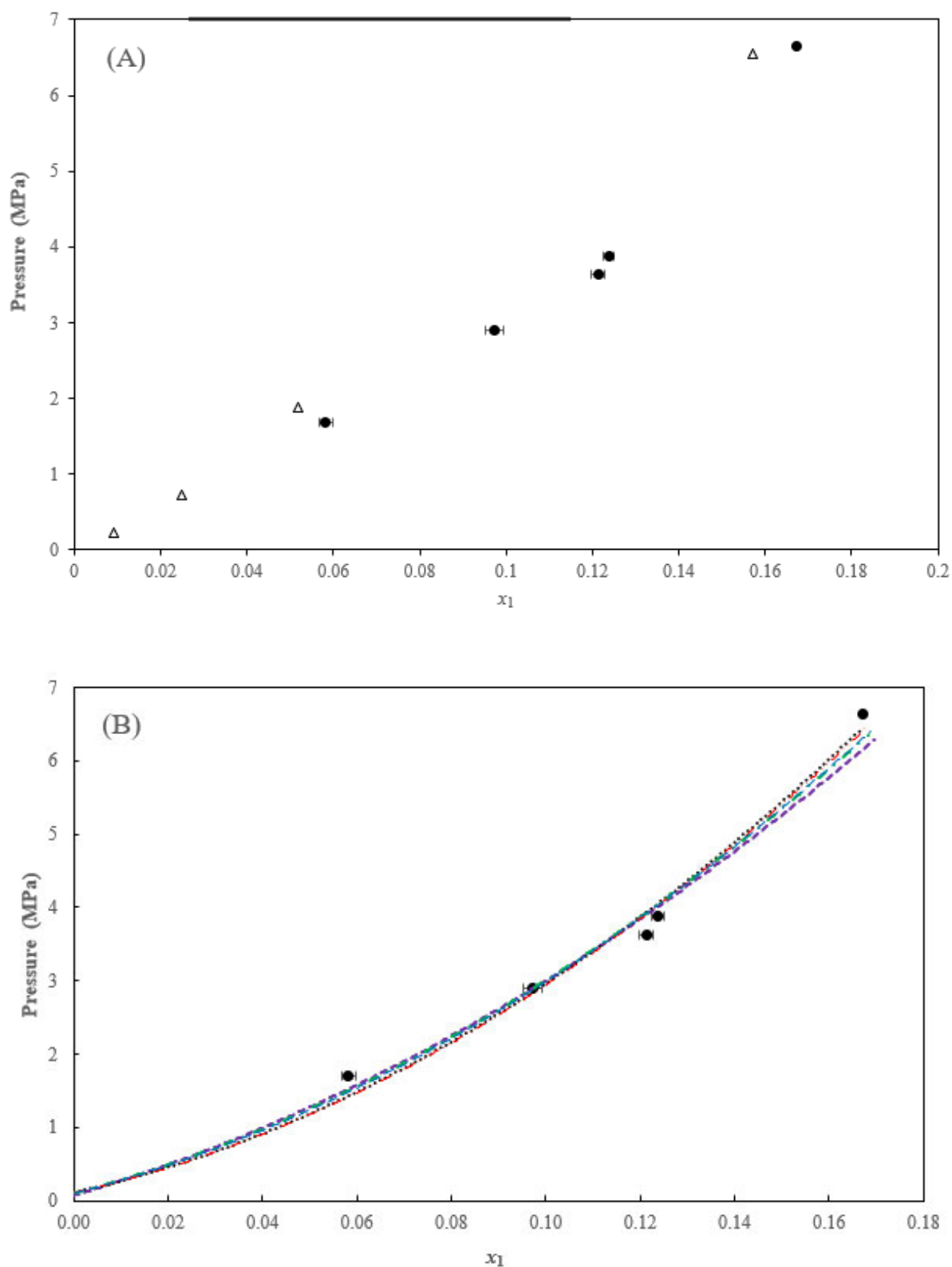


Figure 6-19: TPx plot of the $\text{CO}_2(1) + (\text{H}_2\text{O} (2) / \text{TEG} (3) 10/90 \text{ wt}\%)$ at 298.15 K.
 (A): Experimental data and reported data; This work (\bullet); (Wise and Chapoy, 2016) (Δ). (B):
 Experimental data and model correlation data; PC-SAFT model (\cdots); SRK model ($— — —$); PR model
 ($- \cdot -$); CPA ($- - -$); PRWS ($- \cdot \cdot$).

The experimental data from this work was regressed with the following models: PRWS, PR, CPA, PC-SAFT, and the SRK. Figure 6-19 (B) displays the model correlations, whilst Table 6-18 presents the regressed model parameters and deviations. It can be observed that there is good agreement between the experimental data and all the model correlations considered here, as indicated in Figure 6-19 (B) and values of the AAD and AARD % in Table 6-18. However, the AARD % in pressure for the CPA and PR models are slightly above 1%. All the model correlations were extrapolated to $x_{\text{CO}_2} = 0$ as visible in Figure 6-19 (B).

Table 6-18: Regressed model parameters and deviations for the CO₂ (1) + (H₂O (2) 10 wt.% + TEG (3) 90 wt.%) system.

PRWS model		CPA model		PC-SAFT model	PR model	SRK model
	$T = 298.15$ K		$T = 298.15$ K	$T = 298.15$ K	$T = 298.15$ K	$T = 298.15$ K
k_{12}	-1.08578	k_{12}	2.11478	-0.99445	-1.08	-0.9912
k_{13}	0.23567	k_{13}	0.06795	0.30176	0.46202	0.41651
k_{23}	0.12916	k_{23}	0.87058	-0.00934	-0.16981	-0.15734
A_{12}	2.3754	C_{12}	-0.00047			
A_{21}	1.4973	C_{13}	-0.03512			
A_{13}	2.5117	C_{23}	0.48169			
A_{31}	0.8342					
A_{23}	3.5118					
A_{32}	5.252					
AAD P (MPa)	0.001		0.06	0.01	0.05	0.03
AARD P %	0.04		1.13	0.35	1.07	0.8
AAD x_1	0.0005		0.0012	0.0004	0.0010	0.0009
AARD x_1 %	0.48		1.07	0.43	0.94	0.87
AAD T (K)	0.05		2.88	3.29	6.21	4.85
AARD T %	0.21		11.53	13.14	24.85	19.35

Where C represents the binary cross volume association parameter (CPAVIJ).

It is also important to note that for all the multicomponent systems of this study, for the CPA model, the bubble point pressure was also predicted using binary interaction parameters presented in Table 6-19. This was performed to show that only binary interaction parameters in some cases may not be adequate in describing phase behaviour in multicomponent systems. In the case of the CO₂ (1) + (H₂O (2) 10 wt.% + TEG (3) 90 wt.%) system, the CPA model bubble point predicted data and experimental data are presented in Figure E-3.1 Appendix E. It is evident that the predicted bubble point pressures in

Figure E-3.1 are far off from the experimental data as an error of 39.93 AARD% in pressure was obtained. However, the regressed CPA data are in good agreement with the experimental data as shown in Figure 6-19. This shows that for the CO₂ (1) + (H₂O (2) 10 wt.% + TEG (3) 90 wt.%) system, just fitting binary interaction parameters does not yield satisfactory results.

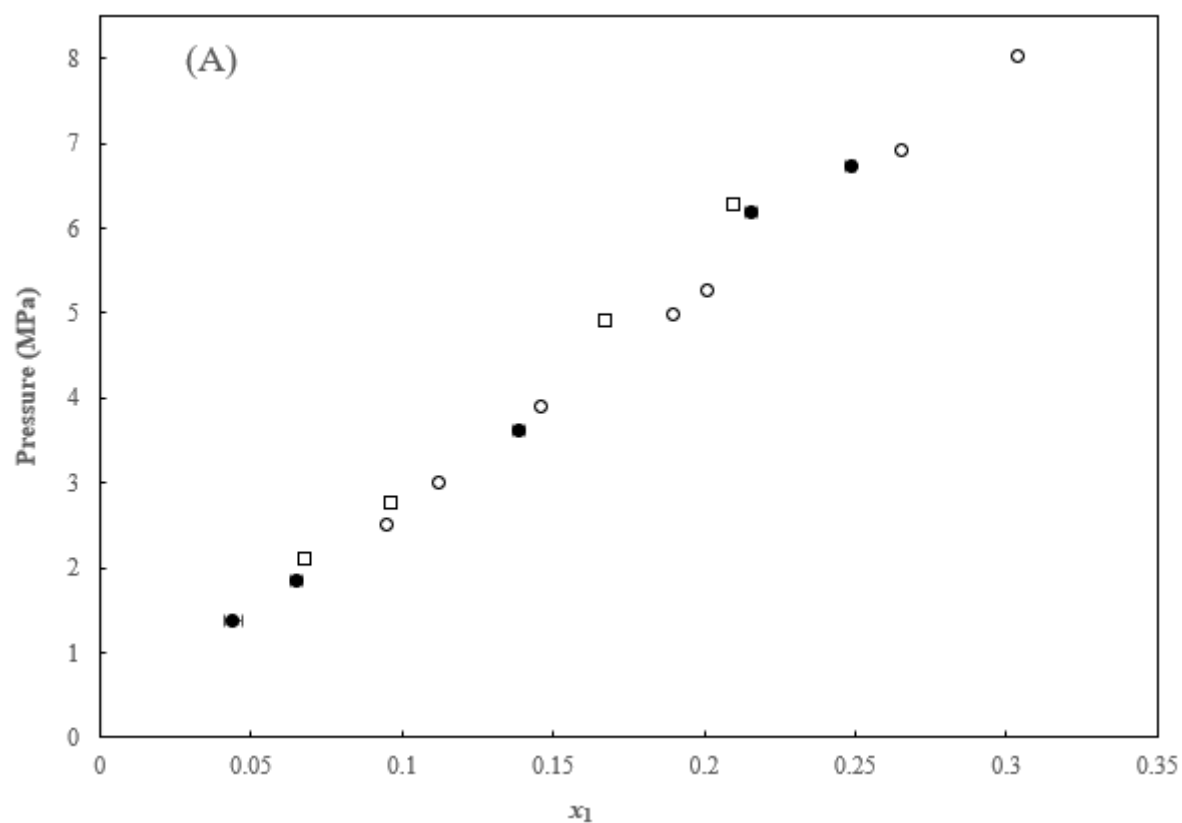
Table 6-19: CPA model parameters used in multicomponent systems bubble predictions in this study.

	k_{ij}
CO ₂ + methanol	-0.1129 ^a
CH ₄ + methanol	0.0405 ^a
CH ₄ + TEG	0.1734 ^a
CO ₂ + TEG	0.0498 ^a
H ₂ O + methanol	-0.094 ^b
H ₂ O + TEG	-0.2010 ^c
C ₃ H ₈ + TEG	0.1251 ^f
C ₃ H ₈ + methanol	0.059 ^d
CH ₄ + water	0.0052 ^d
C ₃ H ₈ + water	0.0432 ^d
CO ₂ + Water	0.1033 ^d
CH ₄ + CO ₂	0.0882 ^e
C ₃ H ₈ + CO ₂	0.1552 ^e
CH ₄ + C ₃ H ₈	0.0097 ^e
^a this work; ^b (Folas et al., 2005); ^c obtained from (Kontogeorgis et al., 2011); ^d (Folas, 2006); ^e (Tsivintzelis and Kontogeorgis, 2016); ^f based on the formula provided by (Arya et al., 2014) Table A.2;	

6.3.6.2 Carbon dioxide (1) + (water (2) / TEG (3) 3.5/96.5 wt.%) test system

The previous test system involving carbon dioxide and aqueous TEG solution showed some slight deviation to the reported data. Takahashi et al. (Takahashi et al., 1984) and Wise and Chapoy (Wise and Chapoy, 2016) presented literature data for this ternary system at 322.04 K and thus, this was included as a test system as well. Takahashi et al. (Takahashi et al., 1984) used a vapour recirculation apparatus for their experimental measurements. The experimental data of this work and reported literature data are displayed in Figure 6-20 (A). It is clear that there is some discrepancy between the reported literature data. This was chosen as a test system due to the scarcity of such data in the open literature. Despite the discrepancies in reported data, Figure 6-20 (A) shows a good comparison of the experimentally measured data and reported data, especially that of Takahashi et al. (Takahashi et al., 1984). The data measured in this work lies between the data indicated by the two literature sources and is closer to the data of Takahashi et al. (Takahashi et al., 1984). Error bars for this work are not visible in Figure 6-20 due to the low compositional uncertainty of carbon dioxide. Wise and Chapoy (Wise and Chapoy, 2016) reported a large composition uncertainty value of $U(x_1) = 0.025$ for which covers the

data of this work and that of Takahashi et al. (Takahashi et al., 1984). This shows that the data measured in this work is comparable with the literature, and hence a sound experimental technique was used. The data measured in this work are listed in Table B.4-7 (Appendix B), together with the associated uncertainties for the measured variables.



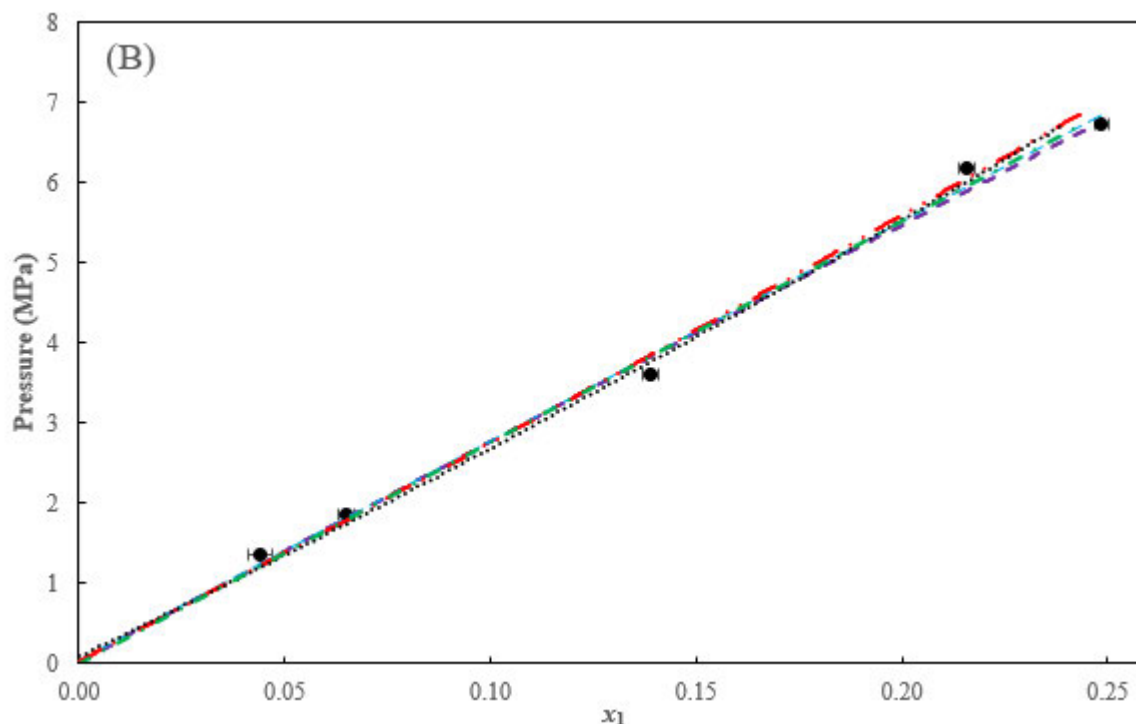


Figure 6-20: TPx graph for the CO_2 (1) + (H_2O (2) / TEG (3) 3.5/96.5 wt.%) at 322.04 K.
 (A): Experimental data and reported; This work (\bullet); (Takahashi et al., 1984) (\circ); (Wise and Chapoy, 2016) (\square). (B): Experimental data and model correlation data; PC-SAFT model (\cdots); SRK model ($-\text{ }-\text{ }-$); PR model ($-\text{ }-\text{ }-$); CPA ($-\text{ }-\text{ }-$); PRWS ($-\text{ } \cdot \text{ } \cdot \text{ } -$)

The experimental data of this work were regressed with the following models: PRWS, PR, CPA, PC-SAFT, and the SRK. Figure 6-20 (B) displays the model correlations, whilst Table 6-20 presents the regressed model parameters and deviations. It can be observed that there is good agreement between the experimental data and all the model correlations considered here as indicated in Figure 6-20 (B) and values of the AAD and AARD % in Table 6-20. The AARD % in pressure values for all the models is less than 2 %. All the model correlations were extrapolated to $x_1 = 0$ as visible in Figure 6-20 (B).

In the case of the CO_2 (1) + (H_2O (2) / TEG (3) 3.5/96.5 wt.%) system, the predicted bubble point data using the CPA model and experimental data are presented in Figure E-3.2 Appendix E. It is evident that the predicted bubble point pressures in Figure E-3.2 are under predicted with respect to experimental data as a model error of 17.55 AARD% in pressure is observed. Comparison of Figures E-32 and 6-20 (B) with respect to the CPA model proves that just fitting binary interaction parameters is not enough to yield satisfactory results. This is because the CPA regressed experimental data presented in Figure 6-20 was in excellent agreement to the experimental data as compared to the results shown in Figure E-32.

Table 6-20: Model parameters for the CO₂ (1) + (H₂O (2) /TEG (3) 3.5/96.5 wt. %) system.

PRWS model		CPA model		PC-SAFT model	PR model	SRK model
	$T = 322.04$ K		$T = 322.04$ K	$T = 322.04$ K	$T = 322.04$ K	$T = 322.04$ K
k_{12}	-1.1608	k_{12}	-4.4595	-0.88574	1.06804	-1.17161
k_{13}	0.6241	k_{13}	0.34926	0.14640	0.23298	0.23737
k_{23}	-0.3814	k_{23}	0.18786	-0.00558	-0.18335	-0.16866
A_{12}	12.1722	C_{12}	-0.05456			
A_{21}	-2.1226	C_{13}	-0.01617			
A_{13}	3.2920	C_{23}	0.11592			
A_{31}	2.7333					
A_{23}	2.0882					
A_{32}	6.3941					
AAD P (MPa)	0.05		0.08	0.02	0.05	0.07
AARD P %	1.62		1.59	0.76	1.48	1.92
AAD x_1	0.0011		0.0025	0.0033	0.0019	0.0028
AARD x_1 %	1.21		1.67	2.10	1.43	2.13
AAD T (K)	1.33		1.97	0.84	2.34	3.13
AARD T %	2.71		4.04	1.71	4.80	6.41

6.4 New systems: VLE data measurement and modelling

Much effort was undertaken to establish if phase equilibrium data of the proposed new systems in this work had been reported in the open literature. A review of the information on Dortmund data bank (DDBST GmbH, 2019) and NIST ThermoData Engine in Aspen Plus V11-12 revealed that no data had been presented or published for the novel system systems to date. This was necessary as it fulfils some of the objectives of the present study, which were to measure VLE for water-methanol-TEG-hydrocarbon systems representative of those encountered in gas processing and model the phase behaviour. In all these measurements, the static synthetic method was used, for which the method was explained in chapter 5, section 5.2.5.3.

6.4.1 New system 1: (methane (1) /propane (2) 95/5 mol%) + methanol (3)

Methanol is commonly found in oil and gas systems where it is used as an additive (O'Brien et al., 2016). The midstream industry's overuse of methanol is of recent concern as they struggle to meet the stringent new natural gas liquids (NGL) product specifications. Sometimes methanol follows propane through fractionation, thus presenting a challenge to the downstream industry since the demand for

propane is now shifting from fuel needs (LPG) into petrochemical markets(O'Brien et al., 2016). As a result, it is necessary to have accurate experimental phase equilibria data for such systems since this aids model development that can accurately predict the distribution of methanol within such systems.

In this work, bubble point pressure data were measured for the (methane (1) / propane (2) 95/5 mol%) + methanol (3) new system at 283.16, 303.16, and 323.15 K. A total of 15 data points were measured for this system. The experimental data of this work are presented in Figure 6-21, and the data is also listed in Table B.5-1 (Appendix B) together with the associated uncertainties for the measured variables. The measured data contributes to the information required for the process design, control, and monitoring of methanol in gas conditioning systems. Error bars represent methane composition uncertainty.

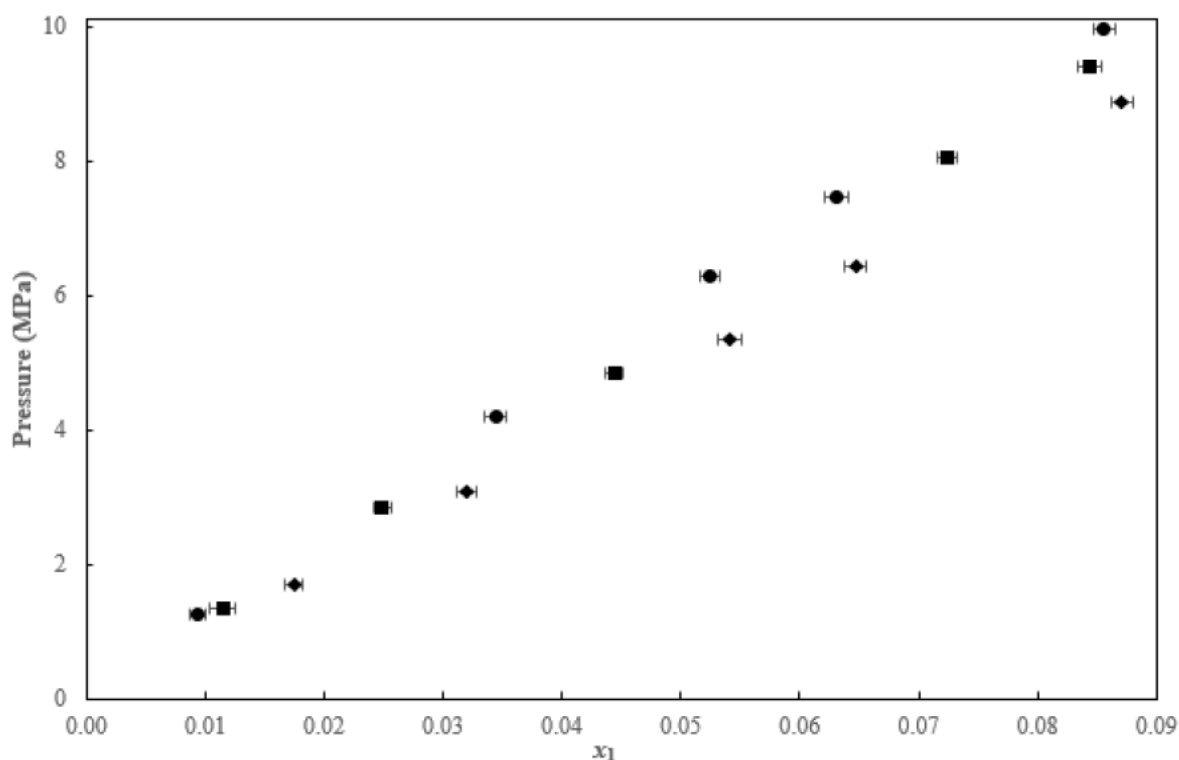
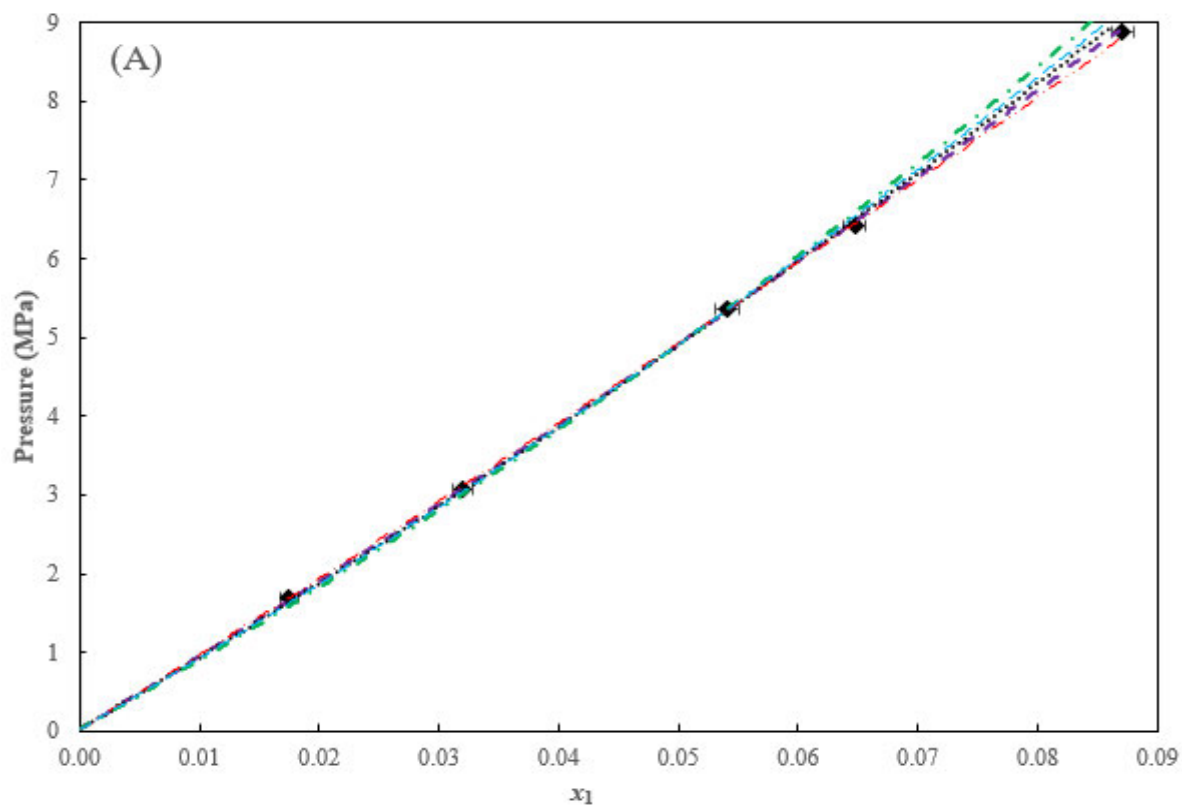


Figure 6-21: TPx graph for the (CH_4 (1) / C_3H_8 (2) 95/5 mol%) + CH_3OH (3) novel system.
283.16 K (◆); 303.16 K (■), 323.15 K (●).

Figure 6-21 shows that for the same composition of methane (x_1), the pressures follow this trend: P at 283.16 K < P at 303.15 K < P at 323.15 K. This implies that the solubility of methane in methanol follows this trend: 283.15 K > 303.16 K > 323.15 K. Thus, it would be wiser to operate such systems at higher temperatures to reduce the quantity of hydrocarbons that can be dissolved in methanol.

The experimental data of this work was regressed with the following models: PR, SRK, PRWS, CPA and the PC-SAFT. Figure 6-22 presents the model correlations at 283.16, 303.16 and 323.15 K, respectively. Table 6-21 presents the regressed model parameters and deviations. All the model correlations were extrapolated to $x_1=0$ as visible in Figure 6-22.



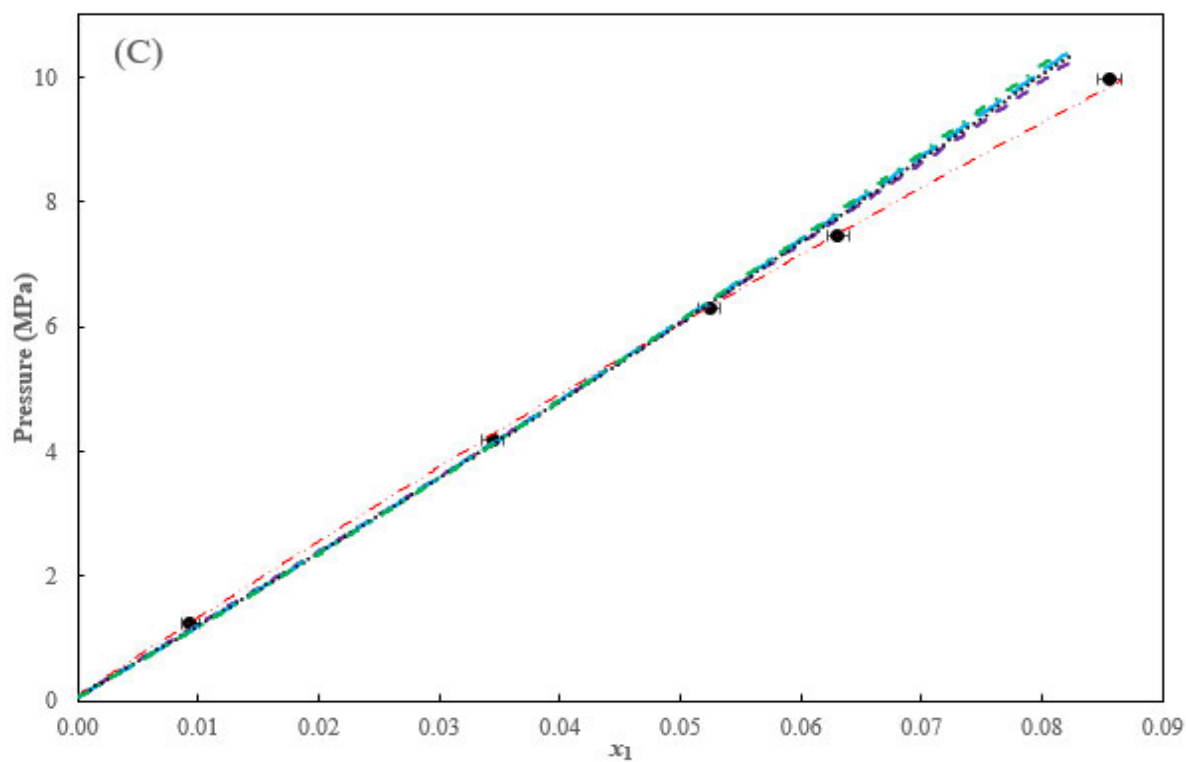
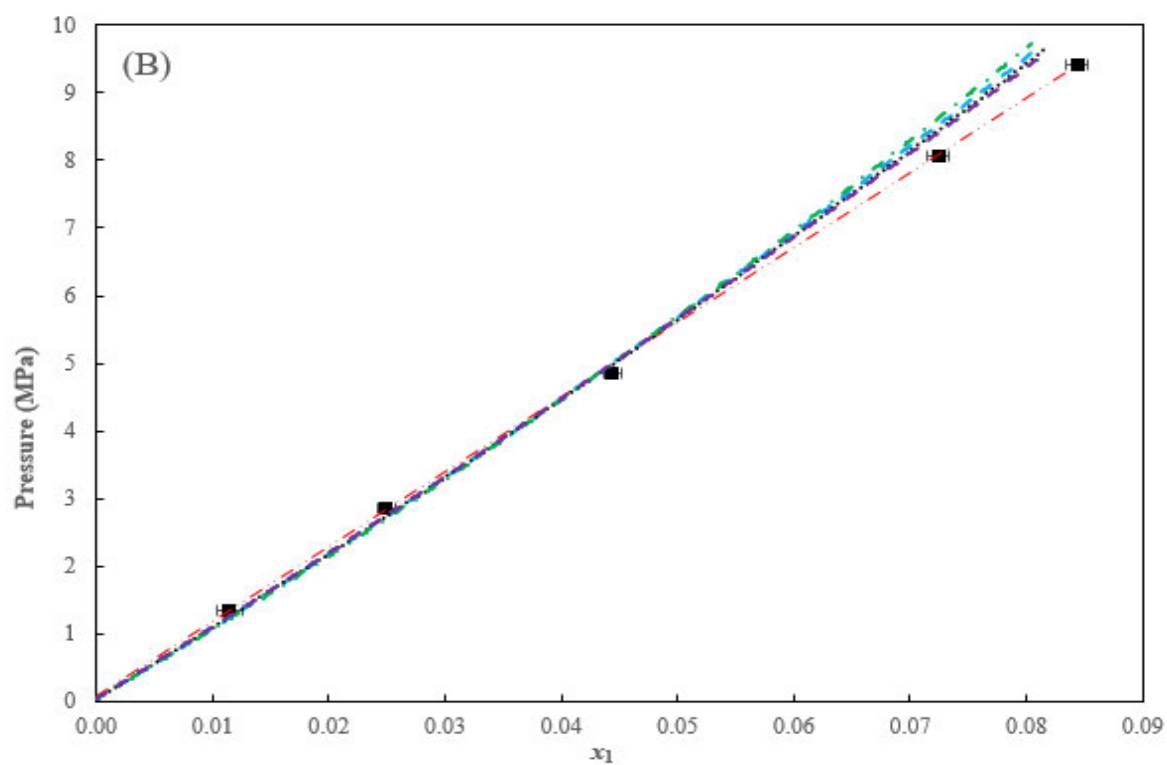


Figure 6-22: Thermodynamic modelling of the (CH₄ (1) / C₃H₈ (2) 95/5 mol%) + CH₃OH (3) system.

(A) $T = 283.16$ K; (B) $T = 303.16$ K; (C) $T = 323.15$ K; Solid symbols (Experimental data) This work; Modelling results: PR model (— · —); SRK model (— — —); PRWS (— · —); CPA (— — —); and PC-SAFT model (·····).

It can be observed from Figures 6-22 that the PRWS yielded the best fit to the experimental data at all isotherms considered. This is further illustrated by the low deviations presented in Table 6-20, where AARD in pressures are all less than or equal to 1% for the PRWS model. The PRWS had nine parameters as compared to other models that had only 3 parameters which were regressed, hence the better performance of the PRWS model. The CPA and PC-SAFT models provided satisfactory correlations at 283.16 K (see Figure 6-22 (A)). This is further illustrated by the AARD % in pressures which are less than 1% (see Table 6-20 b). Overall the majority of the models yielded satisfactory correlations at all isotherms as shown in Figure 6-22 (A), (B) and (C); however, there is some noticeable deviation for the PR and SRK models for data above 6 MPa. The AARD in pressures for the PR and SRK models at 283.16 K are 1.58 % and 1.13% respectively (Table 6-20 (a)).

As the temperature increases from 283.16 to 323.15 K, the AARD % in pressures and deviation from experimental data for the CPA, PC-SAFT, PR, and the SRK models also increases as can be observed in Figure 6-22 and Table 6-20. Large deviation from experimental data for the CPA, PC-SAFT, PR, and SRK can be observed in Figure 6-22 (B) and (C) for data from $x_1 > 0.05$.

The CPA bubble point predictions using k_{ij} reported in Table 6-19 is displayed in Figures E-3.3. A, B and C for the data at 283.16, 303.16 and 323.15K respectively. The AARD % in pressure are 15.83, 8.70 and 8.28 for the data at 283.16, 303.16 and 323.15 K respectively. The observed trends and the AARD % show that as the CPA model prediction yielded better results for the data measured at higher temperatures than at lower temperatures. The CPA model results presented in Figure E-3.3 A, B and C are not as good as those presented in Figure 6-22 A, B and C respectively.

Table 6-21 (a): Regressed model parameters and deviations for the (CH₄ (1) /C₃H₈ (2) 95/5 mol%) + CH₃OH (3) system.

Parameter	PRWS model			PR model			SRK model		
	$T = 283.16$ K	$T = 303.16$ K	$T = 323.15$ K	$T = 283.16$ K	$T = 303.16$ K	$T = 323.15$ K	$T = 283.16$ K	$T = 303.16$ K	$T = 323.15$ K
k_{12}	1.271	1.232	1.346	0.62	0.67	0.705	0.646	0.691	0.726
k_{13}	0.441	0.476	0.524	-0.057	-0.03	-0.008	-0.107	-0.084	-0.065
k_{23}	-3.270	1.932	-1.423	-0.078	-0.069	-0.064	-0.088	-0.079	-0.074
A_{12}	6.895	84.870	8.077						
A_{21}	31.509	59.390	37.673						
A_{13}	0.459	-0.589	-0.776						
A_{31}	0.690	1.885	2.168						
A_{23}	3.399	-3.971	0.550						
A_{32}	6.486	9.982	3.590						

Table 6-21 (a): Regressed model parameters and deviations for the (CH ₄ (1) /C ₃ H ₈ (2) 95/5 mol%) + CH ₃ OH (3) system (Cont)									
Parameter	PRWS model			PR model			SRK model		
	<i>T</i> = 283.16 K	<i>T</i> = 303.16 K	<i>T</i> = 323.15 K	<i>T</i> = 283.16 K	<i>T</i> = 303.16 K	<i>T</i> = 323.15 K	<i>T</i> = 283.16 K	<i>T</i> = 303.16 K	<i>T</i> = 323.15 K
AAD <i>P</i> (MPa)	0.02	0.04	0.03	0.07	0.15	0.17	0.05	0.13	0.15
AARD <i>P</i> %	0.59	1.00	0.72	1.58	3.26	3.37	1.13	2.87	3.09
AAD <i>x</i> ₁	0.0002	0.0004	0.0006	0.0007	0.0016	0.0014	0.0004	0.0014	0.0012
AARD <i>x</i> ₁ %	0.61	1.20	1.55	1.03	3	2.47	0.51	2.5	2.15
AAD <i>T</i> (K)	1.75	0.49	0.11	1.65	1.20	0.83	2.23	1.80	1.03
AARD <i>T</i> %	0.62	0.16	0.03	0.58	0.40	0.26	0.79	0.59	0.32

Table 6-21 (b): Regressed model parameters and deviations for the (CH₄ (1) / C₃H₈ (2) 95/5 mol%) + CH₃OH (3) system cont.

Parameter	CPA model			PC-SAFT model		
	<i>T</i> = 283.16 K	<i>T</i> = 303.16 K	<i>T</i> = 323.15 K	<i>T</i> = 283.16 K	<i>T</i> = 303.16 K	<i>T</i> = 323.15 K
<i>k</i> ₁₂	0.137	0.137	0.137	0.566	0.519	0.497
<i>k</i> ₁₃	0.020	0.030	0.031	0.032	0.039	0.041
<i>k</i> ₂₃	-0.289	-0.309	-0.336	-0.038	-0.043	-0.051
AAD <i>P</i> (MPa)	0.02	0.09	0.12	0.04	0.11	0.14
AARD <i>P</i> %	0.65	2.2	2.55	0.96	2.48	2.78
AAD <i>x</i> ₁	0.0002	0.001	0.001	0.0003	0.0012	0.0011
AARD <i>x</i> ₁ %	0.46	1.72	1.62	0.46	2.10	1.85
AAD <i>T</i> (K)	2.65	2.24	1.99	2.94	2.47	1.95
AARD <i>T</i> %	0.93	0.74	0.62	1.04	0.82	0.60

Trends for the absolute values of the regressed binary interaction parameters for possible binary pairs of this system in Table 6.21 (a) and (b) can be described as follows:

For the PRWS:

Parameter	PRWS model					
	<i>T</i> = 283.16 K		<i>T</i> = 303.16 K		<i>T</i> = 323.15 K	
	Value	<i>σ</i>	Value	<i>σ</i>	Value	<i>σ</i>
<i>k</i> ₁₂	1.271	1.540	1.232	0.199	1.346	6.877
<i>k</i> ₁₃	0.441	0.005	0.476	0.004	0.524	0.028
<i>k</i> ₂₃	-3.27	3.409	1.932	4.291	-1.423	29.151

All values in SI units.

σ represents the standard deviation reported in Aspen Plus V12

- k_{12} at 283.16 K $>$ k_{12} at 303.16 K $<$ k_{12} at 323.15 K, thus there is no clear trend for the interaction parameter of methane and propane between 283.16 and 323.15 K.
- k_{13} at 283.16 K $<$ k_{13} at 303.16 K (a similar trend observed for the methane + methanol binary system in Table 6.11) $<$ k_{13} at 323.15 K. The interaction parameter of methane and methanol between 283.16 and 323.15 K increases with an increase in temperature. The binary interaction parameter between methane + methanol binary pair in the ternary system of 0.47 at 303.16 K is larger than 0.3423 for the methane + methanol binary system at 303.15 K.
- k_{23} at 283.16 K $>$ k_{23} at 303.16 K $>$ k_{23} at 323.15 K. There interaction parameter of propane and methanol between 283.16 and 323.15 K decreases with an increase in temperature.
- At 283.16 and 323.15 K, the standard deviation on the binary interaction parameters for the methane + propane and propane + methanol binary pairs is greater than the absolute value of the respective binary interaction parameters, showing that the data are over fitted (Carlson, 1996). Only the methane + methanol binary interaction parameters are significant to the overall model fitting.
- For the data at 303.16 K, only the propane + methanol binary interaction parameter was insignificant to the overall model fitting. This is because the absolute value of the binary interaction parameter was less than the value of the standard deviation for this binary pair, indicating that the data are over fitted (Carlson, 1996), hence this parameter could be possibly set to 0.

For the PR and SRK models

Parameter	PR model					
	$T = 283.16$ K		$T = 303.16$ K		$T = 323.15$ K	
	Value	σ	Value	σ	Value	σ
k_{12}	0.620	1.013	0.670	1.343	0.705	1.649
k_{13}	-0.057	0.008	-0.030	0.012	-0.008	0.013
k_{23}	-0.078	0.052	-0.069	0.070	-0.064	0.085

All values in SI units.

σ represents the standard deviation reported in Aspen Plus V12

Parameter	SRK model					
	$T = 283.16$ K		$T = 303.16$ K		$T = 323.15$ K	
	Value	σ	Value	σ	Value	σ
k_{12}	0.646	1.170	0.691	1.465	0.726	1.787
k_{13}	-0.107	0.008	-0.084	0.012	-0.065	0.013
k_{23}	-0.088	0.055	-0.079	0.070	-0.074	0.083

All values in SI units.

σ represents the standard deviation reported in Aspen Plus V12

- k_{12} at 283.16 K < k_{12} at 303.16 K < k_{12} at 323.15 K. Thus, the interaction parameters between methane and propane increase with an increase in temperature.
- k_{13} at 283.16 K > k_{13} at 303.16 K > k_{13} at 323.15 K. The interaction parameter between methane and methanol decrease with an increase in temperature.
- k_{23} at 283.16 K > k_{23} at 303.16 K > k_{23} at 323.15 K. The interaction parameter between propane and methanol decrease with an increase in temperature.
- At 283.16 K, 303.16 K and 323.15 K, the absolute value of the binary interaction parameter between methane and propane is less than the reported standard deviation for both the PR and SRK models. This indicates that the data are over fitted, and that the regressed parameter could possibly be set to 0. This might explain the trend observed for the PR and SRK models in Figures 6.22 (A), (B) and (C). For the methane + methanol and propane + methanol binary pairs of the ternary system, the absolute values of the interaction parameters are greater than the standard deviations, which means that these parameters are significant to the overall model fitting.

For the CPA model

Parameter	CPA model					
	$T = 283.16 \text{ K}$		$T = 303.16 \text{ K}$		$T = 323.15 \text{ K}$	
	Value	σ	Value	σ	Value	σ
k_{12}	0.137	0.000	0.137	0.000	0.137	0.000
k_{13}	0.020	0.013	0.030	0.015	0.031	0.016
k_{23}	-0.289	0.043	-0.309	0.052	-0.336	0.054

All values in SI units.

σ represents the standard deviation reported in Aspen Plus V12

- k_{12} at 283.16 K = k_{12} at 303.16 K = k_{12} at 323.15 K. The interaction parameter between methane and propane is independent of temperature between 283.16 and 323.15 K.
- k_{13} at 283.16 K < k_{13} at 303.16 K < k_{13} at 323.15 K. The binary interaction parameter between methane and methanol increase with an increase in temperature. The value of the binary interaction parameter between methane and methanol at 303.16 K of 0.030 reported for this ternary system is significantly less than the 0.0462 reported for the binary system of methane and methanol at 303.15 K of this work (Table 6-15).
- k_{23} at 283.16 K < k_{23} at 303.16 K < k_{23} at 323.15 K. The interaction parameter between propane and methanol increase with an increase in temperature.
- The standard deviation values reported for all the binary parameters shown are less than the absolute values of the regressed binary interaction parameters. This indicates that all the parameters are significant to the overall model fitting (Carlson, 1996).

For the PC-SAFT model

Parameter	PC SAFT model					
	$T = 283.16 \text{ K}$		$T = 303.16 \text{ K}$		$T = 323.15 \text{ K}$	
	Value	σ	Value	σ	Value	σ
k_{12}	0.566	1.122	0.519	1.172	0.497	1.335
k_{13}	0.032	0.008	0.039	0.010	0.041	0.010
k_{23}	-0.038	0.050	-0.043	0.057	-0.051	0.063

All values in SI units.

σ represents the standard deviation reported in Aspen Plus V12

- k_{12} at 283.16 K $>$ k_{12} at 303.16 K $>$ k_{12} at 323.15 K. The interaction parameter between methane and propane decrease with an increase in temperature.
- k_{13} at 283.16 K $<$ k_{13} at 303.16 K $<$ k_{13} at 323.15 K. The interaction parameter between methane and methanol increase with an increase in temperature. The binary interaction parameter between methane and methanol at 303.16 K of 0.519 for this ternary system is comparable to 0.0498 for the methane + methanol binary system at 303.15 K reported in Table 6-15.
- k_{23} at 283.16 K $<$ k_{23} at 303.16 K $<$ k_{23} at 323.15 K. The interaction parameter between propane and methanol increase with an increase in temperature.
- The absolute value of the binary interaction parameter between methane and propane is less than the reported standard deviation at all isotherms for the PC-SAFT model. This indicates that the data are over fitted, and that the regressed parameter could possibly be set to 0. This might explain the trend observed for the PC-SAFT model in Figures 6.22 (A), (B) and (C). For the methane + methanol and propane + methanol binary pairs of the ternary system, the absolute values of the interaction parameters are greater than the standard deviations, which means that the parameters are significant to the overall model fitting.

6.4.1.1 Comparison of the methane + methanol system and the propane-free (methane / propane 95/5 mol%) + methanol system at 303.15 K

The data for the two systems are compared and presented in Figure 6-23. Propane-free (methane / propane 95/5 mol%) + methanol system refers to the fact that only the methane and methanol composition from this ternary system was considered for comparison purposes with the methane + methanol binary system.

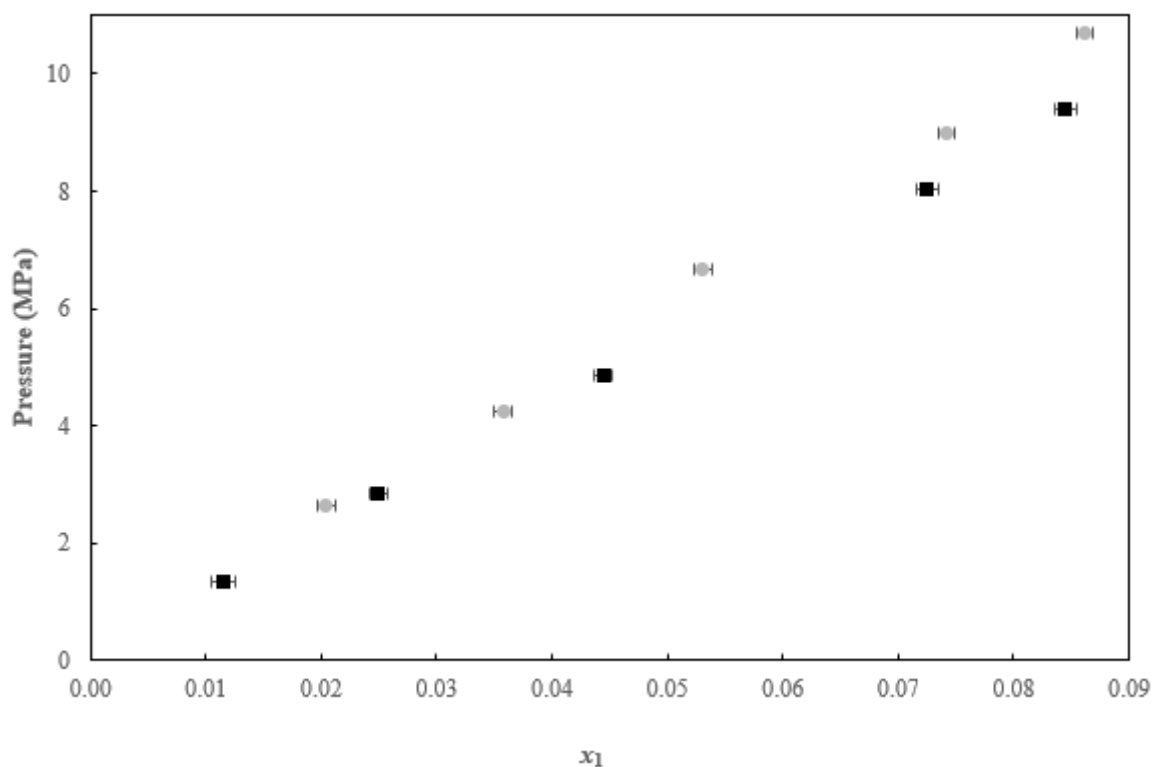


Figure 6-23: Comparison of the TPx data at 303.15 K for:
 (●), $\text{CH}_4(1) + \text{CH}_3\text{OH}(2)$; (■) propane-free ($\text{CH}_4(1)/\text{C}_3\text{H}_8(2)$ 95/5 mol%) + $\text{CH}_3\text{OH}(3)$.

Figure 6.23 shows that the pure methane + methanol system has higher total pressure values as compared to the propane-free (methane / propane 95/5 mol%) + methanol system. As the mole fraction of methane increases, the difference in pressures between the two systems also increases over the range x_1 from 0 to 0.085. Thus, it can be conclusively said that the 5 mol% propane causes an increase in the solubility of methane in methanol, which becomes more pronounced as the mole fraction of methane + propane mixture increases. The addition of propane to the gas mixture led to an increase in the solubility because of the C-H_2 groupings in the mixture of (methane+ propane) + $\text{CH}_3\text{-OH}$ grouping. Error bars represent methane composition uncertainty in each of the systems compared.

6.4.2 New system 2: (methane (1) /propane (2) 95/5mol%) + TEG (3)

Bubble point pressure data for the (methane (1) / propane (2) 95/5 mol%) + TEG (3) new system have been measured at 303.16 and 323.16 K and is displayed in Figure 6-24. A total of 10 data points were measured for this system. The measured data are also listed in Table B.5.2. (Appendix B), together with the associated uncertainties for the measured variables.

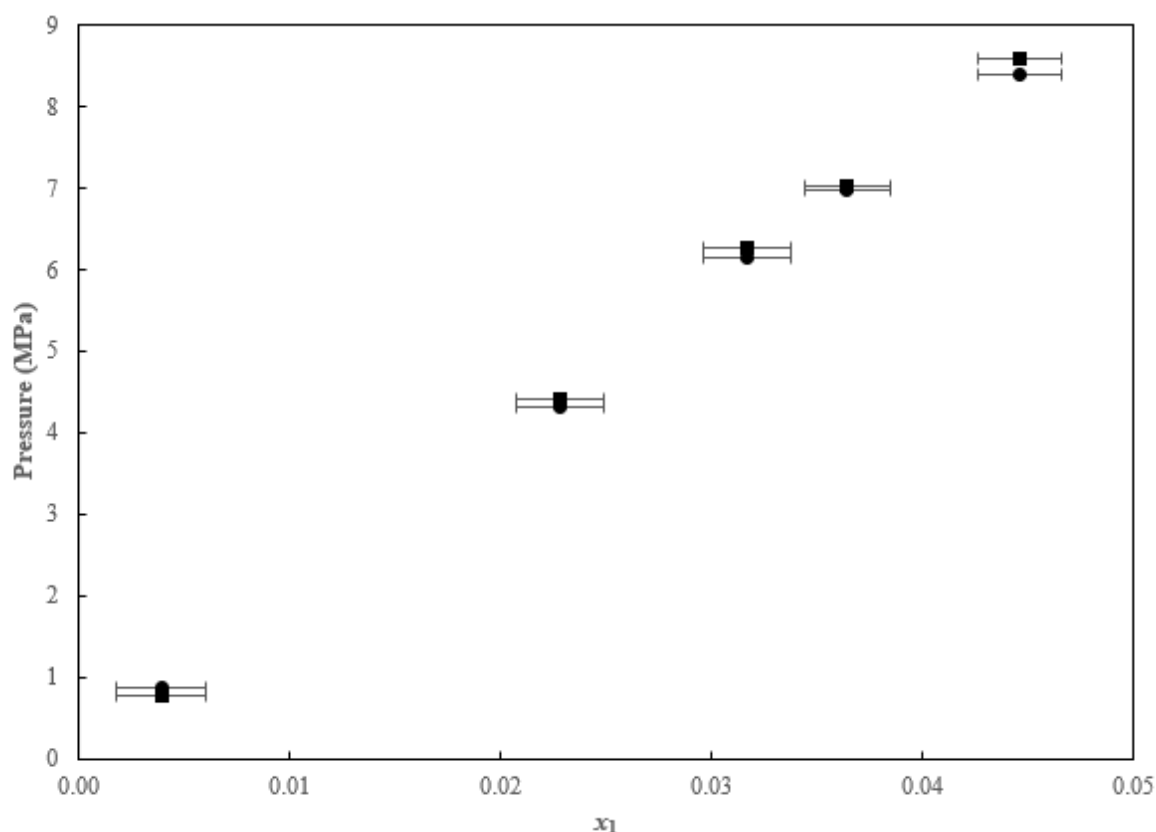


Figure 6-24: TPx plot for the (CH₄ (1) / C₃H₈ (2) 95/5 mol%) + TEG (3) novel system.
303.16 K (■); 323.16 K (●)

Figure 6-24 shows that for the same composition of methane x_1 , there is a minor difference in pressures for the data measured at 303.16 K and that at 323.16 K. The furthest point at x_1 0.0446 indicates that as the mole fraction of methane increases, the difference in pressure values for the data measured at the same composition also increases. The inverse solubility phenomenon in Figure 6-24 has been witnessed for either methane or propane in TEG (Jou et al., 1987; Rasoolzadeh et al., 2020a, 2020b). As temperature increases, some free voids are formed in TEG, such that alkanes are encapsulated in these, hence the increase in solubility of methane in the system as temperature increases.

The measured data in this work were correlated with the PR, SRK PRWS, CPA and PC-SAFT models. Results of the model correlations at 303.16 K and 323.16 K are shown in Figure 6-25 (A) and (B), respectively. All the model correlations were extrapolated to $x_1 = 0$ as visible in Figure 6-25.

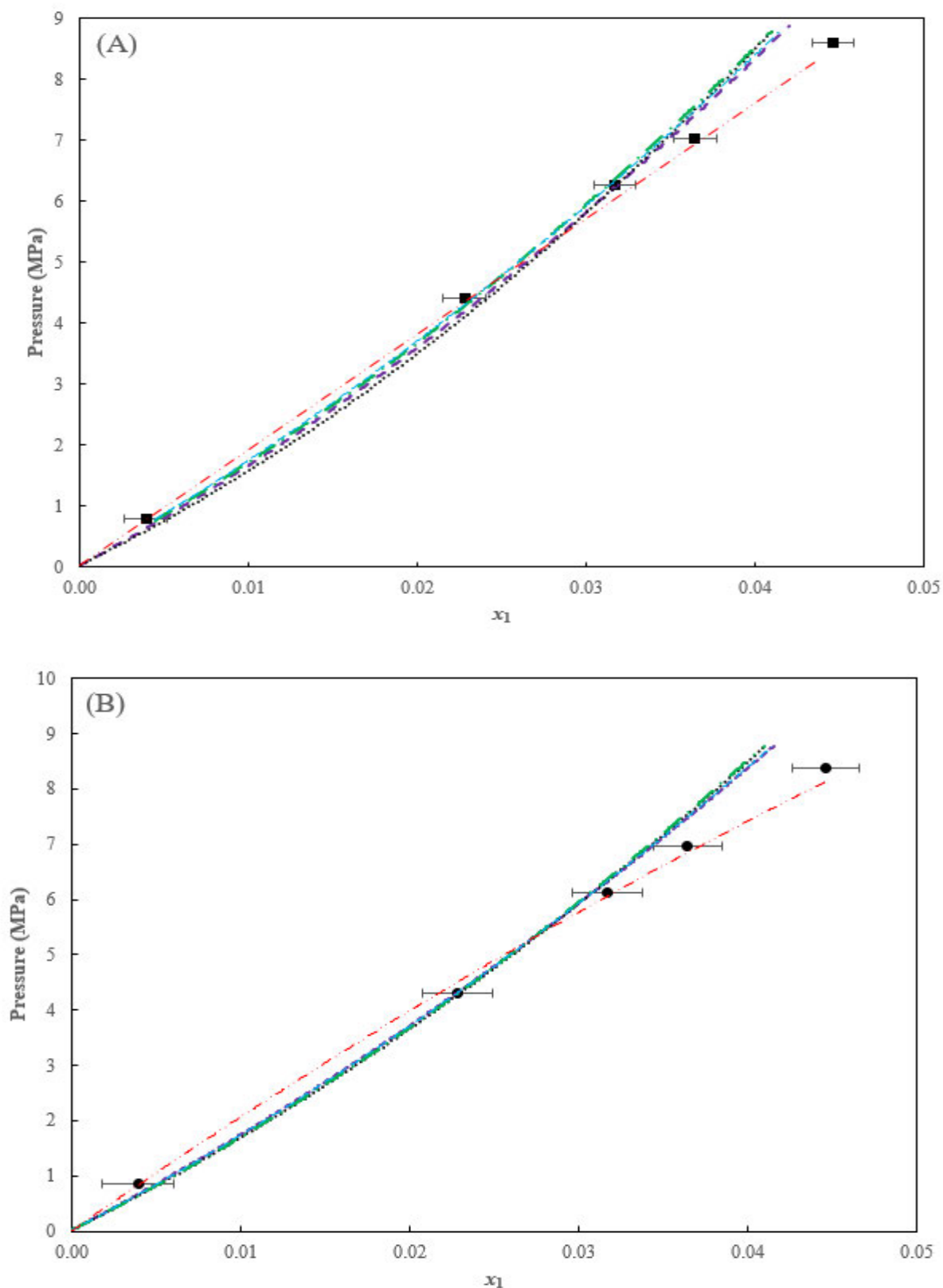


Figure 6-25: Thermodynamic modelling of the (CH₄ (1) / C₃H₈ (2) 95/5 mol%) + TEG (3) system.

(A) Experimental data at 303.16 K (■); (B) Experimental data at 323.16 K (●); and modelling results: PR model (- · - ·); SRK model (- - -); PRWS (- · - ·); CPA (- - -); and PC-SAFT model (·····).

From Figure 6-25, the PRWS model correlation is shown to produce the best fit to the experimental data as all of its correlated data lies within the compositional uncertainty for methane (depicted with error bars). This is further illustrated in Table 6-21, where the regressed model parameters and deviations are presented, with the PRWS giving the least deviations. The PRWS has nine parameters, as shown in Table 6-21, unlike other models that had only 3 fitting parameters. Each fitting parameter is dependent on x_1 , x_2 , x_3 , P , and T . As the temperature increases from 303.16 K to 323.16 K, the AARD in pressures and deviation from experimental data for the CPA, PC-SAFT, PR, and the SRK models also increases as can be observed in Figure 6-25 and Table 6-22. Maximum deviation from experimental data for the CPA, PC-SAFT, PR, and SRK can be observed in Figure 6.25 from $x_1 > 0.03$ at 303.16 K (A) and $x_1 > 0.025$ at 323.16 K (B), and the AARD% in pressure are 4.7, 4.25, 4.32 and 4.11 respectively. For highly non-ideal systems, like the one in this case because of the strongly polar molecule TEG, simple equations of state such as the PR and SRK have always to struggled to describe the phase behaviour of such systems as highlighted in chapter 2, hence the not perfect fitting trends observed in Figure 6-25. The visible error bars in Figure 6-25 represent compositional uncertainties for methane. The error bars are not visible for pressure values since the pressure readings uncertainty of 0.03 MPa is very small.

Table 6-22 (a): Regressed model parameters and deviations for the (CH₄ (1) 95mol% + C₃H₈ (2) 5mol%) + TEG (3) system.

Parameter	PRWS model		PR model		SRK model	
	$T = 303.16 \text{ K}$	$T = 323.16 \text{ K}$	$T = 303.16 \text{ K}$	$T = 323.16 \text{ K}$	$T = 303.16 \text{ K}$	$T = 323.16 \text{ K}$
k_{12}	1.9431	2.0594	0.154	0.154	0.2657	0.2657
k_{13}	0.4699	0.5035	0.22761	0.2437	0.19356	0.2065
k_{23}	-2.3657	-1.6537	0.03796	0.036	0.03345	0.0306
A_{12}	119.4234	91.3660				
A_{21}	119.4114	91.3495				
A_{13}	-1.1099	-1.2383				
A_{31}	3.2529	3.5382				
A_{23}	1.0454	0.4710				
A_{32}	2.9756	2.7222				
AAD P (MPa)	0.11	0.11	0.1	0.16	0.1	0.15
AARD P %	1.83	1.90	3.00	4.32	2.7	4.11
AAD x_1	0.0005	0.0002	0.0012	0.0013	0.0011	0.0011
AARD x_1 %	1.68	0.91	5.26	5.59	4.53	4.92
AAD T (K)	11.70	9.10	6.21	4.16	4.64	3.00
AARD T %	3.86	2.81	2.05	1.29	1.53	0.90

Table 6-22 (b): Regressed model parameters and deviations for the (CH₄ (1) 95mol% + C₃H₈ (2) 5mol%) + TEG (3) system cont.

Parameter	CPA model		PC-SAFT model	
	<i>T</i> = 303.16 K	<i>T</i> = 323.16 K	<i>T</i> = 303.16 K	<i>T</i> = 323.16 K
<i>k</i> ₁₂	0.13704	0.13704	0.35261	0.4309
<i>k</i> ₁₃	0.16793	0.173545	0.0066	0.01971
<i>k</i> ₂₃	-0.04458	-0.05403	-0.02075	-0.0178
AAD <i>P</i> (MPa)	0.1	0.15	0.1	0.15
AARD <i>P</i> %	2.66	4.07	3.1	4.25
AAD <i>x</i> ₁	0.001	0.0011	0.0013	0.0013
AARD <i>x</i> ₁ %	4.29	4.78	5.55	5.66
AAD <i>T</i> (K)	4.45	3.25	4.50	2.91
AARD <i>T</i> %	1.47	1.01	1.48	0.90

Methane compositional uncertainties indicated by visible error bars in Figure 6-25 are large due to the inherent mass balance uncertainty of 0.01 g, considering the very small mass of the gas mixture (methane + propane) which was loaded for the entire range of the data measured.

The CPA bubble point predictions using *k*_{ij} reported in Table 6-19 is displayed in Figures E-3.4. A and B for the data at 303.16 and 323.15K respectively. The AARD% in pressure were 24.55 and 23.56 for the data at 303.16 and 323.15K respectively. In both cases, the bubble point pressure values are over predicted and this trend becomes more pronounced as the methane mole fraction increases.

Trends for the absolute values of the regressed binary interaction parameters for possible binary pairs of the system in Table 6-22 (a) and (b) can be described as follows:

For the PRWS:

Parameter	PRWS model			
	<i>T</i> = 303.16 K		<i>T</i> = 323.16 K	
	Value	σ	Value	σ
<i>k</i> ₁₂	1.9431	0.3865	2.0594	1.8528
<i>k</i> ₁₃	0.4699	0.0011	0.5035	0.0019
<i>k</i> ₂₃	-2.3657	1.2835	-1.6537	3.0076

All values in SI units.

σ represents the standard deviation reported in Aspen Plus V12

- *k*₁₃ at 303.16 K < *k*₁₃ at 323.16 K. The interaction parameter between methane and TEG increases with an increase in temperature. The binary interaction parameter between methane and TEG in this ternary system of 0.5035 at 323.16 K is comparable to the binary interaction

parameter between methane + TEG binary system of 0.5363 at 323.15 K presented in Table 6-16.

- k_{23} at 303.16 K $>$ k_{23} at 323.16 K. The interaction parameter between propane and TEG decreases with increased temperature.
- Only the propane + methanol binary interaction parameter at 323.16 K was insignificant to the overall model fitting. This is because the absolute value of the binary interaction parameter was less than the value of the standard deviation, indicating that the data are over fitted (Carlson, 1996). All the other parameters at 303.16 and 323.16 K were significant to the overall model fitting.

For the PR and SRK models

Parameter	PR model				SRK model			
	$T = 303.16$ K		$T = 323.16$ K		$T = 303.16$ K		$T = 323.16$ K	
	Value	σ	Value	σ	Value	σ	Value	σ
k_{12}	0.1540	0.0000	0.154	0.0000	0.2657	0.0000	0.2657	0.0000
k_{13}	0.2276	0.0241	0.2437	0.0272	0.19356	0.0198	0.2065	0.0250
k_{23}	0.0380	0.0797	0.036	0.0881	0.03345	0.0618	0.0306	0.0753

All values in SI units.

σ represents the standard deviation reported in Aspen Plus V12

- k_{12} at 303.16 K $= k_{12}$ at 323.16 K; a similar trend was observed in Table 6-21. The interaction parameter between methane and propane is independent of temperature.
- k_{13} at 303.16 K $<$ k_{13} at 323.16 K. The interaction parameter between methane and TEG increases with an increase in temperature.
- k_{23} at 303.16 K $>$ k_{23} at 323.16 K. The interaction between propane and TEG decreases with an increase in temperature.
- The methane + propane and methane + TEG binary interaction parameters were significant to the overall model fitting, for both the PR and SRK models. Only the propane + TEG binary interaction parameter was insignificant to the overall model fitting. This was because the magnitude of the standard deviation for the propane + TEG binary pair is greater than the absolute value of the binary interaction parameter.

For the CPA model

- k_{12} at 303.16 K $= k_{12}$ at 323.16 K. The interaction parameter between methane and propane is independent of temperature.
- k_{13} at 303.16 K $<$ k_{13} at 323.16 K. The interaction parameter between methane and TEG increases with an increase in temperature. The binary interaction parameter between methane

and TEG in this ternary system of 0.1735 is slightly less than the binary interaction parameter of 0.2046 for the methane + TEG binary system reported in Table 6-16.

Parameter	CPA model				PC-SAFT model			
	$T = 303.16 \text{ K}$		$T = 323.16 \text{ K}$		$T = 303.16 \text{ K}$		$T = 323.16 \text{ K}$	
	Value	σ	Value	σ	Value	σ	Value	σ
k_{12}	0.1370	0.0000	0.1370	0.0000	0.3526	1.3834	0.4309	1.8600
k_{13}	0.1679	0.0176	0.1735	0.0230	0.0066	0.0112	0.0197	0.0133
k_{23}	-0.0446	0.0589	-0.0540	0.0752	-0.0207	0.0804	-0.0178	0.0946

All values in SI units.

σ represents the standard deviation reported in Aspen Plus V12

- k_{23} at 303.16 K < k_{23} at 323.16 K. The interaction parameter between propane and TEG increases with an increase in temperature.
- For all the CPA model, the absolute values of the binary interaction parameters for propane + TEG are less than the magnitude of the standard deviation. This indicates that the data are over fitted, and the parameters are insignificant to the overall model fitting and could possibly be set at 0.

For the PC-SAFT model

- k_{12} at 303.16 K < k_{12} at 323.16 K. The interaction parameter between methane and propane increases with an increase in temperature.
- k_{13} at 303.16 K < k_{13} at 323.16 K. The interaction parameter between methane and TEG increases with increased temperature. The binary interaction parameter for methane + TEG in the ternary system of 0.0197 at 323.16 K is slightly less than 0.03302 for the methane + TEG binary system reported in Table 6-16.
- k_{23} at 303.16 K > k_{23} at 323.16 K. The interaction parameter between propane and TEG decreases with an increase in temperature.
- For the data at 303.16 K, the methane + TEG and propane + TEG binary parameters were insignificant to the overall model fitting.
- At 323.16 K, the methane + propane binary interaction parameter was insignificant to the overall model fitting.

6.4.2.1 Comparison of the propane-free (methane/propane 95/5 mol%) + TEG system and the methane + TEG system at 323.16 K

To investigate the effect of the 5 mol% propane in the gas solubility of the (methane + propane) mixture in TEG, the data for the two systems are compared and presented in Figure 6-26.

Figure 6-26 shows that the pure methane + TEG system has higher total pressure values as compared to the propane-free (methane/propane 95/5mol%) + TEG system. Propane-free refers to the fact that the mole fraction of propane in the ternary mixture of (methane/propane 95/5 mol%) + TEG) system was not considered for comparison purposes, only that of methane + TEG were considered. As the mole fraction of methane increases from x_1 of 0 to 0.027, the difference in pressures between the two systems is virtually linear (mostly constant) and the data points for the two systems are within composition uncertainty of each other.

From x_1 of 0.027 to 0.045, the difference in pressures between the two systems increases sharply and the data points do not lie within the composition uncertainty of each other. Thus, it can be concluded that the 5 mol% propane has an effect in increasing the solubility of methane in TEG and this becomes more pronounced as the mole fraction of methane + propane mixture increases. Methane is a non-polar component, having a net dipole moment of zero and has one type of bonding (C-H) and thus has the weakest Van der Waals forces (Devi, 2022). As propane is introduced into the mixture, the extent of the dispersion forces likewise increases due to more C-H₂ groupings. Propane molecules and methane molecules experience London intermolecular forces only, which are the weakest Van der Waals forces (Brennan, 2017). The increase in the dispersion forces leads to more interaction of the alkane components with TEG.

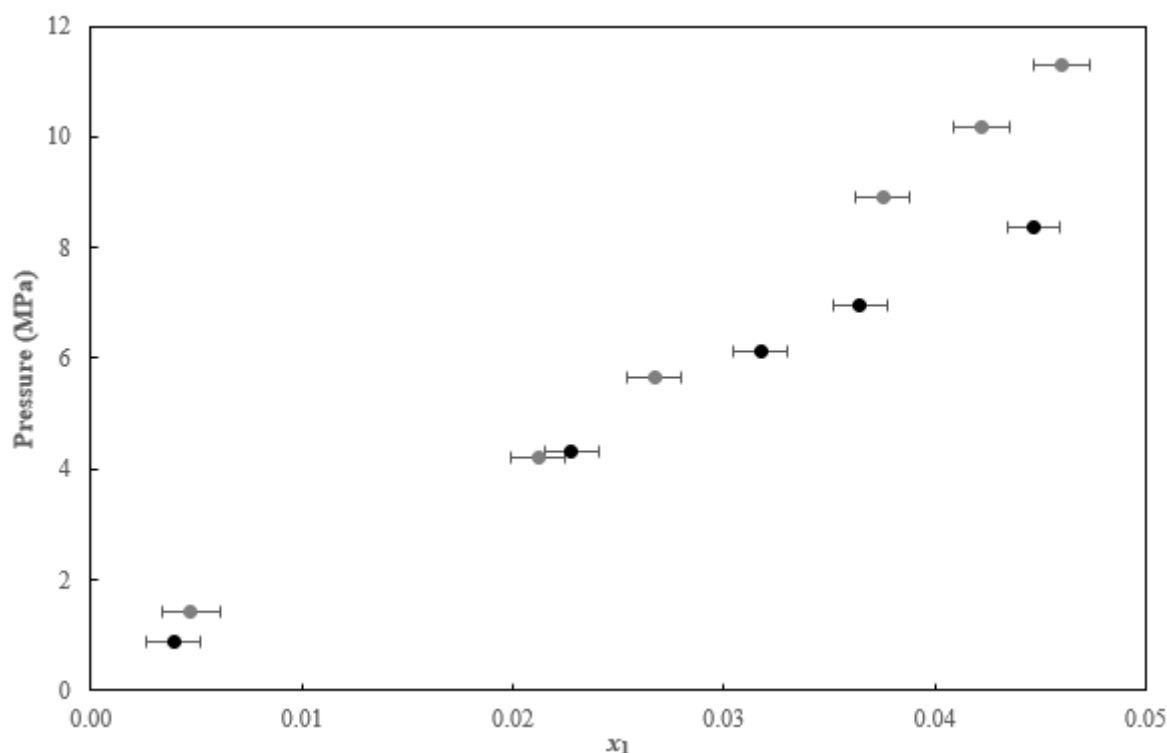


Figure 6-26: Comparison of the TP_x data at 323.16 K for:
 (●), CH₄(1) + TEG(2) ;(●), propane-free (CH₄(1)/ C₃H₈(2) 95/5 mol%) + TEG(3).

6.4.3 New system 3: methane (1) + (methanol (2) / TEG (3) 3.33/96.67 wt.%)

Bubble point measurements were conducted for the methane (1) + (methanol (2) / TEG (3) 3.33/96.67 wt.%) system at 303.16 K and 323.15 K. A total of 12 data points were measured for this system. The (methanol / TEG 3.33/96.67 wt.%) solution was prepared gravimetrically following the method outlined in chapter 5, section 5.2.5.1. The measured data are presented in Figure 6-27. Furthermore, the data is also listed in Table B.5-3 (Appendix B), together with associated uncertainties for the measured variables.

From Figure 6-27, it can be observed that between x_1 of 0.011 and 0.026, the bubble point pressures measured are all slightly higher at 323.15 K than those at 303.15 K. Between x_1 of 0.03 to 0.05 there is a divergence in the trend where the bubble point pressures measured at 323.15 K are lower than those measured at 303.15 K, and the difference in these pressures increases with increase in methane mole fraction. Thus, it can be conclusively said that the solubility of methane (CH₄) in (methanol/TEG 3.33/96.67 wt.%) system is slightly higher at 303.16 K than 323.15 K between x_1 of 0.011 and 0.026 and vice-versa between x_1 of 0.03 to 0.05. At lower pressures less than 8 MPa in this case, the solubility of methane in (methanol /TEG 3.33/96.67 wt.%) is almost independent of temperature. A similar trend was observed on the methane + TEG data measured by Jou et al. (Jou, et al., 1987) presented in Figure 6-16.

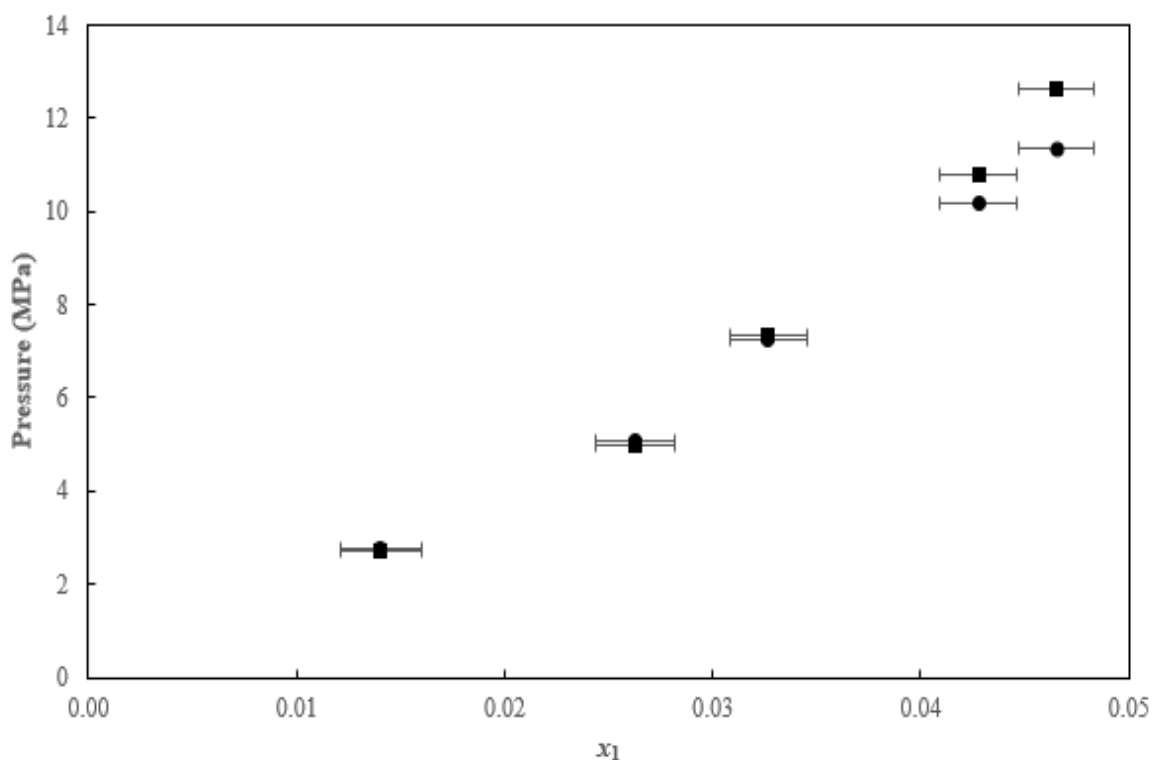


Figure 6-27: TPx graph for the CH_4 (1) + (CH_3OH (2) / TEG (3) 3.33/96.67 wt %) system. 303.16K (■); 323.15K (●).

The measured data from this work was correlated using the PR, SRK, PRWS, CPA, and the PC-SAFT models. Results of the model correlations at 303.16 K and 323.15 K are shown in Figure 6-28 (A) and (B) respectively. Table 6-23 presents the regressed model parameters and deviations. All the model correlations were extrapolated to $x_1=0$ as visible in Figure 6-28.

All the models yielded satisfactory fits to the experimental data at 303.15 K and 323.15 K as can be observed in Figure 6-28. All model correlation data lie within the experimental composition uncertainty of this work, which is represented by error bars. Better fits are observed in Figure 6-28 (B) at 323.15 K as compared to the data at 303.16 K and the trend in model deviations further illustrates this. Table 6-23 shows a decrease in model deviations for both the AAD and the AARD as the temperature increases from 303.16 to 323.15 K on each of the models. The AARD % in pressure at 303.16 K are 0.83, 2.28, 2.01, 2.05 and 2.73 for the PRWS, PR, SRK, CPA and PC-SAFT model correlations, respectively. The AARD % in pressure at 323.16 K are 1.73, 1.32, 1.2, 1.16 and 1.64 for the PRWS, PR, SRK, CPA and PC-SAFT model correlations, respectively. This implies that the PRWS yielded the best fit for this system at 303.16 K, whilst the CPA yielded the best fit at 323.15 K.

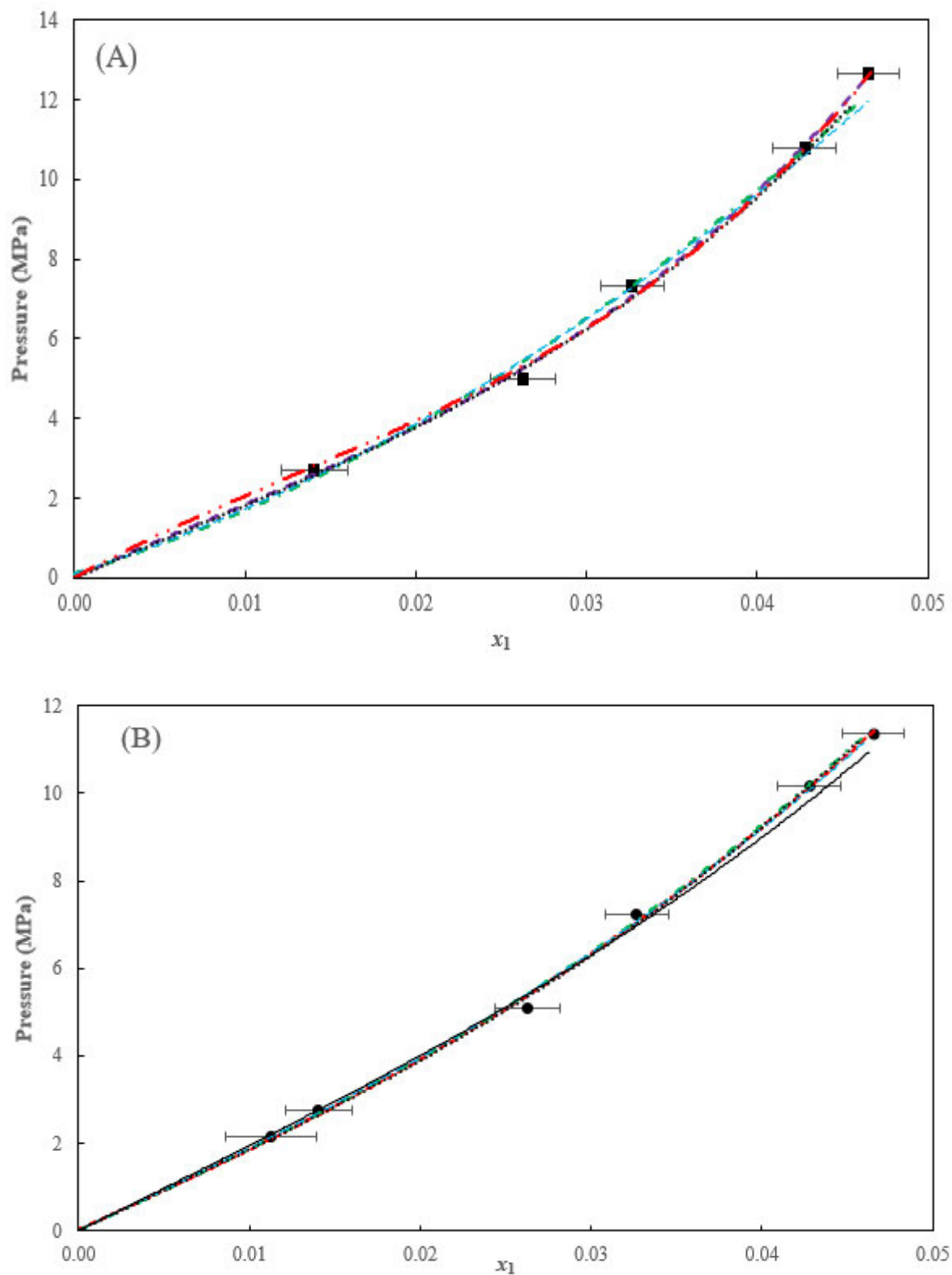


Figure 6-28: Thermodynamic modelling of the CH_4 (1) + $(\text{CH}_3\text{OH}$ (2) / TEG (3) 3.33/96.67 wt%) system.

(A) Experimental data at 303.16 K (■); (B) Experimental data at 323.15 K (●); and modelling results: PR model (-·-·-); SRK model (- - -); PRWS (- · · -); CPA (- - -); and PC-SAFT model (·····).

Table 6-23 (a): Regressed binary parameters and deviations for the various models employed for the CH₄ (1) + (CH₃OH (2) / TEG (3) 3.33/96.67 wt.% system).

Parameter	PRWS model		PR model		SRK model	
	<i>T</i> = 303.16 K	<i>T</i> = 323.15 K	<i>T</i> = 303.16 K	<i>T</i> = 323.15 K	<i>T</i> = 303.16 K	<i>T</i> = 323.15 K
<i>k</i> ₁₂	0.5397	0.9868	0.03706	0.05555	0.07705	0.14076
<i>k</i> ₁₃	0.5931	0.6205	0.25127	0.26515	0.2284	0.24144
<i>k</i> ₂₃	-0.9937	-0.8777	0.05796	0.05664	0.06794	0.06982
<i>A</i> ₁₂	18.6893	2.9453				
<i>A</i> ₂₁	-2.2985	4.6882				
<i>A</i> ₁₃	2.6612	0.5589				
<i>A</i> ₃₁	2.3045	1.1593				
<i>A</i> ₂₃	2.5655	3.1674				
<i>A</i> ₃₂	8.3799	8.0281				
AAD <i>P</i> (MPa)	0.03	0.12	0.2	0.07	0.18	0.07
AARD <i>P</i> %	0.83	1.73	2.28	1.32	2.01	1.2
AAD <i>x</i> ₁	0.0005	0.0004	0.0005	0.0004	0.0003	0.0003
AARD <i>x</i> ₁ %	3.15	1.52	1.84	1.53	1.55	1.3
AAD <i>T</i> (K)	1.98	10.91	6.65	4.70	5.72	3.99
AARD <i>T</i> %	0.65	3.38	2.19	1.46	1.89	1.23

Table 6-23 (b): Regressed binary parameters and deviations for the various models employed for the CH₄ (1) + (CH₃OH (2) / TEG (3) 3.33/96.67 wt.% system) cont.

Parameter	CPA model		PC-SAFT model	
	<i>T</i> = 303.16 K	<i>T</i> = 323.15 K	<i>T</i> = 303.16 K	<i>T</i> = 323.15 K
<i>k</i> ₁₂	0.21683	0.22051	-0.28618	-0.28729
<i>k</i> ₁₃	-0.38916	-0.40812	0.03017	0.04098
<i>k</i> ₂₃	0.16279	0.16279	0.02228	0.01907
AAD <i>P</i> (MPa)	0.18	0.08	0.23	0.1
AARD <i>P</i> %	2.05	1.16	2.73	1.64
AAD <i>x</i> ₁	0.0006	0.0004	0.0005	0.0005
AARD <i>x</i> ₁ %	2.38	1.54	1.93	1.58
AAD <i>T</i> (K)	5.14	3.81	6.12	4.67
AARD <i>T</i> %	1.70	1.18	2.02	1.45

The CPA bubble point predictions using *k*_{ij} reported in Table 6-19 are displayed in Figures E-3.5. A and B for the data at 303.16 and 323.16K respectively. The AARD% in pressure were 10.58 and 8.82 for the data at 303.16 and 323.16K respectively. In both cases, the bubble point pressure values seem to be

slightly over predicted. Comparison of Figures E-3.5 A and B with Figures 6-28 A and B respectively shows that in both cases, the CPA model yielded satisfactory fits to the experimental data.

Trends for the absolute values of the regressed binary interaction parameters for possible binary pairs of this system in Table 6.23 (a) and (b) can be described as follows:

For the PRWS:

Parameter	PRWS model			
	$T = 303.16 \text{ K}$		$T = 323.15 \text{ K}$	
	Value	σ	Value	σ
k_{12}	0.5397	0.2058	0.9868	0.1947
k_{13}	0.5931	0.0012	0.6205	0.0009
k_{23}	-0.9937	0.9793	-0.8777	0.5502

All values in SI units.

σ represents the standard deviation reported in Aspen Plus V12

- k_{12} at 303.16 K < k_{12} at 323.15 K. The interaction parameter between methane and methanol increases with an increase in temperature. The value of the interaction parameter between methane + methanol binary pair of this ternary system of 0.5397 at 303.16 K is significantly larger than 0.3423 for the methane + methanol binary system at 303.15 K reported in Table 6-15.
- k_{13} at 303.16 K < k_{13} at 323.15 K. The interaction parameter between methane and TEG increases with an increased temperature. The value of the interaction parameter between methane + TEG binary pair of this ternary system of 0.6205 is larger than the 0.5363 for the pure methane + TEG binary system at 323.15 K reported in Table 6-16.
- k_{23} at 303.16 K > k_{23} at 323.15 K. The interaction parameter between methanol and TEG decreases with increased temperature.
- At 303.16 K, the methane + methanol and methane + TEG binary interaction parameters were significant to the overall model fitting. The absolute value of the binary interaction parameter for the methanol + TEG binary pair was almost similar to the value of the standard deviation. This indicates that the methanol + TEG binary interaction parameter was insignificant to the overall model fitting (Carlson, 1996).
- At 323.15 K, all the binary interaction parameters were significant to the overall model fitting since the magnitude of the standard deviation was less than the absolute value of the respective binary interaction parameters in the ternary system.

For the PR and SRK models

- k_{12} at 303.16 K < k_{12} at 323.15 K. The interaction parameter between methane and methanol increases with an increase in temperature.
- k_{13} at 303.16 K < k_{13} at 323.15 K. The interaction parameter between methane and TEG slightly increases with an increase in temperature.
- k_{23} at 303.16 K > k_{23} at 323.15 K (PR only). The interaction parameter between methanol and TEG slightly decreases with an increase in temperature.

Parameter	PR model				SRK model			
	$T = 303.16$ K		$T = 323.15$ K		$T = 303.16$ K		$T = 323.15$ K	
	Value	σ	Value	σ	Value	σ	Value	σ
k_{12}	0.03706	1.0445	0.0556	1.0883	0.0771	0.8905	0.1408	0.8953
k_{13}	0.25127	0.0537	0.2652	0.0557	0.2284	0.0453	0.2414	0.0454
k_{23}	0.05796	0.1265	0.0566	0.1105	0.0679	0.0995	0.0698	0.0833

All values in SI units.

σ represents the standard deviation reported in Aspen Plus V12

- k_{23} at 303.16 K < k_{23} at 323.15 K (SRK only). The interaction parameter between methanol and TEG slightly increases with an increase in temperature.
- The magnitude of the standard deviation for the binary interaction parameter between methane + methanol and methanol + propane binary pairs of this ternary system is larger than the values of the binary interaction parameters. This indicates that these parameters are insignificant to the overall model fitting and could possibly be set to 0. The magnitude of the standard deviation for the binary interaction parameter for the methane + TEG binary pair of the ternary mixture is significantly less than the value of the binary interaction parameter at all isotherms considered. This indicates that the methane + TEG binary interaction parameter is significant to the overall model fitting (Carlson, 1996).

For the CPA model

Parameter	CPA model				PC-SAFT model			
	$T = 303.16$ K		$T = 323.15$ K		$T = 303.16$ K		$T = 323.15$ K	
	Value	σ	Value	σ	Value	σ	Value	σ
k_{12}	0.2168	0.0285	0.2205	0.0280	-0.2862	1.0017	-0.2873	1.0177
k_{13}	-0.3892	0.6218	-0.4081	0.6319	0.0302	0.0329	0.0410	0.0322
k_{23}	0.1628	0.0000	0.1628	0.0000	0.0223	0.1069	0.0191	0.0923

All values in SI units.

σ represents the standard deviation reported in Aspen Plus V12

- k_{12} at 303.16 K < k_{12} at 323.15 K. The interaction parameter between methane and methanol slightly increases with an increase in temperature. The value of the binary interaction parameter for the methane + methanol binary pair in the ternary system of 0.2168 at 303.16 K is significantly greater than 0.0462 for the methane + methanol binary system presented in Table 6-15.
- k_{13} at 303.16 K < k_{13} at 323.15 K. The interaction parameter between methane and TEG slightly increases with an increase in temperature. The absolute value of the binary interaction parameter for methane + TEG of 0.4081 at 323.15 K is significantly larger than the 0.2046 at 323.15 K for the pure methane + TEG binary system presented in Table 6-16.
- k_{23} at 303.16 K = k_{23} at 323.15 K. The interaction parameter between methanol and TEG is independent of temperature between 303.16 and 323.15 K.
- The methane + methanol and the methanol + TEG binary interaction parameters are significant parameters to the overall model fitting since their values are significantly greater than the standard deviations. The methane + TEG binary parameter is insignificant to the overall model fitting and could possibly be set to 0, since the magnitude of the standard deviation is greater than the values of the interaction parameters; hence the data are over fitted. This comment applies to both the CPA and PC-SAFT models.

For the PC-SAFT model

- k_{12} at 303.16 K \leq k_{12} at 323.15 K. The interaction parameter between methane and methanol is almost the same, however, with some minor increase as the temperature increases. The absolute value of the binary interaction parameter between methane + methanol binary pair of the ternary system of 0.2862 at 303.16 K is significantly greater than 0.0498 reported in Table 6-15 for the methane + methanol binary system at 303.15 K.
- k_{13} at 303.16 K < k_{13} at 323.15 K. The interaction parameter between methane and TEG increases with an increase in temperature. The absolute value of the binary interaction parameter for methane + TEG of 0.0410 at 323.15 K is larger than the 0.03302 at 323.15 K for the pure methane + TEG binary system presented in Table 6-16.
- k_{23} at 303.16 K > k_{23} at 323.15 K. The interaction parameter between methanol and TEG decreases with an increase in temperature.

Methane is a non-polar molecule, whilst methanol and TEG are polar molecules capable of either self or cross association. With the addition of methanol to the methane + TEG system, the methane solubility is slightly improved. Most likely, the unlike interactions between the methane and -OH groupings result in this behaviour.

Consequently, similar trends are observed on all models for the interaction between methane + methanol and methane + TEG. Similar trends are also observed for the interaction between methanol and TEG except for the SRK and CPA models. The trends are similar because of this narrow composition region.

6.4.3.1 Comparison of the methanol-free (methane + (methanol / TEG 3.33/96.67 wt. %)) system and the methane + TEG system

A comparison of the pure methane + TEG system at 323.15 K and the methanol-free (methane + (methanol / TEG 3.33/96.67 wt. %)) system was performed to observe the effect of the methanol addition in the system. The data are presented in Figure 6-29. Methanol-free refers to the fact that only the composition of methane and TEG were considered from the ternary system of methane + (methanol / TEG 3.33/96.67 wt. %) system.

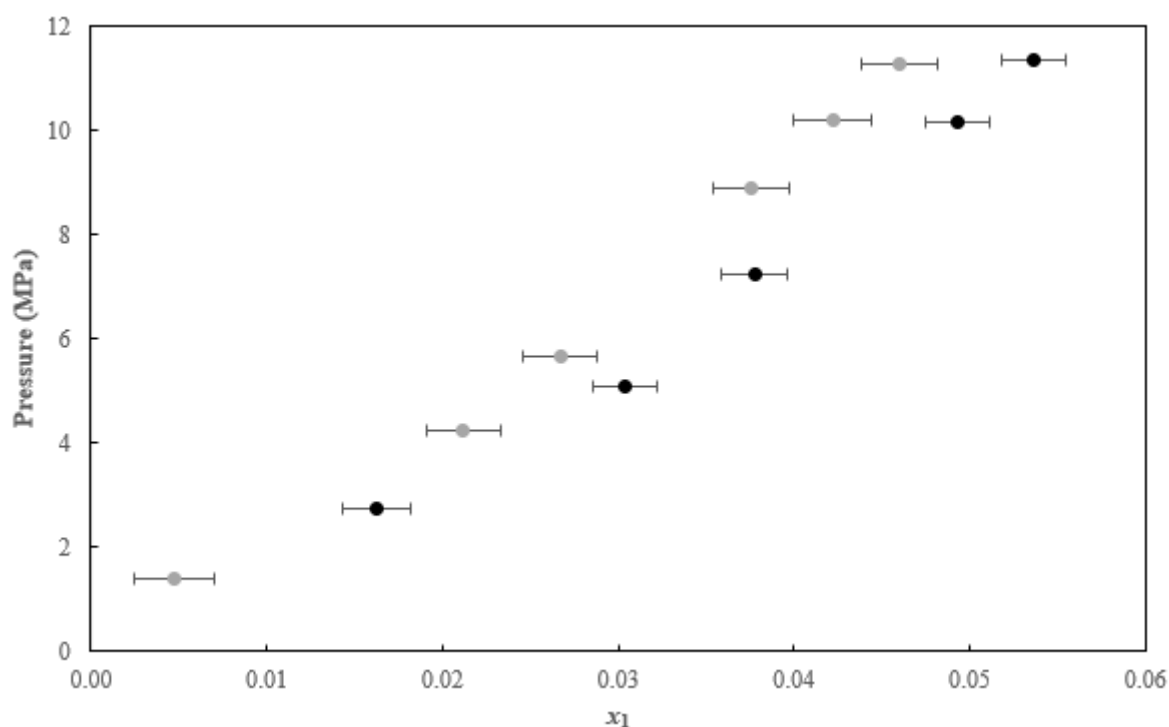


Figure 6-29: Comparison of the TPx data at 323.15 K for:
 (○), CH₄(1) + TEG(2); (●), methanol-free CH₄(1) + (CH₃OH(2) / TEG(3) 3.33/ 96.67 wt. %).

Figure 6.29 shows that the 3.33% methanol added to TEG has an effect of increasing the solubility of methane in TEG. This is because for the same pressure value, the composition of methane in TEG is higher for the ternary system compared to the binary system. This effect is more pronounced as the methane mole fraction increases (see Figure 6-29). To avoid more methane losses via TEG solvent, it will be wise to have process operations where methanol is not present or is kept at minimum levels.

6.4.4 New system 4: Carbon dioxide (1) + (methanol (2) / TEG (3) 3.33/96.67 wt.%)

Bubble point measurements were conducted for the carbon dioxide (1) + (methanol (2) / TEG (3) 3.33/96.67 wt.%) system at 303.16 K and 323.15 K. A total of 11 data points were measured for this system. The measured data are presented in Figure 6.30. Furthermore, the data are also listed in Table B.5-4 (Appendix B), together with associated uncertainties for the measured variables.

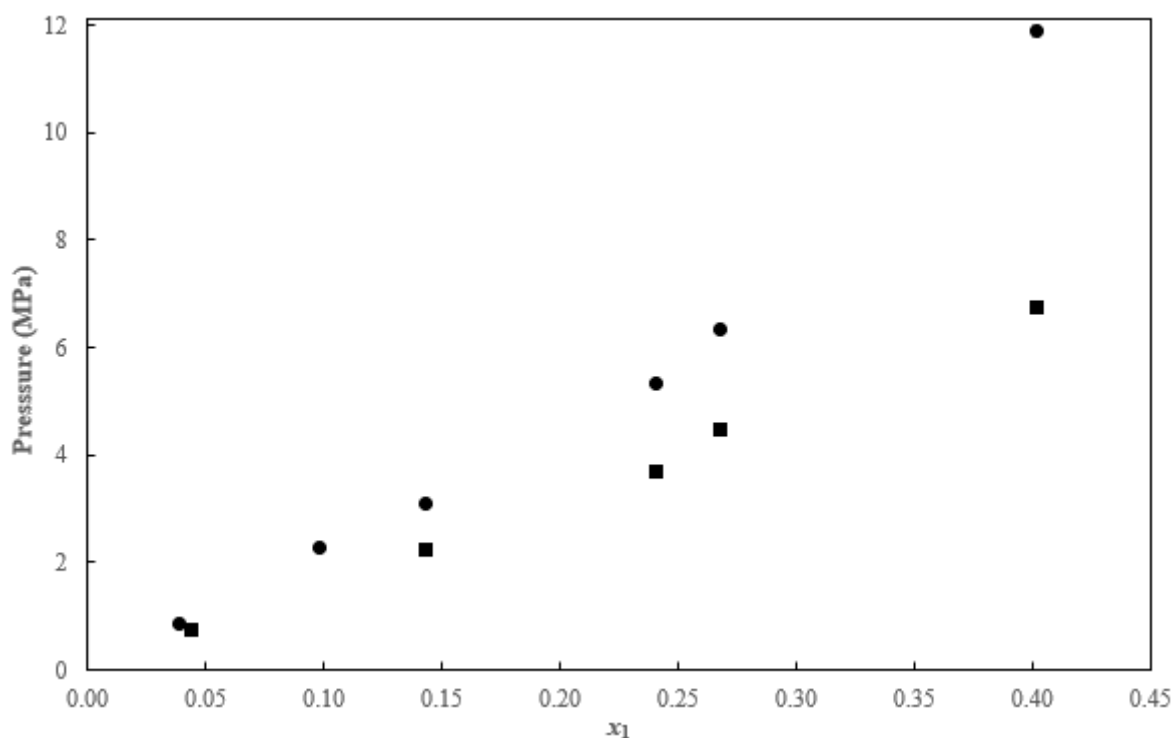


Figure 6-30: TPx graph for the CO_2 (1) + (CH_3OH (2) / TEG (3) 3.33/96.67 wt.%) system.
This work at; 303.16 K (■); 323.15 K (●).

Error bars are not visible in Figures 6-30 due to the small uncertainties in carbon dioxide composition and the measured pressure values. Figure 6-30 shows that at the same liquid mole fraction of carbon dioxide in the system, the equilibrium pressures are always higher for higher temperatures (323.15 K), and they are lower for low temperatures (303.16 K). Also, it is observable that as the liquid mole fraction of carbon dioxide increases in the system, the difference between the bubble point pressures measured at the same liquid mole fraction of carbon dioxide increases. A similar trend was also observed for the carbon dioxide + TEG data measured by Jou et al. (Jou et al., 1987). Therefore, from Figure 6-30, it can be conclusively said that the solubility of carbon dioxide in the (methanol/TEG 3.33/96.67 wt.%) system is greater at 303.16 K than at 323.15 K. At lower pressures, the solubility of carbon dioxide in (methanol/TEG 3.33/96.67 wt.%) system is almost independent of temperature.

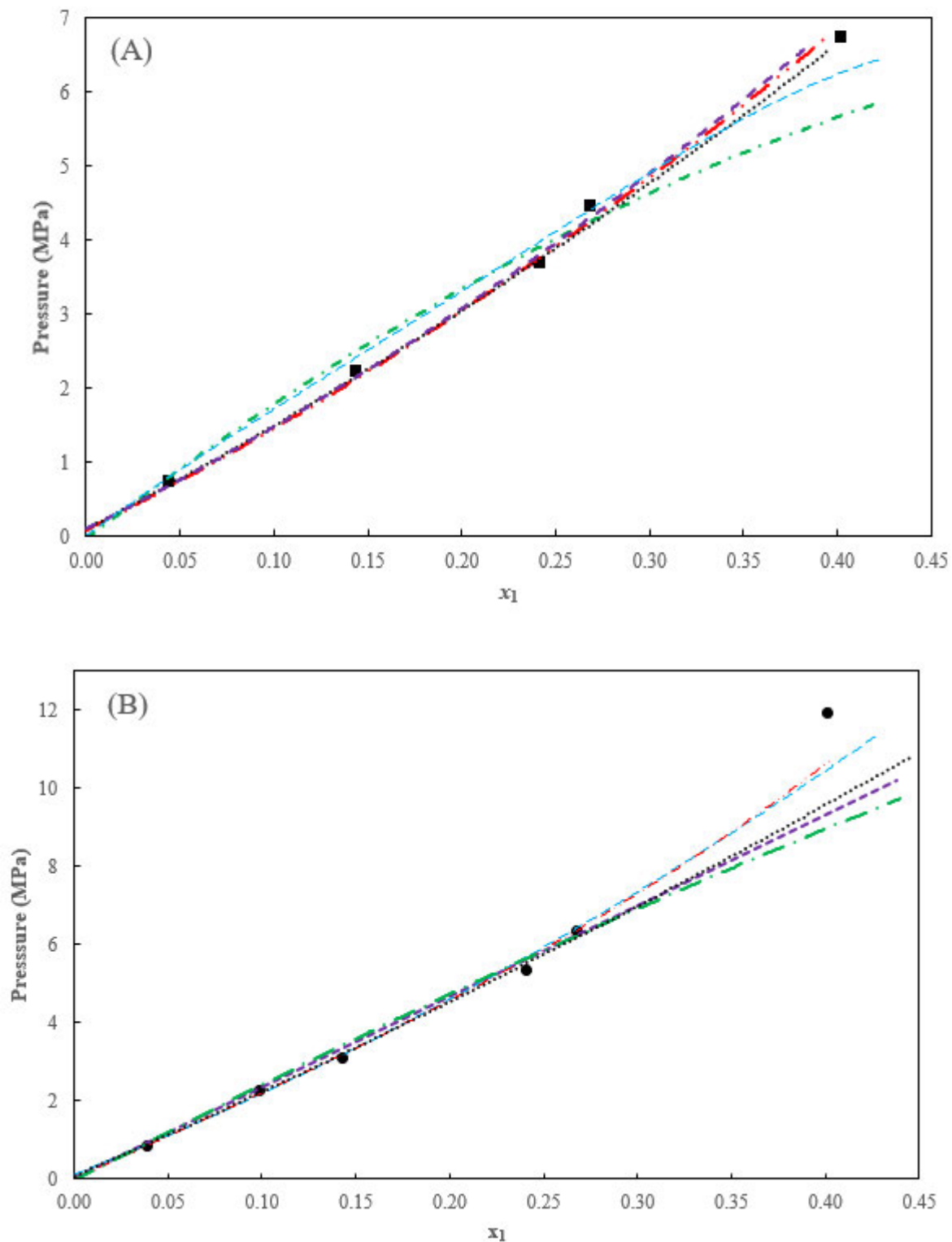


Figure 6-31: Thermodynamic modelling of the CO_2 (1) + $(\text{CH}_3\text{OH}$ (2) /TEG (3) 3.33/96.67 wt.%) system.

(A) Experimental data: 303.16 K (■); (B) Experimental data 323.15 K (●); and model results: PR model (— · —); SRK model (— — —); PRWS (— · · —); CPA (— — —); and PC-SAFT model (·····).

The PR, SRK, PRWS, CPA, and PC-SAFT models were used to correlate the data measured in this work. Results of the model correlations are shown in Figure 6-31 (A) for the data at 303.16 K and (B) for the data at 323.15 K. For the CPA model, the binary interaction parameter k_{ij} for carbon dioxide + TEG of 0.0183 for the data at 303.16 K was evaluated following the method outlined by (Wise & Chapoy, 2016). Table 6-24 presents the regressed model parameters and deviations. All the model correlations were extrapolated to $x_1 = 0$ as visible in Figure 6-31.

Error bars are not visible in Figure 6-31 due to the small uncertainties in carbon dioxide composition and in the pressure values. Figure 6-31 (A) shows that the PRWS, CPA and the PC-SAFT model correlations yielded satisfactory fits to the experimental data over all the range measured at 303.16 K. This is further illustrated by the AARD in pressures which are 1.30%, 1.62% and 1.33% at 303.16 K for the PRWS, CPA and PC-SAFT respectively (Table 6-24). The association models (CPA and PC SAFT) performed well in this case since they account for the hydrogen bonding in the methanol and TEG molecules. The PR and SRK models also yielded good fits for the first four data points from $x_{\text{CO}_2} = 0.04$ to $x_{\text{CO}_2} = 0.28$, after which there is a significant noticeable deviation from the data point at $x_{\text{CO}_2} = 0.40$. For the SRK model, the Weighted least squares initialisation method was used due to convergence issues with the default Deming initialisation method. The AARD in pressures for the PR and SRK at 303.16 K are 4.71 % and 3.00% in that order.

Figure 6-31 (B) shows that the PRWS and SRK models yielded better fits to the experimental data at 323.15 K than all the other models. This is illustrated by the AARD in pressure for the PRWS and SRK models at 323.15 K which are 3.09% and 2.82% respectively (Table 6-24). The PR, CPA and PC-SAFT models did not yield very satisfactory correlations at 323.15 K. For the PC-SAFT model, the Weighted least squares initialisation method was used. This was due to convergence issues with the default Deming initialisation method. The AARD % in pressures for the PR, CPA and PC-SAFT models are 5.65, 4.57 and 3.54 respectively as shown in Table 6-24. In either case, Figure 6-31 (A or B), the PRWS had 9 regressed binary interaction parameters compared to 3 for other models hence the better performance.

Table 6-24 (a): Regressed binary parameters and deviations for the CO₂ (1) + (CH₃OH (2) / TEG (3) 3.33/96.67 wt.%) system.

Parameter	PRWS model		PR model		SRK model	
	<i>T</i> = 303.16 K	<i>T</i> = 323.15 K	<i>T</i> = 303.16 K	<i>T</i> = 323.15 K	<i>T</i> = 303.16 K	<i>T</i> = 323.15 K
<i>k</i> ₁₂	0.6479	0.1261	-0.207	-0.13887	-0.22648	-0.0982
<i>k</i> ₁₃	0.5257	0.8635	0.15942	0.16156	0.15043	0.1476
<i>k</i> ₂₃	-1.5627	-1.6245	0.02105	-0.00022	0.02472	0.0099
<i>A</i> ₁₂	9.8057	17.0168				
<i>A</i> ₂₁	2.0794	-2.6041				
<i>A</i> ₁₃	4.3213	2.2232				
<i>A</i> ₃₁	-0.8365	0.1957				
<i>A</i> ₂₃	1.7601	3.1454				
<i>A</i> ₃₂	8.8895	7.8236				
AAD <i>P</i> (MPa)	0.04	0.25	0.24	0.47	0.12	0.17
AARD <i>P</i> %	1.30	3.09	4.71	5.65	3.00	2.82
AAD <i>x</i> ₁	0.0061	0.0014	0.0086	0.0139	0.0088	0.0096
AARD <i>x</i> ₁ %	2.25	0.74	3.32	5.57	3.49	3.96
AAD <i>T</i> (K)	0.82	15.46	13.13	11.99	11.93	11.61
AARD <i>T</i> %	0.27	4.78	4.33	3.71	3.94	3.59

Table 6-24 (b): Regressed binary parameters and deviations for the CO₂ (1) + (CH₃OH (2) / TEG (3) 3.33/96.67 wt.%) system cont.

Parameter	CPA model		PC-SAFT model	
	<i>T</i> = 303.16 K	<i>T</i> = 323.15 K	<i>T</i> = 303.16 K	<i>T</i> = 323.15 K
<i>k</i> ₁₂	-1.02194	-0.20903	-0.3436	1.87099
<i>k</i> ₁₃	0.0183	0.10352	0.10395	0.02627
<i>k</i> ₂₃	0.12879	0.1145	0.02043	-0.01264
AAD <i>P</i> (MPa)	0.06	0.36	0.06	0.27
AARD <i>P</i> %	1.62	4.57	1.33	3.54
AAD <i>x</i> ₁	0.0027	0.0108	0.0046	0.0106
AARD <i>x</i> ₁ %	1.27	4.49	1.83	3.84
AAD <i>T</i> (K)	4.60	9.20	3.54	7.95
AARD <i>T</i> %	1.52	2.85	1.17	2.46

The CPA bubble point predictions using *k*_{ij} reported in Table 6-19 are displayed in Figures E-3.6. A and B for the data at 303.16 and 323.15 K respectively. The AARD% in pressure were 5.98 and 6.46 for the data at 303.16 and 323.15 K respectively. In both cases, the bubble point pressure values seem to fairly match the experimental data, except for the data point where the carbon dioxide mole fraction was 0.4015. Comparison of Figure E-36 A and B to Figures 6-31 A and B respectively shows that the CPA model yielded satisfactory fits to the experimental data in both scenarios.

Trends for the absolute values of the regressed binary interaction parameters for possible binary pairs of this system in Table 6-24 (a) and (b) can be described as follows:

For the PRWS:

- k_{12} at 303.16 K > k_{12} at 323.15 K. The interaction parameter between carbon dioxide and methanol decreases with an increase in temperature. The binary interaction parameter between carbon dioxide + methanol binary pair of this ternary system, of 0.6479 at 303.16 K is larger and outside of the range of 0.5138 to 0.0984 for the carbon dioxide + methanol binary system from 298.15 K to 313.15 K reported earlier in this work.

Parameter	PRWS model			
	$T = 303.16 \text{ K}$		$T = 323.15 \text{ K}$	
	Value	σ	Value	σ
k_{12}	0.6479	0.3709	0.1261	0.0694
k_{13}	0.5257	0.0034	0.8635	0.0014
k_{23}	-1.5627	1.2339	-1.6245	0.4171

All values in SI units.

σ represents the standard deviation reported in Aspen Plus V12

- k_{13} at 303.16 K < k_{13} at 323.15 K. The interaction between carbon dioxide and TEG increases with an increase in temperature. The binary interaction parameter for carbon dioxide + TEG binary pair of the ternary system of 0.5257 at 303.16 K is significantly large compared to 0.0984 for the carbon dioxide + TEG binary pair reported in this work at 298.15 K.
- k_{23} at 303.16 K < k_{23} at 323.15 K. The interaction between methanol and TEG increases with an increase in temperature.
- The carbon dioxide + methanol, carbon dioxide + TEG and methanol + TEG binary interaction parameters are all significant to the overall model fitting. This is because the absolute values of the interaction parameters for these binary pairs are all larger than the standard deviation.

For the PR model

Parameter	PR model				SRK model			
	$T = 303.16 \text{ K}$		$T = 323.15 \text{ K}$		$T = 303.16 \text{ K}$		$T = 323.15 \text{ K}$	
	Value	σ	Value	σ	Value	σ	Value	σ
k_{12}	-0.2070	0.0000	-0.1389	2.4762	-0.2265	2.6839	-0.0982	1.5613
k_{13}	0.1594	0.0426	0.1616	0.1341	0.1504	0.1443	0.1476	0.0831
k_{23}	0.0211	0.1399	-0.0002	0.2373	0.0247	0.1759	0.0099	0.1714

All values in SI units.

σ represents the standard deviation reported in Aspen Plus V12

- k_{12} at 303.16 K $>$ k_{12} at 323.15 K. The interaction parameter between carbon dioxide and methanol increases with an increase in temperature.
- k_{13} at 303.16 K $<$ k_{13} at 323.15 K. The interaction parameter between carbon dioxide and TEG decreases with an increase in temperature.
- k_{23} at 303.16 K $>$ k_{23} at 323.15 K. The interaction parameter between methanol and TEG increases with an increase in temperature.
- The carbon dioxide + methanol, carbon dioxide + TEG binary interaction parameters are significant to the overall model fitting for the PR model at 303.16 K. This is because the magnitude of the standard deviation is less than the absolute values of the correlated binary interaction parameters. The methanol + TEG binary interaction parameter at 303.16 K is less than the standard deviation indicating that the data are over fitted and this parameter could possibly be set at 0.
- At the 323.15 K for the PR model, the absolute values of all the binary interaction parameters for the possible binary pairs of this ternary system are less than or almost similar to the standard deviation, indicating that the data are over fitted (Carlson, 1996), hence the trend observed in Figure 6-31 (B).

For the SRK model

- k_{12} at 303.16 K $>$ k_{12} at 323.15 K. The interaction parameter between carbon dioxide and methanol decreases with an increase in temperature.
- k_{13} at 303.16 K $>$ k_{13} at 323.15 K. The interaction parameter between carbon dioxide and TEG increases with an increase in temperature.
- k_{23} at 303.16 K $>$ k_{23} at 323.15 K. The interaction parameter between methanol and TEG decreases with an increase in temperature.
- For the SRK model, except for the carbon dioxide + TEG binary interaction parameter at 323.15 K, all the other binary interaction parameters have values less than their standard deviations, indicating that the data are over fitted. This explains the trends observed in Figure 6-31.

For the CPA model

- k_{12} at 303.16 K $<$ k_{12} at 323.15 K. The interaction parameter between carbon dioxide and TEG increases with an increase in temperature. The interaction parameter between carbon dioxide and methanol binary pair of this ternary system 1.02194 (absolute value) at 303.16 K is significantly larger and outside of the range (0.1128 to 0.1159 (absolute values)) for the carbon dioxide + methanol binary system of this work reported over a temperature of 298.10 K to 313.15 K respectively.

- k_{13} at 303.16 K < k_{13} at 323.15 K. The interaction parameter between carbon dioxide and TEG increases with an increase in temperature.

Parameter	CPA model				PC-SAFT model			
	$T = 303.16$ K		$T = 323.15$ K		$T = 303.16$ K		$T = 323.15$ K	
	Value	σ	Value	σ	Value	σ	Value	σ
k_{12}	-1.0219	4.6542	-0.2090	3.6649	-0.3436	5.7514	1.8710	4.5829
k_{13}	0.0899	0.1822	0.1035	0.1413	0.1040	0.2078	0.0263	0.1501
k_{23}	0.1288	0.1593	0.1145	0.2921	0.0204	0.0528	-0.0126	0.1728

All values in SI units.

σ represents the standard deviation reported in Aspen Plus V12

- k_{23} at 303.16 K > k_{23} at 323.15 K. The interaction parameter between methanol and TEG decreases with an increase in temperature.
- The magnitude of the standard deviation for all the possible binary parameters of the ternary system for both the CPA and PC SAFT models is larger than the values of the binary interaction parameters. This indicates that the data are over fitted; hence the trends observed in Figure 6-31.

For the PC-SAFT model

- k_{12} at 303.16 K > k_{12} at 323.15 K. The interaction parameter between carbon dioxide and methanol decreases with an increase in temperature. The binary interaction parameter between carbon dioxide + methanol binary pair of the ternary system of 0.3436 at 303.16 K is significantly larger than 0.0005 (absolute value) for the pure carbon dioxide + methanol system at 298.15 K.
- k_{13} at 303.16 K > k_{13} at 323.15 K. The interaction parameter between carbon dioxide and TEG decreases with an increase in temperature. The binary interaction between carbon dioxide + TEG binary pair of the ternary system at 303.16 K of 0.1039 is comparable to 0.1605 for the carbon dioxide + TEG binary system of this work at 298.15 K.
- k_{23} at 303.16 K > k_{23} at 323.15 K. The interaction parameter between methanol and TEG increases with an increase in temperature.

6.4.4.1 Comparison of the (carbon dioxide + TEG) and methanol-free (carbon dioxide + (methanol/TEG 3.33/96.67 wt.%) system

The effect of the addition of 3.33% methanol to TEG on the solubility of carbon dioxide in TEG is observed by comparing the data of the two data sets of carbon dioxide + TEG measured by Jou et

al.(Jou, et al., 1987) at 323.15 K and the methanol-free (carbon dioxide + (methanol/TEG 3.33/96.67 wt. %)) measured in this work at 323.15 K. Methanol-free (Carbon dioxide + (methanol/TEG 3.33/96.67 wt. %)) means only the composition of carbon dioxide and TEG from this ternary system was considered for comparison purposes. TP_x data for carbon dioxide + TEG data was not measured in this work at 323.15 K, hence reported literature data was used for comparison purposes. The results of the comparison are displayed in Figure 6-32.

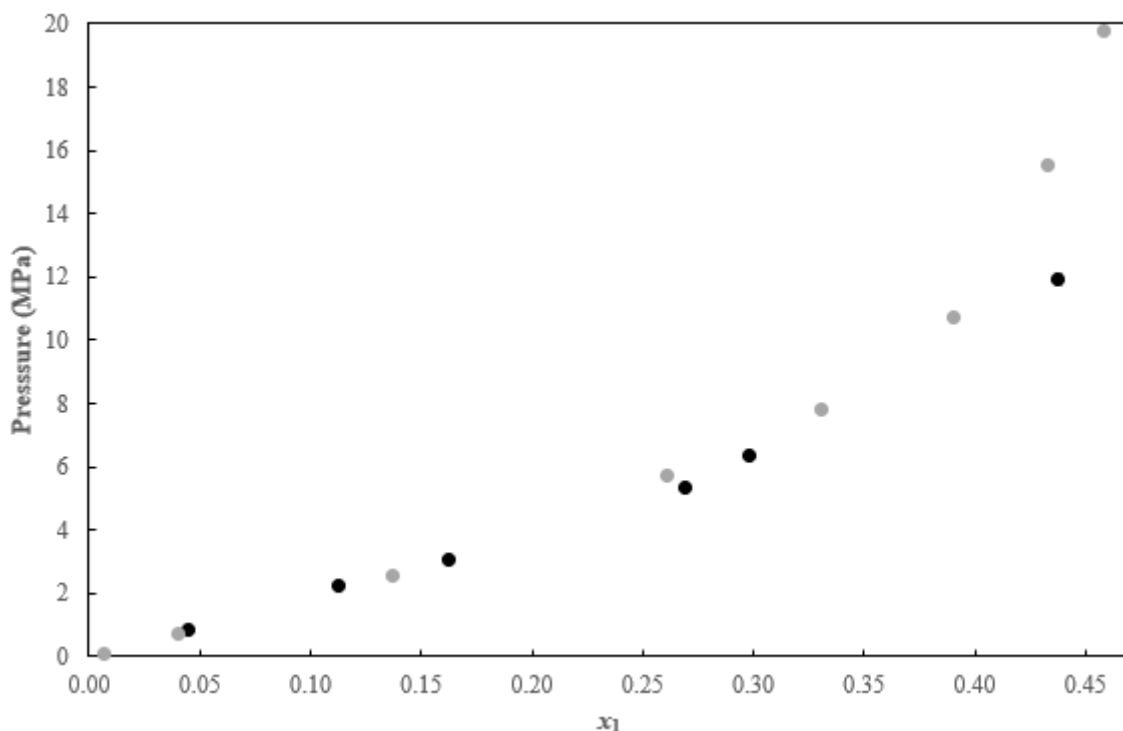


Figure 6-32: Comparison of the TP_x data at $T = 323.15$ K for:
 (●) methanol-free (CO_2 (1) + (CH_3OH (2) / TEG (3) 3.33/96.67 wt. %)), This work; (●), CO_2 (1) + TEG (2) Jou et al. (Jou, et al., 1987)' system.

It can be observed from Figure 6-32 that the addition of methanol is of little significance for the carbon dioxide mole fraction between 0 and 0.1624 since the total pressure values are almost the same between the two systems under comparison. Above the carbon dioxide mole fraction of 0.1624, the added methanol has an effect of increasing the solubility of carbon dioxide in TEG and this becomes more pronounced as the mole fraction of carbon dioxide increases (see the data at x_1 around 0.43 in Figure 6-32). Thus, methanol has an effect of generally increasing the solubility of carbon dioxide in TEG, which could be a non-desirable feature in carbon dioxide dehydration processes since most of the carbon dioxide would be trapped/dissolved in the TEG especially at high pressure operations. Carbon dioxide is a non-polar molecule, whereas methanol and TEG are polar molecules. As a result, the interaction between carbon dioxide and methanol molecules is thermodynamically unfavourable (Zhao, et al., 2000).. Methanol and TEG can either self or cross associate and in the process, form closely packed

structures or clusters (Shukla, et al., 2006) such that the interaction with carbon dioxide is significantly reduced. Shukla et al. (Shukla, et al., 2006) concluded that methanol always forms clusters in a carbon dioxide environment. However, Figure 6-32 shows otherwise.

6.4.5 New system 5: (methane (1)/propane (2) 95/5mol%) + (methanol (3) /TEG (4) 3.33/96.67 wt.%)

Bubble point measurements were conducted for the quaternary system of (methane /propane 95/5 mol%) + (methanol / TEG 3.33/96.67 wt.%) at 283.15, 303.15, and 323.15 K. A total of 15 data points were measured for this system. The experimental method is outlined in chapter 5, section 5.2.5. No literature phase equilibria data was found for the four-component system outlined in this section. Besides the absorption of water, TEG absorbs small quantities of methane, air pollutants, and volatile organic compounds (VOC), which are ultimately released into the atmosphere from the glycol regenerator unit (Arya et al., 2014). Therefore, higher glycol recirculation rates imply that emissions rates will likely increase, resulting in higher operating costs and energy needs for glycol regeneration (Arya et al., 2014). Thus, accurate experimental and model phase equilibria data which is useful to typical gas processing units such as absorber units (high pressure and low temperature) and regenerator units (low pressure and high temperature), is necessary to design and optimize the dehydration unit.

Figures 6-33 to 34 presents the measurement results, which are also listed in Table B.5-5 (Appendix B), together with associated uncertainties for the measured variables.

From the data in Figure 6-33 (A), it is apparent that the solubility of methane in this system is independent of temperature at lower pressures less than 2 MPa. Above 2 MPa, the solubility of methane in the system increases with increasing temperature. For the same composition x_1 , the bubble point pressures follow this trend: P at 283.16 K $>$ P at 303.15 K \gg P at 323.15 K. This trend is more pronounced as the mole fraction of CH_4 increases (see Figure 6-31 (A)).

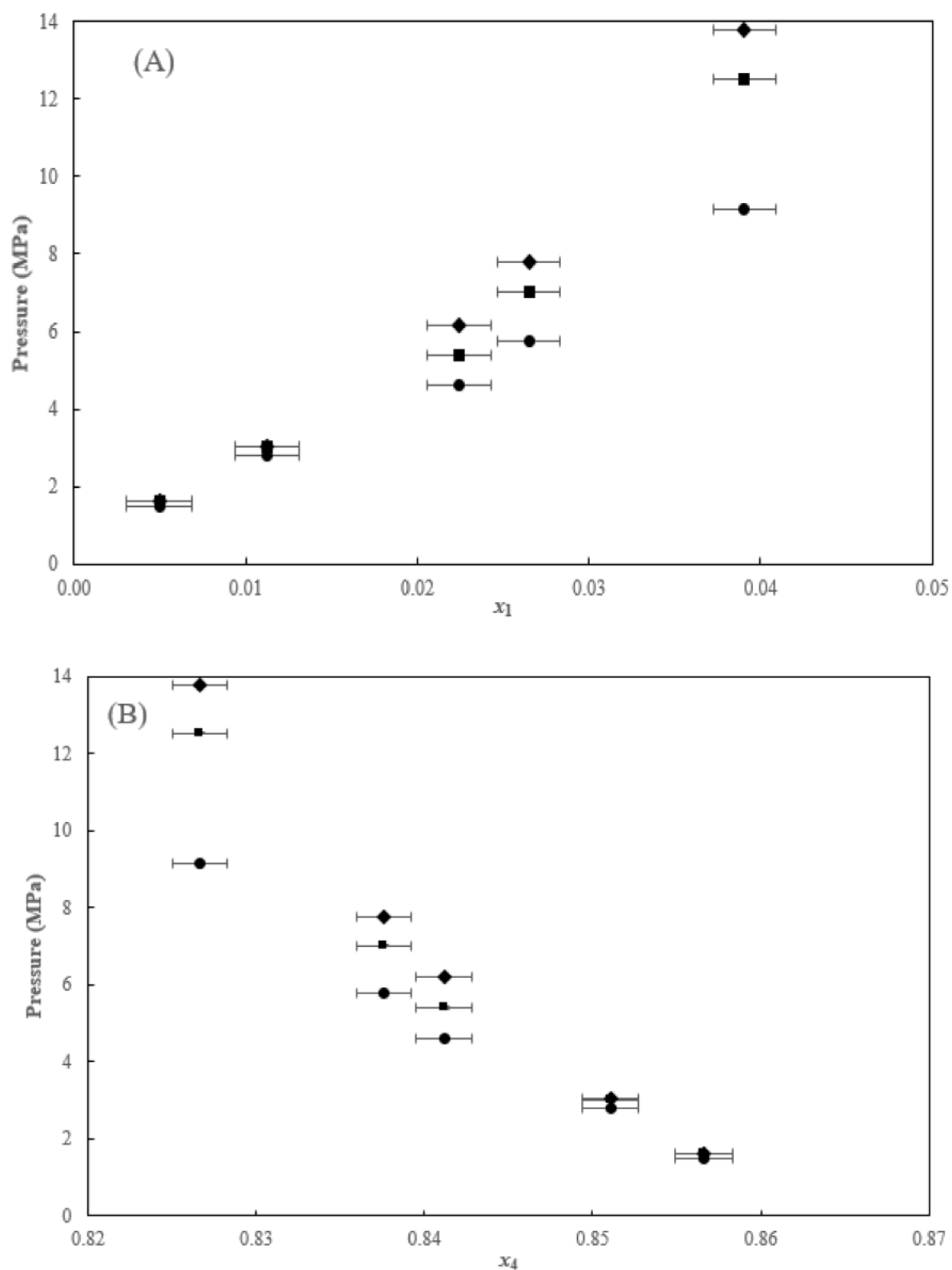
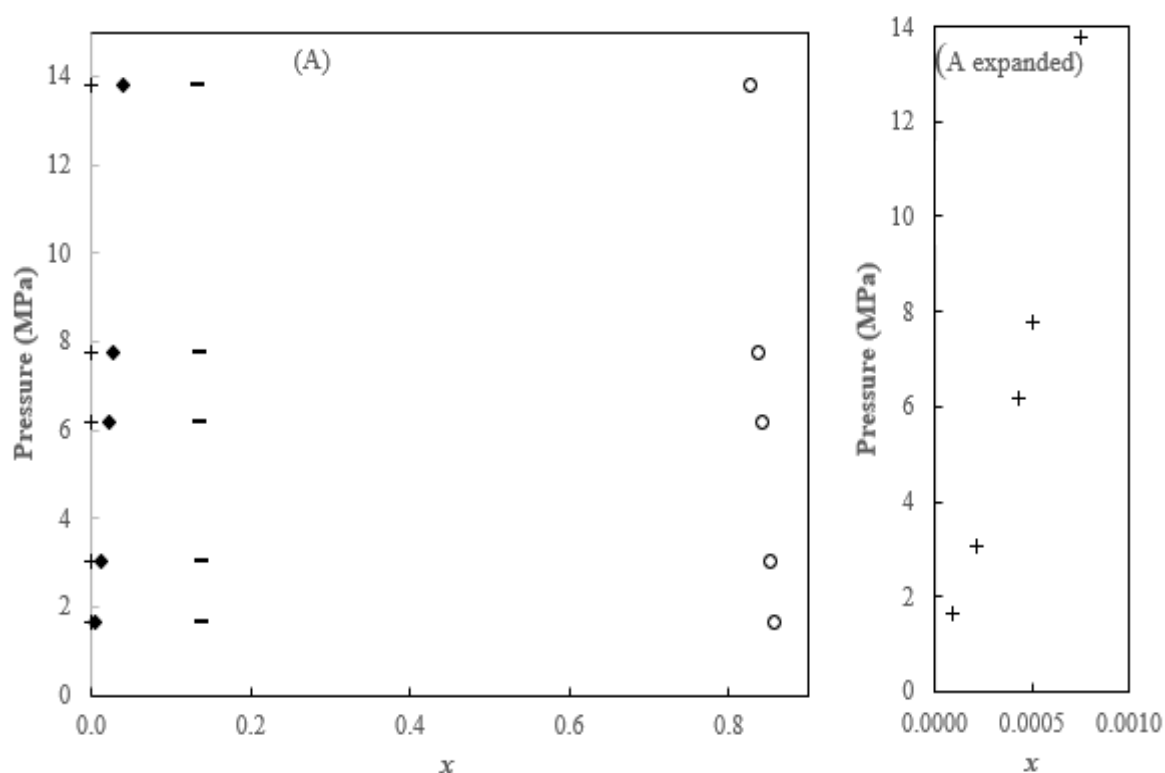


Figure 6-33: TP_x graph for the (CH₄(1)/C₃H₈(2) 95/5mol%) + (CH₃OH(3)/TEG(4) 3.33/96.67 wt%) system.

(A) CH₄ T dependency; (B) TEG T dependency; Symbols represent data at: 283.16 K (◆); 303.16 K (■); 323.15 K (●).

Figure 6-33 (B) shows that at the highest concentration of TEG ($x_4 \sim 0.8570$) in the system, the bubble point pressure values of the system are approximately the same (~ 1.5 MPa) for all the three isotherms considered. For the same composition x_4 , the bubble point pressures follow this trend: P at 283.16 K $>$ P at 303.15 K \gg P at 323.15 K. This trend is more pronounced as the mole fraction of TEG decreases from 0.857 to 0.827. Generally, for each isotherm considered, as the mole fraction of TEG decreases (due to the addition of methane, propane and methanol), the bubble point pressure increases as well. Hence for the same composition of TEG, the decrease in bubble point pressure values at higher temperatures could be due to the breaking down of these strong hydrogen bonds in TEG. Consequently, free voids are thus formed, leading to the encapsulation of alkane molecules in those voids.

More results for this system showing all the components for each of the isotherms are presented in Figure 6-34.



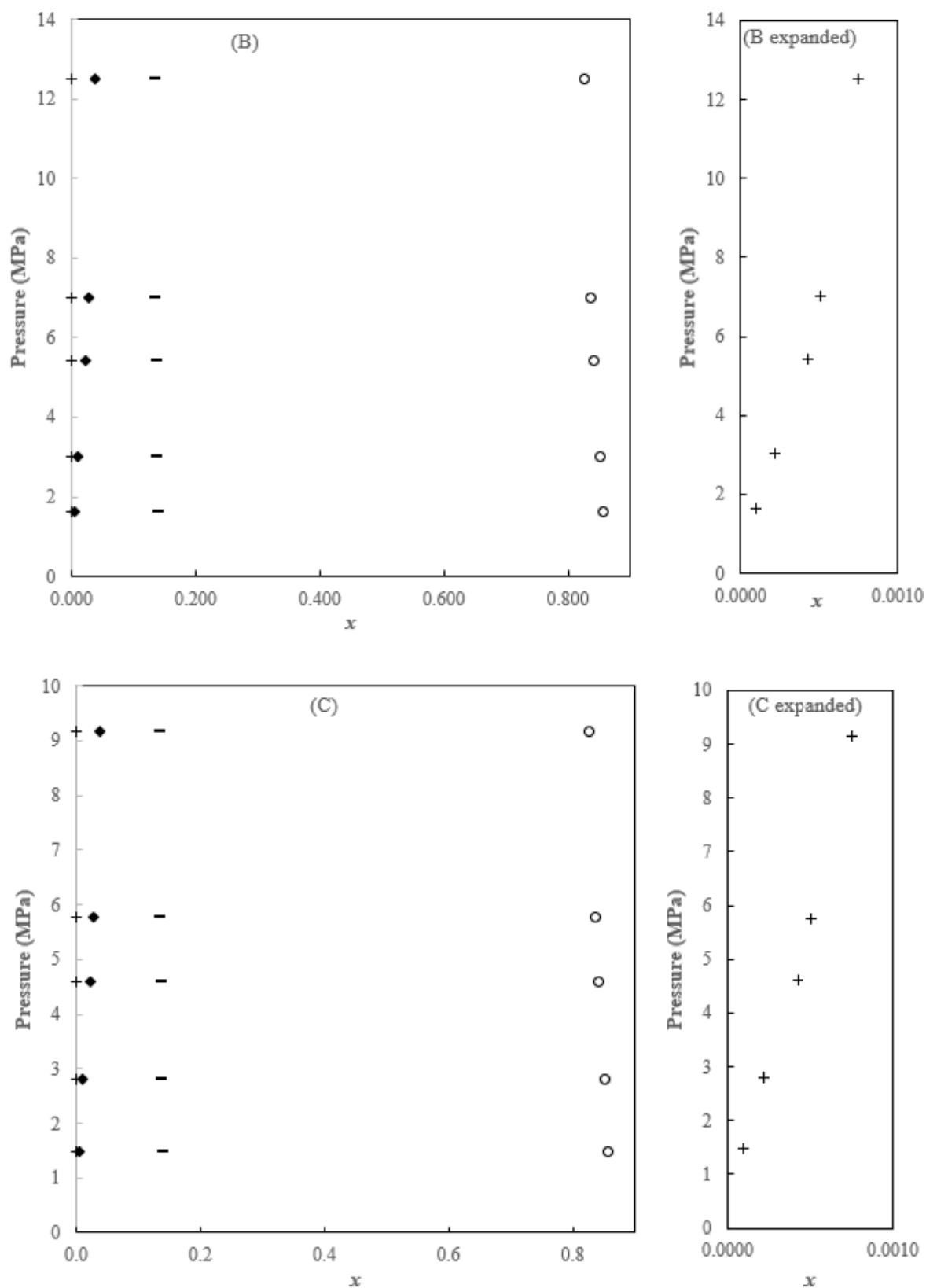
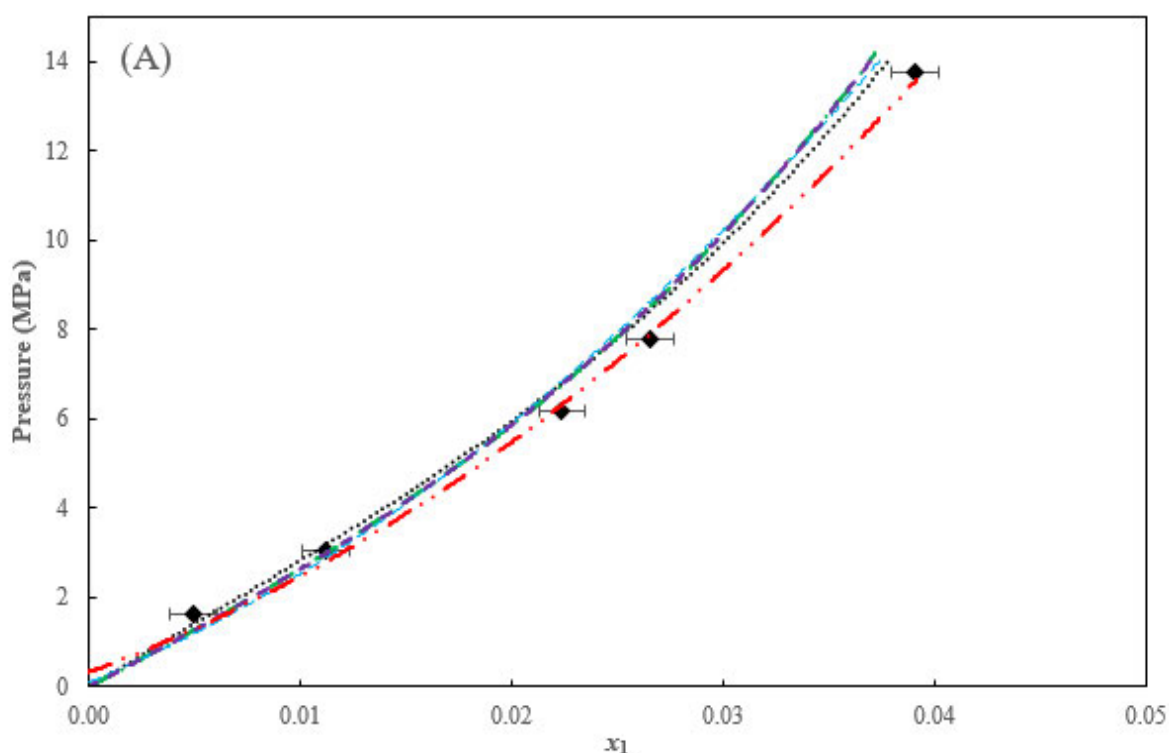


Figure 6-34: TP_x graph for the $(\text{CH}_4 (1) / \text{C}_3\text{H}_8 (2) 95/5\text{mol}\%) + (\text{CH}_3\text{OH} (3) / \text{TEG} (4) 3.33/96.67 \text{ wt.}\%)$ system.

(A) data at 283.16 K; (B) data at 303.16 K; (C) data at 323.15 K; Symbols represent: CH_4 (\blacklozenge); C_3H_8 (+); CH_3OH (—) and: TEG (\circ); expanded represents expanded graphs for propane on each of (A), (B), or (C).

Figure 6-34 shows that the data for each component in the quaternary system follows the same trend at each of the isotherms considered. It can also be observed in Figure 34 that on each of the isotherms, the composition of propane and methanol is pretty steady, whilst notable changes in the composition of methane and TEG can be easily observed with an increase in pressure.

The measured data were correlated using the PR, SRK, PRWS, CPA, and the PC-SAFT models. Results of the model correlations are shown in Figures 6-35 to 37 for data at 283.16, 303.16, and 323.15 K. Table 6-24 presents the regressed model parameters and deviations. Five data points were measured on each of the isotherms although the PRWS has eighteen parameters as shown in Table 6-24. Each fitting parameter is dependent on x_1 , x_2 , x_3 , x_4 , P , and T . All the model correlations were extrapolated to $x_1 = 0$ as visible in Figures 6-35 to 37. Methane and propane are non-polar molecules, whereas methanol and TEG are highly polar components. Introduction of the non-polar alkanes into the polar solution most likely leads to clusters in the methanol or TEG components; hence some models struggle to describe such phase behaviour.



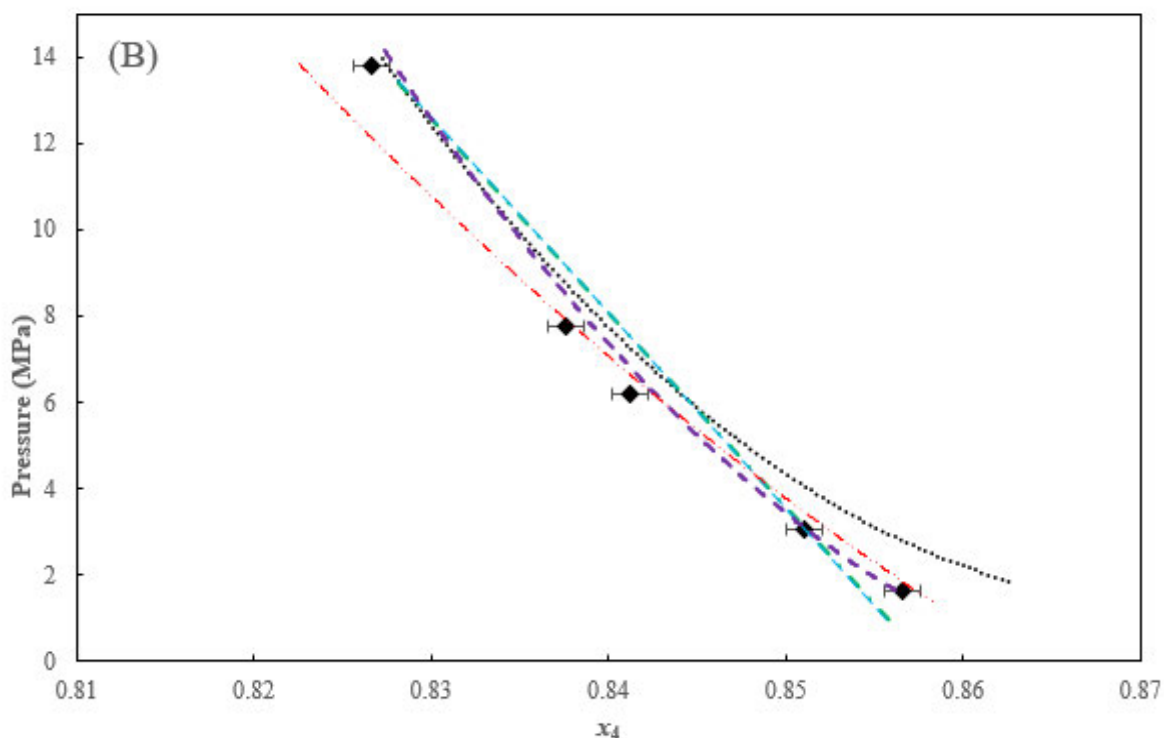


Figure 6-35: Thermodynamic modelling of the (CH₄ (1) /C₃H₈ (2) 95/5mol%) + (CH₃OH (3) /TEG (4) 3.33/96.67 wt%) system at 283.16 K.

(A) CH₄ data; (B), TEG data; Experimental data (◆); and modelling results: PR model (— · —); SRK model (— — —); PRWS (— · · —); CPA (— · —); and PC-SAFT model (·····).

Figure 6-35 (A) shows that at 283.16 K, the PRWS model correlation yielded the best fit to the experimental data alongside the PC-SAFT model correlation since all their regressed data lie within the experimental composition uncertainty of this work (indicated by error bars). The PR, SRK and CPA model correlations also yielded satisfactory fits to the experimental data. This is also illustrated by the AARD in pressures which are 4.43%, 4.35%, 3.14%, 4.47% and 3.8% for the PR, SRK, PRWS, CPA and PC-SAFT model correlations. The regressed model parameters and deviations are presented in Table 6-25. For the PR, SRK, and CPA models, correlations were performed using Aspen Plus V12 and the Deming algorithm was employed instead of the default Britt-Luecke algorithm. This was because with the Britt-Luecke algorithm, the mentioned model correlations were not converging. For the PRWS, the Britt-Luecke algorithm was used together with the weighted least squares initialisation method.

Figure 6-35 (B) shows that all the PR, CPA and SRK model correlations yielded satisfactory fits to the experimental data of TEG in the multicomponent system since all the regressed data lie within the TEG composition uncertainty (indicated by error bars). The PRWS and PC-SAFT model correlations did not yield perfect fits to the experimental data, as shown in Figure 6.35 (A).

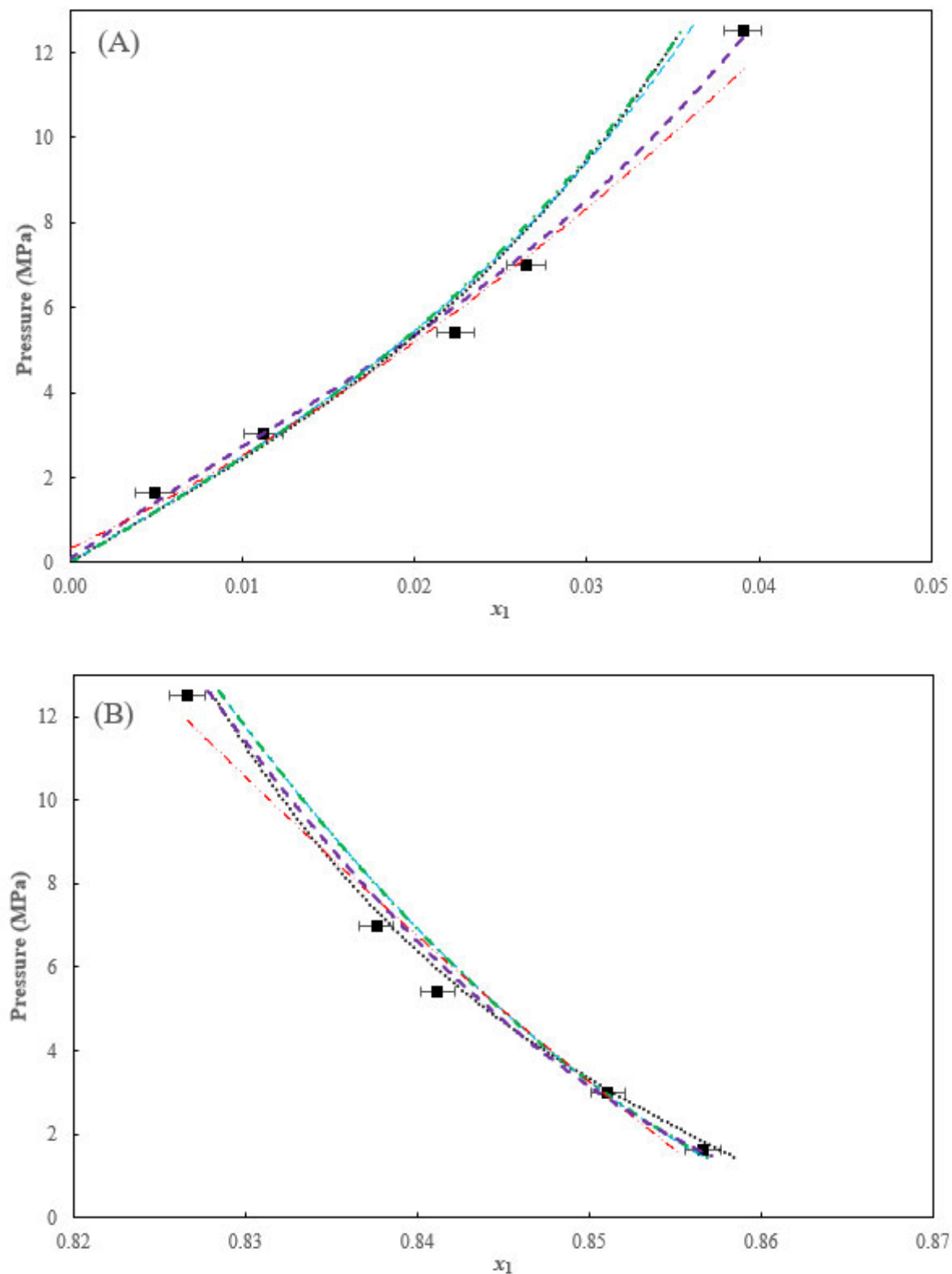


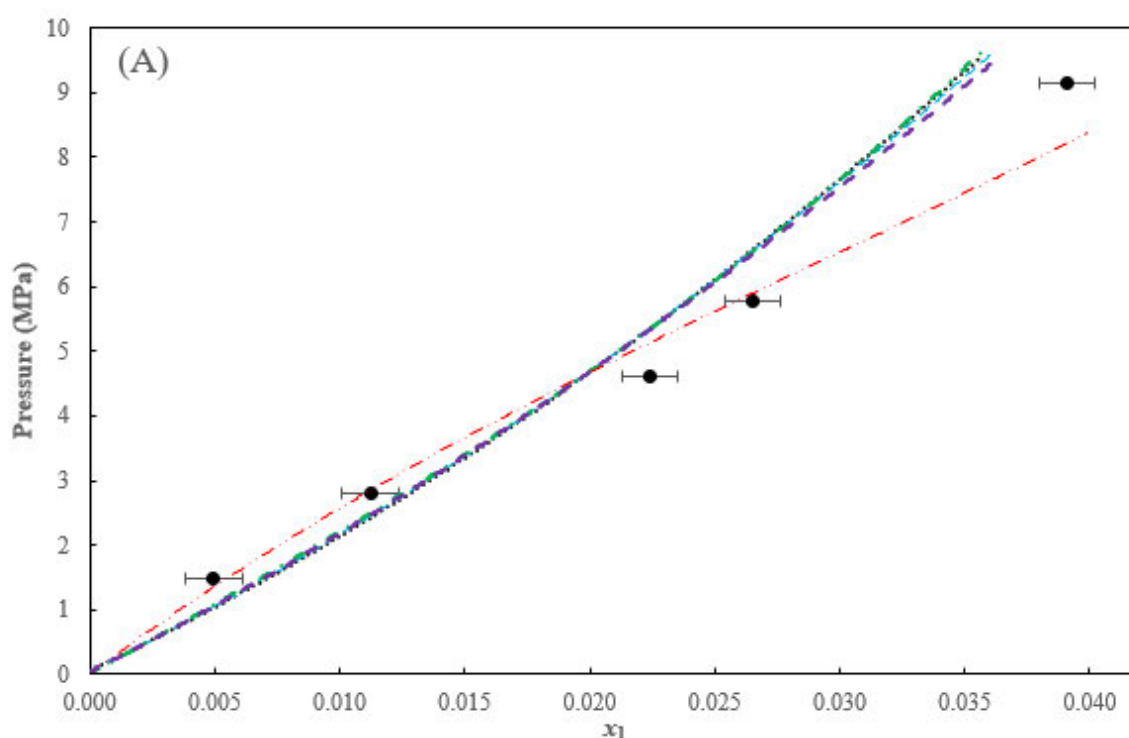
Figure 6-36: Thermodynamic modelling of the (CH₄(1) /C₃H₈(2) 95/5mol%) + (CH₃OH(3) /TEG(4) 3.33/96.67 wt.%) system at 303.16 K.

(A), CH₄ data; (B), TEG data; Experimental data (■); and modelling results: PR model (- · -); SRK model (- - -); PRWS (- · ·); CPA (- - -); and PC-SAFT model (····).

The CPA model correlation yielded the best fit to the experimental data. The AARD in pressure are similar to those presented for Figure 6.35 (A). The AARD in TEG composition are 0.10%, 0.11%, 0.38%, 0.08%, and 0.40% for the PR, SRK, PRWS, CPA and PC-SAFT model correlations in that order.

Figure 6-36 (A) shows that the CPA and PRWS model correlations yielded satisfactory fits to the experimental data of methane in the mixture as their regressed data points all lie within the experimental uncertainty of this work (indicated by error bars). This is also illustrated by the AARD in pressures which are 2.09% and 3.70% for the two models respectively (Table 6-25). As for the PC-SAFT, SRK, and PR model correlations, they all provided relatively good fits on the first 3 data points (from x_{CH_4} of 0.005 to x_{CH_4} of 0.022), after which their correlated data points were out of the compositional uncertainty range of this work at higher pressures as shown in Figure 6-36 (A). The AARD in pressure for the last three models is 5.79%, 5.72%, and 5.81%, respectively.

Figure 6-36 (B) shows that the PR, SRK, PRWS and PC-SAFT model correlations yield better fits to the experimental data of TEG in the mixture as compared to the CPA model correlation. The AARD in TEG composition are 0.13%; 0.13%; 0.14%; 0.43% and 0.15% for the PC-SAFT, SRK, PR, CPA and PRWS model correlations respectively.



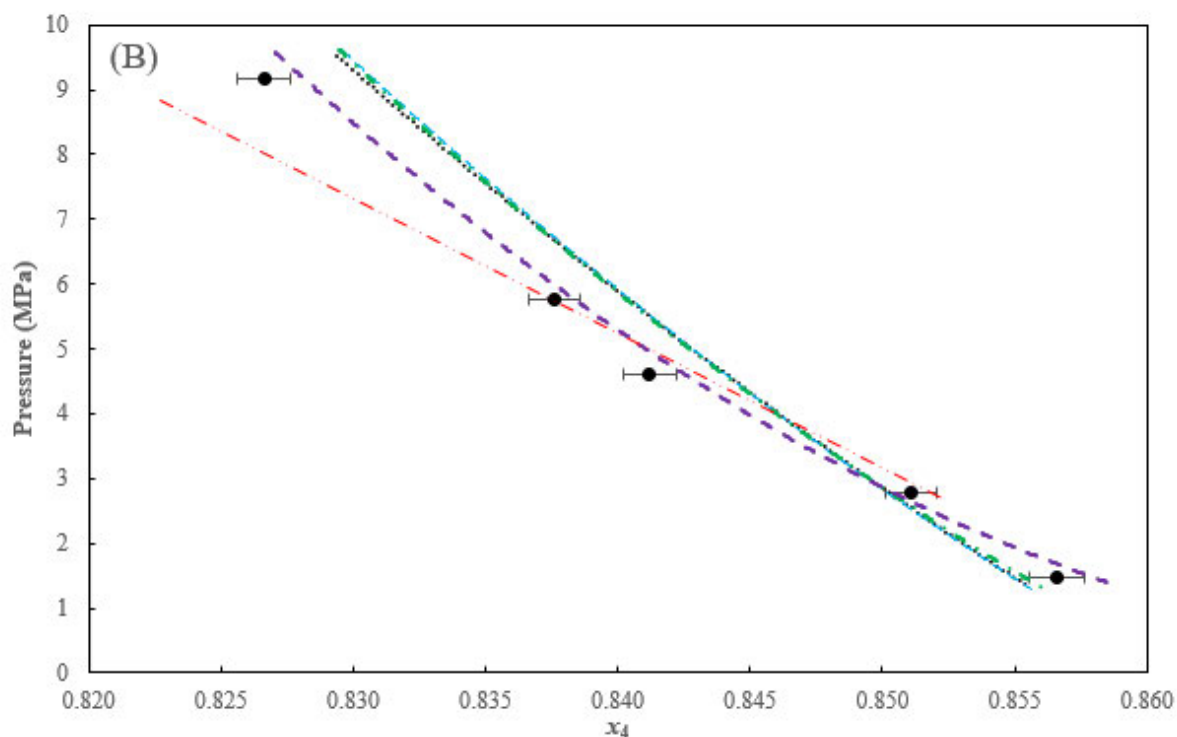


Figure 6-37: Thermodynamic modelling of the (CH₄ (1) /C₃H₈ (2) 95/5mol%) + (CH₃OH (3) /TEG (4) 3.33/96.67 wt.%) system at 323.15 K.

(A), CH₄ data; (B), TEG data; Experimental data (●); and modelling results: PR model (— · —); SRK model (— — —); PRWS (— · · —); CPA (— — —); and PC-SAFT model (·····).

For the data at 323.15 K, Figure 6-37 (A), shows that the PRWS model correlation yielded a satisfactory fit to the experimental data of methane in the mixture over the first four points since the data lie within the compositional uncertainty of this work (indicated by error bars). The AARD in pressure for the PRWS model correlation is 4.45% as shown in Table 6-25. The rest of the models gave relatively good fits to the first two data points, after which their correlated data points were out of the uncertainty range of this work at higher pressures as shown in Figure 6-37 (A). The AARD in pressure for the CPA, PC-SAFT, PR, and SRK models are 7.39%, 7.33%, 7.44%, and 7.25 % respectively.

Figure 6-37 (B), shows that the CPA model correlation yielded a satisfactory fit to the experimental data of TEG in the mixture over all points since the data lie within the compositional uncertainty of this work (indicated by error bars). The AARD in composition of TEG is 0.17%, 0.19%, 0.38%, 0.10% and 0.19% for the PR, SRK, PRWS, CPA and PC-SAFT model correlations respectively.

Table 6-25 (a): Regressed binary parameters and deviations for the (CH₄ (1)/C₃H₈ (2) 95/5 mol %) + (CH₃OH (3) /TEG (4) 3.33/96.67 wt.%) system.

Parameter	PRWS model			PR model			SRK model		
	$T=$ 283.16 K	$T=$ 303.16 K	$T=$ 323.15 K	$T=$ 283.16 K	$T=$ 303.16 K	$T=$ 323.15 K	$T=$ 283.16 K	$T=$ 303.16 K	$T=$ 323.15 K
k_{12}	-1.4441	-3.5121	-0.5072	0.6249	0.154	-0.126	0.7871	-0.2174	-0.2174
k_{13}	-1.3154	0.5166	0.6924	0.7014	0.334	0.4285	0.6656	0.375	0.7151
k_{14}	-0.5449	0.5567	0.4876	0.2769	0.2982	0.2859	0.2503	0.28	0.2546
k_{23}	654.9924	351.8194	81.4439	-439.8	-131.04	-464.4	-329.3	-271.3	-576.55
k_{24}	-6.7925	0.5071	2.1537	25.3021	7.4824	25.9269	18.721	15.153	31.647
k_{34}	3.2535	-1.1608	-0.0057	0.1470	0.1092	0.125	0.1439	0.1214	0.1482
A_{12}	53.1844	-5.1120	61.1680						
A_{21}	133.9939	3.4712	56.7547						
A_{13}	2.9037	1.3010	1.1958						
A_{31}	2.2652	9.9678	7.2048						
A_{14}	-0.7843	-0.5536	-1.0129						
A_{41}	8.1182	3.6073	4.0678						
A_{23}	4.9159	-1.0191	7.7118						
A_{32}	2.0201	0.9976	-1.7690						
A_{24}	-3.4840	-0.7365	-1.6316						
A_{42}	0.0088	0.3897	0.6953						
A_{34}	0.9491	3.1452	1.5257						
A_{43}	-6.0618	8.0930	9.2808						
AAD P (MPa)	0.09	0.24	0.26	0.21	0.21	0.29	0.21	0.21	0.29
AARD P %	3.14	3.70	4.45	4.43	5.81	7.44	4.35	5.72	7.25
AAD x_1	0.0000	0.0005	0.0005	0.0009	0.0016	0.0016	0.0009	0.0014	0.0015
AARD x_1 %	0.28	2.89	2.38	5.75	8.53	8.8	5.52	7.85	8.24
AAD x_4	0.0032	0.0013	0.0032	0.0009	0.0012	0.0014	0.0009	0.0011	0.0016
AARD x_4 %	0.38	0.15	0.38	0.10	0.14	0.17	0.11	0.13	0.19
AAD T (K)	5.38	1.01	11.39	2.09	3.47	2.08	2.97	3.18	1.87
AARD T %	1.90	0.33	3.53	0.74	1.14	0.64	1.05	1.05	0.58

Table 6-25 (b): Regressed binary parameters and deviations for the (CH₄ (1)/C₃H₈ (2) 95/5 mol %) + (CH₃OH (3) /TEG (4) 3.33/96.67 wt.%) system cont.

Parameter	CPA model			PC-SAFT model		
	$T=$ 283.16 K	$T=$ 303.16 K	$T=$ 323.15 K	$T=$ 283.16 K	$T=$ 303.16 K	$T=$ 323.15 K
k_{12}	0.0604	0.0812	0.137	0.30333	0.283	0.3441
k_{13}	0.4882	-0.5173	-0.51732	0.3783	-0.0138	0.3322
k_{14}	0.2533	0.2785	0.2587	0.0472	0.054	0.0407
k_{23}	-192.3	-1.6019	-1.6467	-12.11	-7.339	-5.099
k_{24}	7.54291	0.0449	0.027	0.5424	0.3073	0.1927
k_{34}	0.2910	0.1628	0.1628	0.0667	0.0594	0.0712

Table 6-25 (b): Regressed binary parameters and deviations for the (CH₄ (1)/C₃H₈ (2) 95/5 mol %) + (CH₃OH (3) /TEG (4) 3.33/96.67 wt.%) system cont.						
Parameter	CPA model			PC-SAFT model		
	<i>T</i>=283.16 K	<i>T</i>=303.16 K	<i>T</i>=323.15 K	<i>T</i>= 283.16 K	<i>T</i>=303.16 K	<i>T</i>=323.15 K
AAD <i>P</i> (MPa)	0.22	0.11	0.29	0.19	0.2	0.28
AARD <i>P</i> %	4.47	2.09	7.39	3.8	5.79	7.33
AAD <i>x</i>₁	0.0009	0.0004	0.0014	0.0008	0.0016	0.0016
AARD <i>x</i>₁ %	5.73	1.93	8.09	5.17	8.56	8.71
AAD <i>x</i>₄	0.0007	0.0037	0.0009	0.0034	0.0011	0.0016
AARD <i>x</i>₄ %	0.08	0.43	0.10	0.40	0.13	0.19
AAD <i>T</i> (K)	2.29	1.48	2.90	6.77	3.49	2.05
AARD <i>T</i> %	0.81	0.49	0.90	3.80	1.15	0.63

The CPA bubble point predictions using k_{ij} reported in Table 6-19 are displayed in Figures E-3.7. A, B and C for the data at 283.16 303.16 and 323.15K respectively. The AARD% in pressure were 24.54, 25.68 and 26.98 for the data at 283.16, 303.16 and 323.15K respectively. Generally, the CPA under predicted the bubble point pressure values at all isotherms considered. Comparison of Figures E-3.7 A,B and C with Figures 6-35 to 37 (A) shows that the CPA correlated data in Figures 6-35 A and B is much closer to the experimental data than the predicted data with the help of binary interaction parameters.

Trends for the absolute values of the regressed binary interaction parameters (k_{ij}) for possible binary pairs of this system in Table 6-25 (a) and (b) can be described as follows:

For the PRWS:

- There is no clear trend on the interaction parameter between methane + propane, methane + methanol and methane + TEG. The value of the binary interaction parameter between methane + methanol binary pair at 303.16 K of 0.5166 for the quaternary system is significantly larger than 0.3423 for the methane + methanol binary system at 303.15 K reported in Table 6-15. The value of the interaction parameter for the methane + TEG binary pair of the quaternary system at 323.15 K of 0.4876 is slightly less than 0.5363 for the methane + TEG binary system at 323.15 K reported in Table 6-16.
- The interaction parameter between propane + methanol and propane + TEG and methanol + TEG decreases significantly with an increase in temperature.

Parameter	PRWS model					
	$T = 283.16 \text{ K}$		$T = 303.16 \text{ K}$		$T = 323.15 \text{ K}$	
	Value	σ	Value	σ	Value	σ
k_{12}	-1.4441	11.2516	-3.5121	38.8561	-0.5072	9.7034
k_{13}	-1.3154	0.0872	0.5166	1.0783	0.6924	0.3972
k_{14}	-0.5449	0.0401	0.5567	0.0129	0.4876	0.0186
k_{23}	654.99	403.00	351.82	115.64	81.44	513.61
k_{24}	-6.7925	33.0634	0.5071	32.8950	2.1537	23.5274
k_{34}	3.2535	0.2806	-1.1608	5.6964	-0.0057	0.4311

All values in SI units.

σ represents the standard deviation reported in Aspen Plus V12

- The magnitude of the standard deviation for the binary interaction between methane + propane, propane + TEG at 283.16 K is greater than the absolute values for the binary interaction parameters. This indicates that the data are over fitted and these parameters are insignificant to the overall model fitting and hence they can be set to 0. The other binary interaction parameters are significant to the overall model fitting.
- At 303.16 K, the binary interaction parameter between methane + propane, methane + methanol, propane + TEG, and methanol + TEG are insignificant to the overall model fitting since their absolute values are less than the standard deviation, indicating that the data are over fitted. Only the methane + TEG and propane + methanol binary interaction parameters were significant to the overall model fitting.
- At 323.15 K, the magnitude of the standard deviation between methane + propane, propane + methanol, propane + TEG and methanol + TEG is greater than the values of the binary interaction parameters, indicating that the data are over fitted and hence these parameters can be essentially set at 0, since they are insignificant to the overall model fitting. Only the methane + methanol and methane + TEG binary interaction parameters are significant to the overall model fitting.

For the PR model

- The interaction parameter between methane and propane decreases with an increase in temperature.
- There is no clear trend on the interaction parameter between methane + methanol, methane + TEG, propane + methanol, propane + TEG, and methanol + TEG.
- The magnitude of the standard deviation on all possible binary pairs is significantly less than the absolute values of the binary interaction parameters. This shows that all the binary interaction parameters were significant to the overall model fitting on all the isotherms considered in this study.

Parameter	PR model					
	$T = 283.16 \text{ K}$		$T = 303.16 \text{ K}$		$T = 323.15 \text{ K}$	
	Value	σ	Value	σ	Value	σ
k_{12}	0.6249	0.2009	0.1540	0.0000	-0.1260	0.0000
k_{13}	0.7014	0.0104	0.3340	0.0070	0.4285	0.0237
k_{14}	0.2769	0.0006	0.2982	0.0004	0.2859	0.0014
k_{23}	-439.80	28.64	-131.04	18.29	-464.40	39.28
k_{24}	25.3021	1.6435	7.4824	1.0347	25.9269	2.1886
k_{34}	0.1470	0.0008	0.1092	0.0007	0.1250	0.0008

All values in SI units.

σ represents the standard deviation reported in Aspen Plus V12

For the SRK model

Parameter	SRK model					
	$T=283.16 \text{ K}$		$T=303.16 \text{ K}$		$T=323.15 \text{ K}$	
	Value	σ	Value	σ	Value	σ
k_{12}	0.7871	0.1628	-0.2174	0.0000	-0.2174	0.0000
k_{13}	0.6656	0.0099	0.3750	0.0092	0.7151	0.0198
k_{14}	0.2503	0.0006	0.2800	0.0005	0.2546	0.0012
k_{23}	-329.3	26.67	-271.30	25.33	-576.55	32.35
k_{24}	18.721	1.510	15.153	1.412	31.647	1.774
k_{34}	0.1439	0.0008	0.1214	0.0008	0.1482	0.0009

All values in SI units.

σ represents the standard deviation reported in Aspen Plus V12

- The interaction parameter between methane + propane decreases with an increase in temperature between 283.16 and 303.16 K. Between 303.16 K and 323.15 K, the interaction parameter between methane and propane is independent of temperature.
- The interaction parameter between methane + methanol and methane + TEG decreases with an increase in temperature.
- There is no clear trend on the interaction between propane + methanol, propane + TEG, and methanol + TEG.
- The magnitude of the standard deviation on all possible binary pairs is significantly less than the absolute values of the binary interaction parameters. This shows that all the binary interaction parameters were significant to the overall model fitting on all the isotherms considered in this study.

For the CPA model

- The interaction parameter between methane and propane gradually increases with an increase in temperature. The absolute value of the interaction parameter between methane + methanol

of 0.5173 at 303.16 K for the quaternary system is significantly greater than 0.0462 for the methane + methanol binary system presented in Table 6-15. The value of the interaction parameter for the methane + TEG binary pair of the quaternary system of 0.2587 is slightly larger than 0.2046 for the methane + TEG binary system at 323.15 K reported in Table 6-16.

- There is no clear trend on the interaction parameter between methane + TEG and propane + methanol.

Parameter	CPA model					
	<i>T</i> = 283.16 K		<i>T</i> = 303.16 K		<i>T</i> = 323.15 K	
	Value	σ	Value	σ	Value	σ
k_{12}	0.0604	0.0608	0.0812	0.0104	0.1370	0.0000
k_{13}	0.4882	0.0156	-0.5173	0.0230	-0.5173	0.0000
k_{14}	0.2533	0.0007	0.2785	0.0006	0.2587	0.0001
k_{23}	-192.3	28.496	-1.602	0.370	-1.647	0.000
k_{24}	7.5429	1.1211	0.0449	0.0139	0.0270	0.0005
k_{34}	0.291	0.001	0.1628	0.0021	0.1628	0.0000

All values in SI units.

σ represents the standard deviation reported in Aspen Plus V12

- The interaction parameter between propane and TEG decreases with an increase in temperature.
- The interaction parameter between methanol and TEG decreases with increase in temperature between 283.16 and 303.16 K. However, between 303.16 K and 323.15 K, the interaction parameter between methanol and TEG is independent of temperature.
- At 283.16 K, the magnitude of the standard deviation for the standard deviation is almost similar to the value of the binary interaction parameter, signifying the insignificance of the parameter to the overall model fitting (Carlson, 1996). All other binary interaction parameters are significant to the overall model fitting.
- For 303.16 and 323.15 K, all the binary interaction parameters were significant to the overall model fitting.
- There is no clear trend on the interaction parameter between methane + propane, methane + methanol and methane + TEG. The absolute value of the binary interaction parameter for the methane + methanol binary pair at 303.16 K of 0.0138 is far less than 0.0498 for the methane + methanol binary system reported in Table 6-16, at 303.15 K. The value of the interaction parameter between methane + TEG binary pair of the quaternary system at 323.15 K of 0.0407 is greater than 0.03302 for the methane + TEG binary system at 323.15 K presented in Table 6-16.

- The interaction parameter between propane + methanol, propane + TEG and methanol + TEG decreases with an increase in temperature.

For the PC-SAFT model

Parameter	PC SAFT model					
	<i>T</i> =283.16 K		<i>T</i> =303.16 K		<i>T</i> =323.15 K	
	Value	σ	Value	σ	Value	σ
k_{12}	0.3033	0.0183	0.2830	0.0091	0.3441	0.0794
k_{13}	0.3783	0.0048	-0.0138	0.0057	0.3322	0.0168
k_{14}	0.0472	0.0002	0.0540	0.0002	0.0407	0.0006
k_{23}	-12.1100	0.5657	-7.3390	0.7269	-5.0990	10.1385
k_{24}	0.5424	0.0334	0.3073	0.0350	0.1927	0.4405
k_{34}	0.0667	0.0005	0.0594	0.0006	0.0712	0.0007

All values in SI units.

σ represents the standard deviation reported in Aspen Plus V12

- Except for the propane + methanol and propane + TEG binary interaction parameters at 323.15 K with larger standard deviations showing that the data are over fitted, all the other binary interaction parameters for this quaternary system at all isotherms considered are significant to the overall model fitting since their values are greater than the standard deviation.

6.4.5.1 Comparison of the propane-free (methane /propane 95/5 mol %) + (methanol /TEG 3.33/96.67 wt.%) system and the (methane + (methanol /TEG 3.33/96.67 wt.% system))

A comparison of the TP_x data between the methane + (methanol /TEG 3.33/96.67 wt.%) and the propane-free (methane /propane 95/5 mol %) + (methanol /TEG 3.33/96.67 wt.%) systems for the measured at 323.15 K was carried out and the results are presented in Figure 6-38. Propane-free refers to the fact that the propane composition in the quaternary system (methane /propane 95/5 mol %) + (methanol /TEG 3.33/96.67 wt.%) was not considered in the comparison purposes.

Figure 6-38 (A) shows that the pressure difference between the two systems decreases with increase in composition of methane in the multicomponent mixtures. Between x_1 of 0.03 to 0.04, the difference in pressure for the two systems is fairly constant, after which the pressure values seem to be the same for both systems. The uncertainties in the methane composition for the two systems is approximately the same as indicated by error bars, and the systems are within the methane composition uncertainty of each other over the entire range of the measurements. The addition of propane leads to more alkanes in the (TEG + methanol) solution hence more VdW forces and unlike interactions between the non-polar and

polar components. Thus, methanol and TEG due to hydrogen bonding will form more clusters reducing the interaction with methane and hence the low solubility.

Figure 6-38 (B) shows that at the dilute composition of TEG x_4 0.82 to 0.84, the equilibrium pressure values are almost the same for both systems under comparison. Between x_4 0.84-0.86, the equilibrium pressure for the 4-component system are higher than for the 3-component system and this trend becomes more pronounced as the mole fraction of TEG in the mixtures increases.

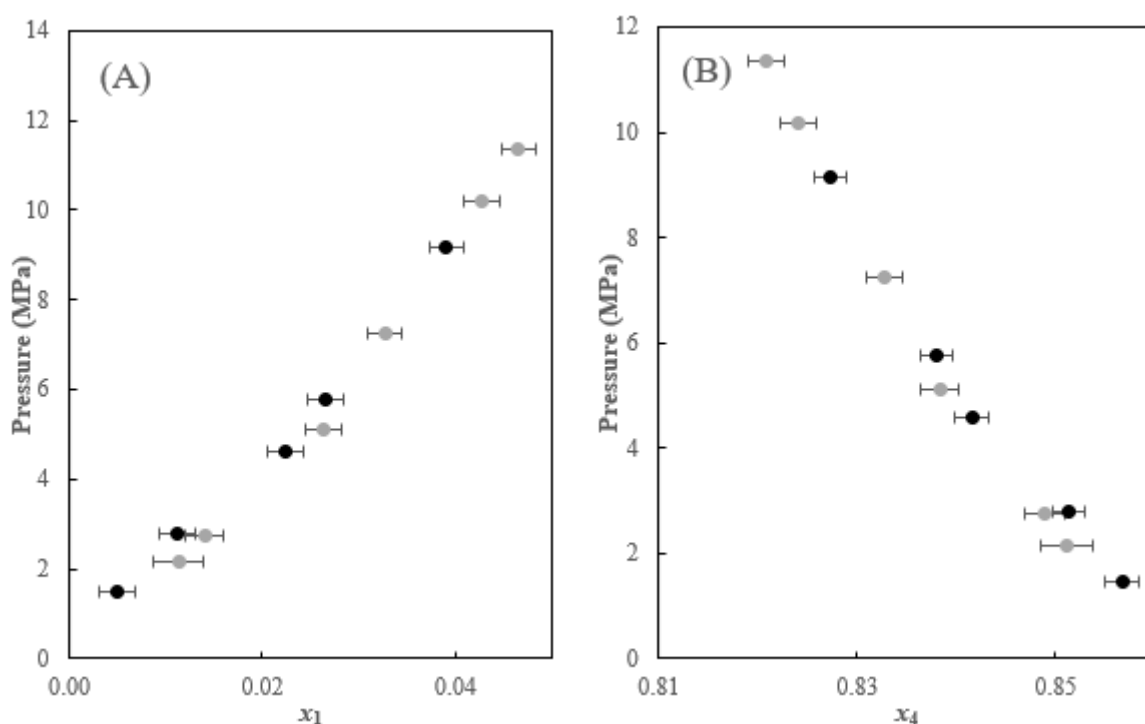


Figure 6-38: Comparison of the TPx data at $T = 323.15$ K for:

Propane-free (CH₄ (1) /C₃H₈ (2) 95/5 mol %) + (CH₃OH (3) /TEG (4) 3.33/96.67 wt.% system), (●); and CH₄ (1) + (CH₃OH (3) /TEG (4)3.33/96.67 wt.% system), (◐); (A), CH₄ data; (B), TEG data.

6.4.6 New system 6: (methane (1)/propane (2) 95/5 mol%) + ((water (3) /TEG (5) 5/95% wt.): methanol (4) 3.33 wt.%)

Bubble point measurements were conducted for the (methane /propane 95/5 mol%) + ((water/TEG 5/95wt%): methanol 3.33 wt.%) system at 283.16, 303.16 and 323.15 K. A total of 20 data points were measured for this system. The (water /TEG 5/95 wt.%) : methanol 3.33wt%) liquid mixture was prepared as outlined in chapter 5, section 5.2.5.2. No published literature data has been found for a system with similar components outlined in this section, although the Dortmund data bank indicates phase equilibria data for this five-component system exists in the proprietary database. The 95 wt.% TEG to 5 wt.% water used in this case is reflective of industrial TEG dehydration units as TEG purity

varies between 95 to 100 wt.% in a dehydration unit (Arya et al., 2014). Figures 6-39 to 40 presents the measurement results.

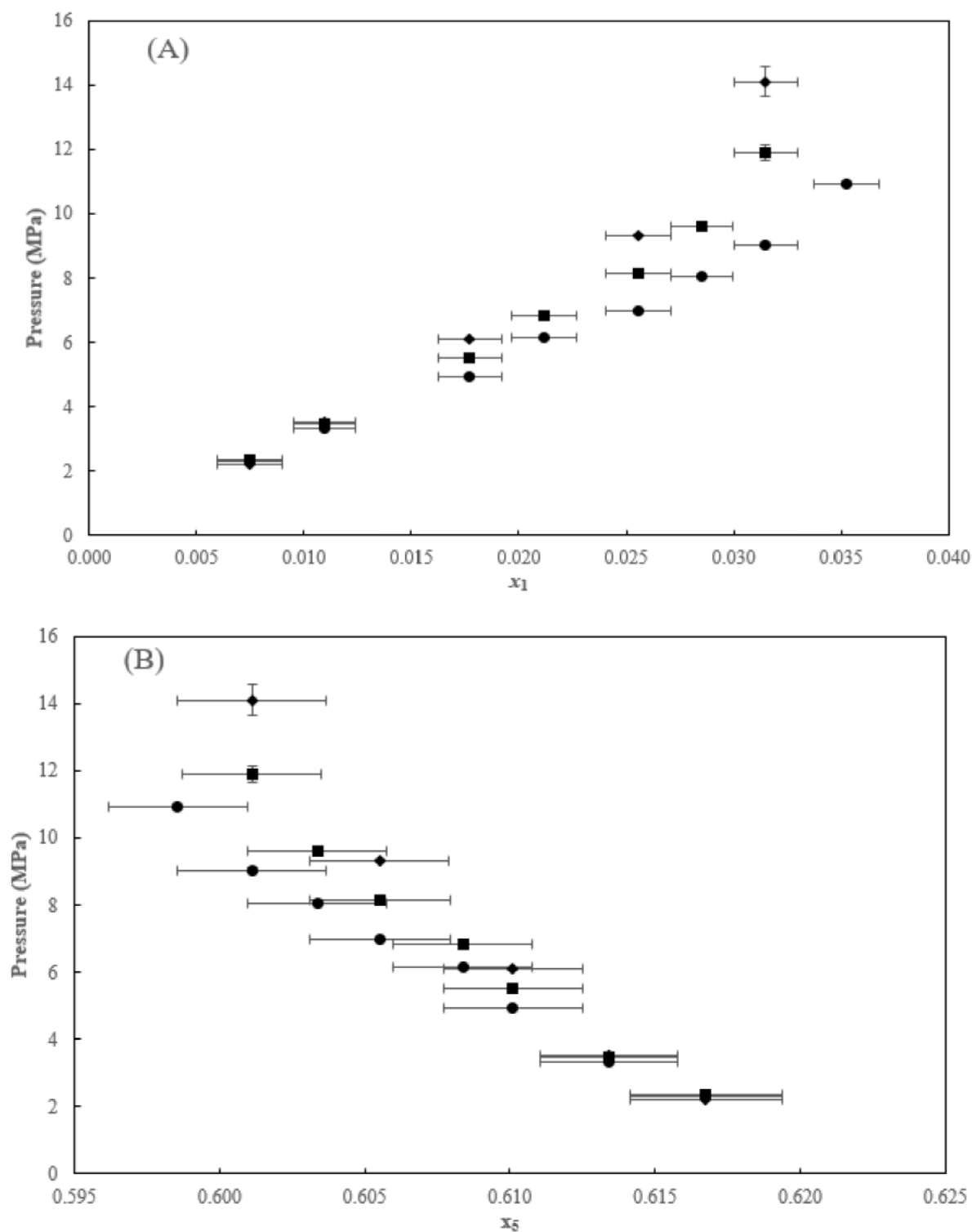


Figure 6-39: TPx graph for the $(CH_4$ (1) / C_3H_8 (2) 95/5mol%) + $((H_2O$ (3) / TEG (5) 5/95 wt.%): CH_3OH (4) 3.33 wt.%) system.

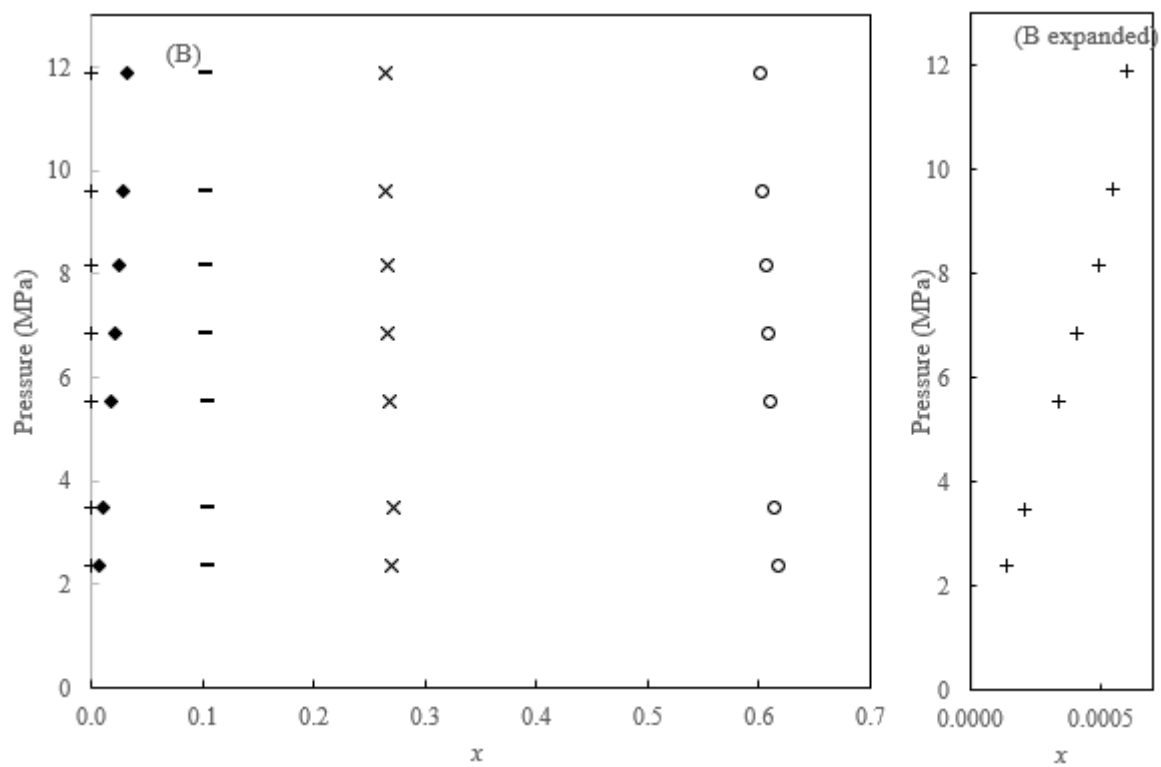
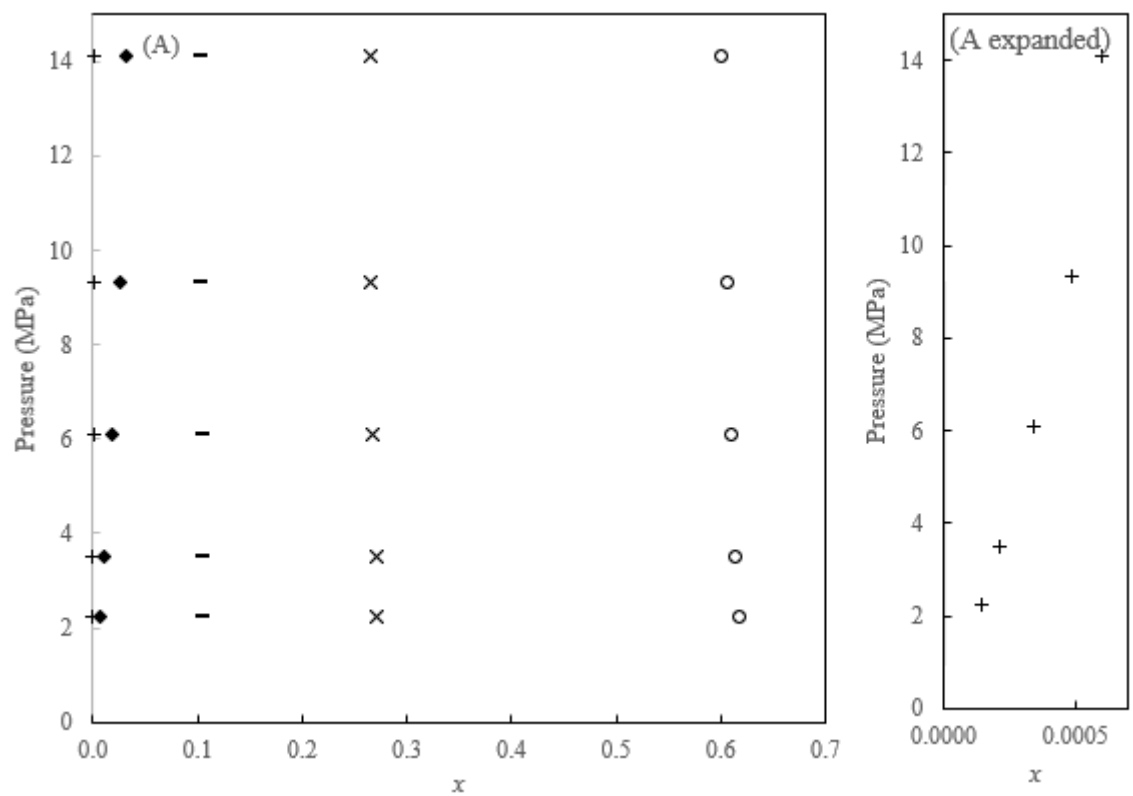
(A) CH_4 T dependency; (B) TEG T dependency; Symbols represent data at: 283.16 K (◆); 303.16 K (■); 323.15 K (●).

Also, the measurement results are listed in Table B.5-6 (Appendix B), together with associated uncertainties for the measured variables. Average expanded uncertainties over all points are: $U(T) = 0.11$ K; $U(P) = 0.03$ MPa, $U(x_1) = 0.0015$, and $U(x_5) = 0.0024$.

From the data in Figure 6-39 (A), it is apparent that the solubility of methane in this multicomponent system is independent of temperature at lower pressures less than 3.52 MPa. Above 3.52 MPa, the solubility of methane increases with an increase in temperature. For the same composition x_1 , the bubble point pressures follow this trend: P at 283.16 K $>$ P at 303.15 K \gg P at 323.15 K. This trend is more pronounced as the mole fraction of methane increases (see Figure 6-39 (A)). This trend could be because as temperature increases, voids are formed in TEG, onto which alkanes are encapsulated, hence the increase in methane solubility. Water, methanol and TEG are polar molecules capable of hydrogen bonding either through self or cross association, whereas methane and propane are non-polar molecules. The non-polar components have the effect of causing the hydrophobic effect when introduced to an aqueous environment.

Figure 6-39 (B) shows that at the highest concentration of TEG ($x_5 \sim 0.6170$) in the system, the bubble point pressure values of the system are approximately the same (~ 2.3 MPa) for all three isotherms considered. For the same composition x_5 , the bubble point pressures follow this trend: P at 283.16 K $>$ P at 303.15 K \gg P at 323.15 K. This trend is more pronounced as the mole fraction of TEG decreases from 0.6170 to 0.5990. Generally, for each isotherm considered, as the mole fraction of TEG decreases (due to the addition of methane, propane, water and methanol), the bubble point pressure increases as well. For the same composition of TEG, the decrease in bubble point pressure values at higher temperatures could be due to the breaking down of these strong hydrogen bonds in TEG.

Additional results for this system showing all the components for each of the isotherms are presented in Figure 6-40.



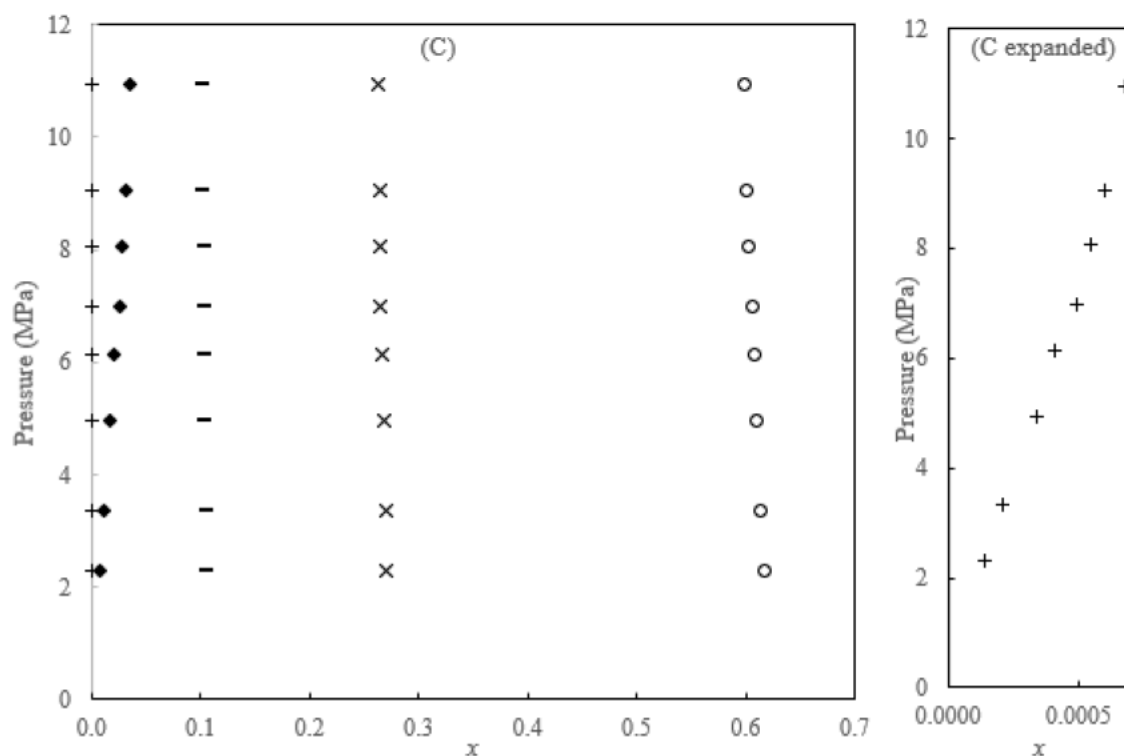


Figure 6-40: TPx graph for the $(\text{CH}_4 (1) / \text{C}_3\text{H}_8 (2) 95/5\text{mol}\%) + ((\text{H}_2\text{O} (3) / \text{TEG} (5) 5/95\% \text{ wt.}): \text{CH}_3\text{OH} (4) 3.33 \text{ wt.}\%)$ system.

(A) data at 283.16 K; (B) data at 303.16 K; (C) data at 323.15 K; Symbols represent: CH_4 (\blacklozenge); C_3H_8 (+); H_2O (x); CH_3OH (—) and: TEG (\circ); expanded represents expanded graphs for propane on each of (A), (B), or (C).

Figure 6-40 shows that the data for each component in the 5-component system follows the same trend at each of the isotherms considered. It can also be observed in Figure 6-40 that on each of the isotherms, the composition of propane, water and methanol is relatively steady, whilst notable changes in the composition of methane and TEG can be easily observed with an increase in pressure.

The measured data in this work was correlated with 5 models, namely the PR, SRK, PRWS, CPA, and the PC-SAFT. Results of the model correlations are shown in Figures 6-41 to 43 for data at 283.16 K, 303.16 K and 323.15 K, respectively. Table 6-26 presents the model parameters and deviations. In this case, the PRWS model has thirty parameters, and each fitting parameter is dependent on x_1 , x_2 , x_3 , x_4 , x_5 , P , and T . All the model correlations were extrapolated to $x_1 = 0$ as visible in Figures 6-41 to 43.

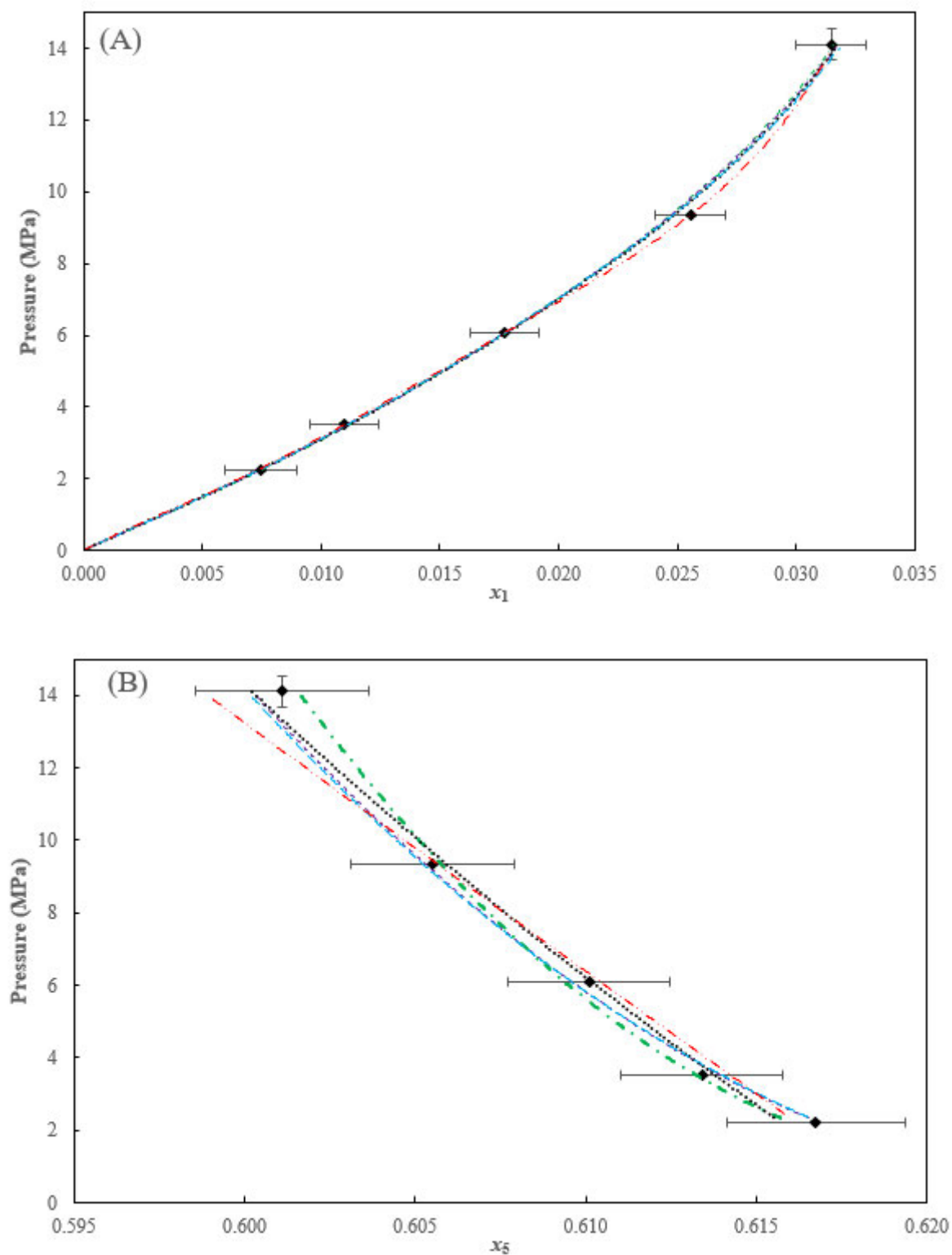
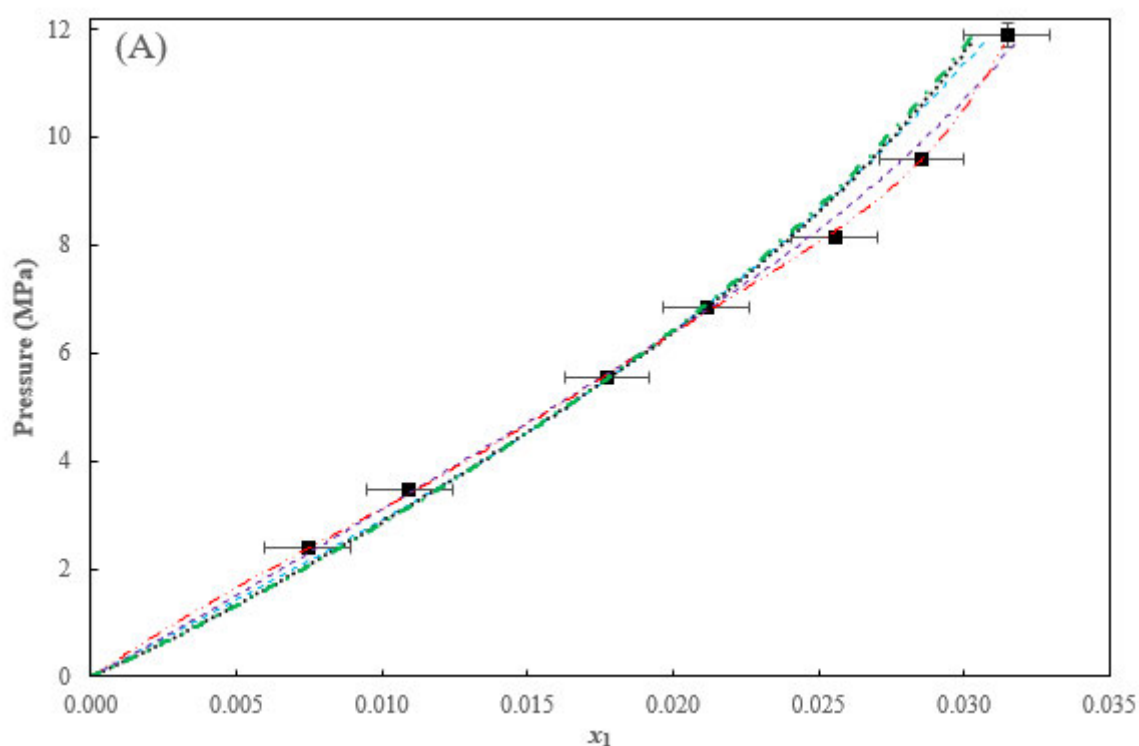


Figure 6-41: Thermodynamic modelling of the (CH₄ (1)/C₃H₈ (2) 95/5mol%) + ((H₂O (3) /TEG (5) 5/95% wt.): CH₃OH (4) 3.33 wt.%) system at 283.16 K.
 (A), CH₄ data; (B), TEG data; Experimental data (◆); and modelling results: PR model (— · —); SRK model (— — —); PRWS (— · · —); CPA (— · —); and PC-SAFT model (·····).

Figure 6-41 both (A) and (B) shows that at 283.16 K, the PR, SRK, PRWS, CPA and PC-SAFT model correlations yielded satisfactory fits to the experimental data since all their regressed data lie within the composition experimental uncertainty of this work (indicated by error bars). This is also illustrated by the AARD in pressures which are all less than 1%. The AARD in pressure are 0.71%, 0.59%, 0.47%, 0.67%, and 0.57% for the PR, SRK, PRWS, CPA and PC-SAFT model correlations respectively. The model correlations presented in Figure 6-41 were performed in Aspen Plus V12. The Deming algorithm was used in this case instead of the default Britt-Luecke algorithm. This was because the Britt-Luecke algorithm did not converge reasonably.



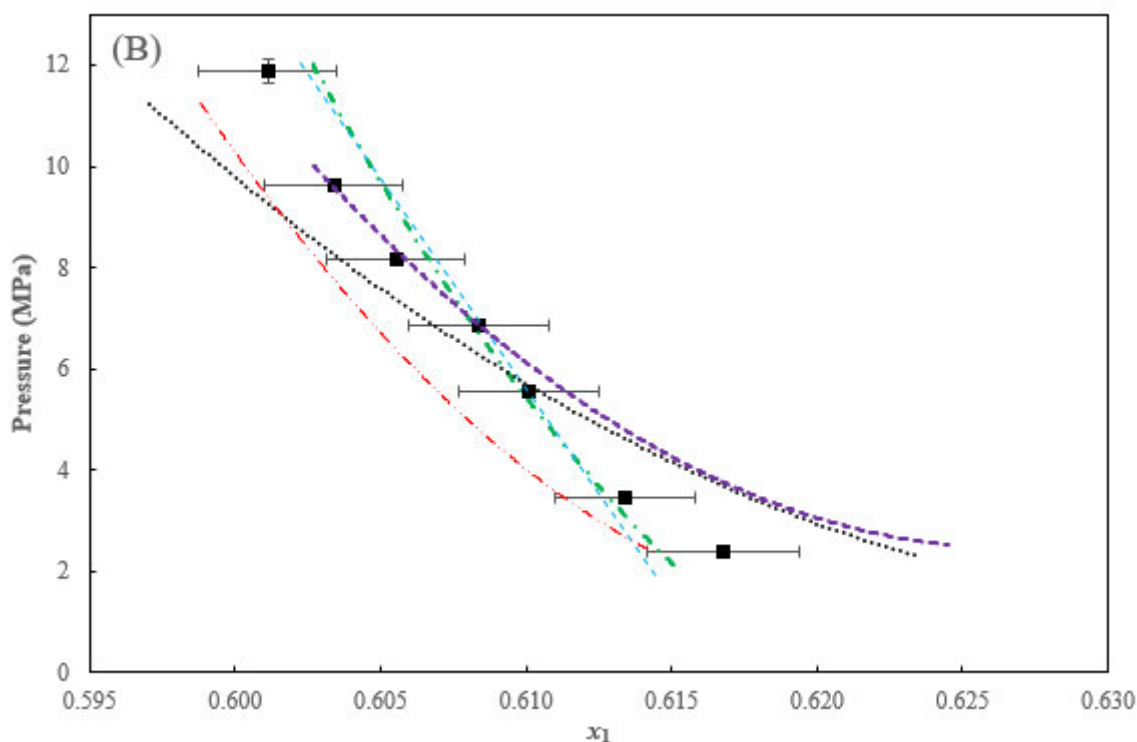


Figure 6-42: Thermodynamic modelling of the (CH₄ (1) /C₃H₈ (2) 95/5mol%) + ((H₂O (3) /TEG (5) 5/95% wt.): CH₃OH (4) 3.33 wt.%) system at 303.16 K.

(A), CH₄ data; (B), TEG data; Experimental data (■); and modelling results: PR model (— · —); SRK model (— — —); PRWS (— · · —); CPA (— — —); and PC-SAFT model (·····).

For the data at 303.16 K, Figure 6-42 (A) for methane in the mixture, shows that all the model correlations considered in this work yielded satisfactory fits to the experimental data as their regressed data points all lie within the experimental uncertainty of this work (indicated by error bars). This is also illustrated by the AARD in pressures which are 2.49%, 2.19%, 0.58% and 2.29% for the PR, SRK, PRWS, CPA and PC-SAFT model correlations respectively. The AARD in methane composition are 3.71%, 3.00%, 0.35%, 1.10%, and 3.45% for the PR, SRK, PRWS, CPA and PC-SAFT model correlations respectively.

Figure 6-42 (B) for TEG composition in the mixture shows that the PR and SRK model correlations yielded fairly satisfactory fits to the experimental data. The association models (CPA and PC-SAFT) model correlations and the PRWS model did not yield very satisfactory fits to the experimental data. The AARD in pressures are similar to those presented for Figure 6.42 (A). The AARD in TEG composition in the mixture are 0.19%, 0.22%, 0.42%, 0.43% and 0.56% respectively for the PR, SRK, PRWS, CPA and PC-SAFT models.

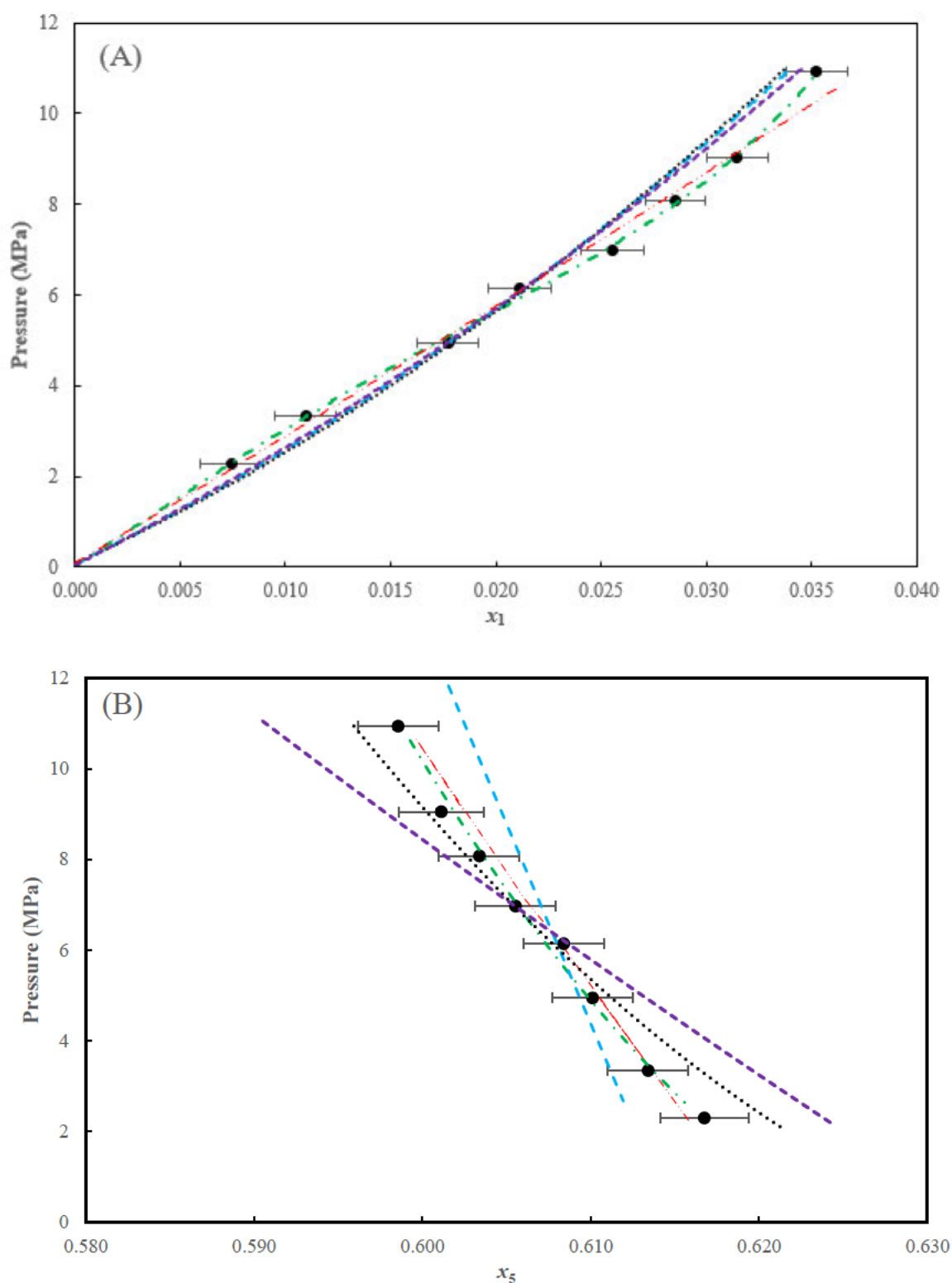


Figure 6-43: Thermodynamic modelling of the (CH₄ (1) /C₃H₈ (2) 95/5mol%) + ((H₂O (3) /TEG (5) 5/95% wt.): CH₃OH (4) 3.33 wt.%) system at 323.15 K.
 (A), CH₄ data; (B), TEG data; Experimental data (●); and modelling results: PR model (— · —); SRK model (— — —); PRWS (— · · —); CPA (— · —); and PC-SAFT model (·····).

It is important to note that for the data at 303.16 K presented in Figure 6-42, the Deming algorithm was used for the PR, PC-SAFT and PRWS model correlations instead of the default Britt-Luecke algorithm. Furthermore, all the model correlations presented in Figure 6-42 were performed using Aspen Plus V12.

For the data at 323.15 K, Figure 6.43 (A) for methane composition in the mixture, shows that all the model correlations considered in this work yielded satisfactory fits to the experimental data over all points since the correlated data lie within the composition uncertainty of this work (indicated by error bars). This is also illustrated by the AARD in pressures which are 0.07%, 3.22%, 1.49%, 2.93% and 3.40% for the PR, SRK, PRWS, CPA and PC-SAFT model correlations respectively. The PR model correlation yielded the best fit as can be observed from Figure 6.43 (A) and its lowest AARD % in pressure presented. The regressed model parameters and deviations are presented in Table 6-26. Modelling of this 5-component system at 323.15 K was performed in Aspen V12, and the Deming algorithm was utilized.

Figure 6-43 (B), for TEG composition in the multicomponent mixture shows that the PR and PRWS model correlations yielded satisfactory fits to the experimental data as their correlated data lies within the TEG composition uncertainty, indicated by error bars. The SRK, CPA and PC-SAFT model correlations did not yield very good fits to the experimental data. The AARD % in pressure are similar to those presented for methane composition in the mixture. The AARD in TEG composition are 0.09%, 0.44%, 0.11%, 0.71%, and 0.34% for the PR, SRK, PRWS, CPA and PC-SAFT model correlations respectively.

Table 6-26(a): Regressed binary parameters and deviations for the (CH₄ (1)/ C₃H₈ (2) 95/5 mol%) + ((H₂O (3) /TEG (5) 5/95 wt.%): CH₃OH (4) 3.33 wt.%) system

Parameter	PRWS model			PR model			SRK model		
	283.16 K	303.16 K	323.15 K	283.16 K	303.16 K	323.15 K	283.16 K	303.16 K	323.15 K
k_{12}	-0.4407	-0.9648	-2.1620	2.0581	0.5395	-3.9196	-0.2060	0.3562	-0.4710
k_{13}	1.1306	3.9271	3.9760	0.5578	-0.2325	-6653.5	0.5419	-0.2026	-0.1894
k_{14}	1.2412	5.4622	6.8474	0.6024	0.2720	42654.8	0.5906	0.2733	0.4951
k_{15}	-0.5808	0.7854	0.8093	0.2284	0.2724	-1763.5	0.2324	0.2629	0.2559
k_{23}	29.7719	7.8509	8.3065	-276.3	-5.8775	-39435	-284.7	11.8365	-13.05
k_{24}	19.4450	16.4612	-0.5919	-231.9	-12.669	253243	-228.7	-31.64	92.85
k_{25}	1.2784	0.4138	0.5644	47.56	1.5057	-10476	47.51	0.4956	-3.8624
k_{34}	-79.434	-92.455	-91.323	-0.4398	3.6156	19.029	-2.6548	1.3892	0.5867
k_{35}	2.4955	2.9628	3.1428	0.0338	-0.3309	-1.8699	0.1931	-0.1597	-0.1044
k_{45}	4.3505	6.5940	6.3487	0.2171	-0.3606	-0.2468	0.5032	-0.0603	0.0454
A_{12}	-0.1447	-5.3570	58.6470						
A_{21}	21.8289	16.2853	5.0389						
A_{13}	3.8080	0.3484	-0.0433						
A_{31}	6.6548	1.9329	3.4435						
A_{14}	3.3947	4.8082	0.2690						
A_{41}	6.6451	2.0188	8.3356						
A_{15}	1.0200	1.9385	-0.7231						
A_{51}	6.2137	1.2300	0.7285						
A_{23}	-2.4357	-1.4695	4.2368						
A_{32}	6.1374	-5.0085	8.2966						
A_{24}	10.7885	-0.6062	-1.9303						
A_{42}	9.3500	-6.8441	9.4704						
A_{25}	-2.3159	-1.0549	2.5977						
A_{52}	2.2980	0.3567	7.5923						
A_{34}	6.5361	7.6985	3.0599						
A_{43}	5.1780	3.2418	4.4165						
A_{35}	4.1102	2.8858	3.5950						
A_{53}	5.1343	5.8804	5.6994						
A_{45}	4.0754	2.8671	3.9716						
A_{54}	6.5052	7.6770	3.8709						
AAD P (MPa)	0.04	0.04	0.10	0.04	0.12	0.00	0.05	0.11	0.17
AARD P %	0.47	0.58	1.49	0.71	2.49	0.07	0.59	2.19	3.22
AAD x_1	0.0000	0.0001	0.0003	0.0002	0.0007	0.0000	0.0002	0.0006	0.0008
AARD x_1 %	0.40	0.35	1.45	0.95	3.71	0.21	1.08	3.00	3.95
AAD x_5	0.0011	0.0026	0.0007	0.0007	0.0011	0.0006	0.0006	0.0014	0.0027
AARD % x_5	0.19	0.42	0.11	0.11	0.19	0.09	0.09	0.22	0.44
AAD T (K)	2.16	0.83	0.53	0.51	3.61	0.65	0.46	3.69	2.53
AARD T %	0.76	0.28	0.16	0.18	1.19	0.20	0.16	1.22	0.78

Table 6-26(b): Regressed binary parameters and deviations for the (CH₄ (1)/ C₃H₈ (2)95/5 mol%) + ((H₂O (3) /TEG (5) 5/95% wt.): CH₃OH (4) 3.33 wt.%) system cont.

Parameter	CPA model			PC-SAFT model		
	283.16 K	303.16 K	323.15 K	283.16 K	303.16 K	323.15 K
k_{12}	0.1849	0.1094	-9.4368	0.0045	0.2883	0.3465
k_{13}	0.0478	-1.3479	-1.1169	0.3755	-0.4090	-0.3500
k_{14}	0.3685	0.0974	0.4487	0.3071	0.0540	0.1433
k_{15}	0.3296	0.3623	0.3252	0.0621	0.0722	0.0659
k_{23}	-270.5674	1.9148	-196.8409	-19.3308	-0.0070	0.3248
k_{24}	-180.0573	-21.4275	-48.7953	-35.3087	-0.5688	-0.8037
k_{25}	25.2340	0.7312	14.1584	19.4254	-0.0003	-0.0198
k_{34}	-8.2656	1.0622	1.2468	-4.3165	2.9237	2.3028
k_{35}	-0.3300	-0.9464	-0.9609	0.3146	-0.0744	-0.0515
k_{45}	0.9032	0.2082	0.2061	0.5914	-0.1518	-0.1070
AAD P (MPa)	0.05	0.06	0.15	0.05	0.11	0.17
AARD P %	0.67	0.85	2.93	0.57	2.29	3.40
AAD x_1	0.0002	0.0002	0.0007	0.0002	0.0007	0.0009
AARD x_1 %	1.08	1.10	3.45	1.03	3.45	4.41
AAD x_5	0.0006	0.0026	0.0043	0.0010	0.0034	0.0021
AARD x_5 %	0.09	0.43	0.71	0.16	0.56	0.34
AAD T (K)	0.36	0.80	2.05	0.30	1.96	1.70
AARD T %	0.13	0.26	0.63	0.11	0.65	0.53

The CPA bubble point predictions using k_{ij} reported in Table 6-19 are displayed in Figures E-3.8. A, B and C for the data at 283.16 303.16 and 323.15K respectively. The AARD% in pressure were 15.22, 9.51, and 7.34 for the data at 283.16, 303.16 and 323.15K respectively. Generally, the CPA under predicted the bubble point pressure values at 283.16 and 303.16 K, especially for the last data point at methane mole fraction of 0.0315. For the data at 323.15 K, the prediction results from the CPA model match well with the experimental data. Comparison of Figures E-3.8 A, B and C to Figures 6-41 to 43 (A) respectively shows that, although the CPA binary interaction parameters yielded good prediction results as observed in Figures E-38 A, B and C, the regressed experimental data in Figures 6-41 to 43 yielded much better results.

Trends for the absolute values of the regressed binary interaction parameters (k_{ij}) for possible binary pairs of this system in Table 6-26 (a) and (b) can be described as follows:

For the PRWS:

- The interaction parameter between methane + propane, methane + water, methane + methanol and methane + TEG increases with an increase in temperature. The value of the binary interaction parameter for the methane + TEG binary pair in the quinary system at 323.15 K of 0.8093 is significantly larger than 0.5363 reported in Table 6-16 for the methane + TEG binary system at 323.15 K. The value of the interaction parameter between methane + methanol binary pair in the quinary system of 5.4622 at 303.16 K is significantly greater than the 0.3423 reported in Table 6-15 for the methane + methanol binary system at 303.15 K.
- There is no clear trend on the interaction parameter between propane + water, propane + TEG, water + methanol, water + TEG and methanol + TEG.
- The interaction parameter between propane + methanol decreases with an increase in temperature.

Parameter	PRWS model					
	<i>T</i> = 283.16 K		<i>T</i> = 303.16 K		<i>T</i> = 323.15 K	
	Value	σ	Value	σ	Value	σ
<i>k</i> ₁₂	-0.4407	12.2630	-0.9648	14.1675	-2.1620	0.8221
<i>k</i> ₁₃	1.1306	0.6334	3.9271	1.9133	3.9760	0.4317
<i>k</i> ₁₄	1.2412	0.7301	5.4622	2.9098	6.8474	0.7941
<i>k</i> ₁₅	-0.5808	0.1311	0.7854	0.0139	0.8093	0.0139
<i>k</i> ₂₃	29.7719	243.2431	7.8509	0.2780	8.3065	3.6925
<i>k</i> ₂₄	19.4450	82.1040	16.4612	0.5241	-0.5919	6.5274
<i>k</i> ₂₅	1.2784	30.4433	0.4138	0.0187	0.5644	0.2754
<i>k</i> ₃₄	-79.4340	51.4400	-92.4550	0.8833	-91.3230	0.8592
<i>k</i> ₃₅	2.4955	1.0737	2.9628	0.0284	3.1428	0.0086
<i>k</i> ₄₅	4.3505	3.7201	6.5940	0.0323	6.3487	0.0318

All values in SI units.

σ represents the standard deviation reported in Aspen Plus V12

- For the data at 283.16 K, the magnitude of the standard deviation for the methane + propane, propane + water, propane + methanol, and propane + TEG binary pairs is smaller than the values of the binary interaction parameters. This shows that the data are over fitted.
- For the data at 303.16 K, only the methane + propane binary interaction parameter is insignificant to the overall model fitting since the value of the binary interaction parameter is less than the standard deviation. This indicates that the data are over fitted.
- For the data at 323.15 K, only the propane + methanol binary interaction parameter is insignificant to the overall model fitting since the absolute value of the binary interaction parameter is less than the standard deviation. This indicates that the data are over fitted and hence this parameter could possibly be set to 0.

For the PR model

- There is no clear trend on the interaction parameter between methane + propane, methane + water, methane + methanol, propane + water, propane + methanol, propane + TEG and methanol + TEG.
- The interaction parameter between methane + TEG, water + methanol and water + TEG increases with an increase in temperature.
- For the data at 283.16 K, all the binary interaction parameters are significant to the overall model fitting since the values of the binary interaction parameters are larger than the standard deviations. Hence a perfect fit can be observed.

Parameter	PR model					
	<i>T</i> = 283.16 K		<i>T</i> = 303.16 K		<i>T</i> = 323.15 K	
	Value	σ	Value	σ	Value	σ
<i>k</i> ₁₂	2.0581	0.3497	0.5395	0.0292	-3.9196	4.4458
<i>k</i> ₁₃	0.5578	0.0102	-0.2325	0.0082	-6653.5	4.1197
<i>k</i> ₁₄	0.6024	0.0084	0.272	0.0107	42654.8	7.8717
<i>k</i> ₁₅	0.2284	0.0016	0.2724	0.0012	-1763.5	0.4583
<i>k</i> ₂₃	-276.3	28.703	-5.8775	3.3357	-39435	22.1595
<i>k</i> ₂₄	-231.9	24.67	-12.669	15.928	253243	91.391
<i>k</i> ₂₅	47.56	4.066	1.5057	0.7740	-10476	2.7065
<i>k</i> ₃₄	-0.4398	0.046	3.6156	0.0256	19.029	1.6066
<i>k</i> ₃₅	0.0338	0.0033	-0.3309	0.0016	-1.8699	0.1411
<i>k</i> ₄₅	0.2171	0.0060	-0.3606	0.0031	-0.2468	0.0900

All values in SI units.

σ represents the standard deviation reported in Aspen Plus V12

- For the data at 303.16 K, only the propane + methanol binary interaction parameter is insignificant to the overall model fitting. This is because the magnitude of the standard deviation is greater than the absolute value of the binary interaction parameter, indicating that the data are over fitted and hence this parameter could possibly be set to 0.
- For the data at 323.15 K, only the methane + propane binary interaction parameter is insignificant to the overall model fitting. This is because the magnitude of the standard deviation is greater than the absolute value of the binary interaction parameter, indicating that the data are over fitted and hence this parameter could possibly be set to 0.

For the SRK model

- The interaction parameter between methane and propane increases with an increase in temperature.
- The interaction parameter between methane + water, water + methanol, water + TEG and methanol + TEG decreases with an increase in temperature.
- There is no clear trend on the interaction parameter between methane + methanol, methane + TEG, propane + water, propane + methanol, propane + TEG.

Parameter	SRK model					
	<i>T</i> = 283.16 K		<i>T</i> = 303.16 K		<i>T</i> = 323.15 K	
	Value		Value		Value	
<i>k</i> ₁₂	-0.2060	0.3850	0.3562	0.0524	-0.4710	0.0793
<i>k</i> ₁₃	0.5419	0.0112	-0.2026	0.0080	-0.1894	0.0135
<i>k</i> ₁₄	0.5906	0.0097	0.2733	0.0090	0.4951	0.0318
<i>k</i> ₁₅	0.2324	0.0018	0.2629	0.0011	0.2559	0.0025
<i>k</i> ₂₃	-284.7	29.983	11.837	3.555	-13.050	8.0094
<i>k</i> ₂₄	-228.7	26.438	-31.640	16.879	92.850	33.490
<i>k</i> ₂₅	47.51	4.2910	0.4956	0.7221	-3.8624	2.1033
<i>k</i> ₃₄	-2.6548	0.0469	1.3892	0.0240	0.5867	0.0256
<i>k</i> ₃₅	0.1931	0.0033	-0.1597	0.0015	-0.1044	0.0015
<i>k</i> ₄₅	0.5032	0.0060	-0.0603	0.0030	0.0454	0.0032

All values in SI units.

σ represents the standard deviation reported in Aspen Plus V12

- At 283.16 K, only the methane + propane binary interaction parameter is insignificant to the overall model fitting since the magnitude of the standard deviation is greater than the absolute value of the binary interaction parameter. This indicates that the data are over fitted, and this parameter could possibly be set to 0.
- For the data at 303.16 K and 323.15 K, all the binary interaction parameters are significant to the overall model fitting.

For the CPA model

- There is no clear trend on the interaction parameter for all binary pairs of the 5-component system. For the methane + methanol binary pair in the quinary system, the value of the binary interaction parameter at 303.15 K of 0.0974 is significantly greater than 0.462 reported in Table 6-15 for the methane + methanol binary system at 303.15 K. For the methane + TEG binary pair of the quinary system, the value of the binary interaction parameter at 323.15 K of 0.3252

is greater than 0.2046 for the methane + TEG binary system at 323.15 K, presented in Table 6-16.

- At 283.15 K, only the methane + propane binary interaction parameter is insignificant to the overall model fitting. This is because the value of the standard deviation is greater than the absolute value of the binary interaction parameter thus, the data are over fitted.

Parameter	CPA model					
	<i>T</i> = 283.16 K		<i>T</i> = 303.16 K		<i>T</i> = 323.15 K	
	Value	σ	Value	σ	Value	σ
k_{12}	0.1849	0.1941	0.1094	0.0467	-9.4368	0.1916
k_{13}	0.0478	0.0273	-1.3479	0.0177	-1.1169	0.0585
k_{14}	0.3685	0.0181	0.0974	0.0146	0.4487	0.0599
k_{15}	0.3296	0.0023	0.3623	0.0019	0.3252	0.0046
k_{23}	-270.5674	44.1638	1.9148	1.1353	-196.8409	37.6090
k_{24}	-180.0573	30.5385	-21.4275	11.7512	-48.7953	41.1890
k_{25}	25.234	3.3939	0.7312	0.4476	14.1584	2.9623
k_{34}	-8.2656	0.1592	1.0622	0.1778	1.2468	0.0814
k_{35}	-0.33	0.0078	-0.9464	0.0092	-0.9609	0.0034
k_{45}	0.9032	0.0112	0.2082	0.0127	0.2061	0.0056

All values in SI units.

σ represents the standard deviation reported in Aspen Plus V12

- For the data at 303.16 K and 323.15 K, all the binary interaction parameters are significant to the overall model fitting.

For the PC-SAFT model

Parameter	PC-SAFT model					
	<i>T</i> = 283.16 K		<i>T</i> = 303.16 K		<i>T</i> = 323.15 K	
	Value	σ	Value	σ	Value	σ
k_{12}	0.0045	0.1074	0.2883	0.0078	0.3465	0.0074
k_{13}	0.3755	0.0103	-0.4090	0.0073	-0.3500	0.0097
k_{14}	0.3071	0.0213	0.0540	0.0123	0.1433	0.0195
k_{15}	0.0621	0.0008	0.0722	0.0008	0.0659	0.0011
k_{23}	-19.3308	4.1971	-0.0070	1.1156	0.3248	0.9156
k_{24}	-35.3087	7.7930	-0.5688	8.3623	-0.8037	8.5126
k_{25}	19.4254	0.6578	-0.0003	0.2526	-0.0198	0.3271
k_{34}	-4.3165	0.0595	2.9237	0.0435	2.3028	0.0411
k_{35}	0.3146	0.0034	-0.0744	0.0014	-0.0515	0.0013
k_{45}	0.5914	0.0077	-0.1518	0.0031	-0.1070	0.0031

All values in SI units.

σ represents the standard deviation reported in Aspen Plus V12

- The interaction parameter between methane + propane increases with an increase in temperature.
- There is no clear trend on the interaction parameter between methane + water, methane + methanol, methane + TEG, propane + water, propane + methanol, propane + TEG. For the methane + methanol binary pair in the quinary system, the value of the interaction parameter of 0.0540 at 303.16 K is comparable to the 0.0498 reported in Table 6-15 for the methane + methanol binary system at 303.15 K. For the methane + TEG binary pair in the quinary system, the value of the binary interaction parameter of 0.0659 at 323.15 K is significantly larger than 0.03302 shown in Table 6-16 for the methane + TEG binary system at 323.15 K.
- The interaction parameter between water + methanol, water + TEG and methanol + TEG decreases with an increase in temperature.
- At 283.16 K, only the methane + propane binary interaction parameter is not significant to the overall model fitting. The magnitude of the standard deviation is greater than the absolute value of the binary interaction parameter, indicating that the data are over fitted. This binary interaction parameter could possibly be set to 0.
- At 303.16 K and 323.15 K, only the propane + methanol and propane + TEG binary interaction parameters are insignificant to the overall model fitting. This is because the absolute value of the binary interaction parameters is less than the standard deviation, indicating that the data are over fitted.

6.4.6.1 Comparison of the water-free (methane / propane 95/5 mol%) + ((water /TEG 5/95 wt.%): methanol 3.33 wt.%) system and the (methane /propane 95/5 mol %) + (methanol /TEG 3.33/96.67 wt.%) system

The data for the four-component system and water-free 5 component systems were compared with respect to the methane and TEG composition in the multicomponent mixtures. Water-free refers to the fact that the water composition in the five-component system was not considered so as to make a fair comparison with the four-component system. The results of the comparison are presented in Figure 6-44.

Figure 6-44 (A) shows that at dilute compositions of methane for both systems (four-component system) or five-component system up to methane mole fraction around 0.0348, equilibrium pressures are almost the same. Above the methane mole fraction of 0.0348, specifically at x_1 of approximately 0.04, the total pressure value for the four component system is higher than that of the water-free five component system. The introduction of water to make a five-component system resulted in a decrease in the bubble

point pressures especially for methane mole fraction equal to or greater than 0.04. Thus, water has the effect of increasing the solubility of methane in this multicomponent system at pressures above 8 MPa. The uncertainties in methane composition for both of the systems are approximately the same, as can be observed by the error bars.

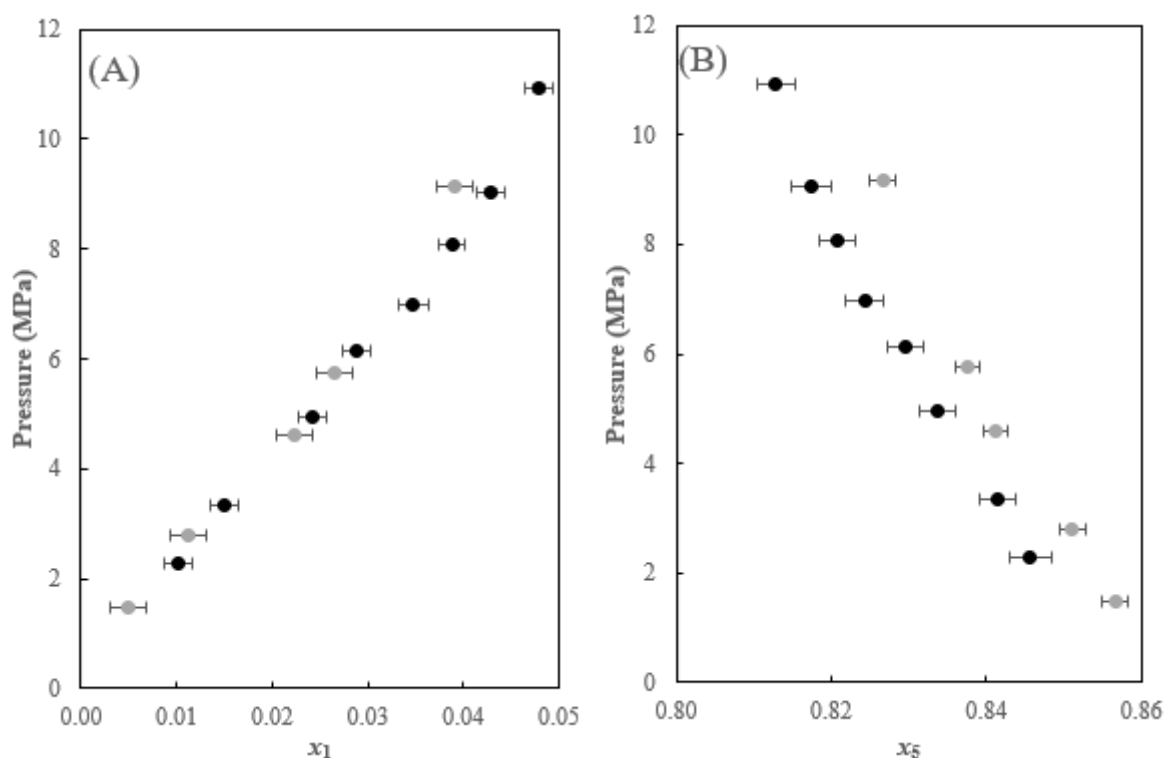


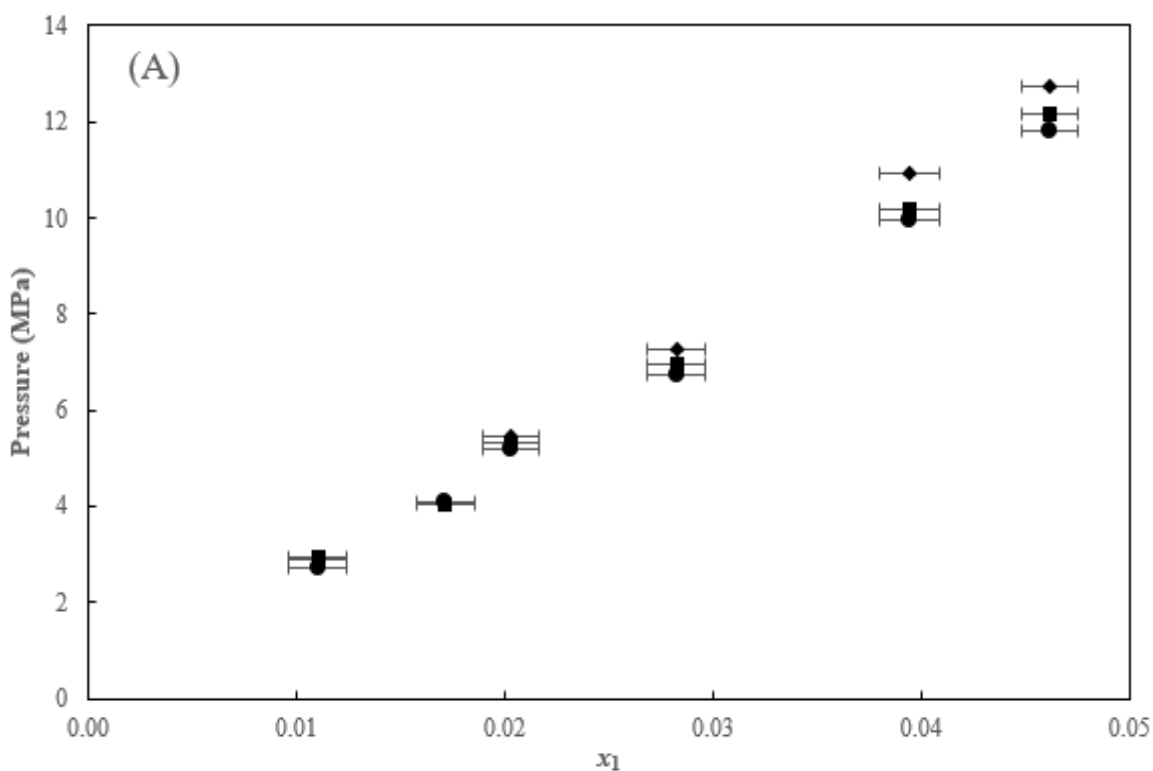
Figure 6-44: Comparison of the TPx data at $T = 323.15$ K for:

Water-free (CH₄ (1)/ C₃H₈ (2) 95/5 mol%) + ((H₂O (3) /TEG (5) 5/95% wt.): CH₃OH (4) 3.33 wt.%) system (●); and the (CH₄ (1)/C₃H₈ (2) 95/5 mol %) + (CH₃OH (3) /TEG (5) 3.33/96.67 wt.%) system (○). (A) CH₄ data; (B) TEG data.

Figure 6-44 (B) shows that the four-component system has generally high total pressure values compared to the water-free five-component system for the pressure range of 0 to 10.93 MPa. Uncertainties in the TEG composition are approximately 0.0016 for both the four-component system and the five-component system. Moreover, the figure shows that for the same equilibrium pressure on both systems, the composition of TEG in the five-component system is always less compared to that of the four-component system. Moreover, for both systems, as the composition of TEG increases, the equilibrium pressure decreases rapidly.

6.4.7 New system 7: (methane (1)/propane (2)/carbon dioxide (3) 90.22/4.60/5.18 mol%) + ((water (4) /TEG (6) 5/95 wt.%): methanol (5) 3.33 wt.%)

No literature data has been found for a system with similar components outlined in this section, although the Dortmund Data Bank indicates phase equilibria data for this six-component system exists in the proprietary database. Bubble point measurements were conducted for the (methane (1) /propane (2) /carbon dioxide (3) 90.22/4.60/5.18 mol%) + ((water (4) /TEG (6) 5/95 wt.%): methanol (5) 3.33 wt.%) system at 283.15, 303.15 and 323.15 K. The methane/propane/carbon dioxide gas mixture was ordered from Afrox (SA). A total of 17 data points were measured for this system. The data measured are presented in Figures 6-45 to 46. The data are also listed in Table B.4-7 (Appendix B), together with the associated uncertainties for the measured variables.



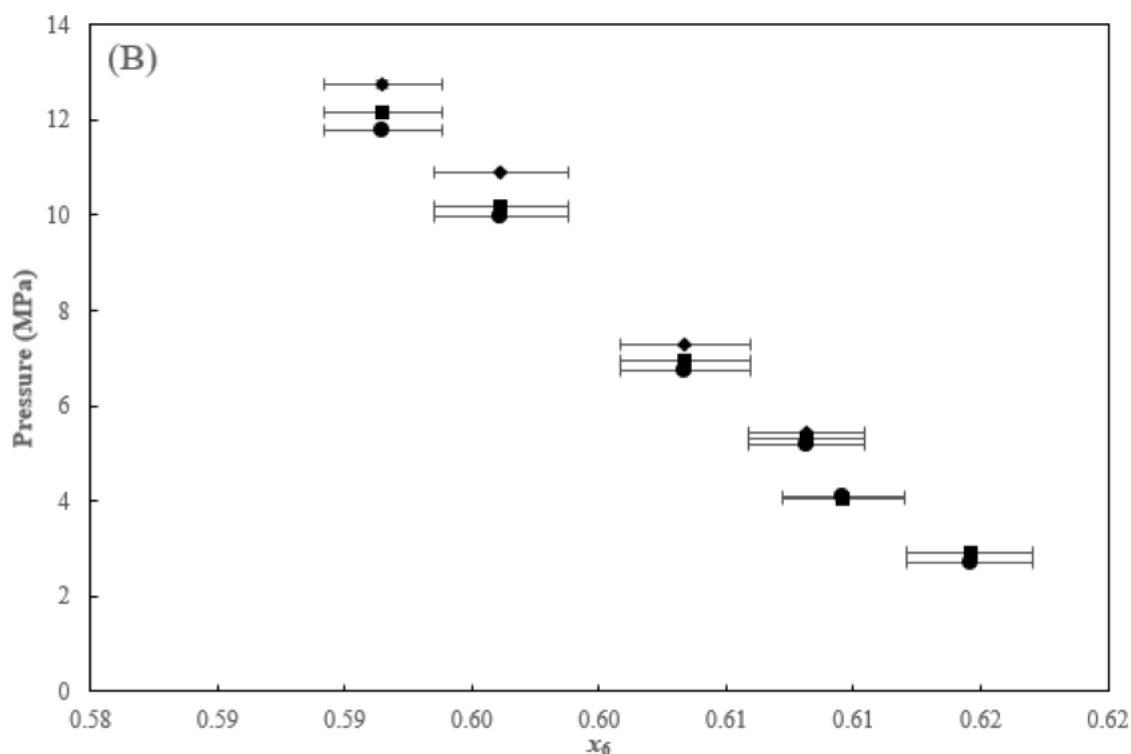


Figure 6-45: TPx graph for the $(\text{CH}_4$ (1) / C_3H_8 (2) / CO_2 (3) 90.22/4.60/5.18 mol%) + $(\text{H}_2\text{O}$ (4) / TEG (6) 5/95% wt.): CH_3OH (5) 3.33 wt.%).
 (A) CH_4 T dependency; (B) TEG T dependency; Symbols represent data at: 283.16 K (◆); 303.16 K (■); 323.15 K (●).

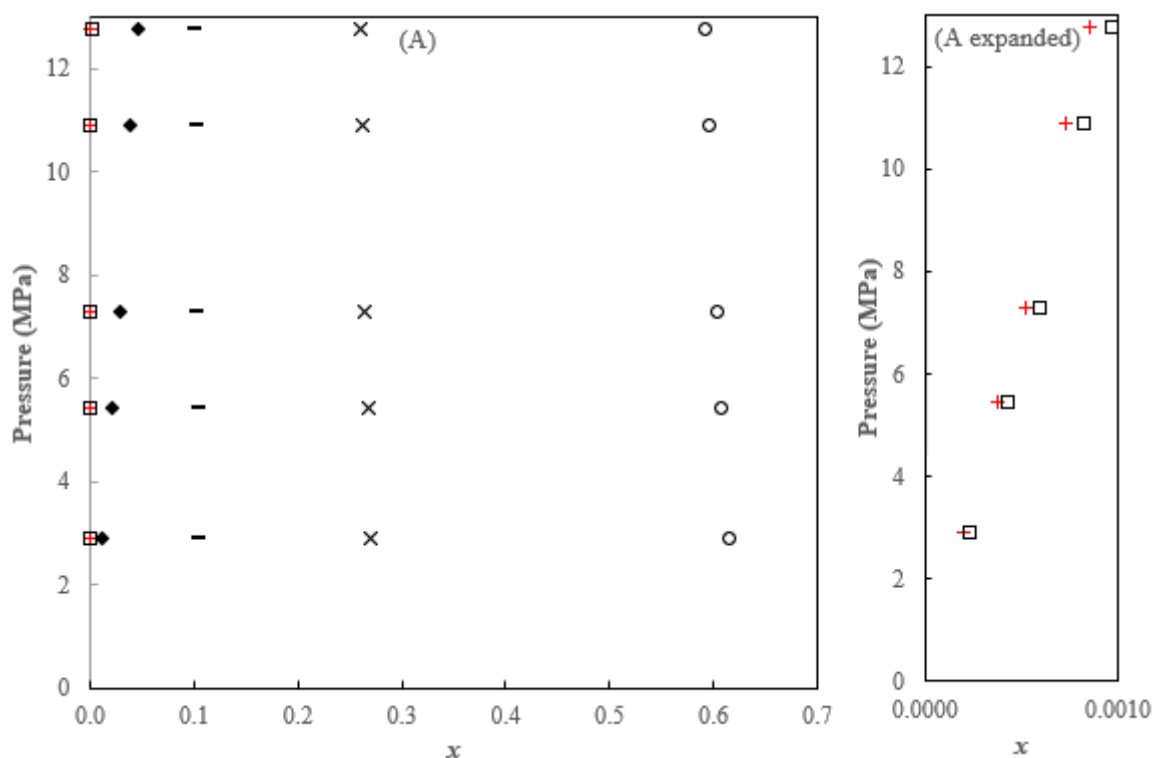
From the data in Figure 6-45 (A), the solubility of CH_4 in this multicomponent system is independent of temperature at lower pressures less than 4.07 MPa. Above 4.07 MPa, the solubility of methane increases with an increase in temperature. For the same composition x_1 , the bubble point pressures follow this trend: P at 283.16 K $>$ P at 303.15 K $>$ P at 323.15 K. This trend is more pronounced as the mole fraction of methane increases (see Figure 6-45 (A)). This trend could be due to the fact that as temperature increases, TEG molecules expand and form voids unto which the non-polar components, including methane, are encapsulated, hence the increase in methane solubility. Moreover, carbon dioxide is a non-polar molecule, hence has an effect of increasing the VdW forces leading to an increased interaction of the polar molecules with (TEG + water + methanol). TEG, water and methanol are polar components capable of either self or cross association.

Figure 6-45 (B) shows that at the highest concentration of TEG ($x_6 \sim 0.6081$) in the system, the bubble point pressure values of the system are approximately the same (~ 2.8 MPa) for all the three isotherms considered. For the same composition x_6 , the bubble point pressures follow this trend: P at 283.16 K $>$ P at 303.15 K $>$ P at 323.15 K. This trend is more pronounced as the mole fraction of TEG decreases from 0.6081 to 0.5915. Generally, for each isotherm considered, as the mole fraction of TEG decreases

(due to the addition of methane, propane, carbon dioxide, water, and methanol), the bubble point pressure increases as well. For the same composition of TEG, the decrease in bubble point pressure values at higher temperatures could be due to the breaking down of these strong hydrogen bonds in TEG.

More results for this system showing all the components for each of the isotherms are presented in Figure 6-46.

Figure 6-46 shows that at each of the isotherms considered, the data for each component in the 6-component system follows the same trend. It can also be observed in Figures 6-46 that on each of the isotherms, the composition of propane, carbon dioxide, water and methanol is relatively steady, whilst notable changes in the composition of methane and TEG can be easily observed with an increase in pressure.



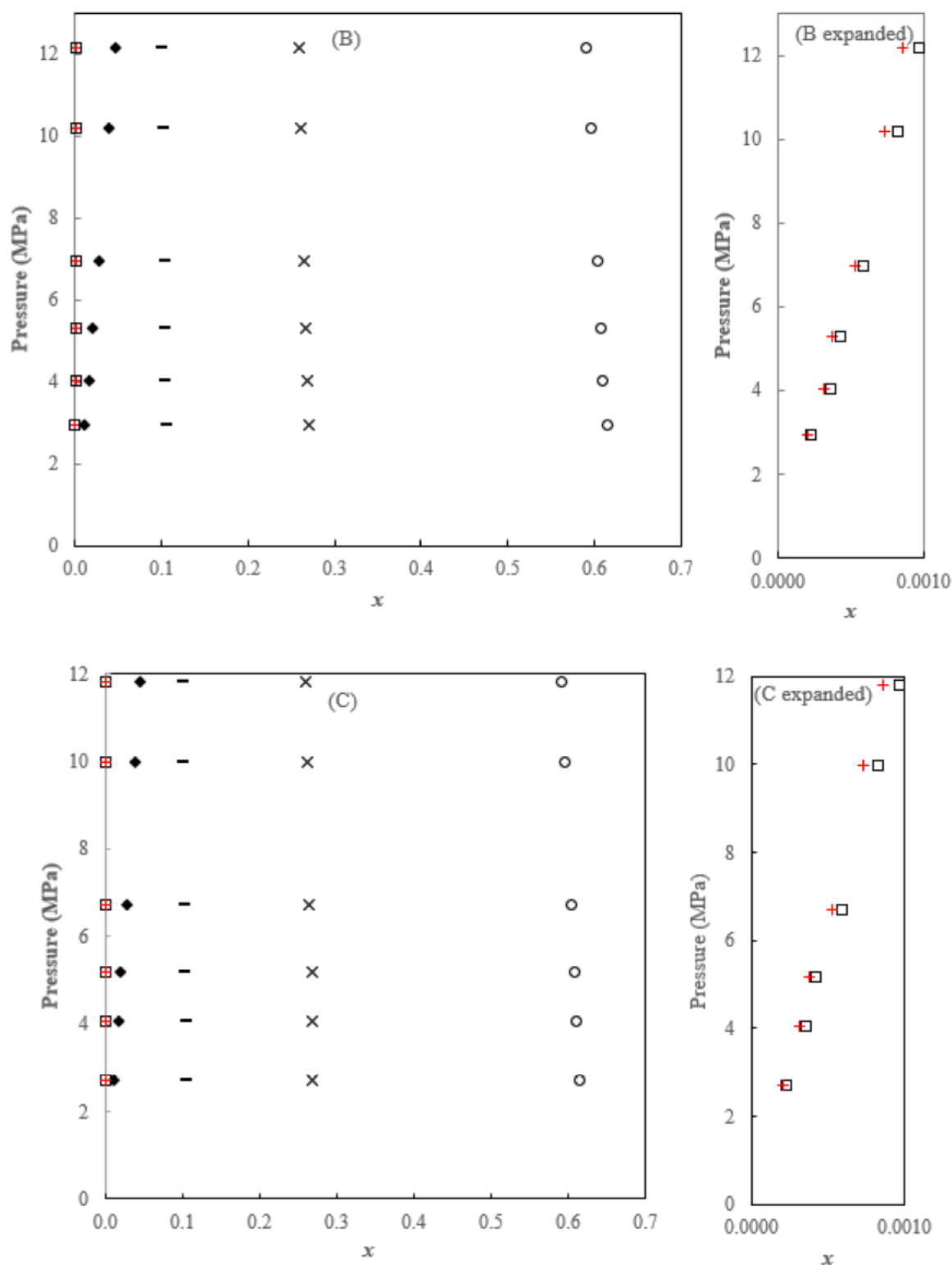
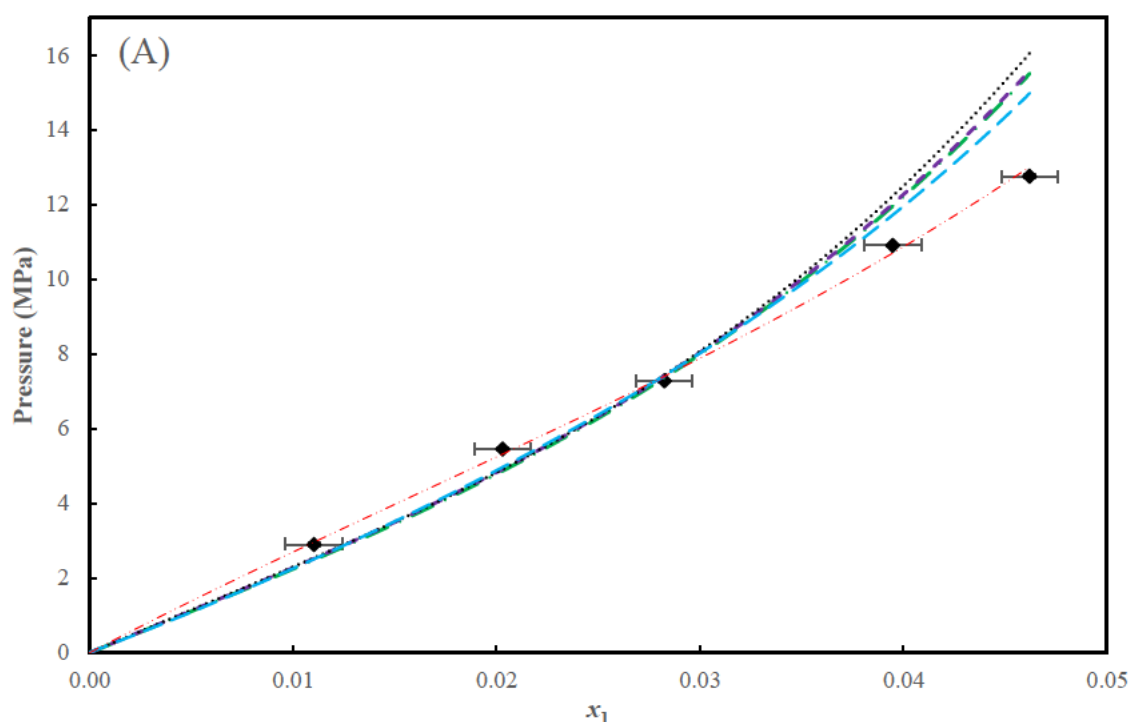


Figure 6-46: TP_x graph for the $(\text{CH}_4$ (1) / C_3H_8 (2) / CO_2 (3) 90.22/4.60/5.18 mol%) + $(\text{H}_2\text{O}$ (4) / TEG (6) 5/95 wt.%): CH_3OH (5) 3.33 wt.% system.
 (A) data at 283.15 K; (B) data at 303.15 K; (C) data at 323.15 K; Symbols represent: CO_2 (\square); C_3H_8 (+); CH_4 (\blacklozenge); CH_3OH (—) H_2O (x); and TEG (\circ); expanded represents expanded graphs for propane and carbon dioxide on each of (A), (B), or (C).

The measured data in this work was regressed with 5 models namely the PR, SRK, PRWS, CPA, and the PC-SAFT. Aspen Plus V12 has the advantage that during regression, analysis profiles (prediction results) are generated simultaneously, hence for this 6-component system, the prediction results are presented. Results of the model predictions are shown in Figures 6-47 to 49 for data at 283.15 K, 303.15 K and 323.15 K respectively. Table 6-27 presents the regressed model parameters and deviations. All the model correlations were extrapolated to $x_1 = 0$ as visible in Figures 6-47 to 49.

Figure 6-47 both (A) and (B) shows that the PRWS model prediction yielded the best fit to the experimental data. The AARD in pressures for the regressed data are 3.96%, 3.62%, 0.48%, 4.15% and 2.35% for the PR, SRK, PRWS, CPA and PC-SAFT models respectively. All the model predictions in this instance were performed in Aspen Plus V12. For the PR and SRK model predictions, the Deming algorithm was employed and the initialisation method used was the weighted least squares.



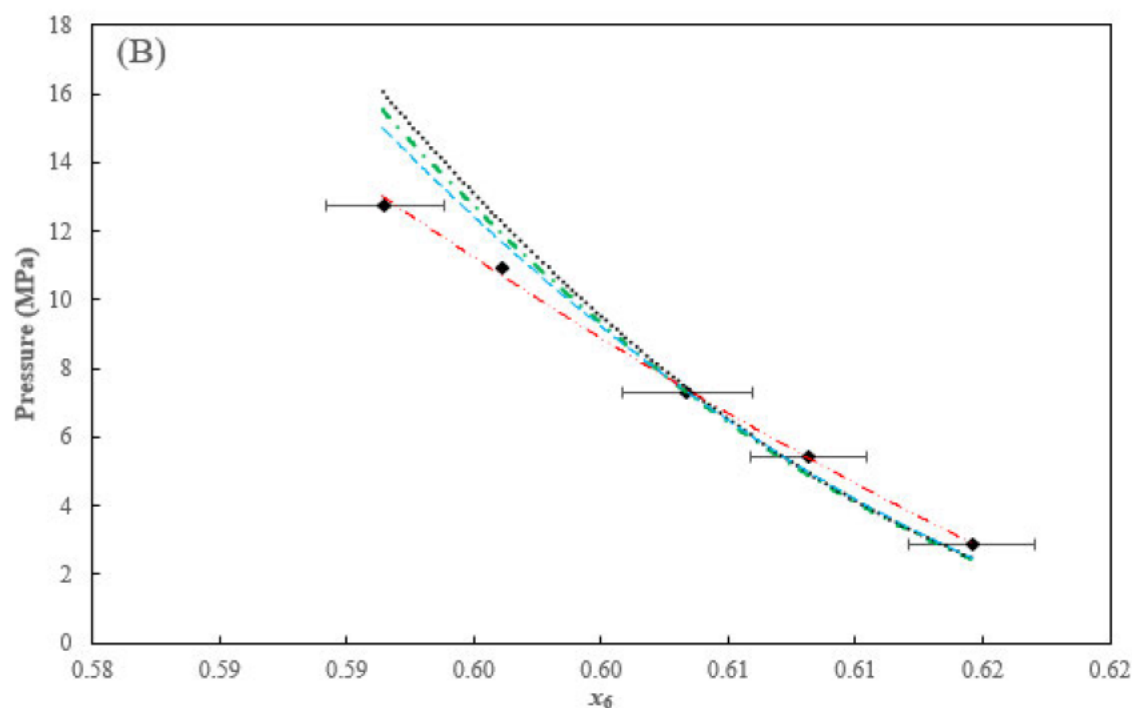
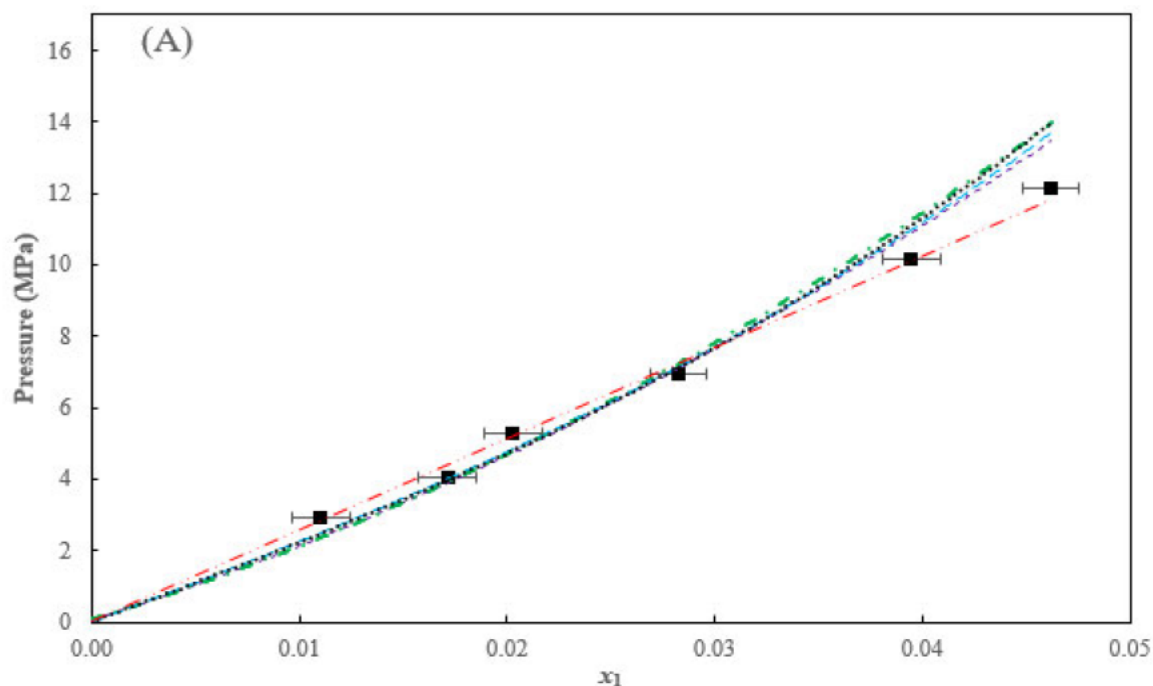


Figure 6-47: Thermodynamic modelling of (CH₄ (1) /C₃H₈ (2) /CO₂ (3) 90.22/4.60/5.18 mol%) + (H₂O (4) /TEG (6) 5/95 wt.%): CH₃OH (5) 3.33 wt.%) system at 283.15 K.
 (A), CH₄ data; (B), TEG data; Experimental data (◆); and modelling results: PR model (— · —); SRK model (— — —); PRWS (— · · —); CPA (— · · ·); and PC-SAFT model (·····).

For the PRWS, CPA and PC-SAFT model predictions, the Deming algorithm was employed, with the Deming initialisation method. Error bars represent compositional uncertainties.



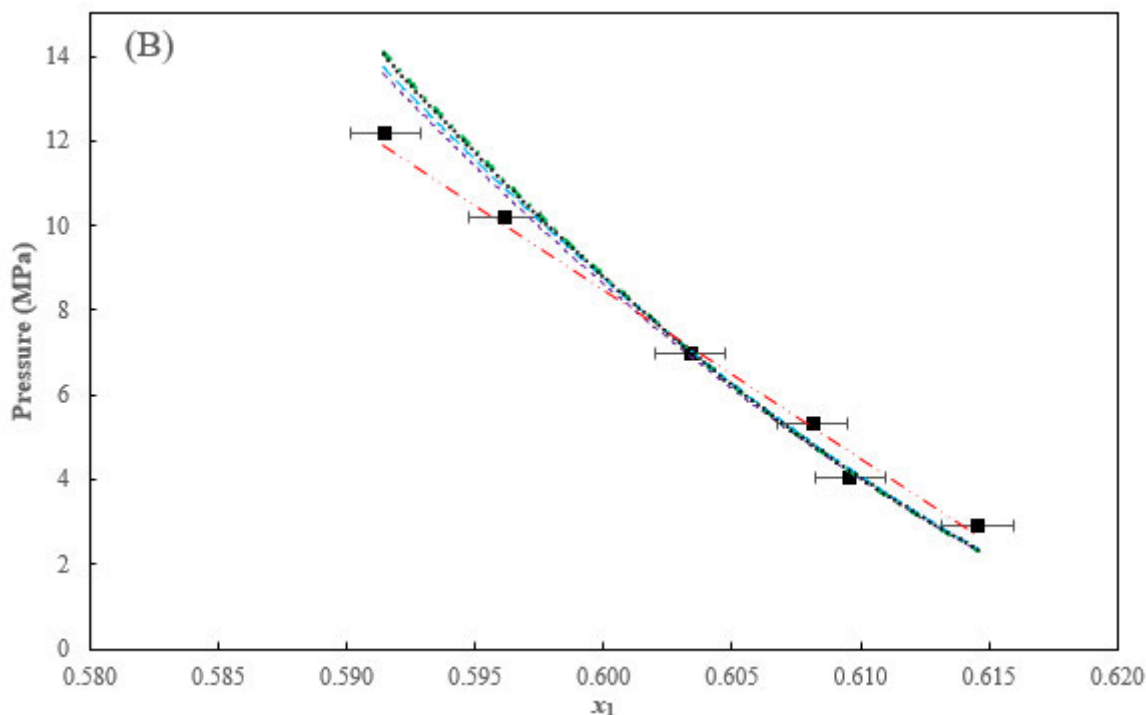


Figure 6-48: Thermodynamic modelling of (CH₄ (1) /C₃H₈ (2) /CO₂ (3) 90.22/4.60/5.18 mol%) + ((H₂O (4) /TEG (6) 5/95 wt.%): CH₃OH (5) 3.33 wt.%) system at 303.15 K.
 (A), CH₄ data; (B), TEG data; Experimental data (■); and modelling results: PR model (---); SRK model (---); PRWS (---); CPA (---); and PC-SAFT model (.....).

Figure 6-48 shows that the PRWS model prediction yielded the best fit to the experimental data as all the predicted data points lie within the experimental composition uncertainty of either methane (A) or TEG (B) indicated by error bars. All the other model predictions performed fairly well especially for the first four data points between 2.45 MPa to 10.18 MPa since the predicted data lie within the composition uncertainty range of this work (indicated by error bars). The AARD in pressures for the regressed data are 3.71%, 3.28%, 3.45%, 2.68% and 3.36% for the PR, SRK, PRWS, CPA and PC-SAFT models. All the model predictions in this instance were performed in Aspen Plus V12. For the PR, SRK, PRWS and PC-SAFT model predictions, the Deming algorithm was used together with the weighted least squares initialisation method. For the CPA model prediction, the Deming algorithm together with the Deming initialisation method were used.

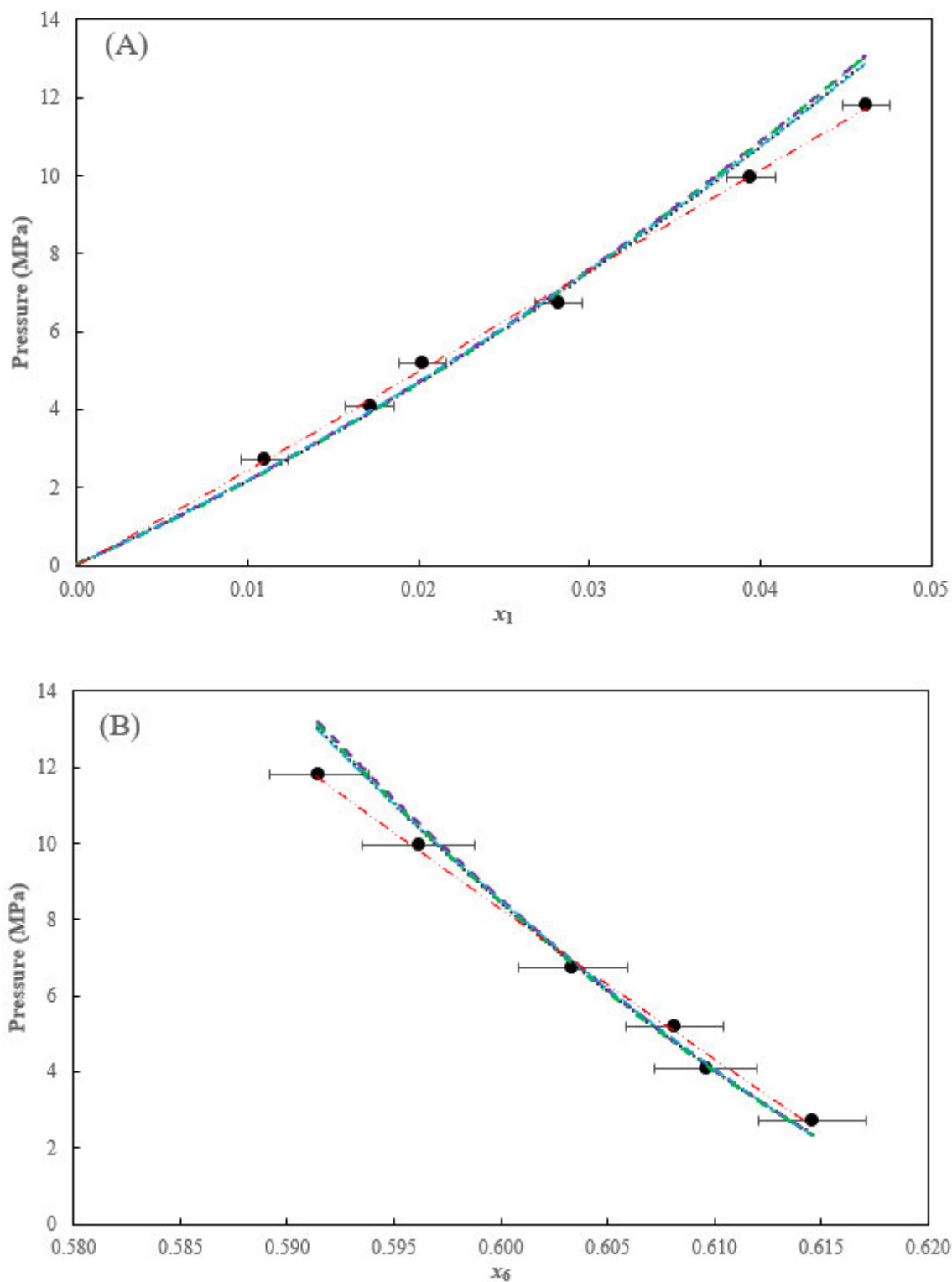


Figure 6-49: Thermodynamic modelling of (CH₄ (1) /C₃H₈ (2) /CO₂ (3) 90.22/4.60/5.18 mol%) + ((H₂O (4) /TEG (6) 5/95 wt.%): CH₃OH (5) 3.33 wt.%) system at 323.15 K.
 (A), CH₄ data; (B), TEG data; Experimental data (●); and modelling results: PR model (— · —); SRK model (— — —); PRWS (— · · —); CPA (· · · · ·).

Figure 6-49 both (A) and (B) shows that PRWS model prediction yielded the best fit to the experimental data as all the predicted data points lie within the experimental composition uncertainty of either

methane (A) or TEG (B) indicated by error bars. The rest of the model predictions performed fairly well especially for the first 5 data points between 2.5 MPa to 9.97 MPa since all the predicted data both for methane and TEG lie within the compositional uncertainty of this work (indicated by error bars). The AARD in pressures for the regressed data are 3.24%, 2.82%, 1.42%, 1.73% and 0.87% for the PR, SRK, PRWS, CPA and PC-SAFT models. All modelling in this instance was performed using Aspen Plus V12. For the PR, SRK and PRWS models, the Deming algorithm together with the weighted least squares initialisation method was used. For the CPA and PC-SAFT models, the Britt-Luecke algorithm, together with the Deming initialisation method were employed.

6.4.7.1 Comparison of the (methane /propane /carbon dioxide 90.22/4.60/5.18 mol%) + ((water /TEG 5/95 wt.%): methanol 3.33 wt.%) system and the (methane / propane 95/5 mol%) + ((water /TEG 5/95 wt.%): methanol 3.33 wt.%) system

The data for the six-component system and five-component systems at 323.15K were compared with respect to the methane and TEG composition in the multicomponent mixtures. The comparison was necessary to observe the effect of the added 5.18 mol% carbon dioxide to the gas mixture. The results of the comparison are presented in Figure 6-50.

Figure 6-50 (A) shows that the six-component system has lower pressure values than the five-component system for the same composition of methane in the multicomponent mixtures. As the mole fraction of methane increases, the difference in the pressure values between the two systems also increases. This shows that the addition of carbon dioxide (5.18 mol %) has an effect of increasing the solubility of methane in the multicomponent mixture. Carbon dioxide is non-polar so in the presence of methane + propane it would seem that the like interactions are preferred.

Figure 6-50 (B) shows that at the same composition of TEG in the multicomponent mixtures, equilibrium pressures are higher for the five-component system, compared to the six-component system. The difference in pressures between the two systems increases with the decrease of TEG composition in the systems. The figure also shows that at the same bubble point pressure value in the multicomponent mixtures, the composition of TEG is always high for the five-component system compared to the six-component system.

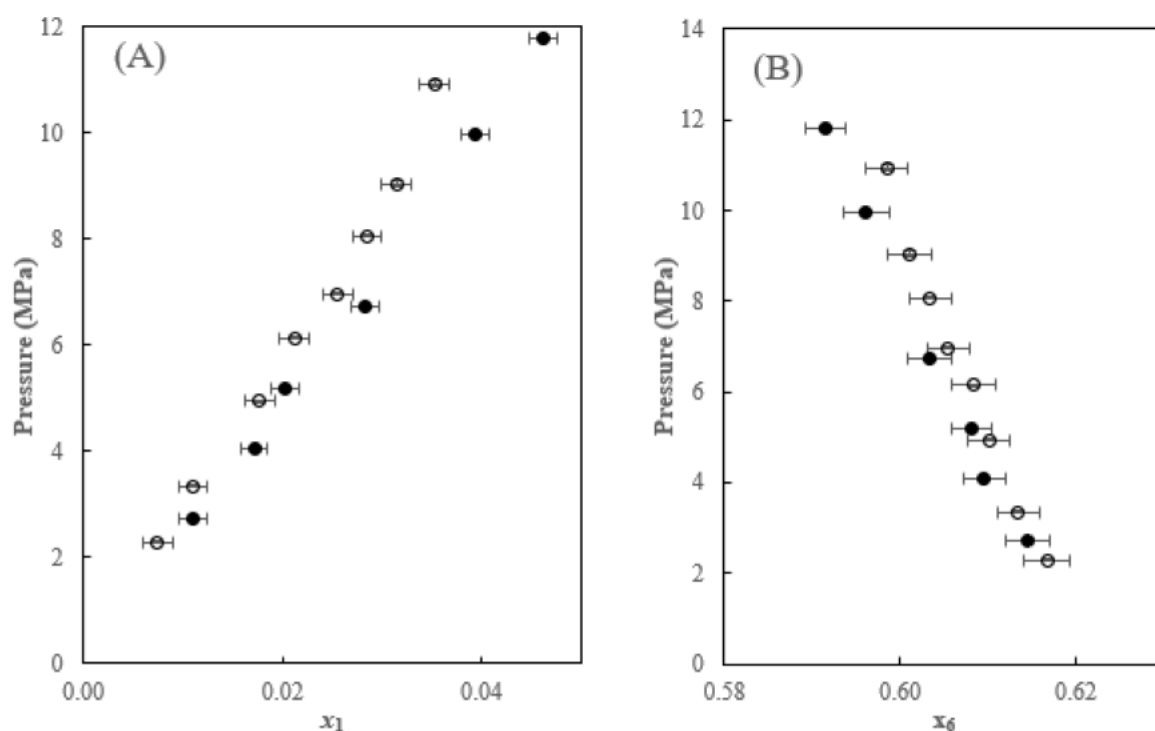


Figure 6-50: Comparison of the TP_x data at $T = 323.15$ K for:
 (CH₄ (1) /C₃H₈ (2) /CO₂ (3) 90.22/4.60/5.18 mol%) + ((H₂O (4) /TEG (6) 5/95 wt.%): CH₃OH (5) 3.33 wt.%) system (●); and the (CH₄ (1) / C₃H₈ (2) 95/5 mol%) + ((H₂O (3) /TEG (6) 5/95 wt.%): CH₃OH (4) 3.33 wt.%) system (○). (A) CH₄ data; (B) TEG data.

Table 6-27 (a): Regressed binary parameters and deviations for the (CH₄(1)/C₃H₈ (2)/CO₂ (3) 90.22/4.60/5.18 mol%) + ((H₂O (4) /TEG (6) 5/95 wt.%): CH₃OH (5) 3.33 wt.%) system.

Parameter	PRWS model			PR model			SRK model		
	$T=283.15$ K	$T=303.15$ K	$T=323.15$ K	$T=283.15$ K	$T=303.15$ K	$T=323.15$ K	$T=283.15$ K	$T=303.15$ K	$T=323.15$ K
k_{12}	0.4735	-0.0829	2.0460	-0.5421	-1.7989	-1.6653	-0.5932	-1.8027	-1.6715
k_{13}	-2.9594	-0.4191	13.9458	0.8544	0.9743	0.8150	0.9319	1.0305	0.8634
k_{14}	0.3251	0.9429	0.7610	0.6592	-0.2539	-0.2489	0.6642	-0.2860	-0.2834
k_{15}	0.5395	1.2855	1.0479	0.2618	-0.0048	0.2002	0.1885	0.0286	0.2322
k_{16}	0.3698	0.8016	0.9273	-0.3241	0.1961	0.2180	-0.4758	0.1860	0.2048
k_{23}	116.2930	766.9130	742.9644	348.62	546.13	409.62	358.21	528.31	394.49
k_{24}	29.0269	6.2455	12.6756	3.0441	22.012	23.1545	2.0780	20.1695	21.412
k_{25}	-9.8869	9.3590	14.2862	-60.984	-3.5171	43.321	-72.206	-4.4040	38.427
k_{26}	0.0237	0.3038	0.3846	3.0107	-2.4659	-5.3669	3.6698	-2.1454	-4.7841
k_{34}	91.2838	8.4989	8.9549	10.620	-21.256	-5.8495	13.846	-20.193	-5.2225
k_{35}	104.2210	6.7820	-15.6203	125.63	46.177	24.250	143.98	32.408	14.272
k_{36}	-0.0709	1.0720	1.3636	-8.9414	-0.0226	-0.5158	-10.372	0.6922	0.0249
k_{45}	30.6047	-102.6011	-95.1676	38.448	5.5241	4.1621	45.817	3.1981	1.9361
k_{46}	1.4471	3.1474	3.1324	-2.5080	-0.4989	-0.3935	-2.9222	-0.3213	-0.2266
k_{56}	-0.3392	6.4455	6.4131	-4.7151	-0.6404	-0.4577	-5.5547	-0.3260	-0.1595
A_{12}	3.0396	7.1658	1.6080						

Table 6-27 (a): Regressed binary parameters and deviations for the (CH₄(1)/C₃H₈ (2)/CO₂ (3) 90.22/4.60/5.18 mol%) + ((H₂O (4) /TEG (6) 5/95 wt.%): CH₃OH (5) 3.33 wt.%) system cont.

Parameter	PRWS model			PR model			SRK model		
	T=283.15 K	T=303.15 K	T=323.15 K	T=283.15 K	T=303.15 K	T=323.15 K	T=283.15 K	T=303.15 K	T=323.15 K
<i>A</i> ₂₁	34.5651	7.0527	14.5908						
<i>A</i> ₁₃	-8.6341	60.0191	63.0157						
<i>A</i> ₃₁	43.3499	36.5285	41.8954						
<i>A</i> ₁₄	7.3997	1.2775	-0.9832						
<i>A</i> ₄₁	6.0582	6.3637	7.5211						
<i>A</i> ₁₅	10.6942	5.3317	-0.7628						
<i>A</i> ₅₁	4.8870	7.8413	9.2697						
<i>A</i> ₁₆	-1.8297	1.8989	0.9242						
<i>A</i> ₆₁	3.2309	4.3997	4.7971						
<i>A</i> ₂₃	-0.2352	454.2156	406.7395						
<i>A</i> ₃₂	46.2125	454.2157	406.7395						
<i>A</i> ₂₄	3.0416	4.7907	0.7727						
<i>A</i> ₄₂	2.2656	7.9210	5.0294						
<i>A</i> ₂₅	7.4379	6.5462	-4.6247						
<i>A</i> ₅₂	-3.8063	9.5067	4.2125						
<i>A</i> ₂₆	3.8031	3.1861	1.5081						
<i>A</i> ₆₂	0.0574	6.6786	4.2188						
<i>A</i> ₃₄	10.2965	-2.9794	-1.8937						
<i>A</i> ₄₃	-2.0967	3.8856	6.4460						
<i>A</i> ₃₅	-5.0317	-2.5271	-4.3385						
<i>A</i> ₅₃	-1.9576	10.7507	9.3692						
<i>A</i> ₃₆	5.3406	-3.0027	-0.3951						
<i>A</i> ₆₃	-1.2646	3.5319	6.0526						
<i>A</i> ₄₅	1.1549	7.0479	7.4038						
<i>A</i> ₅₄	-1.9382	4.9622	5.1898						
<i>A</i> ₄₆	-0.7676	3.9260	3.9284						
<i>A</i> ₆₄	0.8614	5.1680	5.2194						
<i>A</i> ₅₆	1.3939	3.9460	3.9423						
<i>A</i> ₆₅	1.6445	7.0490	6.9840						
AAD <i>P</i> (MPa)	0.04	0.27	0.09	0.28	0.22	0.20	0.26	0.20	0.17
AARD <i>P</i> %	0.48	3.45	1.42	3.96	3.71	3.24	3.62	3.28	2.82
AAD <i>x</i> ₁	0.0002	0.0002	0.0003	0.0014	0.0017	0.0013	0.0013	0.0015	0.0011
AARD <i>x</i> ₁ %	0.74	1.04	1.17	5.15	6.01	4.41	4.58	5.12	3.70
AAD <i>x</i> ₆	0.0008	0.0003	0.0003	0.0011	0.0017	0.0007	0.0008	0.0015	0.0005
AARD <i>x</i> ₆ %	0.13	0.05	0.05	0.18	0.29	0.11	0.14	0.26	0.08
AAD <i>T</i> (K)	0.05	0.05	0.06	0.88	4.82	3.64	0.58	5.02	3.75
AARD <i>T</i> %	0.02	0.02	0.02	0.31	1.59	1.13	0.21	1.66	1.16

Table 6-27 (b): Regressed binary parameters and deviations for the (CH₄ (1)/C₃H₈(2)/CO₂ (3) 90.22/4.60/5.18 mol%) + ((H₂O (4) /TEG (6) 5/95 wt.%): CH₃OH (5) 3.33 wt.%) system cont.

Parameter	CPA model			PC-SAFT model		
	$T = 283.15$ K	$T = 303.15$ K	$T = 323.15$ K	$T = 283.15$ K	$T = 303.15$ K	$T = 323.15$ K
k_{12}	0.1370	0.1370	0.1370	0.4352	0.3760	0.3067
k_{13}	0.4556	0.4984	0.3420	0.2053	0.1691	0.2883
k_{14}	0.0400	-0.0327	-0.0327	0.5876	-0.6734	-0.6766
k_{15}	0.5928	-0.1123	-0.1094	0.2042	-0.1423	-0.0003
k_{16}	0.1256	0.1593	0.4502	-0.0730	0.0125	0.0249
k_{23}	1.4179	1.4179	1.4179	-0.4074	3.6399	3.9994
k_{24}	-1.0215	1.2485	-1.0215	-0.1096	-0.2168	-0.3640
k_{25}	1.3473	1.3473	-1.6467	0.8759	-0.7385	-0.4674
k_{26}	-0.0911	-0.2327	0.2321	-0.0551	-0.0284	-0.0165
k_{34}	0.3927	-0.4799	-0.4799	0.6491	-0.2258	0.5366
k_{35}	0.8521	0.8521	0.8521	4.3446	0.1037	0.7320
k_{36}	0.1468	0.2127	0.3460	-0.0723	0.1138	0.0470
k_{45}	0.4183	0.4183	0.4183	4.2163	10.473	7.4455
k_{46}	-1.3796	-1.3928	1.2567	-0.1414	-0.3998	-0.3515
k_{56}	-0.1498	-0.1990	-0.1000	-0.3990	-0.7199	-0.5705
($\varepsilon^{A_4B_5}$)	0.0035	9.0073E-05	42.666	5.12358E-05	8.76256E-06	4.50294E-05
($\beta^{A_4B_5}$)	-0.0004	9.0431E-05	-0.1256	5.14493E-05	8.79406E-06	4.5183E-05
($\varepsilon^{A_4B_6}$)	-0.0033	0.00214	2086.4	6.97029E-06	-1.20746E-06	9.42978E-07
($\beta^{A_4B_6}$)	-0.1785	0.14607	0.1461	7.01655E-06	-1.20991E-06	1.0132E-06
($\varepsilon^{A_5B_6}$)	0.0005	5.8854E-06	20.6378	6.42129E-06	2.14826E-06	7.03317E-07
($\beta^{A_5B_6}$)	-5.751E-05	5.28E-06	-0.0185	6.47175E-06	2.16994E-06	7.44175E-07
AAD P (MPa)	0.29	0.15	0.11	0.16	0.19	0.08
AARD P %	4.15	2.68	1.73	2.35	3.46	0.87
AAD x_1	0.0015	0.0015	0.0006	0.0009	0.0018	0.0001
AARD x_1 %	5.22	5.06	1.99	3.13	6.11	0.62
AAD x_6	0.0022	0.0081	0.0066	0.0089	0.0023	0.0040
AARD x_6 %	0.36	1.34	1.10	1.47	0.37	0.66
AAD T (K)	1.76	6.14	2.33	1.68	5.36	2.00
AARD T %	0.62	2.03	0.72	0.59	1.77	0.62

Note: All values in SI units.

The CPA bubble point predictions using k_{ij} reported in Table 6-19 are displayed in Figures E-3.9. A, B and C for the data at 283.15, 303.15 and 323.15K respectively. The AARD% in pressure were 32.23, 26.70, and 23.48 for the data at 283.15, 303.15 and 323.15K respectively. Generally, the CPA model over predicted the bubble point pressure values and the trend becomes more pronounced as the methane mole fraction in the mixture increases. Comparison of Figure E-9 to Figures 6-47 to 48 (A) shows that the binary interactions parameters alone may not be adequate for describing phase behaviour in multicomponent systems. This is because the bubble point predictions in Figure E-9 seem to deviate more from the experimental data, than the predicted data in Figures 6-47 to 48 (A).

Trends for the absolute values of the regressed binary interaction parameters (k_{ij}) for possible binary pairs of this system in Table 6-27 (a) and (b) can be described as follows:

For the PRWS:

Parameter	PRWS model					
	$T = 283.15 \text{ K}$		$T = 303.15 \text{ K}$		$T = 323.15 \text{ K}$	
	Value	σ	Value	σ	Value	σ
k_{12}	0.4735	3.8591	-0.0829	0.6101	2.0460	1.0517
k_{13}	-2.9594	6.3014	-0.4191	1.4434	13.9458	1.7266
k_{14}	0.3251	2.4468	0.9429	0.0793	0.7610	0.1126
k_{15}	0.5395	2.1369	1.2855	0.1745	1.0479	0.1741
k_{16}	0.3698	0.4445	0.8016	0.0041	0.9273	0.0052
k_{23}	116.29	2823.1	766.91	260.67	742.96	165.47
k_{24}	29.0269	250.8802	6.2455	3.1138	12.6756	10.7725
k_{25}	-9.8869	623.9194	9.3590	14.7344	14.2862	7.3014
k_{26}	0.0237	2.8564	0.3038	0.1320	0.3846	0.3919
k_{34}	91.2838	125.0944	8.4989	13.6788	8.9549	10.5654
k_{35}	104.2210	183.8032	6.7820	49.4204	-15.6203	18.6182
k_{36}	-0.0709	2.7344	1.0720	0.7610	1.3636	0.1759
k_{45}	30.6047	388.9888	-102.6011	1.5879	-95.1676	1.0658
k_{46}	1.4471	0.9389	3.1474	0.0211	3.1324	0.0207
k_{56}	-0.3392	36.0674	6.4455	0.0670	6.4131	0.0479

All values in SI units.

σ represents the standard deviation reported in Aspen Plus V12

- There is no clear trend on the interaction parameter between methane + propane, methane + carbon dioxide, methane + water, methane + methanol, propane + carbon dioxide, propane + water, propane + methanol, carbon dioxide + water, carbon dioxide + methanol, water + methanol, water + TEG and methanol + TEG. The binary interaction parameter for methane + methanol binary pair in the senary system of 1.2855 at 303.15 K, is significantly greater than

0.3423 at 303.15 K for the methane + methanol binary system reported in Table 6-15. The binary interaction parameter between methane + TEG binary pair in the senary system of 0.9273 at 323.15 K is significantly greater than 0.5363 for the methane + TEG binary system at 323.15 K, reported in Table 6-16. The binary interaction parameter for carbon dioxide + methanol binary pair in the senary system, of 6.7820 at 303.15 K, is not even closer to the range of 0.5401 to 0.5138 reported for the carbon dioxide + methanol binary system at 298.14 K and 313.15 K respectively, reported earlier.

- The interaction parameter between methane + TEG, propane + TEG, carbon dioxide + TEG increases with temperature.
- All binary pairs in the above table where the magnitude of the standard deviation of the binary interaction is greater or similar to the value of the binary interaction parameter indicate that the data are over fitted; hence such binary parameters are insignificant to the overall model fitting and could possibly be set to 0.

For the PR and SRK models

Parameter	PR model						SRK model					
	$T = 283.15 \text{ K}$		$T = 303.15 \text{ K}$		$T = 323.15 \text{ K}$		$T = 283.15 \text{ K}$		$T = 303.15 \text{ K}$		$T = 323.15 \text{ K}$	
	Value	σ	Value	σ	Value	σ	Value	σ	Value	σ	Value	σ
k_{12}	-0.5421	0.1244	-1.7989	0.1359	-1.6653	0.1828	-0.5932	0.1435	-1.8027	0.1520	-1.6715	0.2073
k_{13}	0.8544	0.0428	0.9743	0.0427	0.8150	0.0457	0.9319	0.0503	1.0305	0.0490	0.8634	0.0534
k_{14}	0.6592	0.0184	-0.2539	0.0148	-0.2489	0.0189	0.6642	0.0185	-0.2860	0.0162	-0.2834	0.0210
k_{15}	0.2618	0.0692	-0.0048	0.0500	0.2002	0.0623	0.1885	0.0429	0.0286	0.0546	0.2322	0.0691
k_{16}	-0.3241	0.0257	0.1961	0.0030	0.2180	0.0040	-0.4758	0.0273	0.1860	0.0032	0.2048	0.0043
k_{23}	348.62	36.954	546.13	32.027	409.62	34.080	358.210	40.936	528.31	34.168	394.49	36.611
k_{24}	3.0441	2.1289	22.0120	2.1982	23.1545	2.6119	2.0780	3.0752	20.1695	2.2645	21.4120	2.7041
k_{25}	-60.984	6.2283	-3.5171	6.4063	43.3210	9.3658	-72.2060	15.7320	-4.4040	6.6085	38.4270	9.7082
k_{26}	3.0107	0.3732	-2.4659	0.4019	-5.3669	0.6504	3.6698	1.1746	-2.1454	0.4084	-4.7841	0.6637
k_{34}	10.62	4.8690	-21.2560	2.8098	-5.8495	2.9261	13.8460	4.6371	-20.1930	2.9171	-5.2225	3.0577
k_{35}	125.63	20.3515	46.1770	11.7808	24.2500	11.6751	143.9800	11.1204	32.4080	12.2518	14.2720	12.2661
k_{36}	-8.9414	1.5972	-0.0226	0.6513	-0.5158	0.7038	-10.3720	0.9735	0.6922	0.6680	0.0249	0.7284
k_{45}	38.448	2.1332	5.5241	0.0248	4.1621	0.0270	45.8170	2.1460	3.1981	0.0255	1.9361	0.0278
k_{46}	-2.508	0.1374	-0.4989	0.0016	-0.3935	0.0016	-2.9222	0.1363	-0.3213	0.0016	-0.2266	0.0017
k_{56}	-4.7151	0.2688	-0.6404	0.0032	-0.4577	0.0034	-5.5547	0.2667	-0.3260	0.0032	-0.1595	0.0035

All values in SI units.

σ represents the standard deviation reported in Aspen Plus V12

- There is no clear trend on the interaction parameter between methane + propane, methane + carbon dioxide, methane + water, methane + methanol, methane + TEG, propane + carbon dioxide, propane + methanol, propane + TEG, carbon dioxide + water, carbon dioxide + TEG (PR only),
- The interaction parameter between propane + water increases with an increase in temperature.
- The interaction parameter between carbon dioxide + methanol, carbon dioxide + TEG (SRK only), water + methanol, water + TEG and methanol + TEG decreases with an increase in temperature.
- For the PR model, only the propane + methanol binary parameter at 303.15 K is insignificant to the overall model fitting since the standard deviation value is greater than the value of the binary interaction parameter. This indicates that the data are over fitted. All the other binary parameters at all the isotherms considered are significant to the overall model fitting.
- For the SRK model, only the propane + water binary interaction parameter at 283.15 K, methane + methanol, propane + methanol, carbon dioxide + TEG binary interaction parameters at 303.15 K and carbon dioxide + TEG binary interaction parameter at 323.15 K are insignificant to the overall model fitting. This is because the value of the standard deviation is greater than the value of the binary interaction parameter, indicating that the data are over fitted, and hence these parameters could possibly be set to 0.

For the CPA model

- The interaction parameter between methane + propane, propane + carbon dioxide, carbon dioxide + methanol, water + methanol is independent of temperature.
- There is no clear trend on the interaction parameter between methane + carbon dioxide, propane + water, propane + TEG, water + TEG, and methanol + TEG.
- The interaction parameter between methane + water, carbon dioxide + water, decreases with temperature from 283.15 to 303.15 K. Between 303.15 and 323.15 K, the interaction parameter is independent of temperature.
- The interaction parameter between methane + methanol decreases with an increase in temperature. The absolute value of the binary interaction parameter between methane + methanol binary pair in the senary system of 0.1123, at 303.15 K, is significantly larger than 0.0462 reported in Table 6-15 for the methane + methanol binary system at 303.15 K.
- The interaction parameter between methane + TEG, carbon dioxide + TEG increases with an increase in temperature. The interaction parameter between methane + TEG binary pair of the senary system at 323.15 K, of value = 0.4502 is larger than 0.2046 for the methane + TEG binary system at 323.15 K presented in Table 6-16.

- The interaction parameter between propane + methanol is independent of temperature between 283.15 to 303.15 K. However, from 303.15 to 323.15 K, the interaction parameter increases with an increase in temperature.
- All the binary interaction parameters are significant to the overall model parameter fitting since the magnitude of the standard deviations is less than the values of the binary interaction parameters.

Parameter	CPA model					
	<i>T</i> = 283.15 K		<i>T</i> = 303.15 K		<i>T</i> = 323.15 K	
	Value	σ	Value	σ	Value	σ
<i>k</i> ₁₂	0.137	0.0000	0.1370	0.0000	0.1370	0.0000
<i>k</i> ₁₃	0.4556	0.0118	0.4984	0.0151	0.3420	0.0178
<i>k</i> ₁₄	0.04	0.0000	-0.0327	0.0000	-0.0327	0.0000
<i>k</i> ₁₅	0.5928	0.0112	-0.1123	0.0053	-0.1094	0.0240
<i>k</i> ₁₆	0.1256	0.0177	0.1593	0.0004	0.4502	0.0048
<i>k</i> ₂₃	1.4179	0.0000	1.4179	0.0000	1.4179	0.0000
<i>k</i> ₂₄	-1.0215	0.0000	1.2485	0.0000	-1.0215	0.0000
<i>k</i> ₂₅	1.3473	0.0000	1.3473	0.0000	-1.6467	0.0000
<i>k</i> ₂₆	-0.0911	0.0138	-0.2327	0.0005	0.2321	0.0039
<i>k</i> ₃₄	0.3927	0.0000	-0.4799	0.0000	-0.4799	0.0000
<i>k</i> ₃₅	0.8521	0.0000	0.8521	0.0000	0.8521	0.0000
<i>k</i> ₃₆	0.1468	0.0048	0.2127	0.0015	0.3460	0.0038
<i>k</i> ₄₅	0.4183	0.0000	0.4183	0.0000	0.4183	0.0000
<i>k</i> ₄₆	-1.3796	0.2029	-1.3928	0.0039	1.2567	0.0397
<i>k</i> ₅₆	-0.1498	0.0672	-0.1990	0.0000	-0.1000	0.0161

All values in SI units.

σ represents the standard deviation reported in Aspen Plus V12

For the PC-SAFT model

- The interaction parameter between methane + propane, methane + methanol, propane + methanol, propane + TEG decreases with an increase in temperature. The methane + methanol binary interaction parameter, absolute value of 0.1423 at 303.15 K in the senary system, is significantly larger than 0.0498 for the methane + methanol binary system of this work at 303.15 K, presented in Table 6-15.
- There is no clear trend on the interaction parameter between methane + carbon dioxide, methane + TEG, carbon dioxide + water, carbon dioxide + methanol, carbon dioxide + TEG, water + methanol, water + TEG and methanol + TEG. The binary interaction parameter

between methane + TEG binary pair in the senary system of value = 0.0249 at 323.15 K, is comparable to 0.03302 for the methane + TEG binary system at 323.15 K, presented in Table 6-16.

Parameter	PC-SAFT model					
	<i>T</i> = 283.15 K		<i>T</i> = 303.15 K		<i>T</i> = 323.15 K	
	Value	σ	Value	σ	Value	σ
k_{12}	0.4352	0.0603	0.3760	0.0137	0.3067	0.0157
k_{13}	0.2053	0.0430	0.1691	0.0167	0.2883	0.0325
k_{14}	0.5876	0.0149	-0.6734	0.0098	-0.6766	0.0106
k_{15}	0.2042	0.0256	-0.1423	0.0329	-0.0003	0.0411
k_{16}	-0.073	0.0205	0.0125	0.0013	0.0249	0.0016
k_{23}	-0.4074	20.7752	3.6399	5.0877	3.9994	7.5566
k_{24}	-0.1096	2.2818	-0.2168	1.2114	-0.3640	0.8831
k_{25}	0.8759	12.3739	-0.7385	5.3146	-0.4674	3.8153
k_{26}	-0.0551	0.5676	-0.0284	0.2012	-0.0165	0.0738
k_{34}	0.6491	3.5769	-0.2258	1.7993	0.5366	1.1236
k_{35}	4.3446	9.0707	0.1037	8.4767	0.7320	4.5251
k_{36}	-0.0723	0.4041	0.1138	0.3068	0.0470	0.0847
k_{45}	4.2163	4.6879	10.4730	0.1387	7.4455	0.1979
k_{46}	-0.1414	0.1322	-0.3998	0.0016	-0.3515	0.0042
k_{56}	-0.399	0.2886	-0.7199	0.0029	-0.5705	0.0063

All values in SI units.

σ represents the standard deviation reported in Aspen Plus V12

- The interaction parameter between methane + water, propane + carbon dioxide, propane + water increases with an increase in temperature.
- For the data at 283.15 K, the propane + carbon dioxide, propane + water, propane + methanol, propane + TEG, carbon dioxide + water, carbon dioxide + methanol, carbon dioxide + TEG, water + methanol binary interaction parameters are insignificant to the overall model fitting. This is because the magnitude of standard deviation for the binary parameters is greater than the values of the binary interaction parameters, indicating that the data are over fitted.
- For the data at 303.15 K, the propane + carbon dioxide, propane + methanol, propane + TEG, carbon dioxide + methanol, carbon dioxide + TEG binary parameters are insignificant to the overall model fitting.
- At 323.15 K, the methane + methanol, propane + carbon dioxide, propane + water, propane + methanol, propane + TEG, carbon dioxide + water, carbon dioxide + methanol, carbon dioxide + TEG binary interaction parameters are insignificant to the overall model fitting. This is because the magnitude of standard deviation for the binary parameters is greater than the values of the binary interaction parameters, indicating that the data are over fitted.

Summary of the maximum AARD in pressure for all the data measured in this work.

Table 6-28 presents a summary of the maximum AARD in pressure for all the data measured in this work.

Table 6-28: Summary of the maximum AARD % in pressure for the data measured in this work.

Model	PRWS	PC-SAFT	CPA	PR	SRK
System	Maximum AARD % in Pressure				
Carbon dioxide + n hexane	0.30	0.02	0.08		
Carbon dioxide + n decane	1.62	0.70	0.38		
Carbon dioxide + methanol	0.55	0.82	0.58		
Methane + methanol	1.86	3.32	3.07		
Methane+ TEG	4.89	4.21	4.48		
Carbon dioxide + TEG	3.71	19.7	3.66		
Carbon dioxide + water + TEG	1.62	0.91	2.08	1.07	1.92
Methane + propane + methanol	1.00	2.78	2.55	3.37	3.09
Methane + propane + TEG	1.90	4.25	4.07	4.32	4.11
Methane + methanol + TEG	1.73	2.73	2.05	2.28	2.01
Carbon dioxide + methanol + TEG	3.09	6.77	4.57	9.63	8.67
Methane + propane + methanol + TEG	4.45	7.33	7.39	7.44	7.25
Methane + propane + methanol + water + TEG	1.49	3.4	2.93	2.49	3.22
Methane + propane + carbon dioxide+ methanol + water + TEG	2.72	3.46	4.15	3.96	3.62

From Table 6-28, it can be concluded that the maximum AARD % over all systems measured in this work were 4.89, 19.7, 7.39, 9.63 and 8.67 for the PRWS, PC-SAFT, CPA, PR and SRK model correlations. This implies that generally the PRWS model best describes the phase equilibria data for the systems measured in this work over all the other models.

CHAPTER 7: CONCLUSIONS

This section outlines major conclusions on the work performed in this study. A relatively new experimental apparatus of the variable volume combined static analytic/synthetic method was used and the techniques and reliability of the equipment was confirmed by either TP_x and TP_{xy} measurements for a wide range of test systems. Generally, good agreement was observed between the literature data and the experimental data of this work for the test systems. The maximum AARD in pressure obtained from all data using the PRWS model was 4.89%. The CPA model was also used to predict phase equilibria data for multicomponent systems of this work making use of binary interaction parameters from this work, as well as reported binary interaction parameters. The maximum AARD in pressure using the CPA binary interaction parameters was 39.36%. The results generally showed that binary interaction parameters alone may not be adequate in describing the phase behaviour in multicomponent systems. This was because the regressed experimental data yielded better results with lower errors.

New phase equilibria data (with 100 data points) were measured for 7 systems. For the methane + propane + methanol system measured at 283.15, 303.16, and 323.15 K, as the methane composition in the mixture increased, pressure values increased as well and linear trends were observed. For the same methane composition in the mixture, the total pressure values generally increased with temperature. This means that methane was more soluble in the mixture at lower temperatures compared to higher isotherms. The PRWS yielded better results at all isotherms with an AARD % of ≤ 1 . The average expanded uncertainty over all points in methane composition was $U(x_1) = 0.0009$. Slight variations were observed in the binary interaction parameters on all models considered for the methane + methanol binary pair of the ternary system, compared with the pure methane + methanol binary system measured at 303.16 K.

The system of methane + propane + TEG measured at 303.16 and 323.16 K also showed similar trends of increasing pressures with an increase in methane composition in the mixture. However, for this system, an inverse solubility phenomenon could be observed. Furthermore, slight differences in pressure values were observed for the two isotherms considered. The thermodynamic model which best represented the measured data was the PRWS model, with an AARD of ≤ 1.90 %. The average expanded uncertainty in methane composition over all points was $U(x_1) = 0.0021$. The binary interaction parameter between methane + TEG binary pair of this ternary system is very much comparable to the methane + TEG binary system interaction parameter at 323.15 K, on all the models considered.

For the ternary system of methane + methanol + TEG measured at 303.15 and 323.15 K, as the methane composition increased, total pressure values also increased, with some more pronounced difference in the pressure values for the two isotherms considered. Generally, at low pressures, the solubility of

methane in the mixture was independent of temperature, and as the pressure or methane composition in the mixture increased, the solubility of methane increased with an increase in temperature. The average expanded uncertainty in methane composition over all points was $U(x_1) = 0.0021$. All models yielded satisfactory fits to the measured data with a maximum AARD in pressure of $\leq 2.28\%$. The PRWS model best represented the data and had an AARD of $\leq 1.73\%$. The binary interaction parameters for the binary pairs of methane + TEG at 303.15 K and methane + TEG at 323.15 K, in the ternary mixture are significantly different to those in the respective binary systems for all the models considered.

New data for the carbon dioxide + methanol + TEG system measured at 303.15 and 323.15 K showed that the bubble points curve over the same carbon dioxide composition range, is concave for the data at 323.15 K and a straight line for the data at 303.15 K. At the same carbon dioxide composition, generally the total pressures are low for the data at 303.15 K as compared to the data at 323.15 K, and this difference is more pronounced with an increase in carbon dioxide composition. Methanol has an effect of decreasing the solubility of carbon dioxide in TEG, which could be a desirable feature in carbon dioxide dehydration processes since most of the carbon dioxide would not be trapped/dissolved in the TEG. There is considerable difference between the binary interaction parameters of carbon dioxide + methanol and carbon dioxide + TEG in the ternary system, compared to those from the binary systems for the PRWS, PC-SAFT and CPA models. The average expanded uncertainty in carbon dioxide composition was $U(x_1) = 0.0009$. This ternary system had the worst fits with the maximum AARD in pressure of 9.63 % from the PR model, indicating that simple EOS struggle to describe the data for highly non-ideal systems. The PRWS model yielded the best fit for the data measured with an AARD in pressure of $\leq 3.09\%$.

The methane + propane + methanol + TEG system measured at 283.15, 303.15 and 323.15 K, generally showed concave bubble point curves. The total pressures were low at higher temperatures compared to the lower temperatures at the same methane composition. This shows that the solubility of methane in the multicomponent mixture was higher at high temperatures. The difference in pressure values at the considered isotherms can be described as follows, P at 283.15 K $> P$ at 303.15 K $\gg P$ at 323.15 K. The average expanded uncertainty in methane composition was $U(x_1) = 0.0019$. There is a significant difference on the binary interaction parameter for the methane + methanol binary pair in the quaternary system, compared to those from the respective binary systems for the CPA, PC-SAFT and PRWS models. For the methane + TEG binary pair in the quaternary mixture, slight differences are observed in the binary interaction parameters for the PC-SAFT, PRWS and CPA models, compared to those from the respective binary systems. The PRWS model better represented the measured data, with an AARD in pressure of 4.45%.

For the quinary system of methane + propane + water + methanol + TEG, data measured at 283.15, 303.15 and 323.15 K, similar trends to those presented for the quaternary system above were observed.

The average expanded uncertainty in methane composition was $U(x_1) = 0.0015$. The value of the binary interaction parameter for the methane + TEG binary pair in the quinary system at 323.15 K of 0.8093 is significantly larger than 0.5363 for the methane + TEG binary system at 323.15 K for the PRWS model. The value of the interaction parameter between methane + methanol binary pair in the quinary system of 5.4622 at 303.16 K is significantly greater than the 0.3423 for the methane + methanol binary system at 303.15 K. Similar trends for the binary parameters were also observed for the CPA and PC SAFT models. The PRWS yielded better results at all isotherms with an AARD % of ≤ 1.49 .

New data for the senary system of methane + propane + carbon dioxide + water + methanol + TEG was measured at 283.15, 303.15 and 323.15 K. The average expanded uncertainty in methane composition over all data points was $U(x_1) = 0.0014$. Generally linear trends were observed on all isotherms for the bubble point pressures, which increased with an increase in methane composition. The differences in pressure values at the different isotherms was less pronounced as compared to that observed in the quaternary or quinary systems. The data were best represented by the PRWS model, with an AARD in pressure of ≤ 2.72 %. Significant differences were observed for the binary interaction parameters of methane + methanol, methane + TEG and carbon dioxide + TEG binary pairs in the senary system, compared to those of the respective binary systems measured in this work. This proves that measurement of the multicomponent phase equilibria data was necessary.

Overall, the phase equilibrium data generated for the multicomponent mixtures shows that the solubility of methane in TEG dominated systems increases with an increase in temperature (an inverse solubility phenomenon). The solubility of methane in methanol system and of carbon dioxide in TEG dominated system, decreases with increase in temperature (the conventional solubility phenomenon). For the very dilute region of methane in TEG dominated systems, the relative uncertainty in methane composition was greater than 10%, indicating that the technique adopted may not be appropriate for measurements in that region. The simple EOS with common mixing rules are not satisfactory for describing the phase behaviour of highly non-ideal systems such as the CH_4 + TEG system.

In the multicomponent mixtures, the interactions between methane, propane and carbon dioxide with the (TEG/WATER/methanol) shows high non-ideality due to unlike interactions between the polar and non-polar components. The interactions that takes place between the components are complex. Methane with C-H grouping, propane with C-H₂ grouping and carbon dioxide with C-O grouping are all non-polar components with Van der Waals intermolecular forces. Carbon dioxide has considerable quadrupole moments and can form some weak hydrogen bond with water. Water, methanol and TEG are polar molecules capable of hydrogen bonding either through self or cross association through their

O-H groupings. The non-polar components have the effect of causing the hydrophobic effect when introduced to an aqueous environment. Furthermore, methanol forms clusters in a carbon dioxide environment.

The measured data provides useful information that is required in the design of TEG dehydration and carbon dioxide dehydration units. For the design of TEG dehydration units, when the gas feed rate, gas composition at inlet and outlet of the contactor unit, the lean TEG composition, the TEG circulation rate and equilibrium data for the construction of equilibrium curve are known, then the number of trays or the height of packing can be established. Historically, the equilibrium ratio (K) values for (water/TEG 5/95 wt.%) solution have been used as the basis for the design of glycol dehydration units. Hence, the new chemical mixtures' phase equilibrium data measured in this work contribute to improving dehydration in gas processing technology since the data mimics “real life” processes. Although computational methods are useful, all predictive models presume a large number of accurate binary systems VLE database; however, such data are not enough since predictions must approximate reality.

New binary interaction parameters that have not been previously reported are presented for the following systems: TEG + methanol and TEG + water binary pairs using the PR EOS; methane + methanol, water + methanol, water + propane, carbon dioxide + TEG, methane + TEG, propane + TEG, methanol + TEG and water + TEG using the SRK EOS; carbon dioxide + water; methanol + TEG using the PC-SAFT equation and the methanol + TEG, methane + propane binary pairs, using the CPA model.

It can be concluded that the maximum AARD % in pressures over all systems measured in this work were 4.89, 19.7, 7.39, 9.63 and 8.67 for the PRWS, PC-SAFT, CPA, PR and SRK model correlations. This implies that generally the PRWS model best describes the phase equilibria data for the systems measured in this work over all the other models. This was because the PRWS had the most fitting parameters compared with other models since correlation accuracy usually improves with an increase in the number of adjustable parameters.

CHAPTER 8: RECOMMENDATIONS

This section is devoted to the recommendations that can be made from the current study.

In this work, phase equilibria measurements were performed on a temperature range of 283.15 K to 323.15 K. However, TEG dehydration unit operates effectively at a reboiler temperature of about (448.15 K) (Rasoolzadeh et al., 2020b). Therefore, it is recommended that more phase equilibria measurements for new chemical mixtures of this study be carried out to such high temperatures.

There is a lack of high-pressure phase equilibrium data for the water + TEG binary system, hence it is recommended that the high-pressure data for this system be measured.

The data for the methane + carbon dioxide + methanol is reported at 313.39 K only from one literature source; hence it is recommended that more phase equilibria measurements for this system be measured at other isotherms.

There is limited data for the propane + carbon dioxide + methanol system which has been reported by one literature source at pressures less than 3.5 MPa and temperatures higher than 298.15 K. It is therefore recommended that more measurements be conducted for this system over a wide temperature range, especially low temperature data at isotherms less than 273.15 K which might be of use in industrial processes such as the Rectisol process.

It is also recommended that phase equilibria data be measured for the following systems that have not been previously measured or with data not available in open literature. These were discussed in the literature review and repeated as part of the recommendations, and include:

Methanol + TEG binary system; methane + propane + water; methane + carbon dioxide + TEG; propane + carbon dioxide + TEG; propane + carbon dioxide + water; propane + water + TEG; and water + methanol + TEG ternary systems; methane + propane + carbon dioxide + TEG; methane + propane + carbon dioxide + methanol ; methane + propane + carbon dioxide + water; propane + carbon dioxide + water + TEG; propane + carbon dioxide + water + methanol ; carbon dioxide + water + methanol + TEG ; methane + propane + water + TEG; methane + carbon dioxide + methanol + TEG; methane + carbon dioxide + water + methanol ; methane + water + methanol + TEG ; propane + water + methanol + TEG ; propane + carbon dioxide + methanol + TEG quaternary systems and methane + propane + carbon dioxide + water + methanol; methane + propane + carbon dioxide + water + TEG; methane + propane + carbon dioxide + methanol + TEG; methane + propane + water + methanol + TEG; methane

+ carbon dioxide + water + methanol + TEG; propane + carbon dioxide + water + methanol + TEG quinary systems.

From the data measured, it was observed that for the very dilute methane composition in all the methane + TEG containing systems, the relative uncertainty in methane composition was rather high, i.e., greater than 10% (e.g., 47.41% for methane + TEG system and 23.89% for methane + (methanol /TEG 3.33/96.67 wt.%) system. The high relative uncertainty at dilute methane composition in the mixtures are due to the mass balance uncertainty of 0.01 g considering the very small mass of methane loaded (0.04 g for $x_1 = 0.0113$ for the ternary mixture). For carbon dioxide + TEG containing systems measured in this work, the relative uncertainty in carbon dioxide composition was all less than 10%. Therefore, it is recommended that measurements be conducted at dilute composition for methane + TEG-containing systems using different techniques such as analytic methods or others that do not rely on weighing the loaded methane for composition determination. Examples of such techniques include initially loading a known amount of the liquid component into the equilibrium cell (via either gravimetric or volumetric methods), followed by volumetric loading of gaseous components at a fixed temperature and pressure (Rasoolzadeh et al., 2020a; Wise and Chapoy, 2016) and the use of IR spectroscopy (Sabirzyanov et al., 2001).

For the PRWS modelling, a more in-depth analysis of the significance of the model parameters can be conducted in future work. This will entail reducing the fitting parameters by considering all permutations, until all selected parameters are proved significant by the measure of the standard deviation. Additionally, simultaneous regression of all isotherms can also be conducted in future work, again considering all permutations of parameter combinations and selecting the combination of significant parameters.

Natural gases usually contain hydrogen sulphide as one of the key impurities that is of concern and should be kept at minimum levels, hence it is recommended that phase equilibria data be measured for the chemical mixture combinations of this study + hydrogen sulphide. The measurements may as well include useful gas treating chemical solvents such as MDEA. Such data are helpful in improving gas processing technologies.

The sapphire cylinder that makes up the equilibrium cell used in this study is brittle and expensive, hence extreme caution and training needs to be done before one uses them. If some dents develop or chips wear off the edges of the sapphire, this may compromise the strength of the cell. To preserve the cell in that case, it is recommended to use some little thread tape on the outer edges of the cell and not to pressure the cell to extremely high pressures.

REFERENCES

- Acosta, J.C., Hevia, E., Leipziger, S., 1984. Dew and bubble point measurements for carbon dioxide-propane mixtures. *Journal of Chemical & Engineering Data* 29, 304–309. <https://doi.org/10.1021/je00037a024>
- Afzal, W., Breil, M.P., Tsivintzelis, I., Mohammadi, A.H., Kontogeorgis, G.M., Richon, D., 2012. Experimental study and phase equilibrium modeling of systems containing acid gas and glycol. *Fluid Phase Equilibria* 318, 40–50. <https://doi.org/10.1016/j.fluid.2011.12.025>
- Ahmed, T., 2010. Working Guide to Vapor-Liquid Phase Equilibria Calculations. Gulf Professional Publishing, Burlington, MA 01803, USA.
- Aim, K., 1978. Measurement of vapor-liquid equilibrium in systems with components of very different volatility by the total pressure static method. *Fluid Phase Equilibria* 2, 119–142. [https://doi.org/10.1016/0378-3812\(78\)85004-3](https://doi.org/10.1016/0378-3812(78)85004-3)
- Akers, W.W., Burns, J.F., Fairchild, W.R., 1954. Low-Temperature Phase Equilibria: Methane-Propane System. *Industrial & Engineering Chemistry* 46, 2531–2534. <https://doi.org/10.1021/ie50540a038>
- al Ghafri, S.Z.S., Forte, E., Maitland, G.C., Rodriguez-Henríquez, J.J., Trusler, J.P.M., 2014. Experimental and Modeling Study of the Phase Behavior of (Methane + CO₂ + Water) Mixtures. *The Journal of Physical Chemistry B* 118, 14461–14478. <https://doi.org/10.1021/jp509678g>
- Aniya, V., Singh, A., De, D., Reddy, R., Satyavathi, B., 2015. Experimental isobaric vapor–liquid equilibrium at sub-atmospheric and local atmospheric pressures, volumetric properties and molar refractivity from 293.15 to 313.15K of water+triethylene glycol. *Fluid Phase Equilibria* 405, 132–140. <https://doi.org/10.1016/j.fluid.2015.07.030>
- Arai, Y., Kaminishi, G.-I., Saito, S., 1971. The Experimental Determination of the P-V-T-X Relations for the Carbon Dioxide-Nitrogen and the Carbon Dioxide-Methane Systems. *Journal of Chemical Engineering of Japan* 4, 113–122. <https://doi.org/10.1252/jcej.4.113>
- Arya, A., Maribo-Mogensen, B., Tsivintzelis, I., Kontogeorgis, G.M., 2014. Process Design of Industrial Triethylene Glycol Processes Using the Cubic-Plus-Association (CPA) Equation of State. *Industrial & Engineering Chemistry Research* 53, 11766–11778. <https://doi.org/10.1021/ie501251d>
- Austegard, A., Solbraa, E., de Koeijer, G., Mølnvik, M.J., 2006. Thermodynamic Models for Calculating Mutual Solubilities in H₂O–CO₂–CH₄ Mixtures. *Chemical Engineering Research and Design* 84, 781–794. <https://doi.org/10.1205/cherd05023>
- Avlonitis, D.A., 1992. Thermodynamics of gas hydrate equilibria (Doctoral Thesis). Heriot-Watt University, Edinburgh.
- Bamberger, A., Sieder, G., Maurer, G., 2000. High-pressure (vapor+liquid) equilibrium in binary mixtures of (carbon dioxide+water or acetic acid) at temperatures from 313 to 353 K. *The Journal of Supercritical Fluids* 17, 97–110. [https://doi.org/10.1016/S0896-8446\(99\)00054-6](https://doi.org/10.1016/S0896-8446(99)00054-6)
- Bao, Z., Liu, M., Yang, J., 1995. Measurement and Correlation of Moderate Pressure Vapor-Liquid Equilibrium Data for Mehtanol-Water Binary System. *Journal of Chemical Industry and Engineering-China* 46, 230–233.
- Bell, S., 1999. A Beginner's Guide to Uncertainty of Measurement, 2nd ed. National Physical Laboratory, Teddington, Middlesex, United Kingdom.

- Bengesai, P., 2016. High Pressure Vapour-Liquid Equilibrium Measurements for R116 and Ethane with Perfluorohexane and Perfluorooctane. MSc.Eng. Thesis. University of KwaZulu-Natal, Durban.
- Bernatová, S., Aim, K., Wichterle, I., 2006. Isothermal vapour-liquid equilibrium with chemical reaction in the quaternary water+methanol+acetic acid+methyl acetate system, and in five binary subsystems. *Fluid Phase Equilibria* 247, 96–101. <https://doi.org/10.1016/j.fluid.2006.06.005>
- Best, J.W., 1981. Rigorous Computer Simulation of CO₂ Dehydration Facilities, in: SPE Annual Technical Conference and Exhibition. SPE, San Antonio, Texas. <https://doi.org/10.2118/10284-MS>
- Bian, B., Wang, Y., Shi, J., Zhao, E., Lu, B.C.-Y., 1993. Simultaneous determination of vapor-liquid equilibrium and molar volumes for coexisting phases up to the critical temperature with a static method. *Fluid Phase Equilibria* 90, 177–187. [https://doi.org/10.1016/0378-3812\(93\)85012-B](https://doi.org/10.1016/0378-3812(93)85012-B)
- Blanco, S.T., Velasco, I., Rauzy, E., Otin, S., 2000. Dew points of ternary methane+water+methanol. Measurement and correlation. *Canadian Journal of Chemistry* 78.
- Blanco, S., Velasco, I., Rauzy, E., Otin, S., 2001. Dew Points of Ternary Propane + Water + Methanol: Measurement and Correlation. *Journal of Chemical Engineering of Japan* 34, 971–978. <https://doi.org/10.1252/jcej.34.971>
- Böttger, A., Pérez-Salado Kamps, Á., Maurer, G., 2016. An experimental investigation of the phase equilibrium of the binary system (methane + water) at low temperatures: Solubility of methane in water and three-phase (vapour + liquid + hydrate) equilibrium. *Fluid Phase Equilibria* 407, 209–216. <https://doi.org/10.1016/j.fluid.2015.03.041>
- Breil, M.P., Kontogeorgis, G.M., 2009. Thermodynamics of Triethylene Glycol and Tetraethylene Glycol Containing Systems Described by the Cubic-Plus-Association Equation of State. *Industrial & Engineering Chemistry Research* 48, 5472–5480. <https://doi.org/10.1021/ie801412y>
- Brennan, J., 2017. Intermolecular Forces in the Structure of Propane [WWW Document]. <https://sciencing.com/intermolecular-forces-structure-propane-8236316.html>.
- Brewer, P.J., Brown, R.J.C., Miller, M.N., Miñarro, M.D., Murugan, A., Milton, M.J.T., Rhoderick, G.C., 2014. Preparation and Validation of Fully Synthetic Standard Gas Mixtures with Atmospheric Isotopic Composition for Global CO₂ and CH₄ Monitoring. *Analytical Chemistry* 86, 1887–1893. <https://doi.org/10.1021/ac403982m>
- Bried, E.A., Hennion, G.F., 1938. Some Reactions of Dialkylacetylenes ¹. *J Am Chem Soc* 60, 1717–1719. <https://doi.org/10.1021/ja01275a003>
- Brunner, E., Hültschmidt, W., Schlichthärle, G., 1987. Fluid mixtures at high pressures IV. Isothermal phase equilibria in binary mixtures consisting of (methanol + hydrogen or nitrogen or methane or carbon monoxide or carbon dioxide). *The Journal of Chemical Thermodynamics* 19, 273–291. [https://doi.org/10.1016/0021-9614\(87\)90135-2](https://doi.org/10.1016/0021-9614(87)90135-2)
- Budiman, H., Mulyana, M.R., Zuas, O., 2018. Preparation of calibration standard gas mixtures by primary gravimetric method: a case study on 960 µmol/mol of carbon dioxide in a nitrogen matrix. *Engineering and Applied Science Research* 45, 173–179.
- Burr, B., Lyddon, L., 2008. A Comparison of Physical Solvents for Acid Gas Removal. Bryan Research & Engineering. Inc, Bryan, Texas, USA 137–138.
- Carlson, E.C., 1996. Succeeding At Simulation. Don't Gamble With Physical Properties For Simulations. *Chemical Engineering progress* 35–46.

- Carvalho, P.J., Fonseca, C.H.G., Moita, M.-L.C.J., Santos, Â.F.S., Coutinho, J.A.P., 2015. Thermophysical Properties of Glycols and Glymes. *Journal of Chemical & Engineering Data* 60, 3721–3737. <https://doi.org/10.1021/acs.jced.5b00662>
- Chang, T., Rousseau, R.W., 1985. Solubilities of carbon dioxide in methanol and methanol-water at high pressures: experimental data and modeling. *Fluid Phase Equilibria* 23, 243–258. [https://doi.org/10.1016/0378-3812\(85\)90009-3](https://doi.org/10.1016/0378-3812(85)90009-3)
- Chang, T., Rousseau, R.W., Ferrell, J.K., 1983. Use of the Soave modification of the Redlich-Kwong equation of state for phase equilibrium calculations. Systems containing methanol. *Industrial & Engineering Chemistry Process Design and Development* 22, 462–468. <https://doi.org/10.1021/i200022a021>
- Chapoy, A., 2004. Phase behaviour in water/hydrocarbon mixtures involved in gas production systems, Ph.D. Thesis. École Nationale Supérieure des Mines de Paris)
- Chapoy, A., Mokraoui, S., Valtz, A., Richon, D., Mohammadi, A.H., Tohidi, B., 2004. Solubility measurement and modeling for the system propane–water from 277.62 to 368.16K. *Fluid Phase Equilibria* 226, 213–220. <https://doi.org/10.1016/j.fluid.2004.08.040>
- Chen, D., Chen, W., 1992. Phase equilibria for n-hexane and n-octane in supercritical carbon dioxide. *Huaxue Gongcheng* 1, 66–69.
- Chen, S.J., Randelman, R.E., Seldomridge, R.L., Radosz, M., 1993. Mass spectrometer composition probe for batch cell studies of supercritical fluid phase equilibria. *Journal of Chemical & Engineering Data* 38, 211–216. <https://doi.org/10.1021/je00010a006>
- Chouireb, N., Crespo, E.A., C. Pereira, L.M., Tafat-Igoudjilene, O., Vega, L.F., Coutinho, J.A.P., Carvalho, P.J., 2018. Measurement and Modeling of Isobaric Vapor–Liquid Equilibrium of Water + Glycols. *Journal of Chemical & Engineering Data* 63, 2394–2401. <https://doi.org/10.1021/acs.jced.7b00945>
- Christensen, D.L., 2009. Gas Dehydration. Thermodynamic Simulation of Water/Glycol Mixture. Masters degree Thesis. Aalborg University, Esbjerg Denmark.
- Chung, T.-W., Luo, C.-M., 1999. Vapor Pressures of the Aqueous Desiccants. *Journal of Chemical & Engineering Data* 44, 1024–1027. <https://doi.org/10.1021/je990109q>
- Dahm, K.D., Visco, D.P. (Jr), 2015. Fundamentals of Chemical Engineering Thermodynamics. Timothy Anderson, Cengage Learning, Stamford, USA.
- DDBST GmbH, 2019. Online DDB Search [WWW Document]. <http://dortmundatabank.com/ddb-search.html>.
- de Guido, G., Langè, S., Moioli, S., Pellegrini, L.A., 2014. Thermodynamic method for the prediction of solid CO₂ formation from multicomponent mixtures. *Process Safety and Environmental Protection* 92, 70–79. <https://doi.org/10.1016/j.psep.2013.08.001>
- de Loos, Th.W., Wijen, A.J.M., Diepen, G.A.M., 1980. Phase equilibria and critical phenomena in fluid (propane + water) at high pressures and temperatures. *The Journal of Chemical Thermodynamics* 12, 193–204. [https://doi.org/10.1016/0021-9614\(80\)90130-5](https://doi.org/10.1016/0021-9614(80)90130-5)
- Derawi, S.O., 2002. Modeling of Phase Equilibria Containing Associating Fluids, PhD Thesis. Technical University of Denmark, Lyngby, Denmark.

- Derawi, S.O., Kontogeorgis, G.M., Michelsen, M.L., Stenby, E.H., 2003. Extension of the Cubic-Plus-Association Equation of State to Glycol–Water Cross-Associating Systems. *Industrial & Engineering Chemistry Research* 42, 1470–1477. <https://doi.org/10.1021/ie0206103>
- Devi, S., 2022. CH₄ Intermolecular Forces, *Techie Scientist* [WWW Document]. <https://techiescientist.com/ch4-intermolecular-forces/>.
- Devlikamov, V., Semenova, L.V., Repin, N.N., 1982. Solubility of methane in liquid carbon dioxide. *Izv.Vyssch.Uchebn. Zaved.,Nefi Gaz* 8, 42–46.
- Dhima, A., de Hemptinne, J.-C., Jose, J., 1999. Solubility of Hydrocarbons and CO₂ Mixtures in Water under High Pressure. *Industrial & Engineering Chemistry Research* 38, 3144–3161. <https://doi.org/10.1021/ie980768g>
- Dohrn, R., Brunner, G., 1995. High-pressure fluid-phase equilibria: Experimental methods and systems investigated (1988–1993). *Fluid Phase Equilibria* 106, 213–282. [https://doi.org/10.1016/0378-3812\(95\)02703-H](https://doi.org/10.1016/0378-3812(95)02703-H)
- Dohrn, R., Peper, S., Fonseca, J.M.S., 2010. High-pressure fluid-phase equilibria: Experimental methods and systems investigated (2000–2004). *Fluid Phase Equilibria* 288, 1–54. <https://doi.org/10.1016/j.fluid.2009.08.008>
- Donnelly, H.G., Katz, D.L., 1954. Phase Equilibria in the Carbon Dioxide–Methane System. *Industrial & Engineering Chemistry* 46, 511–517. <https://doi.org/10.1021/ie50531a036>
- DOW chemical company, 2018. Triethylene Glycol-Dow Chemical [WWW Document]. Triethylene Glycol-Dow Chemical.
- Ebrahiminejadhasanabadi, M., 2019. Solubility Studies of Carbon Dioxide in Novel Hybrid Solvents Using a New Static Synthetic Apparatus: PhD Thesis. University of KwaZulu-Natal, Durban.
- Feroiu, V., Sima, S., Geana, D., 2013. High pressure phase equilibrium in carbon dioxide+ethanol system. *UPB Scientific Bulletin, Series B: Chemistry and Materials Science* 75, 53–63.
- Filho, V. de O.C., Chapoy, A., Burgass, R., 2021. Phase Behavior in Natural Gas + Glycol Systems, Part 1: Tri(ethylene glycol) (TEG) and Its Aqueous Solutions. *Journal of Chemical & Engineering Data* 66, 4075–4093. <https://doi.org/10.1021/acs.jced.1c00313>
- Folas, G.K., 2006. Modeling of Complex Mixtures Containing Hydrogen Bonding Molecules. Ph.D. Thesis. Technical University of Denmark (DTU), Kongens Lyngby.
- Folas, G.K., Gabrielsen, J., Michelsen, M.L., Stenby, E.H., Kontogeorgis, G.M., 2005. Application of the Cubic-Plus-Association (CPA) Equation of State to Cross-Associating Systems. *Industrial & Engineering Chemistry Research* 44, 3823–3833. <https://doi.org/10.1021/ie048832j>
- Folas, G.K., Kontogeorgis, G.M., Michelsen, M.L., Stenby, E.H., 2006. Vapor–liquid, liquid–liquid and vapor–liquid–liquid equilibrium of binary and multicomponent systems with MEG. *Fluid Phase Equilibria* 249, 67–74. <https://doi.org/10.1016/j.fluid.2006.08.021>
- Fonseca, J., 2010. Design, Development and Testing of New Experimental Equipment for the Measurement of Multiphase Equilibrium, Ph.D. Thesis. Technical University of Denmark, Lyngby.
- Fonseca, J.M.S., Dohrn, R., Peper, S., 2011. High-pressure fluid-phase equilibria: Experimental methods and systems investigated (2005–2008). *Fluid Phase Equilibria* 300, 1–69. <https://doi.org/10.1016/j.fluid.2010.09.017>

- Fonseca, J.M.S., von Solms, N., 2012. Development and testing of a new apparatus for the measurement of high-pressure low-temperature phase equilibria. *Fluid Phase Equilibria* 329, 55–62. <https://doi.org/10.1016/j.fluid.2012.05.024>
- Fouad, W.A., Berrouk, A.S., 2013. Phase behavior of sour natural gas systems using classical and statistical thermodynamic equations of states. *Fluid Phase Equilibria* 356, 136–145. <https://doi.org/10.1016/j.fluid.2013.07.029>
- Frost, M., Karakatsani, E., von Solms, N., Richon, D., Kontogeorgis, G.M., 2014. Vapor–Liquid Equilibrium of Methane with Water and Methanol. Measurements and Modeling. *Journal of Chemical & Engineering Data* 59, 961–967. <https://doi.org/10.1021/je400684k>
- Frost, M., von Solms, N., Richon, D., Kontogeorgis, G.M., 2015. Measurement of vapor-liquid-liquid phase equilibrium-Equipment and results. *Fluid Phase Equilibria* 405, 88–95. <https://doi.org/10.1016/j.fluid.2015.07.009>
- Galivel-Solastiouk, F., Laugier, S., Richon, D., 1986. Vapor-liquid equilibrium data for the propane-methanol and propane-methanol-carbon dioxide system. *Fluid Phase Equilibria* 28, 73–85. [https://doi.org/10.1016/0378-3812\(86\)85069-5](https://doi.org/10.1016/0378-3812(86)85069-5)
- Gao, J., Zheng, D.-Q., Guo, T.-M., 1997. Solubilities of Methane, Nitrogen, Carbon Dioxide, and a Natural Gas Mixture in Aqueous Sodium Bicarbonate Solutions under High Pressure and Elevated Temperature. *Journal of Chemical & Engineering Data* 42, 69–73. <https://doi.org/10.1021/je960275n>
- Gherwi, W.A. al, Nhaesi, A.H., Asfour, A.-F.A., 2006. Densities and Kinematic Viscosities of Ten Binary Liquid Regular Solutions at 308.15 and 313.15 K. *Journal of Solution Chemistry* 35, 455–470. <https://doi.org/10.1007/s10953-005-9005-x>
- Gil, L., Blanco, S.T., Rivas, C., Laga, E., Fernández, J., Artal, M., Velasco, I., 2012. Experimental determination of the critical loci for {n-C₆H₁₄ or CO₂+alkan-1-ol} mixtures. Evaluation of their critical and subcritical behavior using PC-SAFT EoS. *The Journal of Supercritical Fluids* 71, 26–44. <https://doi.org/10.1016/j.supflu.2012.07.008>
- Gillespie, P.C., Wilson, G.M., 1982. GPA Research Report RR-48. (Gas Processors Association, Tulsa, Oklahoma).
- GPA, 2017. 2017 Cooperative Industry Research, GPA Midstream Association [WWW Document]. <https://gpamidstream.org/assets/gpa/pdf/2017-GPA-Midstream-Research-Brochure.pdf>.
- Grenner, A., Kontogeorgis, G.M., von Solms, N., Michelsen, M.L., 2007. Application of PC-SAFT to glycol containing systems – PC-SAFT towards a predictive approach. *Fluid Phase Equilibria* 261, 248–257. <https://doi.org/10.1016/j.fluid.2007.04.025>
- Gross, J., Sadowski, G., 2002. Application of the Perturbed-Chain SAFT Equation of State to Associating Systems. *Industrial & Engineering Chemistry Research* 41, 5510–5515. <https://doi.org/10.1021/ie010954d>
- Gross, J., Sadowski, G., 2001. Perturbed-Chain SAFT: An Equation of State Based on a Perturbation Theory for Chain Molecules. *Industrial & Engineering Chemistry Research* 40, 1244–1260. <https://doi.org/10.1021/ie0003887>
- Grybat, A., Horstmann, S., Ihmels, C., 2017. Distribution of Methanol in Amine Treating Systems, GPA Research Report RR 235. (Gas Processors Association, Tulsa, Oklahoma).

- Guerrero, H., García-Mardones, M., Pera, G., Bandrés, I., Lafuente, C., 2011. Experimental and Predicted Kinematic Viscosities for Alkane + Chloroalkane Mixtures. *Journal of Chemical & Engineering Data* 56, 3133–3141. <https://doi.org/10.1021/jc200213h>
- Hajiw, M., 2014. Hydrate Mitigation in Sour and Acid Gases, Doctoral Thesis. École Nationale Supérieure des Mines de Paris), Fontainebleau cedex, France.
- Han, X., Yu, Z., Qu, J., Qi, T., Guo, W., Zhang, G., 2011. Measurement and Correlation of Solubility Data for CO₂ in NaHCO₃ Aqueous Solution. *Journal of Chemical & Engineering Data* 56, 1213–1219. <https://doi.org/10.1021/jc1011168>
- Haynes, W.M., 2010. *CRC Handbook of Chemistry and Physics*. CRC Press Inc, Boca Raton, FL.
- Haynes, W.M., Lide, D.R., Bruno, T.J., 2014a. Index of Refraction of Gases, in: *CRC Handbook of Chemistry and Physics*. CRC Press, Boca Raton, pp. 10–248.
- Haynes, W.M., Lide, D.R., Bruno, T.J., 2014b. *CRC Handbook of Chemistry and Physics*, 95th ed. Taylor & Francis Group, Boca Raton, FL.
- Höhler, F., Deschermeier, R., Rehfeldt, S., Klein, H., 2018. Gas solubilities of carbon dioxide in methanol, acetone, mixtures of methanol and water, and mixtures of methanol and acetone. *Fluid Phase Equilibria* 459, 186–195. <https://doi.org/10.1016/j.fluid.2017.12.004>
- Holderbaum, T., Gmehling, J., 1991. PSRK: A Group Contribution Equation of State Based on UNIFAC. *Fluid Phase Equilibria* 70, 251–265. [https://doi.org/10.1016/0378-3812\(91\)85038-V](https://doi.org/10.1016/0378-3812(91)85038-V)
- Hong, J.H., Kobayashi, R., 1988. Vapor—liquid equilibrium studies for the carbon dioxide—methanol system. *Fluid Phase Equilibria* 41, 269–276. [https://doi.org/10.1016/0378-3812\(88\)80011-6](https://doi.org/10.1016/0378-3812(88)80011-6)
- Hong, J.H., Malone, P. v., Jett, M.D., Kobayashi, R., 1987. The measurement and interpretation of the fluid-phase equilibria of a normal fluid in a hydrogen bonding solvent: the methane—methanol system. *Fluid Phase Equilibria* 38, 83–96. [https://doi.org/10.1016/0378-3812\(87\)90005-7](https://doi.org/10.1016/0378-3812(87)90005-7)
- Hou, S.-X., Maitland, G.C., Trusler, J.P.M., 2013. Measurement and modeling of the phase behavior of the (carbon dioxide+water) mixture at temperatures from 298.15K to 448.15K. *The Journal of Supercritical Fluids* 73, 87–96. <https://doi.org/10.1016/j.supflu.2012.11.011>
- Huang, S.H., Radosz, M., 1990. Equation of state for small, large, polydisperse, and associating molecules. *Industrial & Engineering Chemistry Research* 29, 2284–2294. <https://doi.org/10.1021/ie00107a014>
- Im, U.K., Kurata, F., 1972. Solubility of carbon dioxide in mixed paraffinic hydrocarbon solvents at cryogenic temperatures. *Journal of Chemical & Engineering Data* 17, 68–71. <https://doi.org/10.1021/jc60052a027>
- Ishiguro, T., Matsumotu, K., 1947. Studies on the Polyethylene Glycols. XI.* Vapor Pressure and Water Activity of Triethylene Glycol-Water System. https://www.jstage.jst.go.jp/article/yakushi1947/75/11/75_11_1414/_pdf 75, 1414–1417.
- ISO, 2015. Gas analysis- Preparation of calibration gas mixtures. Part 1: Gravimetric method for class I mixtures. Geneva, Switzerland.
- ISO, 2001. Gas analysis- Preparation of calibration gas mixtures- gravimetric method. Geneva, Switzerland.

- Jarne, C., Blanco, S.T., Artal, M., Rauzy, E., Otin, S., Velasco, I., 2004. Dew points of binary carbon dioxide + water and ternary carbon dioxide + water + methanol mixtures Measurement and modelling. *Fluid Phase Equilibria* 216, 85–93. <https://doi.org/10.1016/j.fluid.2003.10.001>
- Jerinić, D., Schmidt, J., Fischer, K., Friedel, L., 2008. Measurement of the triethylene glycol solubility in supercritical methane at pressures up to 9 MPa. *Fluid Phase Equilibria* 264, 253–258. <https://doi.org/10.1016/j.fluid.2007.11.017>
- Jiang, Y., Taheri, M., Yu, G., Zhu, J., Lei, Z., 2019. Experiments, Modeling, and Simulation of CO₂ Dehydration by Ionic Liquid, Triethylene Glycol, and Their Binary Mixtures. *Industrial & Engineering Chemistry Research* 58, 15588–15597. <https://doi.org/10.1021/acs.iecr.9b02540>
- Jiménez-Gallegos, R., Galicia-Luna, L.A., Elizalde-Solis, O., 2006. Experimental Vapor–Liquid Equilibria for the Carbon Dioxide + Octane and Carbon Dioxide + Decane Systems. *Journal of Chemical & Engineering Data* 51, 1624–1628. <https://doi.org/10.1021/jc060111z>
- Jou, F.-Y., Deshmukh, R.D., Otto, F.D., Mather, A.E., 1987. Vapor liquid equilibria for acid gases and lower alkanes in triethylene glycol. *Fluid Phase Equilibria* 36, 121–140. [https://doi.org/10.1016/0378-3812\(87\)85018-5](https://doi.org/10.1016/0378-3812(87)85018-5)
- Joung, S.N., Shin, H.Y., Kim, H.S., Yoo, K.-P., 2004. High-Pressure Vapor–Liquid Equilibrium Data and Modeling of Propane + Methanol and Propane + Ethanol Systems. *Journal of Chemical & Engineering Data* 49, 426–429. <https://doi.org/10.1021/jc0340506>
- Justo-García, D.N., García-Sánchez, F., Díaz-Ramírez, N.L., Romero-Martínez, A., 2008. Calculation of critical points for multicomponent mixtures containing hydrocarbon and nonhydrocarbon components with the PC-SAFT equation of state. *Fluid Phase Equilibria* 265, 192–204. <https://doi.org/10.1016/j.fluid.2007.12.006>
- Kaminishi, G.-I., Arai, Y., Saito, S., Maeda, S., 1968. Vapor-Liquid Equilibria for Binary and Ternary Systems Containing Carbon Dioxide. *Journal of Chemical Engineering of Japan* 1, 109–116. <https://doi.org/10.1252/jcej.1.109>
- Kaminishi, G.-I., Takano, S., Yokoyama, C., Takahashi, S., Takeuchi, K., 1989. Concentration of triethylene glycol, diethylene glycol and ethylene glycol in supercritical carbon dioxide up to 16 MPa at 313. 15 and 333. 15K. *Fluid Phase Equilibria* 52, 365–372. [https://doi.org/10.1016/0378-3812\(89\)80342-5](https://doi.org/10.1016/0378-3812(89)80342-5)
- Kapateh, M.H., Chapoy, A., Burgass, R., Tohidi, B., 2016. Experimental Measurement and Modeling of the Solubility of Methane in Methanol and Ethanol. *Journal of Chemical & Engineering Data* 61, 666–673. <https://doi.org/10.1021/acs.jced.5b00793>
- Kastanidis, P., Romanos, G.E., Stubos, A.K., Economou, I.G., Tsimpanogiannis, I.N., 2017. Two- and three-phase equilibrium experimental measurements for the ternary CH₄ + CO₂ + H₂O mixture. *Fluid Phase Equilibria* 451, 96–105. <https://doi.org/10.1016/j.fluid.2017.08.002>
- Kiepe, J., Horstmann, S., Fischer, K., Gmehling, J., 2003. Experimental Determination and Prediction of Gas Solubility Data for Methane + Water Solutions Containing Different Monovalent Electrolytes. *Industrial & Engineering Chemistry Research* 42, 5392–5398. <https://doi.org/10.1021/ie030386x>
- Kim, J.H., Kim, M.S., 2005. Vapor–liquid equilibria for the carbon dioxide+propane system over a temperature range from 253.15 to 323.15K. *Fluid Phase Equilibria* 238, 13–19. <https://doi.org/10.1016/j.fluid.2005.09.006>

- Kobayashi, R., Katz, D., 1953. Vapor-Liquid Equilibria For Binary Hydrocarbon-Water Systems. *Industrial & Engineering Chemistry* 45, 440–446. <https://doi.org/10.1021/ie50518a051>
- Kohl, A.L., Nielsen, R.B., 1997. *Gas Purification*, 5th ed. Gulf Publishing Company, Houston, Texas.
- Kontogeorgis, G.M., Folas, G.K., 2010. *Thermodynamic Models for Industrial Applications, From Classical and Advanced Mixing Rules to Association Theories*. John Wiley & Sons Ltd, Sussex, United Kingdom.
- Kontogeorgis, G.M., Michelsen, M.L., Folas, G.K., Derawi, S., von Solms, N., Stenby, E.H., 2006. Ten Years with the CPA (Cubic-Plus-Association) Equation of State. Part 1. Pure Compounds and Self-Associating Systems. *Industrial & Engineering Chemistry Research* 45, 4855–4868. <https://doi.org/10.1021/ie051305v>
- Kontogeorgis, G.M., Tsivintzelis, I., Michelsen, M.L., Stenby, E.H., 2011. Towards predictive association theories. *Fluid Phase Equilibria* 301, 244–256. <https://doi.org/10.1016/j.fluid.2010.11.025>
- Kontogeorgis, G.M., Voutsas, E.C., Yakoumis, I. v., Tassios, D.P., 1996. An Equation of State for Associating Fluids. *Industrial & Engineering Chemistry Research* 35, 4310–4318. <https://doi.org/10.1021/ie9600203>
- Kretschmer, C.B., Wiebe, R., 1952. Solubility of Gaseous Paraffins in Methanol and Isopropyl Alcohol. *J Am Chem Soc* 74, 1276–1277. <https://doi.org/10.1021/ja01125a040>
- Kruger, F.J., Danielsen, M. v., Kontogeorgis, G.M., Solbraa, E., von Solms, N., 2018. Ternary Vapor–Liquid Equilibrium Measurements and Modeling of Ethylene Glycol (1) + Water (2) + Methane (3) Systems at 6 and 12.5 MPa. *Journal of Chemical & Engineering Data* 63, 1789–1796. <https://doi.org/10.1021/acs.jced.8b00115>
- Kurata, F., 1974. Solubility of Solid Carbon Dioxide in Pure Light Hydrocarbons and Mixtures of Light Hydrocarbons (GPA Research Report RR-10). Gas Processors Association, Tulsa, Oklahoma.
- Kurata, Fred., Im, K.Un., 1971. Phase equilibrium of carbon dioxide and light paraffins in presence of solid carbon dioxide. *Journal of Chemical & Engineering Data* 16, 295–299. <https://doi.org/10.1021/je60050a018>
- Kurihara, K., Minoura, T., Takeda, K., Kojima, K., 1995. Isothermal Vapor-Liquid Equilibria for Methanol + Ethanol + Water, Methanol + Water, and Ethanol + Water. *Journal of Chemical & Engineering Data* 40, 679–684. <https://doi.org/10.1021/je00019a033>
- Laugier, S., Richon, D., 1986. New apparatus to perform fast determinations of mixture vapor–liquid equilibria up to 10 MPa and 423 K. *Review of Scientific Instruments* 57, 469–472. <https://doi.org/10.1063/1.1138909>
- Lazalde-Crabtree, H., Breedveld, G.J.F., Prausnitz, J.M., 1980. Solvent losses in gas absorption. Solubility of methanol in compressed natural and synthetic gases. *AIChE Journal* 26, 462–470. <https://doi.org/10.1002/aic.690260318>
- Lee, J.M., Lee, B.-C., Cho, C.-H., 2000. Measurement of bubble point pressures and critical points of carbon dioxide and chlorodifluoromethane mixtures using the variable-volume view cell apparatus. *Korean Journal of Chemical Engineering* 17, 510–515. <https://doi.org/10.1007/BF02707158>

- Lee, K.-R., Tan, C.-S., 1998. Vapor–liquid equilibria for the systems propane+m-cresol, propane+p-cresol, and propane+m-cresol+p-cresol at high pressures. *Fluid Phase Equilibria* 143, 125–141. [https://doi.org/10.1016/S0378-3812\(97\)00314-2](https://doi.org/10.1016/S0378-3812(97)00314-2)
- Legoix, L., Ruffine, L., Donval, J.-P., Haeckel, M., 2017. Phase Equilibria of the CH₄-CO₂ Binary and the CH₄-CO₂-H₂O Ternary Mixtures in the Presence of a CO₂-Rich Liquid Phase. *Energies (Basel)* 10, 2034. <https://doi.org/10.3390/en10122034>
- Lemmon, E.W., Bell, I.H., Huber, M.L., McLinden, M.O., 2021. Thermophysical Properties of Fluid Systems in NIST Chemistry WebBook, NIST Standard Reference Database Number 69 [WWW Document]. <https://webbook.nist.gov/chemistry/fluid/>.
- Leu, A.-D., Chung, S.Y.-K., Robinson, D.B., 1991. The equilibrium phase properties of (carbon dioxide + methanol). *The Journal of Chemical Thermodynamics* 23, 979–985. [https://doi.org/10.1016/S0021-9614\(05\)80178-8](https://doi.org/10.1016/S0021-9614(05)80178-8)
- Leu, A.-D., Robinson, D.B., Chung, S.Y.-K., Chen, C.-J., 1992. The equilibrium phase properties of the propane-methanol and n-Butane-methanol binary systems. *The Canadian Journal of Chemical Engineering* 70, 330–334. <https://doi.org/10.1002/cjce.5450700217>
- Li, J., Zhang, Z., Luo, X., Li, X., 2015. Modelling of phase equilibria in CH₄-C₂H₆-C₃H₈-nC₄H₁₀-NaCl-H₂O systems. *Applied Geochemistry* 56, 23–36. <https://doi.org/10.1016/j.apgeochem.2015.02.006>
- Li, Y.-H., Dillard, K.H., Robinson, R.L., 1981. Vapor-liquid phase equilibrium for carbon dioxide-n-hexane at 40, 80, and 120 .degree.C. *Journal of Chemical & Engineering Data* 26, 53–55. <https://doi.org/10.1021/je00023a018>
- Lopez-Castillo, Z.K., Aki, S.N.V.K., Stadtherr, M.A., Brennecke, J.F., 2006. Enhanced Solubility of Oxygen and Carbon Monoxide in CO₂ -Expanded Liquids. *Industrial & Engineering Chemistry Research* 45, 5351–5360. <https://doi.org/10.1021/ie0601091>
- Louder, E.A., Briggs, T.R., Browne, A.W., 1924. Vapor Pressure Curves for Systems Containing Alcohol, Ether, and Water. *Industrial & Engineering Chemistry* 16, 932–935. <https://doi.org/10.1021/ie50177a024>
- Lucile, F., Cézac, P., Contamine, F., Serin, J.-P., Houssin, D., Arpentinier, P., 2012. Solubility of Carbon Dioxide in Water and Aqueous Solution Containing Sodium Hydroxide at Temperatures from (293.15 to 393.15) K and Pressure up to 5 MPa: Experimental Measurements. *Journal of Chemical & Engineering Data* 57, 784–789. <https://doi.org/10.1021/je200991x>
- Manning, F.S., Thompson, R.E., 1991. *Oilfield Processing of Petroleum Volume 1: Natural gas*. PennWell Publishing Company, Tulsa, Oklahoma.
- Mascato, E., Mosteiro, L., Piñeiro, M.M., García, J., Iglesias, T.P., Legido, J.L., 2000. Thermodynamic Properties on Mixing for Hexane + Cyclohexane + 1-Octanol at 298.15 K. *Journal of Chemical & Engineering Data* 45, 1154–1159. <https://doi.org/10.1021/je000155m>
- Mathias, P.M., Copeman, T.W., 1983. Extension of the Peng-Robinson equation of state to complex mixtures: Evaluation of the various forms of the local composition concept. *Fluid Phase Equilibria* 13, 91–108. [https://doi.org/10.1016/0378-3812\(83\)80084-3](https://doi.org/10.1016/0378-3812(83)80084-3)
- May, E.F., Guo, J.Y., Oakley, J.H., Hughes, T.J., Graham, B.F., Marsh, K.N., Huang, S.H., 2015. Reference Quality Vapor–Liquid Equilibrium Data for the Binary Systems Methane + Ethane, + Propane, + Butane, and + 2-Methylpropane, at Temperatures from (203 to 273) K and Pressures

- to 9 MPa. *Journal of Chemical & Engineering Data* 60, 3606–3620. <https://doi.org/10.1021/acs.jced.5b00610>
- McLinden, M.O., Richter, M., 2016. Application of a two-sinker densimeter for phase-equilibrium measurements: A new technique for the detection of dew points and measurements on the (methane + propane) system. *The Journal of Chemical Thermodynamics* 99, 105–115. <https://doi.org/10.1016/j.jct.2016.03.035>
- Mentzer, A.P., 2018. Sciencing, Chemical Formula for Propane [WWW Document]. <https://sciencing.com/chemical-formula-propane-5306559.html>.
- Meyer, C.W., Harvey, A.H., 2015. Dew-point measurements for water in compressed carbon dioxide. *AIChE Journal* 61, 2913–2925. <https://doi.org/10.1002/aic.14818>
- MINESParisTech, 2000. Sampler Injector (ROLSI TM), Centre of Thermodynamics of Processes [WWW Document]. <https://www.ctp.minesparis.psl.eu/Research/Resources/ROLSI-TM/>.
- Mizushima, Y., Nagayama, S., 1957. Interaction of water and urea nitrate. *J. Ind. Explosives Society* 18, 244–248.
- Mohammadian, E., Hamidi, H., Asadullah, M., Azdarpour, A., Motamedi, S., Junin, R., 2015. Measurement of CO₂ Solubility in NaCl Brine Solutions at Different Temperatures and Pressures Using the Potentiometric Titration Method. *Journal of Chemical & Engineering Data* 60, 2042–2049. <https://doi.org/10.1021/je501172d>
- Mokbel, I., Kasehgari, H., Rauzy, E., Jose, J., 1995. Static measurements of the total vapor pressure of water + methanol mixtures at temperatures between 243 and 313 K. *ELDATA: The International Electronic Journal of Physico-Chemical Data* 1, 135–138.
- Mokhatab, S., Poe, W.A., Mak, J.Y., 2019. *Handbook of Natural Gas Transmission and Processing, Principles and Practices*, 4th ed. Gulf Professional Publishing, Joe Hayton, Cambridge, MA 02139, United States.
- Mokhatab, S., Poe, W. A., Speight, J.G., 2006. *Handbook of Natural Gas Transmission and Processing*. Gulf Professional Publishing, Oxford, UK.
- Moosavi, M., Daneshvar, A., Sedghamiz, E., 2015. Rheological properties of {[bmim]PF₆+methanol} mixtures at different temperatures, shear rates and compositions. *Journal of Molecular Liquids* 209, 693–705. <https://doi.org/10.1016/j.molliq.2015.05.029>
- Moosavi, M., Rostami, A.A., 2017. Densities, Viscosities, Refractive Indices, and Excess Properties of Aqueous 1,2-Etanediol, 1,3-Propanediol, 1,4-Butanediol, and 1,5-Pentanediol Binary Mixtures. *Journal of Chemical & Engineering Data* 62, 156–168. <https://doi.org/10.1021/acs.jced.6b00526>
- Mostafazadeh, A.K., Rahimpour, M.R., Shariati, A., 2009. Vapor–Liquid Equilibria of Water + Triethylene Glycol (TEG) and Water + TEG + Toluene at 85 kPa. *Journal of Chemical & Engineering Data* 54, 876–881. <https://doi.org/10.1021/jc800675u>
- Muromachi, S., Shijima, A., Miyamoto, H., Ohmura, R., 2015. Experimental measurements of carbon dioxide solubility in aqueous tetra-*n*-butylammonium bromide solutions. *The Journal of Chemical Thermodynamics* 85, 94–100. <https://doi.org/10.1016/j.jct.2015.01.008>
- Naidoo, P., Ramjugernath, D., Raal, J.D., 2008. A new high-pressure vapour–liquid equilibrium apparatus. *Fluid Phase Equilibria* 269, 104–112. <https://doi.org/10.1016/j.fluid.2008.05.002>
- Najdanovic-Visak, V., Esperança, J.M.S.S., Rebelo, L.P.N., Nunes da Ponte, M., Guedes, H.J.R., Seddon, K.R., Szydłowski, J., 2002. Phase behaviour of room temperature ionic liquid solutions:

- an unusually large co-solvent effect in (water + ethanol). *Physical Chemistry Chemical Physics* 4, 1701–1703. <https://doi.org/10.1039/b201723g>
- Nasr, G.G., Connor, N.E., 2014. *Natural Gas Engineering and Safety Challenges*. Springer International Publishing, Cham. <https://doi.org/10.1007/978-3-319-08948-5>
- National Center for Biotechnology Information, 2021a. PubChem Compound Summary for CID 8058, Hexane [WWW Document]. <https://pubchem.ncbi.nlm.nih.gov/compound/Hexane>.
- National Center for Biotechnology Information, 2021b. PubChem Compound Summary for CID 15600, Decane [WWW Document]. <https://pubchem.ncbi.nlm.nih.gov/compound/Decane>.
- National Center for Biotechnology Information, 2018a. PubChem Compound Summary for CID 887, Methanol [WWW Document]. <https://pubchem.ncbi.nlm.nih.gov/compound/887>.
- National Center for Biotechnology Information, 2018b. PubChem Compound Summary for CID 962, Water [WWW Document]. <https://pubchem.ncbi.nlm.nih.gov/compound/962>.
- National Center for Biotechnology Information, 2018c. PubChem Compound Summary for CID 280, Carbon dioxide [WWW Document]. <https://pubchem.ncbi.nlm.nih.gov/compound/280>.
- National Center for Biotechnology Information, 2018d. PubChem Compound Summary for CID 297, Methane [WWW Document]. <https://pubchem.ncbi.nlm.nih.gov/compound/297>.
- National Center for Biotechnology Information, 2018e. PubChem Compound Summary for CID 6334, Propane [WWW Document]. <https://pubchem.ncbi.nlm.nih.gov/compound/6334>.
- Nelson, W., 2008. The Separation of Hexafluoropropylene and Hexafluoropropylene Oxide Using R-123 and Carbon Dioxide: MSc.Eng. dissertation. University of KwaZulu-Natal, Durban.
- Nelson, W.M., 2012. Separation of Trichlorosilane: Measurement, Modelling And Simulation, Ph.D. Thesis. University of KwaZulu-Natal, Durban.
- Nelson, W.M., Naidoo, P., Ramjugernath, D., 2021. A new high pressure phase equilibrium cell featuring the static-combined method: Equipment commissioning and data measurement. *Journal of Supercritical Fluids* 176. <https://doi.org/10.1016/j.supflu.2021.105291>
- Ngema, P.T., Nelson, W.M., Naidoo, P., Ramjugernath, D., Richon, D., 2014. Isothermal method for hydrate studies using a transparent variable volume cell. *Review of Scientific Instruments* 85, 045123. <https://doi.org/10.1063/1.4871587>
- Ng, H.J., Robinson, D.B., 1983. Equilibrium Phase Composition and Hydrating Conditions in Systems Containing Methanol, Light Hydrocarbons, Carbon Dioxide, and Hydrogen Sulfide (Research Report No. 66). Gas Processors Association.
- Niesen, V.G., Rainwater, J.C., 1990. Critical locus, (vapor + liquid) equilibria, and coexisting densities of (carbon dioxide + propane) at temperatures from 311 K to 361 K. *The Journal of Chemical Thermodynamics* 22, 777–795. [https://doi.org/10.1016/0021-9614\(90\)90070-7](https://doi.org/10.1016/0021-9614(90)90070-7)
- Nourozieh, H., Kariznovi, M., Abedi, J., 2013. Measurement and correlation of saturated liquid properties and gas solubility for decane, tetradecane and their binary mixtures saturated with carbon dioxide. *Fluid Phase Equilibria* 337, 246–254. <https://doi.org/10.1016/j.fluid.2012.09.037>
- Nuñez-Rodriguez, N., 2020. CHE 120 - Introduction to Organic Chemistry - Textbook [WWW Document]. <https://guides.hostos.cuny.edu/che120>.

- O'Brien, D., Mejjorada, J., Addington, L., 2016. Adjusting Gas Treatment Strategies to Resolve Methanol Issues, in: The 66th Laurance Reid Gas Conditioning Conference. Norman, Oklahoma USA.
- Ohgaki, K., Katayama, T., 1976. Isothermal vapor-liquid equilibrium data for binary systems containing carbon dioxide at high pressures: methanol-carbon dioxide, n-hexane-carbon dioxide, and benzene-carbon dioxide systems. *Journal of Chemical & Engineering Data* 21, 53–55. <https://doi.org/10.1021/je60068a015>
- Olson, J.D., 1989. Measurement of vapor-liquid equilibria by ebulliometry. *Fluid Phase Equilibria* 52, 209–218. [https://doi.org/10.1016/0378-3812\(89\)80327-9](https://doi.org/10.1016/0378-3812(89)80327-9)
- Orbey, H., Sandler, S.I., 1998. Modeling Vapor-Liquid Equilibria , Cubic Equations of State and Their Mixing Rules. Cambridge University Press, Cambridge, United Kingdom.
- Ozigagu, C.E., Duben, A.J., 2019. Sensitivity Analysis of Computations of the Vapor-Liquid Equilibria of Methane + Methanol or Glycols at Gas Hydrate Formation Conditions. *Modeling and Numerical Simulation of Material Science* 09, 1–15. <https://doi.org/10.4236/mnsms.2019.91001>
- Patil, N., 2018. Decane, Search Alchetron [WWW Document]. <https://alchetron.com/Decane#decane-fbaff542-0b5a-4d28-83bd-00e58cb7736-resize-750.png>.
- Peng, D.-Y., Robinson, D.B., 1976. A New Two-Constant Equation of State. *Industrial & Engineering Chemistry Fundamentals* 15, 59–64. <https://doi.org/10.1021/i160057a011>
- Peper, S., Dohrn, R., 2012. Sampling from fluid mixtures under high pressure: Review, case study and evaluation. *The Journal of Supercritical Fluids* 66, 2–15. <https://doi.org/10.1016/j.supflu.2011.09.021>
- Peper, S., Fonseca, J.M.S., Dohrn, R., 2019. High-pressure fluid-phase equilibria: Trends, recent developments, and systems investigated (2009–2012). *Fluid Phase Equilibria* 484, 126–224. <https://doi.org/10.1016/j.fluid.2018.10.007>
- Perez, A.G., Coquelet, C., Paricaud, P., Chapoy, A., 2017. Comparative study of vapour-liquid equilibrium and density modelling of mixtures related to carbon capture and storage with the SRK, PR, PC-SAFT and SAFT-VR Mie equations of state for industrial uses. *Fluid Phase Equilibria* 440, 19–35. <https://doi.org/10.1016/j.fluid.2017.02.018>
- Piemonte, V., Maschietti, M., Gironi, F., 2012. A Triethylene Glycol–Water System: A Study of the TEG Regeneration Processes in Natural Gas Dehydration Plants. *Energy Sources, Part A: Recovery, Utilization, and Environmental Effects* 34, 456–464. <https://doi.org/10.1080/15567031003627930>
- Porter, J.A., Reid, L.S., 1950. Vapor-Liquid Equilibrium Data on the System Natural Gas-Water-Triethylene Glycol at Various Temperatures and Pressures. *Journal of Petroleum Technology* 2, 235–240. <https://doi.org/10.2118/950235-G>
- Price, A.R., Kobayashi, R., 1959. Low Temperature Vapor-Liquid Equilibrium in Light Hydrocarbon Mixtures: Methane-Ethane-Propane System. *Journal of Chemical & Engineering Data* 4, 40–52. <https://doi.org/10.1021/je60001a007>
- Price, B., Russell, F.G., Morgan, D.J., Kramer, J.M., Minkinen, A., Heigold, B., Soto, G.A.S., Rivelsrud, H., Bothamley, M., Hall, K., Northrop, S., 2004. Engineering data book; FPS version, Volumes I & II, Section 1-26, 12th ed. Gas Processors Suppliers Association (GPSA), Tulsa, Oklahoma.

- Privat, R., Visconte, M., Zazoua-Khames, A., Jaubert, J.-N., Gani, R., 2015. Analysis and prediction of the alpha-function parameters used in cubic equations of state. *Chemical Engineering Science* 126, 584–603. <https://doi.org/10.1016/j.ces.2014.12.040>
- Qin, J., Rosenbauer, R.J., Duan, Z., 2008. Experimental Measurements of Vapor–Liquid Equilibria of the H₂O + CO₂ + CH₄ Ternary System. *Journal of Chemical & Engineering Data* 53, 1246–1249. <https://doi.org/10.1021/je700473e>
- Qin, X., Cao, X., Guo, Y., Xu, L., Hu, S., Fang, W., 2014. Density, Viscosity, Surface Tension, and Refractive Index for Binary Mixtures of 1,3-Dimethyladamantane with Four C₁₀ Alkanes. *Journal of Chemical & Engineering Data* 59, 775–783. <https://doi.org/10.1021/je4008926>
- Qureshi, M.S., le Nedelec, T., Guerrero-Amaya, H., Uusi-Kyyny, P., Richon, D., Alopaeus, V., 2017. Solubility of carbon monoxide in bio-oil compounds. *The Journal of Chemical Thermodynamics* 105, 296–311. <https://doi.org/10.1016/j.jct.2016.10.030>
- Raal, J.D., Mühlbauer, A.L., 1999. *Phase Equilibria: Measurement and Computation*. Taylor & Francis.
- Raal, J.D., Mühlbauer, A.L., 1994. The Measurement of High Pressure Vapour-Liquid-Equilibria: Part II: Static Methods. *Developments in Chemical Engineering and Mineral Processing* 2, 88–104. <https://doi.org/10.1002/apj.5500020202>
- Rasoolzadeh, A., Raeissi, S., Shariati, A., Peters, C.J., 2020a. Experimental Measurement and Thermodynamic Modeling of Methane Solubility in Triethylene Glycol within the Temperature Range of 343.16–444.95 K. *Journal of Chemical & Engineering Data* 65, 3866–3874. <https://doi.org/10.1021/acs.jced.0c00198>
- Rasoolzadeh, A., Raeissi, S., Shariati, A., Peters, C.J., 2020b. Experimental measurements and thermodynamic modeling of high-pressure propane solubility in triethylene glycol. *Journal of Supercritical Fluids* 163. <https://doi.org/10.1016/j.supflu.2020.104881>
- Rastorguev, Yu.L., Gazdiev, M.A., 1969. Study of the thermal conductivity of manyatomic alcohols. *Inzh.-Fiz. Zh.* 17, 72–79.
- Reamer, H.H., Sage, B.H., Lacey, W.N., 1951. Phase Equilibria in Hydrocarbon Systems. Volumetric and Phase Behavior of the Propane-Carbon Dioxide System. *Industrial & Engineering Chemistry* 43, 2515–2520. <https://doi.org/10.1021/ie50503a035>
- Reamer, H.H., Sage, B.H., Lacey, W.N., 1950. Phase Equilibria in Hydrocarbon Systems. Volumetric and Phase Behavior of the Methane-Propane System. *Industrial & Engineering Chemistry* 42, 534–539. <https://doi.org/10.1021/ie50483a037>
- Reddy, P., 2006. Development of Novel Apparatus for Vapour-liquid Equilibrium Measurements at Moderate Pressures. Ph.D. Thesis. University of KwaZulu-Natal, Durban.
- Renon, H., Prausnitz, J.M., 1969. Estimation of Parameters for the NRTL Equation for Excess Gibbs Energies of Strongly Nonideal Liquid Mixtures. *Industrial & Engineering Chemistry Process Design and Development* 8, 413–419. <https://doi.org/10.1021/i260031a019>
- Renon, H., Prausnitz, J.M., 1968. Local compositions in thermodynamic excess functions for liquid mixtures. *AIChE Journal* 14, 135–144. <https://doi.org/10.1002/aic.690140124>
- Riaz, M., 2011. Distribution of Complex Chemicals in Oil-Water Systems, Ph.D. Thesis. Technical University of Denmark (DTU), Lyngby Denmark.

- Robinson, D.B., Peng, D.-Y., Chung, S.Y.-K., 1985. The development of the Peng - Robinson equation and its application to phase equilibrium in a system containing methanol. *Fluid Phase Equilibria* 24, 25–41. [https://doi.org/10.1016/0378-3812\(85\)87035-7](https://doi.org/10.1016/0378-3812(85)87035-7)
- Rodríguez-Escontrela, I., Rodríguez-Palmeiro, I., Rodríguez, O., Arce, A., Soto, A., 2015. Liquid–liquid–liquid equilibria for water+[P66614][DCA]+dodecane ternary system. *Fluid Phase Equilibria* 405, 124–131. <https://doi.org/10.1016/j.fluid.2015.07.022>
- Sabirzyanov, A.N., Marteau, P., Gumerov, F.M., le Neindre, B., 2001. Phase Equilibria in the Triethylene Glycol– and Tetraethylene Glycol–Supercritical Propane Systems. *Theoretical Foundations of Chemical Engineering* 35, 573–578. <https://doi.org/10.1023/A:1012937510655>
- Sage, B.H., Lacey, W.N., Schaafsma, J.G., 1934. Phase Equilibria in Hydrocarbon Systems II. Methane-Propane System. *Industrial & Engineering Chemistry* 26, 214–217. <https://doi.org/10.1021/ie50290a020>
- Sahki, D., Belaribi, B.F., Ait-Kaci, A., Jose, J., 1999. Static measurements of the total vapor pressure of binary mixtures of morpholine+ heptane and of piperidine or N-methylpiperidine+ heptane or+ decane between 273 K and 353 K. *ELDATA Int. Electron. J. Phys.-Chem. Data* 5, 85–96.
- Sanchez, M., Coll, R., 1978. Water + Propane System of High Pressures and Temperatures: 1.2-Phase Region. *An. Quim* 74, 1329.
- Scauzillo, F.R., 1961. Equilibrium Ratios of Water in the Water-Triethylene Glycol-Natural Gas System. *Journal of Petroleum Technology* 13, 697–702. <https://doi.org/10.2118/1567-G-PA>
- Schlichting, H., Langhorst, R., Knapp, H., 1993. Saturation of high pressure gases with low volatile solvents: experiments and correlation. *Fluid Phase Equilibria* 84, 143–163. [https://doi.org/10.1016/0378-3812\(93\)85121-2](https://doi.org/10.1016/0378-3812(93)85121-2)
- Schmid, B., 2011. Use of a Modern Group Contribution Equation of State for the Synthesis of Thermal Separation Processes (Ph.D. Thesis). Carl von Ossietzky University of Oldenburg, Germany.
- Scurto, A.M., Lubbers, C.M., Xu, G., Brennecke, J.F., 2001. Experimental measurement and modeling of the vapor–liquid equilibrium of carbon dioxide + chloroform. *Fluid Phase Equilibria* 190, 135–147. [https://doi.org/10.1016/S0378-3812\(01\)00599-4](https://doi.org/10.1016/S0378-3812(01)00599-4)
- Secuianu, C., Feroiu, V., Geană, D., 2003. High-Pressure Vapor–Liquid Equilibria in the System Carbon Dioxide and 2-Propanol at Temperatures from 293.25 K to 323.15 K. *Journal of Chemical & Engineering Data* 48, 1384–1386. <https://doi.org/10.1021/jc034027k>
- Sentenac, P., Bur, Y., Rauzy, E., Berro, C., 1998. Density of Methanol + Water between 250 K and 440 K and up to 40 MPa and Vapor–Liquid Equilibria from 363 K to 440 K. *Journal of Chemical & Engineering Data* 43, 592–600. <https://doi.org/10.1021/jc970297p>
- Serpa, F.S., Vidal, R.S., Filho, J.H.B.A., Nascimento, J.F. do, Ciambelli, J.R.P., Figueiredo, C.M.S., Salazar-Banda, G.R., Santos, A.F., Fortuny, M., Franceschi, E., Dariva, C., 2013. Solubility of Carbon Dioxide in Ethane-1,2-diol–Water Mixtures. *Journal of Chemical & Engineering Data* 58, 3464–3469. <https://doi.org/10.1021/jc400736w>
- Shimekit, B., Mukhtar, H., 2012. Natural Gas Purification Technologies - Major Advances for CO₂ Separation and Future Directions, in: *Advances in Natural Gas Technology*. InTech. <https://doi.org/10.5772/38656>

- Shmonov, V.M., Sadus, R.J., Franck, E.U., 1993. High-pressure phase equilibria and supercritical pVT data of the binary water + methane mixture to 723 K and 200 MPa. *The Journal of Physical Chemistry* 97, 9054–9059. <https://doi.org/10.1021/j100137a036>
- Sima, S., Feroiu, V., Geană, D., 2011. New High Pressure Vapor–Liquid Equilibrium and Density Predictions for the Carbon Dioxide + Ethanol System. *Journal of Chemical & Engineering Data* 56, 5052–5059. <https://doi.org/10.1021/je2008186>
- Sima, S., Secuianu, C., Feroiu, V., 2018. Phase equilibria of CO₂ + 1,2-dimethoxyethane at high-pressures. *Fluid Phase Equilibria* 458, 47–57. <https://doi.org/10.1016/j.fluid.2017.11.008>
- Skylogianni, E., Perinu, C., Cervantes Gameros, B.Y., Knuutila, H.K., 2020. Carbon dioxide solubility in mixtures of methyldiethanolamine with monoethylene glycol, monoethylene glycol–water, water and triethylene glycol. *The Journal of Chemical Thermodynamics* 151, 106176. <https://doi.org/10.1016/j.jct.2020.106176>
- Soave, G., 1972. Equilibrium constants from a modified Redlich-Kwong equation of state. *Chemical Engineering Science* 27, 1197–1203. [https://doi.org/10.1016/0009-2509\(72\)80096-4](https://doi.org/10.1016/0009-2509(72)80096-4)
- Song, K.Y., Kobayashi, R., 1989. Water Content Values of a CO₂ - 5.31 Mol Percent Methane Mixture, (GPA Research Report No. 120). Gas Processors Association.
- Soo, C.-B., 2011. Experimental thermodynamic measurements of biofuel-related associating compounds and modeling using the PC-SAFT equation of state. Fontainebleau cedex, France.
- Stewart, M., Arnold, K., 2011. Hydrate Prediction and Prevention, in: *Gas Dehydration Field Manual*. Elsevier, pp. 1–53. <https://doi.org/10.1016/B978-1-85617-980-5.00001-X>
- Suzuki, K., Sue, H., Itou, M., Smith, R.L., Inomata, H., Arai, K., Saito, S., 1990. Isothermal vapor-liquid equilibrium data for binary systems at high pressures: carbon dioxide-methanol, carbon dioxide-ethanol, carbon dioxide-1-propanol, methane-ethanol, methane-1-propanol, ethane-ethanol, and ethane-1-propanol systems. *Journal of Chemical & Engineering Data* 35, 63–66. <https://doi.org/10.1021/je00059a020>
- Takahashi, S., Song, Kyoo.Y., Kobayashi, R., 1984. Experimental Vapor-Liquid Equilibria in the CO₂-Diethylene Glycol-H₂O and CO₂-Triethylene Glycol-H₂O Systems at Feasible Absorption Temperatures and Pressures. *J. Chem. Eng. Data* 29, 23–28.
- Tanaka, K., Higashi, Y., Akasaka, R., Kayukawa, Y., Fujii, K., 2009. Measurements of the Vapor–Liquid Equilibrium for the CO₂ + R290 Mixture. *Journal of Chemical & Engineering Data* 54, 1029–1033. <https://doi.org/10.1021/je800938s>
- Taylor, B.N., Kuyatt, C.E., 1994. Guidelines for Evaluating and Expressing the Uncertainty of NIST Measurement Results; NIST Technical Note 1297. National Institute of Standards and Technology, Gaithersburg.
- Teymouri, S.R.M.B., 2016. Phase Equilibria Measurements and Modelling of CO₂–Rich Fluids/Brine Systems. PhD Thesis. Heriot-Watt University, Edinburgh, Scotland.
- Thiery, R., Kerkhof, A.M. van den, Dubessy, J., 1994. vX properties of CH₄-CO₂ and CO₂-N₂ fluid inclusions: modelling for T less than 30C and P less than 400 bar. *European Journal of Mineralogy* 6, 753–771.
- Tochigi, K., Namae, T., Suga, T., Matsuda, H., Kurihara, K., dos Ramos, M.C., McCabe, C., 2010. Measurement and prediction of high-pressure vapor–liquid equilibria for binary mixtures of

- carbon dioxide+n-octane, methanol, ethanol, and perfluorohexane. *The Journal of Supercritical Fluids* 55, 682–689. <https://doi.org/10.1016/j.supflu.2010.10.016>
- Townsend, F.M., 1955. Equilibrium water contents of natural gas dehydrated by aqueous diethylene-glycol and triethylene-glycol solutions at various temperatures and pressures, PhD Thesis. The University of Oklahoma, Norman, Oklahoma.
- Tsivintzelis, I., Ali, S., Kontogeorgis, G.M., 2014. Modeling Phase Equilibria for Acid Gas Mixtures using the Cubic-Plus-Association Equation of State. 3. Applications Relevant to Liquid or Supercritical CO₂ Transport. *Journal of Chemical & Engineering Data* 59, 2955–2972. <https://doi.org/10.1021/je500090q>
- Tsivintzelis, I., Kontogeorgis, G.M., 2016. Modelling phase equilibria for acid gas mixtures using the CPA equation of state. Part VI. Multicomponent mixtures with glycols relevant to oil and gas and to liquid or supercritical CO₂ transport applications. *The Journal of Chemical Thermodynamics* 93, 305–319. <https://doi.org/10.1016/j.jct.2015.07.003>
- Tsivintzelis, I., Kontogeorgis, G.M., 2015. Modelling phase equilibria for acid gas mixtures using the CPA equation of state. Part V: Multicomponent mixtures containing CO₂ and alcohols. *The Journal of Supercritical Fluids* 104, 29–39. <https://doi.org/10.1016/j.supflu.2015.05.015>
- Tsuji, T., Tanaka, S., Hiaki, T., Saito, R., 2004. Measurements of bubble point pressure for CO₂ + decane and CO₂ + lubricating oil. *Fluid Phase Equilibria* 219, 87–92. <https://doi.org/10.1016/j.fluid.2004.01.019>
- Twu, C.H., Bluck, D., Cunningham, J.R., Coon, J.E., 1991. A cubic equation of state with a new alpha function and a new mixing rule. *Fluid Phase Equilibria* 69, 33–50. [https://doi.org/10.1016/0378-3812\(91\)90024-2](https://doi.org/10.1016/0378-3812(91)90024-2)
- Ukai, T., Kodama, D., Miyazaki, J., Kato, M., 2002. Solubility of Methane in Alcohols and Saturated Density at 280.15 K. *Journal of Chemical & Engineering Data* 47, 1320–1323. <https://doi.org/10.1021/je020108p>
- Vetere, A., 1986. Vapor-liquid equilibria with supercritical gases calculated by the excess Gibbs energy method. *Fluid Phase Equilibria* 28, 265–281. [https://doi.org/10.1016/0378-3812\(86\)80032-2](https://doi.org/10.1016/0378-3812(86)80032-2)
- Wagner, Z., Wichterle, I., 1987. High-pressure vapour—liquid equilibrium in systems containing carbon dioxide, 1-hexene, and n-hexane. *Fluid Phase Equilibria* 33, 109–123. [https://doi.org/10.1016/0378-3812\(87\)87006-1](https://doi.org/10.1016/0378-3812(87)87006-1)
- Wang, L.-K., Chen, G.-J., Han, G.-H., Guo, X.-Q., Guo, T.-M., 2003. Experimental study on the solubility of natural gas components in water with or without hydrate inhibitor. *Fluid Phase Equilibria* 207, 143–154. [https://doi.org/10.1016/S0378-3812\(03\)00009-8](https://doi.org/10.1016/S0378-3812(03)00009-8)
- Wang, Y., Han, B., Yan, H., Liu, R., 1995. Solubility of CH₄ in the mixed solvent t-butyl alcohol and water. *Thermochimica Acta* 253, 327–334. [https://doi.org/10.1016/0040-6031\(94\)02011-C](https://doi.org/10.1016/0040-6031(94)02011-C)
- Webster, L.A., Kidnay, A.J., 2001. Vapor–Liquid Equilibria for the Methane–Propane–Carbon Dioxide Systems at 230 K and 270 K. *Journal of Chemical & Engineering Data* 46, 759–764. <https://doi.org/10.1021/je000307d>
- Wei, M.S.-W., Brown, T.S., Kidnay, A.J., Sloan, E.D., 1995. Vapor + Liquid Equilibria for the Ternary System Methane + Ethane + Carbon Dioxide at 230 K and its Constituent Binaries at Temperatures from 207 to 270 K. *Journal of Chemical & Engineering Data* 40, 726–731. <https://doi.org/10.1021/je00020a002>

- Williams-Wynn, M.D., Naidoo, P., Ramjugernath, D., 2016. Isothermal (vapour + liquid) equilibrium data for binary systems of (n-hexane + CO₂ or CHF₃). *The Journal of Chemical Thermodynamics* 94, 31–42. <https://doi.org/10.1016/j.jct.2015.10.009>
- Wilson, L.C., Wilding, W.V., Wilson, G.M., 1989. Vapor-Liquid equilibrium measurements on four binary mixtures. *AIChE Symp.Ser* 85, 25–43.
- Wise, M., Chapoy, A., 2016. Carbon dioxide solubility in Triethylene Glycol and aqueous solutions. *Fluid Phase Equilibria* 419, 39–49. <https://doi.org/10.1016/j.fluid.2016.03.007>
- Wise, M., Chapoy, A., Burgass, R., 2016. Solubility Measurement and Modeling of Methane in Methanol and Ethanol Aqueous Solutions. *Journal of Chemical & Engineering Data* 61, 3200–3207. <https://doi.org/10.1021/acs.jced.6b00296>
- Wolbach, J.P., Sandler, S.I., 1998. Using Molecular Orbital Calculations to Describe the Phase Behavior of Cross-associating Mixtures. *Industrial & Engineering Chemistry Research* 37, 2917–2928. <https://doi.org/10.1021/ie9707811>
- Wong, D.S.H., Sandler, S.I., 1992. A theoretically correct mixing rule for cubic equations of state. *AIChE Journal* 38, 671–680. <https://doi.org/10.1002/aic.690380505>
- Wu, J., Prausnitz, J.M., 1998. Phase Equilibria for Systems Containing Hydrocarbons, Water, and Salt: An Extended Peng–Robinson Equation of State. *Industrial & Engineering Chemistry Research* 37, 1634–1643. <https://doi.org/10.1021/ie9706370>
- Xia, J., Jödecke, M., Pérez-Salado Kamps, Á., Maurer, G., 2004. Solubility of CO₂ in (CH₃OH + H₂O). *Journal of Chemical & Engineering Data* 49, 1756–1759. <https://doi.org/10.1021/jc049803i>
- Xie, X., Brown, J.S., Bush, D., Eckert, C.A., 2005. Bubble and Dew Point Measurements of the Ternary System Carbon Dioxide + Methanol + Hydrogen at 313.2 K. *Journal of Chemical & Engineering Data* 50, 780–783. <https://doi.org/10.1021/jc0498614>
- Xu, N., Dong, J., Wang, Y., Shi, J., 1992. High pressure vapor liquid equilibria at 293 K for systems containing nitrogen, methane and carbon dioxide. *Fluid Phase Equilibria* 81, 175–186. [https://doi.org/10.1016/0378-3812\(92\)85150-7](https://doi.org/10.1016/0378-3812(92)85150-7)
- Yang, Q., Xu, A., Yang, C., 2017. Isobaric Vapor–Liquid Equilibrium for Two Binary Systems (Methanol + Dibutyl Carbonate) and (n -Butanol + Dibutyl Carbonate) at p = 40.0, 70.0, and 100.0 kPa. *Journal of Chemical & Engineering Data* 62, 148–155. <https://doi.org/10.1021/acs.jced.6b00517>
- Yan, W., Kontogeorgis, G.M., Stenby, E.H., 2007. Application of the CPA Equation of State to Reservoir Fluids in Presence of Water and Polar Chemicals, in: *All Days. SPE*. <https://doi.org/10.2118/110009-MS>
- Yao, J., Li, H., Han, S., 1999. Vapor–liquid equilibrium data for methanol–water–NaCl at 45°C. *Fluid Phase Equilibria* 162, 253–260. [https://doi.org/10.1016/S0378-3812\(99\)00204-6](https://doi.org/10.1016/S0378-3812(99)00204-6)
- Yarym-Agaev, N.L.L.L.Y., Sinyavskaya, R.P., Koliushko, I.I., Levinton, L.Y., 1985. Phase-equilibria in the water methane and methanol methane binary-systems under high-pressures. *Zh. Prikl. Khim* 58, 154–157.
- Ye, K., Freund, H., Sundmacher, K., 2011. Modelling (vapour + liquid) and (vapour + liquid + liquid) equilibria of {water (H₂O) + methanol (MeOH) + dimethyl ether (DME) + carbon dioxide (CO₂)} quaternary system using the Peng–Robinson EoS with Wong–Sandler mixing rule. *The Journal of Chemical Thermodynamics* 43, 2002–2014. <https://doi.org/10.1016/j.jct.2011.07.016>

- Yesavage, V.F., Furtado, A.W., Powers, J.E., 1968. Proc. Annu. Conv. Nat. Gas Process. Assoc. Tech. Pap., 1968, 3, in: Proc. Annu. Conv. Nat. Gas Process. Assoc. Gas Process. Assoc. p. 3.
- Yonemoto, T., Charoensombut-Amon, T., Kobayashi, R., 1989. Triethylene Glycol Vaporization Losses in Supercritical CO₂, RR-119.
- Yoon, J.H., Chun, M.K., Hong, W.H., Lee, H., 1993. High-pressure phase equilibria for carbon dioxide-methanol-water system: experimental data and critical evaluation of mixing rules. *Industrial & Engineering Chemistry Research* 32, 2881–2887. <https://doi.org/10.1021/ie00023a061>
- Yuan, S., Chen, Y., Ji, X., Yang, Z., Lu, X., 2017. Experimental study of CO₂ absorption in aqueous cholinium-based ionic liquids. *Fluid Phase Equilibria* 445, 14–24. <https://doi.org/10.1016/j.fluid.2017.04.001>
- Yucelen, B., Kidnay, A.J., 1999. Vapor–Liquid Equilibria in the Nitrogen + Carbon Dioxide + Propane System from 240 to 330 K at Pressures to 15 MPa. *Journal of Chemical & Engineering Data* 44, 926–931. <https://doi.org/10.1021/jc980321e>
- Zaitsau, D., Paulechka, E., Firaha, D.S., Blokhin, A. v., Kabo, G.J., Bazyleva, A., Kabo, A.G., Varfolomeev, M.A., Sevruck, V.M., 2015. Comprehensive study of the thermodynamic properties for 2-methyl-3-buten-2-ol. *The Journal of Chemical Thermodynamics* 91, 459–473. <https://doi.org/10.1016/j.jct.2015.07.028>
- Zhao, W., Xia, L., Sun, X., Xiang, S., 2019. A Review of the Alpha Functions of Cubic Equations of State for Different Research Systems. *International Journal of Thermophysics* 40, 105. <https://doi.org/10.1007/s10765-019-2567-4>
- Zielkiewicz, J., Oracz, P., 1990. Vapour–liquid equilibrium in the ternary system N,N-dimethylformamide + methanol + water at 313.15 K. *Fluid Phase Equilibria* 59, 279–290. [https://doi.org/10.1016/0378-3812\(90\)80004-U](https://doi.org/10.1016/0378-3812(90)80004-U)
- Žilnik, L.F., Grilc, M., Levec, J., Peper, S., Dohrn, R., 2016. Phase-equilibrium measurements with a novel multi-purpose high-pressure view cell: CO₂ + n-decane and CO₂ + toluene. *Fluid Phase Equilibria* 419, 31–38. <https://doi.org/10.1016/j.fluid.2016.03.010>

APPENDIX A

Uncertainty estimation

A measured value (measurand) is considered complete when it is accompanied by its uncertainty (Bell, 1999). Uncertainty results from quantifying the confidence of the original measurement and is defined as the extent to which the actual value of the measurement has the greatest chances of residing. Since there is always a margin of certainty on any measurement, it is important to know the span of that margin in relation to the measured variable. Two numbers are required to calculate an uncertainty and these are the interval or the width of the margin, and the confidence interval (Bell, 1999). The confidence interval, which states how confident we are that the actual value is within the interval (Bell, 1999). In this work, uncertainty estimation follows the approach outlined by NIST (National Institute of Standard and Technology) authored by Taylor and Kuyatt (Taylor and Kuyatt, 1994) and has been clearly demonstrated by Soo (Soo, 2011) and Nelson (Nelson, 2012).

Classification of components of uncertainty

To evaluate the uncertainty of a measurement, the sources of uncertainty in the measurement are initially identified. This is then followed by an estimation of the size of uncertainty from each of the identified uncertainty sources. Then the distinct standard uncertainties are lumped up to produce an overall quantity (Bell, 1999). The sources/components of uncertainty are classified into two classes, namely type A component and type B components, based on the methods used to evaluate their numerical values.

Type A evaluation:

This is the evaluation of uncertainty by statistical methods, where a statistical analysis of a series of observations is employed. Type A uncertainty may be evaluated from:

$$u(\theta) = \frac{\sigma}{\sqrt{N}} \quad (\text{A-1})$$

Where θ is the measurement parameter which could be composition, pressure or temperature as is the case in this work, σ is the standard deviation of the data, and N is the number of repeated data points.

Type B evaluation:

This is the evaluation of uncertainty by other means. This is generally dependent on scientific judgement utilising all the available pertinent information such as previously measured data, data provided in

calibration reports, manufacturer's specifications and so on. The rectangular distribution is a reasonable default model since there is a 100% likelihood that the value lies within the distribution and is expressed as follows:

$$u_i(\theta) = \frac{b}{\sqrt{3}} \quad (\text{A-2})$$

Where $u_i(\theta)$ is the standard uncertainty of a parameter being evaluated, b is the maximum error induced by the type B uncertainty, e.g., calibration polynomial.

Standard Uncertainty

Every source of uncertainty that adds to the uncertainty of a measurement is best represented by a calculated standard deviation, referred to as standard uncertainty u_i , which is equal to the positive square root of the standard variance u_i^2 (Bell, 1999). Thus, we have standard uncertainty type A and standard uncertainty type B, evaluation of which have been shown in equations (A-1) and (A-2). For evaluation of standard uncertainty type B, if there are high chances that values of the quantity in question are close to the centre of the limits than to the limits a normal distribution or triangular distribution may be a better model and the equation used in this case is different from equation (A-2). Table A-1 lists all the standard uncertainties used in this work.

Combining standard uncertainties

Separate standard uncertainties evaluated by either type A evaluation or type B evaluation are combined validly by the root of sum squares (RSS) (Bell, 1999); some call it the law of propagation of uncertainty. The result of this is the combined standard uncertainty usually denoted by (u_c) . When a quantity (θ) is established from the measurement of other quantities α_i , then the uncertainty $u(\theta)$, will be controlled by the uncertainties that are in each of the measured quantities $u(\alpha_i)$ (Soo, 2011). The RSS is thus expressed as:

$$\theta = f(\alpha_1, \alpha_2 \dots \alpha_n)$$

$$u(\theta) = \sqrt{\left[\left(\frac{\partial \theta}{\partial \alpha_1} \right)_{\alpha_{i \neq 1}} u_{\alpha 1} \right]^2 + \left[\left(\frac{\partial \theta}{\partial \alpha_2} \right)_{\alpha_{i \neq 2}} u_{\alpha 2} \right]^2 + \dots + \left[\left(\frac{\partial \theta}{\partial \alpha_n} \right)_{\alpha_{i \neq n}} u_{\alpha n} \right]^2} \quad (\text{A-3})$$

Table A-1: Values of standard uncertainties used in this study.

Source of uncertainty	Estimate ^a
Temperature (<i>T</i>)	
<i>T</i> standard (K), CTH 6500	0.02
Calibration uncertainty <i>T</i> (K) for main equipment used in this work	0.11
Calibration uncertainty <i>T</i> (K) for liquid vapour pressure equipment	0.01
Pressure (<i>P</i>)	
<i>P</i> standard (MPa), CPC Mensor 8000 (25 MPa gauge)	0.01% ^b
Calibration correlation for (<i>P</i> /MPa)	0.001
Calibration correlation for (<i>P</i> /kPa) for liquid vapour pressure equipment	0.04
Standard uncertainty induced by the pressure transducer (35 MPa)	0.02
Standard uncertainty induced by the pressure transducer (10 MPa)	0.005
Standard uncertainty induced by the pressure transducer (100 kPa)	0.05
Composition uncertainty (<i>x_i</i> and <i>y_i</i> , analytical measurements)	
i. CO ₂ (1) + n-hexane (2) system	
Standard uncertainty due to calibration correlation (vapour phase) <i>u</i> (<i>y₁</i>)	0.0041
Standard uncertainty due to calibration correlation (liquid phase) <i>u</i> (<i>x₁</i>)	0.0013
Standard uncertainty due to the preparation of the calibration mixture (g)	0.01
ii. CO ₂ (1) + n-decane (2) system	
Standard uncertainty due to calibration correlation (vapour phase) <i>u</i> (<i>y₁</i>)	0.0007
Standard uncertainty due to calibration correlation (liquid phase) <i>u</i> (<i>x₁</i>)	0.0015
Standard uncertainty due to the preparation of the calibration mixture (g)	0.01
Composition uncertainty (<i>x_i</i>), Bubble point measurements	
i. Gas-liquid binary system	
Mass balance uncertainty (g)	0.01
ii. Gas-liquid solution (ternary) system	
Mass balance model PA423C (1) uncertainty (g) (liquid solution preparation)	0.003
Mass balance model PX5202 (2) uncertainty (g)	0.01
^a Treated as rectangular distribution unless otherwise stated; ^b Treated as normal distribution	

The simplified combined standard uncertainty of a parameter (θ) is evaluated as follows:

$$u_c(\theta) = \pm \sqrt{\sum_i u_i(\theta)^2} \quad (\text{A-4})$$

Where $u_i(\theta)$ is the standard uncertainty of a parameter being evaluated, such uncertainty due to repeatability, uncertainty induced by calibration standards or references, errors in calibration polynomials and so on.

Coverage factor k

The rescaling of the combined standard uncertainty is achieved by incorporating a coverage factor k . The expanded uncertainty (U_c) is evaluated by multiplying the combined standard uncertainty (u_c) with a coverage factor k (Bell, 1999). The expression for expanded uncertainty is thus presented as:

$$U_c = \pm[k * u_c] \quad (\text{A-5})$$

If $k = 2$, this characterises an interval having 95% level of confidence assuming a normally distributed uncertainty (Bell, 1999). This study assumes mostly the rectangular distributed uncertainty where $k = 1.65$ for a 95% level of confidence.

Temperature uncertainty

The combined standard uncertainty for temperature $u_c(T)$, which was applied to all systems of this study is given by:

$$u_c(T) = \pm \sqrt{u_{rep}(T^2) + u_{calib}(T^2)} \quad (\text{A-6})$$

Where u_{rep} is the standard uncertainty due to measurement repeatability (Type A), and u_{calib} is the uncertainty due to the calibration polynomial and method.

$$u_{calib}(T) = \pm \sqrt{u_{calib\ cor}(T^2) + u_{std}(T^2)} \quad (\text{A-7})$$

Where $u_{calib\ cor}(T)$ is the standard uncertainty due to calibration correlation (Type B), and $u_{std}(T)$ is standard uncertainty induced by the standard temperature probe (Type B).

In the case of $u_{calib\ cor}(T)$, b was taken as the maximum calibration error of the temperature probes used

In the case of $u_{std}(T)$, b was 0.02 K obtained using data from calibration data sheet of the temperature standard.

The expanded uncertainty of the temperature measurements is determined by:

$$U_c(T) = \pm[1.65 * u_c(T)] \quad (\text{A-8})$$

Pressure uncertainty

The combined standard uncertainty of pressure for all pressure measurements in this study is given by:

$$u_c(P) = \pm \sqrt{u_{calib\ cor}(P^2) + u_{std}(P^2) + u_{atm}(P^2) + u_{rep}(P^2)} \quad (A-9)$$

Where:

$u_{atm}(P)$ is the standard uncertainty of the CPC Mensor (barometer), (Type B). and b in this case is 0.001 MPa.

$u_{calib\ cor}(P)$ is the standard uncertainty due to calibration correlation (Type B).

$u_{std}(P)$ is standard uncertainty induced by the pressure transducer, (Type B)

$u_{rep}(P)$ is the standard uncertainty due to measurement repeatability (Type A)

Molar composition uncertainty

Composition uncertainty VLE (T-P-x-y measurements) analytic method: The case of two-component systems

In this case, the combined standard uncertainty was estimated from the uncertainty caused by the TCD calibration correlation (Type B) and the uncertainty of repeatability of sampling using the ROLSI™ sampler (Type A).

$$u_c(x_i) = \pm \sqrt{u_{rep}(x_i^2) + u_{cor}(x_i^2) + u_{calib\ mix}(x_i^2)} \quad (A-10)$$

In this instance, $u_{cor\ x_i}$ is given by (Soo, 2011):

$$u_{cor\ x_i} = |x_{1\ true} - x_{1\ calc}|_{max} \quad (A-11)$$

Where $x_{1\ true}$ is the true mole fraction for component 1, $x_{1\ calc}$ is the evaluated mole fraction for component 1. This is the maximum error observed when using the calibration polynomial. $u_{cor}(x_i)$ is evaluated using the rectangular distribution.

$u_{rep\ x_i}$ is evaluated in a similar way to all other type A uncertainty evaluation.

$u_{calib\ mix}(x_i)$ is uncertainty due to the preparation of the calibration mixture, which depends on three sources namely: Ohaus mass balance uncertainty type B, precision ± 0.01 g; masses of the individual components and thirdly mole fractions. Mole fractions are used since during calibration as outlined in section 5.2.3, a gravimetrically prepared binary mixture of known composition is loaded into the equilibrium cell.

$$u_{calib\ mix} = \pm \sqrt{ub(x_i)^2} \quad (A-12)$$

Where $ub(x_i)$ is uncertainty of the mass balance. Since x_i is dependent on the measurement of the masses m_i and m_j , for component i and j , it follows (Soo, 2011):

$$ub(x_i) = \sqrt{\left[\left(\frac{\partial x_i}{\partial m_1}\right)_{m_2} u(m_1)\right]^2 + \left[\left(\frac{\partial x_i}{\partial m_2}\right)_{m_1} u(m_2)\right]^2} \quad (A-13)$$

Since $x_i = \frac{n_i}{n_i + n_j}$ and $n_i = \frac{m_i}{MM_i}$, where MM is the molar mass, equation (A-13) can be reduced to (Soo, 2011) :

$$ub(x_i) = x_1 x_2 \sqrt{\left(\frac{u(m_1)}{m_1}\right)^2 + \left(\frac{u(m_2)}{m_2}\right)^2} \quad (A-14)$$

$u(m_1)$ and $u(m_2)$ are the standard uncertainties in mass for components 1 and 2 respectively, and these are induced by the internal uncertainty of the mass balance (Nelson, 2012).

In this case the values of $u(m_1)$ and $u(m_2)$ stem from the same balance, hence are equal. The mass balance has a precision of ± 0.01 g and a type B evaluation is employed.

Equation (A-14) can also be applied to evaluate molar composition uncertainty for bubble point measurements of a gas-liquid system.

Likewise, the expanded uncertainty is computed by multiplication of the combined standard uncertainty with a coverage factor (k) of 1.65.

Molar composition uncertainty bubble point (TPx) measurements

Composition uncertainty: The case of a ternary mixture comprised of methane + propane + methanol/TEG

In this case, the combined standard uncertainty is given by the standard uncertainty of the Ohaus mass balance (precision ± 0.01 g), the masses of the respective components, their mole fractions, and the uncertainty provided by the manufacturer for the gas mixture (methane +propane). These are all treated as type B uncertainty.

The combined standard uncertainty u_{ci} is given by

$$u_{ci} = \pm \sqrt{ub_{x_i}^2} \quad (A-15)$$

Where ub_{x_i} is uncertainty of the mass balance, combined with uncertainty of the methane + propane gas mixture which is provided by the manufacturer.

If mm_1 , mm_2 and mm_3 are the masses of the respective components: (methane, propane and liquid component) in that order and MM_1 , MM_2 and MM_3 are the molecular masses of the same components respectively, then applying the root-sum-squared method:

$$ub_{xi} = \pm \sqrt{\left[\frac{dx_1}{dm_1} * u(m_1)\right]^2 + \left[\frac{dx_1}{dm_2} * u(m_2)\right]^2 + \left[\frac{dx_1}{dm_3} * u(m_3)\right]^2} \quad (A-16)$$

Where:

$u(m_1)$ and $u(m_2)$ are estimated using:

$$u(m_i) = \left[\frac{c * m_i + ub * o}{\sqrt{3}} \right] \quad (A-17)$$

Where:

c is the gas composition uncertainty provided by the manufacturer; and b represents the mass balance precision, o represents composition of the gas in the mixture

$$u_{m3} = \frac{ub}{\sqrt{3}} \quad (A-18)$$

The expanded uncertainty in composition in this case is then given by the product of the combined uncertainty and the coverage factor, $k=1.65$ for a 95% level of confidence.

Equation (A-16) is also used in evaluating composition uncertainty for the ternary system comprised of either methane/carbon dioxide + water + TEG or methane/carbon dioxide +methanol + TEG systems, however with some minor changes with respect to the evaluation of $u(m_1)$, $u(m_2)$ and $u(m_3)$, which are evaluated as follows:

$u(m_1)$ is given by equation A – 18;

$$u(m_2) \text{ and } u(m_3) \text{ are : } um_i = \left[\frac{u \text{ prep mix} * mi + ub * wt\%}{\sqrt{3}} \right] \quad (A-19)$$

Where ub precision represents the mass balance precision; $u \text{ prep mix}$ represents uncertainty induced by preparing the liquid-liquid solution; $wt\%_i$ represents the weight percent of component i in the liquid-liquid solution.

It is important to note that for the case of a gas-liquid-liquid system and other systems with multiple liquid mixtures, two Ohaus mass balances are used. One is Ohaus mass balance model PA423C (maximum capacity 420g) with a precision of $\pm 0.003 \text{ g}$ and is for the preparation of the liquid mixture. The second balance is for weighing all the components (prepared liquid mixture of known composition) + gas when loaded in the equilibrium cell, Ohaus mass balance model PX5202 (maximum capacity 5200g) of estimated accuracy $\pm 0.01\text{g}$. These are all treated as type B uncertainty.

For higher systems of this study involving more than three components, the RSS method was used to evaluate composition uncertainty, applying basic principles highlighted in equation (A-17) for gas mixtures and equation (A-19) for liquid mixtures.

Relative volatility uncertainty

Relative volatility is a function of both the liquid mole fraction (x_i) and the vapour mole fraction (y_i) for both components (1) and (2) that were under consideration. The standard relative volatility for a binary system $u(\alpha_{12})$ is given by (Nelson, 2012):

$$u(\alpha_{12}) = \sqrt{\left(\frac{d\alpha_{12} * u(x_1)}{dx_1}\right)^2 + \left(\frac{d\alpha_{12} * u(y_1)}{dy_1}\right)^2} \quad (\text{A-20})$$

Where $u(x_1)$ and $u(y_1)$ are the standard uncertainties estimated using the procedure mentioned in equation A.2 and are further subjected to a Type B evaluation. For calculation, the relative volatility is given by:

$$\alpha_{12} = \frac{y_1(1 - x_1)}{x_1(1 - y_1)} \quad (\text{A-21})$$

Reducing $u(\alpha_{12})$ to:

$$u(\alpha_{12}) = \alpha_{12} \sqrt{\left[\frac{u(x_1)}{x_1 x_2}\right]^2 + \left[\frac{u(y_1)}{y_1 y_2}\right]^2} \quad (\text{A-22})$$

APPENDIX B: TABLES AND GRAPHS OF RESULTS

B.1. Vapour pressure measurement results

Vapour pressure measurements for ambient-liquid compositions were conducted using static synthetic non-visual apparatus made of stainless-steel equilibrium cells. Approximately 30 to 40 cm³ of the degassed liquid sample were loaded to the evacuated cells (70 cm³ capacity). The cells were then submerged into a silicon oil liquid bath, the temperature of which was regulated by a Grant TX temperature controller. Two Pt 100 probes were utilised to measure the bath temperature and hence the temperature of the cell. Each of the cells was equipped with a pressure transducer that operates within the 0-100 kPa range. Before use, both the temperature probes and the pressure transducers were calibrated (results presented in this report). The equipment has a stirrer that helps to rapid attainment of equilibrium. Pressure and temperature readings were recorded when stable lines were observed for over 10 minutes, indicating the vapour and the liquid phase were in equilibrium. Vapour pressure measurements were conducted for the following liquid components: water, methanol and n-hexane. Vapour pressure measurements could not be conducted for TEG since the available pressure transducers would not be able to measure extremely low pressures required for TEG. n-decane sample was used up; hence vapour pressure measurements were not performed.

For gaseous components, vapour pressure measurements for carbon dioxide only was conducted. Carbon dioxide vapour pressure measurement was conducted in the main equipment used in this work, which is described in section 5.1. Carbon dioxide was loaded into the evacuated equilibrium cell after purging the feeding lines. The cell was cooled by ice bath, so that the carbon dioxide gas loaded turns into liquid and this was done until the cell was half-filled since the contents could be observed. The equilibrium cell was then submerged into a water bath, the temperature of which was regulated by a Grant TX temperature controller. Pressure and temperature readings were recorded when stable lines were observed for over 10 minutes, indicating the vapour and the liquid phase were in equilibrium.

Table B.1-1 to 2 and Figures B.1-1 to 2 presents calibration polynomials and errors for both the temperature probes and pressure transducer calibrations for the apparatus that had been used for liquid component vapour pressure measurements.

Table B.1-1: Calibration polynomials for the temperature probes T104 and T105.

Probe	Correlation	R ² value	ΔT (max): K
T104	$Y = 4E-06x^2 + 0.9990x - 1.2324$	$R^2 = 1.000$	0.012
T105	$Y = 2E-05x^2 + 0.9949x - 1.2774$	$R^2 = 1.000$	0.012

Y represents the calculated temperature value in K, x represents the displayed temperature value in K.

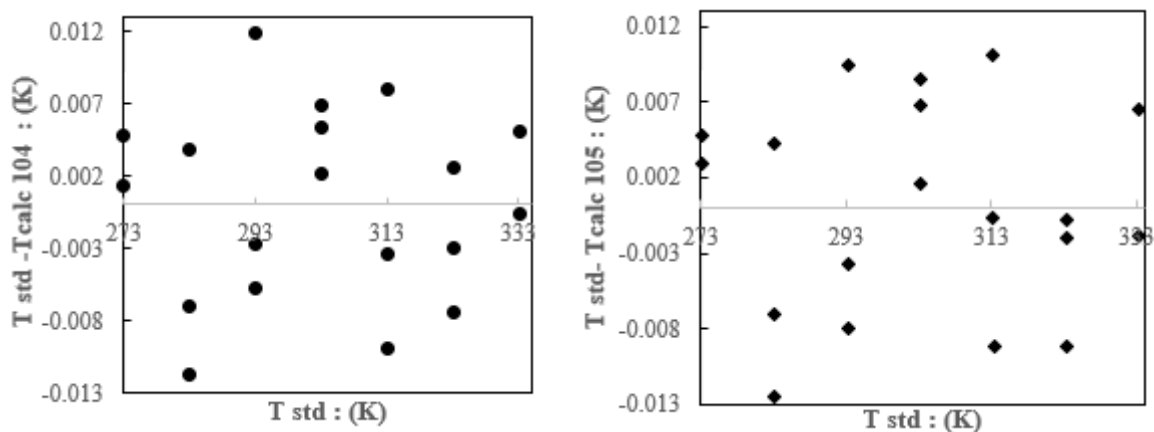


Figure B.1-1: Plot of deviation between the standard temperature (T std) and calibrated calibrated temperature (T calc) for the probes used in this work.

(Left) probe T104; (Right) probe T105.

Figure B.1-1 shows that the calibration polynomial for probe T104 yielded a maximum deviation reading of ± 0.012 K. Calibration polynomial for probe T105 gave a maximum deviation reading of ± 0.012 K.

Table B.1-2: Pressure transducer calibration polynomials.

Transducer	Correlation	R ² value	ΔP(max): kPa
P121	$Y = -3.651E-04x^2 + 1.0015x + 0.0007$	$R^2 = 1.000$	0.03
P122	$Y = -3E-04x^2 + 1.0013x + 0.0006$	$R^2 = 1.000$	0.04

Y represents the calculated pressure value in kPa, x represents the displayed pressure value in kPa for each transducer.

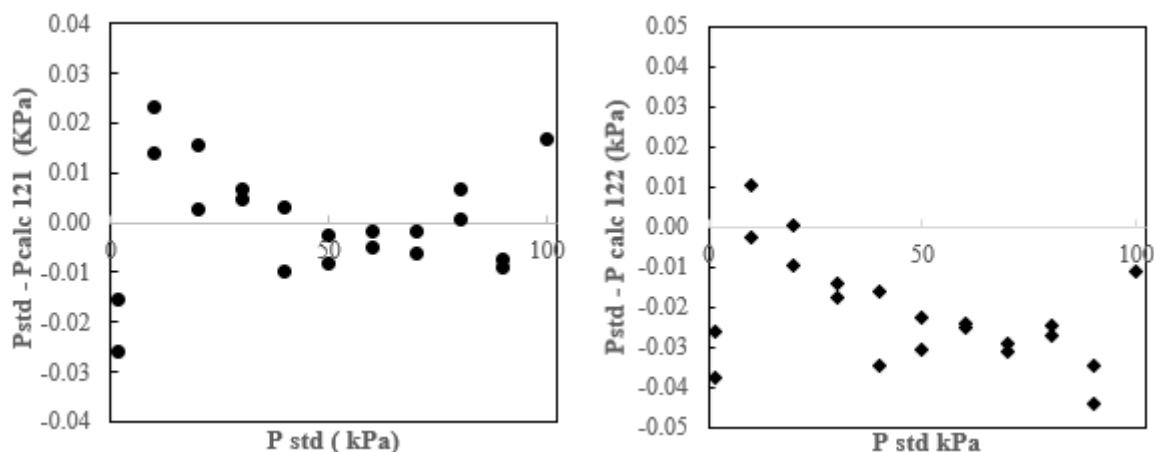


Figure B.1-2: Plot of the deviation between the standard pressure (Pstd) and the calculated calibrated pressure (Pcalc) for the transducers used in this work.
(Left) transducer P121; (Right) transducer P122.

Figure B.1-2 shows that pressure transducer P121 calibration polynomial gives a maximum deviation reading of ± 0.03 kPa, pressure transducer P122 calibration polynomial gave a maximum deviation reading of ± 0.04 kPa.

B.1.1. Water vapour pressure

Water vapour pressure measurement results are displayed in Figure B.1-3 and are also presented in Table B.1-3 together with the reported literature data. The data of this work agrees well with the reported literature data as the AARD % is less than 1%, see Table B.1-4.

Table B.1-3: Vapour pressure measurement results for water.

T (K)	P (kPa)	P (kPa) Lit*	ΔP (kPa)
283.19	1.245	1.2532 ^a ; 1.228 ^b	-0.008
293.16	2.419	2.3198 ^a ; 2.339 ^b	0.099
298.18	3.22	3.160 ^a ; 3.182 ^c	0.060
303.19	4.273	4.293 ^a ; 4.245 ^b	-0.020
313.19	7.32	7.386 ^a ; 7.376 ^b	-0.066
323.14	12.19	12.359 ^a ; 12.334 ^b	-0.169

$U(T) = 0.02$ K; $U(P) = 0.072$ kPa; a: Obtained from NIST ThermoData Engine (TDE version 10.2, database version 10.12) in Aspen Plus V11 (Louder et al., 1924); b: Obtained from NIST ThermoData Engine (TDE version 10.2, database version 10.12) in Aspen Plus V11 (Mizushima and Nagayama, 1957); c: : Obtained from NIST ThermoData Engine (TDE version 10.2, database version 10.12) in Aspen Plus V11 (Zaitsau et al., 2015).

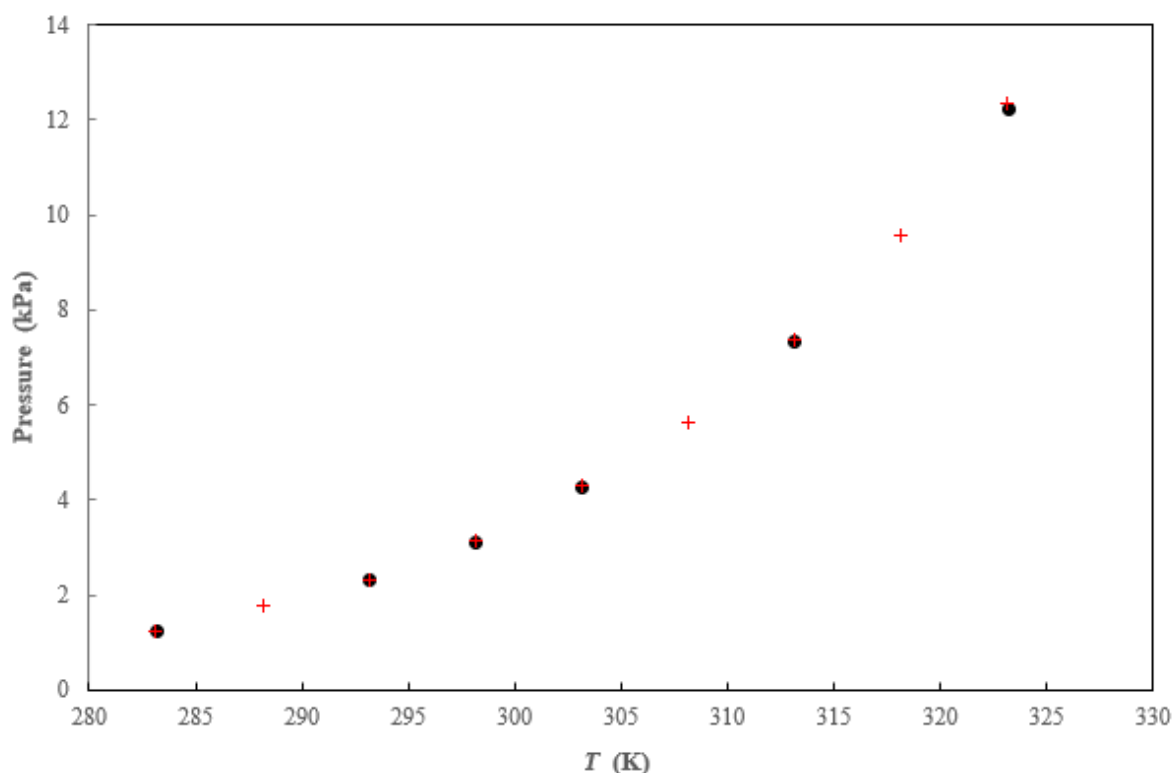


Figure B.1-3: Water vapour pressure measurement results.

This work (●); (Louder et al., 1924)(+).

Table B.1-4: AAD and AARD for water between this work and literature data of (Louder et al., 1924).

Component	AAD (kPa)	AARD
Water	0.047	0.91%

B.1.2. Methanol vapour pressure results

Methanol vapour pressure measurement results are displayed in Figure B.1-4 and are also presented in Table B.1-5 together with the reported literature data. The data of this work agrees well with the reported literature data as the AARD % is less than 1%, see Table B.1-6.

Table B.1-5: Vapour pressure measurement results for methanol.

T (K)	P (kPa)	Lit*	ΔP (kPa)
283.16	7.442	7.443	-0.001
293.20	12.985	13.039	-0.054
298.15	16.917	16.981	-0.064
303.16	21.807	21.914	-0.107
313.15	35.511	35.518	-0.007
323.16	55.238	55.684	-0.446

$U(T) = 0.02$ K; $U(P) = 0.072$ kPa; Lit* : data obtained from NIST TDE (Lemmon et al., 2021)

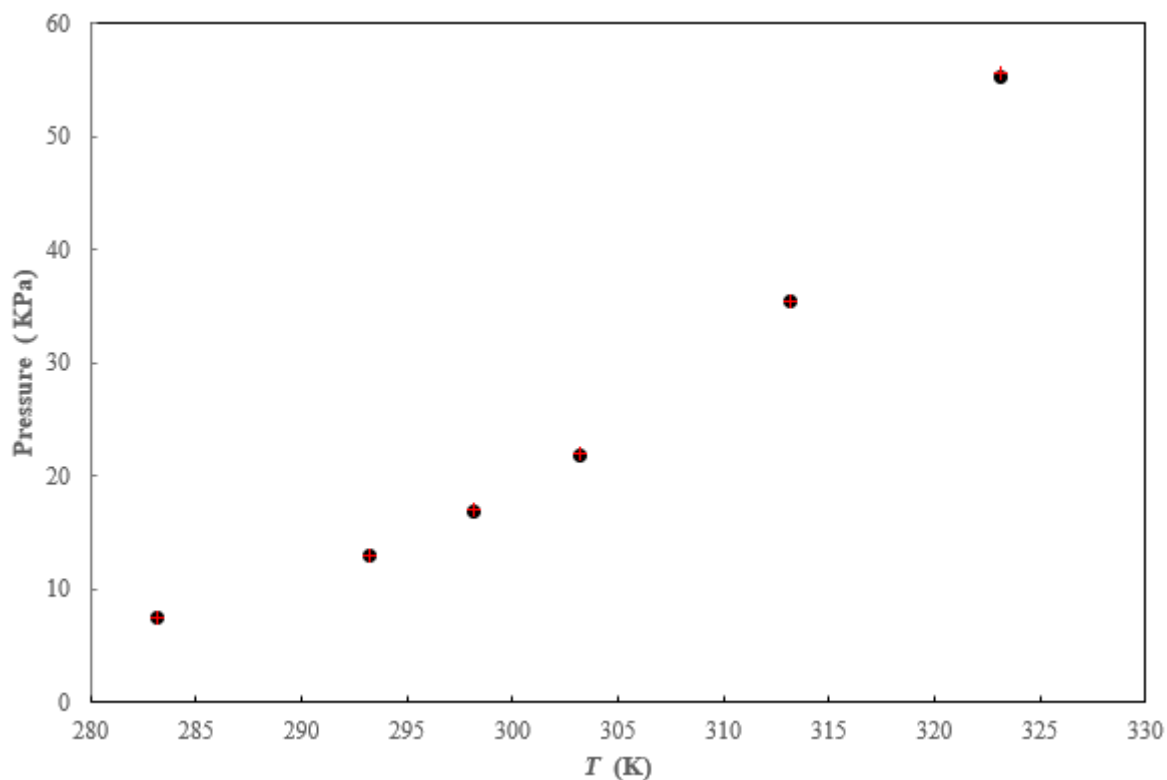


Figure B.1-4. Methanol vapour pressure measurement results.

This work (●); NIST TDE (Lemmon et al., 2021) (+).

Table B.1-6: AAD and AARD for methanol between this work and literature data from NIST TDE (Lemmon et al., 2021)

Component	AAD (kPa)	AARD
Methanol	0.113	0.35%

B.1.3. n-Hexane vapour pressure results

n-Hexane vapour pressure measurement results are displayed in Figure B.1-5 and are also presented in Table B.1-7 together with the reported literature data. The data of this work agrees well with the reported literature data as the AARD % is less than 2%, see Table B.1-8.

Table B.1-7: Vapour pressure measurement results for n-hexane.

<i>T</i> (K)	<i>P</i> (kPa)	Lit*	ΔP (kPa)
283.16	10.455	10.092	0.363
293.20	16.316	16.165	0.151
298.15	20.814	20.164	0.650
303.13	25.040	24.946	0.094
313.16	37.646	37.283	0.363
323.16	54.298	54.089	0.209

$U(T) = 0.02$ K; $U(P) = 0.072$ kPa; Lit* : data obtained from NIST TDE (Lemmon et al., 2021)

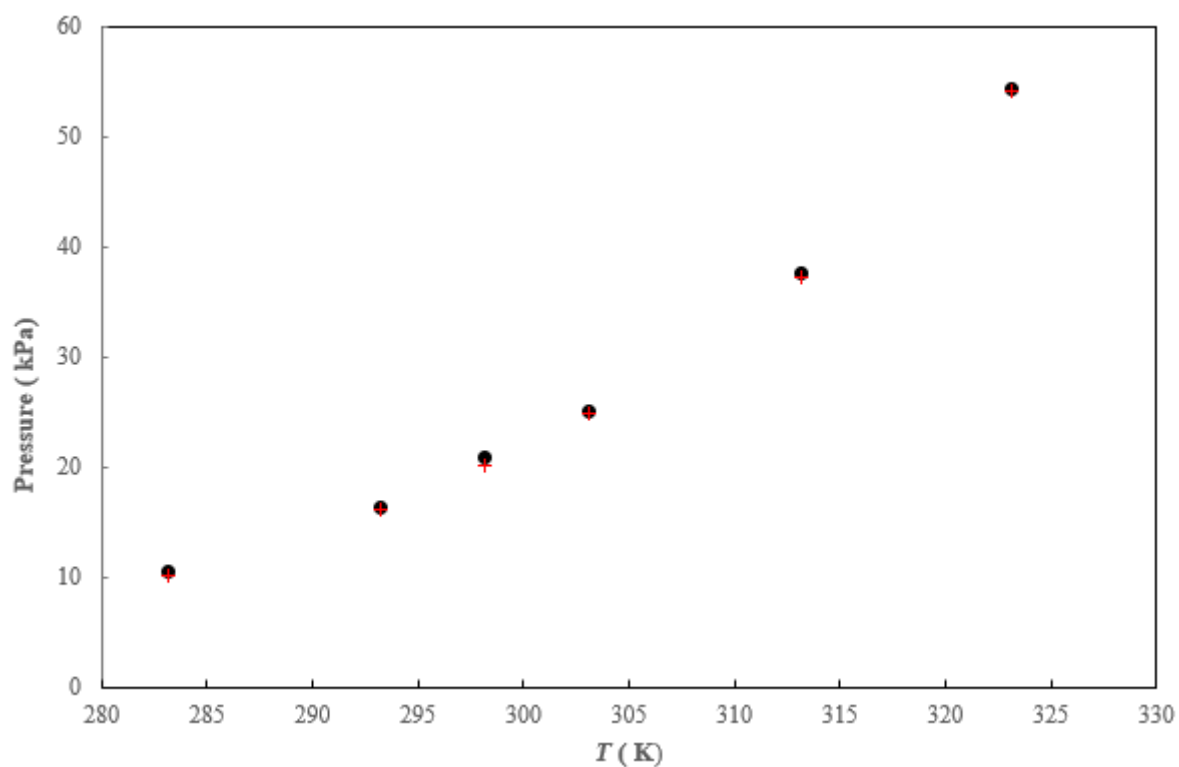


Figure B.1-5. n-Hexane vapour pressure measurement results.

(●) This work; NIST (Lemmon et al., 2021) (+).

Table B.1-8: AAD and AARD for n-hexane between this work and literature data from NIST (Lemmon et al., 2021)

Component	AAD (kPa)	AARD
n-Hexane	0.305	1.54%

B.1.4. Carbon dioxide vapour pressure results

Measurement of carbon dioxide vapour pressure was conducted using the new equipment of this work, which has been described in section 5. The results are presented in Figure B.1-6 and Table B.1-8, together with reported literature data.

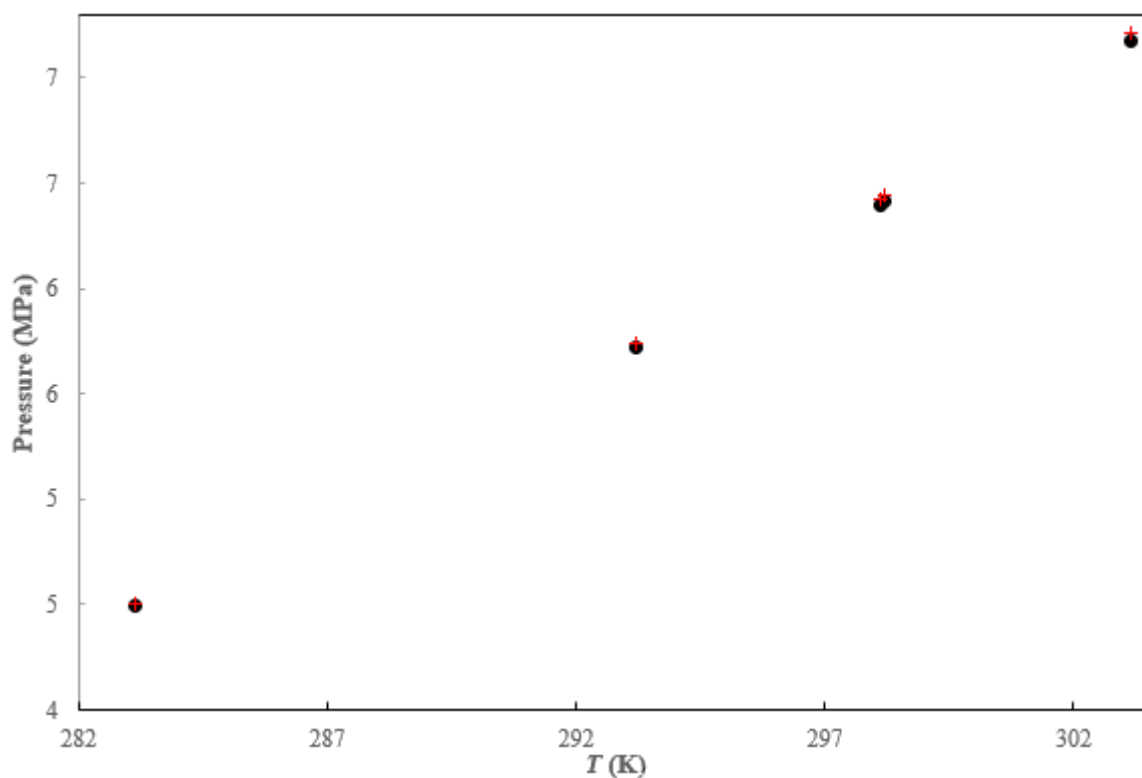


Figure B.1-6: CO₂ vapour pressure measurement results.
This work (●); NIST TDE (Lemmon et al., 2021) (+).

Table B.1-9: Vapour pressure measurement results for CO₂.

<i>T</i> (K)	<i>P</i> (MPa)	Lit* (MPa)	ΔP (MPa)
283.15	4.50	4.50	-0.01
293.20	5.72	5.74	-0.02
298.11	6.40	6.43	-0.03
298.21	6.41	6.44	-0.03
303.16	7.17	7.22	-0.04

$U(T) = 0.11$ K; $U(P) = 0.02$ MPa ; Lit*: data obtained from NIST TDE (Lemmon et al., 2021)

Table B.1-10: AAD and AARD for CO₂ between this work and literature data from NIST TDE (Lemmon et al., 2021)

Component	AAD (MPa)	AARD
CO ₂	0.03	0.40%

B.2. Gas mixture composition validation

The gas mixtures composition verification was performed to check the supplier's stated purities. In this work, all calculations presented in the main text are based on the supplier's stated gas composition (for cases where gas mixtures are involved). Composition validation was made possible through:

- Injection of pure gases (methane) /carbon dioxide at a set volume
- Injection of the gas mixture at a similar volume to that used for the pure component
- dividing the peak area in gas mixture for either methane/carbon dioxide to the peak area of the same pure component injection
- This was done for three different volumes (i.e 200 μ l ; 300 μ l and 400 μ l) and the averaged results are taken as the true composition.

The gases were injected at the same conditions into the Shimadzu 2010 GC equipped with a HayeSep Q packed column with a TCD detector. A 500 μ l HAMILTON GASTIGHT® syringe was used for the injections.

The following compositions were determined:

6. Methane + propane gas mixture

Table B.2-1: CH₄ + C₃H₈ gas mixture validation.

Component	mol%	Rel S.D. %	U_y
Methane	94.28	0.50	0.85%
Propane	5.72	0.68	0.65%

Where Rel S.D % represents the relative standard deviation in peak areas, U is the expanded uncertainty for the respective gas component in a given mixture.

2. Methane + carbon dioxide + propane gas mixture

Table B.2-2: CH₄ + CO₂ + C₃H₈ gas mixture validation.

Component	mol%	Rel.S.D %	U_y
Methane	90.14	0.46	0.83%
Carbon dioxide	4.92	0.98	1.01%
Propane	4.94	1.03	0.98%

The column operating conditions for this test are presented in Table B.2-3.

Table B.2-3: GC equipment conditions.

GC condition	Value	Units
T injection	513.15	K
Pessure	115.4	kPa
Total flow	20	cm ³ /min
Purge flow	3	cm ³ /min
T column	363.15	K
T detector	513.15	K
Make up flow	8	cm ³ /min
Column	HayeSep Q	
Length	2	m
ID	2	mm
Film thickness	1	μm
Current	70	ma
Carrier gas	H ₂	
Detector	TCD	

In this case, since compositions were evaluated through comparison of peak areas of individual components (methane/carbon dioxide) in the respective gas mixtures to the peak areas of pure components injection, uncertainties in the peak areas (relative std dev) play a crucial role in the determination of composition uncertainty.

For methane / carbon dioxide uncertainty in the gas mixture:

Using the RSS method, methane/carbon dioxide composition standard uncertainty was estimated as follows

$$u_{xi} = \sqrt{\theta_{pure}^2 + \theta_{mix}^2} \quad (B.2-1)$$

Where i is component in this case either methane or carbon dioxide in the gas mixture; θ_{pure} represents relative standard deviation in peak areas for the pure component injection; θ_{mix} represents relative standard deviation in peak areas for component i in a gas mixture.

For propane in the gas mixtures

$$ux_i = \sqrt{\theta_{mix}^2} \quad (B.2-2)$$

Assuming a rectangular distribution, $k= 1.65$ and hence the expanded uncertainties were evaluated by multiplying either equation 1 or 2 by k . The uncertainties were all treated as type B.

B.3. Pure component parameters

Table B .3-1: Critical properties and acentric factors for components of interest in this study.

All values obtained from NIST ThermoData Engine (TDE version 10.2, database version 10.12)
in Aspen Plus V11.

Chemical Component	<i>T</i> critical (K)	<i>U</i> <i>T</i> (K)	<i>P</i> critical (MPa)	<i>U</i> <i>P</i> (MPa)	Acentric factor
Carbon dioxide	304.18	0.05	7.38	0.02	0.22547
Methanol	512.68	0.41	8.06	0.98	0.56196
TEG	777.20	32.6	3.29	0.20	0.70002
Water	647.11	0.05	22.07	0.05	0.34416
Methane	190.56	0.01	4.61	0.01	0.01131
Propane	369.90	0.13	4.26	0.03	0.15251
n-Hexane	507.55	0.14	3.03	0.04	0.30031
n-Decane	618.05	0.92	2.11	0.60	0.48767

Table B.3-2: Critical properties and acentric factors for components of interest in this study. All values were obtained from Aspen Plus V12, DB PURE 38.

Parameter	Units	CO ₂	CH ₃ OH	H ₂ O	TEG	CH ₄	C ₃ H ₈	C ₆ H ₁₄	C ₁₀ H ₂₂
Omega		0.22362	0.56583	0.34486	0.75595	0.01155	0.15229	0.30126	0.49233
<i>P</i> critical	MPa	7.38	8.08	22.06	3.32	4.60	4.25	3.03	2.11
<i>T</i> critical	K	304.21	512.50	647.10	769.50	190.56	369.83	507.60	617.70

Table B.3-3: Mathias Copeman alpha function Parameters.

Parameter	CO ₂	CH ₄	C ₃ H ₈	C ₆ H ₁₄	C ₁₀ H ₂₂	H ₂ O	CH ₃ OH	TEG
<i>C</i> ₁	0.749	0.417	0.610	0.842	1.090	0.919	1.236	2.135
<i>C</i> ₂	-1.761	-0.182	-0.096	-0.312	-0.265	-0.333	-0.419	8.218
<i>C</i> ₃	15.088	0.374	0.357	0.874	0.871	0.325	-0.009	22.727

MC parameters obtained from Aspen Plus V12-aspenONE, DB-PURE 38.

B.4 Vapour liquid equilibria measurement results: test systems

Table B.4-1: Experimental VLE data, relative volatility (α_{12}), and uncertainty information for the CO₂ (1) + n-hexane (2) system for both synthetic (bubble point) and analytic methods of measurement, U represents the expanded uncertainty.

P [MPa] Visual	P [MPa] Breaking	x_1	Ux_1	P (MPa)	x_1	Ux_1	y_1	Uy_1	α_{12}	$U \alpha_{12}$
P-x data at 313.20 K (Synthetic method)				P-x-y data at 313.19 K (Analytic method)						
0.70	0.70	0.0651	0.0008	2.05	0.2105	0.0047	0.9743	0.0043	142.48	14.37
1.90	1.89	0.1941	0.0007	3.47	0.3783	0.0093	0.979	0.0043	76.65	11.17
2.13	2.14	0.2131	0.0006	4.57	0.515	0.0052	0.9814	0.0044	49.83	6.91
2.40	2.38	0.2447	0.0007	5.77	0.6818	0.0043	0.9812	0.0044	24.39	3.35
3.42	3.42	0.3582	0.0004	6.75	0.8271	0.0052	0.9801	0.0043	10.31	1.35
4.15	4.16	0.4577	0.0003	7.24	0.8895	0.0056	0.9771	0.0056	5.31	0.79
4.96	4.98	0.5661	0.0002	7.34	0.8998	0.0056	0.9801	0.0044	5.49	0.73
5.54	5.56	0.6503	0.0002	7.21	0.8895	0.0056	0.9786	0.0044	5.69	0.71
6.89	6.87	0.846	0.0002	3.39	0.3783	0.0093	0.9807	0.0044	83.36	11.18
7.39	7.42	0.9116	0.0002							

$U(T) = 0.04$ K; $U(P) = 0.01$ MPa.

For the analytic method, composition uncertainty is based on the repeatability of sampling using the RolsiTM sampler (Type A) and the calibration correlation used (Type B). These are all evaluated following guidance from (Nelson, 2012; Soo, 2011) who also followed the National Institute of Standard and Technology (NIST) guidelines on the estimation of uncertainty. The coverage factor k of 1.65 was used throughout.

Table B.4-2: Experimental VLE data, relative volatility, and uncertainty information for the CO₂ (1) + n-decane (2) system at 319.22 K.

$P(\text{MPa})$	x_1	Ux_1	y_1	Uy_1	α_{12}	$U\alpha_{12}$
1.257	0.1111	0.0016	0.9979	0.0007	3851.96	759.85
2.115	0.1942	0.0055	0.9988	0.0007	3378.98	1114.09
2.462	0.2289	0.0032	0.9988	0.0007	2714.77	894.55
3.448	0.3293	0.0049	0.9984	0.0007	1286.71	342.81
4.09	0.3858	0.0051	0.9985	0.0008	1036.09	308.77
5.003	0.4619	0.0061	0.9984	0.0008	710.46	203.5
5.773	0.5309	0.0078	0.9986	0.0008	613.33	191.12
6.854	0.6321	0.0084	0.9982	0.0008	317.92	80.00
8.04	0.764	0.0100	0.9977	0.0007	131.93	23.36
8.078	0.764	0.0100	0.9964	0.0007	86.24	10.74
8.327	0.8163	0.0108	0.997	0.0007	75.08	10.74

$U(T) = 0.04 \text{ K}$; $U(P) = 0.005 \text{ MPa}$.

Table B.4-3: Experimental VLE data and uncertainty information for the CO₂ (1) + methanol (2) system.

$P(\text{MPa})$ Visual	$P(\text{MPa})$ Breaking	x_1	Ux_1	$P(\text{MPa})$ Visual	$P(\text{MPa})$ Breaking	x_1	Ux_1
$T = 298.10 \text{ K}$				$T = 313.15 \text{ K}$			
0.71	0.71	0.049	0.0003	0.43	0.43	0.02	0.0003
2.84	2.83	0.2037	0.0002	1.81	1.82	0.096	0.0002
0.45	0.45	0.0289	0.0003	4.42	4.41	0.239	0.0002
3.4	3.4	0.2605	0.0003	5.87	5.89	0.367	0.0003
5.03	5.03	0.4517	0.0003	7.79	7.79	0.68	0.0003
5.77	5.77	0.6744	0.0007				

$U(T) = 0.07 \text{ K}$; $U(P) = 0.01 \text{ MPa}$.

Table B.4-4: Experimental VLE data and uncertainty information for the CH₄ (1) + CH₃OH system.

<i>P</i> (MPa) Visual	<i>P</i> (MPa) Breaking	<i>x</i> ₁	<i>Ux</i> ₁	<i>P</i> (MPa) Visual	<i>P</i> (MPa) Breaking	<i>x</i> ₁	<i>Ux</i> ₁
<i>T</i> = 298.15 K				<i>T</i> = 303.15 K			
1.27	1.26	0.0087	0.0007	2.63	2.63	0.0204	0.0008
3.00	2.98	0.0239	0.0008	4.26	4.26	0.0357	0.0008
4.51	4.51	0.036	0.0008	6.67	6.67	0.053	0.0007
7.06	7.06	0.0585	0.0008	8.99	8.98	0.0742	0.0007
13.08	13.07	0.1025	0.0007	10.69	10.68	0.0862	0.0007

U(*T*) = 0.11 K; *U*(*P*) = 0.02 MPa.

Table B.4-5: Experimental VLE data and uncertainty information for the CH₄ + TEG system.

<i>P</i> (MPa) Visual	<i>P</i> (MPa) Breaking	<i>x</i> ₁	<i>Ux</i> ₁	<i>P</i> (MPa) Visual	<i>P</i> (MPa) Breaking	<i>x</i> ₁	<i>Ux</i> ₁
<i>T</i> = 298.15 K				<i>T</i> = 323.15 K			
1.32	1.32	0.0047	0.0022	1.41	1.41	0.0047	0.0022
4.54	4.54	0.0212	0.0021	4.23	4.22	0.0212	0.0021
6.15	6.14	0.0267	0.0021	5.65	5.65	0.0267	0.0021
9.14	9.13	0.0376	0.0021	8.90	8.90	0.0376	0.0021
10.15	10.15	0.0422	0.0022	10.18	10.18	0.0422	0.0022
11.92	11.92	0.0460	0.0022	11.29	11.28	0.0460	0.0022

U(*T*) = 0.11 K; *U*(*P*) = 0.03 MPa

Table B.4-6: Experimental VLE data and uncertainty information for the CO₂ + TEG test system.

<i>P</i> (MPa) Visual	<i>P</i> (MPa) Breaking	<i>x</i> ₁	<i>Ux</i> ₁
<i>T</i> = 298.15 K			
2.77	2.77	0.1940	0.0006
4.00	4.00	0.2623	0.0005
4.76	4.75	0.3251	0.0004
5.25	5.25	0.3559	0.0004
5.73	5.72	0.3758	0.0003

U(*T*) = 0.11 K; *U*(*P*) = 0.01 MPa.

The standard uncertainty in composition for this particular apparatus is dependent on the standard uncertainty of the Ohaus mass balance (maximum error 0.01g), the masses of the respective components, and their mole fractions.

Table B.4-7: Experimental VLE data and uncertainty information for the CO₂ (1) + H₂O (2) + TEG (3) test systems.

<i>P</i> (MPa) Visual	<i>P</i> (MPa) Breaking	<i>x</i> ₁	<i>x</i> ₂	<i>x</i> ₃	<i>Ux</i> ₁
Data for the CO₂ (1) + (H₂O (2) 10 % wt. + TEG (3) 90 % wt.) system at 298.15 K					
1.69	1.69	0.0582	0.451	0.4908	0.002
2.89	2.89	0.0973	0.4361	0.4667	0.0015
3.63	3.62	0.1213	0.4245	0.4543	0.0014
3.89	3.88	0.1238	0.4203	0.456	0.0016
6.65	6.66	0.1672	0.4125	0.4203	0.0013
Data for the CO₂ (1) + (H₂O (2) 3.5 % wt. + TEG (3) 96.5 % wt.) system at 322.04 K					
1.37	1.36	0.0441	0.222	0.734	0.003
1.85	1.85	0.0649	0.217	0.7181	0.0018
3.62	3.61	0.1387	0.1997	0.6615	0.002
6.19	6.18	0.2157	0.182	0.6023	0.0019
6.73	6.73	0.2485	0.1745	0.577	0.0018

$U(T) = 0.11$ K; $U(P) = 0.02$ MPa

B.5. Vapour liquid equilibria measurement results: novel systems

Table B.5-1: Experimental VLE data and uncertainty information for the (CH₄ (1) /C₃H₈ (2) 95/5 mol%) + CH₃OH (3) system.

<i>P</i> (MPa) Visual	<i>P</i> (MPa) Breaking	<i>x</i> ₁	<i>x</i> ₂	<i>x</i> ₃	<i>U_{x1}</i>
<i>T</i> = 283.16 K					
1.7	1.69	0.0175	0.0003	0.9822	0.0008
3.07	3.07	0.032	0.0006	0.9674	0.0008
5.36	5.34	0.0541	0.001	0.9449	0.0009
6.42	6.41	0.0647	0.0012	0.9341	0.0009
8.88	8.87	0.0871	0.0017	0.9113	0.001
<i>T</i> = 303.16 K					
1.35	1.35	0.0115	0.0002	0.9883	0.0007
2.86	2.87	0.0249	0.0005	0.9746	0.0008
4.85	4.83	0.0444	0.0008	0.9548	0.0009
8.05	8.05	0.0724	0.0014	0.9262	0.0011
9.4	9.39	0.0844	0.0016	0.914	0.001
<i>T</i> = 323.15 K					
1.26	1.25	0.0093	0.0002	0.9905	0.0007
4.19	4.18	0.0345	0.0007	0.9649	0.0009
6.28	6.27	0.0524	0.001	0.9466	0.0009
7.45	7.45	0.0631	0.0012	0.9357	0.0009
9.97	9.96	0.0856	0.0016	0.9128	0.001

U(*T*) = 0.11 K; *U*(*P*) = 0.02 MPa.

Table B.5-2: Experimental VLE data and uncertainty information for the (CH₄ (1) 95 % mol + C₃H₈ (2) 5 % mol) + TEG (3) system.

<i>P</i> (MPa) Visual	<i>P</i> (MPa) Breaking	<i>x</i> ₁	<i>x</i> ₂	<i>x</i> ₃	<i>U_{x1}</i>
<i>T</i> = 303.16 K					
0.78	0.78	0.0039	0.0001	0.9960	0.0021
4.41	4.4	0.0228	0.0004	0.9768	0.0021
6.26	6.25	0.0317	0.0006	0.9677	0.0021
7.03	7.02	0.0364	0.0007	0.9629	0.0021
8.59	8.58	0.0446	0.0009	0.9545	0.002
<i>T</i> = 323.16 K					
0.87	0.87	0.0039	0.0001	0.9960	0.0021
4.31	4.31	0.0228	0.0004	0.9768	0.0021
6.14	6.14	0.0317	0.0006	0.9677	0.0021
6.97	6.96	0.0364	0.0007	0.9629	0.0021
8.38	8.38	0.0446	0.0009	0.9545	0.002

U(*T*) = 0.11 K; *U*(*P*) = 0.03 MPa.

Table B.5-3: Experimental VLE data and uncertainty information for the CH₄ (1) + (CH₃OH (2) 3.33 wt.% +TEG (3) 96.67 wt. % (3) system.

<i>P</i> (MPa) Visual	<i>P</i> (MPa) Breaking	<i>x</i> ₁	<i>x</i> ₂	<i>x</i> ₃	<i>Ux</i> ₁
<i>T</i> = 303.16 K					
2.04	2.04	0.0113	0.1376	0.8511	0.0027
2.70	2.70	0.014	0.137	0.8489	0.0020
4.98	4.98	0.0263	0.1354	0.8383	0.0019
7.32	7.32	0.0327	0.1346	0.8328	0.0019
10.81	10.80	0.0428	0.1332	0.8241	0.0018
12.64	12.64	0.0465	0.1327	0.8208	0.0018
<i>T</i> = 323.15 K					
2.14	2.14	0.0113	0.1376	0.8511	0.0027
2.75	2.75	0.014	0.137	0.8489	0.0020
5.10	5.10	0.0263	0.1354	0.8383	0.0019
7.17	7.16	0.0327	0.1346	0.8328	0.0019
10.17	10.17	0.0428	0.1332	0.8241	0.0018
11.35	11.35	0.0465	0.1327	0.8208	0.0018

U(*T*) = 0.11 K; *U*(*P*) = 0.03 MPa.

Table B.5-4: Experimental VLE data and uncertainty information for the CO₂ (1) + (CH₃OH (2) 3.33 wt.% +TEG (3) 96.67 wt. % (3) system.

<i>P</i> (MPa) Visual	<i>P</i> (MPa) Breaking	<i>x</i> ₁	<i>x</i> ₂	<i>x</i> ₃	<i>Ux</i> ₁
<i>T</i> = 303.16 K					
0.75	0.74	0.0437	0.133	0.8233	0.0007
2.25	2.24	0.143	0.1192	0.7377	0.0008
3.70	3.69	0.241	0.1056	0.6534	0.0009
4.47	4.47	0.2678	0.1019	0.6303	0.0009
6.75	6.75	0.4015	0.0832	0.5152	0.0011
<i>T</i> = 323.15 K					
0.85	0.84	0.0391	0.1337	0.8273	0.0007
2.26	2.25	0.0983	0.1254	0.7763	0.0008
3.08	3.07	0.143	0.1192	0.7377	0.0008
5.34	5.34	0.241	0.1056	0.6534	0.0009
6.33	6.32	0.2678	0.1019	0.6303	0.0009
11.91	11.9	0.4015	0.0832	0.5152	0.0011

U(*T*) = 0.11 K; *U*(*P*) = 0.02 MPa

Table B.5-5: Experimental VLE data and uncertainty information for the (CH₄ (1) /C₃H₈ (2) 95/5 mol%) + (CH₃OH (3) /TEG (4) 3.33/96.67 wt. %) system.

<i>P</i> (MPa) Visual	<i>P</i> (MPa) Breaking	<i>x</i> ₁	<i>x</i> ₂	<i>x</i> ₃	<i>x</i> ₄	<i>Ux</i> ₁	<i>Ux</i> ₄
<i>T</i> = 283.16 K							
1.63	1.63	0.005	0.0001	0.1383	0.8566	0.0019	0.0017
3.05	3.04	0.0112	0.0002	0.1375	0.8511	0.0019	0.0017
6.18	6.18	0.0224	0.0004	0.136	0.8412	0.0019	0.0017
7.77	7.77	0.0265	0.0005	0.1353	0.8376	0.0018	0.0016
13.79	13.78	0.0391	0.0007	0.1336	0.8266	0.0018	0.0016
<i>T</i> = 303.16 K							
1.63	1.63	0.005	0.0001	0.1383	0.8566	0.0019	0.0017
3.02	3	0.0112	0.0002	0.1375	0.8511	0.0019	0.0017
5.4	5.4	0.0224	0.0004	0.136	0.8412	0.0019	0.0017
7	7	0.0265	0.0005	0.1353	0.8376	0.0018	0.0016
12.52	12.51	0.0391	0.0007	0.1336	0.8266	0.0018	0.0016
<i>T</i> = 323.15 K							
1.47	1.46	0.005	0.0001	0.1383	0.8566	0.0019	0.0017
2.79	2.78	0.0112	0.0002	0.1375	0.8511	0.0019	0.0017
4.6	4.6	0.0224	0.0004	0.136	0.8412	0.0019	0.0017
5.76	5.76	0.0265	0.0005	0.1353	0.8376	0.0018	0.0016
9.16	9.15	0.0391	0.0007	0.1336	0.8266	0.0018	0.0016

U(*T*) = 0.11 K; *U*(*P*) = 0.02 MPa

Table B.5-6: Experimental VLE data and uncertainty information for the (CH₄ (1)/C₃H₈ (2) 95/5 mol%) + ((H₂O (3) /TEG (5) 5/95 wt.%): CH₃OH (4) 3.33 wt.%).

<i>P</i> (MPa) Visual	<i>P</i> (MPa) Breaking	<i>x</i> ₁	<i>x</i> ₂	<i>x</i> ₃	<i>x</i> ₄	<i>x</i> ₅	<i>U</i> <i>x</i> ₁	<i>U</i> <i>x</i> ₅
<i>T</i> = 283.16 K								
2.23	2.23	0.0074	0.0001	0.2707	0.1049	0.6168	0.0015	0.0026
3.52	3.52	0.011	0.0002	0.271	0.1044	0.6134	0.0015	0.0024
6.09	6.08	0.0177	0.0003	0.2682	0.1037	0.6101	0.0015	0.0024
9.33	9.33	0.0256	0.0005	0.2654	0.103	0.6055	0.0015	0.0024
14.11	14.1	0.0315	0.0006	0.2646	0.1022	0.6011	0.0015	0.0025
<i>T</i> = 303.15 K								
2.38	2.38	0.0074	0.0001	0.2707	0.1049	0.6168	0.0015	0.0026
3.47	3.46	0.011	0.0002	0.271	0.1044	0.6134	0.0015	0.0024
5.54	5.54	0.0177	0.0003	0.2682	0.1037	0.6101	0.0015	0.0024
6.86	6.86	0.0212	0.0004	0.2667	0.1034	0.6084	0.0015	0.0024
8.15	8.15	0.0256	0.0005	0.2654	0.103	0.6055	0.0015	0.0024
9.61	9.6	0.0285	0.0005	0.2649	0.1026	0.6034	0.0014	0.0024
11.89	11.88	0.0315	0.0006	0.2646	0.1022	0.6011	0.0015	0.0025
<i>T</i> = 323.16 K								
2.3	2.29	0.0074	0.0001	0.2707	0.1049	0.6168	0.0015	0.0026
3.34	3.34	0.011	0.0002	0.271	0.1044	0.6134	0.0015	0.0024
4.94	4.94	0.0177	0.0003	0.2682	0.1037	0.6101	0.0015	0.0024
6.14	6.13	0.0212	0.0004	0.2667	0.1034	0.6084	0.0015	0.0024
6.97	6.98	0.0256	0.0005	0.2654	0.103	0.6055	0.0015	0.0024
8.07	8.07	0.0285	0.0005	0.2649	0.1026	0.6034	0.0014	0.0024
9.05	9.05	0.0315	0.0006	0.2646	0.1022	0.6011	0.0015	0.0025
10.93	10.93	0.0353	0.0007	0.2636	0.1019	0.5986	0.0015	0.0024

U(*T*) = 0.11 K; *U*(*P*) = 0.07 MPa.

Table B.5-7: Experimental VLE data and uncertainty information for the (CH₄ (1)/C₃H₈ (2)/CO₂ (3) 90.22/4.60/5.18 mol%) + ((H₂O (4) /TEG (6) 5/95 wt.%): CH₃OH (5) 3.33 wt.%) system.

<i>P</i> (MPa) Visual	<i>P</i> (MPa) Breaking	<i>x</i> ₁	<i>x</i> ₂	<i>x</i> ₃	<i>x</i> ₄	<i>x</i> ₅	<i>x</i> ₆	<i>U</i> _{<i>x1</i>}	<i>U</i> _{<i>x6</i>}
<i>T</i> = 283.15 K									
2.89	2.89	0.0110	0.0002	0.0002	0.2694	0.1046	0.6146	0.0014	0.0025
5.45	5.44	0.0203	0.0004	0.0004	0.2674	0.1034	0.6081	0.0014	0.0023
7.28	7.27	0.0282	0.0005	0.0006	0.2646	0.1026	0.6034	0.0014	0.0026
10.91	10.9	0.0395	0.0007	0.0008	0.2614	0.1015	0.5962	0.0014	0.0026
12.76	12.75	0.0462	0.0009	0.0010	0.2599	0.1006	0.5915	0.0014	0.0023
<i>T</i> = 303.15 K									
2.93	2.93	0.0110	0.0002	0.0002	0.2694	0.1046	0.6146	0.0014	0.0025
4.03	4.02	0.0171	0.0003	0.0004	0.2688	0.1038	0.6096	0.0014	0.0024
5.3	5.3	0.0203	0.0004	0.0004	0.2674	0.1034	0.6081	0.0014	0.0023
6.96	6.96	0.0282	0.0005	0.0006	0.2646	0.1026	0.6034	0.0014	0.0026
10.18	10.18	0.0395	0.0007	0.0008	0.2614	0.1015	0.5962	0.0014	0.0026
12.17	12.16	0.0462	0.0009	0.0010	0.2599	0.1006	0.5915	0.0014	0.0023
<i>T</i> = 323.15 K									
2.72	2.72	0.0110	0.0002	0.0002	0.2694	0.1046	0.6146	0.0014	0.0025
4.07	4.06	0.0171	0.0003	0.0004	0.2688	0.1038	0.6096	0.0014	0.0024
5.17	5.16	0.0203	0.0004	0.0004	0.2674	0.1034	0.6081	0.0014	0.0023
6.72	6.72	0.0282	0.0005	0.0006	0.2646	0.1026	0.6034	0.0014	0.0026
9.97	9.97	0.0395	0.0007	0.0008	0.2614	0.1015	0.5962	0.0014	0.0026
11.8	11.8	0.0462	0.0009	0.0010	0.2599	0.1006	0.5915	0.0014	0.0023

U(*T*) = 0.11 K; *U*(*P*) = 0.03 MPa.

APPENDIX C: P-y PLOTS

C.1 Carbon dioxide + n-hexane system

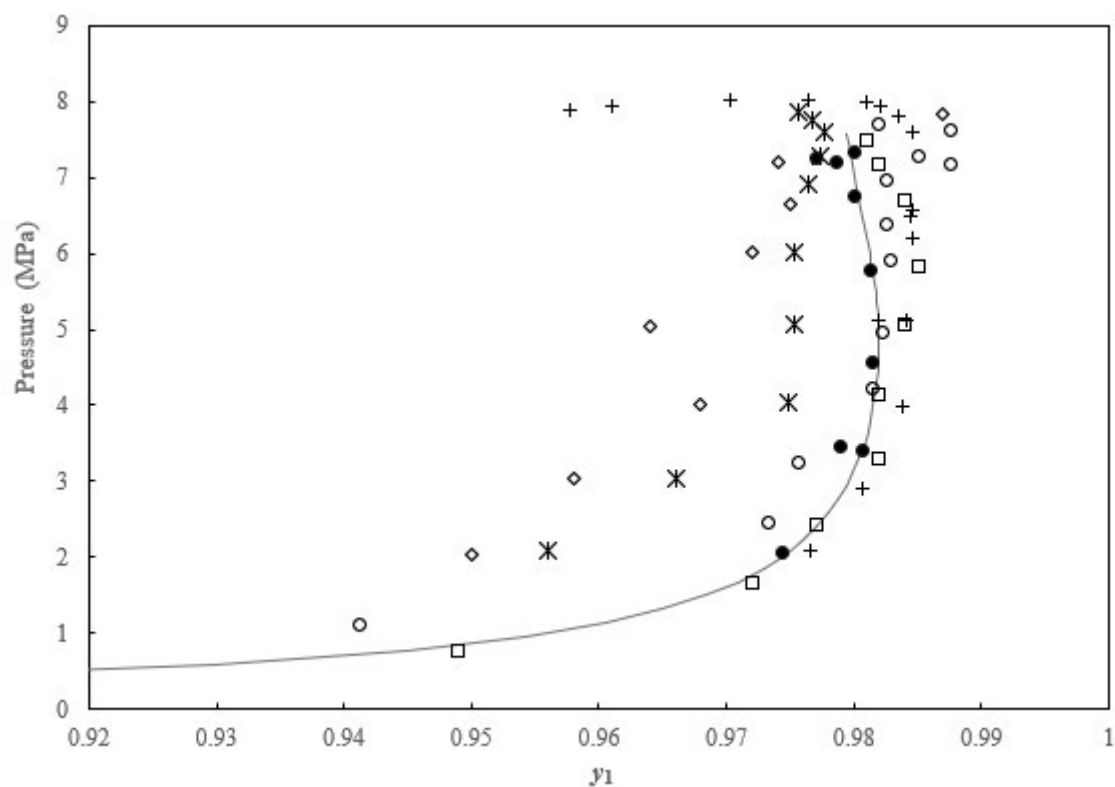


Figure C-1: *P*-*y* plot of CO₂ (1) + n-hexane (2) system.

This work at 313.19 K (●); Williams-Wynn et al. (Williams-Wynn et al., 2016) at 313.12 K (○); Chen and Chen (Chen and Chen, 1992) at 313.15 K (◇); Li et al. (Li et al., 1981) at 313.14 K (□); Wagner and Wichterle (Wagner and Wichterle, 1987) at 313.14 K (⋈); Nelson et al. (Nelson et al., 2021) at 313.15 K (+); PRSK model at 313.15 K (Solid continuous black line).

C.2 Carbon dioxide (1) + n-decane (2) system

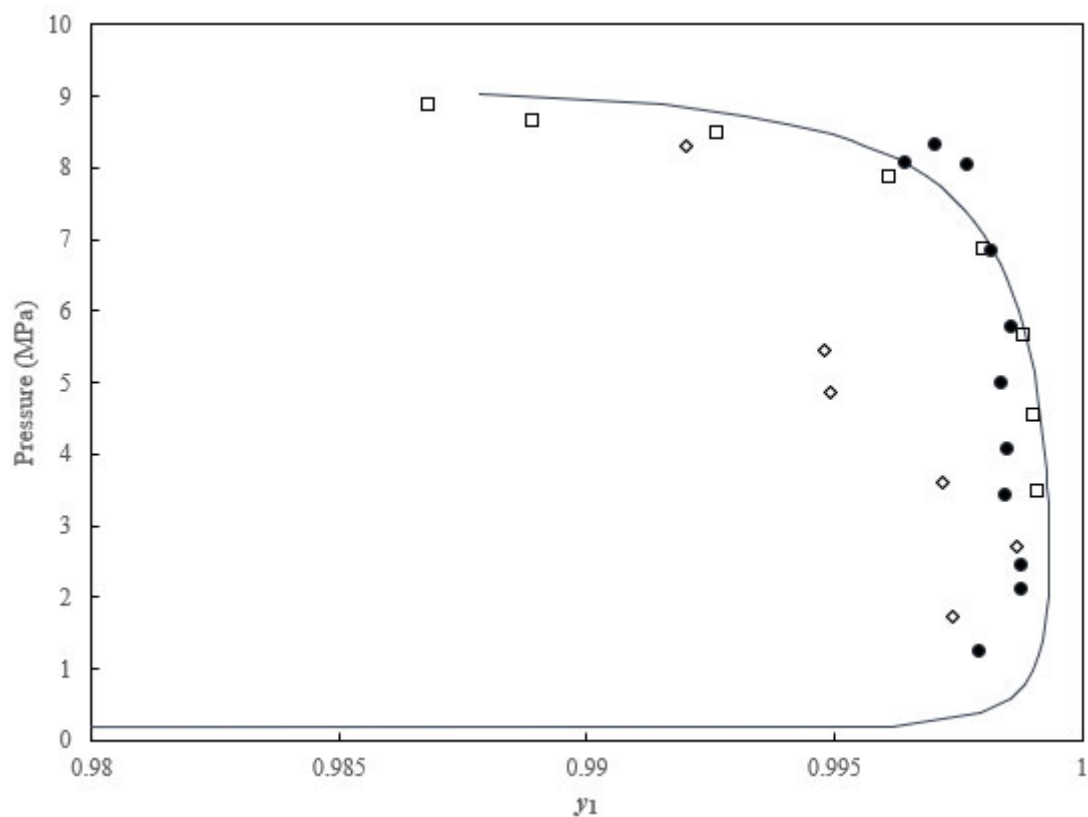


Figure C 2: *P*-*y* plot for the CO₂ (1) +n-decane (2) test system.

Figure C-2: *P*-*y* plot for the CO₂ (1) + n-decane (2) test system: This work at 319.23 K (●); Jimenez-Gallegos et al. (Jiménez-Gallegos et al., 2006) at 319.11 K (□); Zilnik et al. (Žilnik et al., 2016) at 319.10 K (◇); PRSK model at 319.15 K (continuous solid black line).

APPENDIX D. DESCRIPTION OF THERMODYNAMIC MODELS APPLIED IN THIS WORK

D.1. Equations of state (EsOS) models

An equation of state is a mathematical expression that relates pressure to the volume, absolute temperature or internal energy of a system (Ahmed, 2010; Avlonitis, 1992). An EOS plays a key part in VLE thermodynamic modelling for hydrocarbon fluids, particularly at high and moderate pressures (Orbey and Sandler, 1998).

D.1.1. Cubic equations of state

Cubic EsOS are equations that are cubic in volume and can describe both the liquid and the vapour phases. The formulation of the empirical cubic equation of state is centred on the expression of pressure as a sum of two terms namely attraction pressure ($P_{\text{attraction}}$) and repulsion pressure ($P_{\text{repulsion}}$) (Peng and Robinson, 1976). The $P_{\text{repulsion}}$ term is expressed using the Van der Waals (VdW) hard-sphere equation (Peng and Robinson, 1976):

$$P_{\text{repulsion}} = \frac{RT}{V - b} \quad (\text{D-1})$$

Where R is the gas constant, T is the temperature, V is the actual molar volume of a fluid, and b the minimum molar volume of a fluid; in other terms, b is defined as the co-volume (Ahmed, 2010; Dahm and Visco, 2015).

The $P_{\text{attraction}}$ term can be expressed as:

$$P_{\text{attraction}} = \frac{a}{g(V)} \quad (\text{D-2})$$

Where a is a constant which represents intermolecular attraction force between the molecules (Ahmed, 2010), and $g(V)$ is a function of molar volume (V).

A more general form for the representation of any form of the equation of state is given by:

$$P = P_{\text{repulsion}} - P_{\text{attraction}} \quad (\text{D-3})$$

Substituting equations (D-1) and (D-2) into equation (D-3) gives:

$$P = \frac{RT}{V - b} - \frac{a}{g(V)} \quad (\text{D-4})$$

In this work, the cubic equations of state applied were the SRK of (Soave, 1972) and the PR of (Peng and Robinson, 1976). Table D-1 represents these two classical cubic EsOS used in study.

Table D-1: SRK and PR EOS (Orbey and Sandler, 1998)

Equation of state	Expression
Soave-Redlich-Kwong (SRK)	$P = \frac{RT}{V-b} - \frac{a(T)}{V(V+b)}$ (D-5)
Peng-Robinson (PR)	$P = \frac{RT}{V-b} - \frac{a(T)}{V(V+b)+b(V-b)}$ (D-6)

Where parameters of equations (D-5) and (D-6) are defined in Table D-2.

The main weakness of the SRK EOS is the unrealistic universal value of 0.333 for the critical compressibility on all components. Therefore, the molar volumes are usually overestimated and, thus, densities are underestimated (Ahmed, 2010). The PR EOS predicts liquid densities better than the SRK EOS hence its more popular (Avlonitis, 1992). This is due to a more realistic constant critical compressibility factor value obtained by a suitable alteration of the attractive term. For all components, the SRK equation estimates critical compressibility to be equal to 0.333, while the PR equation yields 0.307. However, for most fluids, the experimental critical compressibility factor Z_c is approximately 0.28 (Avlonitis, 1992). Some of the limitations of the PR EOS are poor representation in the critical region, inaccurate liquid densities and that they are inapplicable to highly polar fluids such as water and electrolytes (Wu and Prausnitz, 1998).

Table D-2: Parameters for the SRK and PR EOS.

Parameter	Value	Units
P (Pressure)	System parameter	Pa
V (Molar volume)	System parameter	$\text{m}^3.\text{mol}^{-1}$
T (Temperature)	System parameter	K
R (Universal gas constant)	8.314	$\text{J mol}^{-1} \text{K}^{-1}$
a	Attractive parameter of component i	$\text{J.m}^3.\text{mol}^{-2}$
b	Co-volume of component i.	$\text{m}^3.\text{mol}^{-1}$

Evaluation of the attractive parameter (a)

The attractive parameter is a constant for the VdW equation of state, while for the PR and SRK EsOS, it is temperature dependent (Hajiw, 2014).

$$a(T) = \alpha a(T_c) \quad (\text{D-7})$$

and,

$$a(T_c) = \Omega a \frac{R^2 T_c^2}{P_c} ; \alpha = \left(1 + k \left(1 - \sqrt{\frac{T}{T_c}} \right) \right)^2 \quad (\text{D-8})$$

Where

- T_c and P_c are pure component critical temperature and critical pressure parameters.
- k is a constant characteristic of each component.
- α is the alpha function of the cubic EOS.

Alpha functions of EOS

As researchers sought improvements to the predictive accuracy of cubic equations of state, many variations of the alpha function were proposed. Alpha functions have an effect on the predictive capabilities of cubic equations of state for the thermodynamic properties (Zhao et al., 2019), and most of them are aimed at predicting specific components. A good alpha function can improve the prediction of the vapour pressure of pure compounds and the VLE of mixtures. This work made use of the Mathias Copeman function (MC); hence it is briefly discussed in this section. The expression for the MC function proposed by (Mathias and Copeman, 1983) is presented as:

$$\alpha = \left[1 + c_1(1 - \sqrt{T_r}) + c_2(1 - \sqrt{T_r})^2 + c_3(1 - \sqrt{T_r})^3 \right]^2 \quad (\text{D-9})$$

Where c_1 , c_2 , and c_3 are adjustable parameters that depend on the considered component and are determined from VLE data and is similar to k in equation (D-8); T_r is the reduced temperature which is expressed as T/T_c in equation (D-8).

Thus equation (D-8) is obtained when c_2 and c_3 are equal to zero in equation (D-9). (Mathias and Copeman, 1983) stated that the additional parameters c_2 and c_3 were necessary to correlate the vapour pressure of highly polar components such as methanol and water. For these reasons, the MC function was used in this work in the PR and PRWS models. The MC alpha function is used in the PSRK. For further details on alpha functions, the reader is referred to (Mathias and Copeman, 1983; Privat et al., 2015; Twu et al., 1991; Zhao et al., 2019).

Table D-3: Parameters of the attractive parameter (Hajiw, 2014)

Equation of State	Ωa	k
SRK	≈ 0.42748	$k = 0.48508 + 1.551716\omega_i - 0.15613\omega_i^2$ (D-10)
PR	≈ 0.47236 Or = 0.45724 according to (Peng and Robinson, 1976)	$\text{if } \omega_i \leq 0.491$ $k_i = 0.37464 + 1.54226\omega_i - 0.26992\omega_i^2$ (D-11) $\text{if } \omega_i > 0.49$ $k_i = 0.379642 + 1.48503\omega_i - 0.164423\omega_i^2 + 0.016666\omega_i^3$ (D-12)

Where ω_i is the acentric factor of component i .

Calculation of the co-volume parameter (b)

Unlike the attractive parameter a , which is temperature dependant, the co-volume parameter b is temperature independent (Mathias and Copeman, 1983).

The expression for the co-volume parameter (b) for the PR and SRK EsOS is presented as:

$$b = \Omega_b \frac{RT_c}{P_c} \quad (\text{D-13})$$

Table D-4 presents parameters for the co-volume parameter for both the SRK and PR EOS.

Table D-4: Parameters of the co-volume parameter (Hajiw, 2014).

Equation of State	Ω_b
SRK	0.08664
PR	0.07780

Compressibility factor (Z)

To calculate the fugacity coefficients, the EOS is expressed in terms of the compressibility factor Z . This is done by replacing the molar volume in equations (D-5) and (D-6) with (ZRT/P) and rearranging. In this form the SRK EOS is:

$$Z^3 - Z^2 + Z(A - B - B^2) - AB = 0 \quad (\text{D-14})$$

Where

$$A = \frac{aP}{R^2T^2} \quad (D-15)$$

$$B = \frac{bP}{RT} \quad (D-16)$$

$$Z = \frac{PV}{RT} \quad (D-17)$$

The PR EOS is presented in the form (Peng and Robinson, 1976):

$$Z^3 - (1 - B)Z^2 + Z(A - 3B^2 - 2B) - (AB - B^2 - B^3) = 0 \quad (D-18)$$

Equations (D-14) and (D-18) produces one or three roots subject to the number of phases in the system (Ahmed, 2010; Peng and Robinson, 1976). Using an appropriate method, the roots of Z for a two-phase system are computed with the greatest value assigned to the vapour phase, the intermediate value has no physical meaning, and the lowest value is assigned to the liquid phase. The coefficients A and B for the PR EOS are computed using the same equations above for the SRK EOS.

Fugacity coefficient from cubic EOS

For the SRK EOS, the fugacity coefficient for a pure component is given by (Ahmed, 2010)

$$\ln \phi = Z - 1 - \ln(Z - B) - \frac{A}{B} \ln \left(\frac{Z + B}{Z} \right) \quad (D-19)$$

For the PR EOS, fugacity coefficient for a pure component is given by (Orbey and Sandler, 1998) :

$$\ln \phi = (Z - 1) - \ln(Z - B) - \frac{A}{2\sqrt{2}B} \ln \left(\frac{Z + (1 + \sqrt{2})B}{Z + (1 - \sqrt{2})B} \right) \quad (D-20)$$

The PR fugacity coefficient of component *i* in a mixture is given by (Orbey and Sandler, 1998):

$$\ln \bar{\phi}_i = \frac{b_i}{b_{mix}} (Z - 1) - \ln(Z - B) - \frac{A}{(2\sqrt{2}) * B} \left(\frac{2 \sum_{i=1}^n x_i a_{ik}}{a_{mix}} - \frac{b_i}{b_{mix}} \right) \ln \left(\frac{Z + 2.414B}{Z - 0.414B} \right) \quad (D-21)$$

D.1.1.1. Classical mixing rules

Besides being applicable to pure components, equations (D-5) and (D-6) are applicable to multicomponent systems provided mixing rules are utilised in determining the mixture co-volume and the attraction parameters. Mixing rules are the rules that govern the combination of composition and pure component parameters to derive mixture properties (Avlonitis, 1992). The combination of two-

parameter cubic EsOS with the classical Van der Waals mixing rules is the most widely used modelling tool by practising engineers for the VLE of hydrocarbons with organic gases and hydrocarbon mixtures (Orbey and Sandler, 1998). Van der Waals mixing rules are shown below (Avlonitis, 1992; Haji, 2014).

$$a_{mix} = \sum_i \sum_j x_i x_j a_{ij} \quad (D-22)$$

Where

$$a_{ij} = \sqrt{a_i a_j} (1 - k_{ij}) \quad (D-23)$$

and

$$b_{mix} = \sum_i x_i b_i \quad (D-24)$$

Where k_{ij} is the binary interaction parameter.

The conventional Van der Waals mixing rules are easy to use; however, their limitation is that they struggle to correlate or predict VLE of complex mixtures (Orbey and Sandler, 1998).

D.2. Activity coefficient models

D.2.1 The Non-random two liquid (NRTL) activity coefficient model

The NRTL model was proposed by (Renon and Prausnitz, 1968) . The NRTL expression for the excess Gibbs energy of a binary mixture is a function of mole fractions x_i and x_j and is expressed as (Kontogeorgis and Folas, 2010; Renon and Prausnitz, 1969, 1968) :

$$\frac{g^E}{RT} = x_i x_j \left(\frac{\tau_{ij} G_{ij}}{x_j + x_i G_{ij}} + \frac{\tau_{ji} G_{ji}}{x_i + x_j G_{ji}} \right) \quad (D-25)$$

Where:

$$G_{ij} = \exp(-a_{ij} \tau_{ij}) \quad (D-26)$$

$$G_{ji} = \exp(-a_{ij} \tau_{ji}) \quad (D-27)$$

$$\tau_{ij} = \frac{g_{ij} - g_{jj}}{RT} \quad (D-28)$$

$$\tau_{ji} = \frac{g_{ji} - g_{ii}}{RT} \quad (D-29)$$

with

$$g_{ij} = g_{ji} \quad (D-30)$$

g_{ij} represents the energy of interaction between components i and j .

Thus equation (D-25) has two temperature-dependent parameters, namely, $(g_{ij} - g_{jj})$ and $(g_{ji} - g_{ii})$ plus a non-randomness parameter a_{ij} which is temperature independent and is usually estimated from nature of components i and j .

The activity coefficient for a component i in a binary mixture of components i and j is determined after differentiating equation (D-25) and is expressed as:

$$\ln \gamma_i = x_j^2 \left[\tau_{ji} \left(\frac{G_{ji}}{x_i + x_j G_{ji}} \right)^2 + \frac{\tau_{ij} G_{ij}}{(x_j + x_i G_{ij})^2} \right] \quad (D-31)$$

Where x_i is the liquid mole fraction;

$$a_{ij} = c_{ij} + d_{ij}(T - 273.15) \quad (D-32)$$

Where T is the temperature in Kelvins; d_{ij} is set to zero in this work; c_{ij} can be considered an unadjustable parameter and is usually fixed at 0.3. Parameter c_{ij} is unitless. Some of Renon and Prausnitz's recommendations for a_{ij} are as follows (Renon and Prausnitz, 1968):

- 0.2 for polar non-associated components with saturated hydrocarbons
- 0.3 for polar components-water, polar mixtures and non-polar components
- 0.47 for strongly self-associated components-non-polar components, two polar components, self-associated component-water. These systems exhibit a high degree of non-randomness. For such systems, better fits are produced when a_{ij} is used as an adjustable parameter, with optimum values in the range of 0.40 to 0.55.

D.3. Wong Sandler (WS) mixing rules and its application in the PRWS model

The Wong-Sandler mixing rules use the following approximation:

$$A_{EOS}^E(T, P = \infty, x) = A_{\gamma}^E(T, P = \infty, x) = A_{\gamma}^E(T, low P, x) = G_{\gamma}^E(T, low P, x) \quad (D-33)$$

Where subscripts EOS and γ represents the equation of state and activity coefficient models, respectively.

For the co-volume parameter, the mixing rule parameter b_m is defined as:

$$b_m = \frac{RT \sum_i \sum_j x_i x_j \left(b_{ij} - \frac{a_{ij}}{RT} \right)}{RT - \left[\sum_i x_i \frac{a_i}{b_i} + \frac{A_{EOS}^E(T, P = \infty, x_i)}{C^*} \right]} \quad (D-34)$$

Where $A_{EOS}^E(T, P = \infty, x_i)$ is the Helmholtz free energy at infinite pressure from the EOS, which is assumed to be similar to the excess Gibbs energy of the activity coefficient model at low pressure. The mixing rule energy parameter a_{mix} is defined as:

$$a_{mix} = b_m \left(\sum_i x_i \frac{a_i}{b_i} + \frac{A_{EOS}^E(T, P = \infty, x_i)}{C^*} \right) \quad (D-35)$$

For the Peng-Robinson (PR) EOS, C^* is

$$C^* = -\frac{1}{\sqrt{2}} \ln(1 + \sqrt{2}) \quad (D-36)$$

And

$$\left(b - \frac{a}{RT} \right) = \sum_i \sum_j x_i x_j \left(b_{ij} - \frac{a_{ij}}{RT} \right) \quad (D-37)$$

with

$$\left(b_{ij} - \frac{a_{ij}}{RT} \right) = \frac{1}{2} \left[\left(b_i - \frac{a_i}{RT} \right) + \left(b_j - \frac{a_j}{RT} \right) \right] (1 - k_{ij}) \quad (D-38)$$

The unitless binary interaction parameter k_{ij} for the second virial coefficient in equation (D-38) is incorporated into the mixing rule and therefore the equation of state. Generally, excellent results have been obtained for polar (symmetric compounds) with the WS mixing rule (Kontogeorgis and Folas, 2010).

The excess Helmholtz free energy at infinite pressure from the EOS, $A_{EOS}^E(T, P = \infty, x_i)/RT$ is:

$$\frac{A_{EOS}^E(T, P = \infty, x_i)}{C^* RT} = \frac{a_m}{b_m RT} - \sum_i x_i \frac{a_i}{b_i RT} \quad (D-39)$$

The mixture's thermodynamic properties can now be computed. The fugacity coefficient can now be calculated using:

$$\ln \varphi_i = \int_V^\infty \left[\frac{1}{RT} \left(\frac{\partial P}{\partial n_i} \right)_{T, V, n_j} - \frac{1}{V} \right] dV - \ln \left(\frac{PV}{RT} \right) \quad (D-40)$$

For the PR EOS, after derivations described in (Wong and Sandler, 1992), the following results:

$$\frac{\partial nD}{\partial n_i} = \frac{a_i}{b_i RT} + \frac{\ln \gamma_{\infty i}}{C^*} \quad (\text{D-41})$$

Where D is:

$$D = \left(\sum_i x_i \frac{a_i}{b_i RT} + \frac{A_{EoS}^E(T, P = \infty, x_i)}{C^* RT} \right) \quad (\text{D-42})$$

with

$$\ln \gamma_{\infty i} = \frac{1}{RT} \frac{\partial n A_{EoS}^E(T, P = \infty, x_i)}{\partial n_i} \quad (\text{D-43})$$

For the excess Gibbs free energy model (NRTL) in this study, $A_{\gamma}^E(T, P = \infty, x_i)/RT$ is:

$$\frac{A_{\gamma}^E(T, P = \infty, x_i)}{RT} = \sum_i x_i \left(\frac{\sum_j x_j \tau_{ji} G_{ji}}{\sum_k x_k G_{ki}} \right) \quad (\text{D-44})$$

The partial derivative of $A_{\gamma}^E(T, P = \infty, x_i)/RT$ with respect to the mole number of each component, which is the logarithm of the component activity coefficient is given by:

$$\ln \gamma_{\infty i} = \frac{\sum_j x_j \tau_{ji} G_{ji}}{\sum_k x_k G_{ki}} + \sum_j \frac{x_j G_{ij}}{x_k G_{kj}} \left(\tau_{ij} - \frac{\sum_i x_i \tau_{ij} G_{ij}}{\sum_k x_k G_{ki}} \right) \quad (\text{D-45})$$

D.4 Association models

D.4.1. The Perturbed-Chain Statistical Associating Fluid Theory (PC-SAFT) model

For pure compounds, a maximum of five parameters are needed to employ the model. These parameters are:

- i. (m) the segment number, or the number of segments per chain (PCSFTM)
- ii. (σ) the segment diameter in Å, or the segment size parameter (PCSFTV)
- iii. (ϵ) the segment energy parameter in K, (PCSFTU)
- iv. ($\beta^{A_i B_i}$) the association volume parameter, (PCSFAV)
- v. ($\epsilon^{A_i B_i}$) the association energy parameter in K, (PCSFAU)

Note that the abbreviations in brackets are the representative terminologies used in aspen.

Geometric parameters (i to iii) are needed for every component, whilst association parameters (iv and v) are only needed if the component is self-associating and hence, the association scheme of the

component must be established. Association parameters can be computed from molecular orbital calculations or based on experimental measurements of the entropy and enthalpy of hydrogen, whilst the geometric parameters can be fitted to liquid densities and vapour pressures (Kontogeorgis and Folas, 2010).

The segment diameter is usually a constant for the different compounds, whilst “*the segment energy usually increases with molecular weight and becomes a constant for heavier molecules of a homologous series*” (Kontogeorgis and Folas, 2010). Generally, the parameters show a well-defined trend for compounds of the same homologous series (Kontogeorgis and Folas, 2010).

The crucial relation in Wertheim’s theory concerns the fraction of molecules not bonded at a specific site X^A and the residual Helmholtz energy due to association. X^A is related to the association strength, and $\Delta^{A_i B_j}$, which is defined as (Kontogeorgis and Folas, 2010):

$$\Delta^{A_i B_j} = d_{ij}^3 g_{ij}(d_{ij})^{seg} K^{A_i B_j} \left[\exp\left(\frac{\varepsilon^{A_i B_j}}{kT}\right) - 1 \right] \quad (D-46)$$

where g is the radial distribution function.

The association strength is represented by a square well potential and is characterised by two parameters, which are the association energy ($\varepsilon^{A_i B_i}$); and the association volume ($\beta^{A_i B_i}$ or $K^{A_i B_j}$). These properties can be related to spectroscopic properties.

The association term represented by Z , the compressibility factor, is expressed as follows

$$Z^{as} = -\frac{1}{2} \left(1 + \rho \frac{\partial \ln g}{\partial \rho} \right) \sum_i x_i \sum_{A_i} (1 - X_{A_i}) \quad (D-47)$$

The residual Helmholtz energy is defined as (Kontogeorgis and Folas, 2010):

$$a^{res} = a^{sg} + a^{chn} + a^{as} \quad (D-48)$$

Where a^{res} is the residual Helmholtz energy; a^{sg} is the Helmholtz energy of the segment which includes both the dispersion and the hard-sphere reference terms; a^{chn} is the chain formation contribution; and a^{as} is the contribution from association.

In the different forms of the SAFT equation, Wertheim’s contributions account for the expression of the chain and association terms. The chain term is expressed as (Kontogeorgis and Folas, 2010):

$$\frac{a^{chn}}{RT} = \sum_i x_i (1 - m_i) \ln(g_{ii} (d_{ii})^{hs}) \quad (D-49)$$

Where m is the number of segments or chain length; d is the segment diameter,

The association term is defined as (Kontogeorgis and Folas, 2010):

$$\frac{a^{as}}{RT} = \sum_i x_i \left[\sum_{A_i} \left(\ln X^{A_i} - \frac{X^{A_i}}{2} \right) + \frac{1}{2} M_i \right] \quad (D-50)$$

Where X^{A_i} represents fraction of molecules i not bonded to site A; M_i represents the number of association sites on molecule i .

X^{A_i} is related to the association strength $\Delta^{A_i B_j}$ between two sites of two different components, in this case, site A of component i and site B of component j .

$$X^{A_i} = \frac{1}{1 + \rho \sum_j x_j \sum_{B_j} X_{B_j} \Delta^{A_i B_j}} \quad (D-51)$$

B_j represents summation over all sites

ρ is the molar density of the fluid, x_j is the mole fraction of component j .

$\Delta^{A_i B_j}$ is the association strength.

X_B represent the fractions of all other kind of association sites B.

Both X^{A_i} and $\Delta^{A_i B_j}$ depend on the structure of the molecule and the type and number of sites.

X^{A_i} has been defined in equation (D-51), from where the association strength $\Delta^{A_i B_j}$ is defined as (Kontogeorgis and Folas, 2010):

$$\Delta^{A_i B_j} = d_{ij}^3 g_{ij} (d_{ij})^{sg} k^{A_i B_j} \left[\exp \left(\frac{\varepsilon^{A_i B_j}}{kT} \right) - 1 \right] \quad (D-52)$$

Where k is the Boltzmann factor; T is temperature; g_{ij} or sometimes is the radial distribution function.

The simplified version of the radial distribution function g_{ij} or sometimes $g(\rho)$ is given by the expression (Kontogeorgis et al., 2006):

$$g(\rho) = \frac{1}{1 - 1.9\eta} \quad (D-53)$$

Where η is the reduced fluid density, which is given by (Hajiw, 2014):

$$\eta = \frac{1}{4} b \rho = \frac{b}{4V} \quad (\text{D-54})$$

Where ρ is the fluid density b is the co-volume parameter which is believed to be temperature independent.

For the PC-SAFT equation which has been employed in this work, the temperature-independent diameter (σ) is employed in the association strength term. The temperature dependency of the size parameter has a physical meaning since real molecules are not hard spheres (Kontogeorgis and Folas, 2010). At high temperatures, there is some interpenetration of molecules, consequently, the effective hard-sphere diameter of a segment is reduced (Kontogeorgis and Folas, 2010). However, the effect of this is small in practical applications (Kontogeorgis and Folas, 2010). The simplified radial distribution function defined in equation (D-53) is used for the simplified PC-SAFT equation of state. The Helmholtz energy for the dispersion term in the PC-SAFT EOS is given by the expression (Kontogeorgis and Folas, 2010):

$$\frac{a^{dsp}}{kTN} = \frac{A_1}{kTN} + \frac{A_2}{kTN} \quad (\text{D-55})$$

Where:

$$\frac{A_1}{kTN} = -2\pi\rho m^2 \left(\frac{\varepsilon}{kT}\right) \sigma^3 \int_1^\infty \check{u}(x) g^{hc} \left(m; \frac{x\sigma}{d}\right) x^2 dx \quad (\text{D-56})$$

$$\frac{A_2}{kTN} = -\pi\rho m \left(1 + Z^{hc} + \rho \frac{\partial Z^{hc}}{\partial \rho}\right)^{-1} m^2 \left(\frac{\varepsilon}{kT}\right)^2 \sigma^3 \frac{\partial}{\partial \rho} \left[\rho \int_1^\infty \check{u}(x) g^{hc} \left(m; \frac{x\sigma}{d}\right) x^2 dx \right] \quad (\text{D-57})$$

Where $= \frac{r}{\sigma}$; $\check{u}(x) = \frac{u(x)}{\varepsilon}$ is the reduced intermolecular potential.

Expressions for the radial distribution function in equation (D-52) and the simplification of integrals in equations (D-56) and (D-57) are detailed in (Kontogeorgis and Folas, 2010).

(Solms, et al., 2003) proposed a simplified PC-SAFT equation of state to ease programming and computational effort without affecting the model's performance. The simplified PC-SAFT considers that segment diameters are normally alike for segments of different molecules, thus enabling it to employ simple mixing rules (Grenner et al., 2007). Consequently, the simplified PC-SAFT is similar to the original PC-SAFT in the case of non-associating molecules; however, in the case of associating molecules and multicomponent mixtures in general, it is different to the original PC-SAFT

(Kontogeorgis and Folas, 2010). This also means that the pure compound parameters of the original and simplified PC-SAFT are the same (Kontogeorgis and Folas, 2010).

The Helmholtz energy for a mixture of associating compounds is expressed as follows under the simplified PC-SAFT EOS (Kontogeorgis and Folas, 2010):

$$a^{res} = ma^{hs} + a^{chn} + a^{dsp} + a^{as} \quad (D-58)$$

Where m is the average chain length; a^{hs} is the hard-sphere reference; a^{chn} is the chain contribution term; a^{dsp} is the dispersion term; and a^{as} is the association term.

The diameter of segments is evaluated by setting the volume fraction = ζ_3 ; where (Grenner et al., 2007):

$$\eta = \frac{\pi \rho d^3}{6} \sum_i x_i m_i \quad (D-59)$$

And d is given by (Grenner et al., 2007; Kontogeorgis and Folas, 2010)

$$d = \left(\frac{\sum_i x_i m_i d_i^3}{\sum_i x_i m_i} \right)^{\frac{1}{3}} \quad (D-60)$$

The hard-sphere and association equations are simplified, thus radial distribution function equation and the Carnahan-Starling equation for the hard-sphere mixture reference system, all presented by (Kontogeorgis and Folas, 2010), reduces respectively to:

$$g^{hs}(d^+) = \frac{2 - \eta}{2(1 - \eta)^3} \quad (D-61)$$

$$a^{hs} = \frac{4\eta - 3\eta^2}{(1 - \eta)^2} \quad (D-62)$$

The necessary equations for calculating fugacity using the simplified PC-SAFT EOS are available in (Kontogeorgis and Folas, 2010), and thus not presented in this work. Reported pure component parameters for the PC-SAFT EOS are shown in Table D-5

Table D-5: Pure component parameters for the PC-SAFT EOS.

All water and glycols were modelled using the 4C scheme. For methanol, a 2B scheme has been used.

Reference	Component	m	σ (Å)	ϵ (K)	$\beta^{A_i B_i}$	$\epsilon^{A_i B_i}$ (K)
a	Methane	1.0000	3.7039	150.03		
a	Propane	2.0020	3.6184	208.11		
a	n-Hexane	3.0576	3.7983	236.77		
a	n-Decane	4.6627	3.8384	243.87		
a	CO ₂	2.7852	2.0729	169.21		
b	Water	1.50	2.6273	180.30	0.0942	1804.22
c	Methanol	1.5255	3.2300	188.90	0.035176	2899.50
b	TEG	3.18092	4.0186	333.17	0.0235	2080.03
d	TEG	3.4039	3.921111	324.78	0.01963	2148.16

References: a: (Gross and Sadowski, 2001); b: (Grenner et al., 2007); c:(Gross and Sadowski, 2002) ; d: (Teymouri, 2016)

D.4.1.1. Mixtures

Mixing rules are not needed in the association and chain terms of the PC-SAFT EOS. Mixing rules are required in the dispersion term. Furthermore, combining rules are required in the diameter (or volume) and segment energy parameters and the Lorentz–Berthelot rules are normally used (Kontogeorgis and Folas, 2010). A binary interaction parameter k_{ij} is mostly utilised in the combining rule for the energy parameter (Kontogeorgis and Folas, 2010). Mostly the Van der Waals one-fluid mixing rules are used.

The Lorentz–Berthelot combining rules, as used for PC–SAFT are presented as (Kontogeorgis and Folas, 2010):

$$\epsilon_{ij} = \sqrt{\epsilon_i \epsilon_j} (1 - k_{ij}) \quad \sigma_{ij} = \frac{\sigma_i + \sigma_j}{2} \quad (D-63)$$

Where k_{ij} is corrects the dispersion energies of dissimilar components. k_{ij} must be optimised from experimental data (Kontogeorgis and Folas, 2010).

For the PC-SAFT EOS, a slight positive k_{ij} required is needed to obtain an excellent correlation (Kontogeorgis and Folas, 2010). The same k_{ij} value can successfully be utilised for diverse gas-alkane systems depending only on the gas and not the alkane used (Kontogeorgis and Folas, 2010). Combining rules are required for association parameters of cross-associating molecules. The two successful ones are the CR-1 rule and Elliott’s rule (Folas et al., 2005; Wolbach and Sandler, 1998), presented in equations (D-64) and (D-65) respectively

$$\epsilon^{A_i B_j} = \frac{\epsilon^{A_i B_i} + \epsilon^{A_j B_j}}{2} \quad \beta^{A_i B_j} = \sqrt{\beta^{A_i B_i} \beta^{A_j B_j}} \quad (D-64)$$

$$\epsilon^{A_i B_j} = \frac{\epsilon^{A_i B_i} + \epsilon^{A_j B_j}}{2} \quad \beta^{A_i B_j} = \sqrt{\beta^{A_i B_i} \beta^{A_j B_j}} \left(\frac{\sqrt{\sigma_i \sigma_j}}{\sigma_{ij}} \right)^3 \quad (D-65)$$

Equation (D-64) above is similar to the square root of the cross-association strength.

$$\Delta^{A_i B_j} = \sqrt{\Delta^{A_i B_i} \Delta^{A_j B_j}} \quad (\text{D-66})$$

The difference between equations (D-64) and (D-65) is expected to be small except when applying the cubic plus association model described below. This is because the segment diameter values are alike even for distinct components (Kontogeorgis and Folas, 2010).

D.4.2. Cubic Plus Association (CPA) EOS

The CPA, is a sum of the association and the SRK terms and can be expressed as (Kontogeorgis and Folas, 2010):

$$P = \frac{RT}{V_m - b} - \frac{a(T)}{V_m(V_m + b)} - \frac{1}{2} \frac{RT}{V_m} \left(1 + \rho \frac{\partial \ln(g)}{\partial \rho} \right) \sum_i x_i \sum_{Ai} (1 - X^{Ai}) \quad (\text{D-67})$$

Where P is the pressure

ρ is the molar density ($= \frac{1}{V_m}$)

X^{Ai} is the mole fraction of site A, on component i , not bonded to other active sites (Frost et al., 2014).

x_i is the mole fraction of component i .

X^{Ai} is related to the association strength $\Delta^{A_i B_j}$ between two sites of two different components, in this case, site A of component i and site B of component j and is presented in equation (D-51).

Both X^{Ai} and $\Delta^{A_i B_j}$ depend on the structure of the component and the type and number of sites.

The association (binding) strength between site A on molecule i , and site B on molecule j is expressed as:

$$\Delta^{A_i B_j} = g(\rho) \left[\exp \left(\frac{\varepsilon^{A_i B_j}}{RT} \right) - 1 \right] \beta^{A_i B_j} b_{ij} \quad (\text{D-68})$$

Where $g(\rho)$ is the radial distribution function, $\beta^{A_i B_j}$ and $\varepsilon^{A_i B_j}$ are the volume parameter of the CPA and the association energy, respectively, b is the co-volume parameter from the cubic part of the model,

b_{ij} is given by

$$b_{ij} = \frac{b_i + b_j}{2} \quad (\text{D-69})$$

The simplified version of the radial distribution function applied in the CPA is presented in equation (D-53). The energy parameter $a(T)$ of the CPA EOS is obtained using a Soave-type temperature dependency, while b is temperature independent.

$$a(T) = a_0(1 + c_1(1 - \sqrt{T_r}))^2 \quad (D-70)$$

Where T_r is equal to T/T_c and T_c is the critical temperature.

Thus, the CPA has five parameters, two of which are used for associating components only and these are the $\beta^{A_i B_j}$ association volume parameter (CPAAV) and $\varepsilon^{A_i B_j}$ the association energy parameter (CPAAU). Then the three parameters applicable to all components are: a_0 the attractive parameter of component i , b the co-volume parameter of component i , and c a constant characteristic of each component. Instead of the last three parameters, the monomer critical temperature (CPATC), CPAPC (the critical pressure), and CPAM which is the M parameter of the alpha function of the CPA model is sometimes required. In this work, the CPA binary cross volume association parameter (CPAVIJ) is represented by C_{ij} for the components i and j . The conventional mixing rules are applied in the physical term (SRK) for the energy and co-volume parameters when the CPA is applied to mixtures. An alternate approach that can be used so as to evaluate equation (D-70) without the inconvenience of having to know the experimental critical temperature is the estimation of the three monomer parameters using the conventional SRK expressions (Kontogeorgis et al., 2006).

$$a = \Omega_A \left(\frac{R^2 T_{cm}^2}{P_{cm}} \right) \left[1 + m_m \left(1 - \sqrt{\frac{T}{T_{cm}}} \right) \right]^2 \quad (D-71)$$

$$b = \Omega_B \left(\frac{RT_{cm}}{P_{cm}} \right) \quad (D-72)$$

Where $\Omega_A = 0.42748$ and $\Omega_B = 0.08664$

The critical parameters and the “m” (monomer) parameters can be evaluated from liquid density and vapour pressure data (Kontogeorgis et al., 2006). From equations (D-71) and (D-72), the following expressions are obtained:

$$m_m = c_1 \sqrt{\frac{a_0 \Omega_B}{b_{CPA} R T_c \Omega_A}} \quad (D-73)$$

$$T_{cm} = T_c \left[\frac{1 + \left(\frac{1}{c_1} \right)}{1 + \left(\frac{1}{m_m} \right)} \right]^2 \quad (\text{D-74})$$

$$P_{cm} = \frac{\Omega_B R T_{cm}}{b_{CPA}} \quad (\text{D-75})$$

Using the equations (D-73 to D-75), and the CPA parameters (a_0 , b_{CPA} , c_1), the resultant monomer parameters can be estimated and this means that the monomer critical pressure, temperature and m parameters can be used instead.

Mixing and combining rules for the CPA EOS

As has been previously shown for cubic EOS, mixing rules are needed to extend the EOS to mixtures, and the same also applies for the CPA EOS. In the CPA EOS, mixing rules are needed for the physical part (SRK) part in this case. The mixing and combining rules for a and b are the classical VdW one fluid theory and have already been defined in equations (D-22 to D-24).

Combining rule: Cross associating mixtures

Combining rules are needed for the association energy term ε^{AiBj} and volume β^{AiBj} parameters between different cross associating molecules such as (glycol + water or alcohol + water) systems. These enable the computation of the association strength. These are similar to those presented for the PC-SAFT EOS in equations (D-64) and (D-65).

APPENDIX E MODELLING RESULTS

E.1. CPA analysis and flash results comparison using either literature k_{ij} or k_{ij} from this work for binary systems of interest

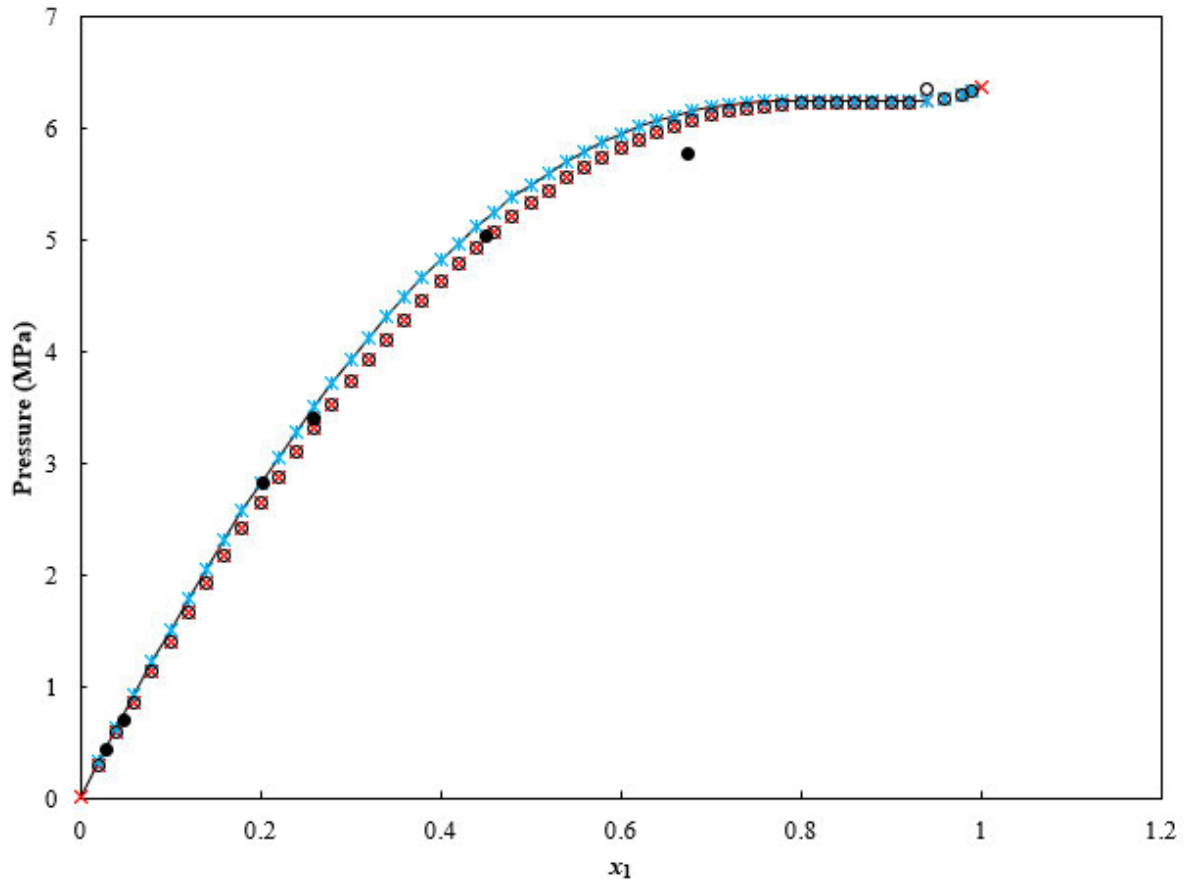


Figure E-1.1: CPA flash and analysis results comparison for thermodynamic modelling of the CO₂ (1) + CH₃OH (2) test system at 298.10 K.

(●) Experimental data, this work; (○) Flash results using k_{ij} from this work; (x) Analysis results using k_{ij} from this work; (⋈) Flash results using literature k_{ij} ; (—) Analysis results using literature k_{ij} .

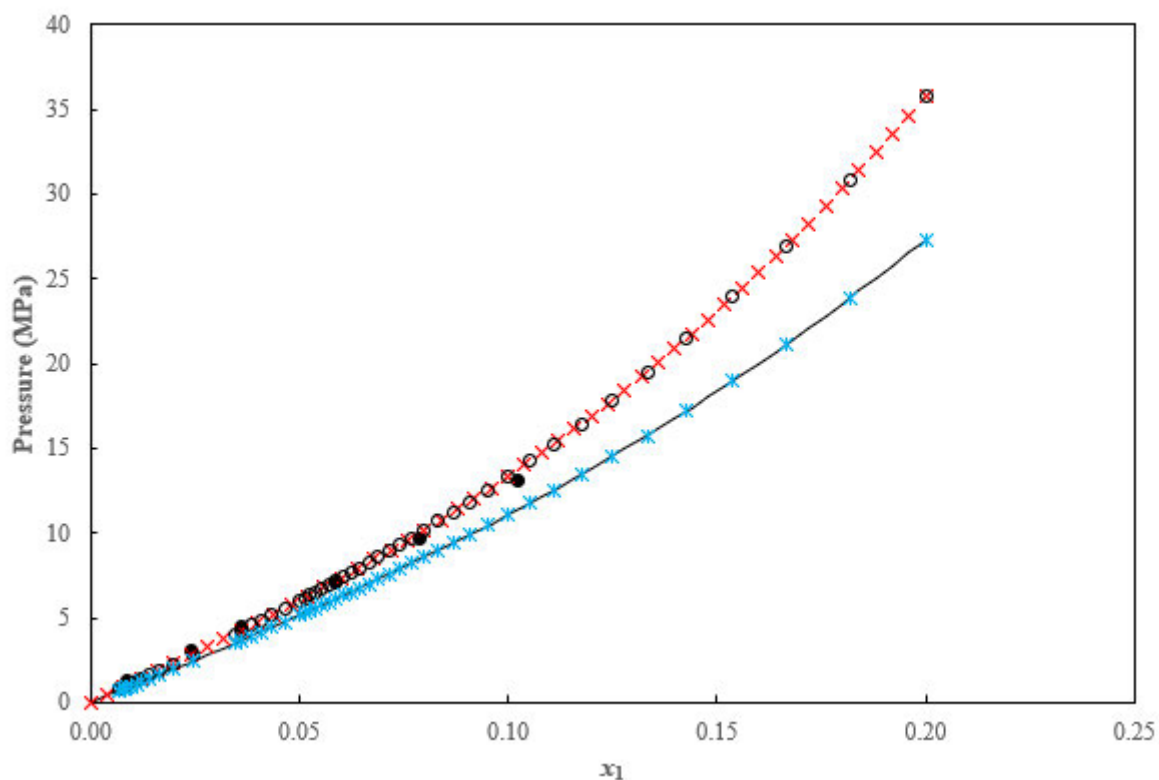


Figure E-1.2: CPA flash and analysis results comparison for thermodynamic modelling of the CH_4 (1) + CH_3OH (2) test system at 298.15 K.

(●) Experimental data, this work; (○) Flash results using k_{ij} from this work; (x) Analysis results using k_{ij} from this work; (x) Flash results using literature k_{ij} ; (—) Analysis results using literature k_{ij} .

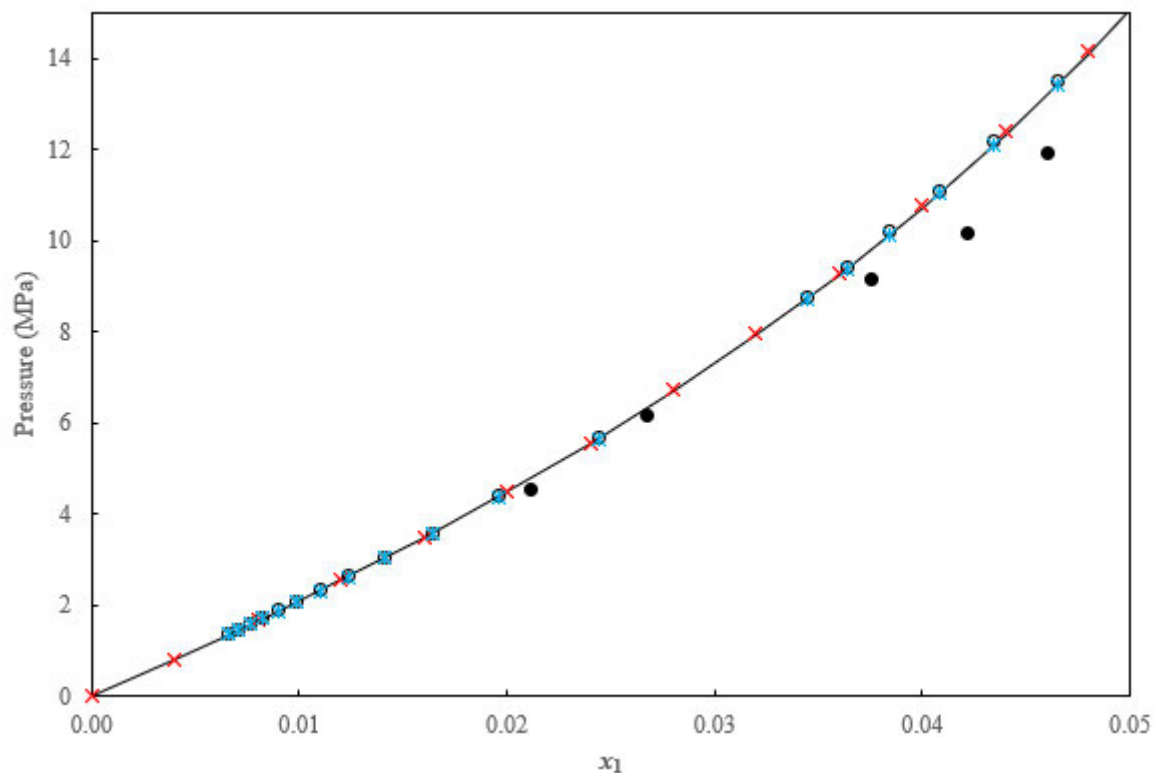


Figure E-1.3: CPA flash and analysis results comparison for thermodynamic modelling of the CH_4 (1) + TEG (2) test system at 298.15 K.

(•) Experimental data, this work; (○) Flash results using k_{ij} from this work; (x) Analysis results using k_{ij} from this work; (x) Flash results using literature k_{ij} ; (—) Analysis results using literature k_{ij} .

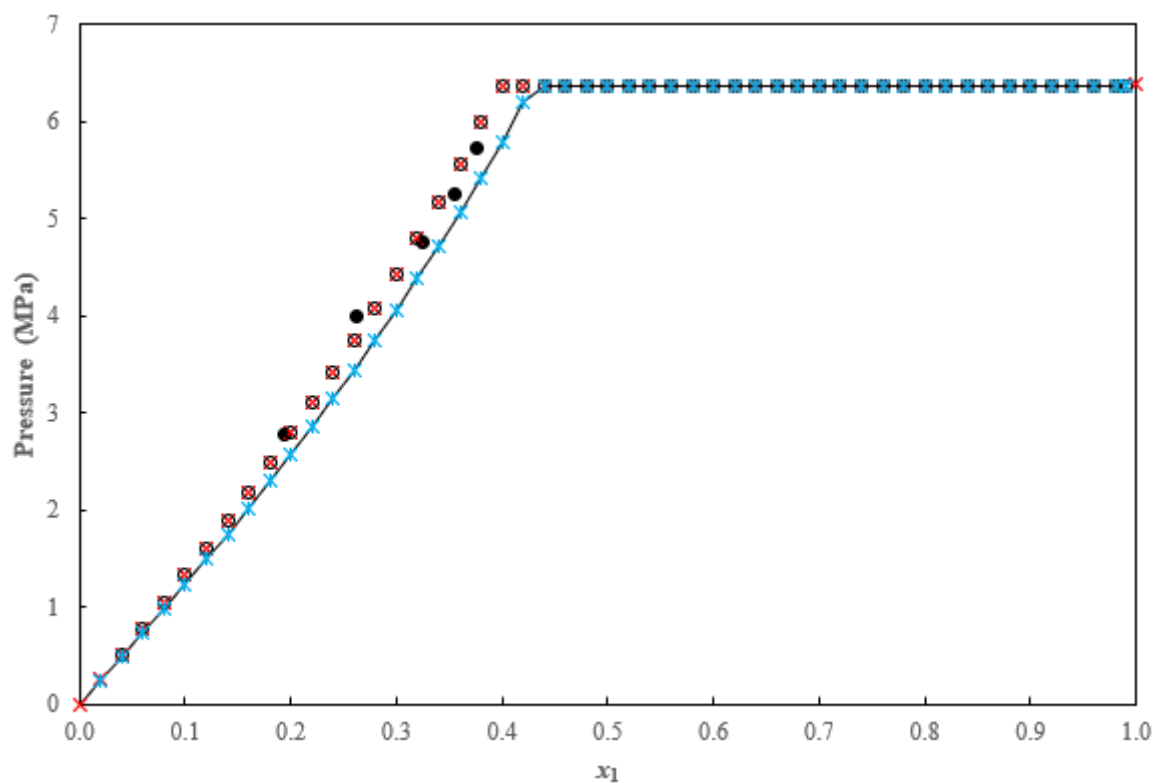


Figure E-1.4: CPA flash and analysis results comparison for thermodynamic modelling of the CO_2 (1) + (2) TEG test system at 298.15 K.

(●) Experimental data, this work; (○) Flash results using k_{ij} from this work; (x) Analysis results using k_{ij} from this work; (x) Flash results using literature k_{ij} ; (—) Analysis results using literature k_{ij} .

E.2. Graphical representation of the statistical significance of k_{ij} on the methane + methanol system.

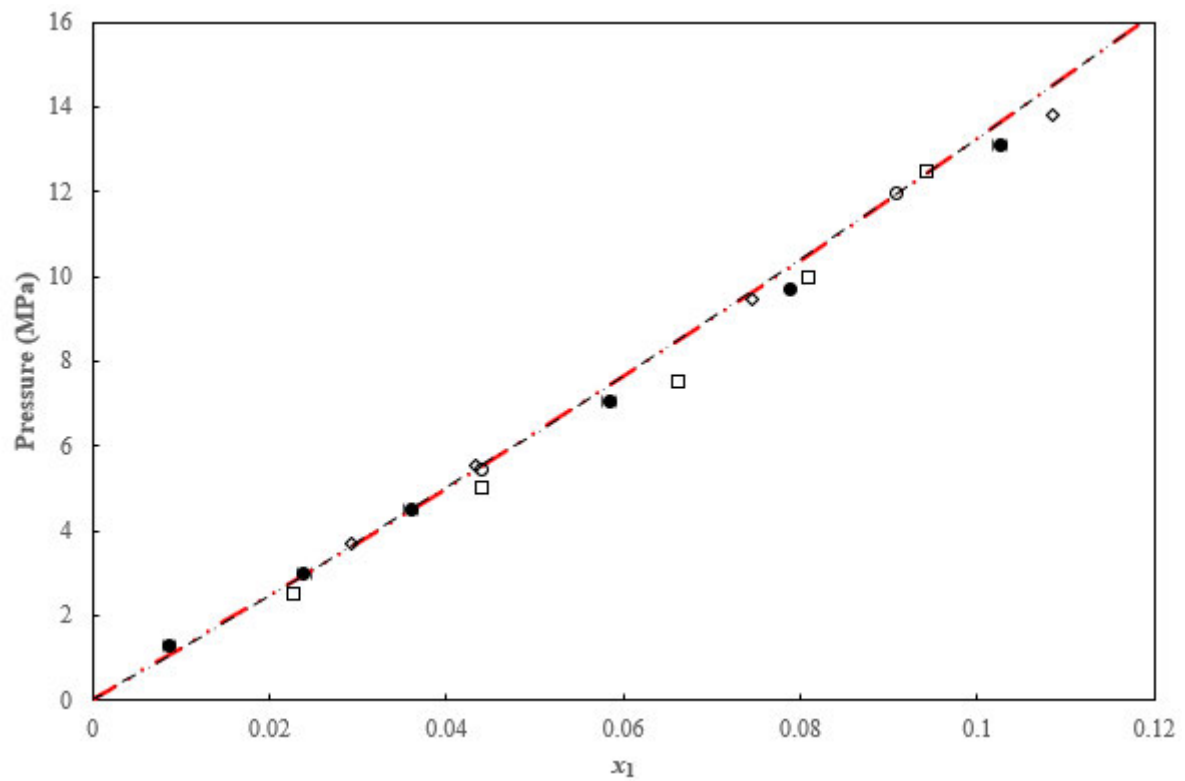


Figure E-2.1: PRWS thermodynamic modelling of the CH₄ (1) + CH₃OH (2) test system at 298.15 K.

(●) This work; (□) Yarym-Agaev et al. (Yarym-Agaev, et al., 1985); (○) Brunner et al. (Brunner, et al., 1987); (◇) Frost et al. (Frost, et al., 2015) ; (— · —) PRWS model using regressed k_{ij} from experimental data at 298.15 K; (— · —) PRWS model using regressed k_{ij} from experimental data at 303.15 K.

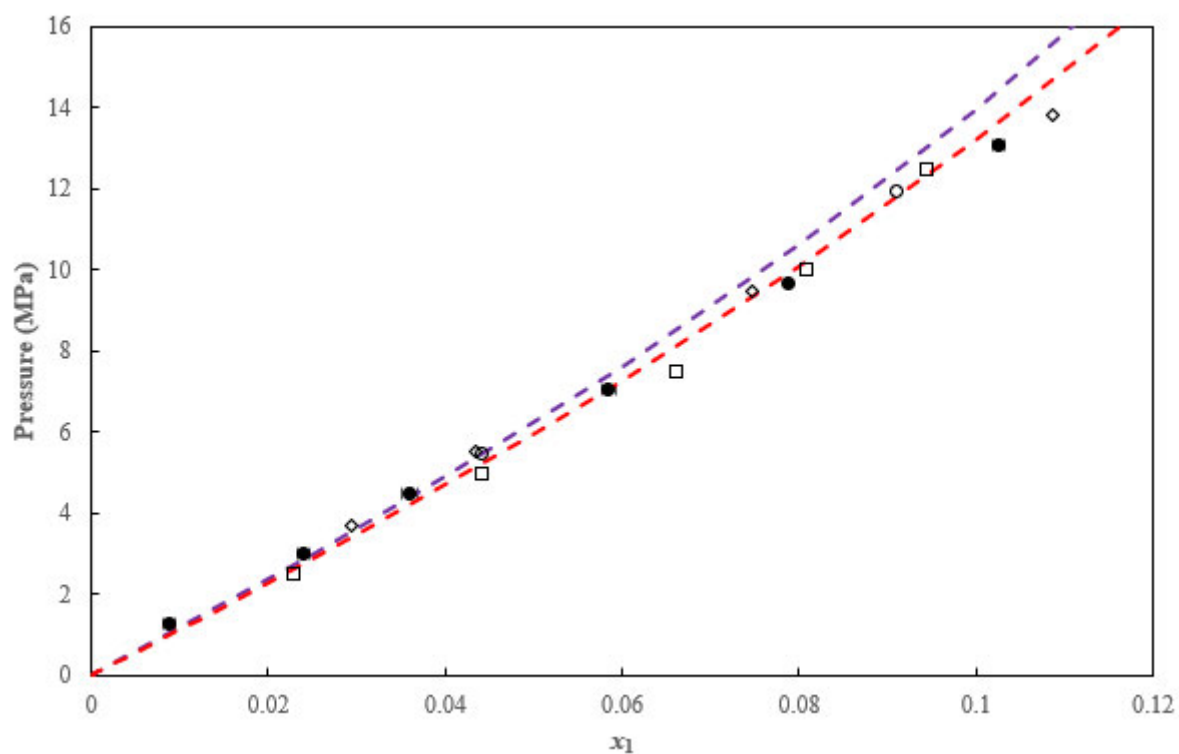


Figure E-2.2: CPA thermodynamic modelling of the CH_4 (1) + CH_3OH (2) test system at 298.15 K.

(●) This work; (□) Yarym-Agaev et al. (Yarym-Agaev, et al., 1985); (○) Brunner et al. (Brunner, et al., 1987); (◇) Frost et al. (Frost, et al., 2015) ; (---) CPA model using regressed k_{ij} from experimental data at 298.15 K; (---) CPA model using regressed k_{ij} from experimental data at 303.15 K.

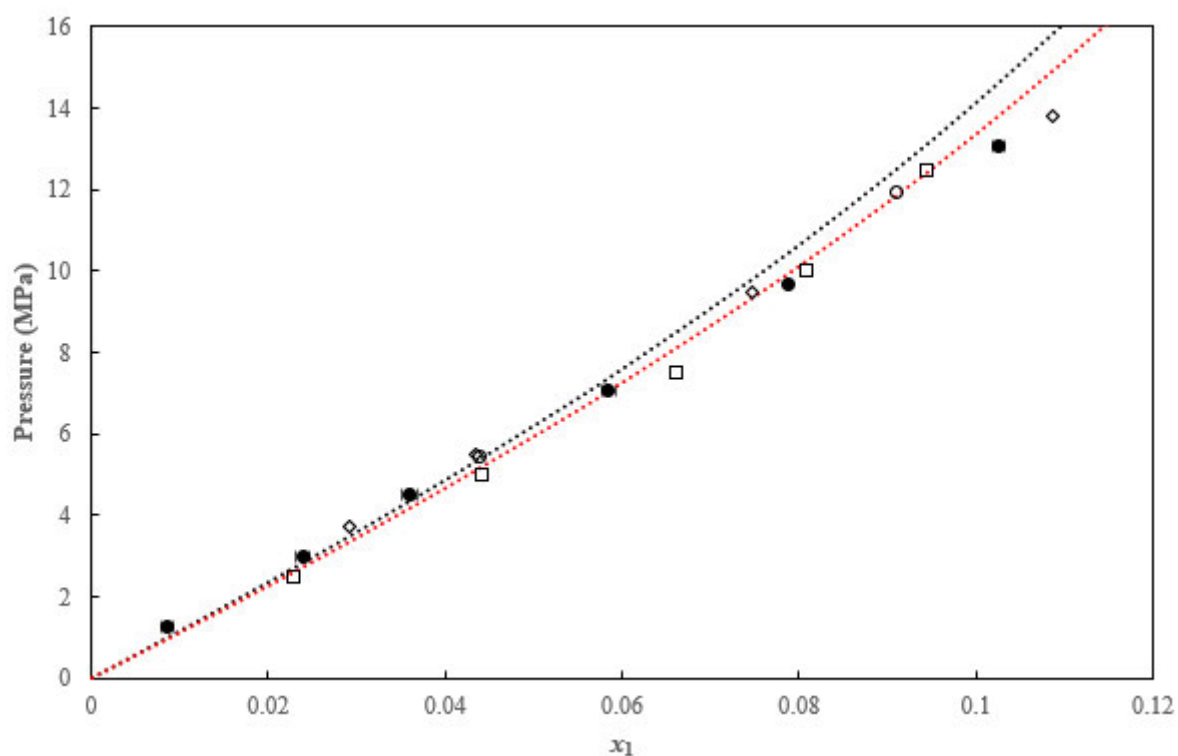


Figure E-2.3: PC-SAFT thermodynamic modelling of the CH_4 (1) + CH_3OH (2) test system at 298.15 K.

(●) This work; (□) Yarym-Agaev et al. (Yarym-Agaev, et al., 1985); (○) Brunner et al. (Brunner, et al., 1987); (◇) Frost et al. (Frost, et al., 2015) ; (····) PC-SAFT model using regressed k_{ij} from experimental data at 298.15 K; (····) PC-SAFT model using regressed k_{ij} from experimental data at 303.15 K.

E.3. CPA multicomponent systems bubble point predictions using k_{ij} s reported in table 6-19

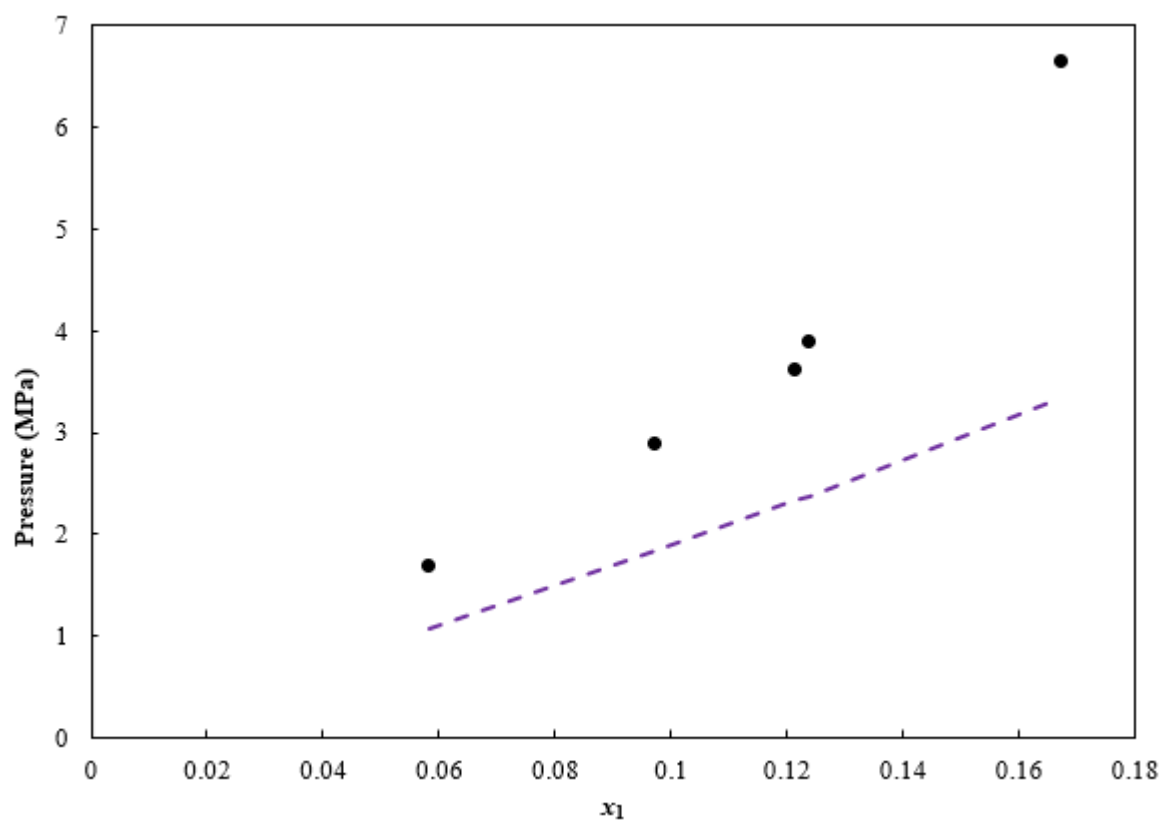


Figure E-3.1: CPA Thermodynamic modelling of the CO₂ (1) + (H₂O (2) /TEG (3) 10/90 wt% TEG) at 298.15 K.

(●) This work; (---) CPA model prediction using k_{ij} s reported in Table 6-19.

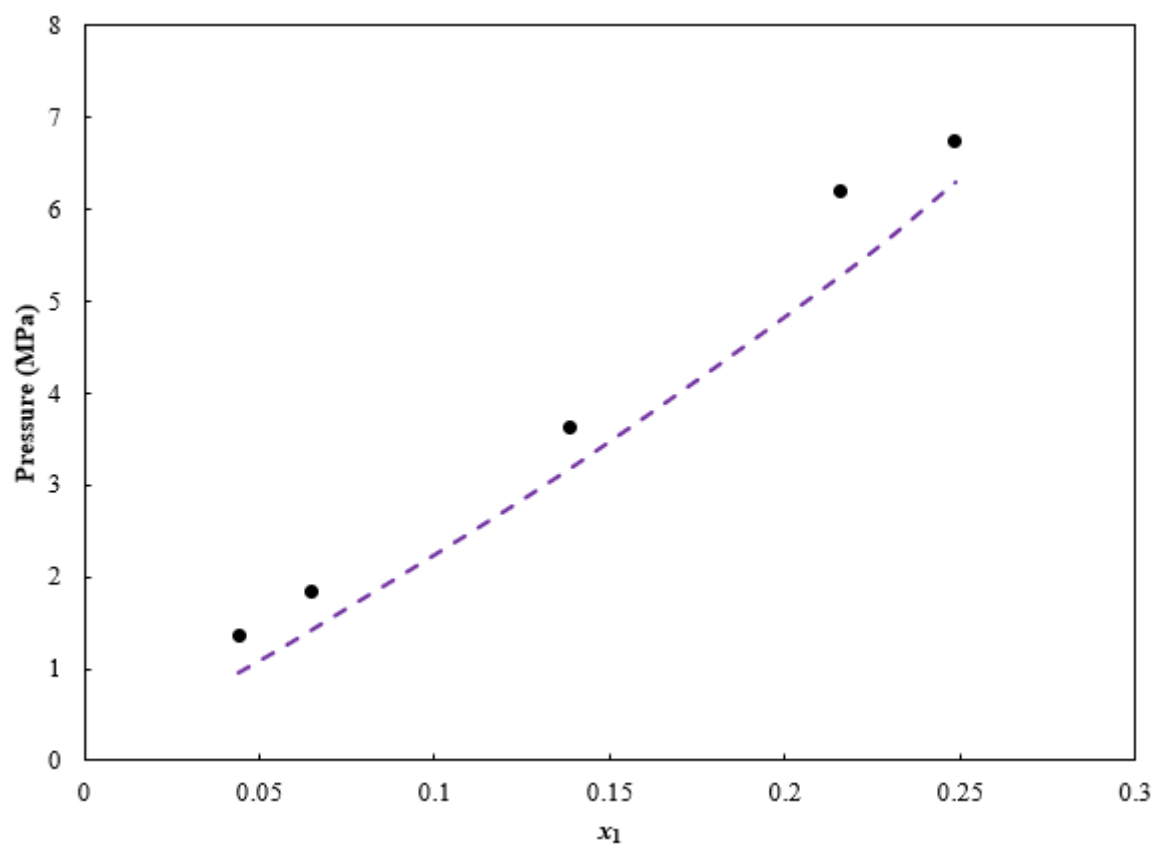
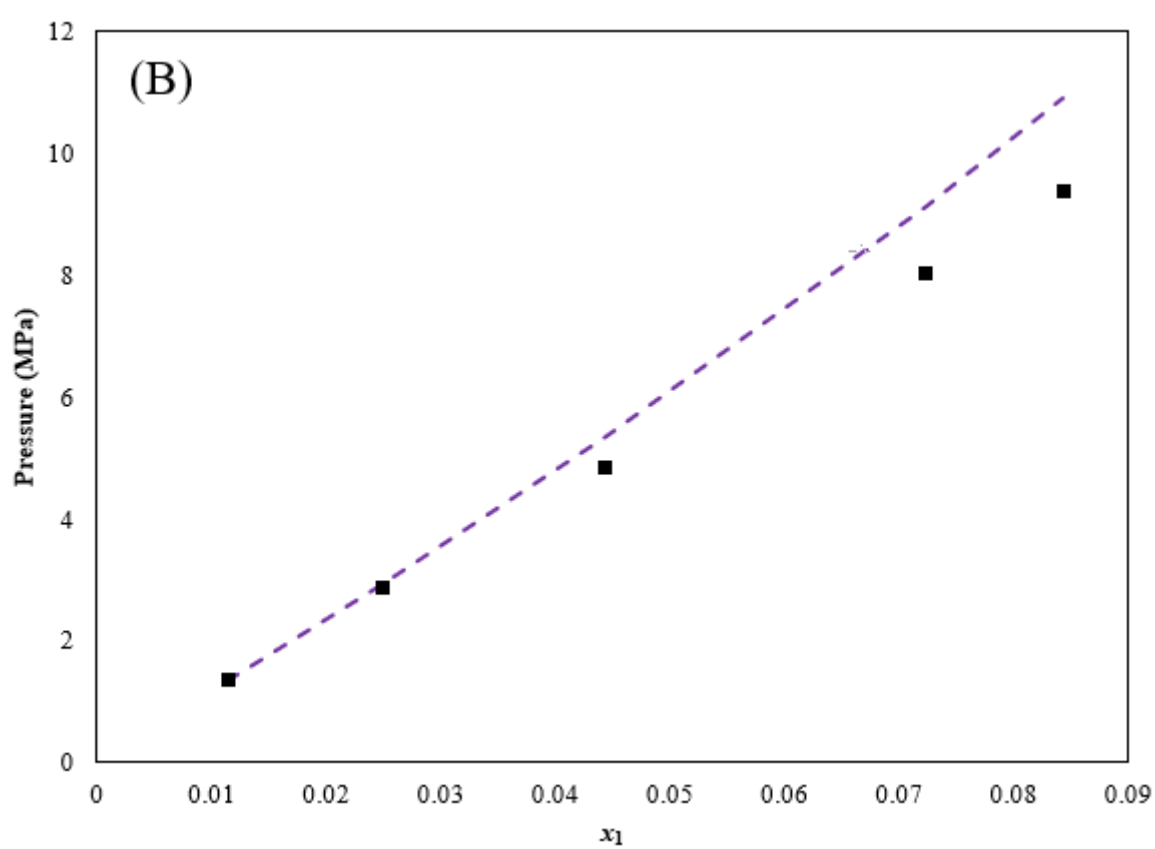
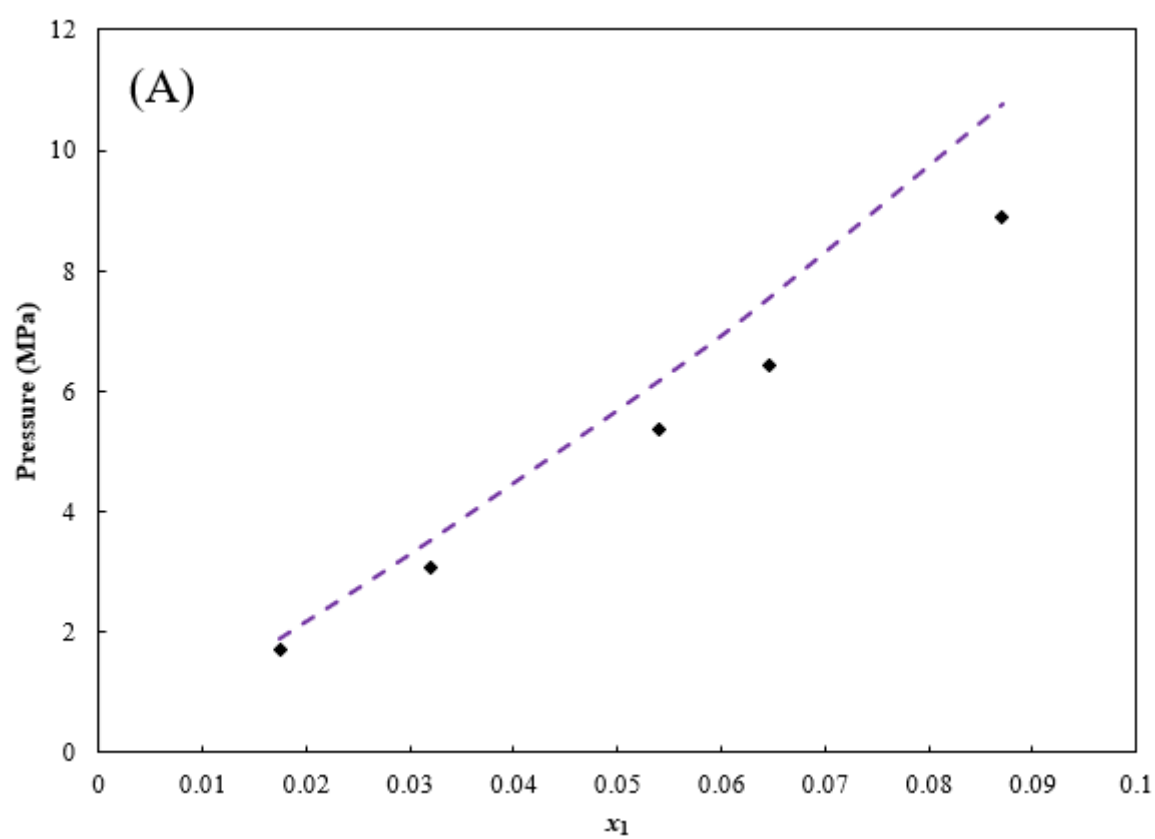


Figure E-3.2: CPA Thermodynamic modelling of the CO₂ (1) + (H₂O (2) /TEG (3) 3.5/96.5 wt.%) at 322.04 K.

(●) This work; (---) CPA model prediction using k_{ij} s reported in Table 6-19.



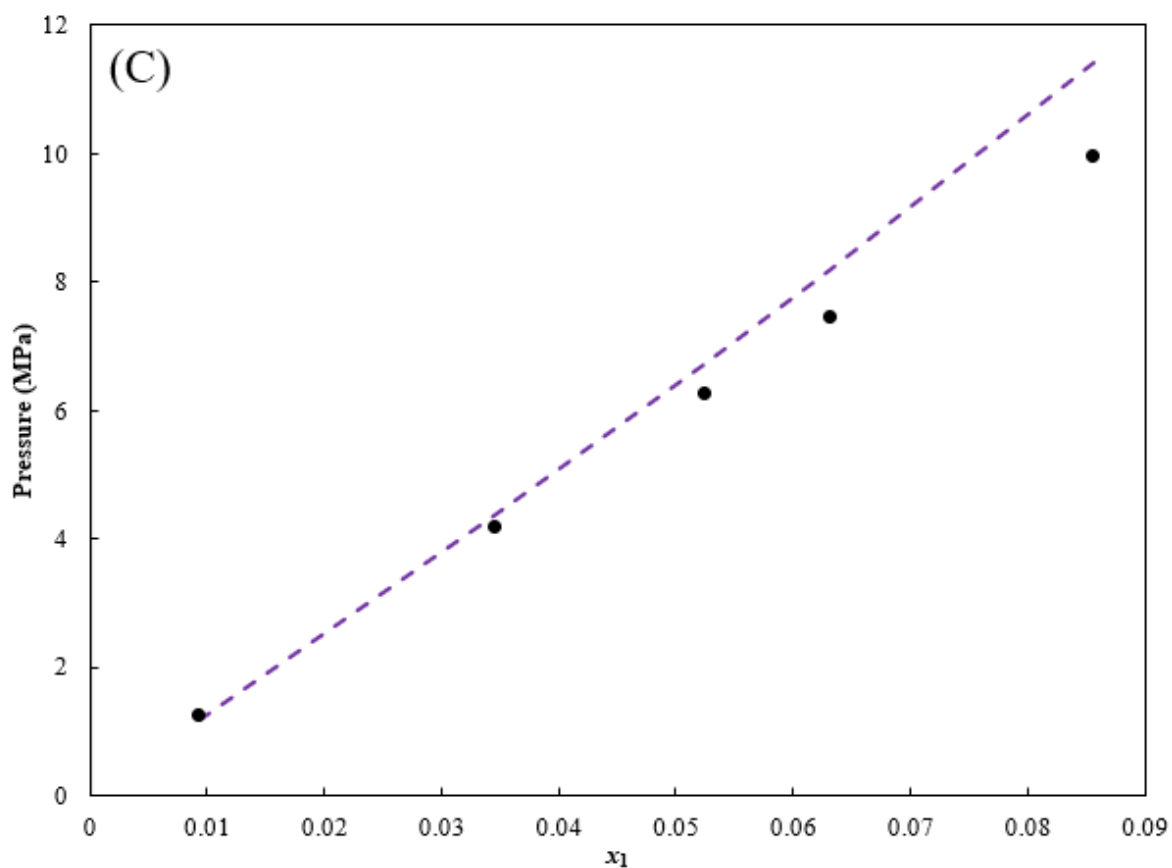


Figure E-3.3: CPA Thermodynamic modelling of the (CH_4 (1) / C_3H_8 (2) 95/5 mol%) + CH_3OH (3) system.

(A) $T = 283.16 \text{ K}$; (B) $T = 303.16 \text{ K}$; (C) $T = 323.15 \text{ K}$; Solid symbols (Experimental data) This work; (---) CPA model prediction using k_{ij} s reported in Table 6-19.

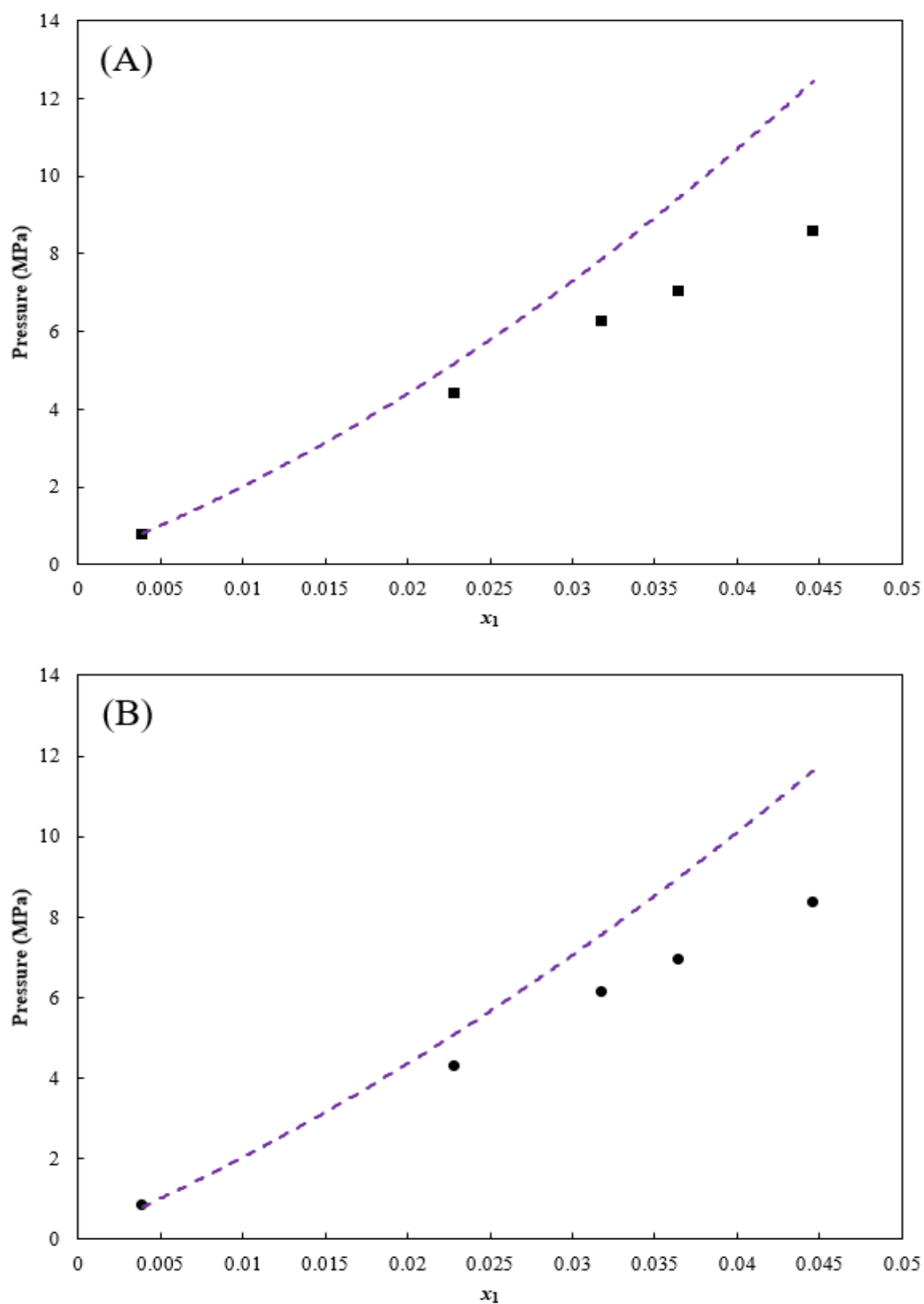


Figure E-3.4: CPA Thermodynamic modelling of the (CH₄ (1) / C₃H₈ (2) 95/5 mol%) + TEG (3) system.

(A) $T = 303.16$ K; (B) $T = 323.15$ K; Solid symbols (Experimental data) This work; (---) CPA model prediction using k_{ij} s reported in Table 6-19.

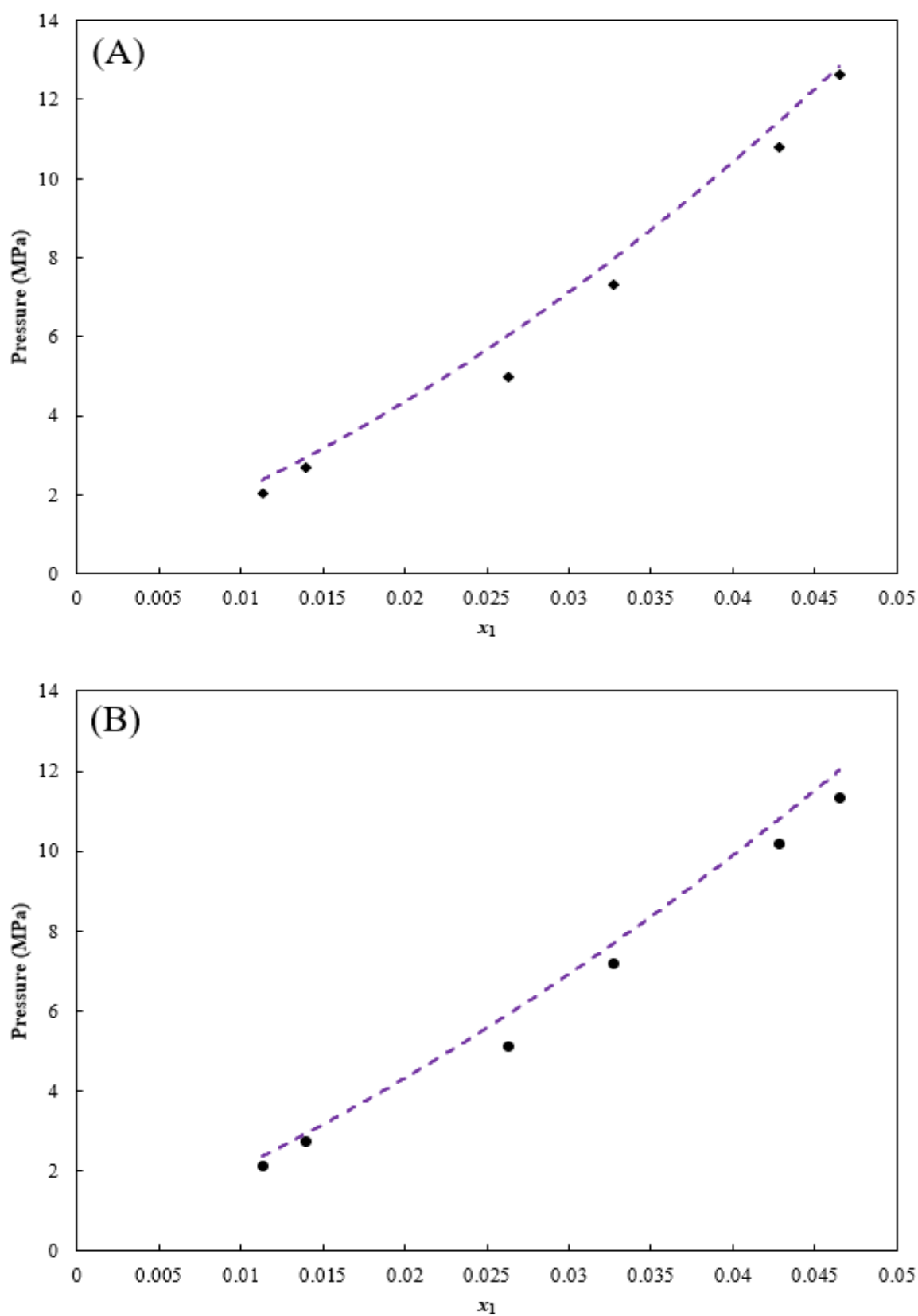


Figure E-3.5: CPA Thermodynamic modelling of the CH_4 (1) + $(\text{CH}_3\text{OH}$ (2) / TEG (3) 3.33/96.67 wt.%) system.

(A) $T = 303.16$ K; (B) $T = 323.16$ K; Solid symbols (Experimental data) This work; (---) CPA model prediction using k_{ij} s reported in Table 6-19.

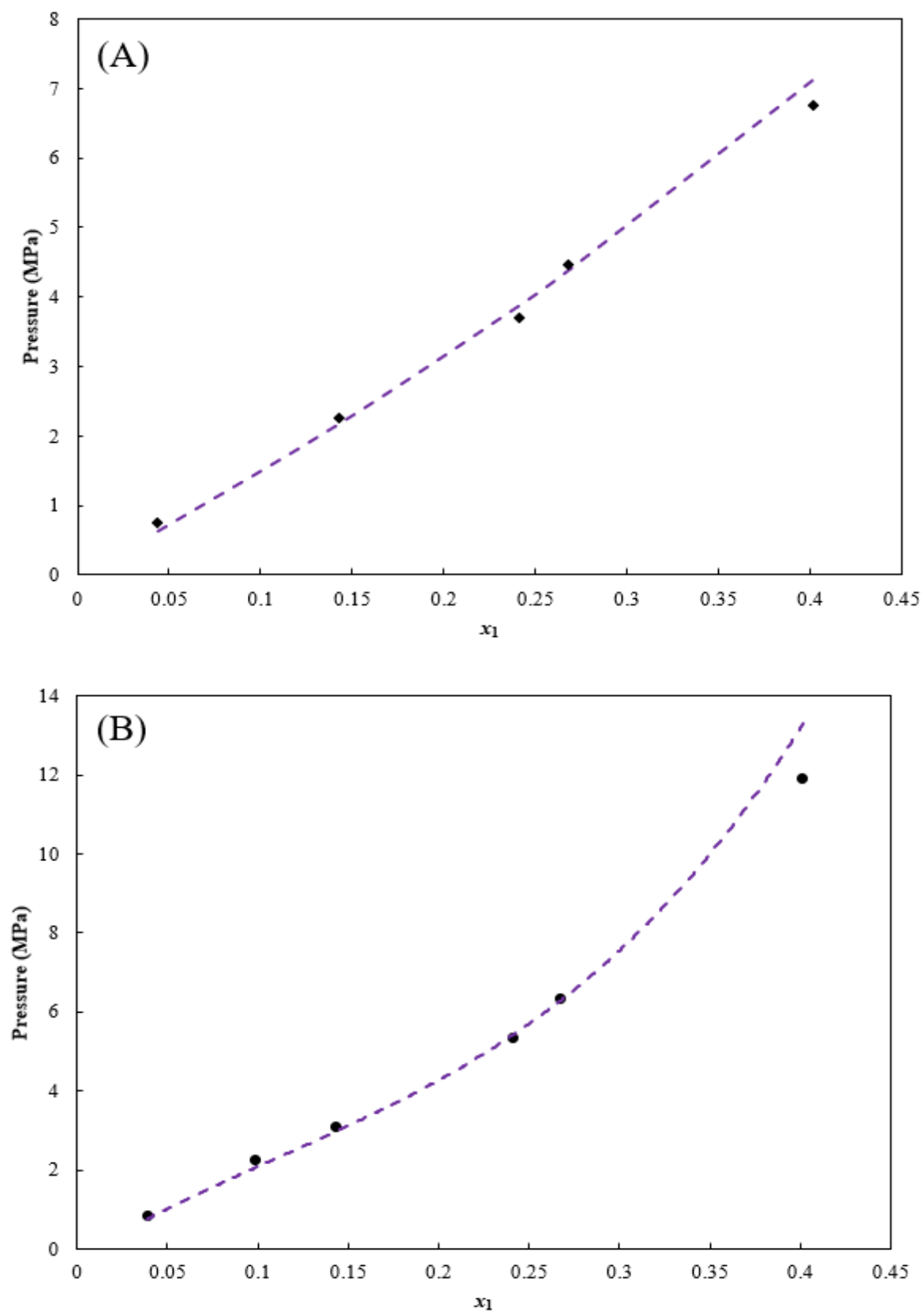
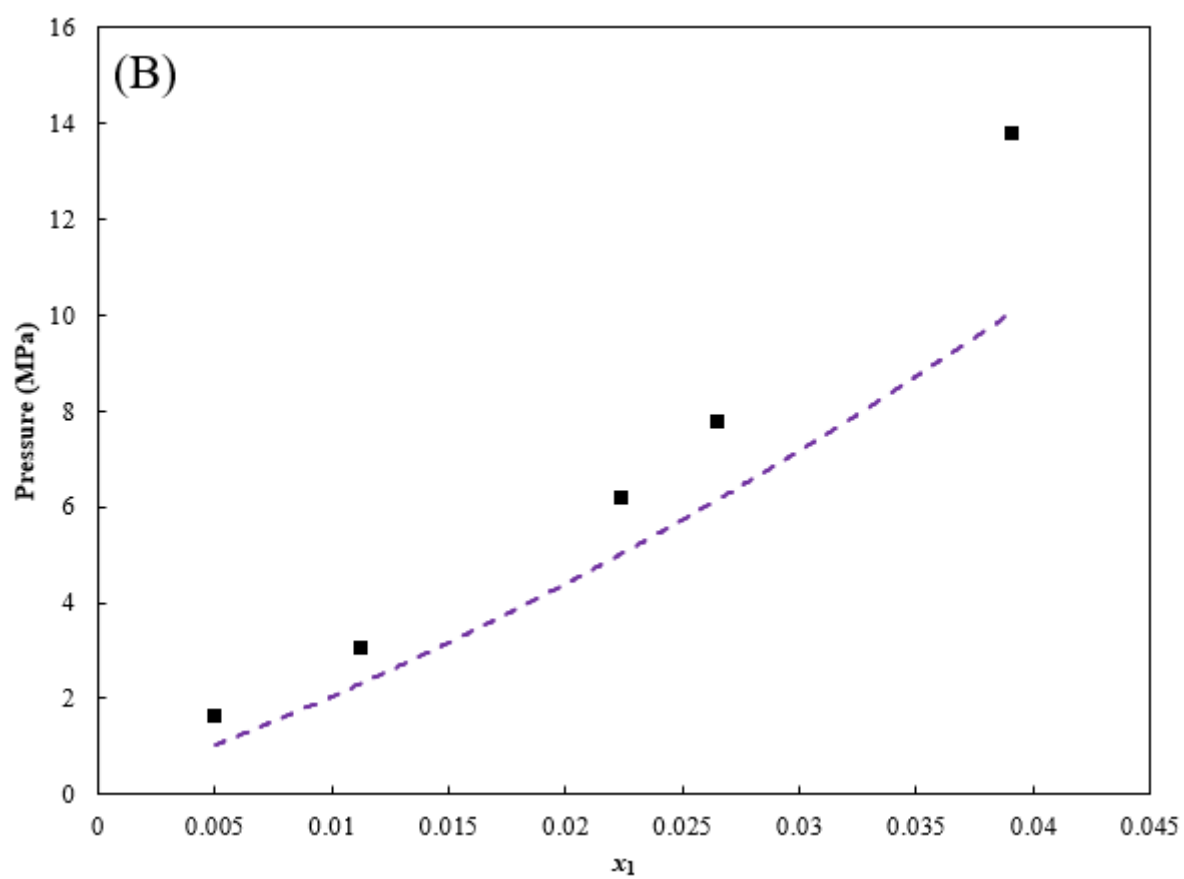
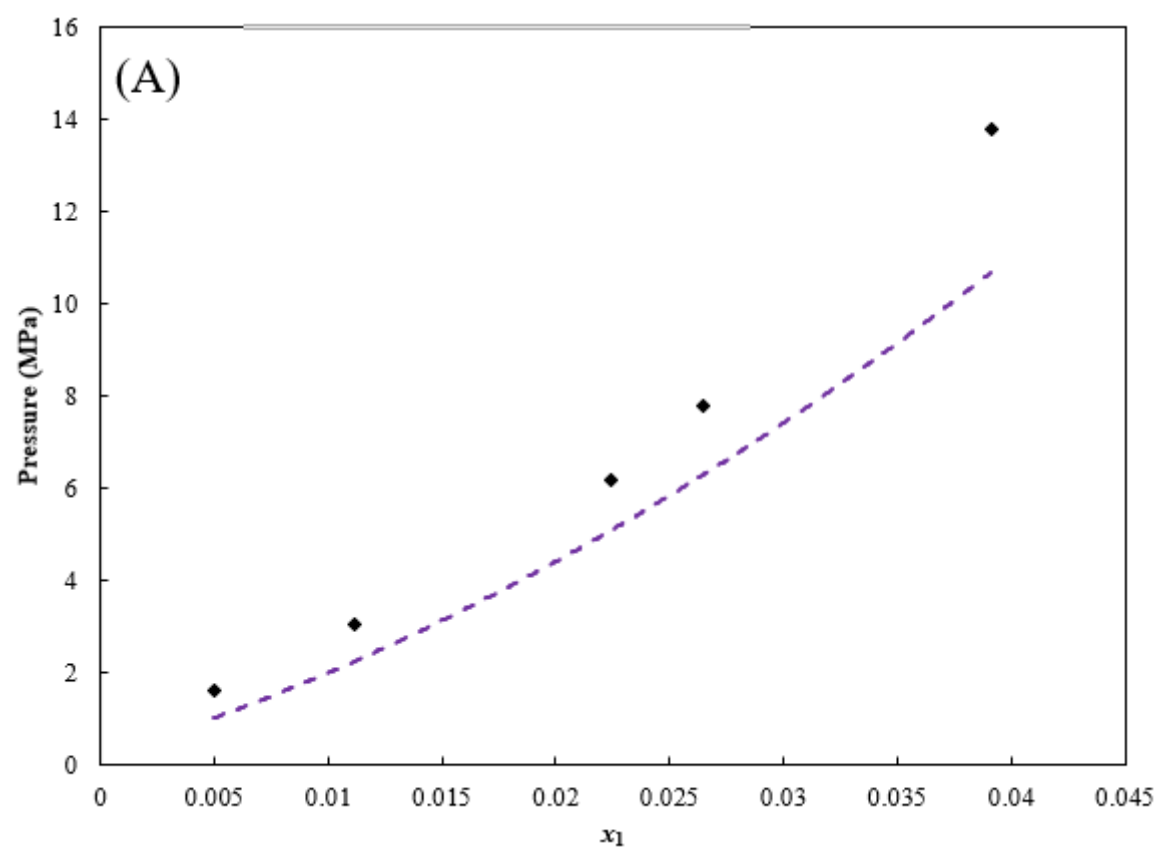


Figure E-3.6: CPA Thermodynamic modelling of the CO_2 (1) + $(\text{CH}_3\text{OH}$ (2) / TEG (3) 3.33/96.67 wt.%) system.

(A) $T = 303.16$ K; (B) $T = 323.15$ K; Solid symbols (Experimental data) This work; (---) CPA model prediction using k_{ij} s reported in Table 6-19.



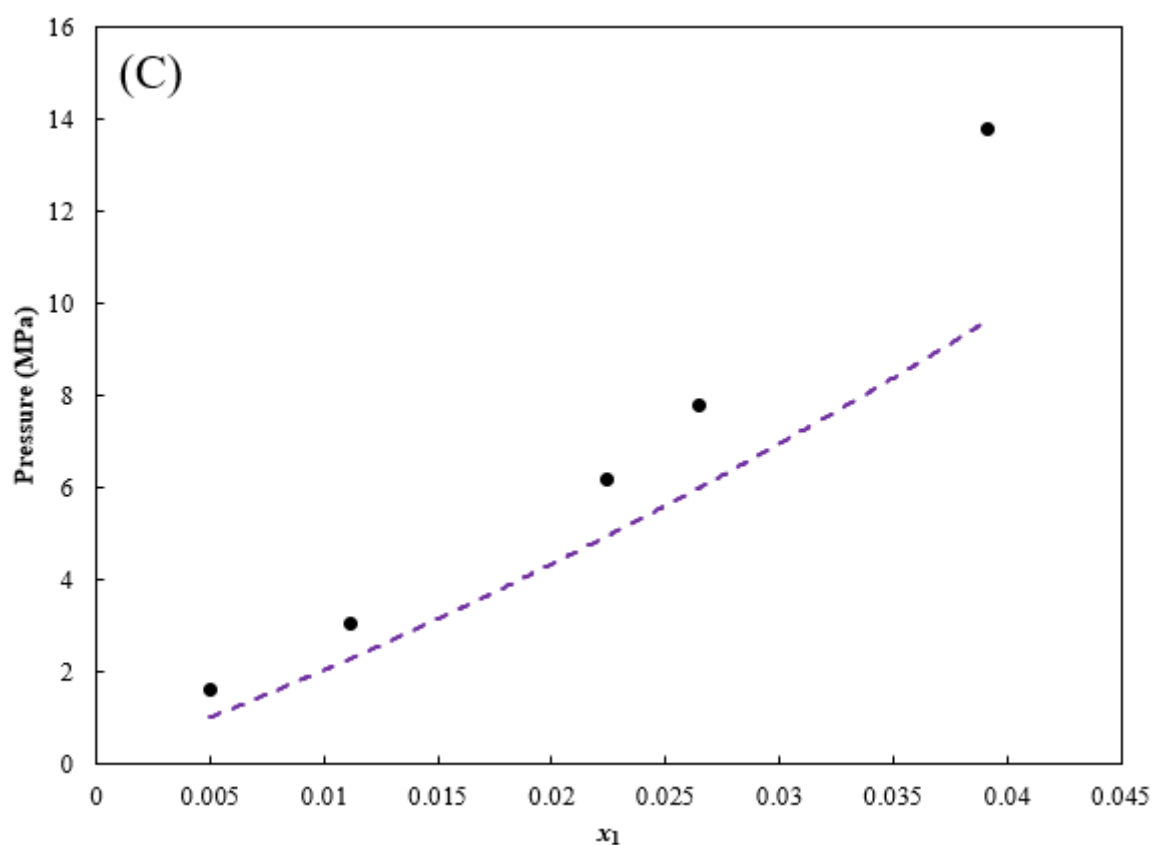
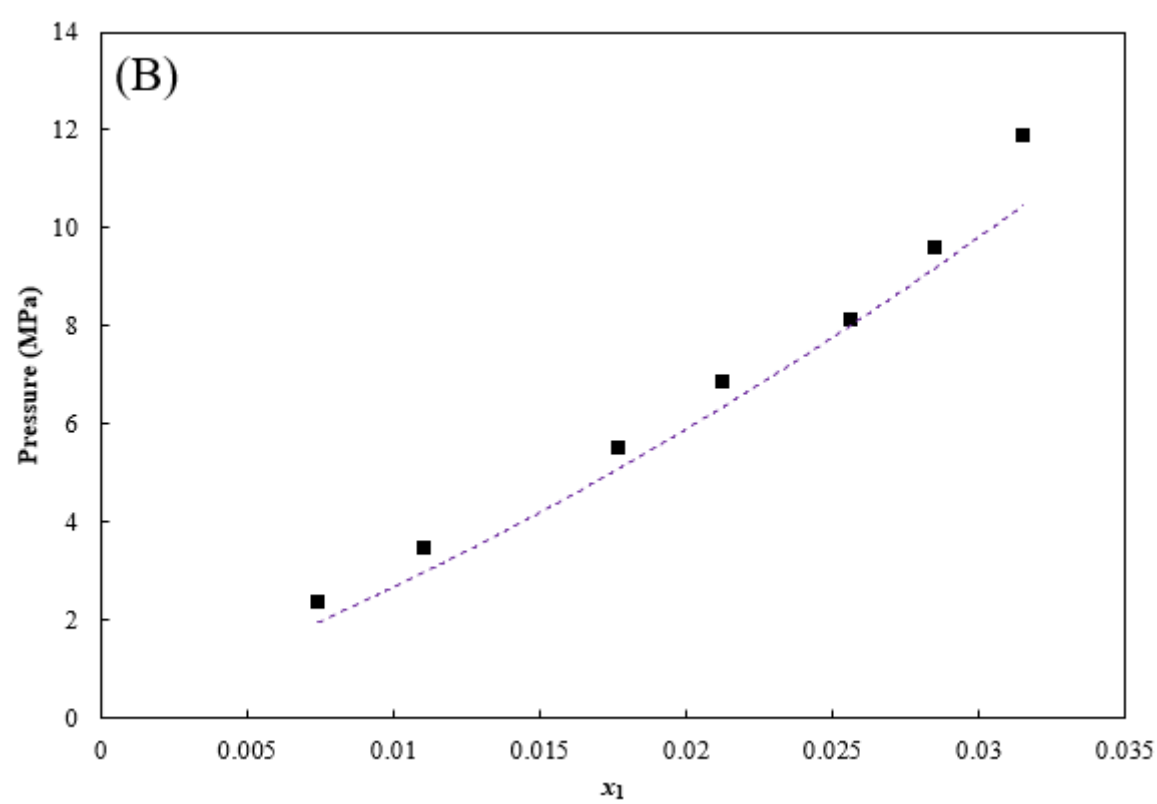
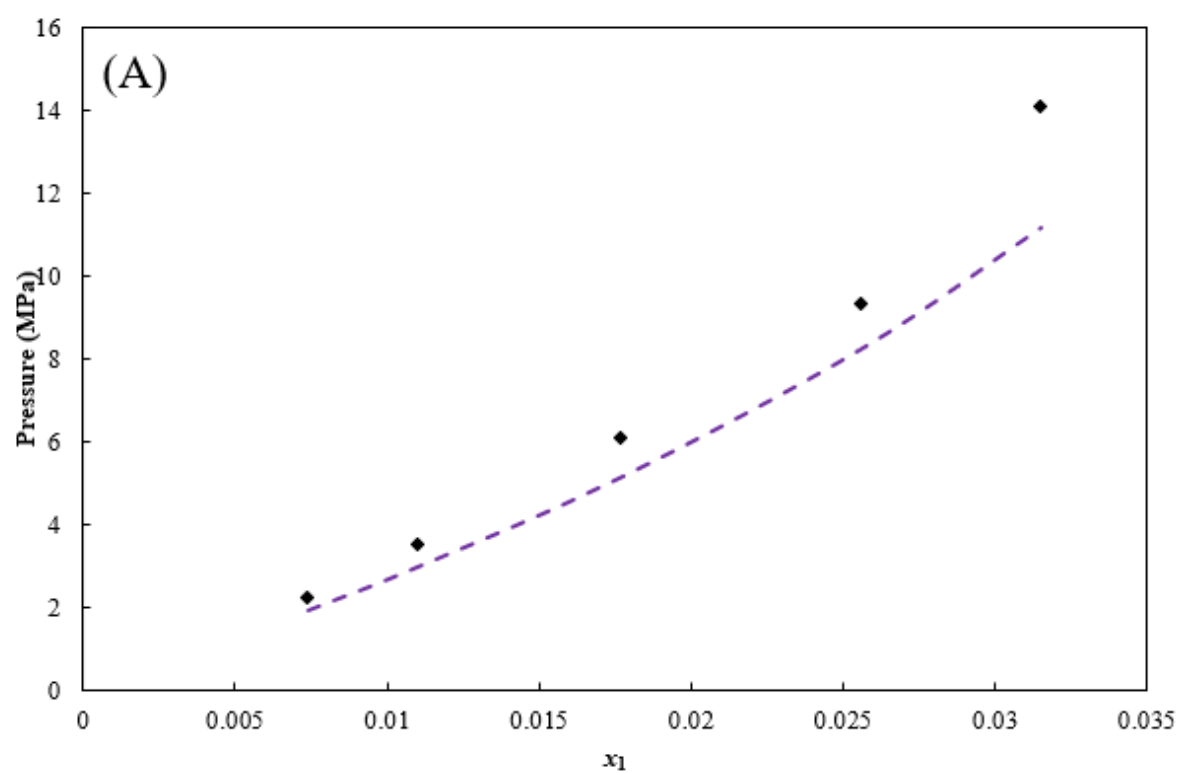


Figure E-3.7: CPA Thermodynamic modelling of the (CH₄ (1) /C₃H₈ (2) 95/5mol%) + (CH₃OH (3) /TEG (4) 3.33/96.67 wt.%) system.

(A) $T = 283.16$ K; (B) $T = 303.16$ K; (C) $T = 323.16$ K; Solid symbols (Experimental data) This work; (---) CPA model prediction using k_{ij} s reported in Table 6-19.



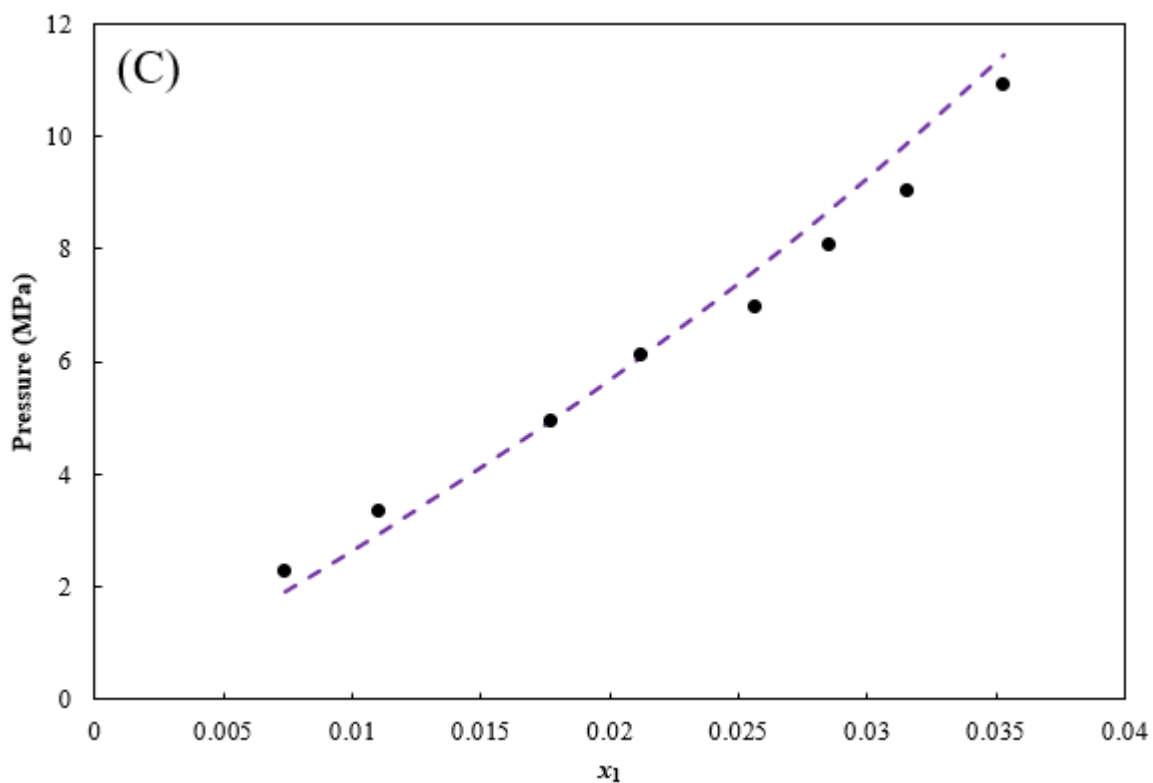
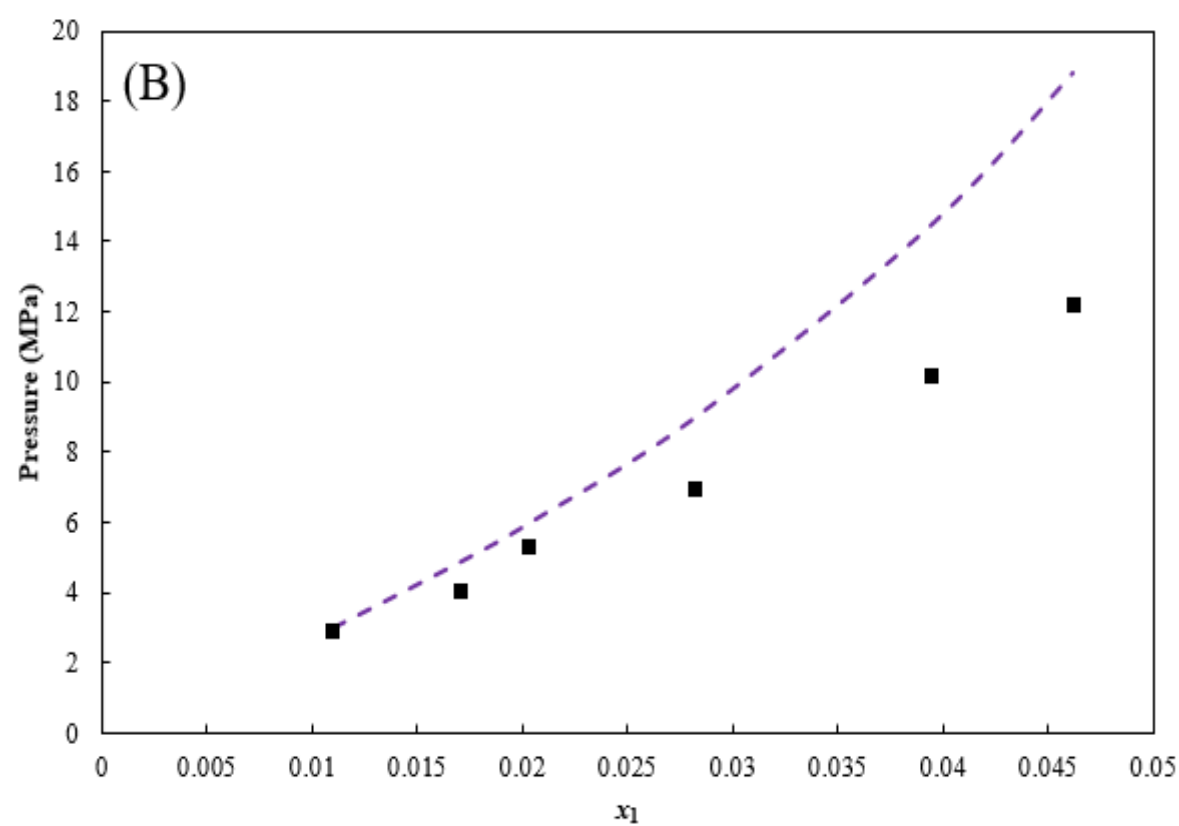
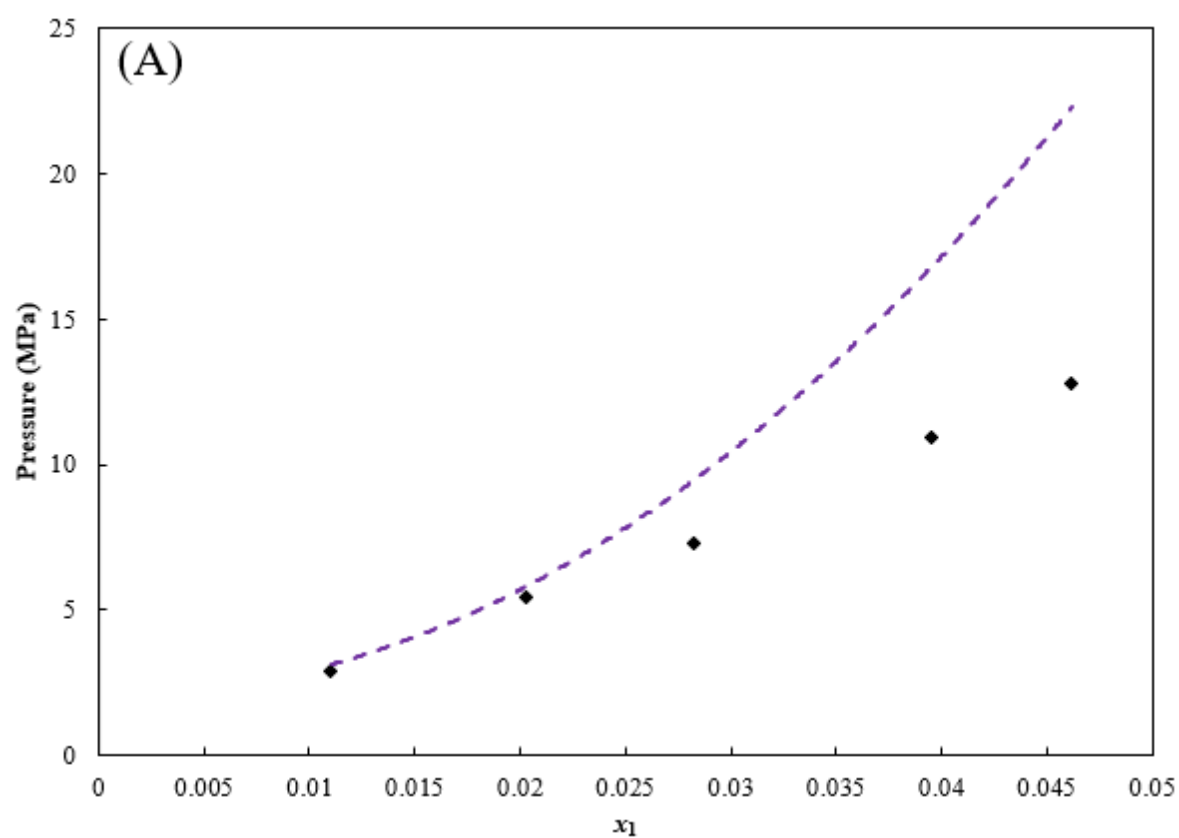


Figure E-3.8: CPA Thermodynamic modelling of the (CH_4 (1)/ C_3H_8 (2) 95/5mol%) + (H_2O (3) /TEG (5) 5/95% wt.): CH_3OH (4) 3.33 wt.%) system.

(A) $T = 283.16$ K; (B) $T = 303.16$ K; (C) $T = 323.15$ K; Solid symbols (Experimental data) This work;
 (---) CPA model prediction using k_{ij} s reported in Table 6-19.



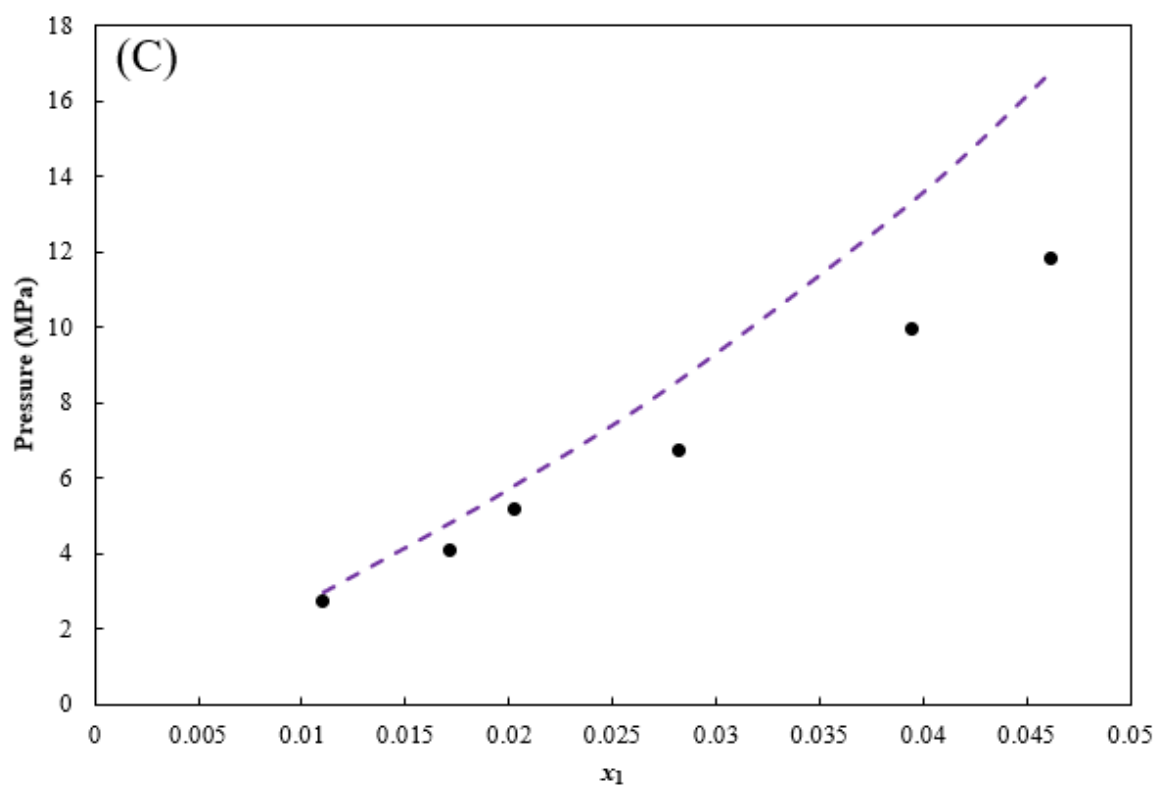


Figure E-3.9: CPA Thermodynamic modelling of the (CH₄ (1)/C₃H₈ (2)/CO₂ (3) 90.22/4.60/5.18 mol%) + ((H₂O (4) /TEG (6) 5/95 wt.%): CH₃OH (5) 3.33 wt.%) system.

(A) $T = 283.15$ K; (B) $T = 303.15$ K; (C) $T = 323.15$ K; Solid symbols (Experimental data) This work;
 (---) CPA model prediction using k_{ij} s reported in Table 6-19.

APPENDIX F: CPA PURE COMPONENT VAPOUR PRESSURE AND DENSITY PREDICTIONS

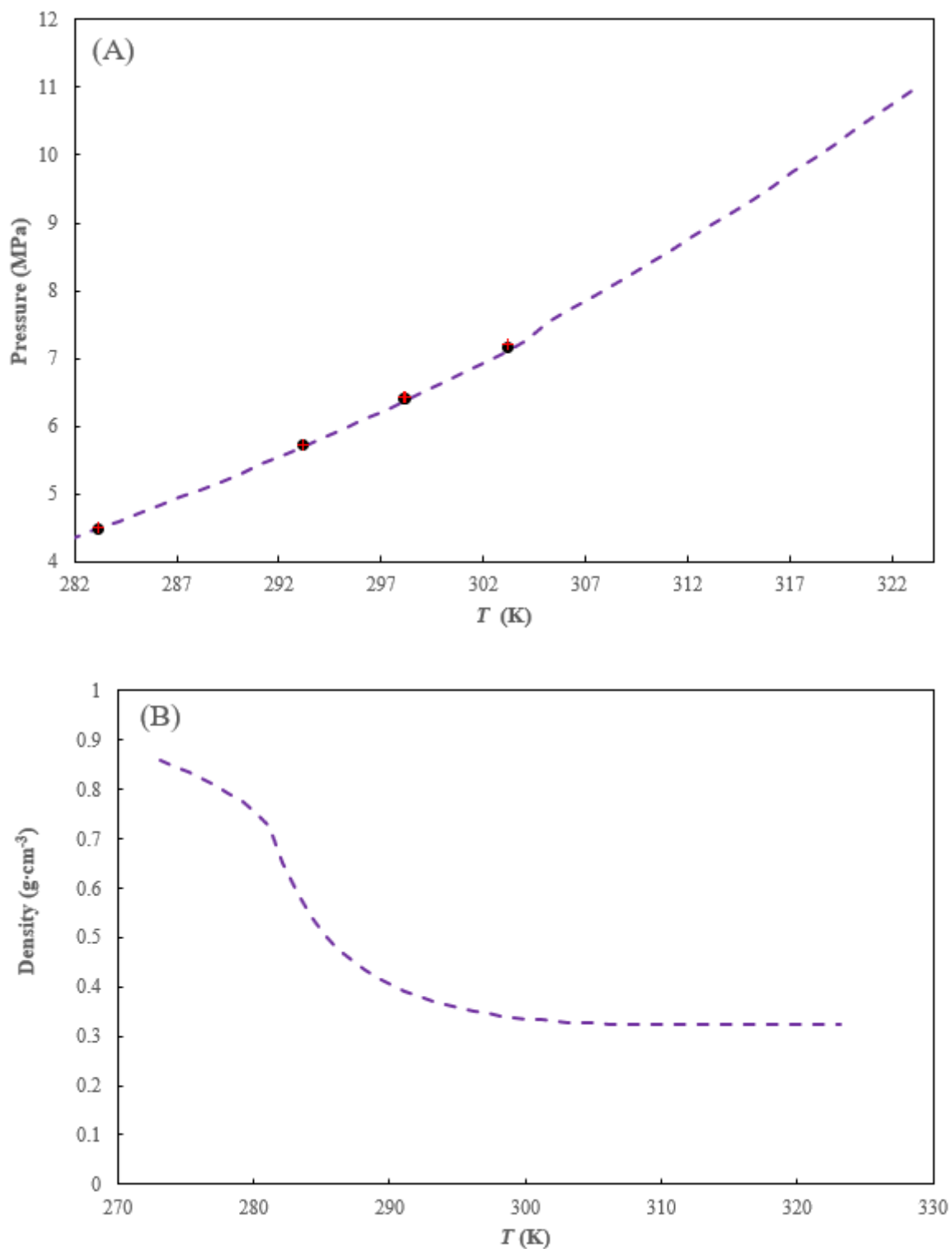


Figure F-1: Carbon dioxide pure component properties.
(A) Vapour pressure; (B) Density; This work (●); NIST TDE (Lemmon et al., 2021) (+); CPA (- - -).

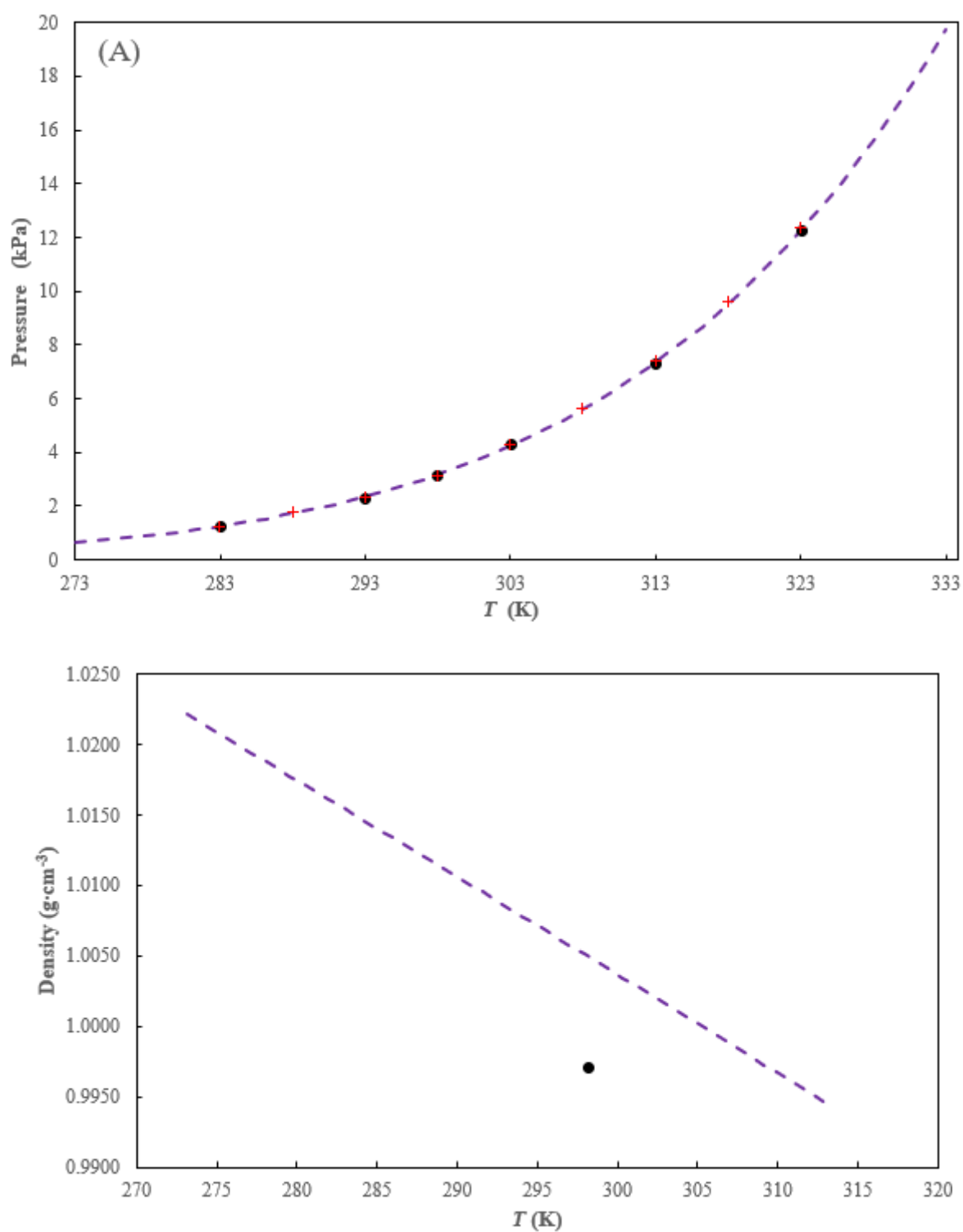


Figure F-2: Water pure component properties.

(A) Vapour pressure; (B) Density; This work (●);(Louder, et al., 1924) (+); CPA (- - -).

Figure F-2 shows that the CPA model over predicted the density of water at 298.15 K as compared to the experimental data of this work.

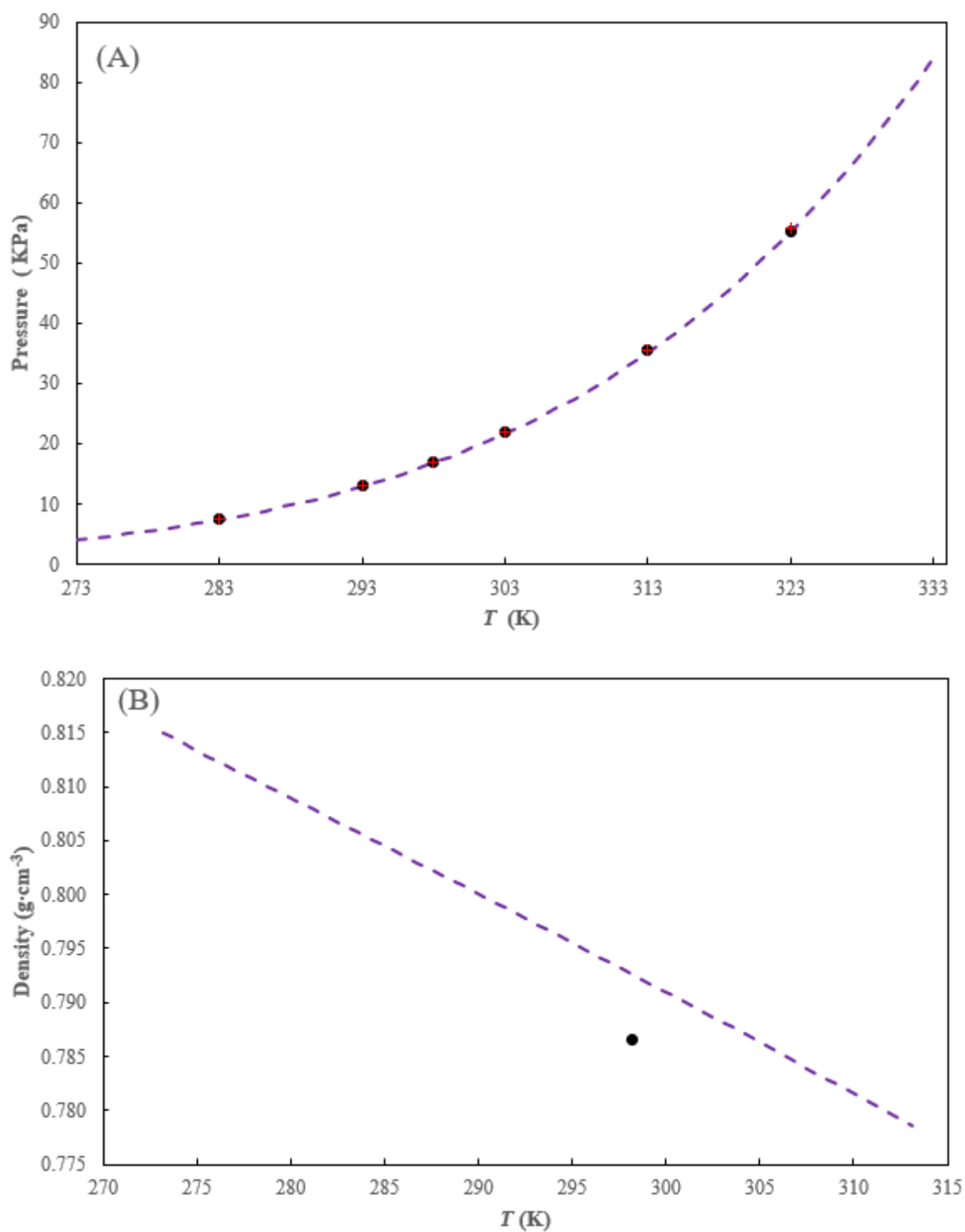


Figure F-3: Methanol pure component properties.

(A) Vapour pressure; (B) Density; This work (●); NIST TDE (Lemmon et al., 2021) (+); CPA (- - -).

Figure F-3 shows that the CPA model over predicted the density of methanol at 298.15 K compared to the experimental data of this work.

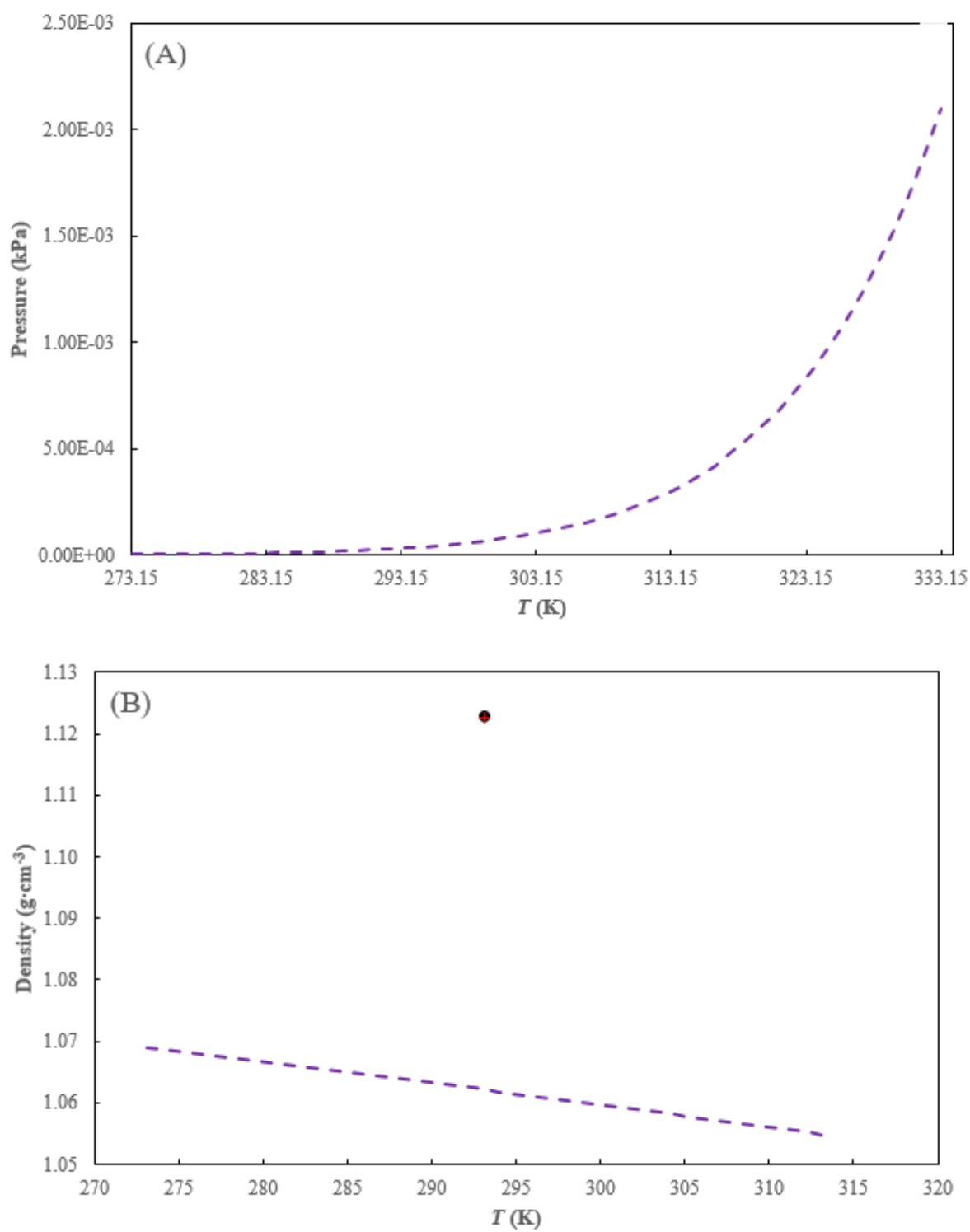


Figure F-4: TEG pure component properties.

(A) Vapour pressure; (B) Density; This work (●); (Rastorguev and Gazdiev, 1969) (+); CPA (- - -).

Figure F-4 shows that the CPA model under predicted the density of TEG at 293.15 K compared to the experimental data of this work and the literature data of (Rastorguev and Gazdiev, 1969).

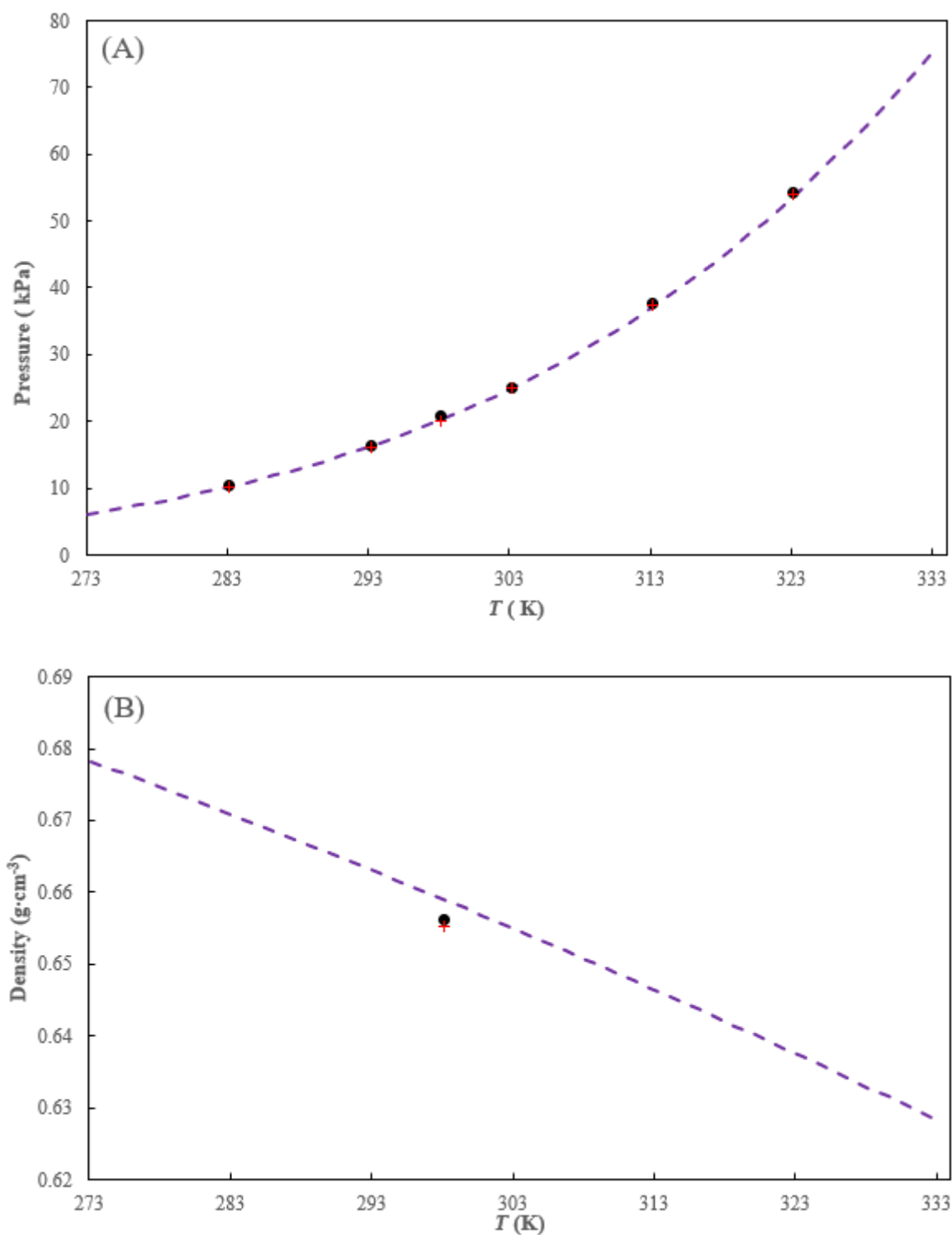


Figure F-5: Hexane pure component properties.

(A) Vapour pressure; (B) Density; This work (●); NIST (Lemmon et al., 2021) (+) for Figure (A); (Mascato et al., 2000) (+) for Figure (B); CPA (---).

Figure F-5 (B) shows that the CPA model slightly over predicted the density of hexane at 298.15 K compared to the data of this work, as well as the literature data.

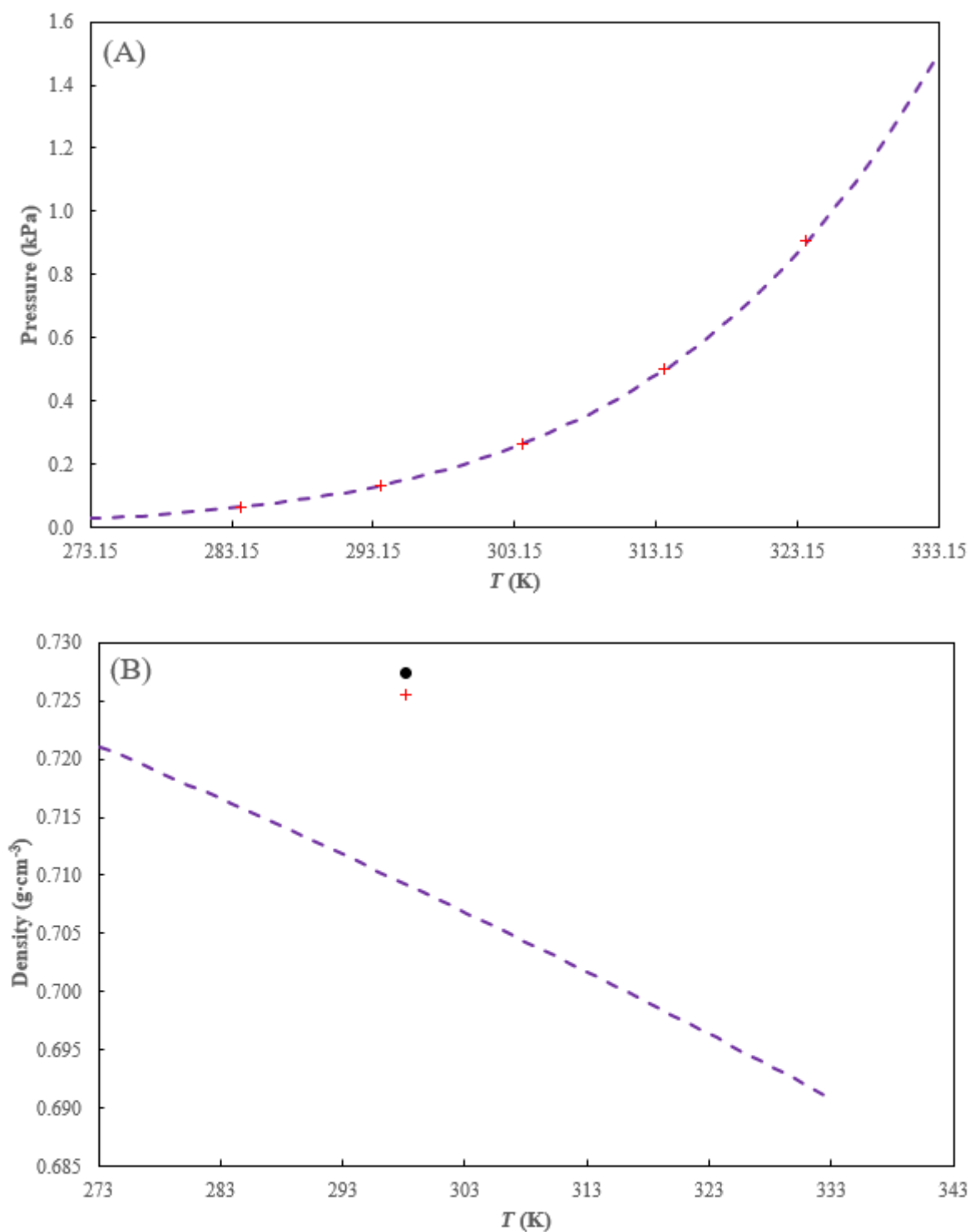


Figure F-6: Decane pure component properties.

(A) Vapour pressure; (B) Density; This work (●); (Sahki et al., 1999) (+) for Figure (A); (Haynes et al., 2014b) (+) for Figure (B); CPA (- -).

Figure F-6 (B) shows that the CPA model under predicted the density of n-decane at 298.15 K compared to the data of this work, as well as the literature data of (Haynes et al., 2014b).